DAΦNE '95

Frascati, April 4-7, 1995

Second Workshop on Physics and Detectors for DAΦNE

FRASCATI PHYSICS SERIES

Series Editor
Vincenzo Valente

Technical Editor
Luigina Invidia

Volume IV

Istituto Nazionale di Fisica Nucleare – Laboratori Nazionali di Frascati
Divisione Ricerca – SIS – Ufficio Pubblicazioni
P.O. Box 13, I–00044 Frascati (Roma) Italy
email: sispub@vaxlnf.lnf.infn.it

FRASCATI PHYSICS SERIES

SECOND WORKSHOP ON PHYSICS AND DETECTORS FOR DAΦNE

Copyright © 1995, by INFN Laboratori Nazionali di Frascati
SIS – Ufficio Pubblicazioni

All rights reserved. No part of this publication may be reproduced, stored in a retrieval system or transmitted, in any form or by any means, electronic, mechanical, photocopying, recording or otherwise, without the prior permission of the copyright owner.

ISBN 88-86409-05-02

Printed in Italy

FRASCATI PHYSICS SERIES

Volume IV

WORKSHOP ON PHYSICS AND DETECTORS FOR DAΦNE '95

Editors
R. Baldini, F. Bossi, G. Capon, G. Pancheri

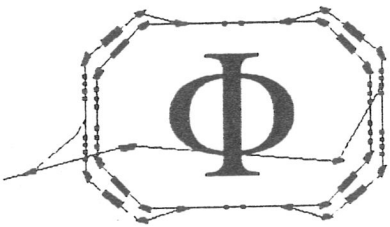

Proceedings of the "Workshop on Physics and Detectors for DAΦNE"
Frascati, April 4-7, 1995

International Advisory Committee

G. Alexander	*(Tel Aviv)*
G. Bellettini	*(Pisa)*
K. Berkelman	*(Cornell)*
T. Bressani	*(Torino)*
S. Donnachie	*(Manchester)*
C. Dover	*(Brookhaven)*
P. Franzini	*(Roma)*
D.R. Gill	*(Triumf)*
M. Greco	*(L'Aquila)*
J. Haissinski	*(Orsay)*
E. Iarocci	*(Frascati)*
W. Kluge	*(Karlsruhe)*
L. Maiani	*(Roma)*
R.D. Peccei	*(Ucla)*
B. Richter	*(Slac)*
G. Salvini	*(Roma)*
A.N. Skrinsky	*(Novosibirsk)*
G. Vignola	*(Frascati)*

Local Organizing Committee

R. Baldini
S. Bertolucci
C. Bloise
F. Bossi
G. Capon
R. De Sangro
F.L. Fabbri
P. Gianotti
G. Nicoletti
G. Pancheri
V. Patera
M. Piccolo
V. Valente

Secretariat

M.C. D'Amato
S. Giromini
G. Zaratti

FOREWORD

The Second Workshop for Physics and Detectors for DAΦNE was held in Frascati from April 4th, 1995, and was attended by about 200 physicists.

DAΦNE is the ϕ–factory under construction in Frascati, to be commissioned in the spring of 1997.

The aim of the Workshop was to review theory and experiments on CP violation, K interactions and decays, light hadrons spectroscopy, hypernuclear physics, tests of Quantum Mechanics and all the other issues which are part of the experimental program at DAΦNE.

Status reports on the approved experiments, KLOE and FINUDA, were given, as well as the first proposal for a measurement of the kaonic hydrogen atom energy levels, to become the DEAR experiment.

We thank all the participants for their contribution to the success of the Workshop. We also notice that the Workshop would not have been possible without the dedication and the efforts of the Laboratory staff, and in particular of the Workshop secretariat, who have greatly helped in the organization.

We are looking forward to the next Workshop in which real data from DAΦNE will be presented and discussed.

The Editors

QUANTUM MECHANICS AND TIME EVOLUTION OF THE $K\bar{K}$ SYSTEM 235

PARALLEL SESSION

Y.N. Srivastava	Real and Virtual Strange Processes	237
P.H. Eberhard	EPR Paradox and Tests of Quantum Mechanics at DAΦNE	247
L. Stodolski	EPR Effects without Collapse of the Wavefunction	267
N.E. Mavromatos	Experimental Tests of CPT Symmetry and Quantum Mechanics at CPLEAR	269
L. Khalfin	CP Violation Problem Beyond Approximate Lee–Ohme–Yang Theory	287
J. Bogdanowicz	On the Concept of the Life Time of Unstable Particles (The Φ Delayed Decay)	289

HYPERNUCLEI AND K–N INTERACTIONS 291

PLENARY SESSION

A. Zenoni	Status Report on FINUDA	293
A. Gal	Hypernuclei: A Theoretical Review	315
B.R. Holstein	Weak Hypernuclear Decay	333
T. Yamazaki	Present Status of Hypernuclear Studies	347
C. Guaraldo	How to Solve at DAΦNE The "Kaonic Hydrogen Puzzle"	349
A. Olin	KN Scattering at DAΦNE?	379

PARALLEL SESSION

A. Molinari	About the Decay of the Λ in a Nucleus	393
A. Ramos	One–And Two–Nucleon Induced Λ Decay	405
R. Alzetta	Non Leptonic Λ Weak Decays in Light to Medium Hypernuclei	415
R. Sawafta	Σ Hypernuclei	427
B. Saghai	Low Energy K^-–Proton Interactions	435
T. Barnes	KN Scattering in the Nonrelativistic Quark Model	445
R.C. Barrett	Relativistic Equations for Kaon–Nucleus Interactions	459
M. Iwasaki	Measurement of Kaonic Hydrogen X–Rays at KEK	461

HADRONIC PHYSICS 471

PLENARY SESSION

J. Gasser — Prospects of Chiral Perturbation Theory 473
L. Montanet — Open Problems in Meson Spectroscopy, Which Should be Solved at DAΦNE 495
A. Courau — Two–Photon Physics at DAΦNE 505
G. Altarelli — The QED Running Coupling and DAΦNE 523
P. Spillantini — Experimental Search for Antimatter in the Universe 535
C. Rubbia — Matter Lifetime 537

PARALLEL SESSION

E.P. Solodov — Recent Results of the ϕ–Meson Study with CMD–2 AT VEPP–2M and Relevance to Future CP, CPT Φ –Factory Studies 541
V.N. Ivanchenko — Review of Radiative Decays Study 559
G.V. Fedotovich — Measurement of the $e^+e^- \to \pi^+\pi^-$ Coss Section in the Energy Range Between ρ and Φ Meson 571
V. Fliaguine — Results in K Decays from Serpukhov PS 583
S. Dubnicka — An Improved Evaluation of Hadronic Contributions to the Anomalous Magnetic moment of Charged Leptons 593
J. Stern — How to see the Chiral Structure of QCD Vacuum in Low Energy π–π Scattering 609
M. Finkemeier — Radiative Corrections to π_{l2} and K_{l2} 623
P. Kokkas — Measuremet of the Difference of the K^o–$\overline{K}^o$ Forward Scattering Amplitudes in Carbon at Low Momentum with the CPLEAR Detector 635
N.N. Achasov — Do the Proofs of Appreciable $\varphi\omega$ Mixing Exist? 646

Participants 655

CP VIOLATION: MACHINE, EXPERIMENTS, THEORY

PLENARY SESSION

A.N. Skrinsky	VEPP–2M Status and Prospects and Φ–Factory Project at Novosibirsk	3
G. Vignola	Status Report on DAΦNE	19
J. Lee–Franzini	Status Report on KLOE	31
P. Pavlopoulos	Measurements of CP and T Violation Parameters in the Neutral Kaon System at CPLEAR	55
B. Winstein	Status of KTEV	73
M. Calvetti	Experimental Search for Direct CP–Violation Status Report on NA48 at CERN	81
A. Dzierba	Measuring Rare Radiative Decays of the ϕ Meson at CEBAF	99
R.D. Peccei	CP Violation: A Theoretical Review	119
P. Roudeau	Expectations and Measurements of CP Violation in the D System Using the Tau/CHARM Factory Facility	147
A. Ali	Determination of the CKM Matrix from B Decays	163

VEPP–2M STATUS AND PROSPECTS AND Φ–FACTORY PROJECT AT NOVOSIBIRSK

A.N. Skrinsky
Budker Institute for Nuclear Physics
630090 Lavrentiev 11, Novosibirsk, Russia

1 VEPP-2M collider

Electron-positron collider VEPP-2M is the world first pre-Factory, constructed to rise sharply luminosity in already explored energy domain, and the only e^+e^- machine for last 20 years operating in the energy range 2E from 0.4 to 1.4 GeV, covering the energy of resonance production of lightest quarkonia ρ, ω, ϕ. Collider complex VEPP-2M (Fig. 1) consists of an injector part with 3 MeV linear accelerator ILU and 250 MeV electron synchrotron B-3M, 900 MeV synchrotron BEP for accumulation of electrons and positrons and 700 MeV collider VEPP-2M [1]. The maximum luminosity of VEPP-2M depends on its energy in accordance with E^4 law, and at the energy of 2E = 1000 MeV it is equal to $5 \cdot 10^{30} \mathrm{cm}^{-2}\mathrm{sec}^{-1}$. Several different type detectors have operated at the VEPP-2M starting from 1974.

It is worth to mention the best intensity results at VEPP-2M and BEP in a single beam single bunch mode: 0.2 A ($0.8 \cdot 10^{11}$ per bunch) and 0.6 A ($3 \cdot 10^{11}$ per bunch) at the collider and the booster, correspondingly.

The previous longest experimental run was performed at VEPP-2M with a Neutral Detector (ND) [2]. The physics results obtained with ND were based on 19 inverse picobarns of integrated luminosity [3]. In 1992 experiments with CMD-2 detector [4] started, and in early 1995 a new nonmagnetic Spherical Neutral Detector [5] began data acquisition as well. Now both CMD-2 and SND detectors, located in opposite straight sections of VEPP-2M, take data in parallel.

2 CMD-2 detector

The CMD-2 detector has been described in more detail in other presentations [6, 7]. The cross section of the detector is shown in Figure 2. The CsI barrel calorimeter

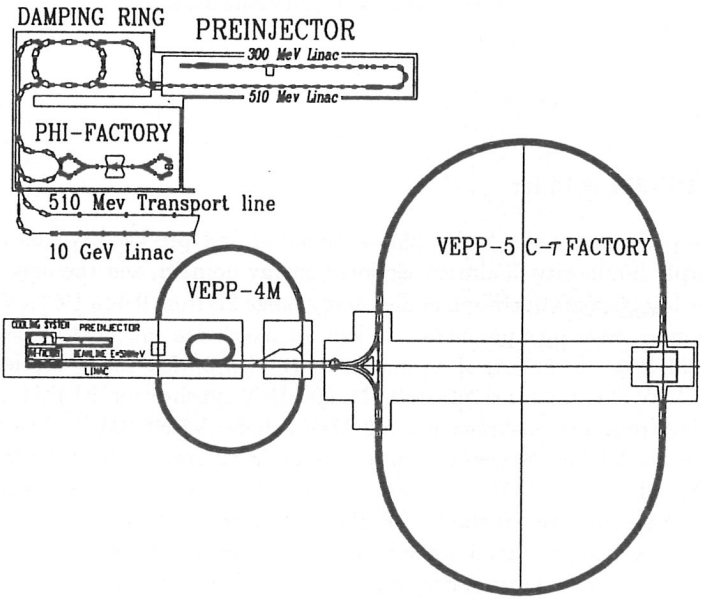

Figure 1: Layout of VEPP-2M complex

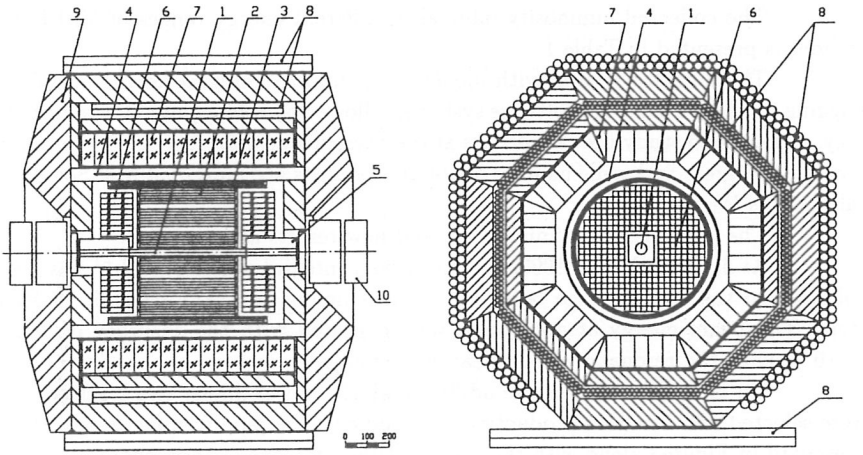

Figure 2: Horizontal and vertcal cross sections of the CMD-2 detector. 1 - vacuum chamber; 2 - drift chamber; 3 - Z-chamber; 4 - superconducting solenoid; 5 - compensating solenoid; 6 - storage ring lenses; 7- calorimeter; 8-muon range system; 9 - magnet yoke (the scale in mm).

with 6x6x15 cm crystal size is placed outside a superconducting solenoid with a 1 Tesla azimuthally symmetric magnetic field (coil thickness 0.4 r.l.). The endcap calorimeter is made of 2.5 x 2.5 x 15 cm BGO crystals and was not installed for the data presented here. The drift chamber inside the solenoid with 30 cm outer radius and 44 cm length has about 200 μ resolution transverse to the beam and 0.5-0.6 cm longitudinally. The vertex reconstruction resolution in case of neutral kaon decays into charged particles is about 0.2 cm radially. After reconstruction a momentum uncertainty of 4-5%/p for 250 MeV/c charged particles, and energy resolution of 10% for photons in the CsI calorimeter have been obtained.

A vacuum beam tube is made of Be with 0.077 cm wall thickness and has 3.4 cm outer diameter and may be considered as a target for the kaon interaction study.

The collected luminosity integral in different energy ranges of VEPP-2M collider is presented in Table 1.

The detector started with moderate luminosity integral for the initial debugging of all hardware and software systems, followed by taking data at ϕ-meson energy, sufficient to study the rare decays at the present world average level. The analisys is in progress and some number of obtained results are presented in E.Solodov's talk at this Workshop.

The analysis is not finished yet and new results are expected.

At January-March 1995, the luminosity integral about 300 nb^{-1} has been collected in the energy range between ρ and ϕ-mesons by scanning with 10 MeV step. The beam energy at each point was measured with the accuracy of about $1 \cdot 10^{-4}$ using the resonance depolarization technique.

Up to April 1995, for the off-line analysis only collinear two tracks events were selected and two pion production was studied. The pion formfactor values are presented in Figure3 along with the results of the previous experiments.

The statistical error of the $e^+e^- \to \pi^+\pi^-$ cross section at each energy point is better than 3%. The total systematic error at the moment is estimated to be about 1.5%. The main part of this error comes from the detector solid angle unsertainty (1%) and from the calculation of the radiative corrections for the Bhabha events (1%), which are using for the normalization. We hope to decrease the systematic error to the level of 0.5%. This level of accuraccy is nesesery for the calculation of the hadrinic vacuume polarization to g-2 of muons, to be able to interpret the result of the E821 experiment now in preparation at BNL. In this experiment the g-2 of muon is planned to be measured with extremely high accuracy of 0.35 ppm.

	c.m. energy range MeV	Triggers	Integrated Luminosity nb^{-1}
$\rho - \omega$–mesons	390 – 900	$5.5 \cdot 10^6$	20
ϕ–meson	1009 – 1028	$12.8 \cdot 10^6$	310
background	994	$0.45 \cdot 10^6$	20
	1993 runs		
ϕ–meson	1013 – 1040	$52.7 \cdot 10^6$	1400
background	994	$6.6 \cdot 10^6$	120
	1994 runs		
scanning with 10 MeV step	1000 – 786	$20.0 \cdot 10^6$	290
	1995/96 runs (before round beams at VEPP-2M)		
scanning with	780 – 360		300
10 MeV step	1000 – 1400		10000
ϕ–meson	1013 – 1040		10000

Table 1: List of the CMD-2 runs.

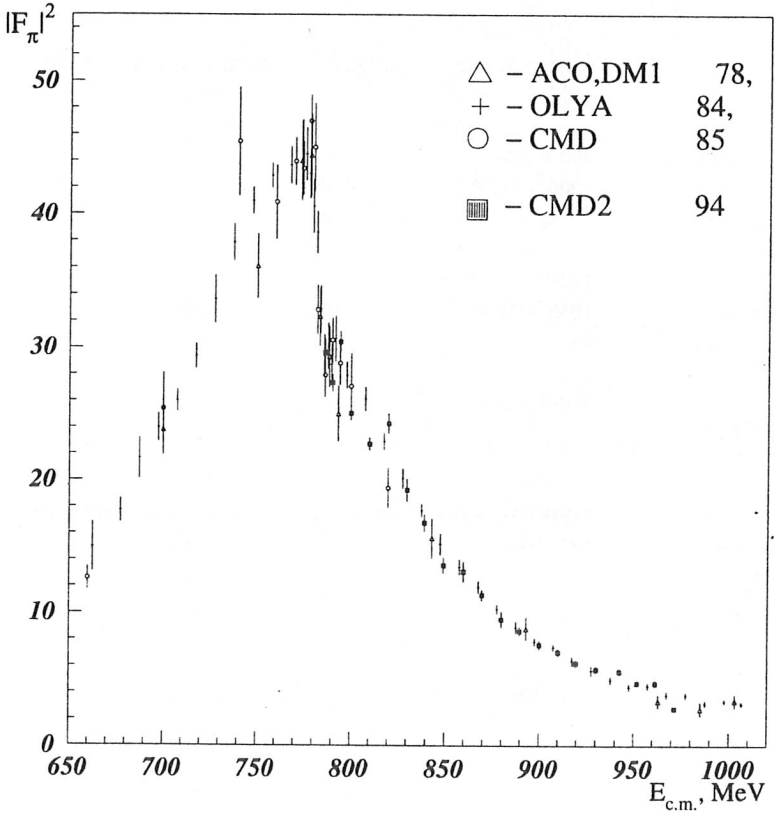

Figure 3: The experimental data for $|F_\pi|^2$.

3 SND detector

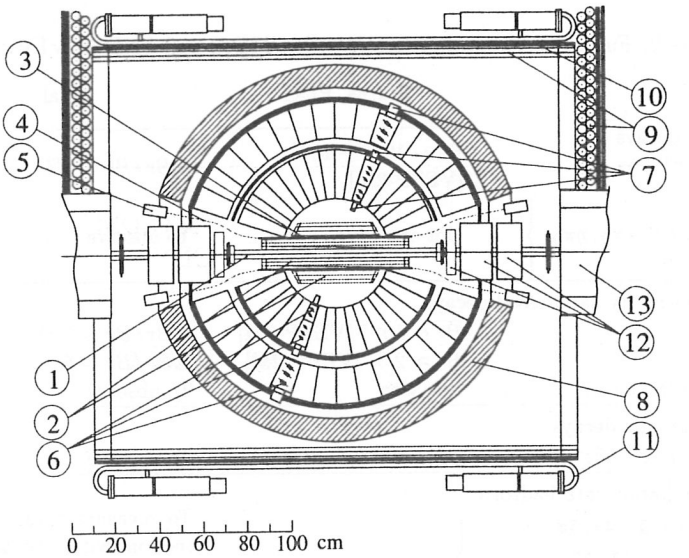

Figure 4: Detector SND — view transverse to the beam; 1 — beam pipe, 2 — drift chambers, 3 — scintillation counters, 4 — fiber lightguides, 5 — PMTs, 6 — NaI(Tl) counters, 7 — vacuum phototriodes, 8 — iron absorber, 9 — streamer tubes, 10 — 1 cm iron plates, 11 — scintillation counters, 12 — magnetic lenses, 13 bending magnets

In February 1995 experiments have been started with Spherical Neutral Detector (SND). SND (Fig. 4) is nonmagnetic wide purpose detector, intended to study e^+e^- annihilation at VEPP-2M. The main part of the SND is a three layer spherical NaI(Tl) calorimeter, consisted of 1680 individual crystals. The calorimeter thickness is 14 radiation lengths and its total mass is 3.6 tons. The energy resolution, expected for photons in the range of 50-500 MeV, is 4-6(rms), the angular resolution is 1.5 degrees. Inner part of the detector is a cylindrical drift chamber system for charge particles tracking with the accuracy of about 0.4 degrees in azimuthal and polar direction. Outside the calorimeter 11 cm iron absorber and muon/veto detector are installed, which consists of streamer tubes and scintillation counters. The last system is used as cosmic veto counter in events with neutral particles.

The parameters of SND detector allow to study wide range of physical processes, in spite of absence of magnetic field. The important part of the program is study of radiative decays of vector mesons, including both already measured magnetic dipole decays and still not observed electric dipole decays. The careful measurement of e^+e^- annihilation cross section into hadrons is another important point of the program. This cross section significantly contributes into hadronic

vacuum polarization for muon (g-2) factor. The Table 2 shows full physics program for CMD-2 and SND detectors at VEPP-2M.

Table 2: Full experimental program with CMD-2 and SND at VEPP-2M

	Status, PDG	Goal
Radiative decays		
$\rho, \omega, \phi \to \pi^0\gamma, \eta\gamma$	Br $\sim 10^{-4} \div 10^{-1}$ [VEPP-2M]	$\Delta Br/Br \sim 1\%$
$\phi \to \eta'\gamma$ $\phi \to a_0\gamma, f_0\gamma, \pi\pi\gamma, \eta\pi\gamma$ $\rho, \omega \to \pi\pi\gamma$	Not seen	To observe
OZI and G-parity suppressed decays		
$\phi \to \pi\pi$	$Br \sim 10^{-4}$ [VEPP-2M]	$\Delta Br/Br \sim 5\ \%$
$\omega \to \pi\pi$	$Br \approx 2\ \%$ [VEPP-2M]	$\Delta Br/Br \sim 5\ \%$
$\phi \to \omega\pi, \eta\pi\pi; \rho \to 3\pi$	Not seen	To observe
Electromagnetic decays		
$\rho, \omega, \phi \to \eta e^+e^-, \pi^0 e^+e^-$	Only $\phi \to \eta ee$ seen	To observe
e^+e^- annihilation into hadrons		
$e^+e^- \to 2\pi, 3\pi, 4\pi, 5\pi$ $e^+e^- \to \omega\pi, \eta\pi\pi, \phi\pi$ $e^+e^- \to K^+K^-, K_SK_L, KK\pi$		To measure total cross section with 1% accuracy and partial cross sections
Test of QED		
$e^+e^- \to 3\gamma, e^+e^-\gamma$ $(2 \to 3)$ $e^+e^- \to 4\gamma, e^+e^-\gamma\gamma, 4e$ $(2 \to 4)$		To study with accuracy $\sim 1\%$
$e^+e^- \to 5\gamma, 3\gamma e^+e^-, 4e\gamma$ $(2 \to 5)$		To observe
Search for rare K_S decays		
$K_S \to 2\gamma$	$Br \sim 10^{-6}$	$\Delta Br/Br \sim 20\ \%$
$K_S \to 3\pi^0, 2\pi^0\gamma, \pi^0\gamma\gamma, \pi^0e^+e^-$	Not seen	$Br \leq 10^{-5}$
Search for rare η decays		
$\eta \to 3\gamma, e^+e^-, 4e$	Not seen	$Br \leq 10^{-4}$
Search for C-even reactions		
$e^+e^- \to \eta', a_0, f_0, a_2, f_2$	Not seen	To lower limit to $\sigma \leq 10^{-36} cm^2$

4 Round beams and VEPP-2M

In the recent years electron–positron colliders with luminosities $L \sim 10^{33} cm^{-2} s^{-1}$ at the energy of 510 MeV, so called Φ-factories, are in consideration at different laboratories and under construction at Frascati and at Novosibirsk. In the Novosibirsk project the high luminosity level will be achieved with round colliding beams [8, 9]. What does mean "round beams"?

1. The equal and small $\beta_0 = \beta_x, \beta_z$ values.

2. The equal emittances ϵ_x, ϵ_z excited by quantum fluctuations independently.

3. The equal betatron tunes ν_x, ν_z and "zero" coupling.

4. The small positive non-integer tune fractions.

5. The small tunable synchrotron frequency ν_s.

As a result of items 1, 2 and 3, the angular momentum is conserved, thus converting transversal motion to "one-dimensional" one, with less beam-beam resonances which cause beam-beam blow-up and/or degrade their life-time. Items 4 and 5 proved to be important also in rising the maximal beam-beam tune shift ξ_max, which does not damage luminosity. We hope to rise its value, at least, up to 0.1, in comparing with 0.05 achieved now for flat beams. The additional useful effect arises due to the simple fact, that beam-beam tune shift for given counting bunch density is 2 times lower for round beams than for smaller dimension of flat beams.

There are many arguments for advantages of the round beam option. The best way to prove all significant arguments *pro* and *contra* round beam concept is an *experimentum crucis*. We have found a unique possibility to test them experimentally at VEPP-2M storage ring [12].

The present magnetic lattice of VEPP-2M has four symmetric periods with low β^*-functions (β_z = 5cm; β_x= 40cm) at interaction regions (IR), which are provided by two quadrupole doublets. Two opposite IRs are occupied by the detectors CMD-2 and SND detectors. Two remaining low-β straights are occupied by RF-cavity and SC wiggler. The superconducting wiggler has 5 poles with magnetic field up to 80 kG. The correction coils system can compensate the optics distortion from the wiggler and the solenoids of CMD-2 detector.

The main idea of VEPP-2M lattice modification to round beam mode is to replace the quadrupole doublets by SC solenoids accomodated inside the detectors (Fig. 5). The solenoids will provide the equal β^*-functions in the beam collision points, and besides rotate by $\pi/2$ the planes of the betatron oscillations. This will result in alternation of vertical and horizontal orientations of the planar betatron eigen-modes over each half-turn, similarly to the Novosibirsk ϕ-factory design. Weakening by ca.10 per cent the remaining 8 quadrupoles will transform the half-turn bends into achromats to provide for zero dispersion in the both IRs at the expense of enhanced dispersion in the bends (maximum of 140 cm vs. 70 cm at present) (Fig. 6). The momentum compaction factor will be left practically unchanged.

The chromaticity correction is performed by sextupoles placed on either side of the remaining quadrupole doublets. The natural chromaticity of betatron tunes with solenoids is:

$$\gamma \cdot \frac{\partial \nu_x}{\partial \gamma} = -12, \; \gamma \cdot \frac{\partial \nu_z}{\partial \gamma} = -13.$$

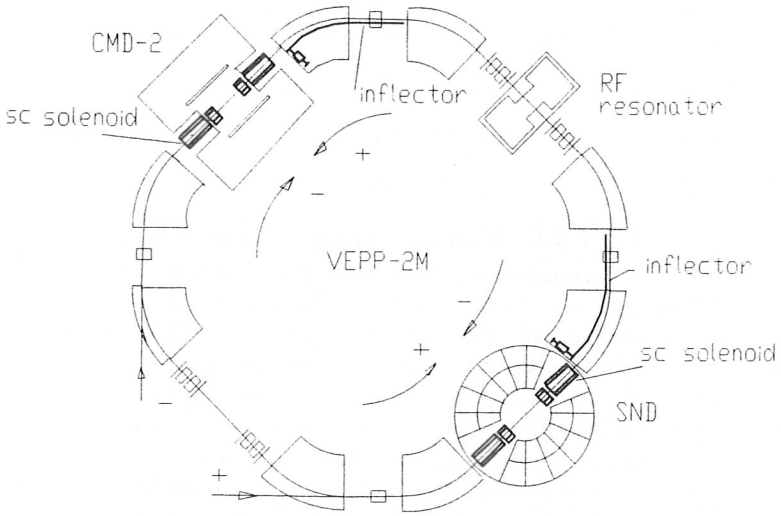

Figure 5: The VEPP-2M modification for round beam operation. The SC solenoids will be installed on both sides of existing detectors.

As far as the dispersion is zero over the IR, the compensation of the betatron tune chromaticities is possible only in the arcs by the appropriate sextupoles correction families S_x and S_z. The VEPP-2M round beam lattice was optimized to compensate the betatron tune chromaticity by minimizing the possible effect of sextupole correctors on the dynamic aperture. To determine the dynamic aperture limitation the particle motion was tracked in the lattice with averaging over initial betatron phases.

The computer simulations of the beam-beam interaction inherent in the dynamics of round beam collision encourage for the design goal of $\xi \sim 0.1$ ($N \sim 6.7 \cdot 10^{10}$) for the attainable beam-beam parameter. With the beam emittances of $\epsilon_x = \epsilon_z = 1.5 \cdot 10^{-5} cm \cdot rad$ this will hopefully come to luminosities of $L \sim 10^{32} cm^{-2} s^{-1}$ at the energy of 510 MeV.

The existing and proposed beam and optics parameters are summarized in the Table 3.

4.1 Specific Goals

This move will let us learn - just now! - such a non-traditional storage ring optics and study its tolerances, reach real gain in ξ_{max} and in luminosity, rising it from current $5 \cdot 10^{30}\mathrm{cm}^{-2}\mathrm{sec}^{-1}$ to $1 \cdot 10^{32}\mathrm{cm}^{-2}\mathrm{sec}^{-1}$. This improvement will give also a possibility to operate detectors at already very high fluxes of useful events, and, consequently, to collect many important experimental data.

VEPP-2M: BEAM AND OPTICS PARAMETERS			
Parameters		**flat beam**	**round beam**
Circumference, m	C	17.88	17.88
RF frequence, MHz	f_0	200	200
Momentum compaction	α	0.167	0.18
Emittances, $cm \cdot rad$	ε_x	$4.6 \cdot 10^{-5}$	$1.5 \cdot 10^{-5}$
	ε_z	$5.5 \cdot 10^{-7}$	$1.5 \cdot 10^{-5}$
Energy loss/turn, keV	ΔE_0	9.1	5.0
Dimensionless	δ_z	$9.8 \cdot 10^{-6}$	$4.8 \cdot 10^{-6}$
damping	δ_x	$8.5 \cdot 10^{-6}$	$4.8 \cdot 10^{-6}$
decrements	δ_s	$2.1 \cdot 10^{-5}$	$1.2 \cdot 10^{-5}$
Energy spread	σ_ε	$6 \cdot 10^{-4}$	$3.5 \cdot 10^{-4}$
β_x at IP, cm	β_x	48	5
β_z at IP, cm	β_z	4.5	5
Betatron tunes	ν_x, ν_z	3.05,3.1	3.1,3.1
Particles/bunch	e^-, e^+	$2 \cdot 10^{10}$	$6.7 \cdot 10^{10}$
Tune shifts	ξ_x, ξ_z	0.02,0.05	0.1,0.1
Luminosity, $cm^{-2} \cdot s^{-1}$	L_{max}	$\sim 5 \cdot 10^{30}$	$\sim 1 \cdot 10^{32}$

Table 3: Comparative parameters of VEPP-2M beams for flat beams option ("wiggler-on") and round beams option.

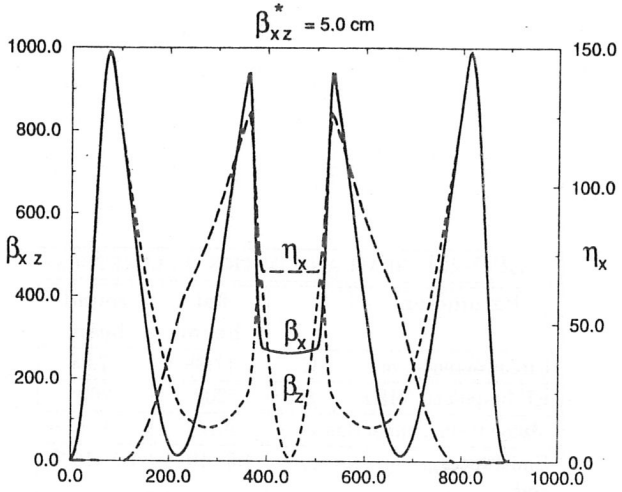

Figure 6: Optical functions for VEPP-2M round beam mode.

5 Four-wing ϕ-factory

Firstly, we summarize the status of the injection part of VEPP-5 complex envisaged for use by ϕ-factory, VEPP-4M and Charm/Tau Factory.

The civil engineering progress is rather fast: by now the halls of the injection linac and of the damping ring are constructed, as well as the rooms for all electric equipment and the control room, the klystron gallery and the main VEPP-5 linac tunnel. The ϕ-factory hall construction is about its finish. The equipment for the injection linac and transfer lines is partly installed. The SLAC klystron is tested for its nominal power. The major part of the damping ring magnetic system is machined. However, the pace of the project on the whole is apparently rather slow due to insufficient dedicated budgeting.

The concept of round colliding beams is still the highlight of the Novosibirsk approach to the ultra-high luminosities [8]. Meanwhile, the last year resulted in a serious revision of the ϕ-factory project: we switched to the double-ring machine with the electrostatic orbit separation. The 50 kV/cm electrostatic separator plates are 2 meters in length and provide ± 2 cm aperture. Similarly to the previous "Siberian Butterfly" scheme, the interaction region is a common straight section with the axi-symmetric solenoidal focusing, envisaged for direct and reversed passages of colliding bunches (*i.e.* the bunches are in two-way head-on collision, see Fig. 7).

With the design RF harmonic number $h = 110$ ($\lambda = 42.8$ cm) two modes are possible for head-on collision of N bunches:

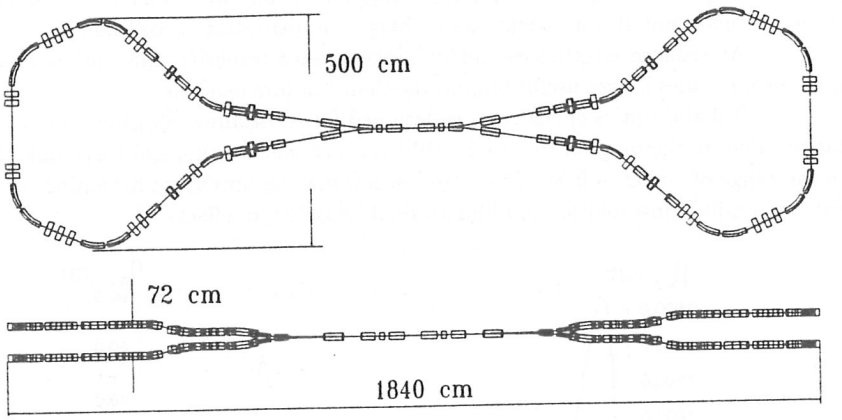

Figure 7: The ϕ-factory design.

• At $N = 11$ (*i.e.* the bunches are spaced by 9 empty RF buckets) we will collide only electrons with positrons. The closest parasitic collision of $e^+ e^+$, $e^- e^-$ occurs at a distance of 2.5 λ from the *I*nteraction *P*oint (IP), and the orbits are horizontally separated with magnetic field. The parasitic $e^+ e^-$ collision is 5 λ apart from the IP, it is electrostatically separated in the vertical plane.

At emittances about $1.25 \cdot 10^{-5} cm \cdot rad$ the luminosity should reach $2.5 \cdot 10^{33} cm^{-2} s^{-1}$.

• At $N = 10$ (10 empty RF buckets between the bunches) the $e^+ e^-$ collisions at the IP (half of luminosity) are simultaneous with the $e^+ e^+$ and $e^- e^-$ collisions (another half). In this collision mode all the parasitic collisions take place 5.5 λ apart from the IP. Here we have certain hopes for attaining a higher effective beam-beam parameter ξ as a result of overlapping of uni-directional $e^+ e^-$ bunches prior collisions and of consequent space charge compensation at collision.

At reduced emittances and/or higher bunch intensity, this option should give several times higher useful luminosity than the previous one.

Tunable optics of the rings is designed for controlling both the beam emittance values in the range of $(0.5 \rightarrow 2) \cdot 10^{-5}$ $cm \cdot rad$ and the momentum compaction in the range of $-0.02 \rightarrow 0.06$. The latter option may be important in taming coherent longitudinal instabilities and longitudinal beam-beam effects [13].

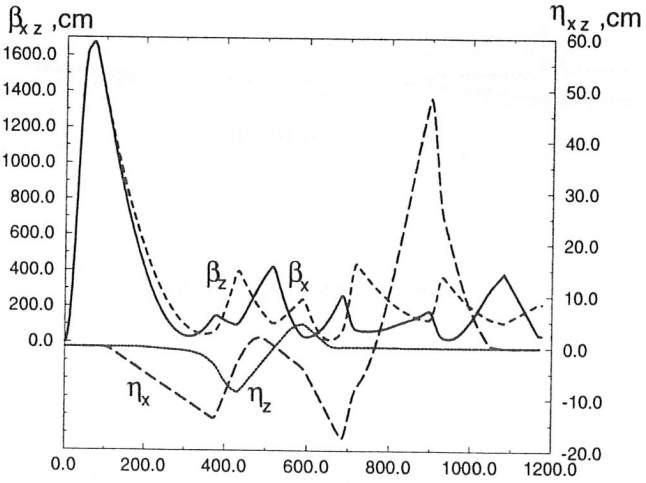

Figure 8: Optical functions of ϕ-factory.

The optical functions of the ring(s) are shown in Fig. 8. Note that the negative contribution to the momentum compaction comes from the vertical bends. Their purpose is to compensate for the (unwanted) vertical dispersion which originates from the electrostatic separator. The main parameters of the ϕ-factory are

MAIN PARAMETRS OF PHI—FACTORY		
Circumference, m	C	47.08
RF frequence, MHz	f_0	700.4
RF voltage, kV	V	100
RF harmonic number	q	110
Momentum compaction	α	-0.02...0.06
Synchrotron tune	ν_s	0.012 ($\alpha = 0.04$)
Emittances, $cm \cdot rad$	ε_x	$1.25 \cdot 10^{-5}$
	ε_z	$1.25 \cdot 10^{-5}$
Energy loss/turn, keV	ΔE_0	13.5
Dimensionless	δ_z	$1.25 \cdot 10^{-5}$
damping	δ_x	$1.25 \cdot 10^{-5}$
decrements	δ_s	$2.92 \cdot 10^{-5}$
Energy spread	σ_ε	$4.3 \cdot 10^{-4}$
β_x at IP, cm	β_x	1.0
β_z at IP, cm	β_z	1.0
Betatron tunes	ν_x, ν_z	8.1,6.1
Particles/bunch	e^-, e^+	$5.0 \cdot 10^{10}$
Bunches/beam		11
Tune shifts	ξ_x, ξ_z	0.1,0.1
Luminosity, $cm^{-2} \cdot s^{-1}$	L_{max}	$2.5 \cdot 10^{33}$

Table 4: The main parameters of ϕ-factory.

presented in Table 4 .

References

1. G.M. Tumaikin et al., *Proc. of the 10th Int. Conf. on High Energy Acc.*, Serpukhov (1977), v.1, p.443
2. V.B.Golubev et al., *NIM*, 227 (1984), p.467
3. S.I.Dolinsky et al., *Phys. Rep.*, 202, No.3, (1991), p.99
4. CMD-2 Collaboration, *ICFA Instrumentation Bulletin*, 5, (1988), p.18
5. V.V.Anashin et al., *Proc. of 5th Int. Conf. on Instrumentation for Colliding Beam Physics*, Novosibirsk (1990), p.360
6. G.A.Aksenov et al., *INP Preprint 85-118*, Novosibirsk (1985)
7. E.V. Anashkin et al., *ICFA Instrumentation Bulletin 5* (1988), p.18
8. L.M.Barkov et al., *Proc.of the 14th Int. Conf. High Energy Acc.*, Tsukuba (1989), p.1385
9. L.M.Barkov et al., *Proc. of the IEEE Particle Accelerator Conference*, San Francisco (1991), p.183
10. I.B.Vasserman et al., *INP Preprint 79-74*, Novosibirsk (1979)
11. N.S.Dikansky et al., *Proc. of the IEEE Particle Accelerator Conference*, San Francisco (1991), p.523
12. A.N.Filippov et al., *Proc. of the 15th Int. Conf. High Energy Acc.*, Hamburg (1992), p.1145
13. V.V.Danilov et al., *Workshop on Beam-Beam and Beam-Radiation interactions*, UCLA (1991), p.1

STATUS REPORT ON DAΦNE

The DAΦNE Project Team*

presented by G. Vignola

INFN, Laboratori Nazionali di Frascati (LNF), C.P. 13, 00044 Frascati, Italy

ABSTRACT

The e^+e^- Φ-factory DAΦNE has been approved in 1990; the detailed engineering design started in 1991 and the construction is proceeding steadily.

The beginning of the collider commissioning, with a short term luminosity goal $L = 1.3\ 10^{32}\ cm^{-2}\ sec^{-1}$, is scheduled for the end of 1996.

I. INTRODUCTION

The main features of the e^+e^- Φ-factory DAΦNE have been described in detail elsewhere [1]. The project was approved and funded in 1990 and the detailed engineering design started in 1991. The construction of machine and experiments is proceeding steadily.

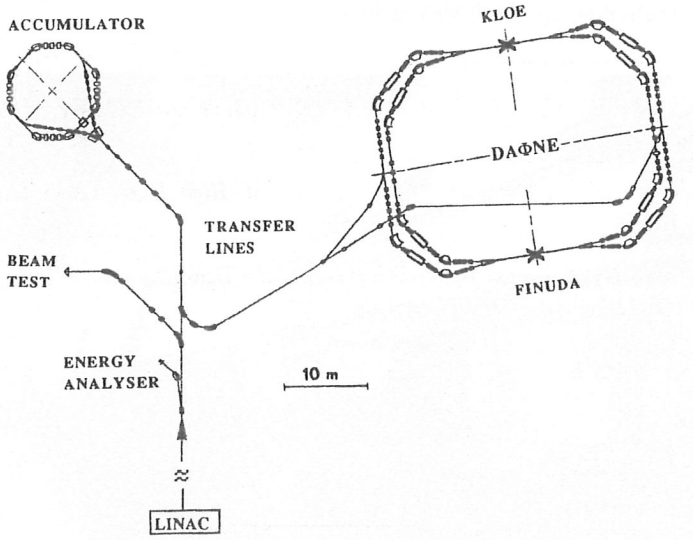

Figure 1: Layout of DAΦNE Accelerator Complex.

---

* M. Bassetti, M.E. Biagini, C. Biscari, R. Boni, A. Cattoni, V. Chimenti, A. Clozza, S. De Simone, G. Di Pirro, H. Dong, A. Drago, S. Faini, A. Gallo, A. Ghigo, S. Guiducci, Y. He, H. Hsieh, F. Marcellini, C. Marchetti, M.R. Masullo, M. Migliorati, C. Milardi, M. Modena, L. Palumbo, L. Pellegrino, M. Preger, H. Qu, G. Raffone, C. Sanelli, F. Sannibale, M. Serio, F. Sgamma, B. Spataro, A. Stecchi, L. Trasatti, C. Vaccarezza, M. Verola, M. Vescovi, S. Vescovi, G. Vignola, D. Yao, M. Zobov.

The accelerator complex layout is shown in Fig. 1. It consists of:

- $e^+ e^-$ LINAC;
- $e^+ e^-$ Accumulator/damping ring;
- twin ring collider (DAΦNE).

The tender phase is almost complete and all the various components are under construction. The beginning of the collider commissioning is scheduled for the end of 1996, and the start of experimental runs for mid 1997.

The design luminosity $L = 5.2\ 10^{32}\ cm^{-2}\ sec^{-1}$ should be achieved in a period of at least 2 years of continuous operation by pushing up the current and, at the same time, by fine tuning all machine parameters.

In the following, we will discuss briefly the main features and the status of the three accelerators and, in some more detail, the vacuum system, the RF cavity and the longitudinal feedback system for the collider.

II. LINAC

The LINAC [2] is an S-band structure with a pulse compression system (SLED) capable of accelerating electrons up to 800 MeV at 50 pps.

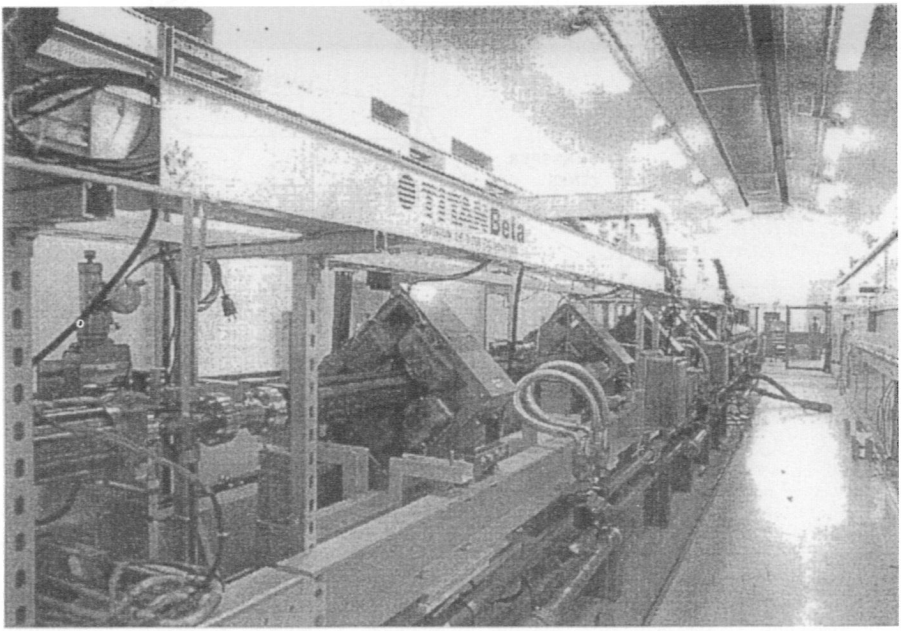

Figure 2: DAΦNE LINAC during installation (April 95).

In the positron mode of operation the first part of the LINAC (from the gun to the positron converter) is used to accelerate a 4A-10ns electron pulse at 250 MeV.

The high-current performances of the LINAC have been successfully tested at the TITAN Beta factory.

The LINAC (see Fig. 2) is now being installed at LNF and the beam tests are scheduled for May 95. It will be fully operational by December 95.

III. ACCUMULATOR

The main parameters of the Accumulator/damping ring are shown in Table I. It has a compact 4 period structure, with a total length 1/3 of DAΦNE.

Table I - DAΦNE Accumulator Main Parameters

Energy (MeV)	510.0
Circumference [m]	32.56
Emittance, ε_o [mm·mrad]	0.26
Betatron tune, ν_x/ν_y	3.12/1.14
RF frequency, f_{RF} [MHz]	73.65
Bunch average current [mA]	150
RF voltage [kV]	200
Bunch length σ_z [cm]	3.8
Synchrotron radiation loss [keV/turn]	5.2
Damping time, τ_E/τ_x [ms]	10.7/21.4

The Accumulator is used to store at 50 pps the required number of electrons (positrons) in one RF bucket and to damp the transverse and longitudinal emittance of the LINAC beam. The damped beam is extracted at ~ 1 pps and injected into a single bucket in DAΦNE.

Oxford Instr. is the main contractor for the construction and the installation of the Accumulator, whose magnets are built by Tesla Eng.

The series production of magnets (designed and measured by LNF), vacuum chambers and other components is complete. The installation of the Accumulator, due to ~ 1 year delay in the delivery of the Transfer Lines, built by Ansaldo Energia, is scheduled for September 95, while the beam tests will begin in January 96.

Due to the excellent magnetic field quality measured on the first Accumulator quadrupole (see Fig. 3), we have decided to use in the DAΦNE long straights the same type of quadrupoles.

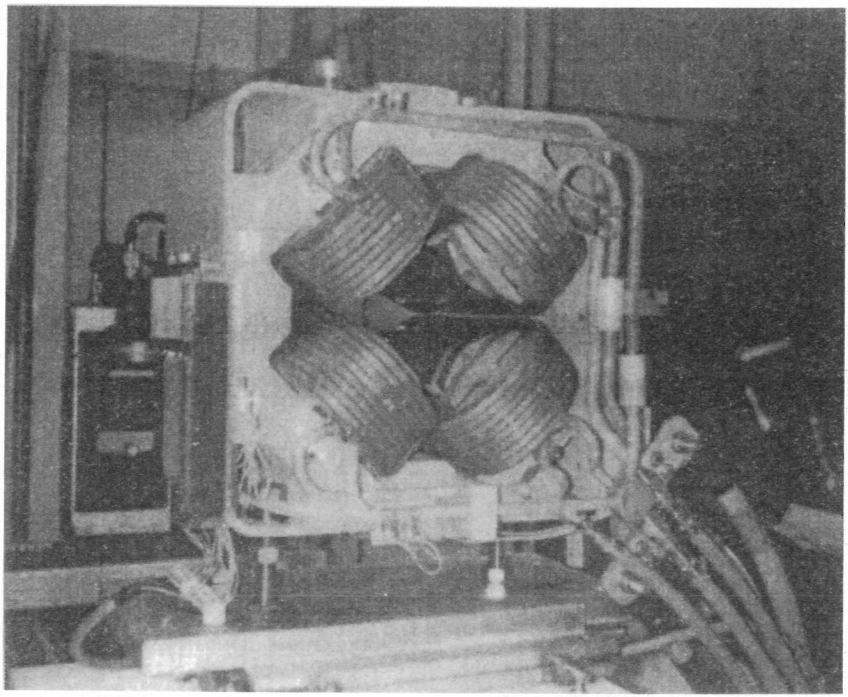

(*) TESLA Quadrupole field quality

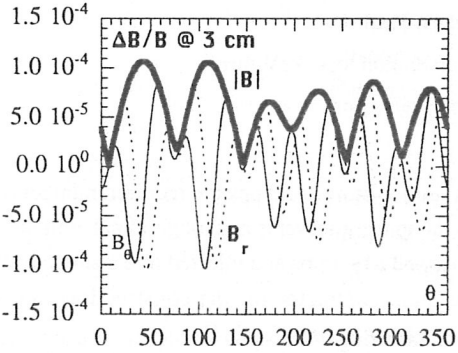

Multipole	6	8	10	12	20
ΔB/B @ 3 cm	6.5×10^{-6}	3.5×10^{-5}	2.1×10^{-5}	1.8×10^{-5}	4.6×10^{-5}

(*) 60 of these quadrupoles will be installed in the Main Rings.

Figure 3: Accumulator quadrupole and field quality measurement ($\Delta B/B = \pm10^{-4}$ @ ±3 cm, instead of $\pm5\cdot10^{-4}$ requested by the Specs).

IV. DAΦNE

The major physics motivation for the construction of DAΦNE is the observation of direct CP-violation in K_L decays, i.e. the measurements of ε'/ε with accuracy in 10^{-4} range by the KLOE detector [3]. To achieve this result, a luminosity $L = 5\ 10^{32}\ cm^{-2}\ sec^{-1}$ integrated over an effective year of 10^7 seconds is required.To get such a luminosity DAΦNE is designed as a high current double ring system with a maximum number of 120 bunches/beam. The high current approach, adopted also by PEP-II [4], allows to use single bunch parameters quite conservative from an accelerator physics point of view, but it moves the difficulties to engineering challenges (vacuum, RF, multibunch). In DAΦNE electrons and positrons are stored in two separated storage rings laying in the same horizontal plane with horizontal crossing in 2x10m long interaction regions, at an angle of ± 12.5 mrad. The main DAΦNE parameters are shown in Table II.

Table II - DAΦNE Main Parameters

Energy (MeV)	510.0
Trajectory length [m]	97.69
Emittance, $\varepsilon_x/\varepsilon_y$ [mm·mrad]	1/0.01
Beta function at crossing, β^*_x/β^*_y [cm]	450/4.5
Beam-beam tune shift, ξ_x/ξ_y	0.04/0.04
Betatron tune, ν_x/ν_y	5.13/6.10
RF frequency, f_{RF} [MHz]	368.25
Max. number of bunches, h_{RF}	120
Minimum bunch separation [cm]	81.4
Bunch average current [mA]	43.7
RF voltage [kV]	250
Bunch length σ_z [cm]	3.0
Synchrotron radiation loss [keV/turn]	9.3
Damping time, τ_ε/τ_x [ms]	17.8/36.0
Luminosity [$cm^{-2}\ s^{-1}$]	5.2×10^{32}

The regular lattice of each ring consists of 4 achromats, each housing a 2 m long, 1.8 T normal conducting wiggler to increase radiation damping and tune beam emittance.

The straight sections orthogonal to the interaction regions are used for injection, RF, feedbacks and a scrapers system [5] optimized for reducing the lost particles background inside the detectors.

The betatron tune working point [6], with equal vertical betatron phase advance between the two interaction points, is almost insensitive to resonances and shows negligible beam blow-up.

The second interaction region is assigned to a smaller size detector, FINUDA [7], for study of hypernuclei formation and decay.

The installation of three beam lines for soft X-rays [8] is also planned.

V. VACUUM SYSTEM

The DAΦNE vacuum system [9] is dimensioned for an operating pressure of ~ 1 nTorr with ~ 5 A of circulating current. A design, similar to ALS, has been adopted for the vacuum vessel inside the achromat, consisting of two chambers connected through a narrow slot. The beam circulates in the first chamber, while the synchrotron radiation photons hit a system of copper absorbers located in the second one (antechamber) in such a way that more than 95% of the photon flux is intercepted in the antechamber.

The achromat vessel (~10 m long) is made by two halves of Al alloy 5083-H321 plates, which, after machining, are welded along the middle plane. The total weight of each chamber is ~ 1.5 ton. The inner surface is mirror finished (roughness = 0.2 Ra).

Figure 4 shows one half of the arc vacuum vessel, fully machined.

Right close to each copper absorber there is a pumping station based on Ti sublimation pump (TSP). In addition, sputter ion pumps are used to pump down CH_4 and noble gases. The total pumping speed installed in each storage ring is ~ 125000 l/s.

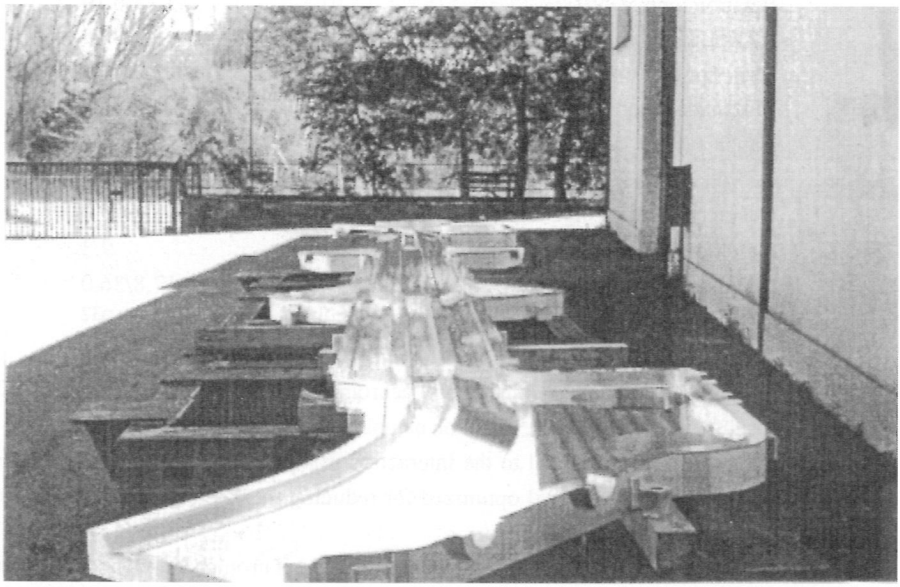

Figure 4: Arc Al vacuum vessel, one half, before welding.

VI. RF SYSTEM

The RF system of each ring consists of a normal conducting single cell cavity, fed by a 150 kW/cw klystron developed by Thomson. The klystron is protected against the reflected cavity power by a ferrite circulator.

To reduce the high order mode (HOM) impedance [10], the RF cavity is equipped with long tapered beam tubes and three waveguides (WG) to couple out the parasitic modes that are then dissipated into external 50 Ω loads. The central body of the RF cavity (see Fig. 5) is obtained from a single forged OFHC copper billet and the internal surface is fully manufactured with an automatic milling machine. Power test of the first cavity is foreseen in Summer 1995.

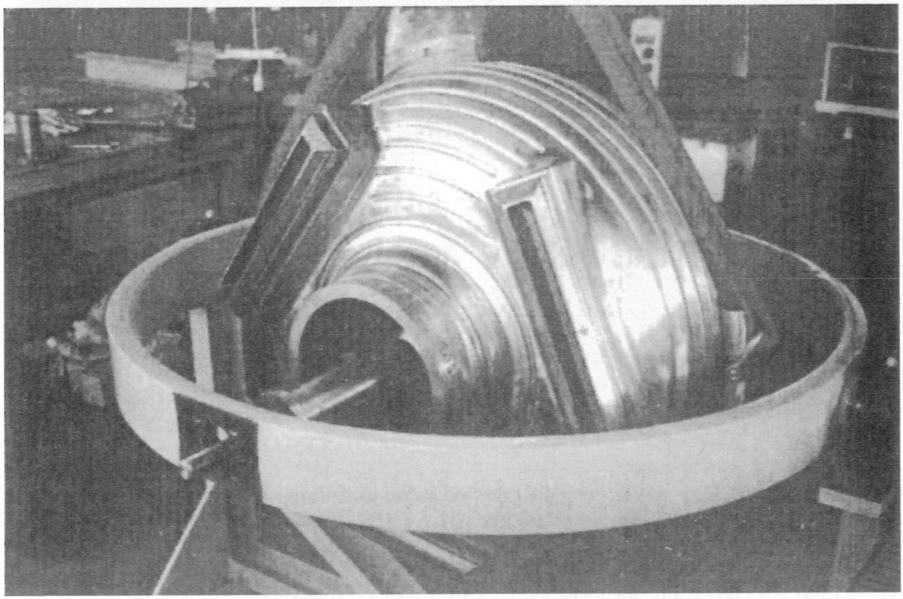

Figure 5: DAΦNE RF cavity during fabrication.

The low power tests, performed on a copper cavity prototype, have shown that a considerable reduction of the HOM Qs over a 2 GHz bandwidth is achieved. For symmetry reasons, the WGs, whose cut off is above the accelerating mode frequency, are applied 120° apart onto the cavity body. They are broadband transitions from rectangular WG slots to coaxial, terminated on the other side with 7/8" ceramic windows [11] which allow to dissipate the HOM power on standard 50 Ω loads in air.

The WGs (see Fig. 6), also made of OFHC copper, have been power tested successfully on bench under vacuum. The 7/8" coaxial output port is a wide band 50 Ω ceramic window designed at LNF.

The rectangular WG flanged slots on the cavity central body are clearly visible in Fig. 5.

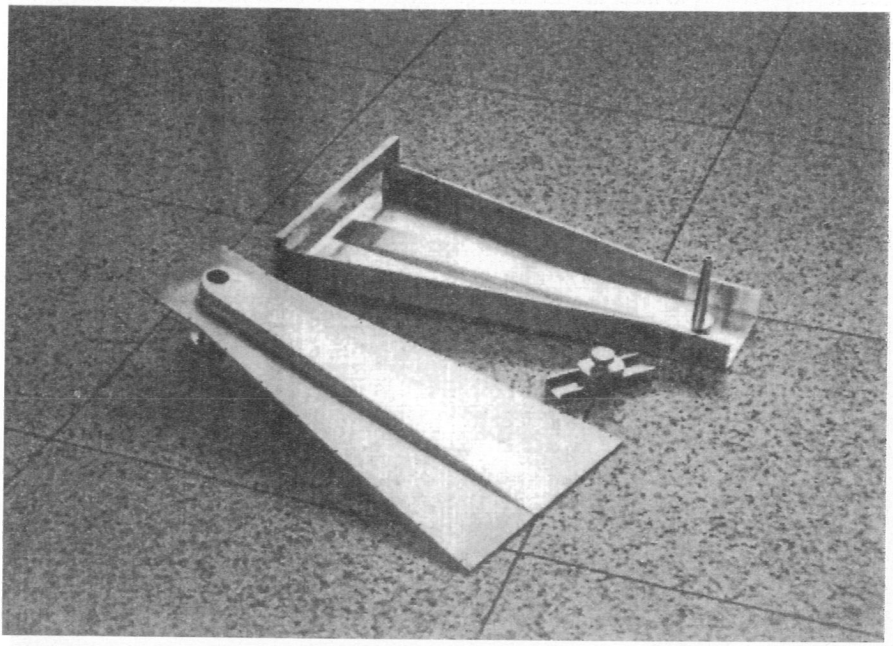

Figure 6: HOM waveguide transition.

VII. LONGITUDINAL FEEDBACK SYSTEM

The basic design choice of achieving the required luminosity with a very high current, distributed over a large number of bunches (30 -> 60 -> 120), makes the operation very critical with respect to longitudinal coupled bunch instabilities caused by parasitic higher order modes in the ring, mainly in the RF cavity. These instabilities have been identified since the very beginning of the project as a potentially severe limit to the ultimate achievable luminosity. Even though the HOMs in the accelerating cavity are heavily damped, the probability for a damped HOM to cross a coupled bunch mode frequency is large and, due to the large total current, the growth rate of unstable modes can be stronger than the radiation damping rate by up to two orders of magnitude.

The required additional damping is provided via a time domain, bunch by bunch feedback system [12] based on digital signal processors (DSP).

The digital section is under construction at SLAC in the framework of a collaboration with the SLAC-LBL PEP-II group on feedback systems for the next generation of "factories" with intense beams and a large number of bunches. In fact, the design specifications are set to meet the ultimate performance specifications of ALS, PEP-II and DAΦNE.

A prototype system with a single-board digital section is running at ALS and the complete modular system has passed the pre-production test.

The maximum power at the kicker is determined by the voltage gain needed to achieve the required damping rate and the maximum synchrotron phase error allowed during injection.

Due to difficulties in building and tuning a stripline kicker we have designed an RF kicker with a resonant frequency of 1.2 GHz, (3.25 times the main RF frequency) [13].

Figure 7 shows a view of a prototype cavity. The 88 mm diameter beam tube opens into a 200 mm diameter, 72 mm long, pill-box cavity. To obtain the very large bandwidth required (~180 MHz at least, for 120 bunches operation), the cavity is loaded by 6 ridged waveguides followed by broadband transitions to 7/8" standard coax, very similar to those in the main RF cavity, except that in this case the coupling is extended to the fundamental mode.

The 6 waveguides are placed symmetrically with respect to the accelerating mode. Three WGs are used as input ports and the other three as termination loads. In this way, thanks to the symmetry, the system is perfectly matched.

Being broadband, the kicker cavity does not need to be tuned in operation, nor cooled, since almost all the power is dissipated in the external loads. Moreover, the damping waveguides couple out the HOMs as well. Not being the kicker cavity a directional device like the stripline kicker, it extracts power from the beam. Ferrite circulators are then necessary to isolate the output section of the power amplifier feeding the cavity.

The geometry of the kicker cavity has been defined. A peak shunt impedance of 750 W, together with a bandwidth larger than 220 MHz, have been calculated with 3D simulations with the HFSS code by HP.

The mechanical design is under preparation at LNF and we intend to place an order to industry for two pieces (one per ring) for the initial operation at a reduced number of bunches. According to simulations with realistic values of the HOM impedances, a large band-width power amplifier of ~ 200 Watt is enough to damp an initial offset of 100 ps of the injected bunch with the other 29 bunches at the full design current.

Two cavities per ring will eventually be installed for operation at the full nominal current with a 3x200 Watt power amplifiers per cavity, each feeding separately a waveguide coupler.

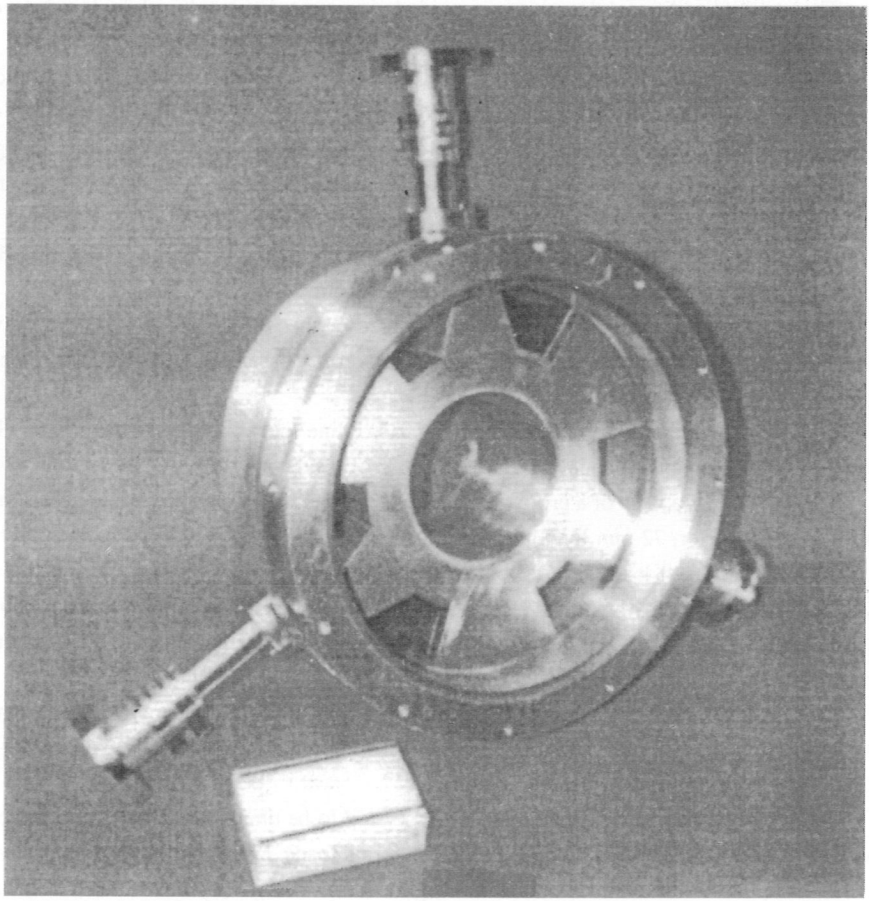

Figure 7: View of the overdamped kicker cavity prototype.

VIII. ACKNOWLEDGMENTS

I like to thank the DAΦNE Machine Review Committee (Andrew Hutton - Chairman, Franco Bonaudi, Daniel Boussard, Giorgio Brianti, Jean-Pierre Delahaye, Albin Wrülich) for their constant advice; Enzo Iarocci - LNF Director, Dolores Federici and Fernando Pacciani - LNF Administrative Office, for their continuous support to this Project.

I am also pleased to acknowledge all the personnel of the LNF Accelerator Division for their enthusiastic commitment, and Pina Possanza for her outstanding secretarial and administrative management.

IX. REFERENCES

[1] The DAΦNE Project Team, "DAΦNE, The Frascati Φ-factory", Proceedings of PAC 93, p. 1993.

[2] K. Whitham et al., "Design of the e^+ e^- Frascati Linear Accelerator for DAΦNE", Proceedings of PAC 93, p. 611.

[3] The KLOE Collaboration, "KLOE, a General Purpose Detector for DAΦNE", Frascati Internal Note LNF-92/019 (IR), April 1992.

[4] PEP II - An Asymmetric *B* Factory, Conceptual Design Report, June 1993, LBL-PUB-5379, SLAC-418, CALT-68-1869, UCRL-ID-114055, UC-IIRPA-93-01.

[5] S. Guiducci, "Background evaluation in DAΦNE", DAΦNE Technical Note IR-6 (1995).

[6] M.E. Biagini, M. Zobov, "A better working point for DAΦNE", DAΦNE Technical Note G-32 (1995).

[7] The FINUDA Collaboration, "FINUDA, a Detector for Nuclear Physics at DAΦNE", Frascati Internal Note LNF 93/021 (IR), May 1993.

[8] A. Balerna et al., "DAΦNE-L: Proposta per l'utilizzazione di DAΦNE come sorgente di luce di sincrotrone", Frascati Internal Note LNF-91/083 (IR), October 1991.

[9] V. Chimenti et al., "The DAΦNE Main Ring Vacuum System", Proceedings of PAC 93, p. 3906.

[10] S. Bartalucci et al., "Analysis of Methods for Controlling Multibunch Instabilities in DAΦNE", Particle Accelerator, Vol. 48, 4 (1995), p. 213.

[11] R. Boni et al., "A Broadband Waveguide to Coaxial Transition for High Order mode Damping in Particle Accelerator RF Cavities", Particle Accelerator, Vol. 45, 4 (1994), p. 195.

[12] G. Oxoby et al., "Bunch by Bunch Longitudinal Feedback System for PEP-II", Proceedings of EPAC 94, p. 1616.

[13] A. Gallo et al., "Overdamped Cavity for the DAΦNE Longitudinal Feedback", DAΦNE Technical Note RF-17 (1995).

STATUS REPORT ON KLOE

Juliet Lee–Franzini
Laboratori Nazionali di Frascati
Via Enrico Fermi 40 - 00044 - Frascati, Italy
Physics Department, State University of New York at Stony Brook
Stony Brook, New York 11794, U.S.A.

ABSTRACT

A general purpose detector, KLOE, is being constructed. While it is designed primarily for CP violation measurements and other symmetry studies, it is also capable of doing a whole spectrum of other experiments, from tests of chiral pertubation predictions to detailed light meson spectroscopy. Its physics program and present status are discussed.

1 – KLOE'S Physics Program

1. 1 CP and CPT by quantum interferometry

Consider the process $\phi \to K\overline{K} \to f_1, t_1 + f_2, t_2$ where a K^0 meson decays into a state f_1 at time t_1 and the other into a state f_2 at time t_2, as illustrated below.



The decay intensity to f_1, f_2, as a function of $\Delta t = t_1 - t_2$ and for $\Delta t > 0$, is:

$$I(f_1,\ f_2;\ \Delta t) =$$
$$\frac{1}{2\Gamma}|\langle f_1|\, K_S\rangle\langle f_2|\, K_S\rangle|^2\Big(|\eta_1|^2 e^{-\Gamma_L \Delta t} + |\eta_2|^2 e^{-\Gamma_S \Delta t}$$
$$- 2|\eta_1||\eta_2| e^{-\Gamma \Delta t/2}\cos(\Delta m \Delta t + \phi_1 - \phi_2)\Big)$$

where $\eta_i =< f_i/K_L > / < f_i/K_S >$ and a similar expression holds for $\Delta t < 0$. The interference term is sensitive to Δm, the magnitudes of the amplitude ratios η's and their phase difference, while the complete distribution depends also on the K_S and K_L lifetimes. One can thus perform a whole spectrum of precision "kaon-interferometry" experiments at DAΦNE by measuring the above decay intensity distributions for appropriate choices of the final states f_1, f_2. Four examples are listed below.

1. With f_1=f_2 one measures Γ_S, Γ_L and Δm, since all phases cancel. Rates can be measured to $\times 10$ improvement in accuracy and Δm to $\times 2$.
2. With f_1=$\pi^+\pi^-$, f_2=$\pi^0\pi^0$, one measures $\Re(\epsilon'/\epsilon)$ at large time differences, and $\Im(\epsilon'/\epsilon)$ for $|\Delta t| \leq 5\tau_s$. Fig. 1 shows the interference pattern for this case.
3. With $f_1 = \pi^+\ell^-\nu$ and $f_2 = \pi^-\ell^+\nu$, one can measure the CPT–violation parameter δ_K:[1] its real part at large time differences and the imaginary part for $|\Delta t| \leq 10\tau_s$. Fig. 2 shows the interference pattern.
4. For $f_1 = 2\pi$, $f_2 = \pi^+\ell^-\nu$ or $\pi^-\ell^+\nu$ small time differences yield Δm, $|\eta_{\pi\pi}|$ and $\phi_{\pi\pi}$, while at large time differences, the asymmetry in K_L semileptonic decays provides tests of T and CPT. The *vacuum regeneration* interference is shown in fig. 3.

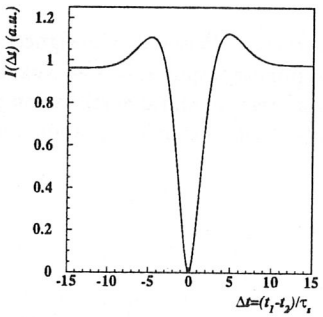

Fig. 1. Interference for f_1=$\pi^+\pi^-$, f_2=$\pi^0\pi^0$.

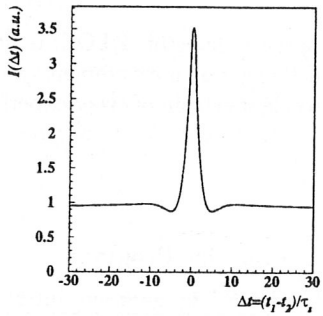

Fig. 2. Interference for $f_1 = \ell^-, \phi_2 = \ell^+$.

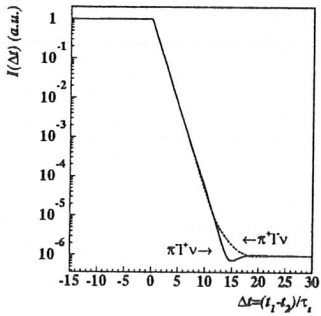

Fig. 3. Interference pattern for $\phi_1 = 2\pi, f_2 = \ell^\pm$.

In all, by choosing appropriate f_1 and f_2 channels one can determine 16 independent parameters describing the neutral K system. If the validity of the $\Delta S = \Delta Q$ rule is

assumed there are only 13 parameters to be determined. Experiments at DAΦNE can thus test CPT invariance, in addition to studying CP violation. Should however the $\Delta S = \Delta Q$ rule not hold (it is expected to be violated to only one part in 10^7 in the Standard Model), there are in fact 17 independent parameters.[2] Therefore we will need to use strangeness tagged K^0's, which can be obtained from charge exchange of K^+ mesons, in turn tagged by observation of a K^- meson from the copious decay $\phi \to K^\pm$.

1. 2 Measuring $\mathcal{R}^\pm/\mathcal{R}^0$

We can also use the classical method of the double ratio $\mathcal{R}^\pm/\mathcal{R}^0 = 1 + 6 \times \Re(\epsilon'/\epsilon)$, and other ways of measuring $\Re(\epsilon'/\epsilon)$ from selected final states. Very different systematics are involved, thus allowing a self–check of the results. In fact, one can illustrate the statistical accuracy achievable at DAΦNE easily using the double ratio method (recall that the tagging efficiency drops out identically here and thus do not contribute to systematic errors).

In abbreviated form, the double ratio is

$$\mathcal{R}^\pm/\mathcal{R}^0 = \frac{N_L^\pm/N_S^\pm}{N_L^0/N_S^0} \approx 1 + 6\mathrm{Re}\frac{\epsilon'}{\epsilon},$$

where each N refers to the number of $K_{L,S}$ decaying to two charged or neutral pions. The N_S numbers will evidently be much larger then the N_L; thus, the statistical errors coming from them will be negligible compared to those coming from the N_L. We thus have

$$\delta\left(\frac{\epsilon'}{\epsilon}\right) = \frac{1}{6}\sqrt{(\Delta N_L^\pm)^2 + (\Delta N_L^0)^2} = \frac{1}{6}\sqrt{\frac{1}{N_L^\pm} + \frac{1}{N_L^0}} = \frac{1}{6}\sqrt{\frac{3}{2N_L^0}},$$

since by isospin symmetry there are twice as many charged two–pion decays as neutral two pion decays. N_L^0 is given by the ϕ cross-section, times the integrated luminosity per year, times the efficiency for K_L tags, times $BR(\phi \to K_L K_S)$, times $BR(K_L \to \pi^0\pi^0)$, times the number of K_L's that are within the fiducial volume (i.e., that are detectable):

$$N_L^0 = 5\ \mu\mathrm{b} \times 10^{10}\ \mu\mathrm{b}^{-1} \times 2/3 \times 0.34 \times 10^{-3} \times (1 - e^{-150/350}) = 4 \times 10^6,$$

which gives as claimed,

$$\delta\left(\frac{\epsilon'}{\epsilon}\right) = 1 \times 10^{-4}.$$

1. 3 Other CP violating process/decays

So far CP violation has only been seen in K_L decays ($K_L \to \pi\pi$ and semileptonic decays). DAΦNE can look for $K_S \to \pi^0\pi^0\pi^0$, the counterpart to $K_L \to \pi\pi$. The branching ratio for this process is proportional to $\epsilon + \epsilon'_{000}$ where ϵ'_{000} is a quantity similar to ϵ', signalling direct CP violation. It is not as suppressed as the normal ϵ', perhaps a factor of twenty less. Nonetheless, as the expected BR is 2×10^{-9}, the whole signal will be at the 30 event level, and therefore there is here only the possibility to see the CP impurity of K_S, never observed before, not direct CP violation. The current limit on this BR is 3.7×10^{-5}. Another possibility is to look at the difference in rates between $K_S \to \pi^+ l^- \nu$ and $K_S \to \pi^- l^+ \nu$, which is expected to be $\sim 16 \times 10^{-4}$, measurable in one year's running at DAΦNE, to an accuracy of $\sim 4 \times 10^{-4}$. Again this would be only a measurement of ϵ, not ϵ', but the observation for the first time of CP violation in two new channels of K_S decay would be nonetheless of considerable interest.

Evidence for direct CP violation can be also be obtained from the decays of charged kaons which are copiously produced at DAΦNE. CP invariance requires equality of the partial rates for $K^\pm \to \pi^\pm\pi^+\pi^-$ ($\tau^\pm$) and for $K^\pm \to \pi^\pm\pi^0\pi^0$ ($\tau'^\pm$). One can improve the present rate asymmetry measurements by two orders of magnitude. One can also observe differences in the Dalitz plot distributions for K^+ and K^- decays in both the τ and τ' modes; at DAΦNE one could reach sensitivities of $\sim 10^{-4}$. Finally, differences in rates in the radiative two pion decays of $K^\pm$, $K^\pm \to \pi^\pm\pi^0\gamma$, are also proof of direct CP violation. At DAΦNE the sensitivity reachable is $\sim 1.4 \times 10^{-3}$.

1. 4 Chiral perturbation theory

In the last decade chiral perturbation theory (CHPT) has been extended to the next order terms in the chiral expansion ($\mathcal{O}(m^4)$, $\mathcal{O}(p^4)$, $\mathcal{O}(m^2p^2)$). Many new amplitudes can then be predicted.[3] At lowest order the CHPT relation predicts the slope of the scalar form factor, λ_0. There is at present disagreement of experiment with the CHPT prediction, 0.017 ± 0.004. One can measure λ_0 for K_L to an accuracy of 1.4×10^{-5}. Similar accuracies are obtainable for $K^\pm$ and for λ_+. There is only one measurement of the relevant $K_{\ell 4}$ form factors. These decays provide an unique opportunity for the determination of the $\pi\pi$ phase shift.[4] The amplitudes for $K_{\ell 2,\gamma}$, $K_{\ell 2,e^+e^-}$ and $K_{\ell 3,\gamma}$ depend on the K charge radius. The rate for $K^\pm \to \pi^\pm\gamma\gamma$ and the $\gamma\gamma$ distributions are uniquely predicted by the chiral lagrangian approach. Dalitz decays of K mesons and two photon production of pions are also of great interest.

1. 5 Radiative ϕ decays

Many other physics topics can be studied, especially at the DAΦNE start–up time, when the number of beam bunches will be approximately a quarter (30) of the final design value. An example is the study of light meson spectroscopy. Precise measurements of the $\eta - \eta'$ mixing have important bearings on quark models and QCD, in particular on the question of whether there are gluonic components in the η and η' wave functions.[5] In this regard, measurements of the radiative ϕ decays to η and to η', which are feasible with great sensitivity using KLOE, can lead to a really decisive test, when combined with the information coming from other sources such as the analogous J/Ψ decays and the two-photon decays of η and η'. To complete the determination of the η' parameters we need measurements of the rare transition $\phi \rightarrow \eta'\gamma$. There is some room for a non-vanishing gluonic component in the η'. To give an idea of the expected order of magnitude of the branching ratio, for no gluonium in the η' and a mixing angle of 20° we expect BR($\phi \rightarrow \eta'\gamma$)$\sim 1.2\times10^{-4}$. A Monte Carlo study[6] shows that KLOE can reach, during the commissioning year of DAΦNE, BR's of $\sim 10^{-6}$.

At the end of 1996, DAΦNE will begin delivering of the order of 500 ϕ - mesons/sec. This provides a unique opportunity to study the $f_0(975)$ in ϕ radiative decays, even for branching ratios which in some estimates could be as low as 1×10^{-6}. The unique, lightest scalar meson state $f_0(975)$ is poorly described by current models. By Monte Carlo studies we show that the branching ratio above can easily be measured in the neutral decay channel $f_0 \rightarrow \pi^0\pi^0$.[7] In decays to $\pi^+\pi^-$, there are backgrounds from continuum processes.[8] Interference between one of these processes and the f_0 amplitude leads to very interesting and complex patterns.[9] A complete study of the photon spectrum from $e^+e^- \rightarrow \pi^+\pi^-\gamma$ at the ϕ peak, after suppression of continuum contributions by suitable kinematics and angular cuts, can determine the sign of the $\phi f_0\gamma$ coupling even for the smallest branching ratio, thus providing a totally new piece of information for the investigation of the nature of the f_0.[7]

1. 6 e^+e^- annihilations into hadrons from threshold to 1.5 GeV

Precise measurements of $\sigma(e^+e^- \rightarrow \text{hadrons})$ up to energies of $\sim$1.5 GeV are necessary for the calculation of the muon anomaly a_μ.[10] The required accuracy for the measurements[11] of $\sigma(e^+e^- \rightarrow \text{hadrons})$ is $\sim$ 0.5%, readily accessible to KLOE.

1. 7 Other decays

DAΦNE will be a unique source of pure K_S, thanks to tagging, providing up to 10^{10} kaons per year, and allowing measurements of rare K_S decay modes, most of which have not been measured yet, down to the 10^{-8} or 10^{-9} level. Rare charged K decay modes will also be studied. It will be a place to study many rare decays, such as $\phi \to \eta\gamma$, and η decays. In table 1 some of the improvements that may be made in rare decay BR limits are listed.

Table 1. Rare decays.

Decay mode	To date	Limits that can be achieved at DAΦNE
$\eta \to 3\gamma$	BR $< 5 \times 10^{-4}$	1.4×10^{-8}
$\eta \to \omega\gamma$	BR $< 5 \times 10^{-2}$	10^{-9}
$\phi \to \rho\gamma$	BR $< 2 \times 10^{-2}$	10^{-9}
$\phi \to \pi^+\pi^-\gamma$	BR $< 7 \times 10^{-3}$	10^{-9}
$\eta \to \pi^0 e^+ e^-$	BR $< 4 \times 10^{-5}$	1.4×10^{-8}
$\eta \to \pi^0 \mu^+ \mu^-$	BR $< 5 \times 10^{-6}$	1.4×10^{-8}

2 – The KLOE Design

2. 1 The KLOE LOGO

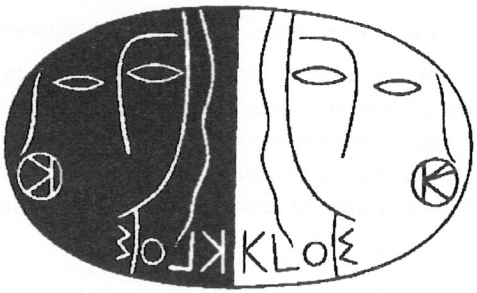

Fig. 4. KLOE LOGO.

The KLOE-Detector, with its distinctive logo, was proposed to the LNF's Scientific committee and given stage-I approval April 28, 1992.[12] A technical design proposal was submitted to the same committee on January 12, 1993.[13] It was

fully approved on March 19, 1993. Two additional addenda were written to amplify design concerns specific to the central drift chamber,[14] and to the data acquisition system.[15] These four documents by the KLOE Collaboration are the source materials containing the full evolutionary details of the KLOE design. Here, I have extracted the salient features and the parameters of the main components of the final detector. I also list some of the interesting results obtained during our prototyping and test work, to give a flavor of how much has been achieved and what still remains to be done.

The KLOE detector requirements are:

1. Collect enough statistics
2. Measure the path length of the K_S, K_L decays to the required accuracy
3. Reject backgrounds at the desired level
4. Be self-calibrating, using various K decay modes, in addition to Bhabha scattering events.

Its scale is driven by a fundamental parameter, the mean decay path length of the long lived K^0-meson $L(K_L)$: at DAΦNE, $\beta(K)$=0.216 and $L(K_L) = \gamma\beta c\tau = 3.44$ m.

2. 2 The KLOE Collaboration

A. Aloisio[e], A. Andryakov[b], A. Antonelli[b], M. Antonelli[b], F. Anulli[b], C. Avanzini[h], D. Babusci[b], C. Bacci[j], R. Baldini-Ferroli[b], G. Barbiellini[m], M. Barone[h], K. Barth[c], V. Baturin[e], H. Beker[h], G. Bellettini[g], G. Bencivenni[b], S. Bertolucci[b], C. Bini[h], C. Bloise[b], V. Bocci[i], V. Bolognesi[g], F. Bossi[b], P. Branchini[k], L. Bucci[h], A. Calcaterra[b], R. Caloi[h], P. Campana[b], G. Capon[b], M. Carboni[b], G. Cataldi[d], S. Cavaliere[e], F. Ceradini[j], L. Cerrito[i], M. Cerù[h], F. Cervelli[g], F. Cevenini[e], G. Chiefari[e], G. Ciapetti[h], M. Cordelli[b], P. Creti[d], A. Doria[e], F. Donno[b], R. De Sangro[b], P. De Simone[b], G. De Zorzi[h], D. Della Volpe[e], A. Denig[c], G. Di Cosimo[h], A. Di Domenico[h], E. Drago[e], V. Elia[d], O. Erriquez[a], A. Farilla[a], G. Felici[b], A. Ferrari[g], M. L. Ferrer[b], G. Finocchiaro[b], D. Fiore[e], P. Franzini[h,f], A. Gaddi[b], C. Gatto[e], P. Gauzzi[h], E. Gero[b], S. Giovanella[h], V. Golovyatuk[d], E. Gorini[d], F. Grancagnolo[d], W. Grandegger[b], E. Graziani[k], U. v. Hagel[c], R. Haydar[b], M. Imhof[c], M. Incagli[g], C. Joram[c], L. Keeble[b], W. Kim[l], W. Kluge[c], F. Lacava[h], G. Lanfranchi[h], P. Laurelli[b], J. Lee-Franzini[b,l], A. Martini[b], A. Martinis[m], M. M. Massai[g], R. Messi[i], L. Merola[e], A. Michetti[h], S. Miscetti[b], S. Moccia[b], F. Murtas[b], M. Napolitano[e], A. Nisati[h], E. Pace[b], G. F. Palamà[d], M. Panareo[d], L. Paoluzi[i], A. Parri[b],

E. Pasqualucci[i], M. Passaseo[h], A. Passeri[k], V. Patera[b], F. Pelucchi[b], E. Petrolo[h], M. C. Petrucci[h], M. Piccolo[b], M. Pollack[l], L. Pontecorvo[h], M. Primavera[d], F. Ruggieri[a], P. Santantonio[b], R. D. Schamberger[l], A. Sciubba[h], F. Scuri[m], A. Smilzo[e], S. Spagnolo[d], E. Spiriti[k], C. Stanescu[k], L. Tortora[k], P. M. Tuts[f], E. Valente[h], P. Valente[b], G. Venanzoni[g], S. Veneziano[h], S. Weseler[c], R. Wieser[c], S. Wölfle[b], Y. G. Xie[n], A. Zallo[b], C. D. Zhang[n], J. Q. Zhang[n]

[a] Dipartimento di Fisica dell'Università e Sezione INFN, Bari
[b] Laboratori Nazionali di Frascati dell'INFN, Frascati
[c] Institut für Experimentelle Kernphysik, Universität Karlsruhe
[d] Dipartimento di Fisica dell'Università e Sezione INFN, Lecce
[e] Dipartimento di Scienze Fisiche dell'Università e Sezione INFN, Napoli
[f] Physics Department, Columbia University, New York
[g] Dipartimento di Fisica dell'Università e Sezione INFN, Pisa
[h] Dipartimento di Fisica dell'Università e Sezione INFN, Roma I
[i] Dipartimento di Fisica dell'Università e Sezione INFN, Roma II
[j] Dipartimento di Fisica dell'Università di Roma III e Sezione INFN, Roma I
[k] Istituto Superiore di Sanità and Sezione INFN, ISS, Roma.
[l] Physics Department, State University of New York at Stony Brook
[m] Dipartimento di Fisica dell'Università e Sezione INFN, Trieste/Udine
[n] Institute of High Energy Physics of Academica Sinica, Beijing, China, joined in 1995

2. 3 Systematics constraints

Since the observation[16] in 1964 that the long lived K^0 meson decays into two pions, the search for direct CP violation has failed. In terms of physical observables, if the direct CP violating amplitude $\langle \pi\pi | K_2 \rangle$, where K_2 is CP-odd, vanishes, then:

$$\mathcal{R}_S \equiv \frac{\Gamma(K_S \to \pi^+\pi^-)}{\Gamma(K_S \to \pi^0\pi^0)} = \mathcal{R}_L \equiv \frac{\Gamma(K_L \to \pi^+\pi^-)}{\Gamma(K_L \to \pi^0\pi^0)},$$

otherwise, in general, $|\mathcal{R}_S - \mathcal{R}_L| = \Delta\mathcal{R} \neq 0$ and $|\Delta\mathcal{R}/\mathcal{R}| = 6 \times |\mathrm{Re}(\epsilon'/\epsilon)|$.

The aim of KLOE is to reach a sensitivity in $\Delta\mathcal{R}/\mathcal{R}$ of $\sim 6 \times 10^{-4}$, which from the statistical point of view, is achievable at DAΦNE at full luminosity in about one year. The two formidable tasks for KLOE to face are the controlling of efficiencies for the decays of interest and the rejection of background from the copious K_L decays to states other than two pions. The relation between measurements and BR's, assuming tagging is used, is:

$$\underbrace{N^{\pm,0}_{L,S}}_{\text{observed}} - \underbrace{BK^{\pm,0}_{L,S}}_{\text{estimated}} = \underbrace{N_{KK} \times \varrho_{L,S}(\text{tag})}_{\text{cancelsinratio}} \times \underbrace{BR^{\pm,0}_{L,S}}_{\text{desired}} \times \underbrace{\langle \varrho^{\pm,0}_{L,S} \rangle}_{\langle\text{efficiency}\rangle} \times \iint_{\text{FV}} g(l-l')I(l)\,\mathrm{d}l\,\mathrm{d}l'.$$

The double integral is a convolution of the decay intensity $I(l)$ and the experimental resolution $g(l-l')$ in the measurement of the decay path length and an integration over the fiducial volume, FV, of the detector. The four backgrounds $BK^{\pm,0}_{L,S}$ and the averaged efficiencies $\langle \varrho^{\pm,0}_{L,S} \rangle$ are different. They must be known to an accuracy of $\mathcal{O}(1/3000)$.

2. 4 Fiducial volumes

As will be described later, our detector consists of an electromagnetic calorimeter, a large tracking chamber and a vertex detector. The calorimeter has a central part which is a cylinder of 2 m radius and 3.5 m length, closed by two end caps, covering ~98% of the solid angle. The chamber, with inner wall of 25 cm radius, provides tracking for $30 < r < 200$ cm. The whole detector is immersed in a solenoidal field of 0.6 T. Regeneration in walls (beam pipe, chamber walls) is $\leq 1\%$. Use of a large beam pipe, 10 cm radius, inside which all K_S's decay, and rejection of K decays up to 6 cm (10 τ_S) past any wall eliminate the effects of $K_L \to K_S$ regeneration. The fiducial volume (FV) for K_S and K_L decays are idealized below in fig. 5.

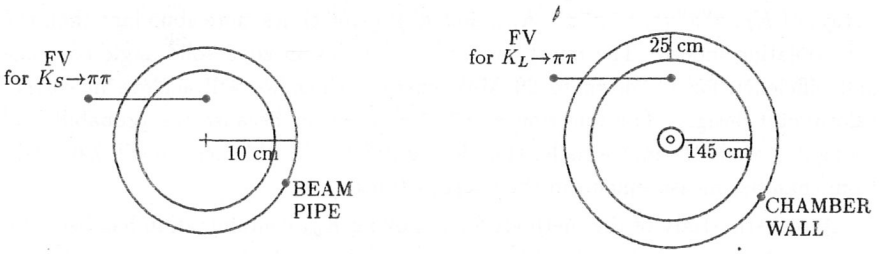

Fig. 5. Fiducial Volumes for K_S and K_L decays.

A helium based chamber is both the decay volume for K_L's and measures angle and momenta for charged particles. The fiducial volume for K_L decays, in cylindrical coordinates, is taken as:

$$30 < r < 175 \text{ cm}$$
$$-125 < z < 125 \text{ cm}$$

If the integral over the FV equation could be carried out to infinity, FV bound-

ary and resolution would not contribute any error. This is essentially the case for K_S decays. A K_L signal guarantees the presence of a K_S. The beam pipe has radius equivalent to $\geq$13–17 lifetimes. Therefore without imposing, ideally, any fiducial volume cut on the data, the integrals are "1", independently of flight path resolution. Efficiencies for $\pi^+\pi^-$ and $\pi^0\pi^0$ decays are $\geq$99% and are well–controlled. Backgrounds are at the level of 10^{-3}, before any cuts are applied.

The case is quite different for K_L decays, since the fiducial volume has dimensions, $\sim$145 cm, which are about half the mean decay path of $\sim$350 cm. A small error on the determination of the boundary of the fiducial volume can introduce large errors on $\mathcal{R}_L$, at the accuracy of interest. What is relevant is the relative error in the determination of the boundaries of the fiducial volumes for $K_L \to \pi^+\pi^-$ and $K_L \to \pi^0\pi^0$, since different methods are used to obtain the K_L path length. $K_L \to K_S$ regeneration at the chamber's inner wall provides in fact an excellent check of the correct knowledge of the inner boundary of the fiducial volumes. To achieve a sensitivity of 6×10^{-4} in $\Delta\mathcal{R}/\mathcal{R}$, we must insure that the outer boundaries of the fiducial volumes for charged and neutral decays are equal to better then 0.5 mm. The most effective way to ensure this is to use K_L decays for which both a "neutral" and a "charged" decay vertex is measurable, such as $K_L \to \pi^+\pi^-\pi^0$. Decays of charged K's, $K^\pm \to \pi^\pm\pi^0$, can also be used over part of the FV, see section on calibration.

2. 5 Backgrounds

The main sources of background in CP experiments are the non– CP violating decays of K_L, $\pi^0\pi^0\pi^0$, $\pi^+\pi^-\pi^0$, $K_{\mu 3}$, and K_{e3}, $\sim$100 times more abundant than the CP–violating modes. The rejection of $\pi^0\pi^0\pi^0$ relies on good solid angle coverage and efficiency for γ's down to 20 MeV energy, which we will achieve in correct calorimeter design. The rejection of $\pi^+\pi^-\pi^0$ is easier because the probability of losing 2/2 γ's is 15 times smaller than losing 2/6 γ's; in addition, we will have help from chamber measurements of the charged tracks.

A realistic study of the methods for removing $K_{\mu 3}$ contamination has been developed. A large sample, 1.35×10^7 $K_{\mu 3}$ and 10^5 $K_L \to \pi^+\pi^-$ events, was generated using the standard size of the luminous region, $\sigma_x = 0.2$ cm, $\sigma_y = 20$ μm, $\sigma_z = 3$ cm. $K \to K_{\mu 3}$ and $K \to \pi^+\pi^-$ events are distinguished by the use of a χ^2 function constructed using the measured variables corresponding to all the kinematical constraints available. A double Gaussian parameterization has been applied to the resolution functions (in p_T, ϕ, $\cot(\theta)$, vertex position) obtained from reconstructed GEANFI[17] generated tracks, using the ARGUS–KLOE program for a 84 layer stereo chamber, to take tails into account. The χ^2 function is peaked at very low

values for $K_L \to \pi^+\pi^-$ decays, while for $K_{\mu 3}$ events it vanishes at 0 and extends to very high values. This calculation has been repeated for several values of the magnetic field, 4 to 8 kG. The rejection factor at 6 kG is approximately 4.5×10^{-4} with a $\pi^+\pi^-$ signal efficiency of 98.8%.[14] The K_{e3} decays are more easily distinguished and removed, partly because $m_e \ll m_\mu$, and the energy deposition pattern of an electromagnetic shower in the calorimeter is very distinctive.

2. 6 Trigger

Triggering at DAΦNE will be an entirely new experience. At full luminosity, the ϕ–event rate is ~5 kHz while the machine produced background when properly masked, can be estimated, scaling from other machines, to be ~10% of this value. All events in principle must be passed to the digitizing electronics (FEE) and data acquisition system (DAQ). The calorimeter can provide an adequate trigger for most events of interest, especially when complemented with some tracking information. Bhabha scattering at angles $10° < \theta < 20°$ and cosmic ray events must be recognized and rejected or prescaled not to overload FEE and DAQ. Both these two classes of events are important for detector calibration. We will employ calorimeter information and simple combinatorial logic to reject/scale these events.

2. 7 Calibration

At DAΦNE a general purpose detector capable of measuring all decay modes of the ϕ has a wealth of processes useful for the calibration of its efficiencies. Furthermore the availabilty of abundant Bhabha scatterings observed in the detector allows a complete calibration of energy and time scales. The following table summarizes the accuracies to which the key parameters can be monitored by various methods. We conclude that KLOE is truly a "self-calibrating" detector!

Table 2. Detector Calibration

Parameter	Method, Process	Accuracy/m
Energy Scale	Continuous, absolute: BHABHA	1%/cluster
Time Scale	– same – : BHABHA	$12ps$/cluster
Tracking Efficiency	– same – : e^+e^-, $\mu^+\mu^-$, $K \to$ 3body	10^{-3}/track
Photon Efficiency	– same – : $K^\pm \to \pi^\pm\pi^0, K^0 \to \pi^+\pi^-\pi^0$	10^{-3}/cluster
F.V. $\pi^0\pi^0/\pi^+\pi^-$	Cont., relative: $K^\pm \to \pi^\pm\pi^0, K^0 \to \pi^+\pi^-\pi^0$	10^{-3}/global

3 – The KLOE Detector

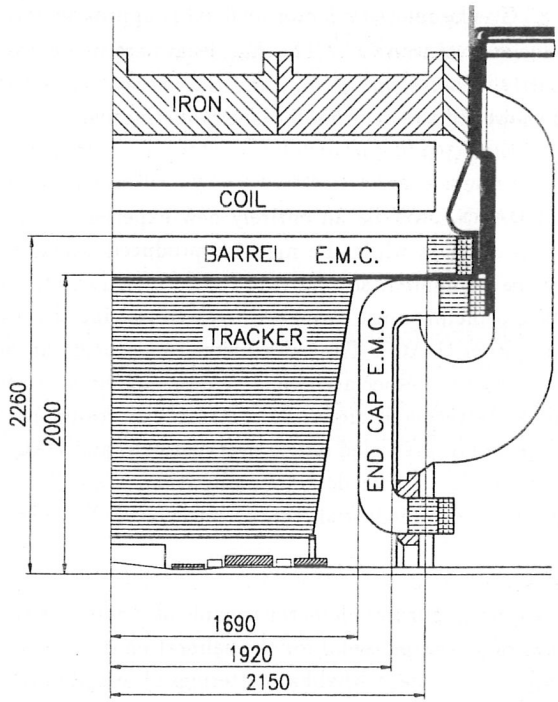

Fig. 6. KLOE cross section along the beam axis.

From the discussions of the previous chapter we conclude that KLOE must be able to track charged particles of momenta between 50 and 250 MeV/c. It must also detect with very high efficiency γ's with energy as low as 20 MeV, measure their energies with a resolution $\delta E_\gamma / E_\gamma \sim 15\%$ at 100 MeV, and provide the space coordinates of the photon conversion point so that the K_L decay path can be determined to within $\sim$1 cm. Thus while the general features of the KLOE detector are similar to those of a *typical* general purpose collider's apparatus: a cylindrical structure surrounding the beam pipe, consisting of a highly efficient, large tracking device for detecting the charged K^0 decay products, an electromagnetic calorimeter with exceptional timing ability, which also provides some particle identification, all enclosed in a solenoidal field, each component has its own unusual features. The KLOE cross section is shown in fig. 6. We discuss the components, in order of

increasing radius. The radius of the beam pipe around the luminous point is 10 cm. This allows the definition of a fiducial region for K_S decays without complication from regeneration. The beam pipe is made of 0.5 mm thick beryllium to minimize multiple scattering, energy loss for charged kaons and regeneration. The enlargment of the beam pipe at the interaction point, visible in fig. 6 as a trapezoidal structure, is in fact a technical challenge for DAΦNE because it could act as a free wheeling RF cavity, with all the attending problems. In figure 6 we also show that the low β insertion permanent magnets are mounted directly on the beam pipe, inside KLOE, another difficult technical problem to be solved.

4 – Central Tracking Chamber

The design of the large tracking chamber for the KLOE detector is driven for the most part by the following considerations:

1. Maximize the homogeneity and isotropy of the active tracking volume because of the long decay path of the K_L and the isotropic angular distribution of the charged decay products.
2. Achieve a high and a well controlled efficiency for the reconstruction of $K_L \to \pi^+\pi^-$ decays.
3. Maximize, without forgetting the points above, the fiducial volume for decay detection, to obtain the largest event sample for a given delivered luminosity.
4. Optimize resolution at low momentum values.
5. Minimize the number of wires, both sense and field, in order to ease the difficulties of building a transparent chamber shell, minimize multiple scattering and maintain the electronics channels count within reasonable limits.

The decay length of K_L's, λ_D=350 cm, requires that a long decay path be available to observe a significant fraction of their decays. A reasonable compromise is to detect K_L decays in a big, cylindrical chamber of radius $\sim$ 2 m and length 370 cm. The above tracking volume is located inside a 15 X_0 thick, lead-scintillating fiber e.m.calorimeter, surronded in turn by a superconducting coil providing a solenoidal field of 0.6 T.

The uniform distribution of K_L decay vertices and secondary tracks in the chamber volume requires a constant size drift cell. This is achieved by using only alternating stereo layers, with constant inward radial displacement at the chamber center. This results in a stereo angle which increases with radius, 50 mrad $\leq \theta_{st} \leq$ 120 mrad, and an approximately constant, square cell shape along z, with constant wire gain. A possible configuration, assuring good tracking also for $K_S \to \pi^+\pi^-$ decays,

might consist of twelve layers in the inner part of the chamber with 1.5×1.5 cm^2 cells, followed by 3×3 cells. The number of cell layers for this case is 61 for a total number of cells of ~13,000. This choice is not too far from an optimal configuration.

Because of the low momenta of the decay products, <300 MeV, we have tested helium-based gas mixtures to minimize multiple scattering. A satisfactory choice

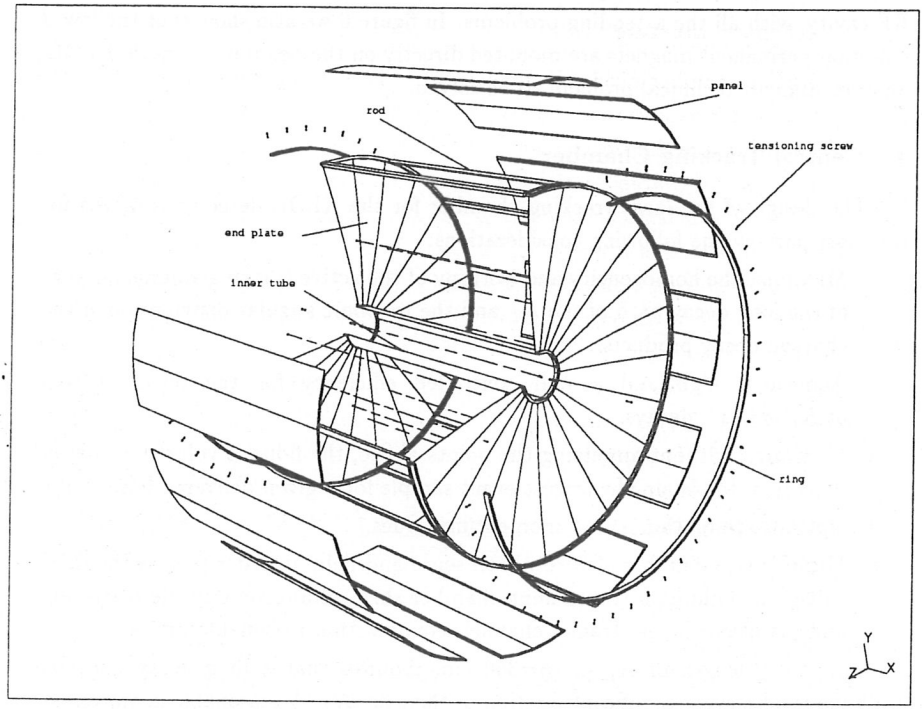

Fig. 7. Exploded View of the KLOE Chamber.

is a 90-10 mixture of He-iC_4H_{10} whose radiation length is X_0=1300 m. The wires, W for sense and Al for field, result in a final value X_0=900 m. The choice of a relatively big drift cell of 3 × 3 cm^2 helps in reducing the total amount of material in the chamber, while still maintaining a proper time-space correlation over most of the cell. Drift velocity is generally not saturated. For an expected resolution on any single measurement of $\sigma_{r\phi} \leq 200$ μm, the $K_L \to \pi^+\pi^-$ vertex is expected to be reconstructed with accuracies $\sigma_{x,y} \leq 500$ μm, $\sigma_z \leq$1–2 mm. The resolution for the reconstructed K_L mass is $\sigma_M \sim 1$ MeV. The low drift velocity of He gas mixtures, and the smallness of the Lorentz angle, implies that the magnetic field will only

change the time-space correlation without loss in either resolution or efficiency. This was confirmed during a beam test using a drift chamber prototype located inside a magnet, which could produce a field of 0.6 T, exposed to a beam at CERN. The effect of the magnetic field is measured to be small ($\simeq 5 \div 10\%$ change in drift velocity).

4. 1 Mechanical structure

The KLOE chamber needs all its walls and the preamplifiers mounted on the chamber end plates to have the smallest possible thickness, in order to minimize photon conversions before the electromagnetic calorimeter as well as multiple scattering and energy losses of charged particles entering the chamber. While some bending of the end plates can be acceptable, flat plates are unacceptably thick. The plate deformation under load is strongly helped by properly attaching the plate outer rim to a torsionally stiff ring. The end plates of the KLOE chamber are kept apart by twelve rods attached to an outer ring. Gas seal is completed by twelve panels which will be mounted after chamber stringing and an inner cylinder. This last is attached to the end plates via two rings at the center of the plates which also provide support for the low β insertion. Panels and inner cylinder carry no loads in our chamber design, see figure 7. The mechanical structure of the drift chamber, with spherical end plates, can withstand without deformation the tension of some 50,000 wires with good transparency ($\leq 0.1 X_0$) to photons from π^0 decays, to be detected in the calorimeter.

4. 2 Prototype 1

In order to acquire first hand experience about all problems concerning materials, stringing procedure, gas tightness, signal and HV, etc. we have built a full length prototype. The prototype, built with carbon fiber plates furnished by STESALIT A. G. of Zullwil, Switzerland, is 3.2 m long with 1 m^2 end plates. Five hundred single sense wire square cells, 3cm by 3cm and 1.5cm by 1.5cm, arranged in thirty layers, are strung at stereo angles in the range 50-120 mrad between two conical shaped carbon fiber end-plates.[18] Cosmic ray and beam test results confirm that it is invaluable for acquiring experience about all phases of the project.

4. 3 Chamber parameters

The performance required of the KLOE tracking device is given below:

Table 3. Central Chamber Performance.

Drift Chamber,	He gas mix, thin walls
δpoint	$= 200\ \mu$m, r and ϕ
	$= 2$ mm, z
δp_t	$= 0.5\% \times p_t$
$\delta(\tan(\theta))$	$= (3.5 \oplus 2.5) \times 10^{-4}$

5 – Calorimeter

Reconstruction of the $\pi^0\pi^0$ decay mode of a 110 MeV/c momentum K, the determination of its decay point and the efficient rejection of the three π^0 decays make designing the electromagnetic calorimeter, EmC, a most challenging project. Unique to the KLOE experiment, is the method of determining the flight path of K_L, the segment ID in fig. 8, by time measurements. I is the ϕ decay point, the direction of ID is given by $-\mathbf{p}_{K_S}$, and A is the photon conversion apex in the calorimeter. As illustrated in fig. 8, the flight time measurements for even a single photon of the four from $\pi^0\pi^0$allow the determination of the K_L decay path. The time of arrival of a photon gives the flight path of the K^0 to an accuracy $\delta l = \beta_K c\, \delta t \sim 6 \times 10^{-3}$ cm $\times\ \delta t$(ps). For a 510 MeV K^0, that is for four photons with $\sum E_\gamma = 510$ MeV, one expects a time resolution of ~100 ps and a path resolution of 0.6 cm. Observation of only three out of four photons still allows an over-constrained determination of both the K^0 mass and the flight path, using time, position and energy measurements.

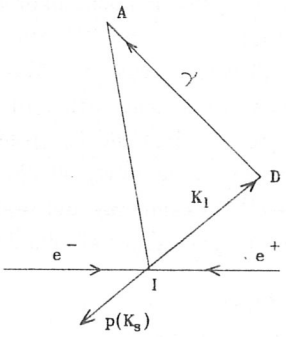

Fig. 8. Measuring the K_L decay length.

The KLOE EmC is a very fine sampling lead-scintillating fiber calorimeter, with photomultipliers (PMs) read-out. The central part, barrel, approximates a cylindrical shell of 4 m inner diameter, 4.3 m active length and 23 cm thicknes. The barrel covers the polar angle region $49° < \theta < 131°$ and consists of 24 sectors with trapezoidal cross section, ~60 cm wide. Two end-caps, 4 m in diameter and 23 cm thick, close hermetically the calorimeter. Each end-cap consists of 26 "C" shaped modules which run vertically along the chords of the circle inscribed in the barrel. At the two ends they are bent at 90°, becoming parallel to the barrel ends, to decrease the effects of the magnetic field on the PMs and to increase hermeticity, see figures 6 and 9.

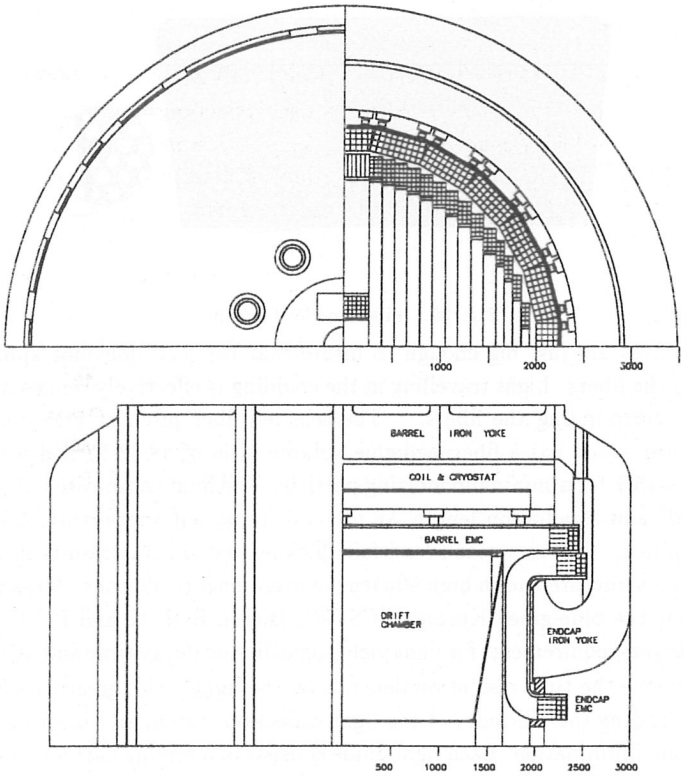

Fig. 9. Partial KLOE views.

Partial KLOE views are shown in figure 9. The top figure shows an endview of the top half with half of the return iron yoke cut away, the lower figure shows a side

view, again with half of the iron yoke cut away.

In our EmC fibers run mostly transversely to the particle trajectories. This reduces sampling fluctuations due to channeling, resulting in improved resolution particularly important at low energies. Each module of the KLOE EmC is built by glueing 1 mm diameter blue scintillating fibers between thin grooved lead plates, obtained by passing 0.5 mm thick lead foils through rollers of proper shape. The grooves in the two sides of the lead are displaced by one half of the pitch so that fibers are located at the corners of adjacent, quasi-equilateral triangles resulting in optimal uniformity of the final stack, see fig. 10.

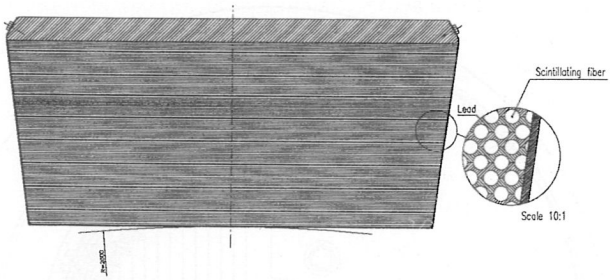

Fig. 10. Fiber and lead layout.

The grooves are just big enough to insure that the lead does not apply direct pressure on the fibers. Light travelling in the cladding is effectively removed because of the glue surrounding the fibers. The selected fiber pitch of 1.35 mm results in a structure which has a fiber:lead:glue volume ratio of 48:42:10 and a sampling fraction of $\sim$15% for a minimum ionizing particle. The final composite has a density of $\sim$5 g/cm^3 and a radiation length X_0 of $\sim$1.6 cm, is self–supporting, and can be easily machined. The very small lead foil thickness ($< 0.1\,X_0$) results in a quasi–homogeneous structure and in high efficiency for low energy photons. Measurements indicate that the blue-green Kuraray SCSF-81, Bicron BCF-12 and Pol.Hi.Tech-46 fiber, satisfy our requirements for light yield, scintillation decay time and attenuation length.[19] Since the time resolution depends on the light yield, great care has been put in maximizing the efficiency of the light collection system and insuring uniform photocathode illumination. Each light guide consists of a mixing part and a Winston cone concentrator.[20] We are thus able to match the calorimeter elements to the PM photocathodes, with an area reduction factor of up to $\sim$4, without losses, because of the small 22° divergence angle of the light travelling in the fibers.

5. 1 Module Ø

All the machinery for building the *barrel* calorimeter have been designed and built by the KLOE calorimeter group, mostly at LNF. The first full size *barrel* module, with dimensions of 23 cm×60 cm×430 cm and trapezoidal cross section, called module Ø, was then succesfully built, also at Frascati. The machinery has been turned over to a company which will assemble all modules of the *barrel* calorimeter. The front half of module Ø is built with Kuraray SCSF-81 fibers and the back half with Pol.Hi.Tech-46 fibers.

The module read–out consists of five planes of 12 elements each, of ~4.4×4.4 cm^2, varying slowly in size across the module face. Each element is viewed through light pipes which provide mixing and terminate with a Winston concentrator coupled to mesh photomultipliers. The PMs are manufactured to KLOE specifications by Hamamatsu (R2021, mod.). KLOE needs to use these special tubes because they can operate in moderate magnetic field.[21] As shown in fig. 6, they are inside the return yoke where they see up to 0.15 T inclined less than 25° with respect to the PM's axis.[22] These PMs have a measured quantum efficiency of only ~60% of the conventional tubes like the ones used in the previous prototypes.[23]

Module Ø employs the final KLOE electronics. The PM base contains the voltage divider for the PMs working with grounded cathode to allow grounding of the tube shieldings and an A.C. coupled preamp which drives the cables carrying the signals outside of the magnet yoke. The signals enter three way splitters, providing input to a constant fraction discriminator, a driver for amplitude measurements and first level analog sums for trigger generation. All these functions are mounted on a 9U VME card, containing 30 complete channels. Signals from this card go to the KLOE designed 12 bit ADC's, 2 V×10 ns full scale, and 12 bit TDC's, 25 ps per count.[15] A description of KLOE electronics can be found in ref. 15.

Module Ø was exposed to a test beam at PSI this past July. Analysis of the collected data is underway at present. Preliminary results indicate that $\sigma_E/E \sim 5\%/\sqrt{E\ (\mathrm{GeV})}$ and $\sigma_T \sim 66\mathrm{ps}/\sqrt{E\ (\mathrm{GeV})}$. These results are precisely the expected resolutions taking into account the length of the full module (4.3 m) and the reduced quantum efficiency of the mesh PM's, halving the number of photoelectrons.

In sum, we have studied extensively the performance of both the *barrel* and *end-cap* prototypes of the KLOE calorimeter and confirmed the findings with module Ø. Aside from the measured energy and time resolutions quoted, we found the energy resolution to be independent of the incidence angle and we expect very little dependence of the time resolution on incidence. We have verified that the calorimeter

can provide some added means to identify pions and muons. Finally, the KLOE electronics performed extremely well at the PSI test, fully to specifications and with very low noise. Therefore, we have succeeded in the design of a calorimeter which satisfy, with some safety margins, the requirements of the KLOE experiment.

5. 2 Calorimeter performance

Table 4. Calorimeter Performance.

δ(Shower Apex)	=1 cm
$\delta E/E$	$= 5\%/\sqrt{E\ (\mathrm{GeV})}$
δt	$= 66$ ps$/\sqrt{E\ (\mathrm{GeV})}$

6 – Magnet

Of crucial importance in rejecting contamination of the $K_L \to \pi^+\pi^-$ sample is the ability of performing good measurements of momenta in the range 155–268 MeV/c. In particular $K_{\mu 3}$ decays overlap kinematically $K_L \to \pi^+\pi^-$ decays when the laboratory muon momentum is ~250 MeV. A simple argument predicts that kinematical overlaps decrease as the cube of the field value. This has been proved by full Monte Carlo calculations. A possible argument against high field is the loss of tracking efficiency and accuracy in vertexing for spiraling tracks. Again we barely see a loss in tracking efficiency beginning at 7 kG, ~0.2% as well as some saturation in the $K_{\mu 3}$ background rejection. This justifies our choice of 6 kG, which provides good rejection without impairing other detector functions. The chamber and calorimeter are inside a superconducting coil and the iron return yoke has deep cavities hollowed out so that the magnetic field therein is reduced and axial, to allow the proper functioning of the mesh photomultipliers employed in the EmC readout. Economical reasons, *i.e.*, power consumption, made us choose a superconducting coil.

7 – Front-end Electronics

The KLOE detector contains 5,000 photomultipliers, PMs, for the readout of the calorimeter, and ~13,000 wires for the tracking chamber. The PM signals are amplified in the PMs' bases and sent to analog boards of 30 channels each. The outputs of this board are connected to ADCs, TDCs and to the trigger processor. The chamber signals are preamplified at the wire feed-through and sent to boards of 48 channels each. The output of two of these boards are connected to a 96 channel TDC board for drift time measurements.

Module Ø tested to great satisfaction the following chain of the final KLOE electronics at PSI in June 1994: PM bases containing the voltage divider and an A.C. coupled preamp which drives the cables carrying the signals to the outside, splitters which provide input to a constant fraction discriminator and to a driver for amplitude measurements, the KLOE designed 12 bit ADC's and 12 bit TDC's.

The TDC chips for the KLOE chamber digitization will reside in groups of three (96 channels) on modules fitting into the KLOE custom crates and readout scheme. Most of the functionality, digitization and event buffering, is integrated into a VLSI chip. The measurement of the signal drift-time coming from the chamber is performed by a custom integrated circuit, which is under development by the INFN Sezione di Roma1. The circuit is a multichannel common start/stop TDC, with 32 channels per chip. In KLOE the drift-time measurement is done by recording, for each signal, its time of arrival with respect to a stop signal, which is common to all channels and generated by the trigger. The TDC integrated circuit will be developed as a full-custom device in 0.5 micron CMOS technology. Its working frequency is a function of an external reference clock that must be supplied to the circuit and it can be as high as 1 GHz (1 nsec LSB). The circuit is capable of detecting rising/falling edges, with a double edge resolution of 10 nsec or better. A programmable number of hits, from 1 to 16, can be stored for each channel. The hits are recorded as 16 bit words and every registered hit is stored in the chip for a programmable time interval. If during this time the chip does not receive a stop command the hit is removed, otherwise, the hit is kept for the read-out. The chip has also a multi–event buffering capability, 4 events deep, which is used only if at least one hit is present in one of the 32 channels, in a time window associated with a stop signal. Dedicated prompt trigger output lines inform the read-out of the presence in the chip of data to be read. The read-out of the data passes through the I/O port at a maximum speed of 50 MHz. The empty channels are automatically skipped during the read-out phase and for each registered hit the chip gives its absolute time value with respect to the stop signal and its channel number. Additional chip functions include an event counter, masking of the individual channels, and a self–test facility.

8 – Data Acquisition

ϕ decays and calibration events represent, at full DAΦNE luminosity, a very large load for the data acquisition system. At 10,000 events per second, each event consisting of 2 to 4 kBytes, we estimate that 20,000 MIPS equivalent computing power will be necessary to digest the data. The universal approach appears to be farms of the new powerful μ–processors. We are looking at the α–VAX product

of DEC, capable of 120 MIPS, amongst possible choices. We intend to write to tape all raw data, and we need to perform Monte Carlo simulations at the 10^8, or greater, event level. The data produced in one year at full $\mathcal{L}$ is $\sim 4 \times 10^{14}$ Bytes, to be stored at a bandwidth of 50–100 MBytes/s. The new Digital Linear Tapes, DLT by DEC, seems capable of such task. Due to the Monte Carlo simulation needs and the inevitable necessity of running production more than once we plan on two 20,000 MIPS farms. The major components of the KLOE DAQ system are briefly presented in the following.[15] An overall view is given in fig. 11.

Data comes from ~25,000 Front End Electronics channels housed in some 40 9U-VME crates. Signal conditioning and digitization is performed in a fixed time of $\mathcal{O}(2\ \mu s)$, to avoid biases depending on event configuration. Every FEE channel contains buffers of appropriate depth, in order to eliminate data overflows and to allow asynchronous read-out. Data from the FEE are transferred to an on-line farm of Single Board Computers, SBC, using a two level concentration scheme. The first one is performed at crate level via a custom bus in the backplane, the AUXbus, and a hardwired read-out controller, ROCK, located in the crate itself. The ROCK implements the function of a sparse readout scanner collecting data related to each single trigger. The second level of concentration is performed by a ROCK manager, ROCKM, connected to chains of crates of suitable length with a cable bus, Cbus. Each ROCKM resides in a 6U-VME crate together with a VME processor which prepares sub-events for transmission to a given farm element. A commercial VME interconnector, VIC, connects all the crates in a chain allowing VME processors to program, check and debug FEE, ROCK's etc. The components of the DAQ system are interconnected via Ethernet for low bandwidth operations (controls, downloading, monitoring) and via FDDI for data transmission. A DEC FDDI GIGAswitch, with bridge functionality, is used to provide parallel paths between the VME processors and the farm in a scalable way. The number of switch ports dedicated to chains is chosen taking into account two factors: the maximum acceptable read-out ROCKM time and the throughput of the communication protocol achievable at VME and farm level. In order to improve the performance of the communication protocol, the sub-events related to the same group of consecutive trigger numbers are packed in sub-event-strings that must be gathered by a single SBC. The farm SBC's build and test the integrity of each event, implement the final event formatting, and perform quality control on samples of the data. The address of each farm element is assigned by an additional VME processor, the data flow controller, DFC, connected also via VIC channels to the ROCKM crates. The DFC manages the load of all the VME processors, maintaining a table which maps groups of trigger

numbers and SBC addresses. DAQ resets and buffer flush-out commands are generated when misalignment is detected at farm level. Other error conditions will be similarly handled. The farm is based on SBC's organized in crates. Each crate has a dedicated output SBC which manages the crate I/O to the storage devices. The total CPU power required for the whole farm is estimated to be about 16,000 Specint'92. CPU boards adequate for this are beginning to appear in the market. We wait for a final decision upon the outcome of a joint project between INFN and DEC designing a custom SBC using the DEC Alpha chip.

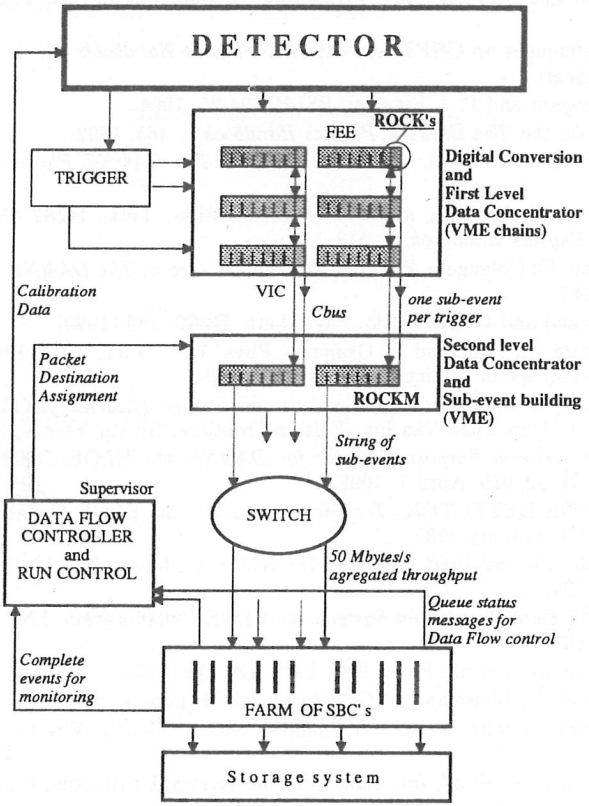

Fig. 11. System Architecture and Information Flow.

Acknowledgments

I wish to acknowledge and thank all my KLOE colleagues for their brilliant, wonderful and heroic efforts to realize KLOE. I also wish to thank Paula J. Franzini for help in preparing this paper.

REFERENCES

1. C. D. Buchanan *et al.*, Phys. Rev. **D45**, 4088 (1992).
2. L. Maiani, *The DAΦNE Physics Handbook*, L. Maiani *et al.* Eds., Frascati, 1992, V. I, p. 21.
3. For all references on CHPT, see *DAΦNE Physics Handbook*, ed. L. Maiani *et al.*, LNF, Frascati.
4. M. Baillargeon and P. J. Franzini, PSI-PR-94-25, 1994.
5. F. E. Close, the *The DAΦNE Physics Handbook*,p. 465, 1992.
6. J. Lee-Franzini, W. Kim, and P. J. Franzini, *The DAΦNE Physics Handbook*, p. 533.
7. J. Lee-Franzini, W. Kim, and P. J. Franzini, Phys. Lett. **B287** 259 (1992); *The DAΦNE Physics Handbook*, p. 513.
8. A. Bramon, G. Colangelo, P. J. Franzini and M. Greco, *The DAΦNE Physics Handbook*, p. 487.
9. P. J. Franzini and G. Colangelo, Phys. Lett. **B289**, 189 (1992).
10. T. Kinoshita, B. Nižić and Y. Okamoto, Phys. Rev. D **31**, 2108 (1985), and references therein; see in particular their reference 28.
11. P. Franzini, *'89 Electroweak Interactions and Unified Theories, XXIV Rencontre de Moriond*, J. Tran Than Van Ed., Edition Frontière, Gif-sur-Yvette, 1989.
12. *KLOE, A General Purpose Detector for DAΦNE*, the KLOE Collaboration, LNF Report LNF-92/019, April 1, 1992.
13. "THE KLOE DETECTOR, *Technical Proposal.*" the KLOE Collaboration, LNF-93/002 (IR), January 1993.
14. *The KLOE Central Drift Chamber*, the KLOE Collaboration, LNF Report LNF-94/028, 1994.
15. *The KLOE Data Acquisition System*, the KLOE Collaboration, LNF Report LNF-95/014, 1995.
16. J. H. Christenson *et al.*, Phys. Rev. Lett. **13**, 138 (1964).
17. A. Antonelli, C. Bloise and A. Calcaterra, KLOE note 3, 23.
18. F. Grancagnolo, with the KLOE Chamber Group, Vienna Wire Chamber Conference 1995.
19. G. de Zorzi, *Proc. of 4th Int. Conf. on Calorimetry*, La Biodola, Italy (1993).
20. A. Di Domenico *et al.*, KLOE Notes 83 and 84.
21. C. Bini *et al.*, KLOE Notes 42, 50, 60, and 78; G. Barbiellini *et al.*, KLOE Notes 56 and 81.
22. F. Bossi, KLOE notes 54 and 91.
23. L. Keeble, G. Lanfranchi and M. Anelli, KLOE Notes 90, 96 and 109.

MEASUREMENTS OF CP AND T VIOLATION PARAMETERS IN THE NEUTRAL KAON SYSTEM AT CPLEAR

Panagiotis Pavlopoulos
Institute for Physics, University of Basel, Klingelbergstr. 82, CH-4056 Basel, Switzerland
For the CPLEAR Collaboration [1].

ABSTRACT

The CPLEAR experiment at CERN studies the CP, T and CPT symmetries in the neutral kaon system by measuring the time dependent decay rate asymmetries of initially pure K^0 and $\overline{K}^0$ states. Results on η_{+-}, η_{+-0}, Δm and x are reported, as well as on the first direct test of T violation and CPT invariance in K^0-$\overline{K}^0$ oscillations. Our results are consistent with CPT invariance and allow for an improved limit on the K^0-$\overline{K}^0$ mass difference.

1 Introduction

The CPLEAR experiment [1)] investigates CP, T and CPT symmetries in the neutral kaon system. Contrary to the traditional experiments, CPLEAR uses initially pure K^0 and $\overline{K}^0$ and measures the difference between the rates of their decays to a variety of final states, $\pi^+\pi^-$, $\pi^0\pi^0$, $\pi e\nu$ and $\pi^+\pi^-\pi^0$. The CP, T and CPT violation parameters can be extracted from the time dependent decay rate asymmetries:

$$A_f(t) \equiv \frac{R_{\overline{K}^0\to f}(t) - R_{K^0\to f}(t)}{R_{\overline{K}^0\to f}(t) + R_{K^0\to f}(t)}$$

The use of such asymmetries has the advantage of cancelling many systematic effects related to the detector acceptances. CPLEAR measures the CP violation parameters η_{+-} for $\pi^+\pi^-$ and η_{+-0}

[1]The CPLEAR Collaboration

R. Adler[2], T. Alhalel[11], A. Angelopoulos[1], A. Apostolakis[1], E. Aslanides[11], G. Backenstoss[2], C.P. Bee[9], O. Behnke [17], A. Benelli [9], V. Bertin[11], F. Blanc[7,13], P. Bloch[4], C. Bula[13], P. Carlson[15], M. Carroll[9] J. Carvalho[5], E. Cawley[9], S. Charalambous[16], M. Chardalas[16], G. Chardin[14], M.B. Chertok[3], A. Cody[9], M. Danielsson[15], S. Dedoussis[16], M. Dejardin[14], J. Derre[14], J. Duclos[14], A. Ealet[11], B. Eckart[2], C. Eleftheriadis[16], I. Evangelou[8], L. Faravel [7], P. Fassnacht[11], J.L. Faure[14], C. Felder[2], R. Ferreira-Marques[5], W. Fetscher[17], M. Fidecaro[4], A. Filipčič[10], D. Francis[3], J. Fry[9], E. Gabathuler[9], R. Gamet[9], D. Garreta[14], H.-J. Gerber[17], A. Go[3,15], C. Guyot[14], A. Haselden[9], P.J. Hayman[9], F. Henry-Couannier[11], R.W. Hollander[6],E. Hubert[11], K. Jon-And[15], P.-R. Kettle[13], C. Kochowski[14], P. Kokkas[2], R. Kreuger[6], R. Le Gac[11], F. Leimgruber[2],A. Liolios[16], E. Machado[5], I. Mandić[10], N. Manthos[8], G. Marel[14], M. Mikuž[10], J. Miller[3], F. Montanet[11], T. Nakada[13], A. Onofre[5], B. Pagels [17], I. Papadopoulos[16], P. Pavlopoulos[2], J. Pinto da Cunha[5], A. Policarpo[5], G. Polivka[2], R. Rickenbach[2], B.L. Roberts[3], E. Rozaki[1], T. Ruf[4], L. Sakeliou[1], P. Sanders[9], C. Santoni[2], K. Sarigiannis[1], M. Schäfer[17], L.A. Schaller[7], A. Schopper[4], P. Schune[14], A. Soares[14], L. Tauscher[2], C. Thibault[12], F. Touchard[11], C. Touramanis[4], F. Triantis[8], E. Van Beveren[5], C.W.E. Van Eijk[6], G. Varner[3], S. Vlachos[2], P. Weber[17], O. Wigger[13], M. Wolter[17], C. Yeche[14], D. Zavrtanik[10] and D. Zimmerman[3]
[1]University of Athens, [2]University of Basel, [3]Boston University, [4]CERN, [5]LIP and University of Coimbra, [6]Delft University of Technology, [7]University of Fribourg, [8]University of Ioannina, [9]University of Liverpool, [10]J. Stefan Inst. and Phys. Dep., University of Ljubljana, [11]CPPM, IN2P3-CNRS et Université d'Aix-Marseille II, [12]CSNSM, IN2P3-CNRS, Orsay, [13]Paul-Scherrer-Institut(PSI), [14]CEA, DSM/DAPNIA, CE-Saclay, [15]KTH Stockholm, [16]University of Thessaloniki, [17]ETH-IPP Zürich

for $\pi^+\pi^-\pi^0$, Δm, the K_L-K_S mass difference, and the parameter x (to test the validity of the $\Delta S = \Delta Q$ rule) from the semileptonic decays. The possibility of measuring the strangeness of the neutral kaon at its production and at its decay is a superior tool for directly measure T violation, as well as for directly testing CPT invariance. Moreover such a tool potentially allows the study of discrete symmetries in various parameters and form factors of the semileptonic decays as presented by Lee and Wu [14]. An indirect test of CPT invariance is made by comparing φ_{+-}, the phase of η_{+-}, to φ_{sw}, the superweak phase. First results have been obtained, including data up to middle '94, for the time dependent asymmetries in the $\pi^+\pi^-$, the semileptonic and 3π channels, from which the CP, T and CPT parameters have been evaluated with statistical significance better than of many existing measurements. In some cases the results are unique.

2 Experimental Setup

The K^0 and $\overline{K}^0$ mesons are produced in equal amounts in $\overline{p}p$ annihilations at rest, through the channels:

$$\overline{p}p \rightarrow K^-\pi^+K^0$$

$$\overline{p}p \rightarrow K^+\pi^-\overline{K}^0$$

each one with a branching ratio of $\approx 2 \cdot 10^{-3}$. The strangeness of the neutral kaon $K^0(\overline{K}^0)$ at t=0 is defined by the companion charged kaon $K^-(K^+)$.

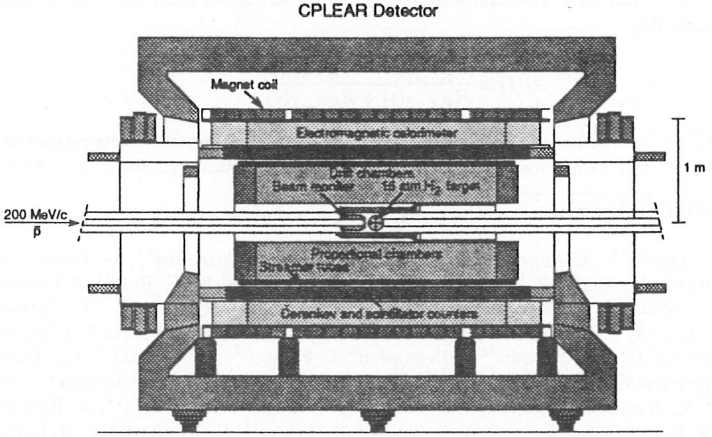

Figure 1: The CPLEAR detector.

The CPLEAR detector [2] is shown in Fig. 1. The detector has a cylindrical geometry and is mounted inside a solenoid magnet of 3.6 m length and 1 m radius, producing a field of 0.44 T. It allows the detection of neutral kaon decays for the eigentime range $0 \leq \tau \leq 20\tau_S$ (τ_S is the K_S mean life). The 200 Mev/c antiprotons from the Low Energy Antiproton Ring (LEAR) of CERN at a rate $\approx 10^6 s^{-1}$ stop and annihilate inside a gaseous hydrogen target (16 bar pressure) at the center of the detector. Viewed from the target to the outside, the detector consists of two multiwire proportional chambers and six drift chambers which are the tracking devices, two layers of streamer tubes giving a fast information of the z coordinate for each track, a scintillator(S1)-Cerenkov(CE)-scintillator(S2) sandwich (PID) which provides identification of charged kaons, pions and electrons, and an electromagnetic calorimeter to detect photons. The electromagnetic showers are detected

in the lead/gas sampling calorimeter using 17280 tubes, each with one wire, working in a limited streamer mode. It consists of three segments, each of 120°, and of 18 layers in depth. Each layer of tubes is sandwiched between two layers of pick-up strips (±30° with respect to the tubes). Special care was taken in the design and construction of the detector to minimize the material in the decay volume and hence the effects due to regeneration and absorption of the neutral kaons.

A multi-level trigger system, including custom-made hardwired processors, provides a fast event selection. The trigger is based on particle identification, kinematical selection and shower counting, and provides a rejection factor of ≈ 1000 in less than $5\mu s$.

3 Detemination of Δm and x from $K^\circ(\overline{K}^\circ) \to \pi e \nu$ decays.

The CPLEAR experiment has the capacity to determine the strangeness of the neutral kaons both at their production and at their decays. Therefore is able to measure the four decay rates R, as a function of the decay eigentime τ of the kaon, depending on the strangeness of the neutral kaon (K^0or $\overline{K}^0$) at the production time, $\tau = 0$, and on the charge of the decay lepton (e^+or e^-):

$$R^+(\tau) \equiv R[K^0_{(\tau=0)} \to e^+\pi^-\nu](\tau) \qquad \overline{R}^-(\tau) \equiv R[\overline{K}^0_{(\tau=0)} \to e^-\pi^+\overline{\nu}](\tau) \qquad (1)$$

$$R^-(\tau) \equiv R[K^0_{(\tau=0)} \to e^-\pi^+\overline{\nu}](\tau) \qquad \overline{R}^+(\tau) \equiv R[\overline{K}^0_{(\tau=0)} \to e^+\pi^-\nu](\tau) \qquad (2)$$

The $K_L - K_S$ mass difference Δm is obtained from the asymmetry

$$A_{\Delta m}(\tau) = \frac{[R^+(\tau)+\overline{R}^-(\tau)]-[\overline{R}^+(\tau)+R^-(\tau)]}{[R^+(\tau)+\overline{R}^-(\tau)]+[\overline{R}^+(\tau)+R^-(\tau)]} = \frac{2\cos(\Delta m\tau)e^{-\frac{1}{2}(\tau/\tau_L+\tau/\tau_S)}}{(1+2\mathrm{Re}(x))e^{-\tau/\tau_S}+(1-2\mathrm{Re}(x))e^{-\tau/\tau_L}}, \qquad (3)$$

where a possible violation of the $\Delta S = \Delta Q$ rule is taken into account by the parameter $\mathrm{Re}(x)$ [4], and τ_S (τ_L) denotes the mean life of K_S (K_L).

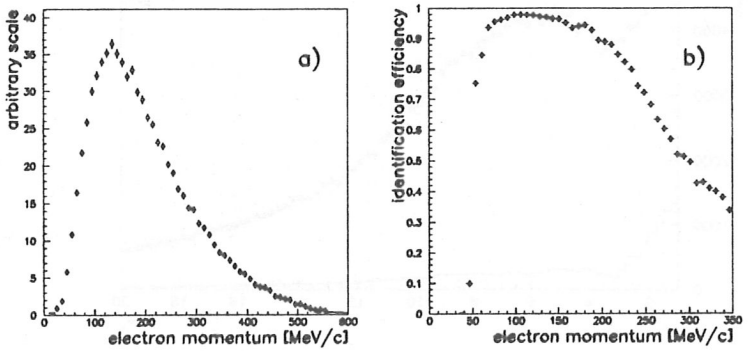

Figure 2: a) Expected electron momentum spectrum in semileptonic decays of neutral kaons. b) Electron identification efficiency versus momentum when 2% of pions fake electrons.

The effect of the strangeness normalisation and the semileptonic channel identification is particularly small due to the manner of construction of the asymmetry $A_{\Delta m}$ (Eq. 3) which compares two sets of data containing both $K^0$and $\overline{K}^0$and also $e^+$and e^-. Similarly, the rates entering $A_{\Delta m}$ do not need to be corrected for regeneration in the detector material, since in the construction of $A_{\Delta m}$ all terms linear in the regeneration amplitude cancel.

A first selection requires four tracks with zero total charge, good track quality and at least one charged kaon candidate. The annihilation vertex (primary vertex) must lie within the beam stopping distribution and a separate vertex for the decay of the neutral kaon (secondary vertex) is required. A cut on the minimum distance between the two vertices (1 cm in the transverse plane) is applied to remove ambiguities on the track assignment to either vertex, and to reduce the background from other $\bar{p}p$ annihilation channels to less than 1% for decay times greater than 1 τ_S. A kinematical fit requiring the K^0 missing mass at the primary vertex is performed to validate the hypothesis of the $(K^{\pm}\pi^{\mp}K^0)$ channel.

The semileptonic decay channel is selected by identifying one of the secondary tracks as an electron or a positron. Electron-pion separation is based on the energy loss in S1 and S2, the number of photo-electrons per unit path length in CE and the time of flight of the particle from the decay vertex to S1. The selection has been optimized using electron data from converted photons and pions from decays of neutral kaons into $\pi^+\pi^-$. The expected electron momentum spectrum obtained from Monte Carlo is shown in Fig. 2 a). The electron identification efficiency versus momentum is shown in Fig. 2 b). This efficiency is obtained requiring that less than 2% of pions are misidentified as electrons, independently of the momentum. Under these conditions, muons have an average probability of $\approx 15\%$ to be misidentified as electrons. A constrained fit requiring energy-momentum conservation under the assumption of a missing neutrino and the alignment of the K^0 momentum vector with the line joining the two vertices is performed. This fit also improves the resolution of the decay time and fixes the absolute time scale of the neutral kaon with a precision better than 2×10^{-4}. Simulation studies show that the decay time resolution varies from 5 ps to 15 ps as a function of the neutral kaon decay radius. Finally, events which fit to the $(K\pi K^0,\ K^0 \to \pi^+\pi^-)$ hypothesis with high probability are removed in order to reduce the $\pi^+\pi^-$background which is dominant at short decay times. The final sample contains $\approx 700,000$ $(K^0,\ \overline{K}^0 \to \pi e \nu)$ events collected up to mid 1994.

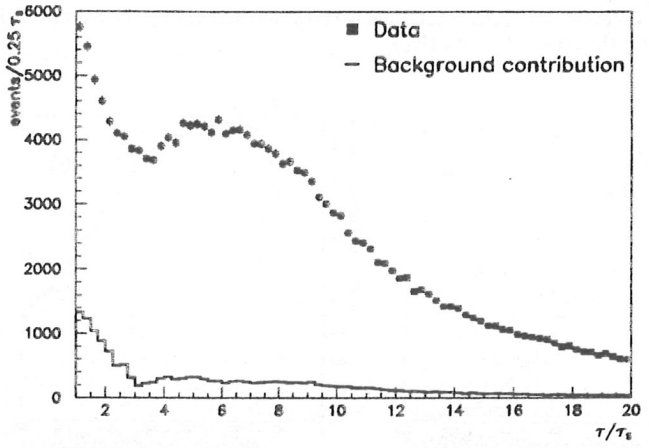

Figure 3: Decay time distribution for real data (squares) and expected background contribution obtained from simulation (solid line).

Due to the different strong interaction cross-sections of K^+ and K^-, as well as of π^+ and π^-, the detection efficiencies of a $(K^+\pi^-)$ pair and a $(K^-\pi^+)$ pair are not identical. The difference of the overall $(K^+\pi^-)$ and $(K^-\pi^+)$ efficiencies is of the order of 15%. To restore the initial K^0-$\overline{K}^0$ production symmetry, we have to correct for this difference in the tagging efficiencies. Let ξ denote the ratio of the two efficiencies, $\xi = \epsilon(K^+\pi^-)/\epsilon(K^-\pi^+)$, which depends on the momenta of the primary pion and kaon $[\xi(\vec{p}_K, \vec{p}_\pi)]$. This ratio is independent of the decay mode and is determined

from the decay rates of neutral kaons into $\pi^+\pi^-$. The weight ξ is then applied event by event to the semileptonic data. The error on Δm due to the uncertainty of this procedure is smaller than $0.00002 \times 10^{10}\hbar/s$.

We have also studied the difference in the detection efficiencies of the two possible final states $(\pi^+e^-\overline{\nu})$ and $(\pi^-e^+\nu)$. Using data from photon conversions, we have not observed any difference in the detection of e^+ and e^-. On the other hand, the difference between the π^+ and π^- cross-sections with matter leads to the detection of a small excess of π^+. We define the parameter η as the ratio of the two detection efficiencies $\epsilon(\pi^+)$ and $\epsilon(\pi^-)$. This ratio is measured as a function of the transverse and longitudinal momentum of the pion by selecting kinematically, in minimum bias events, the annihilation pionic channel and applying subsequently all the online and offline pion selection criteria. We find that η never deviates from unity by more than 2.5%, inducing, at the present stage of the analysis, an uncertainty on Δm of $0.0001 \times 10^{10}\hbar/s$.

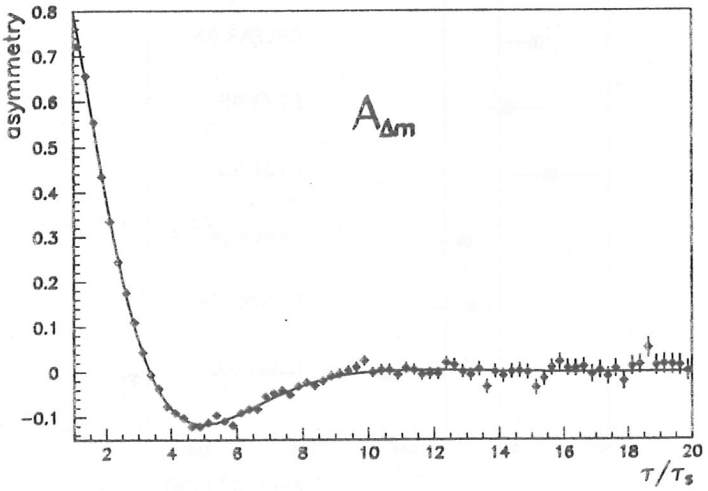

Figure 4: The asymmetry $A_{\Delta m}$ versus the decay time (in unit of τ_S). The solid line represents the result of the fit.

The signal consists of correctly reconstructed $\pi e\nu$ events and of $\pi\mu\nu$ events seen as $\pi e\nu$ ($\approx$ 10% of the signal). The background is determined from a Monte Carlo simulation. The main background source consists of residual neutral kaon decays to $\pi^+\pi^-$ and is concentrated at short decay times. At large decay times there are contributions from $\pi^+\pi^-\pi^0$ decays and from $\pi l\nu$ decays where the pion and the lepton assignments are exchanged. In the simulation, each channel is scaled to the same number of generated $\overline{p}p$ annihilations. The sum of the background contributions normalized by the weight ξ as the signal (since both the signal and the background result from neutral kaon decays) is displayed in Fig. 3 by the solid line. The background causes a dilution in the asymmetry $A_{\Delta m}$ of Eq. 3, which is accounted for by the factor $f_b(\tau)$:

$$f_b(\tau) = \frac{1 + \frac{B^+(\tau)+\overline{B}^-(\tau)-B^-(\tau)-\overline{B}^+(\tau)}{R^+(\tau)+\overline{R}^-(\tau)-R^-(\tau)-\overline{R}^+(\tau)}}{1 + \frac{B^+(\tau)+\overline{B}^-(\tau)+B^-(\tau)+\overline{B}^+(\tau)}{R^+(\tau)+\overline{R}^-(\tau)+R^-(\tau)+\overline{R}^+(\tau)}}, \tag{4}$$

computed by simulation from the background rates $\overset{(-)}{B}{}^{\pm}(\tau)$, and the associated signal $\overset{(-)}{R}{}^{\pm}(\tau)$ (Eqs. 1 and 2).

The diluted asymmetry $A_{\Delta m}(\tau) \times f_b(\tau)$, folded with the decay time resolution, is fitted to the real data asymmetry $A_{obs}(\tau)$ leaving Δm and $\mathrm{Re}(x)$ as free parameters:

$$A_{\Delta m}(\tau) \times f_b(\tau) = A_{obs}(\tau) \; . \tag{5}$$

In order to reduce the systematic error related to the background knowledge, and to minimize the correlation between Δm and $\mathrm{Re}(x)$, the fit is performed above 2 τ_S. The value of $\mathrm{Re}(x)$ resulting from the fit is $Re(x) = (12.4 \pm 11.9_{stat}) \times 10^{-3}$ and we obtain $\Delta m = (0.5274 \pm 0.0029_{\mathrm{stat.}}) \times 10^{10}\hbar/\mathrm{s}$. The correlation coefficient between Δm and $\mathrm{Re}(x)$ is 0.068, and the value and the error of Δm do not change by fixing the value of $\mathrm{Re}(x)$ to zero. The asymmetry $A_{\Delta m}$ (eq. 3) is plotted in Fig. 4, using the value of Δm found by the fit, together with the data points corrected for $f_b(\tau)$.

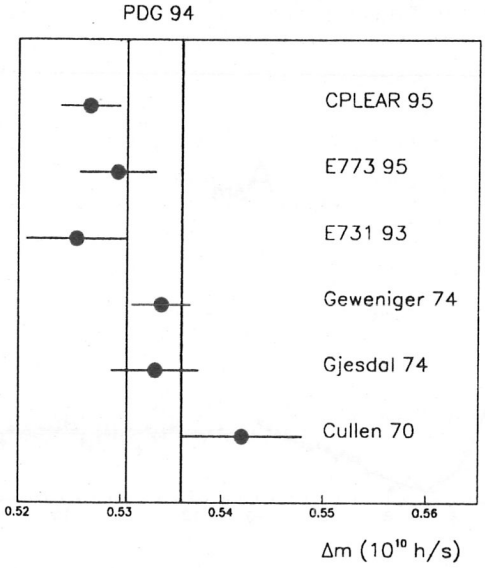

Figure 5: Δm values from CPLEAR[9] and other experiments[4,5]. The two vertical lines correspond to the PDG '94 value $\pm 1\sigma$.

Table 1: Systematic errors

Source of systematic error	Known precision	$\Delta(\Delta m)$ $[10^{10}\hbar/\mathrm{s}]$
background level	$\pm 10\%$	± 0.0004
background asymmetry	$\pm 1.0\%$	± 0.0001
decay time resolution	$\pm 10\%$	± 0.0001
η correction	$\pm 2.5\%$	± 0.0001
τ_S precision [4]	$\pm 0.0012 \times 10^{-10}$s	± 0.0001
total		± 0.0005

The systematic errors of the measurement are listed in Table 1. The main source of systematic uncertainty arises from the Monte Carlo estimation of the background, in particular at short decay times, where the $\pi^+\pi^-$ final state has to be rejected by a large factor ($> 10^3$).

The simulation shows that, for all the background channels, the misidentification of a pion as an electron results from a large error in the track momentum evaluation. To check our simulation, we have relaxed the cuts on the $\pi^+\pi^-$channel so that the background becomes comparable to the signal. The simulation still agrees with the data within 10%. We can thus assume a 10% accuracy on the estimation of the various types of background which are used to compute the background dilution factor $f_b(\tau)$.

A possible charge asymmetry in the remaining background has been studied with the pion data used to calibrate the e/π separation [3]. This sample shows a difference of $(3.0 \pm 1.0)\%$ between the number of π^+which are misidentified as positrons and the number of π^-which are misidentified as electrons. This asymmetry is taken into account in the fit and the corresponding uncertainty on Δm is $0.0001 \times 10^{10}\hbar/s$.

Folding the decay time resolution in the $A_{\Delta m}$ asymmetry resulted in a shift of $+0.0009 \times 10^{10}\hbar/s$ to the value of Δm. The uncertainty on this correction due to the Monte Carlo statistics is $\pm 0.0001 \times 10^{10}\hbar/s$. In conclusion, our final result [3] is

$$\Delta m = (0.5274 \pm 0.0029_{stat.} \pm 0.0005_{syst.}) \times 10^{10}\hbar/s, \tag{6}$$

$$Re(x) = (12.4 \pm 11.9_{stat} \pm 6.9_{syst}) \times 10^{-3}$$

which does not depend on the value of ϕ_{+-} and is the most precise value obtained using semileptonic final states [4], see Fig. 5. Adding this new value and the most recent one [5] to the previous values used by the PDG [4], we obtain

$$\Delta m = (0.5310 \pm 0.0019) \times 10^{10}\hbar/s$$

where the error is scaled by a factor 1.2 following the PDG procedure.

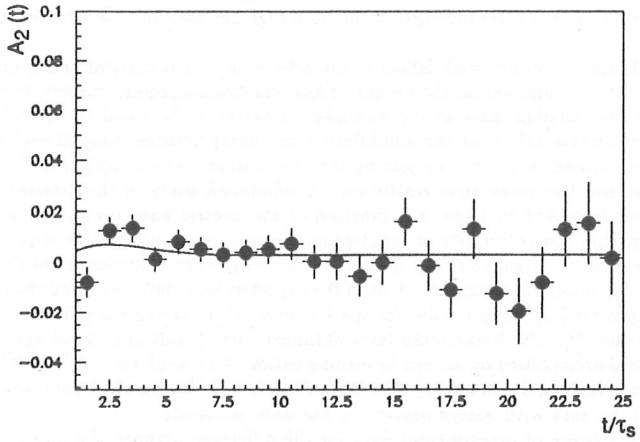

Figure 6: The asymmetry $A_2(t)$ vs the decay time. The line represents the result of the fit.

The asymmetry $A_2(t)$ is sensitive to $Im(x)$ and is shown in Fig. 6,

$$A_2(t) \equiv \frac{\overline{R}^-(t) + \overline{R}^+(t) - R^-(t) - R^+(t)}{\overline{R}^-(t) + \overline{R}^+(t) + R^-(t) + R^+(t)} \simeq$$

$$2Re(\epsilon_T) + 4e^{-\gamma t}\frac{Im(x)sin(\Delta mt) - Re(\epsilon_T)cos(\Delta mt)}{e^{-\gamma_S t} + e^{-\gamma_L t}}$$

where $\gamma = (\gamma_S + \gamma_L)/2$, $Re(x) = 0$ and $\delta_{CPT} = 0$ and ε_T describes CP violation in the kaon matrix. The fit yields:

$$\mathbf{Im(x) = (4.8 \pm 4.3_{stat} \pm 0.6_{syst}) \times 10^{-3}} \quad (7)$$

This value has to be compared with the world average value which is $Im(x) = (-3 \pm 26) \times 10^{-3}$ [4].

4 $K^\circ(\overline{K}^\circ) \to \pi^+\pi^-$ decay mode.

The rates for initially pure K^0 and $\overline{K}^0$ decaying into the $\pi^+\pi^-$ final state, $R(\tau)$ and $\overline{R}(\tau)$ respectively, can be expressed as a function of the decay eigentime τ by:

$$R(\tau), \overline{R}(\tau) \propto \frac{1 \mp 2\mathrm{Re}(\varepsilon_T)}{2} \left[e^{-\tau/\tau_S} + |\eta_{+-}|^2 e^{-\tau/\tau_L} \pm 2|\eta_{+-}| e^{-\frac{1}{2}(\tau/\tau_L + \tau/\tau_S)} \cos(\Delta m\tau - \phi_{+-}) \right], \quad (8)$$

where $\tau_L(\tau_S)$ is the $K_L(K_S)$ mean life and ε_T describes CP violation in the kaon mixing matrix. Since $R(\tau)$ and $\overline{R}(\tau)$ are the decay rates of CP conjugate hadronic final states, any difference between the two is a sign of CP violation. In Fig.7 the decay rates measured by our experiment are shown separately for K^0 and $\overline{K}^0$. Such a difference between the behavior in the world and the antiworld, where the world observed in the "CP-mirror" is referred to as the antiworld, is first direct demonstration of the known violation of CP-invariance graphically.

The K_L–K_S interference term in Eq.8 is isolated by forming the asymmetry of the observed number of K^0 and $\overline{K}^0$ decays to $\pi^+\pi^-$, $N(\tau)$ and $\overline{N}(\tau)$, as a function of the decay time:

$$A_{+-}(\tau) = \frac{\overline{N}(\tau) - \alpha N(\tau)}{\overline{N}(\tau) + \alpha N(\tau)} = -2\frac{|\eta_{+-}| e^{\frac{1}{2}(\tau/\tau_S - \tau/\tau_L)} \cos(\Delta m\tau - \phi_{+-})}{1 + |\eta_{+-}|^2 e^{(\tau/\tau_S - \tau/\tau_L)}}. \quad (9)$$

The acceptances common to K^0 and $\overline{K}^0$ cancel in the asymmetry, thus reducing the systematic uncertainties. The normalization factor α includes the tagging efficiency ξ of $\overline{K}^0$ relative to K^0, $\alpha \simeq [1 + 4\mathrm{Re}(\varepsilon)] \times \xi$, and is determined from the data together with the CP violation parameters $|\eta_{+-}|$ and ϕ_{+-}.

In addition to online and offline event selections, a kinematical and geometrical fit with nine constraints is imposed on the events. These constraints require conservation of energy and momentum, the missing mass at the annihilation vertex to be equal to the K^0 mass, the intersections of two track helices at the annihilation and decay vertices, respectively, and the K^0 momentum to be colinear with the line joining the two vertices. The fit improves the signal–to–background ratio and the decay–time resolution. A simulation study of the detector shows this resolution varying from 4 ps to 10 ps as a function of the neutral kaon decay radius. The only remaining background source consists of semileptonic decays, which are further reduced by using electron identification [2]. Figure 8 shows the sum of the decay–time distributions of K^0's and $\overline{K}^0$'s in which the K_S–K_L interference cancels. A fit of the expected kaon decay rate and the background shape (Fig. 5, open circles) yields a value for the K_S mean life in agreement (within 1%) with the world average value [4]. The background level obtained with this fit is in good agreement with Monte Carlo calculations based on known branching ratios. A total of 1.6×10^7 $K^0(\overline{K}^0) \to \pi^+\pi^-$ events in the time interval between $1\tau_S$ and $20\tau_S$ remain after background subtraction (only a small fraction of the data with decays below $1\,\tau_S$ has been analysed).

In the absence of experimental data for the difference between the forward scattering amplitudes of K° and $\overline{K}^\circ$ in the momentum region of the present experiment (<800 MeV/c), we have used the values calculated recently by Eberhard and Uchiyama [6]. The values used for hydrogen as input to their calculation on heavy nuclei are consistent with others [7], from which we estimate an average uncertainty smaller than 13% on the magnitude and 9° on the phase for hydrogen and for heavy nuclei [8]. We have corrected our data on an event–by–event basis depending on the measured momentum of the neutral kaon as well as on the detector materials traversed (see [3]). Diffractive regeneration and absorption are found to be negligible in our experimental set–up. In 1996 a dedicated measurement of the difference of the $K^\circ - \overline{K}^\circ$ forward

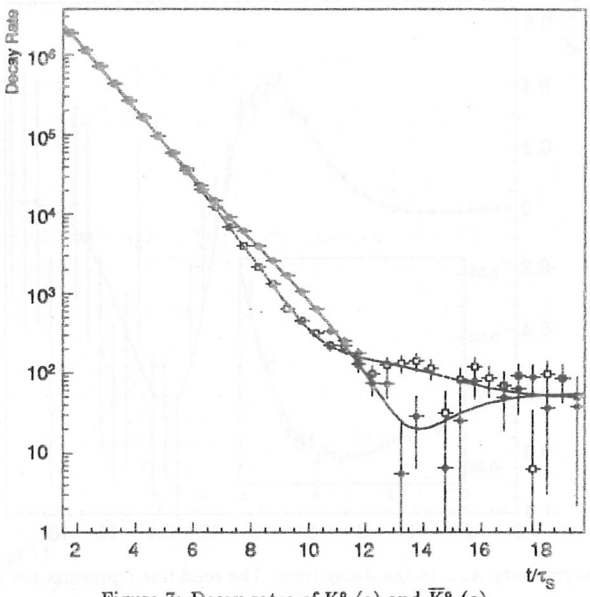

Figure 7: Decay rates of K° (•) and $\overline{K}^\circ$ (○).

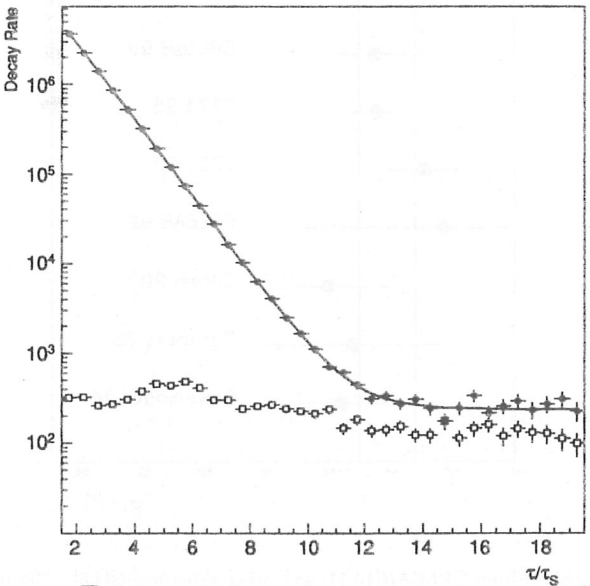

Figure 8: Sum of K° and $\overline{K}^\circ$ decay rates (●) (normalized and corrected for $K \to \pi^+\pi^-$ acceptance). The solid line is a fit with two exponential functions for K_S and K_L, and the background distribution (□) obtained from a simulation.

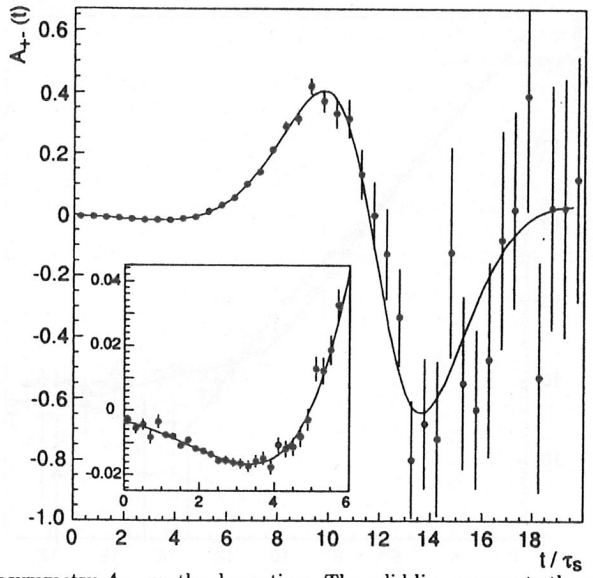

Figure 9: The asymmetry A_{+-} vs the decay time. The solid line represents the result of the fit.

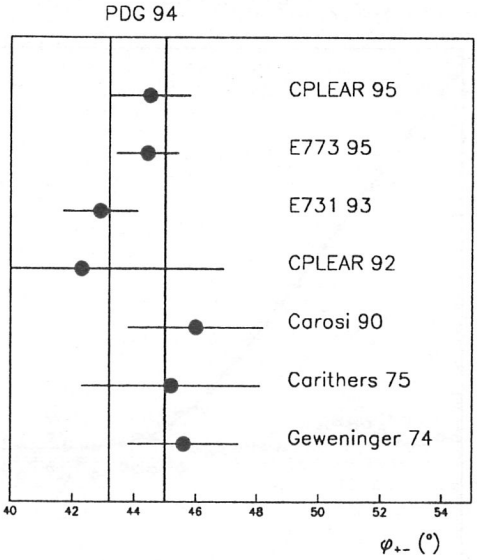

Figure 10: φ_{+-} values from CPLEAR[10,11] and other experiments[4,5]. The two vertical lines correspond to the PDG '94 value $\pm 1\sigma$. We note that K.Kleinknecht et al. [Phys. Let.336B (1995) 581] claims that the systematic error of E731 and E773 should be increased due to regeneration corrections. These claims, however, have been responded to in the literature [R.A.Briere and B.Winstein, Phys. Rev. Lett. 75 (1995) 402].

scattering amplitudes in carbon at low momentum will be done with the CPLEAR detector [9]. After this measurement the systematic error on φ_{+-} due to regeneration effects is expected to decrease by a factor more than 2.

Figure 9 shows the asymmetry $A_{+-}(t)$. The data entering $A_{+-}(t)$ are corrected, on an event by event basis, for the momentum dependence of the tagging efficiency of K^0 relative to $\overline{K}^0$ (determined at short decay-times) and for regeneration effects. The K^0 and $\overline{K}^0$ tagging efficiences are not equal due to the different interactions of K^+ and K^-, and of π^+ and π^-, in the detector material.

Equation 9 folded with the decay time resolution is fitted to the asymmetry shown in Fig.9 with $|\eta_{+-}|$, ϕ_{+-} and α as free parameters. The values of ϕ_{+-} and $|\eta_{+-}|$ obtained by the fit, together with their dependence on Δm (in units of $10^7\,\hbar s^{-1}$) and τ_S (in units of ps), are:

$$|\eta_{+-}| = (2.312 \pm 0.043 - 0.001[\Delta m - 527.4] + 0.091[\tau_S - 89.26]) \times 10^{-3} \quad (10)$$

$$\phi_{+-} = 42.7 \pm 0.9^\circ + 0.316[\Delta m - 527.4]^\circ + 0.30[\tau_S - 89.26]^\circ, \quad (11)$$

where we used $\Delta m = (527.4 \pm 2.9) \times 10^7 \hbar s^{-1}$ measured recently by the CPLEAR collaboration using semileptonic decays [3] (see section 2) and $\tau_S = (89.26 \pm 0.12)$ ps [4]. The correlation coefficient between ϕ_{+-} and $|\eta_{+-}|$ given by the fit is 12%. Floating Δm in the fit gives $\Delta m = (529.5 \pm 6.7) \times 10^7 \hbar s^{-1}$, in good agreement with the value used. By changing the background level, the decay time resolution, the regeneration amplitude, Δm and τ_S within their estimated uncertainties we derive the systematic errors shown in Table 2. Our results are [10]:

$$|\eta_{+-}| = (2.312 \pm 0.043_{\mathrm{stat.}} \pm 0.030_{\mathrm{syst.}} \pm 0.011_{\tau_S}) \times 10^{-3} \quad (12)$$

$$\phi_{+-} = 42.7^\circ \pm 0.9^\circ_{\mathrm{stat.}} \pm 0.6^\circ_{\mathrm{syst.}} \pm 0.9^\circ_{\Delta m}\,. \quad (13)$$

$$\alpha = 0.9989 \pm 0.0006$$

The external error on $|\eta_{+-}|$ is dominated by the uncertainty on the value of τ_S ($0.08926 \pm 0.00012\ ns$) [4], while that on φ_{+-} by the uncertainty on Δm. Our systematic errors result mainly from the present uncertainty on the difference between the forward scattering amplitudes of K^0 and $\overline{K}^0$ and the uncertainty on the value of Δm.

The value of ϕ_{+-} obtained with our value of Δm agrees well with the superweak phase computed with the same Δm and $\Delta\Gamma$ from [4]:

$$\phi_{SW} = \tan^{-1}\frac{2\Delta m}{\Delta\Gamma} = 43.30^\circ \pm 0.16^\circ, \quad (14)$$

being consistent with CPT symmetry.

Table 2: Systematic errors of the presented ϕ_{+-} and $|\eta_{+-}|$ values

Source	ϕ_{+-}	$\|\eta_{+-}\| \times 10^3$
Background level	0.05^0	0.02
Decay time resolution	0.10^0	0.01
Normalization procedure	0.05^0	0.005
Regeneration	0.60^0	0.02
Total syst.	$\mathbf{0.61^0}$	**0.030**
$\sigma(\Delta m)$	0.92^0	0.003
$\sigma(\tau_S)$	0.04^0	0.011

Using the PDG [4] value of $\Delta m = (533.3 \pm 2.7) \times 10^7 \hbar s^{-1}$, we find $|\eta_{+-}| = 2.311 \times 10^{-3}$ and $\phi_{+-} = 44.5^\circ$. The errors remain the same except for the error on ϕ_{+-} resulting from the uncertainty of Δm which reduces to 0.8°.

Figure 10 shows our result on φ_{+-} in comparison with previous measurements[4,5] for the same Δm value [4].

5 The correlation of the φ_{+-} measurements from Δm.

The comparison of the phase ϕ_{+-} of the CP violation parameter η_{+-} with the superweak phase $\varphi_{SW} \equiv \tan^{-1}(2\Delta m/\Delta\Gamma)$, yields the world's best limits of CPT violation. The phase ϕ_{+-} has been measured by many experiments over the last 30 years. It is important to notice that the experimental value of φ_{+-} has a different dependence on Δm for different experiments. Averaging Δm and ϕ_{+-} independently [4] is not an adequate method as these two parameters are correlated. We have evaluated both parameters, Δm and ϕ_{+-} by taking into account the correlations. Since the values of ϕ_{+-} depend on the value of τ_S, we leave τ_S as an additional free parameter in the fit. However its value is constrained to the world average of $< \tau_S >= (0.8926 \pm 0.0012) \times 10^{-10}$s [4].

Using as input to our fit the experimental data published up to 1994, we find similar results as the independent averaging method of PDG [4] although our error for $< \Delta m >$ is smaller compared to the PDG result due to the additional information used, and in contrast to PDG we do not need to scale the error of Δm by 1.2 since the χ^2/degree of freedom (dof) for the combined average of ϕ_{+-} and Δm is 1.0, For Δm we find $< \Delta m >= (532.2 \pm 1.8 \pm 0.1) \times 10^7 \hbar/s$ and for ϕ_{+-} the value $< \phi_{+-} >= 44.5^\circ \pm 1.0^\circ \pm 0.1^\circ$, where the second error reflects the uncertainty of the correlation between ϕ_{+-} and Δm.

I believe that a complete evaluation of Δm and ϕ_{+-} from a correlation analysis of the different experiments including the two Δm values [3, 10] and the ϕ_{+-} value [10], from CPLEAR as well as the Δm and ϕ_{+-} value from E773 [5] will improve considerably both the precisions on $\phi_{+-} - \phi_{SW}$ and the agreement of the data with the CPT invariance.

6 Indirect CPT test.

From our present knowledge of weak interactions, the three discrete symmetries C, P and T are not exact symmetries in our universe, and the same applies to the combined symmetries CP, CT and PT. This fact is well accomodated in the Standard Model and is well established experimentally. However, in the framework of a local field theory of Lorenz invariance any order of the triple product CPT represents an exact symmetry. In some cases as spontaneously broken symmetries with degenerated vacuum, fields with infinite many components and non local theories, the CPT invariance could be in first or higher order not exact.

The best limit on CPT violation is obtained by comparing the phase of η_{+-} with the superweak angle $\varphi_{sw} = tan^{-1}(\frac{2\Delta m}{\Delta\Gamma})$, where $\Delta\Gamma = \gamma_S - \gamma_L$. Note that if we take the available data [4] the phase difference between φ_{+-} and φ_{sw} can be as large as 3° [19] even in the absence of CPT violation. The equation that relates η_{+-} and ϵ_T is:

$$\eta_{+-} = \epsilon_T + \delta_\perp + i\varphi_0 + \epsilon'$$

where ϵ_T has a phase φ_{sw} and $\delta_\perp$ describes the component of the CPT violation parameter δ perpendicular to ϵ_T,

$$-\delta_\perp \equiv \frac{i\Delta\Gamma - 2\Delta m}{4\Delta m^2 + \Delta\Gamma^2}(M_{22} - M_{11} + \frac{\Delta m}{\Delta\Gamma}(\Gamma_{22} - \Gamma_{11}))$$

where $M_{ij} - \frac{1}{2}\Gamma_{ij}$ are the elements of the kaon mixing matrix. The term φ_0 is derived to be:

$$\varphi_0 = \frac{\gamma_L}{\gamma_S}[2BR(\mathrm{K_L} \to \pi l\nu) Im(x) + BR(\mathrm{K_L} \to 3\pi) Im(\eta_{3\pi} - \eta_{+-})]$$

The term ϵ' describes the CP violation in the decay amplitude and can be neglected since $|\epsilon'| < 10^{-5}$ [20] and the phase difference between the isospin two (δ_2) and zero (δ_0) amplitudes is [4] $(\delta_2 - \delta_0) = (-45 \pm 15)^\circ$). Figure 11 shows the relation between the CP violating parameters η_{+-}, ϵ_T, $\delta_\perp$, φ_0 and ϵ'.

Using our improved limits for $Im(\eta_{+-0})$ and $Im(x)$, our measurements of φ_{+-} and Δm, and $\Delta\Gamma$ from [4], we find:

$$|\delta_\perp| < 10^{-4} (90\%\text{C.L.})$$

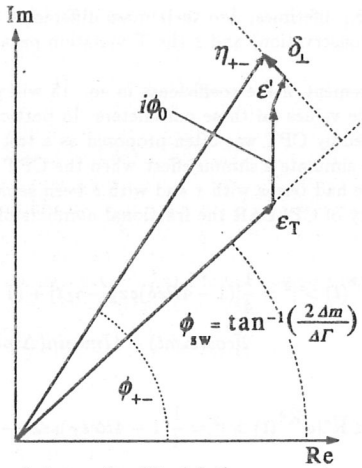

Figure 11: The relation between the CP violating parameters η_{+-}, ϵ_T, $\delta_\perp$, φ_0 and ϵ'.

Assuming CPT conservation in the decay amplitude related to the smallness of $\phi_{+-} - \phi_{00}$ [4], we obtain the preliminary value from the present CPLEAR results:

$$|\frac{M_{\overline{K}^0} - M_{K^0}}{M_K}| < 2.0 \cdot 10^{-18}$$

This is the best limit on a particle-antiparticle mass difference arising from the measurements of one single experiment without any phenomenological assumption on any parameter.

Results from the comparison of ϕ_{+-} with ϕ_{00} are used frequently as a test of CPT invariance. Here I would like to make clear that the measurement of $(\phi_{+-} - \phi_{00})$ test only the CPT invariance in the decay, i.e. the CPT violating components of $\epsilon\prime$, but the measurement of $\phi_{+-} - \phi_{SW}$ is testing the combined effect of both the CPT violating component δ and ReB_2/ReA_0 [12, 13] Referring to the work of Barmin et al. [12] we stress that only for the case of $|\epsilon\prime| \neq 0$, the measurement of the phase difference $\phi_{+-} - \phi_{00}$ provides a test for the CPT violating decay parameters. Even if $\phi_{+-} - \phi_{00}$ could be measured to be exactly zero, this would not allow any conclusion to be drawn regarding CPT invariance [13]. Therefore, for the case of very small or vanishing values of $|\epsilon\prime|$, the best and more complete test of CPT invariance [13] is the phase difference of η_{+-} relative to the superweak angle, i.e. $(\phi_{+-} - \phi_{SW})$.

7 Separate CPT and T violation.

The most accurate CPT tests, such as lifetime and mass equalities between particles and antiparticles, do not verify the full extent of CPT invariance since they do not involve helicity or complex conjugation [14]. The neutral kaon complex is a superior tool for making detailed tests of CPT symmetry [14].

Many authors have dealt with the description of the K^0-$\overline{K}^0$ complex and with many consequences of CP, T and CPT violation [14]. The Wigner-Weisskopf approximation is usally used to obtain the evolution in time of the system. After Lee, Oehme and Yang [15], it is customary to consider the total number of neutral K-mesons as a function of time, starting initially with pure K^0 (or $\overline{K}^0$),

$$N^{\pm}(t) = \frac{1}{2}[[1 \mp 2Re(\varepsilon_T + \delta)]exp[-\gamma_L t] + [1 \mp 2Re(\varepsilon_T - \delta)]exp[-\gamma_S t] \pm 2[(Re\varepsilon_T + iIm\delta)exp[i\Delta m t] + c.c.]exp[-\frac{1}{2}(\gamma_L + \gamma_S)t]] \quad (15)$$

where γ_S^{-1},γ_L^{-1} are the K_S, K_L lifetimes, Δm their mass difference, δ the Lee-Wu CPT violation parameter ($\delta = 0$ for CPT conservation) and ε the T violation parameter. The upper sign is for K°, and the lower for $\overline{K}^\circ$.

Clearly, a measurement of the coefficients in eq. 15 will give combinations of ε and δ and will enable one to deduce values for these parameters. In particular, the reversal of sigh of δ in the oscillation term implied by CPT was often proposed as a test for CPT invariance. But, as noted by Michel [16], T may simulate a similar effect when the CPT violation is small. The effect would be much more decisive had terms with ε and with δ been separated.

Given the capacity of CPLEAR the fractional numbers of K° or of $\overline{K}^\circ$ particles in the beam may be calculated:

$$R^{K^\circ}(K^\circ,t) = |< K^\circ|\psi^{K^\circ}(t)>|^2 = \frac{1}{4}[(1-4Re\delta)exp[-\gamma_L t] + (1+4Re\delta)exp[-\gamma_S t] + 2[cos(\Delta mt) - 4Im\delta sin(\Delta mt)]exp[-\frac{1}{2}(\gamma_L+\gamma_S)t] \tag{16}$$

$$R^{K^\circ}(\overline{K}^\circ,t) = |< \overline{K}^\circ|\psi^{K^\circ}(t)>|^2 = \frac{1}{4}(1-4Re\varepsilon_T)(exp[-\gamma_L t] + exp[-\gamma_S t] - 2cos(\Delta mt)exp[-\frac{1}{2}(\gamma_L+\gamma_S)t]) \tag{17}$$

In these equations, $|\psi^{K^\circ}(t)>$ is the state vector starting from pure K° at $t = 0$. $R^{K^\circ}(K^\circ,t)$ denotes the fractional number of K°'s in this beam, while $R^{K^\circ}(\overline{K}^\circ,t)$ denotes the fractional number of $\overline{K}^\circ$'s in it at the proper time t. The change of K° to $\overline{K}^\circ$ in all expressions will cause the change of signs of both ε and δ.

Clearly, the sum of eqs. 16 and 17 gives eq. 15. The obvious advantage from CPLEAR (eqs. 16 and 17) lies in the separation of the CPT parameter δ and the T parameter ε_T. A measurement of these quantities may thus serve as the independent test of T violation and CPT invariance.

The CPLEAR experiment, assuming the validity of the $\Delta S = \Delta Q$ rule, can perform the experimental measurement of the ratio between the first two coefficients of eq. 16, which is independent of the flux of the beam, which will give directly $Re\delta$, and the oscillating term will give $Im\delta$. A measurement of the flux in eq. 17 will give $Re(\varepsilon_T)$.

8 Direct measurement of T violation (Kabir test).

Since weak interactions do not conserve strangeness (hypercharge), a K° meson can, and does occasionally, transform itself into a $\overline{K}^\circ$ meson in the course of time. Similarly, a state produced initially as $\overline{K}^\circ$ may be found later to have changed into K°. Time reversal invariance, or microscopic reversibility (sometimes also called reciprocity) would require, as proposed by Kabir, all details of the second process to be deducible from the first; in particular, it should proceed at a rate exactly equal to that of the $K^\circ \rightarrow \overline{K}^\circ$ transformation, since time reversal simply reverses the process in this case.

A convenient way to make the measurement is to take advantage of the $\Delta S = \Delta Q$ rule. Then $\pi^- l^+ \nu$ and $\pi^+ l^- \overline{\nu}$ decays in a neutral kaon beam provide indicators of the K° and $\overline{K}^\circ$ content, respectively. The first could be used in decays of a beam produced initially as $\overline{K}^\circ$ to measure $\overline{K}^\circ \rightarrow K^\circ$ conversion while the second would similary yield the rate of $K^\circ \rightarrow \overline{K}^\circ$ transitions. Therefore, we are able to compare the probability $|< K^\circ|M - i\Gamma|\overline{K}^\circ>|^2$ to the probability $|< \overline{K}^\circ|M - i\Gamma|K^\circ>|^2$ by forming the asymmetry using eq. 17:

$$A_T(t) \equiv \frac{\overline{R}^+(t) - R^-(t)}{\overline{R}^+(t) + R^-(t)} \tag{18}$$

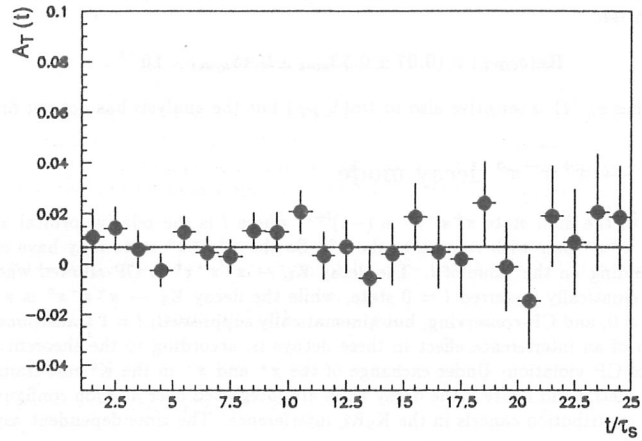

Figure 12: The asymmetry $A_T(t)$ vs the decay time. The line represents the result of the fit.

where the parameter x is assumed to be zero and M and Γ are the usual mass and decay matrix respectively, as defined in the textbooks. These probabilities are related as:

$$\begin{aligned} &< \mathrm{K^o}|M - i\Gamma|\overline{\mathrm{K}}^o >=< T\mathrm{K^o}|T(M - i\Gamma)|\overline{\mathrm{K}}^o >^*= \\ &< T\mathrm{K^o}|T(M - i\Gamma)T^{-1}|T\overline{\mathrm{K}}^o >^*=< T\mathrm{K^o}|(TMT^{-1}) + i(T\Gamma T^{-1})|T\overline{\mathrm{K}}^o >^*= \\ &< T\overline{\mathrm{K}}^o|(TMT^{-1})^\dagger + (iT\Gamma T^{-1})^\dagger|T\mathrm{K^o} >=< T\overline{\mathrm{K}}^o|(M_T)^\dagger + (i\Gamma_T)^\dagger|T\mathrm{K^o} >= \\ &< T\overline{\mathrm{K}}^o|M_T - i\Gamma_T|T\mathrm{K^o} >=< \overline{\mathrm{K}}^o|M_T - i\Gamma_T|\mathrm{K^o} > \end{aligned} \tag{19}$$

with $M_T(\Gamma_T) = TM(\Gamma)T^{-1}$ and $|\mathrm{K^o} >= T|\mathrm{K^o} >$, $|\overline{\mathrm{K}}^o >= T|\overline{\mathrm{K}}^o >$ within a phase angle. These probabilities are equal if the underlying theory is invariant under T transformation without any additional assumption on CPT inavriance. Figure 12 shows the asymmetry $A_T(t)$. A fit to this asymmetry gives:

$$\mathbf{A_T = (6.3 \pm 2.1_{stat} \pm 1.8_{syst}) \times 10^{-3}} \tag{20}$$

It is important that time reversal invariance can be checked directly because everyone beleives T is violated, although no empirical evidence existed for this. The effect of T violation is expected at level of 10^{-3} since CP is known to be violated at this degree and everyone believes CPT invariance is exact, although there is no evidence for this either.

9 Direct test of CPT invariance in the $\mathrm{K^o}$ - $\overline{\mathrm{K}}^o$ mixing.

CPT invariance implies, independent of T invariance, that $M_{11} = M_{22}$ and $\Gamma_{11} = \Gamma_{22}$. By using $|\overline{\mathrm{K}}^o >= CPT|\mathrm{K^o} >$ within an arbitrary phase and similarely to eqs. 19, it can be proven that the asymmetry:

$$A_{CPT}(t) \equiv \frac{\overline{R}^-(t) - R^+(t)}{\overline{R}^-(t) + R^+(t)} \tag{21}$$

is a direct measure of CPT-violation, where we used $x = 0$ and eq. 16. This is because CPT invariance requires that the fraction of $\mathrm{K^o}$'s which survive as $\mathrm{K^o}$ is exactly equal to that of $\overline{\mathrm{K}}^o$'s

which remain $\overline{K}^0$. A fit to $A_{CPT}(t)$ for large life times gives for $Re(\delta_{CPT})$ a preliminary value compatible with zero,

$$\mathbf{Re(\delta_{CPT}) = (0.07 \pm 0.53_{stat} \pm 0.45_{syst}) \times 10^{-3}} \quad (22)$$

For short lifetimes eq. 21 is sensitive also to $Im(\delta_{CPT})$ but the analysis has not yet finished.

10 $K^0(\overline{K}^0) \to \pi^+\pi^-\pi^0$ decay mode.

The CP-parity of the final state $\pi^+\pi^-\pi^0$ is $(-1)^{l+1}$, where l is the relative orbital angular momentum of the $\pi^+\pi^-$ pair with respect to the π^0. So the $\pi^+\pi^-\pi^0$ state may have even or odd CP-parity depending on the value of l. The decay $K_L \to \pi^+\pi^-\pi^0$ is CP-allowed when the final state is the kinematically preferred $l = 0$ state, while the decay $K_S \to \pi^+\pi^-\pi^0$ is a mixture of CP-violating, $l = 0$, and CP-conserving, but kinematically suppressed, $l = 1$ transitions. However, any observation of an interference effect in these decays is, according to the theorem of ref. [17], a direct prove of CP violation. Under exchange of the π^+ and π^- in the K^0 rest frame the $l = 1$ state is antisymmetric and hence if the decay rates are integrated over all pion configurations, the CP-allowed K_S contribution cancels in the $K_S K_L$ interference. The time dependent asymmetry:

$$A_{+-0}(t) \equiv \frac{R_{\overline{K}^0 \to \pi^+\pi^-\pi^0}(t) - R_{K^0 \to \pi^+\pi^-\pi^0}(t)}{R_{\overline{K}^0 \to \pi^+\pi^-\pi^0}(t) + R_{K^0 \to \pi^+\pi^-\pi^0}(t)} =$$

$$\simeq 2Re(\epsilon_T + \delta_{CPT}) - 2e^{-1/2(\gamma_S - \gamma_L)t}[Re(\eta_{+-0})cos(\Delta mt) - Im(\eta_{+-0})sin(\Delta mt)]$$

is shown in Fig. 13. The total number of events is 1.5×10^5. From a fit to this asymmetry we obtain as preliminary result:

$$\mathbf{Re(\eta_{+-0}) = (-4 \pm 17_{stat} \pm 3_{syst}) \times 10^{-3}}$$

$$\mathbf{Im(\eta_{+-0}) = (-16 \pm 20_{stat} \pm 8_{syst}) \times 10^{-3}}$$

The value of $Re(\eta_{+-0})$ is consistent with been equal to $Re(\eta_{+-})$. Figure 14 shows our result, in comparison with the results from other experiments.

11 Summary

CPLEAR provides information on the CP, T and CPT violation parameters. The parameters φ_{+-} and Δm are measured in an independent way, with a precision comparable to the one of the best published results. Improved values for η_{+-0} as well as for $Re(x)$ and $Im(x)$ are determined. CPLEAR provides also the first direct measurement of T violation through a comparison of K^0, $\overline{K}^0$ decay rates, and a direct test of CPT invariance. Finally taking into account all our results we can perform one of the best indirect tests of CPT invariance. The full analysis of the data (including the data to be collected up to 1996) will decrease our statistical errors by a factor ≥ 2. A dedicated measurement of the regeneration parameters in 1996 will help to decrease our systematic error in φ_{+-} by more than a factor of 2.

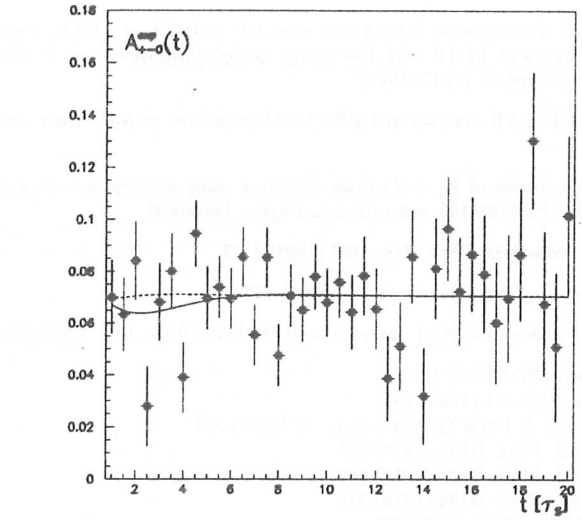

Figure 13: The asymmetry $A_{+-0}(t)$ vs the decay time. The solid (dotted) line represents the result of the fit when we float $Re(\eta_{+-0})$ and $Im(\eta_{+-0})$ (only $Im(\eta_{+-0})$ with the constraint $Re(\eta_{+-0}) = Re(\eta_{+-})$).

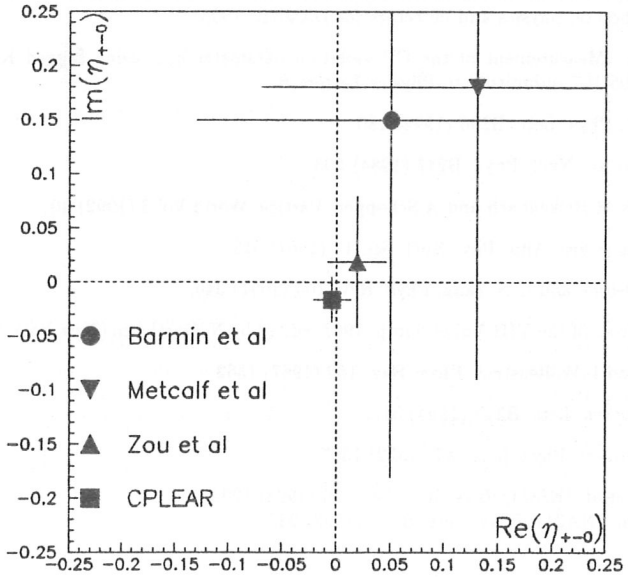

Figure 14: $Im(\eta_{+-0})$ vs $Re(\eta_{+-0})$ for CPLEAR (preliminary) and other experiments[4,18].

References

1. E. Gabathuler and P. Pavlopoulos, Strong and weak CP violation at LEAR, Proccedings of the Workshop on physics at LEAR with low energy cooled antiprotons, ed. U. Gastaldi and R. Klapish, Plenum publisher, p.747 (1982).

2. R.Adler et al., The CPLEAR detector at CERN, to be submitted to Nucl. Instr. and Methods A.

3. R.Adler et al., Measurement of $K_L - K_S$ mass difference using semileptonic decays of tagged neutral kaons, CERN-PPE/95-103, submitted to Physics Letters B.

4. Review of Particle Properties, Phys. Rev. D50 (1994) 1173.

5. B.Schwingenheuer et al., Phys. Rev. Lett. 74 (1995) 4376.

6. P.H.Eberhard and F.Uchiyama, Nucl. Instrum. and Methods, Phys. Res. A350 (1994) 144.

7. J. Antolin, Phys.Rev. 35D (1987) 122;
   J. Antolin, J. Math. Phys. 31 (1990) 791;
   J. Antolin and A.Cruz, J. Phys. G: Nucl. Phys. 12 (1986) 297;
   P. Baillon et al., Nucl. Phys. B105 (1976) 365;
   P. Baillon et al., Nucl. Phys. B107 (1976) 189;
   P. Baillon et al., Nucl. Phys. B134 (1978) 31;
   A.D. Martin, Nucl. Phys. B179 (1981) 33.

8. CPLEAR internal note, CP/PHY-034 (1994);
   CERN/SPSLC/95-47, SPSLC/M561 (1995).

9. P.Kokkas (for the CPLEAR coll.), Measurement of the difference of the $K^\circ - \overline{K}^\circ$ forward scattering amplitudes in carbon at low momentum with the CPLEAR detector, Proc. of the second workshop on physics and detectors for DAΦNE (1995).

10. R.Adler et al., Measurement of the CP violation parameter η_{+-} using tagged K° and $\overline{K}^\circ$, CERN-PPE/95-107, submitted to Physics Letters B.

11. R.Adler et al., Phys. Lett. B286 (1992) 180.

12. V.V.Barmin et al., Nucl. Phys. B247 (1984) 293.

13. P.Pavlopoulos, R.Rickenbach and A.Schopper, Particle World Vol.3 (1992) 40.

14. T.D.Lee and C.S.Wu, Ann. Rev. Nucl. Sci. 17 (1967) 513.

15. T.D.Lee, R.Oehme and C.N.Yang, Phys. Rev. 106 (1957) 340.

16. L.Michel in Proc. of the VIII Nobel Sump, 1968, edited by N.Svartholm (New York.1968), 345.

17. L.M.Seghal and L.Wolfenstein, Phys. Rev. 162 (1967) 1362.

18. Y.Zou et al., Phys. Lett. B329 (1994) 519.

19. L.Lavoura, Modern Phys. Lett. A7 (1992) 1367.

20. L.K.Gibbons et al. (E731), Phys. Rev. Lett. 70 (1993) 1203.
    G.D.Barr et al. (NA31), Phys. Lett. B317 (1993) 233.

STATUS OF KTEV

B. Winstein
The University of Chicago, The Enrico Fermi Institute,
5640 South Ellis, Avenue, Chicago, IL 60637

Introduction

In this lecture, I will review some aspects of KTeV at Fermilab. This will include a mention of our goals, methods, and then the status of many of the crucial components. I will present the latest schedule for the completion of the beam and detector and the start of commissioning and data taking. Finally, I will close on a personal note about Φ factories.

KTeV Goals

The goals for KTeV arise naturally out of the efforts that have recently been completed in our kaon program at Fermilab.

World-wide, over the period covered by the current generation of experiments in this field (about five years), there have been approximately 50 new measurements including those from FNAL, CERN, BNL, and KEK. This represents something of a renaissance in kaon physics. Of these results, about 25 have come from FNAL with experiments E621, E731, E773, and E799 contributing. Eight of these results are related to the 2π decay modes (ε'/ε, Δm, τ_S, etc.) while the bulk of the others are related to rarer K_L decays.

In this lecture, I will concentrate upon the measurement of ε'/ε; indeed, most of the design of the new beam and detector is driven by the requirements of this measurement.

In E731, we measured[1] $\mathrm{Re}(\varepsilon'/\varepsilon) = (7.4 \pm 5.9) \times 10^{-4}$; the error was dominated by statistics and KTeV is designed to use the same techniques to reach about a factor of five smaller uncertainty. Those techniques include:

1) Taking K_S and K_L decays simultaneously;

2) Using regeneration to provide K_S;

3) Understanding the beam and detector just short of "as much as is possible" but a bit beyond "only what is necessary;" and

4) Produce other results (particularly with the 2π decay modes) to help corroborate the ε'/ε measurement.

Other Recent Results

There were two short runs with essentially the same apparatus since E731; these were E773 - a study of CPT violation, and E799-I, a study of rarer K decays.

E773 has published[2] results on the K_S lifetime, the K_L - K_S mass difference, and the phases Φ_{+-} and Φ_{00} of the 2π amplitudes. Regarding the rare K decays, E731 and E799 have:

A) published first results on $K_L \to \mu\mu\gamma$,[3] $K_L \to \mu\mu ee$,[4] $K_L \to \pi^{\pm}\pi^0 e\nu$ form factors,[5] $K_{L,S} \to \pi\pi\gamma$ interference,[6] and $K_L \to 3\pi^0$ structure;[7]

B) published the best results on $K_L \to 4e$,[8] $K_L \to ee\gamma\gamma$,[9] and $\pi^0 \to ee$;[10]

C) published the first limits on $K_L \to \pi^0 \nu \bar{\nu}$[11] and $K_L \to \pi^0 \mu e$;[12] and,

D) published the best limits on $K_L \to \pi^0 ee$ and $K_L \to \pi^0 \mu\mu$.[13]

This collaboration also made measurements of $K_L \to \pi^0\gamma\gamma$, $K_L \to \pi^0\pi^0\gamma$ and $K_L \to \pi^0 ee$ but these have since been bettered, by NA31.

For the rare decay program in KTeV, the goal is to reach single event sensitivities approaching 10^{-11}.

The KTeV Detector

The KTeV Detector is shown in the Figure. It will observe decays from the two entering beams, one of which strikes an active regenerator. The decay products are detected by means of a magnetic spectrometer and CsI crystal calorimeter. The detector is housed in a new building under construction.

The detector is being constructed by a collaboration from Chicago, Colorado, Elmhurst, Fermilab, Osaka, Rice, Rutgers, UCLA, UCSD, Virginia, and Wisconsin. I will briefly give the characteristics and status of some of the key elements of the detector.

The CsI calorimeter consists of 3100 crystals supplied from France, Japan, and the U.S. At present, nearly all of the crystals are in hand and have been processed. They are wrapped to a uniformity of

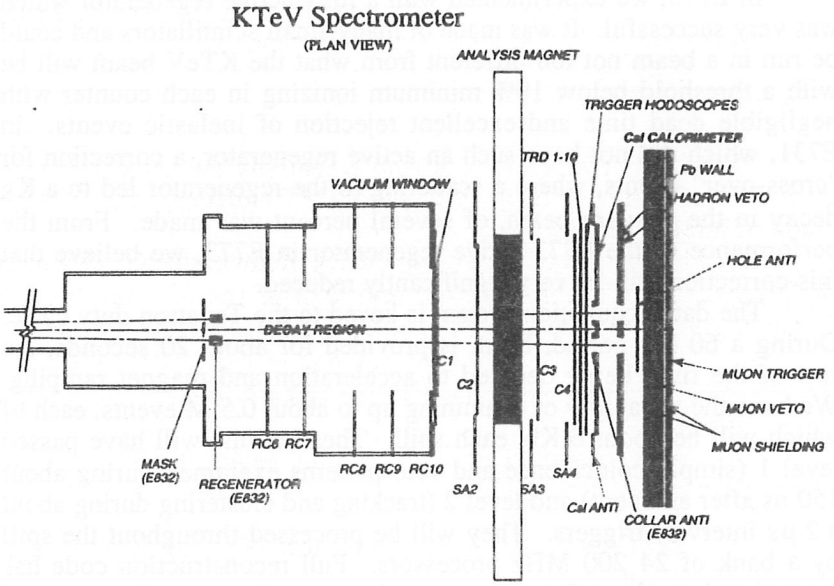

about 5% over their length of 27 rl. They are to be read out with a flash ADC mounted in the phototube base, providing 8 bits of precision over a 16 bit dynamic range, roughly 1 MeV to 70 GeV. A small array of the calorimeter was tested[14] last summer at CERN with a prototype of the readout electronics with good resolution (see section on detector resolutions). The digitization is done at the RF frequency of the beam, 53 MHz, so that one also has a great deal of information of the time structure of pulses in each of the crystals readout.

There is an extensive veto system to detect γ's, primarily from $3\pi^0$ decays. These are made of a lead, scintillating tile sandwich which provides roughly 40 p.e. per 100 MeV energy deposit.

The analysis magnet has been constructed and tested at full current; it provides about 450 MeV/c which is significantly greater than in past K decay experiments.

The drift chambers are the same that were used in the past series of experiments where they achieved, at best, 80 μm resolution per wire plane. (In fact, this is the only "old" element of the KTeV detector.) However, they have been restrung with Al wires, and thinner windows, and equipped with new, higher gain electronics.

In E773, we experimented with a fully active regenerator which was very successful. It was made of many small scintillators and could be run in a beam not too different from what the KTeV beam will be with a threshold below 10% minimum ionizing in each counter with negligible dead time and excellent rejection of inelastic events. In E731, which did not have such an active regenerator, a correction for "cross-over" events, where a scattering in the regenerator led to a K_S decay in the vacuum beam, of several percent was made. From the performance of the E773 active regenerator in E773, we believe that this correction will be very significantly reduced.

The data acquisition system is keyed to the Tevatron duty cycle. During a 60 sec period, beam is provided for about 20 seconds, the rest of the time being devoted to acceleration and magnet ramping. We have the capability of examining up to about 0.5 M events, each of which will be about 6 Kb, each spill. These events will have passed level 1 (simple coincidence and veto patterns examined during about 150 ns after an event) and level 2 (tracking and clustering during about a 2 μs interval) triggers. They will be processed throughout the spill by a bank of 24 200 MHz processors. Full reconstruction code has been timed at about 3 ms per event on one processor; the expected output will be approximately 50 K events per spill.

Detector Resolutions

One measure of performance (but not the only important one!) is detector resolution. The following table makes some relevant comparisons.

Table I: $\pi^{\pm}$ momentum resolutions for several experiments

EXPERIMENT	MOMENTUM RESOLUTION
E731/E773	$0.0046 \oplus 0.0028 \frac{p}{30 GeV/c}$
KEK137	$0.0033 \oplus 0.0021 \frac{p}{1.5 GeV/c}$
BNL791	$0.0035 \oplus 0.0024 \frac{p}{3 GeV/c}$
KTeV	$0.0016 \oplus 0.0014 \frac{p}{30 GeV/c}$

The improvement in the momentum resolution in KTeV with respect to that in E731 comes from the higher bend and less material presented to multiple scatter the particles (multiple scattering contributes exclusively to the first terms in the table). The resolution is expected to be even better than those of two very high rate rare decay experiments. (For all cases, the second term is expressed at a momentum which is the rough average for the experiment in question.) The figure for KTeV assumes that the magnetic field is understood sufficiently accurately, however; for BNL791, for example, there is a significant contribution in the quoted resolution from residual uncertainties in the magnetic field which could be better determined.[15]

The resolution in E731 for photons was given approximately by

$$\Delta E/E \approx 2\% \oplus \frac{4.5\%}{\sqrt{E}} \text{ (E731, photons).}$$

The "constant" term was as large as it is because of rather large nonuniformities in the light collection coupled with longitudinal fluctuations in shower development for photons. For electrons, this term was closer to 1%.

For KTeV, the crystals are wrapped to make them highly uniform -- a much easier task with the isotropically emitted scintillation light. As a result, the resolution and response should be almost exactly the same for photons as it is for electrons. From our beam test together with the noise properties of our electronics, we can parameterize the response of the KTeV array to photons as follows:

$$\Delta E/E \approx \frac{0.6\%}{E} \oplus \frac{0.7\%}{\sqrt{E}} \oplus \frac{1.0\%}{\sqrt[4]{E}} \text{(KTeV, photons).}$$

Here, the first term is due to electronic noise, the second term is due to photostatistics, and the final term is due to fluctuations in shower leakage (transverse at low energy, longitudinal at high energy).

Thus at a typical photon energy of 16 GeV, we can expect a little over 0.5% resolution in KTeV to be compared with about 2.5% in E731. Of course we must obtain the same level of noise rejection in the full calorimeter as in the test beam to reach this figure.

Systematic Errors

We reproduce here a table of the contributions to the systematic error on ε'/ε from E731 together with a listing of where improvements are expected to come from.

TABLE 1: Systematic Uncertainties on ε'/ε

SYSTEMATIC EFFECT	UNCERTAINTY $[10^{-4}]$ (E731)	MAJOR IMPROVEMENTS (KTeV)
ACCEPTANCE	1.19	more statistics
ENERGY CALIBRATION	1.60	CsI resolution
ACCIDENTALS	1.07	cleaner beam; flash ADCs
$3\pi^0$ BACKGROUND	0.60	CsI; vetoes
REGENERATOR SCATTERING	0.84	fully active
REGENERATOR ANTI COUNTER POSITION	0.51	better surveying
TRIGGER PLANE EFFECTS	1.22	removed
CHARGED BACKGROUND	0.29	CsI
BEAM SCATTERING	0.30	better collimation
TOTAL	2.85	<1 (?)

The largest uncertainty came from the neutral energy calibration; this will be addressed with the much superior performance of the calorimeter.

The next largest came from scattering and regeneration in a trigger plane in the middle of the E731 decay region; there will be no such plane in KTeV.

The next largest came from uncertainties in the detector acceptance. The parameters of the acceptance are determined from K_{e3} decays. The greater statistics will help in studying any residual problems. But it is now anticipated that this will be the dominant systematic.

Accidentals also accounted for a sizable uncertainty. In KTeV it is expected that the beams will be significantly cleaner. In addition, the flash ADCs on every calorimeter channel will add greatly to the ability to study accidental effects.

Backgrounds are not anticipated to be a serious problem; these will be significantly reduced with the superior veto system and the superior track and calorimeter resolutions.

Scattering from the regenerator will be greatly reduced since it will be totally active.

Schedule

Many of the detector components are now complete. The building is scheduled for completion in mid August 1995 at which time our installation begins. Six months later (2/15/96), we should be 95% installed and only awaiting some electronics. First beam is expected beginning somewhere between April and June; the running is planned to consist of four approximately five month long periods over a period of roughly two years.

Personal Note

I was very pleased to be able to come to Frascati for the first time and meet with those pursuing the same physics we are with the beautiful system at the Φ meson. Ever since I first read Lipkin's 1968 paper[16] around 1975, I too have been completely fascinated with this wonderful quantum mechanical system, compiling many pages of notes, including considering various patterns of regenerators, etc., over the years, each time convincing myself that it is simply too hard to do the measurement at a Φ Factory. But I keep coming back to the system and I am happy to say that, from what I saw at Frascati, this dream of making the measurement at the Φ that has been shared by so many looks much better than ever! I want to thank Rinaldo, Sergio, Paulo, Juliet and all the others for a wonderful meeting of just the right size and wish you the best of luck in your efforts.

---

[1]E731 result (L.K. Gibbons *et al*, Phys. Rev. Lett. **70**, 1203 (1993))
[2]E773 results (B. Schwingenheuer *et al.*, Phys. Rev. Lett. **74**, 4376 (1995))
[3]M.B. Spencer *et al.*, Phys. Rev. Lett. **74**, 3323 (1995)
[4]In preparation
[5]G. Makoff *et al.*, Phys. Rev. Lett. **70**, 1591 (1993)
[6]E.J. Ramberg *et al.*, Phys. Rev. Lett. **70**, 2529 (1993); J.N. Matthews *et al.*, accepted by Phys. Rev. Lett. (1995)
[7]S.V. Somalwar *et al.*, Phys. Rev. Lett. 68, 2567 (1992)
[8]P. Gu *et al.*, Phys. Rev. Lett. **72**, 3000 (1994)
[9]T. Nakaya *et al.*, Phys. Rev. Lett. **73**, 2169 (1994)
[10]K.S. McFarland *et al.*, Phys. Rev. Lett. **71**, 31 (1993); see BNL 777 result: A. Deshpande *et al.*, Phys. Rev. Lett. **71**, 27 (1993)
[11]M. Weaver *et al.*, Phys. Rev. Lett. **72**, 3758 (1994)
[12]In preparation
[13]D.A. Harris *et al.*, Phys. Rev. Lett. **71**, 3914 (1993); D.A. Harris *et al.*, Phys. Rev. Lett. **71**, 3918 (1993); see BNL 845 result: K.E. Ohl *et al.*, Phys. Rev. Lett. **64**, 2755 (1990)
[14]R. Kessler *et al.*, to appear in Nucl. Instr. and Meth. (1995)
[15]Bill Molzon, private communication.
[16]H. Lipkin, Phys. Rev. D **176**, 1715 (1968)

EXPERIMENTAL SEARCH FOR DIRECT CP–VIOLATION STATUS OF THE NA48 EXPERIMENT AT CERN

Cagliari-Cambridge-CERN-Dubna-Edinburgh-Ferrara-Firenze-Mainz-Orsay-Perugia-Pisa-Saclay-Siegen-Torino-Vienna-Warsaw

presented by M.Calvetti
Dipartimento di Fisica - Universita' di Firenze

INTRODUCTION

One of the open problems in modern high energy physics is to obtain experimental evidence of direct CP-violation in particle decays.

So far CP-violation (not direct) has been observed only in K-decays, the only place at the moment, in which nature makes a difference between matter and antimatter.

This is why three new experiments are now under construction, one at FERMILAB (KTEV), one at CERN (NA48) and one in FRASCATI (KLOE).

The first two are quite similar ; they detect $\pi^0\pi^0$ and $\pi+\pi-$ from two collinear and simultaneous KL and KS beams while the FRASCATI experiment, also described in this conference, uses a dedicated storage ring e+ e- --> Ø --> K0-K0bar to generate kaons.

The effects of direct CP-violation on the K decay branching ratios are so small (10-3) and , because making such experiments is so difficult, it is necessary to have several independent measurements.

I shall describe the CERN NA48 detector now under construction at CERN.

The first data are expected to be collected in '97. Two or three years will be necessary to collect enough events to reduce the statistical error to the required accuracy (10-4). First results will probably be available in '98 - '99 when the B-factory in SLAC starts operations.

Direct CP violation will manifest itself in the difference from 1 of the parameter R :

$$R=1-6R(\varepsilon'/\varepsilon)$$

the ratio of the ratios of the branching ratios KL over KS for the neutral and charged decays.

The Superweak Model predicts no direct violation while in the Standard Model, a prediction is difficult due to uncertainties in the hadronic contributions to the decay diagrams and to the imperfect knowledge of the CKM matrix elements.

Different calculations place ε'/ε into the interval 10**-4 / 10**-3 depending on the top quark mass.

Our present experimental knowledge is based on the results of the NA31 and E731 collaborations at CERN and FNAL. They are:

$$\mathrm{Re}\,(\varepsilon'/\varepsilon) = (23 \pm 6{,}5)\ 10\text{-}4 \qquad \text{NA31}$$

$$\mathrm{Re}\,(\varepsilon'/\varepsilon) = (7.4 \pm 5.9)\ 10\text{-}4 \qquad \text{E731}$$

the average of the two experiments is

$$Re\,(\varepsilon'/\varepsilon) = (\,14.8 \pm 4.3\,)\,10\text{-}4$$

To confirm this result a new generation of experiments is necessary , aiming at a final error of about 10-4 .

To achieve this precision in NA48 we believe it necessary :

- to work at high rate to have high statistics (1MHz rate in the detectors) .
- to have simultaneous KL and KS beams to be insensitive to variation of detection efficiencies and have the same effects on KL and KS decays from accidental overlapping of multiple events.
- to have collinear KL-KS beams, with the same momentum distributions, to have equal detection efficiencies. The space and momentum distributions of the reconstructed events for KL and KS , are "equalised" using weighting methods .
- to know the absolute energy scale, for charged and neutral decays , better than few 10-4.
- to have a low background from three body decays.

In the following a brief description of the NA48 experiment is given.

NA48 STATUS REPORT

THE BEAM

The two beams are generated using the same primary protons as shown in fig1. About 10**12protons, with a momentum of 450 Gev/c , are extracted from the SPS ring every 14 sec in a 2.4 seconds extraction and sent onto a Be-target , 1.5 interaction length long.

The target is 250 m upstream the detectors in such a way that only KL's, neutrons and photons can reach them.

Of the non interacting primary protons a fraction 10**-5 is channeled in the lattice planes of a bent silicon crystal located behind the target.

The Si-crystal is part of the optics to progagate the emerging 10**7 protons onto the second Be-target used to produce the KS-beam, 120 m downstream the crystal.

At the exit of the last defining collimator the two beams are separated vertically by 72 mm and are converging to coincide in space at the entrance of the electromagnetic calorimeter.

The non exact collinearity and divergence of the two beams will induce a second order correction to the result since the acceptances are not exactly equal .

Some of the characteristics of the combined Kaon beams are listed in Table 1. The two beams are completed and have been used in a test run in the summer '95 . The number of kaons produced, and the rates measured in the detectors, are as expected.

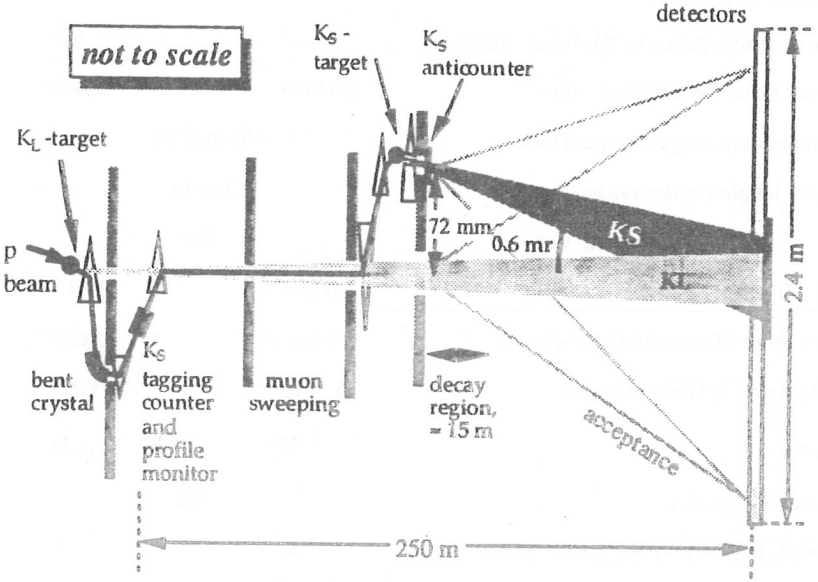

Figure 1 – Conceptual layout of the NA48 experiment (side view).

TABLE1

MEASURED PARAMETERS WITH SIMUNTANEOUS KS-KL BEAMS IN '95

	KL	KS
Protons per pulse on target	1.5x10**12	3x10**7
Spill 2.5 s , Cycle time 14.4 s		
Momentum P0 Gev/c	450	450
Production angle mrad	2.4	4.2
Angle of convergence to KL beam mrad	------	0.6
Radius of beam at detector mm	36+-5	45+-25
K0 momentum range accepted Gev/c	70<p<170	
Fiducial lenght for decays m	3ts=18	
at mean momentum Gev/c	110	
Total K0 per pulse at exit last coll.	2x10**7	2x10**2
K0 per pulse of accepted momentum	6.4x10**6	1.5x10**2
and decaying in fiducial length	3.3x10**4	1.4x10**2
to πo πo	30	45
Detector acceptance	0.2	
USEFUL DECAY PER PULSE p0p0	6	9
HOUR p0p0	1.5x10**3	2.3x10**3
PER 120 DAYS at 50% EFFICIENCY	2.2x10**6	3.3x10**6
RATES		
with incident protons	6x10**11	1.2x10**7
KO decays into detector s-1	3x10**5	4x10**2
muons through detector	1.5x10**5	10**3
Total rate into detector MHz	1.5	0.1

THE SPECTROMETER

An expanded view of the NA48 detector is shown in Fig.2 .

The beams and the decay fragments propagate in a vacuum tube (10**-5 mbar, 2.5m diameter) untill they cross a thin window separating the vacuum from one atm of He. The volume in between the four wire chambers of the spectrometer, two before and two after the magnet, and the magnet field volume itself filled with He. (The He is used to reduce the multiple Coulomb scattering of the charged pions).

The solid angle outside the detector acceptance is covered with seven rings of scintillation counters to reject photons from KL-->3π0 decays.

To avoid interactions in air of the surviving Kaons and of the accompanying neutrons and photons , a 16 cm diameter tube continues the vacuum across the apparatus from the thin window to the beam dump.

The four wire chambers measure the position of the crossing pions with an accuracy of 100 μ in the transverse plane.

The position of the decay vertex along the beam line and in the transverse plane, is calculated using the information of the two chambers in front of the magnet. The expected longitudinal resolution is about 50 cm and it is dominated by Coulomb scattering .

The dipole magnet produces a vertical magnetic field of 0,86 T.m to measure the momentum with an accuracy $\Delta p/p = 0.6\%$ p.

Some properties of the magnetic field are listed here:

I = 1200 A
B= 0.3712 Tesla
B*l = 0.858 Tm
Pt= 257.4 Mev/c
Leff= 2.31 m

In September '95 we have taken data with KL and KS beams using only three chambers (out of four).

The obtained kaon invariant mass distribution is shown in fig.3. The Kaon mass is measured with a resolution of 3Mev.

The reconstructed transverse position of the charged vertex is shown in Fig.4 .

The two distributions are vertically separated since most of the KS decay at the beginning of the decay region where the two beams are not overlapping.

The final alignment of the chambers has still to be done but we can already say that the quality of the spectrometer is as good as expected.

The results are still preliminary.

Since the NA48 spectrometer is similar to the one used by the FNAL collaboration in the E 731 experiment we think that with our (hopefully better) electron identification in the liquid krypton , we should keep the Ke3 background in the $\pi+\pi-$ sample lower than 10-4.

In the summer '96 we shall have a complete spectrometer with the final charged trigger. We are planning to run the system at nominal intensity.

THE ELECTROMAGNETIC CALORIMETER

The two π^o's coming from the kaons are identified measuring the position and the energy of the 4 photons in the electromagnetic calorimeter, placed downstream the spectrometer immediately after the trigger hodoscope.

The calorimeter is a homogeneous detector with 27 radiation lengths of liquid Krypton (22 tons of Krypton). The active region has the shape of an octagon which has inscribed a circle of 121 cm radius.

The sensitive volume is filled with 27 thousand ribbons, 2 cm high and 40 μ thick, of copper with 1% berillium, separated by 1 cm . The ribbons, 130 cm long, are stretched,

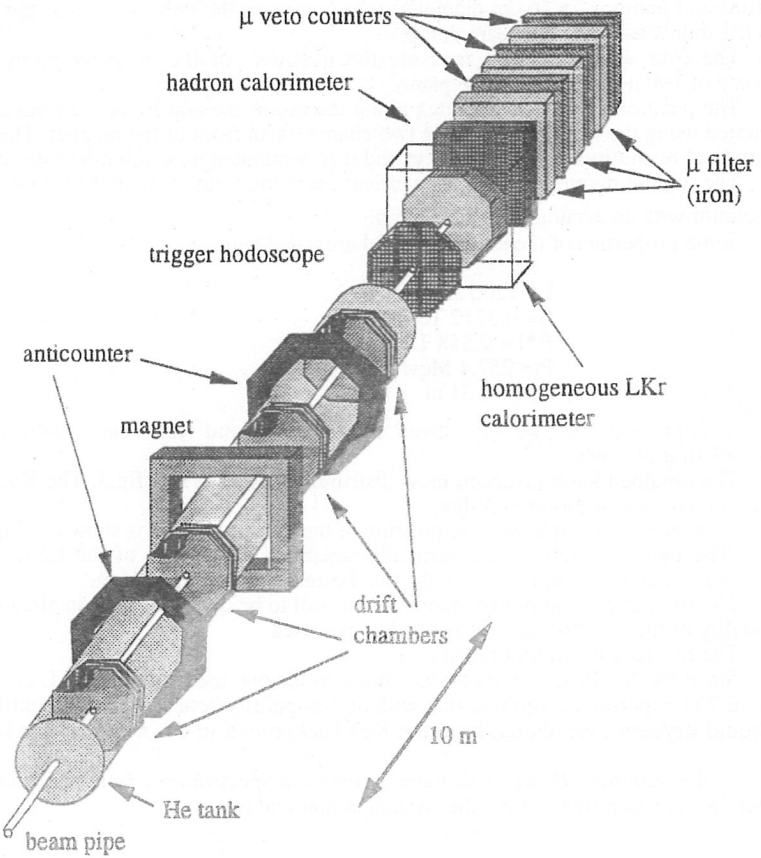

Figure 2 – Perspective view of the NA48 detecor.

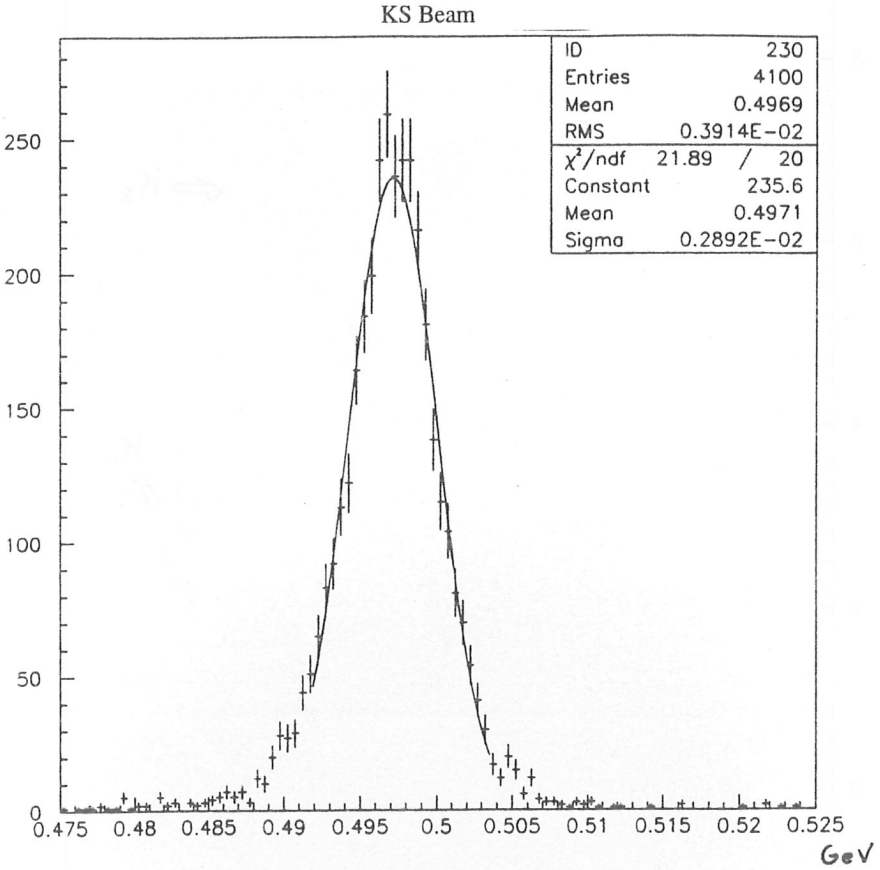

Figure 3 – k mass, cut on p^+/p^-.

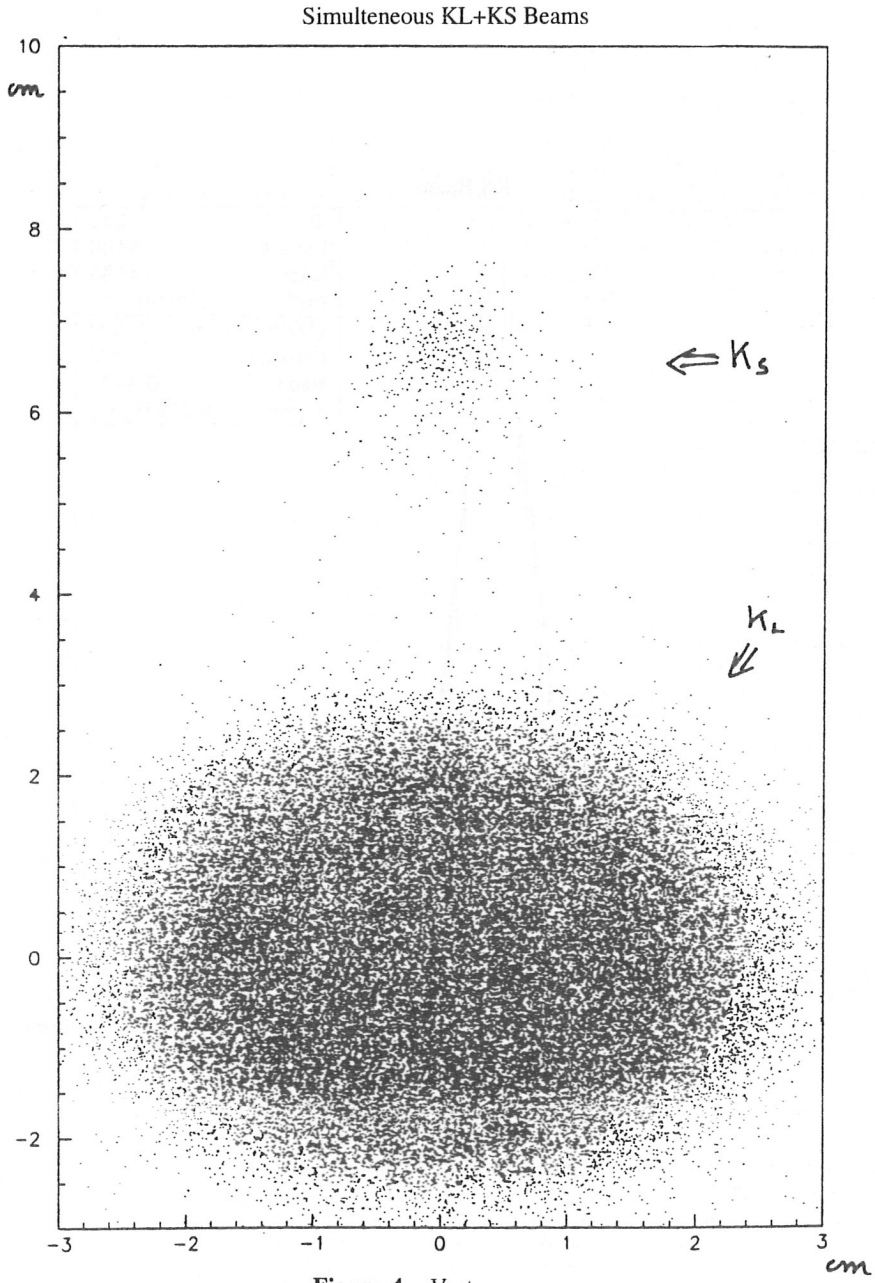

Figure 4 – Vertex x vs y.

with a tension of 200 gr, between the entrance plate and the back-plate of the electrodes supporting structure (in Stesalit).

The basic cell has one central ribbon (the anode), connected to the HV(8KV), and two side ribbons connected to ground . A decoupling capacitor connects the central anode to the input of the preamplifier located at the back-end of the ribbon into the Krypton. The calorimeter has 14500 cells.

Five intermediate grids, used to keep the ribbons in position and parallel to each other , make the ribbons follow a zig-zag (left and right) to avoid having the shower development parallel to the electrodes (in such a case we would have a strong position dependence of the measured energy when the photon is near to the anode).

To reduce the sensitivity of the measurement of the position of the photons to longitudinal shower fluctuations , the cells are not parallel to each other, but pointing to the center of the fiducial decay region, 100m upstream (projective geometry).

The central anode and the two side grounded cathodes constitute a transmission line. The induced signal on the line, produced by the drift of the electrons under the action of the electric field , propagates toward the preamplifier at the end of the ribbon, together with the front edge of the developing electromagnetic cascade.

Half of the energy of the induced signal reaches the preamplifier within 2 nsec from the crossing of the photons (the other half will arrive after reflection at the open end). The detector has unprecedented potential precision in the measurement of the arrival time of the photons .

The energy in each cell is measured, after amplification and shaping, with the use of a 10 bits FADC driven at 40 MHz . The amplification is a function of the pulse height of the incoming signal. There are 4 different amplifications, the overall dynamic range corresponds to a 14 bits FADC. The signal is shaped to have a rise time of 80 nsec.

The amplitude is proportional to the induced initial current in the gap of the cell which in turns is proportional to the total energy released.

A fit with two free parameters, the amplitude and the phase with respect to the clock, is performed. The total energy of the photon is calculated summing the amplitudes obtained by fitting the signals of about 122 cells (11x11 box) most of them with very little energy deposited.

On average 30% -40% of the photon energy is released in a single central cell .

The arrival time is obtained fitting the signal of the central cell, while the position of the photon is calculated weighting the position of the 3x3 central cells with their energies.

The energy, position and time resolutions measured in the prototype of the calorimeter are presented in figs 5, 6 and 7.

The geometry after cooling, is measured extrapolating the track of the electron from KL decays.

The distance of the decay vertex from the calorimeter is calculated using the transverse positions and the energies of the four photons imposing on them the kaon invariant mass .

The absolute energy scale is calibrated using a scintillation counter used as a veto in the trigger, preceded by a Pb-converter at the exit of the final KS defining collimator.

The veto defines the beginning of the fiducial volume both for charged and neutral decays.

The reconstructed longitudinal position must be an exponential distribution (at fixed momentum and after acceptance correction) starting at the position of the lead. The fine tuning of the global energy calibration constant is obtained imposing this condition. The channel to channel responce is calibrated electronically.

A cross check of the calibration can be done using the electrons since the momentum is measured in the spectrometer and compared with the energy measured in the calorimeter.

We hope (and need) to calibrate the neutral energy scale to better than 5x10**-4

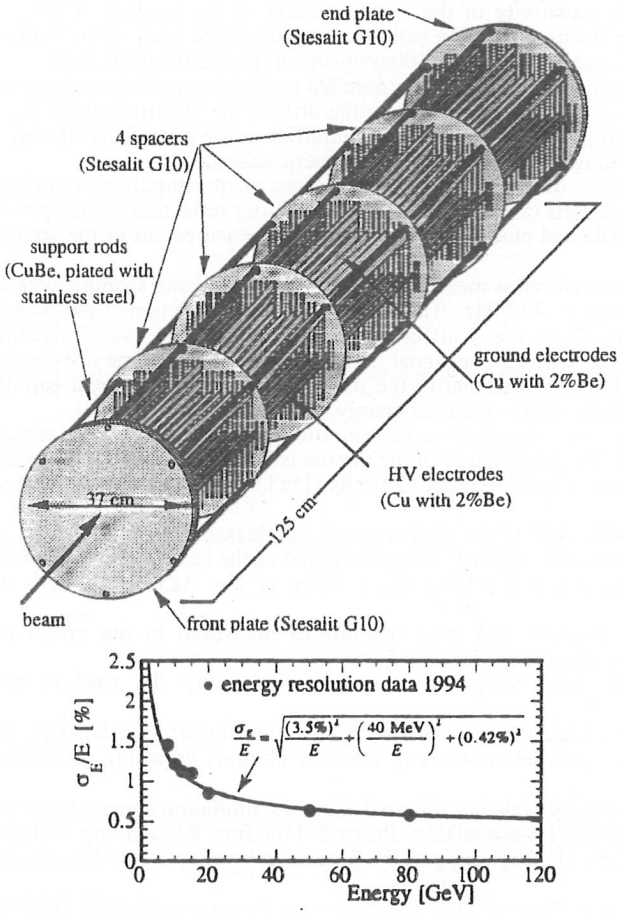

Figure 5 – Energy resolution of the Lkr prototype calormenter obtained from electron test beam data in 1994.

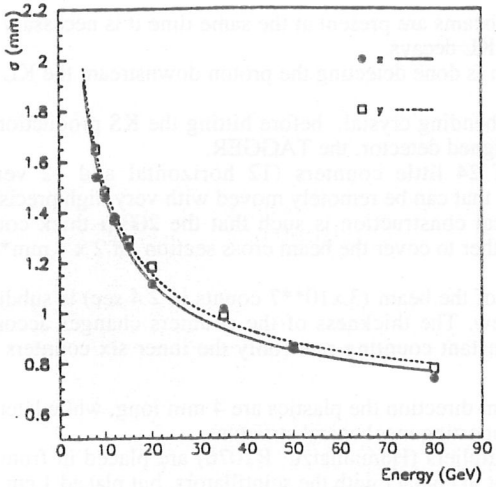

Figure 6 – Space resolution as function of the electron beam energy.

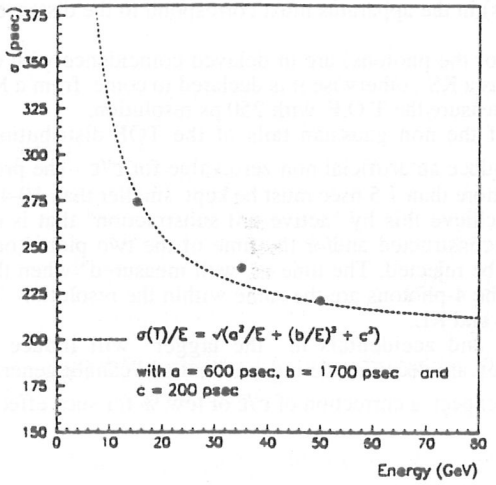

Figure 7 – Energy dependence of the time resolution (a trigger resolution of 180 ps has been subtracted in quadrature).

THE TAGGER

Since the two beams are present at the same time it is necessary to have a method to distinguish KS from KL decays.

The distinction is done detecting the proton downstream the KL Be-target in the KS proton beam line.

After the Si-bending crystal, before hitting the KS production target, the protons cross a specially designed detector, the TAGGER.

It consists of 24 little counters (12 horizontal and 12 vertical) placed on a mechanical structure that can be remotely moved with very high precision, see fig 8.

The mechanical construction is such that the 200 μ thick counters are placed in space one after the other to cover the beam cross section of 2 x 4 mm**2 with 50μ overlap .

The total rate of the beam (3.x10**7 counts in 2.4 sec) is subdivided among the 12 counters of each view. The thickness of the counters changes accordingly to the beam profile to have a constant counting rate (only the inner six counters have a thickness of 200μ).

Along the beam direction the plastics are 4 mm long, while laterally they are 15 mm wide to reach the supporting mechanical structure.

The photomultipliers (Hamamatzu R2076) are placed in front of the 4 x 15 mm2 surface . They are not in contact with the scintillators, but placed 1 cm away in air, in order not to be in the beam profile and halo. The light is received directly through the air . The analog pulse of each PM is sampled with 8 bits, 960 Mhz FADC. The amplitude and the arrival time of the pulses with respect to the clock are obtained by fitting their shape (see Fig.9).

The optical path of the photons to the photocathode is so small (1-2cm) that we have a very good light yield (400 photoelectrons) and hence a very good time resolution (100 ps) with a two pulses separation of 8 nsec .

The time (T.O.F) between the passage of the proton in the tagger and the crossing of the pions (or photons) in the apparatus must correspond to the distance of the tagger to the detectors.

If the pions (or the photons) are in delayed coincidence with one proton then the decay is interpreted as a KS , otherwise it is declared to come from a KL.

We hope to measure the T.O.F with 250 ps resolution.

Differences of the non gaussian tails of the TOF distributions for charged and neutral events can induce an artificial non zero value for ε'/ε . The probability to measure wrongly the T.O.F more than 1.5 nsec must be kept smaller than 10-4.

We hope to achieve this by "active tail substraction" that is events in which the tagger is not well reconstructed and/or the time of the two pions (or 4-photons) are not well measured, will be rejected. The time is "well measured" when the crossing times of the two pions or of the 4-photons are the same within the resolution. The rejection should be symmetric for KS and KL.

Inefficiencies and accidentals in the tagger will induce errors in the kaon identification but they are decay-mode independent and cannot generate an artificial non-zero value of ε'. We expect a correction of ε'/ε of few % for such effects.

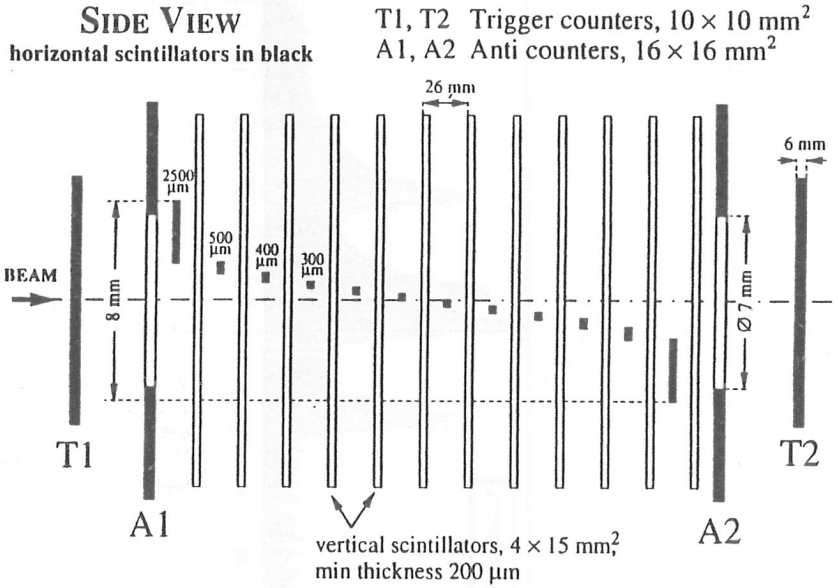
SIDE VIEW
horizontal scintillators in black
T1, T2 Trigger counters, 10 × 10 mm²
A1, A2 Anti counters, 16 × 16 mm²
26 mm
6 mm
2500 µm
500 µm
400 µm
300 µm
BEAM
8 mm
Ø 7 mm
T1
T2
A1
A2
vertical scintillators, 4 × 15 mm²
min thickness 200 µm

Figure 8

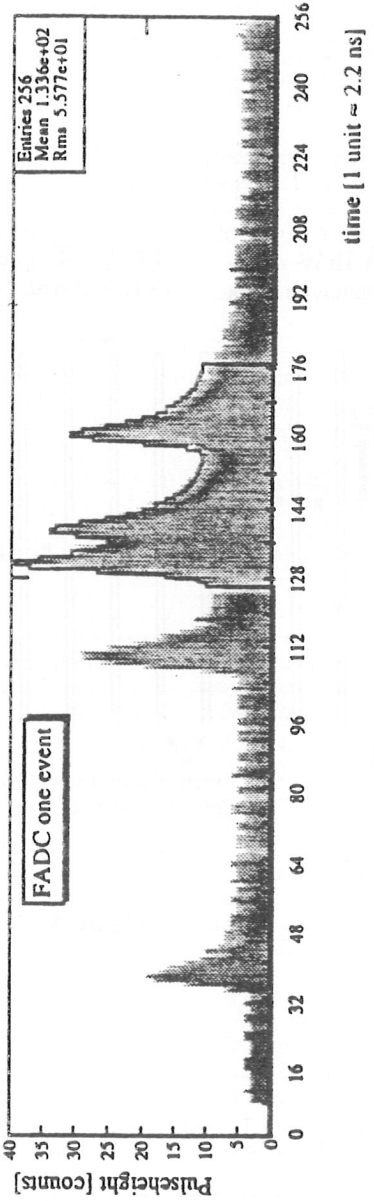
FADC one event
Entries 256
Mean 1.336e+02
Rms 5.577e+01
Pulseheight [counts]
time [1 unit ≈ 2.2 ns]
0
5
10
15
20
25
30
35
40
0
16
32
48
64
80
96
112
128
144
160
176
192
208
224
240
256

Figure 9

TRIGGER AND DATA FLOW

The trigger system works in pipeline mode. Several events can be stored in the buffers where they can wait for the time necessary for the processors to take the decision .

The first level trigger makes use of the muon veto, photon anticounters and fast energy information. The expected rate is less than 100KHz, the information is available in less than 500nsec. The "level 1" signal starts the "level 2" trigger processors. The trigger flow is coordinated by the "Trigger Supervisor".

Charged trigger.

To select the $\pi+\pi-$ final states we require two opposite quadrants in the trigger hodoscope, with a total energy measured in the calorimeters, hadronic plus electromagnetic, bigger than 30 Gev.

The second level charged trigger system perform an on line reconstruction in less than 100 μs). The position of the vertex and the invariant mass of the two pions is calculated. Charged decay candidates are selected according to Pt balance, vertex, energy and invariant mass.

Neutral trigger.

To select the $\pi 0\pi 0$ events we use the calorimeter information. The analog signals of the 14.500 channels of the liquid krypton readout, are summed together in tiles of 16 elements (2 x 8). Each sum is digitised via 10 bits, 40 MHz FADC, to calculate the total energy, the first and second moments of the spatial energy distribution and the number of photons impinging in the calorimeter. The number of photons is calculated on line using the x and y projections of the energy deposited in the tiles. A specially dedicated processor, the Data Concentrator, is used for the zero suppression. It identifies the cells fired event by event (about 450 cells) making the pattern recognition on line to take care of overlapping showers.

The neutral trigger processor is able to take the decision in less than 10μs at a rate of 2 KHz.

In the case of the neutral trigger a "level2B" processor runs a complete event reconstruction which is an integral part of the data acquisition system.

The trigger rate is dominated by three body decays from KL and only a handfull of good $\pi\ \pi$ events are collected per burst (see table 1) . Including KS decays, calibration, downscaling and rare decay, the likely (accepted) trigger rate is 10 KHz.

The Trigger Supervisor controls the trigger flow and provides a set of special triggers (downscaling) to record useful events to monitor the performances of the detectors.

The trigger efficiency must be the same for KL and KS decays.

The choice of which kind of events we have to record and many of each kind, is one of the major issues of the experiment.

At the beginning of each extraction a scaler in the Trigger Supervisor starts counting the clock of the experiment at a frequency of 40 MHz.

For every clock pulse each subdetector readout electronics store the relevant information in successive locations of circular memories (there is a general reset at the beginning of each extraction) . When the trigger conditions are satisfied the Trigger Supervisor generates a Time Stamp, which is the number of the time window in which the event has occurred, and broadcast it to the subdetectors.

Asynchronously each subdetector uses the Time Stamp to read the corresponding time windows and sends the data to the Data Merger, via an optical link, 150 m away in the control room of NA48.

The information of the subdetectors for the entire spill are stored in the Data Merger (fig.10). The system is designed to work in a pipelined mode to have no dead time.

The event data size is dominated by the liquid-Krypton calorimeter and depends critically on the suppression of the empty channels. With 10 KB per event and 10 KHz of rate we have 100MB/s to be sustained by the Data Merger during the 2.4 s of the extraction.

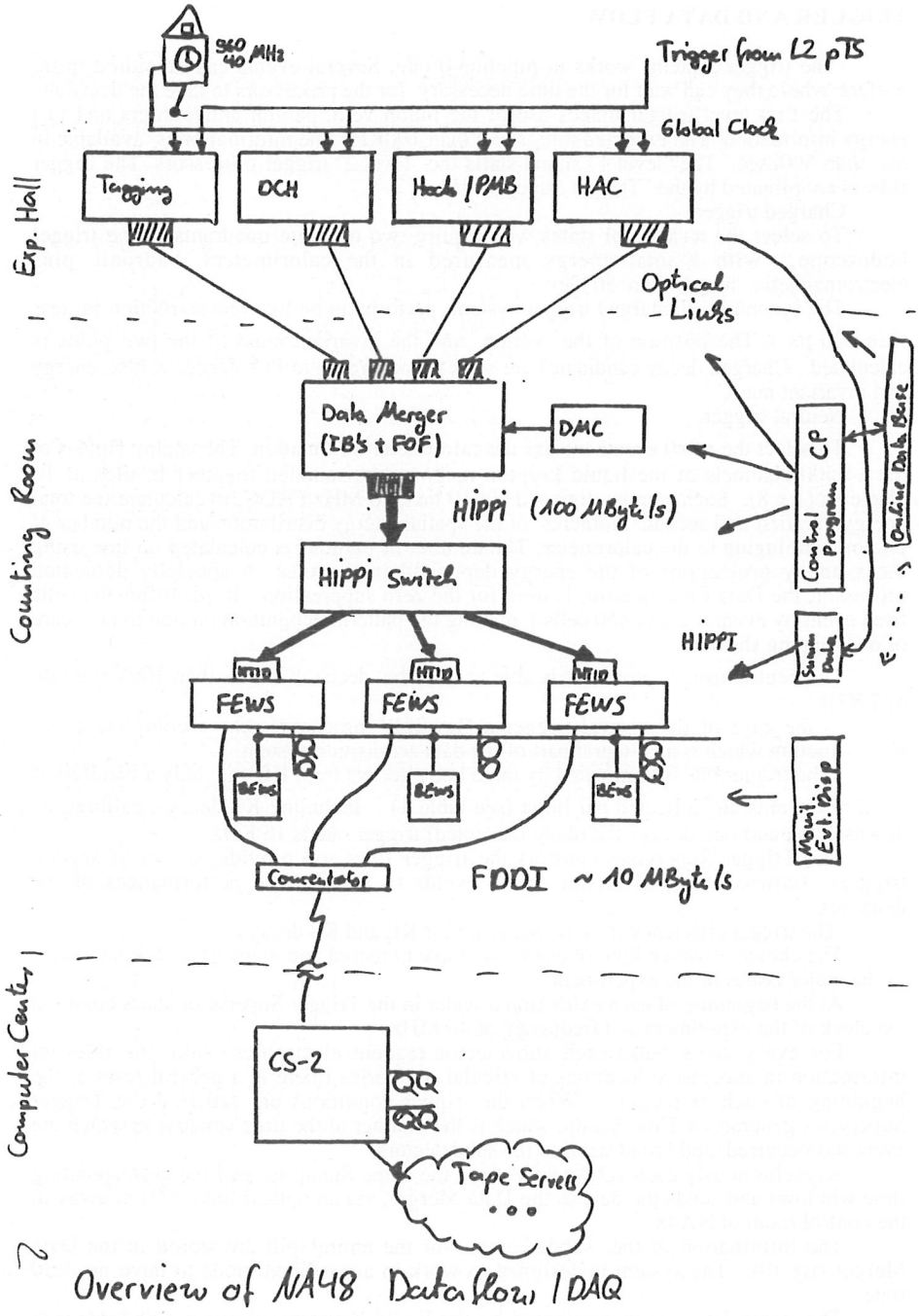

960 40 MHz
Trigger from L2 pTS
Global Clock
Tagging
DCH
Hodo / PMB
HAC
Exp. Hall
Optical Links
Data Merger (IB's + FOF)
DMC
Counting Room
HIPPI (100 MByte/s)
HIPPI Switch
Control Program
CP
Online Data Base
HIPPI
Sum Data
HTID
FEWS
BEWS
Monit. Evt. Disp
Concentrator
FDDI ~ 10 MByte/s
Computer Center
CS-2
QQ
Tape Servers
Overview of NA48 Dataflow / DAQ

Figure 10

The subevents of each subdetector are stored in the Data Merger, which then builds the complete event. The events are then sent via the Hippi Switch to the memory of the Front End Workstation. At the end of the burst the information is sent via an FDDI link to the CERN computer center, while the next FEWS records the data of the following burst. No significant local storage of the data is performed. The data flow takes advantage of the SPS duty cycle to reduce by a factor 6 the output rate from the FEWS.

The data are received at the CERN computer center via an FDDI ring and a Gigaswitch into the memory of the MEIKO CS2 (cerncs2-ESPRIT Project GPMIMD2) computer fully dedicated to NA48.

In the CS2 we run the reconstruction program to filter the events, to produce calibration constants, to monitor the experiment and to store the relevant informations on local appropriate media.

In the test run last September, we used the sysyem as described.

The data were fully analysed 5 minutes after they were taken. In this sense the CERN computer center was part of the experiment.

The data rate, and the expected volume of data recorded, place the NA48 experiment between the current LEP experiments and the LHC projects.

In our case we believe necessary to have a dedicated powerful computer and a massive data storage capacity directly at CERN since only preselected and limited data samples can be analysed in the local institutions. The CS2 can also be used for the Montecarlo simulation of the experiment when it is not used for data taking or reconstruction.

CONCLUSIONS

The NA48 experiment is very well on schedule. The hodoscope for charged decays, the muon and photon anticounters , the hadron calorimeter, the spectrometer , the trigger, the tagger, the Data Merger and the D.A.Q have been installed and successfully tested in the new "K12" beam line. We expect to install the electromagnetic calorimeter in the beam area in the summer '96 with 20% of its readout electronics. The forthcoming test in '96 will be dedicated to the running of the charged particle spectrometer and of the Krypton calorimeter. Installation of the complete readout electronics for the calorimeter is foreseen end of '96 and beginning of '97. In '97 NA48 will start data taking.

REFERENCES

1 -G.Barr et al., Proposal of the NA48 collaboration, CERN/SPSC/90-22,SPSC/P253,20july 1990
2 -T.White et al, Description of the muon veto. NA48 Note 94-1
3 -G.Barr et al., Desciption of the neutral trigger. NA48 Note 94-4
4 -I.Augustin et al, Readout of wire chambers in NA48, NA48 Note 94-33
5 -P.Debu et al, Description of a detailed simulation of a liquid Krypton calorimeter prototype, NA48 Note 94-18
6 -R.Moore et al, The muon veto trigger, NA48 Note 95-3
7 -G.Unal , Neutral Reconstruction, NA48 Note 95-10
8 -E.Griesmayer et al, Comparison of field calculations and measurements of a spectrometer magnet, NA48 Note 95-11
9 -C.Avanzini et al , The Peaksum Processing System for the NA48 Experiment, NA48 Note 95-12
10-N.Doble et al, A novel application of bent crystal channeling to the production of simultaneous particle beams , NA48 Note 95-13,CERN SL/95-16(EA)
11-M.Jeitler et al, Clock Control and Signal Distribution System for NA48, NA48 Note 95-14
12-H.Bluemer, Search For Direct CP Violation: The NA48 Experiment At CERN, NA48 Note 95-16
13-G.Unal, Event Weighting and Neutral Energy Scale Systematic Error on e'/e, NA48 Note 95-20
14-F.Bal et al, The Calorimeter Pipeline Digitizer CPD F690C, NA48 Note 95-23
15-A.Ceccucci et al, The NA48 Electromagnetic Calorimeter:Some Simulation Results, NA48 Note 95-27
16-T.Beier et al, A Proton Tagging Detector for the NA48 Experiment, CERN-PPE/94-11, N.I.M A 344(1994) 487-491
17-G.Barr et al, Performance of an Electromagnetic Liquid Krypton Calorimeter based on a Ribbon Electrode Tower Structure, CERN-PPE/95-64
18-H.Bluemer, C.Ebersberger, A scintillating fiber profile monitor for intense proton beams, N.I.M A 365 (1995) 268-272

MEASURING RARE RADIATIVE DECAYS OF THE Φ MESON AT CEBAF

Alex R. Dzierba
Indiana University
Bloomington, IN 47405, USA

Abstract

At CEBAF, preparations are underway for an experiment to measure rare radiative decays of the ϕ meson. Among the goals of this experiment is a determination of the sub-structure of the $f_0(975)$ and $a_0(980)$ mesons by determining the ratio $\phi \to a_0\gamma / \phi \to f_0\gamma$. A $6\ GeV$ tagged photon beam, with intensity $5 \cdot 10^7\ \gamma's/sec$ will yield about $30\ \phi's/sec$ via the photoproduction process: $\gamma p \to \phi p$. With a relatively modest electromagnetic calorimeter to detect the all-photon decay modes of the ϕ, branching ratio sensitivities of order 10^{-4} to 10^{-5} will be achieved. The experiment technique is described along with a discussion of expected backgrounds from electromagnetic and hadronic processes. The virtues of building a tagged ϕ facility are also discussed.

1 – Introduction

Discussions, at this and earlier workshops on the physics and detectors for DAΦNE, point to the rich physics to be uncovered in studying the decays of the ϕ meson. The potential for CP and CPT investigations is very exciting. There is also the opportunity for answering open questions in light-quark meson spectroscopy. As an historical example, the measurement of the ratio $\phi \to 3\pi\ /\ \phi \to K\overline{K}$ led to the OZI rule. Expected to be especially interesting for spectroscopy are the radiative decays of the ϕ. The radiative decays of the heavier vectors, the J/ψ and Υ, have certainly added to our understanding of light and heavy quark spectroscopy.

The decays of the ϕ into $K\bar{K}$ or 3π account for $98.8\ \%$ of the observed modes. There are seven meson states with masses lighter than that of the ϕ and therefore energetically possible as a decay product of the ϕ, along with a photon. Of these states, two (the ρ and ω) are vectors but the decays $\phi \to \rho\gamma$ and $\phi \to \omega\gamma$ are prohibited by the conservation of the C quantum number. Of the remaining five allowed states, only the decays $\phi \to \pi^o\gamma$ and $\phi \to \eta\gamma$ have been observed. Although the former is favored over the latter by pure phase space considerations, the branching ratio for $\phi \to \eta\gamma$ is larger than that for $\phi \to \pi^o\gamma$ by an order of magnitude because of the content of the η. The remaining three decays: $\phi \to \eta'\gamma$, $\phi \to f_0\gamma$ and $\phi \to a_0\gamma$ have not been observed and will be discussed below.

The subject of ϕ radiative decays will be discussed in more detail in Section 2, especially as it pertains to the scalar states, the f_0 and a_0. The complementarity of using boosted $\phi's$, from the photoproduction reaction, with $\phi's$ at rest, from e^+e^- collisions, will be investigated. In Section 3, the experimental study of these decays in a CEBAF experiment will be described. The virtue, and limitations, of restricting the study to all-photon decay products will be explored. Electromagnetic backgrounds in using a tagged photon beam and expected hadronic backgrounds will be discussed. Since the technique calls for use of a lead glass calorimeter to detect and measure the photon products of the ϕ decays, some recent all-neutral meson results of an experiment at the Brookhaven AGS by some members of the CEBAF experiment, also using a lead calorimeter will be presented in Section 3. In Section 4, possibilities of a future tagged ϕ facility at CEBAF are examined.

2 – ϕ Decays in a Photoproduction Experiment

At CEBAF energies realizable in the near future, photon energies in the 4 - $6\ GeV$ range are well above threshold for production of the ϕ in the reaction $\gamma p \to \phi p$.[1] In the vector dominance picture, which describes the data well, the photon ($J^{PC} = 1^{--}$) turns into a ϕ ($J^{PC} = 1^{--}$) which, in turn, elastically scatters off the proton. The cross section ($\approx\ 0.5\ \mu b$) is approximately constant with energy and the ϕ is produced

strongly peaked in the forward direction with a steeply falling t distribution:

$$\frac{d\sigma}{d|t|} \propto e^{-\alpha|t|} \tag{1}$$

where t is the square of the momentum transferred from the incoming γ to the outgoing ϕ and $\alpha \approx 6 \text{ to } 8 \ GeV^{-2}$. The $\phi's$ emerge roughly in the direction of, and with the energy of the incident photon beam. The high intensity, high energy CW accelerator at CEBAF makes possible the production of a beam of $\phi's$. For example, in late 1996, the tagged photon beam in Hall B at CEBAF will be delivering $5 \cdot 10^7 \ \gamma's/sec$. Incident on a $30 \ cm \ LH_2$ target, this will yield about $30 \ \phi's/sec$, which is equivalent to an e^+e^- collider operating with a luminosity of $\approx 10^{31} \ cm^{-2} \cdot sec^{-1}$. With some effort, a factor of 10 to 20 increase in yield should be possible. CEBAF affords the opportunity of studying the decays of $\phi's$ with yields comparable to that of a *ϕ-factory* and with very different systematics since the $\phi's$ are boosted (in photoproduction) instead of at rest (at an e^+e^- collider). This is especially evident in radiative decays.

2.1 Radiative Decays and Kinematics

Consider the decay:

$$\phi \rightarrow X\gamma \tag{2}$$

If the ϕ is produced at rest, the energy of the radiated photon, E_γ is given by:

$$E_\gamma = \frac{m_\phi^2 - m_X^2}{2m_\phi} \tag{3}$$

For example, for $\phi \rightarrow f_0\gamma$, $E_\gamma \approx 45 \ MeV$, making the detection of the radiated photon a challenge. If, on the other hand, the ϕ is moving with $\gamma_\phi = E_\phi / m_\phi$, the energy of the

radiated photon in the LAB is boosted by a factor as high as $2 \cdot \gamma_\phi$ ($\approx$ *12* for a *6 GeV* electron beam).

If X is a scalar or pseudoscalar, the decay (2) is an electric dipole (E1) or magnetic dipole (M1) transition and the width is given by:

$$\Gamma(E1 \text{ or } M1) \propto E_\gamma^3 \cdot |\langle f|E1 \text{ or } M1|i\rangle|^2 \tag{4}$$

The E_γ^3 factor strongly damps the branching ratio if $m_X \approx m_\phi$. For example, consider the effect of on the ratio of branching ratios:

$$\frac{BR(\phi \to \eta'\gamma)}{BR(\phi \to \eta\gamma)} = \left[\frac{m_\phi^2 - m_{\eta'}^2}{m_\phi^2 - m_\eta^2}\right]^3 \Re = 4 \times 10^{-3} \cdot \Re$$

where $\Re$ is the ratio of the squares of the amplitudes. The paucity of results on ϕ radiative decays can be understood. The rates are low and the radiated photons are difficult to detect.

2.2 Probing the Substructure of the Scalar Mesons

The scalar states, the a_0 and f_0 have been the focus of much attention, of late. The first of these scalar states is an isovector and the second is an isoscalar. They are nearly degenerate in mass. For completeness their properties [2] are:

$$\left.\begin{array}{l} a_o: \; I^G = 1^- \;\; J^{PC} = 0^{++} \;\; m = 980 \;\; MeV \;\; \Gamma = 57 \;\; MeV \\ f_o: \; I^G = 0^+ \;\; J^{PC} = 0^{++} \;\; m = 975 \;\; MeV \;\; \Gamma = 47 \;\; MeV \end{array}\right\} \tag{5}$$

The isoscalar state decays into $\pi\pi$ while the isovector state decays into $\eta\pi$. Both states also couple to $K\overline{K}$. The question of the interpretation of these states as $q\bar{q}$ states is an intriguing one and has attracted much theoretical attention. For example, their

masses and widths are too low for a ${}^3P_o$ $q\bar{q}$ nonet. Moreover the ${}^3P_o$ $q\bar{q}$ nonet is oversubscribed with recent results from the Crystal Barrel of an isoscalar $f_0(1365)$ [3] and an isovector $a_0(1450)$ [4]. These recent data may allow the $f_0(975)$ and $a_0(980)$ to be jettisoned from the ground-state scalar nonet, adding to the real possibility that these may be $non-q\bar{q}$ states, for example $qq\bar{q}\bar{q}$ or $K\bar{K}$ molecules. The $\gamma\gamma$ couplings of these states are also too small to be consistent with a ${}^3P_o$ $q\bar{q}$ nonet. [5,6] Weinstein and Isgur [7] have proposed a $K\bar{K}$ molecular picture of these states. The issue of whether these states mix via their common coupling to $K\bar{K}$ has been examined by Achasov and others. [8] Gribov and collaborators [9] have also discussed the possibility that the $f_0(975)$ and $a_0(980)$ might be novel states constructed of negative energy Dirac levels.

Close, Isgur and Kumano [10] show how a measurement of the ratio of branching ratios of ϕ radiative decays can provide information on the makeup of these scalar states. In the conventional ${}^3P_o$ $q\bar{q}$ picture, we expect $(\phi \to a_o\gamma)/(\phi \to f_o\gamma) = 0$ because of OZI suppression. The $K\bar{K}$ *molecule vs* $qq\bar{q}\bar{q}$ pictures can be distinguished by the electric dipole nature of these decays (which probes the electric charges of the constituents weighted by the distance from the overall *cm*) through the relative phases in $I = 0$ and $I = 1$ wave functions and through the relative spatial distributions of quarks and antiquarks. To summarize:

$$\left.\begin{array}{l} {}^3P_o \;\; q\bar{q} \;\; nonet: \\ a_o = (u\bar{u} - d\bar{d})/\sqrt{2} \\ f_o = some \;\; s\bar{s} \end{array}\right\} \Rightarrow \frac{\phi \to a_o\gamma}{\phi \to f_o\gamma} = 0 \qquad (6)$$

$$K\bar{K} \;\; molecule:$$

$$\left.\begin{array}{l} a_o \\ f_o \end{array}\right\} = \frac{1}{\sqrt{2}}\left[(u\bar{s})(\bar{u}s) \mp (d\bar{s})(\bar{d}s)\right] \Rightarrow \frac{\phi \to a_o\gamma}{\phi \to f_o\gamma} = 1 \qquad (7)$$

$$qq\bar{q}\bar{q}:$$

$$\left.\begin{array}{l} a_o \\ f_o \end{array}\right\} = \frac{1}{\sqrt{2}}\left[(us)(\bar{u}\bar{s}) \pm (ds)(\bar{d}\bar{s})\right] \Rightarrow \frac{\phi \to a_o\gamma}{\phi \to f_o\gamma} = 9 \qquad (8)$$

2.3 Other Physics

The measurements of the branching ratios discussed above is important information for CP studies at a $\phi - factory$. A determination of the branching ratio for $\phi \to (a_0 \ or \ f_0)\gamma$ will allow a determination of the branching ratio for $\phi \to (K_S^o K_S^o \ or \ K_L^o K_L^o)\gamma$. [10] The latter could be an insidious background for doing CP studies since the radiated photon will be very low in energy ($24 \ MeV \ at \ most$) and will likely go undetected causing confusion with:

$$\phi \xrightarrow[CP-violating]{} K_S^o K_S^o \ or \ K_L^o K_L^o \tag{9}$$

The $\phi \to \eta'\gamma$ decay mode is strongly damped because of the mass of the η' relative to the ϕ. The measurement of this branching ratio is important in providing information on the gluonic and $s\bar{s}$ content of the η'. [11]

The modes $\phi \to \rho\gamma$ and $\phi \to \omega\gamma$ are C-violating but the current limits are very imprecise and of order several percent. The sensitivity of this CEBAF experiment is such that the limit on $\phi \to \omega\gamma$ should be improved by 2 to 3 orders of magnitude.

3 – Experimental Setup

Figure 1 shows a schematic of the experiment [12] which includes a 25×25 element lead glass detector (LGD) in the Hall B tagged photon beam in front of the CLAS detector (not used for this experiment). The LGD is similar to a prototype LGD [13] built for Brookhaven AGS Experiment E852. [14] The beam will be incident on a *1-in* thick Be target, which will be followed by a charged particle veto (CPV), downstream of the target. The CPV will be used to veto on the presence of charged particles in the final state. The array will be large enough to match the transverse dimensions of the lead glass array but will not intercept recoil protons from the ϕ production reaction: $\gamma p \to \phi p$. The charged particle veto is just upstream of the LGD. The lead glass detector and the CPV will have holes for passage of the non-interacting photon beam.

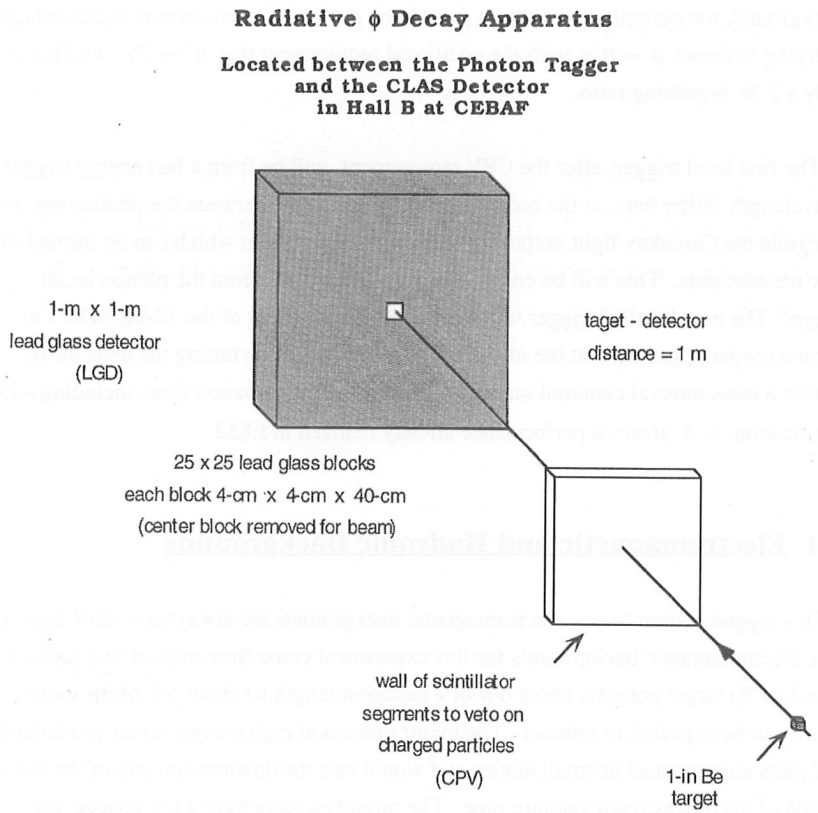

Figure 1: Schematic of the apparatus for the radiative ϕ decay experiment at CEBAF

A *4-cm* diameter vacuum pipe will be used between the target and the LGD to minimize material presented to the non-interacting photon beam between the target and LGD. The restriction to all-neutral decays of the ϕ has the advantage that no magnetic field is required so the impact from pair-production in the bremsstrahlung beam is minimized. The all-neutral requirement also removes a large fraction of hadronic

background, for example, from $\gamma p \to \rho p$ where $\rho \to \pi^+\pi^-$ An obvious disadvantage is in trying to detect $\phi \to \eta'\gamma$ with the additional requirement that $\eta' \to 2\gamma$, which has only a 2 % branching ratio.

The first level trigger, after the CPV requirement, will be from a fast energy trigger. Wavelength shifter bars, at the back end of the glass array, between the phototubes, will integrate the Cerenkov light output for an energy requirement which can be formed in a few nanoseconds. This will be correlated with information from the photon beam tagger. The next level of trigger will use the digitized output of the 12-bit ADC's to form a trigger requiring that the effective mass of all photons hitting the detector be within a mass interval centered on m_ϕ. This trigger determination time, including ADC digitization, is $5\ \mu sec$, a performance already realized in E852.

3.1 Electromagnetic and Hadronic Backgrounds

In a tagged photon beam, electromagnetic backgrounds are always a serious concern. The electromagnetic backgrounds for this experiment come from at least two sources. The *1-in* Be target presents about *6%* of a radiation length so about *6%* of the incident beam can be expected to interact. The major process at high energy is pair production. All pairs are produced at small angles and would exit the downstream end of the target inside of the downstream vacuum pipe. The produced pairs have a 6% chance, on average, of re-scattering in the target. This gives rise to a *0.4%* background. In general only one of the particles in the pair will scatter and so the event would be below trigger threshold. This background scales as the square of the target thickness so the signal to noise could be optimized at the expense of a loss in event rate. The presence of re-scattered pairs makes it essential that the vacuum pipe be extended downstream of the target to at least the end of the detector. The second source of background comes from the large number of photons with energies well below those of interest for ϕ production. Photons with energies below the tagger threshold are still present in the beam and pass through the target. While they will never produce triggerable energy depositions they do contribute to the radiation exposure of the detector and the general noise.

GEANT was used to simulate electromagnetic processes with an incident photon spectrum given by the Bethe-Heitler formula. A tagged photon rate between *4 GeV* and *6 GeV* of $5 \cdot 10^7 / sec$ was assumed. The width of the ADC gate is *250 nsec*. The results are that for blocks at *6 cm* radius (i.e. the innermost layer) we expect an average of *2.4 MeV* per block per ADC gate, from beam-induced background. The average *hit* energy that produces this is *10-15 MeV*. Thus the average of *2.4 MeV* (Poisson-distributed) means that many blocks have nothing, but about *20 %* have a *10-15 MeV* photon. Since a real shower is spread over several blocks, one must add up over (typically) nine blocks to get the photon energy. Thus there is a pedestal to the ADC signals of order *25 MeV*. This is negligible compared to the resolution of the lead-glass. The same calculation at *20 cm* radius (near the middle of the detector) gives an order-of-magnitude lower average energy, i.e. completely negligible.

Assuming a $1/E_\gamma$ spectrum for photons, $E_\gamma^{max} = 6\ GeV$ and $5 \times 10^7\ photons/sec$ in the range $4.5 < E_\gamma < 6.0\ GeV$, the total hadronic production rate is $\approx 150\ KHz$. In this experiment, we will trigger only on events with no charged forward particles into the LGD. The hadronic rate for processes yielding only photons in the forward direction is $\leq 100\ KHz$ and is dominated by $\gamma n \rightarrow \pi^o n$ and $\gamma p \rightarrow \pi^o p$ which accounts for $\approx 75\ KHz$. The effective mass trigger processor will reject the great majority of single π^o events in the trigger. Our off-line mass resolution of $\sigma = 10\ MeV$ at the π^o mass is more that adequate to reject this background.

The major contributor to other hadronic processes yielding forward photons are the production of the vector mesons: ρ, ω and ϕ. The photoproduction cross sections are in the ratio:

$$\sigma(\gamma p \rightarrow \rho p) : \sigma(\gamma p \rightarrow \omega p) : \sigma(\gamma p \rightarrow \phi p) \approx 36 : 4 : 1 \qquad (10)$$

This ratio, convolved with the fraction of ρ, ω and ϕ decays into all photons, yields the following:

$$N(\rho \rightarrow photons) : N(\omega \rightarrow photons) : N(\phi \rightarrow photons) \approx 3.8 : 34 : 1. \qquad (11)$$

Since the trigger will require that the energy deposited in the detector be a large fraction of the tagged photon energy, the trigger rate will be dominated by neutral decays of vector mesons other than the ϕ. The unknown branching ratios for $\phi \rightarrow f_0\gamma$ and $\phi \rightarrow a_0\gamma$ were chosen so that 2000 events would be generated by the Monte-Carlo program for these decays assuming a branching ratio of 10^{-4}. Corresponding to this, all other all-photon decays of the ρ, ω and ϕ were generated consistent with production cross-sections (equations 10 and 11). The photon 4-vectors were generated using conservation of energy and momentum in a sequential decay tree. The angular distributions used to populate the decay phase space took into account the polarization of the initial state vector mesons. Flat angular distributions were used for the spinless daughters of the primary meson.

The above scheme was used to estimate energy deposited in block of the LGD. In addition, GEANT-generated electromagnetic background was also used to estimate energies in the blocks. The electromagnetic events were randomly mixed in to 'spoil' the events from pure hadronic processes. On average, 9.5 electromagnetic events contributed to every hadronic event, based on a $250\ nsec$ integration time for the ADC's. These 'spoiled' Monte Carlo events were then passed on to the pattern recognition and hypothesis-sorting software used in E852.

This process yielded an estimate of the overall acceptance which takes into account (1) geometry; (2) cuts on minimum photon energies ($\approx 100\ MeV$) and photon separation ($\approx 6\ cm$); and (3) pattern recognition and hypothesis sorting. The results are summarized in Table 1. The most problematic background comes from $\phi \rightarrow \eta\gamma \rightarrow 3\pi^o\gamma$. Some fraction of the time, events of this sample mimic $\phi \rightarrow a_0\gamma \rightarrow \eta\pi^o\gamma$, with 5 photons in the LGD reconstructing to a mass near m_ϕ and 4 of the photons satisfying the $\eta\pi^o$ hypothesis. Techniques have been developed to understand and remove this background.

Table 1: Yield estimates based on the assumptions described in the text.

Decay Mode $\phi \rightarrow$	BR(%)	BR in all photons 10^{-4}	Number of photons	A [a] (%)	$A \cdot BR$ 10^{-4}	Yield of Events
$\pi^o\gamma$	0.13	13	3	35	4.5	38,000
$\eta\gamma$	1.3	52	3	35	18.2	150,000
$\eta'\gamma$ [b,c]	0.04	0.09	3	30	0.03	250
$\omega\gamma$ [b]	5	43	4	20	8.6	75,000
$a_0\gamma \rightarrow \eta\pi^o\gamma$ [b]	0.10	10	5	7	1	5,300
$f_0\gamma \rightarrow \pi^o\pi^o\gamma$ [b]	0.20	20	5	10	2	15,000

[a] A = acceptance as defined in the text.

[b] the measured limit is used for BR.

[c] For the $\eta'\gamma$ mode the prediction is about 15 % of the current measured limit.

The following BR are also used :

$\eta \rightarrow 2\gamma$ (39 %); $\eta' \rightarrow 2\gamma$ (2.2 %); $\omega \rightarrow \pi^o\gamma \rightarrow 3\gamma$ (8.5 %)

3.2 Results from E852

In estimating our efficiency for extracting the radiative decay signals from the expected hadronic electromagnetic backgrounds, we made use of pattern recognition and hypothesis-sorting software developed for E852. This software is still undergoing improvements. Several results from E852 analysis are presented here. In Figures 2 and 3 we present the $\pi^o\pi^o$ and $\pi^o\eta$ effective mass distributions from:

$$\pi^- p \rightarrow \pi^o\pi^o n \rightarrow 4\gamma n \qquad (12)$$

$$\pi^- p \rightarrow \pi^o\eta n \rightarrow 4\gamma n \qquad (13)$$

respectively, at an incident momentum of $18\ GeV$. The mass plots are corrected for acceptance. The data shown in these and other plots represent about 10 % of the total E852 sample.

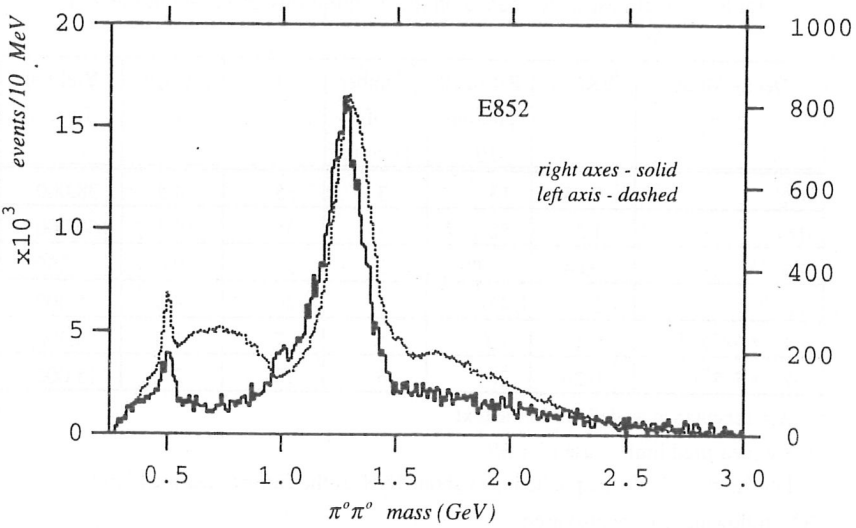

Figure 2: $\pi^o\pi^o$ mass distribution. The dashed histogram is for all events and the solid histogram is for events with $0.4 < |t_{\pi\to\pi\pi}| < 5.0\ GeV^2$.

In Figure 2, the shaded histogram shows a peak at the K_S^o mass and at the $f_2(1275)$. A dip in the distribution occurs at the mass of the $f_0(975)$. This phenomenon has been seen by others and is due to at least two resonances, one broad with a mass near $1\ GeV$ and another, whose phase rapidly goes through 90°, also near $1\ GeV$. The solid histogram is for events satisfying the requirement on the momentum transfer squared from the incident π^- to the outgoing $\pi^o\pi^o$ system: $0.4 < |t_{\pi\to\pi\pi}| < 5.0\ GeV^2$. In this case, a bump appears in the distribution near $1\ GeV$. When fitted to two Breit-Wigners, the mass of the bump occurs at $988 \pm 10\ MeV$ with a width of $61 \pm 7\ MeV$. A partial wave analysis of these data is in progress.

In Figure 3, the $a_0(980)$ and $a_2(1320)$ are clearly seen. The fit of the distribution to two Breit-Wigners and a quadratic background yields the following masses and widths:

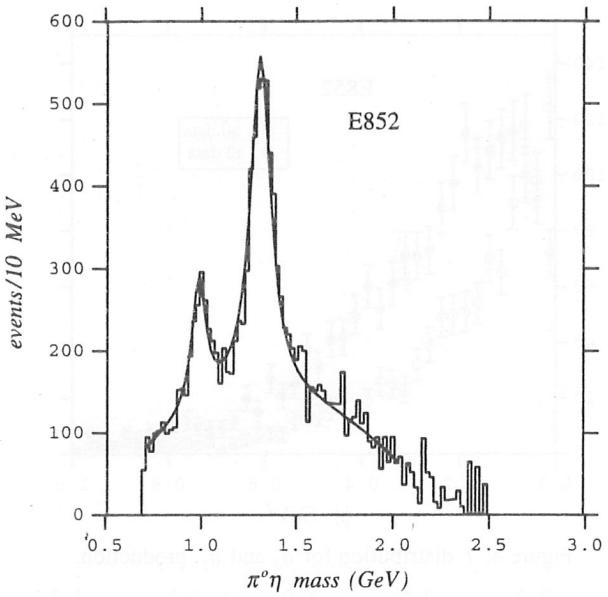

Figure 3: $\pi^o\eta$ mass distribution. The fits are described in the text.

$$a_0: \; m = 986 \pm 5 \;\; MeV \;\; and \;\; \Gamma = 90 \pm 11 \;\; MeV$$
$$a_2: \; m = 1311 \pm 2 \;\; MeV \;\; and \;\; \Gamma = 130 \pm 7 \;\; MeV$$

The distributions in $|t_{\pi\to\pi\eta}|$ are shown in Figure 4 for events in the a_0 and a_2 mass peaks. The difference in these distributions is striking. The production characteristics of processes (12) and (13) near *1 GeV* may indicate $f_0 \leftrightarrow a_0$ mixing (see the references of [8]) or *G-parity regeneration.* [15] As an indication of the resolution in the *t* variable, the E852 measurement on the *t* - distribution for the charge exchange reaction:

$$\pi^- p \to \pi^o n \to 2\gamma n \qquad (14)$$

is compared in Figure 5 with two other experiments [16,17] nearby in energy.

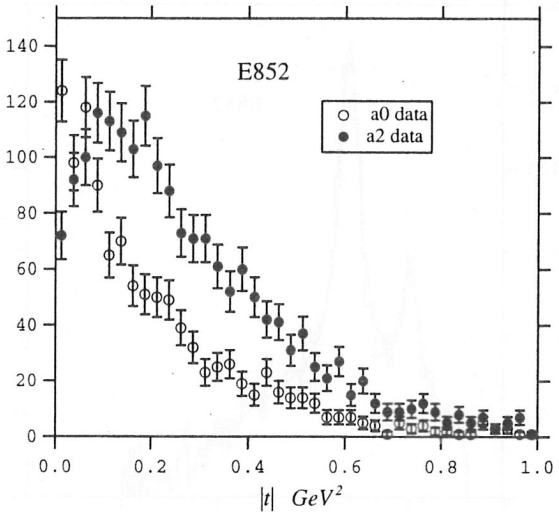

Figure 4: t distribution for a_0 and a_2 production.

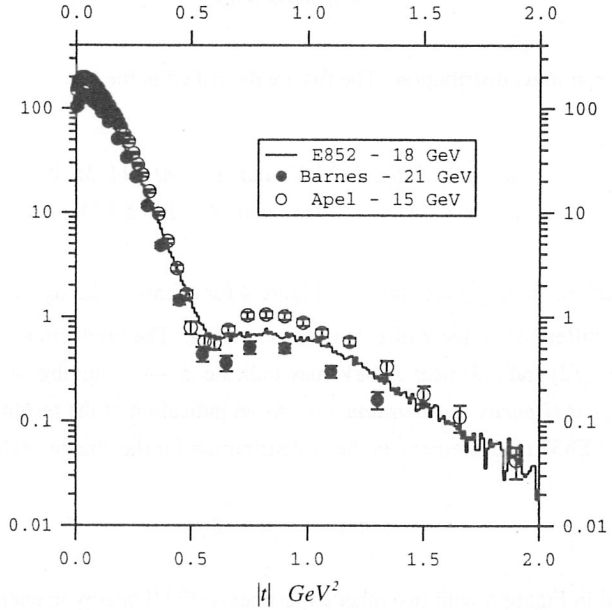

Figure 5: The t distribution for $\pi^- p \to \pi^o n$ measured by E852 and compared to results of references [16] and [17].

Finally, as an example of a radiative decay, the distribution in the $\pi^o\gamma$ effective mass for the sub-sample of five cluster events corresponding to the reaction $\pi^- p \to \pi^o\pi^o\gamma n$ is shown in Figure 6. The $\omega \to \pi^o\gamma$ is clearly observed. For six cluster events corresponding to the reaction $\pi^- p \to \pi^o\pi^o\eta n$, the $\pi^o\pi^o\eta$ effective mass is shown in Figure 7. The $\eta' \to \pi^o\pi^o\eta$ decay is clearly observed.

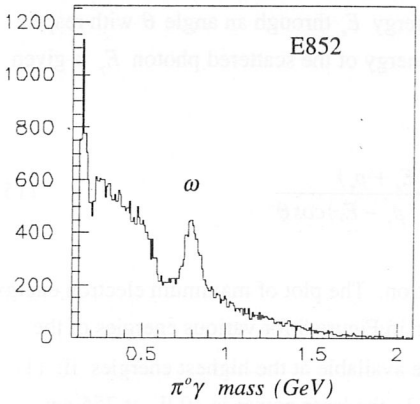

Figure 6: $\pi^o\gamma$ effective mass distribution from the reaction : $\pi^- p \to \pi^o\pi^o\gamma n$. The ω is clearly observed.

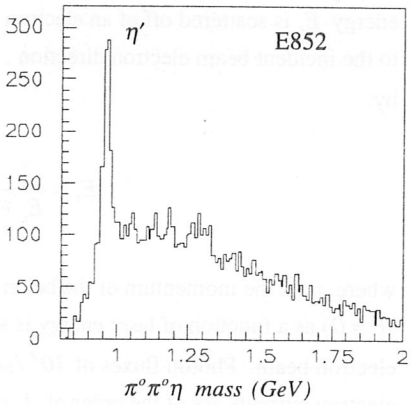

Figure 7: $\pi^o\pi^o\eta$ effective mass distribution from the reaction : $\pi^- p \to \pi^o\pi^o\eta\, n$. The η' is clearly observed.

4 – A Tagged ϕ Facility

The point of the discussion in Section 3 is that there are advantages in boosting the to study its rare radiative decays. One does not have to deal with the delicate radiated photon as in the case of a ϕ produced at rest. In any case, photoproduction is certainly a complementary method. In this section, the possibility of using the photoproduction reaction, $\gamma p \to \phi p$, to produced tagged $\phi's$, and, therefore correlated sources of K^+K^- or $K_S^o K_L^o$ is considered. [18]

4.1 Photon Beams

Tagged bremsstrahlung photon beams have advantages in being able to achieve high energies but the electromagnetic background accompanying the beam can create problems for detectors. An attractive alternative is to create a photon beam by Compton backscattering of laser beam from an electron beam.[19] If a photon from a laser of energy E_t is scattered off of an electron of energy E_e through an angle θ with respect to the incident beam electron direction , the energy of the scattered photon E_γ is given by:

$$E_\gamma = \frac{E_t(E_e + p_e)}{E_e + E_t - (p_e - E_t)\cos\theta} \tag{15}$$

where p_e is the momentum of the beam electron. The plot of maximum electron energy ($\theta = 0$) as a function of laser energy is shown in Figure 8 for various energies of the electron beam. Photon fluxes of $10^8/sec$ are available at the highest energies if: (1) electron currents are of the order of $3\ \mu A$; (2) the laser power is $10\ W$ at $256\ nm$ (coherent doubling of $512\ nm$); (3) high quality mirrors can be developed at $256\ nm$; and (4) multiple (2-3) lasers can be used. There are many advantages including

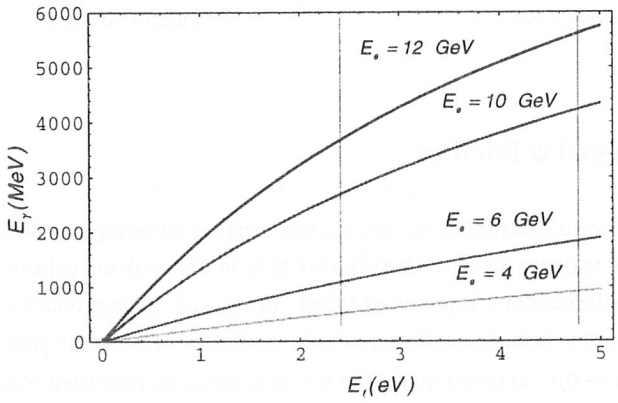

Figure 8: Backscattered photon energy (max) as a function of laser energy for various values of the beam energy. The first line corresponds to the $2.4\ eV$ green line in an Ar-ion laser and the second line to a frequency doubled $2.4\ eV$ line.

(1) 100 % tagging efficiency; (2) all the photons available are in the energy region of interest; (3) there is little background; and (4) the tagger is simpler. It may also be possible to exploit the polarization of the photon beam. A disadvantage is that such a beam requires better shielding of the beam dump to handle the higher currents.

4.2 Recoil Proton Tag

Indeed, a double-tagging may be employed by considering the dependence of the recoil proton angle *vs* momentum for the recoil proton as shown in Figure 9. The plot shows the recoil proton for $\gamma p \rightarrow \phi p$ as well as for $\gamma p \rightarrow \rho\, p$ at *6 GeV* incident photons. The same production mechanism is assumed and the natural widths of the ρ and ϕ are included. It should not be difficult to use the combined measurement of the recoil proton momentum and angle, along with event-by-event photon information to kinematically identify the process $\gamma p \rightarrow \phi p$ as part of a first-level trigger.

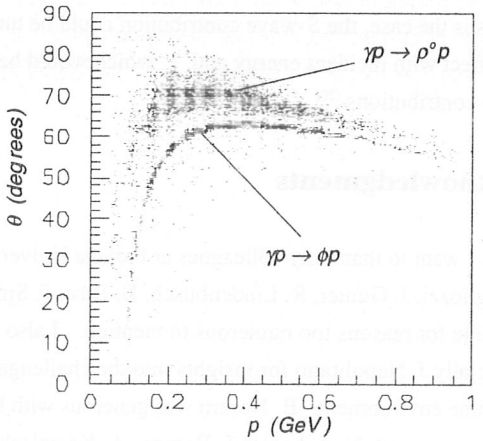

Figure 9: Recoil proton kinematics for *6 GeV* incident photons

4.3 Physics Opportunities

Physics opportunities with a tagged ϕ facility include:

(1) low-energy $K^{\pm}N$ scattering;

(2) rare decays of K_S^o by tagging on the K_L^o; and

(3) CP or CPT studies.

A complication with the latter is that the CP-violation signature is the process (9).

However, it is possible to directly produce K-pairs in an S-wave which would yield:

$$\gamma p \rightarrow \left(K_S^o K_S^o \ \ or \ \ K_L^o K_L^o\right) p \tag{16}$$

with a K-pair mass near m_ϕ. It may be that the interference of the CP-violating amplitude for (9) could interfere with the S-wave amplitude to enhance CP-violation effects. If this is the case, the S-wave contribution could be tuned by studying the variation of the effect with incident energy and t, which would be used to select the ratio of S and P wave contributions.[20]

Acknowledgments

First, I want to thank my colleagues at Indiana University: B. Brabson, R. Crittenden, P. Figliozzi, J. Gunter, R. Lindenbusch, D. Rust, P. Smith, E. Scott, T. Sulanke and S. Teige for reasons too numerous to mention. I also thank my E-94-016 colleagues, especially J. Napolitano for insights into the challenges of working in an electron machine environment. B. Norum was generous with his ideas. I also learned a lot from discussions with N. Achasov, T. Barnes, A. Kostelecky, M. Pennington and J. Speth. Finally, I want to thank the conference organizers for their generous invitation to speak at and attend this Workshop. Frascati is a joy ! This work was supported by a grant from the Department of Energy, DEFG0291ER40661, Task D.

References

[1] H. J. Behred *et al.,* Nucl. Phys. **B144**, 22 (1978); D. Aston *et al,* Nucl. Phys. **B172**, 1 (1978); D. P. Barber *et al,* Z. Phys. **C12**, 1 (1982). The measurements reported in these references span photon energies from 2.8 to 36 GeV.

[2] L. Montanet *et al.,* Review of Particle Properties, Phys Rev. **D50** (1994). This reference also contains material on the $f_0(975)$ in a mini-review of the $f_0(1300)$ on pg. 1478 and the mini-review of the $a_0(980)$ is on pg. 1465.

[3] V. V. Anisovich *et al.,* Phys. Lett. **B323**, 33 (1994).

[4] C. Amsler *et al.*, Phys. Lett. **B333**, 277 (1994).

[5] M.R.Pennington, University of Durham report DTP-94/26 (April 1994), to appear in Proceedings of the Meeting on Two-Photon Physics from DAΦNE to LEP200 and Beyond, eds. F.Kapusta and J.Parisi (Paris, February 1994).

[6] T.Barnes, Phys. Lett. **165B**, 434 (1985); E.P.Shabalin, Yad. Fiz. **46**, 852 (1987); T.N.Truong, in Proceedings of the HADRON '89 International Meeting on Hadron Spectroscopy (Ajaccio, 1989), pp.645; N.Brown and F.E.Close, Rutherford Laboratory report RAL-91-085.

[7] J.Weinstein and N.Isgur, Phys. Rev. Lett. **48**, 659 (1982); Phys. Rev. **D27**, 588 (1983); see also A.Astier *et al.*, Phys. Lett. **B25**, 294 (1967); A.B.Wicklund *et al.*, Phys. Rev. Lett. **45**, 1469 (1980); J.Weinstein and N.Isgur, Phys. Rev. **D41**, 2236 (1990); J.Weinstein, Phys. Rev. **D47**, 911 (1993).

[8] N. N. Achasov, S. A. Devyanin and G. N. Shestakov, Sov. Phys. Usp. **27 (3)**, 161 (1984); Phys. Lett. **88B,** 367 (1979); Modern Phys. Lett. A **8 (25),** 2343 (1993); Yad. Fiz. **33,** 1337 (1981); Sov. J. Nucl. Phys. **33(5),** May 1981, 1982 American Institute of Physics.

[9] V.N.Gribov, Lund report LU-TP 91-7 (March 1991); F.E.Close, Yu.L.Dokshitzer, V.N.Gribov,V.A.Khoze and M.G.Ryskin, Phys. Lett. **B319**, 291 (1993).

[10] F. Close, N. Isgur and S. Kumano, Nucl. Phys. **B389**, 513 (1993).

[11] J. L. Rosner, Phys. Rev. **D27**, 1101 (1983).

[12] The CEBAF E-94-016 proposal to PAC-8 (1994) and the Update to PAC-9 (1995). The collaboration consists of H. Crannell, J. O'Brien and D. Sober *(Catholic University of America, Washington, DC 20064),* M. Kossov, B. Niczyporuk and E. Smith *(Continuous Beam Accelerator Facility, Newport News, VA 23606),* B. Brabson, R. Crittenden, A. Dzierba, P. Figliozzi, J. Gunter, R. Lindenbusch, D. Rust, P. Smith, E. Scott, T. Sulanke and S. Teige *(Indiana University, Bloomington, IN 47405),* J. Bishop, N. Cason, J. Kolata, J. LoSecco, A. Sanjari and W. Shephard *(University of Notre Dame, Notre Dame, IN 46556),* G. Adams, J. Napolitano and M. Witkowski *(Rensselaer Polytechnic Institute, Troy, NY 12180),* B. Bonner, G. Mutchler and S. Ahmad

(Bonner Nuclear Physics Lab at Rice University, Houston, TX 77251), G. Gilfoyle, P. Rubin and M. Vineyard *(University of Richmond, Richmond, VA 23173),* E. Frlez and D. Pocanic *(University of Virginia, Charlottesville, VA 22901), and* D. Armstrong *(College of William and Mary, Williamsburg, VA 23187).* The Spokesman is A. Dzierba and the Co-Spokesman is J. Napolitano.

[13] B. Brabson *et al.,* Nucl. Instr. & Meth. **A332**, 419 (1993).

[14] A. R. Dzierba, CERN Courier **30**, 15 (1990) and ASG Proposal E852 (S. U. Chung and A. R. Dzierba, Co-Spokesmen).

[15] T. Barnes, Phys. Lett. **165B**, 434 (1985).

[16] A. Barnes *et al.,* Phys. Rev. Lett. **37**, 76 (1976).

[17] Apel *et al.,* Phys. Lett. **72B**, 132 (1977).

[18] A. R. Dzierba, Proceedings of the Workshop on CEBAF at Higher Energies (ed. N. Isgur and P. Stoler), 13 (1994). This reference contains a more speculative discussion of the physics possibilities with a Flying ϕFactory.

[19] Private conversations with B. E. Norum and B. E. Norum and T. P. Welch, CEBAF Hall B Letter of Intent to the CEBAF PAC (1993).

[20] Private conversations with N. Isgur and A. Kostelecky.

CP VIOLATION: A THEORETICAL REVIEW

R.D. Peccei
Department of Physics, University of California at Los Angeles,
Los Angeles, CA 90095–1547

Abstract

This review of CP violation focuses on the status of the subject and its likely future development through experiments in the Kaon system and with B-decays. Although present observations of CP violation are perfectly consistent with the CKM model, we discuss the theoretical and experimental difficulties which must be faced to establish this conclusively. In so doing, theoretical predictions and experimental prospects for detecting $\Delta S = 1$ CP violation through measurements of ϵ'/ϵ and of rare K decays are reviewed. The crucial role that B CP-violating experiments will play in elucidating this issue is emphasized . The importance of looking for evidence for non-CKM CP-violating phases, through a search for a non-vanishing transverse muon polarization in $K_{\mu 3}$ decays, is also stressed.

1 Introduction

The discovery more than 30 years ago of the decay $K_L \to 2\pi$ by Christianson, Cronin, Fitch and Turlay [1] provided the first indication that CP, like parity, was also not a good symmetry of nature. It is rather surprising that, for such a mature subject, we have still so little experimental information available. Indeed, the only firm evidence for CP violation to date remains that deduced from meausurements in the neutral Kaon system. Here there are five parameters meausured: the values of the the two complex amplitude ratios for the decays of K_L and K_S to $\pi^+\pi^-$ ($\eta_{+-} = \epsilon + \epsilon'$) and to $\pi^o\pi^o$ ($\eta_{oo} = \epsilon - 2\epsilon'$), plus the semileptonic asymmetry in

K_L decays (A_{K_L}) [1]. However, in fact, these five numbers at present give only one **independent** piece of dynamical information. To a very good approximation [3], η_{+-} and η_{oo} are equal in magnitude

$$|\eta_{+-}| \simeq |\eta_{oo}| \simeq 2 \times 10^{-3} ,$$

and in phase

$$\phi_{+-} \simeq \phi_{oo} \simeq 44^\circ ,$$

with the ratio

$$\epsilon'/\epsilon \leq 10^{-3} .$$

Because the two pion intermediate states dominate the neutral Kaon width, assuming CPT conservation [4] the phases ϕ_{+-} and ϕ_{oo} are approximately equal to the superweak phase

$$\phi_{SW} = \tan^{-1} \frac{2\Delta m}{\Gamma_S - \Gamma_L} = (43.64 \pm 0.14)^\circ .$$

CPT conservation also fixes the value of the semileptonic asymmetry in terms of Re ϵ [5]. Since ϵ' is so small, effectively one has [4]

$$A_{K_L} \simeq 2Re\ \eta_{+-}.$$

Thus the dynamical information we have today is, essentially, that obtained in the original discovery experiment [1], augmented by the statement that there is little or no $\Delta S = 1$ CP violation!

The above statement is a bit of an exaggeration, since in the last 30 years we have learned very much more about CP violation **outside** the neutral Kaon complex. In particular, very strong bounds have been established for the electric dipole moments of the neutron and the electron [3]

$$d_e, d_n \leq 10^{-25} \text{ ecm} .$$

Furthermore, we have uncovered the fundamental role that CP violation plays in the Universe, to help establish the observed matter-antimatter asymmetry [6]. In addition, we have a variety of bounds on a host of other CP violating parameters, like the amplitude ratios η_{+-o} and η_{ooo} for $K \to 3\pi$ decays , or the transverse muon polarization $< P_\perp^\mu >$ in $K_{\mu 3}$ decays. These bounds, however, are too insensitive to provide much dynamical information.

In the modern gauge theory paradigm CP violation can have one of two possible origins. Either,

i) the full Lagrangian of the theory is CP invariant, but this symmetry is not preserved by the vacuum state: CP $|0\rangle \neq |0\rangle$. In this case CP is a spontaneously broken symmetry [7].

[1] CP Lear [2] has presented recently a preliminary meausurement of the K_S semileptonic asymmetry, A_{K_S}, which agrees with A_{K_L} within 10%.

Or

ii) there are terms in the Lagrangian of the theory which are not invariant under CP transformations. CP is explicitly broken by these terms and is no longer a symmetry of the theory.

The first possibility, unfortunately, runs into a potential cosmological problem [8]. As the universe cools below a temperature T^* where spontaneous CP violation occurs, one expects that domains of different CP should form. These domains are separated by walls having a typical surface energy density $\sigma \sim T^{*3}$. The energy density associated with these walls dissipates slowly as the universe cools further and eventually contributes an energy density to the universe at temperature T of order $\rho_{\rm wall} \sim T^{*3}T$. Such an energy density today would typically exceed the universe closure density by many orders of magnitude:

$$\rho_{\rm wall} \sim 10^{-7} \left(\frac{T^*}{\rm TeV}\right)^3 {\rm GeV}^{-4} \gg \rho_{\rm closure} \sim 10^{-46}\ {\rm GeV}^{-4}\ .$$

One can avoid this difficulty by imaging that the scale where CP is spontaneously violated is very high, so that T^* is above the temperature where inflation occurs. In this case the problem disappears, since the domains get inflated anyway. Nevertheless, there are still problems since it proves difficult to connect this high energy spontaneous breaking of CP with observed phenomena at low energies. What emerges, in general, are models which are quite complex [9], with CP violation being associated with new interactions much as in the original superweak model of Wolfenstein [10].

If, on the other hand, CP is explicitly broken the phenomenology of neutral Kaon CP violation is a quite natural result of the standard model of the electroweak interactions. There is, however, a requirement emerging from the demand of renormalizability which bears mentioning. Namely, if CP is explicitly broken then renormalizability requires that all the parameters in the Lagrangian which can be complex must be so. A corollary of this observation is that the number of possible CP violating phases in a theory increases with the complexity of the theory, since there are then more terms which can have imaginary coefficients.

In this respect, the three generation ($N_g = 3$) standard model with only one Higgs doublet is the simplest possible model, since it has only one phase. With just one Higgs doublet, the Hermiticity of the scalar potential allows no complex parameters to appear. If CP is not a symmetry, complex Yukawa couplings are, however, allowed. After the breakdown of the $SU(2) \times U(1)$ symmetry, these couplings produce complex mass matrices. Going to a physical basis with real diagonal masses introduces a complex mixing matrix in the charged currents of the theory. For the quark sector, this is the famous Cabibbo-Kobayashi Maskawa (CKM) matrix [11].[2] This $N_g \times N_g$ unitary matrix contains $N_g(N_g-1)/2$ real angles and $N_g(N_g+1)/2$

[2] If the neutrinos are massless, there is no corresponding matrix in the lepton sector since it can be reabsorbed by redefining the neutrino fields.

phases. However, $2N_g - 1$ of these phases can be rotated away by redefinitions of the quark fields leaving only $(N_g - 1)(N_g - 2)/2$ phases. Thus for $N_g = 3$ the standard model has only one physical complex phase to describe all CP violating phenomena.[3]

If CP is broken explicitly, it follows by the renormalizability corollary that any extensions of the SM will involve further CP violating phases. For instance, if one has two Higgs doublets, Φ_1 and Φ_2, then the Hermiticity of the scalar potential no longer forbids the appearance of complex terms like

$$V = \ldots \mu_{12}\Phi_1^\dagger \Phi_2 + \mu_{12}^* \Phi_2^\dagger \Phi_1 \ .$$

Indeed, if one did not include such terms the presence of complex Yukawa couplings would induce such terms at one loop.

2 CP Violation in the Standard Model: Expectations and Challenges

The gauge sector of the $SU(3) \times SU(2) \times U(1)$ Standard Model contains no explicit phases since the gauge fields are in the adjoint representation, which is real, leading to real gauge couplings. Nevertheless, the nontrivial nature of the gauge theory vacuum [12] introduces a phase structure (θ vacua [13]) which allows for the presence of effective CP-violating interactions, involving the non Abelian gauge field strengths and their duals:

$$\mathcal{L}_{\text{CP viol.}} = \theta_{\text{strong}} \frac{\alpha_s}{8\pi} F_a^{\mu\nu} \tilde{F}_{a\mu\nu} \ + \ \theta_{\text{weak}} \frac{\alpha_2}{8\pi} W_a^{\mu\nu} \tilde{W}_{a\mu\nu} \ .$$

The weak vacuum angle θ_{weak} is actually irrelevant since the electroweak theory is chiral and through a chiral rotation this angle can be set to zero [14]. The phase angle θ_{strong}, on the other hand, is problematic. First of all, what contributes physically is not θ_{strong}, since this angle receives additional contributions from the weak interaction sector as a result of the chiral rotations that render the quark mass matrices diagonal. Thus, in reality, the CP-violating efffective interaction is

$$\mathcal{L}_{\text{CP viol.}} = \bar{\theta} \frac{\alpha_s}{8\pi} F_a^{\mu\nu} \tilde{F}_{a\mu\nu},$$

where $\bar{\theta} = \theta_{\text{strong}} + \text{Arg det M}$ and M is the quark mass matrix. The presence of such an interaction in the Standard Model gives rise to a large contribution to the neutron electric dipole moment. One has, approximately [15],

$$d_n \simeq \frac{e}{M_n} \left(\frac{m_q}{M_n}\right) \bar{\theta} \ ,$$

with m_q a typical light quark mass. Thus, to respect the existing experimental bounds on d_n [3], $\bar{\theta}$ must be extremely small:

$$\bar{\theta} \leq 10^{-9} - 10^{-10}.$$

[3] This is not quite true. In the SM there is also another phase related to the QCD vacuum angle which leads to a CP violating interaction involving the gluonic field strength and its dual. We return to this point in the next section.

Why this should be so is unclear and constitutes the strong CP problem [16].

There are three possible attitudes one can take regarding the strong CP problem:

i) One can just ignore this problem altogether. Afterall, $\bar{\theta}$ is yet another uncalculable parameter in the Standard Model, no different say than the unexplained ratio $m_e/m_t \sim 10^{-6}$. So why should one worry about this parameter explicitly?

ii) One can try to calculate $\bar{\theta}$ and thereby "explain" the size of the neutron electric dipole moment. To do so, one must imagine that CP is spontaneously broken, so that indeed $\bar{\theta}$ is a finite calculable quantity. However, as was mentioned earlier, then one runs into the domain wall problem. Models that avoid this problem and which, in principle, produce a tiny calculable $\bar{\theta}$ exist. However, they are quite recondite [9] and the price one pays for solving the strong CP problem this way is to introduce considerable hidden underlying structure beneath the Standard Model.

iii) One can try to dynamically remove $\bar{\theta}$ from the theory. This is my favorite solution, which I suggested long ago with Helen Quinn [17]. Quinn and I proposed solving the strong CP problem by imagining that the Standard Model has an additional global chiral symmetry. The presence of this, so called, $U(1)_{PQ}$ symmetry allows one to rotate away $\bar{\theta}$, much as the chiral nature of the $SU(2) \times U(1)$ electroweak theory allows one to rotate away θ_{weak}. However, this solution also requires that axions exist [18] and these elusive particles have yet to be detected [16]! An alternative possibility along this vein is that the Standard Model has a natural chiral symmetry built in, which removes $\bar{\theta}$ because $m_u = 0$ [19].However, this solution appears unlikely, as $m_u = 0$ is disfavored by current algebra analyses [20].

It is fair to say that there is no clear understanding of what to do about the strong CP problem at the moment. My own view is that the existence of this unresolved problem is something that should not be ignored. There is a message here and it may simply be that we do not understand CP violation at all!

In the Standard Model, with one Higgs doublet and three generations of quarks and leptons, besides the strong CP phase $\bar{\theta}$ there is only one other CP-violating angle in the theory. This is the combination of phases in the Yukawa couplings of the quarks to the Higgs doublet which remains after all redefinition of quark fields, leading to a diagonal mass matrix, are done. This weak CP-violating angle appears as a phase in the CKM mixing matrix, V, which details the coupling of the quarks to the charged W-bosons:

$$\mathcal{L}_{CC} = g_2 \bar{u}_i \gamma_\mu (1 - \gamma_5) V_{ij} d_j W^\mu \; + \; h.c. \; .$$

However, one does not really know if the complex phase present in the CKM matrix is responsible for the CP violating phenomena observed in the neutral Kaon system. Indeed, one does not know either whether there are further phases besides the CKM

phase. Nevertheless, it is remarkable that, as a result of the hierarchial structure of the CKM matrix and of other dynamical circumstances, one can **qualitatively** explain all we know experimentally about CP violation today on the basis of the CKM picture.

2.1 Testing the CKM Paradigm

In what follows, I make use of the CKM matrix in the parametrization adopted by the PDG [3] and expand the three real angles in the manner suggested by Wolfenstein [21] in powers of the sine of the Cabibbo angle λ. To order λ^3 one has then

$$V = \begin{vmatrix} 1 - \frac{\lambda^2}{2} & \lambda & A\lambda^3(\rho - i\eta) \\ \lambda & 1 - \frac{\lambda^2}{2} & A\lambda^2 \\ A\lambda^3(1 - \rho - i\eta) & -A\lambda^2 & 1 \end{vmatrix}$$

with A, ρ and η being parameters one needs to fix from experiments—with $\eta \neq 0$ signalling CP violation.[4]

This matrix, with is hierarchical interfamily structure, naturally accounts for the three principal pieces of independent information that we have today on CP violation. As we discussed earlier, these are:

i) The value of the mass mixing parameter $|\epsilon| \sim 10^{-3}$, which characterizes the strength of the K_L to K_S amplitude ratios.

ii) The small value of the ϵ' parameter which typifies direct ($\Delta S = 1$) CP violation, with the ratio $\epsilon'/\epsilon \leq 10^{-3}$.

iii) The very strong bounds on the electric dipole moments of the neutron and the electron, which give $d_e, d_n \leq 10^{-25}$ ecm.

One can "understand" the above three facts quite simply within the Standard Model and the CKM paradigm. In the model the parameter ϵ is determined by the ratio of the imaginary to the real part of the box graph of Fig. 1a. It is easy to check that this ratio is of order

$$\epsilon \sim \lambda^4 \sin\delta \sim 10^{-3} \sin\delta \ .$$

That is, ϵ is naturally small because of the suppression of interfamily mixing without requiring the CKM phase δ to be small.

The explanation of why ϵ'/ϵ is small is a bit more dynamical. Basically, this ratio is suppressed both because of the $\Delta I = 1/2$ rule and because ϵ' arises through the Penguin diagrams of Fig.1b. These diagrams involve the emission of virtual gluons (or photons [5]), which are Zweig suppressed [22]. Typically this gives

$$\frac{\epsilon'}{\epsilon} \sim \frac{1}{20} \cdot \left[\frac{\alpha_s}{12\pi} \ln \frac{m_t^2}{m_c^2}\right] \sim 10^{-3} \ .$$

[4] It is often convenient instead of using $\rho - i\eta$ to write this in terms of a magnitude and phase: $\rho - i\eta = \sigma e^{-i\delta}$, with δ being the CP violating CKM phase.

[5] The contribution of the electroweak Penguin diagrams are not suppressed by the $\Delta I = 1/2$ rule, but these diagrams are only of $O(\alpha)$, not $O(\alpha_s)$.

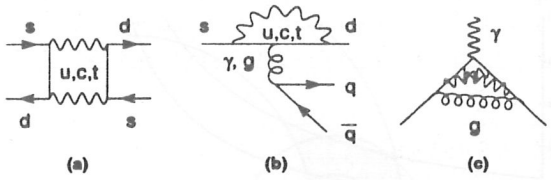

Figure 1: Graphs contributing to ϵ, ϵ' and $d_{q,e}$

Finally, in the CKM model the electric dipole moments are small since the first nonvanishing contributions [23] occur at three loops, as shown in Fig. 1c, leading to the estimate [24]

$$d_{q,e} \sim e m_{q,e} \left[\frac{\alpha^2 \alpha_s}{\pi^3}\right] \left[\frac{m_t^2 m_b^2}{M_W^6}\right] \lambda^6 \sin\delta \sim 10^{-32} \text{ ecm} .$$

One can, of course, use the precise value of ϵ measured experimentally to determine an allowed region for the parameters entering in the CKM matrix. Because of theoretical uncertainties in evaluating the hadronic matrix element of the $\Delta S = 2$ operator associated with the box graph of Fig. 1a, this parameter space region is rather large. Further restrictions on the allowed values of CKM parameters come from semileptonic B decays and from $B_d - \bar{B}_d$ mixing. Because the parameter A, related to V_{cb}, is better known, it has become traditional to present the result of these analyses as a plot in the $\rho - \eta$ plane. Fig. 2 shows the results of a recent analysis, done in collaboration with my student, K. Wang [25]. The input parameters used, as well as the range allowed for certain hadronic amplitudes and other CKM matrix elements is detailed in Table 1

Table 1: Parameters used in the $\rho - \eta$ analysis of [25]

$\lvert\epsilon\rvert$	=	$(2.26 \pm 0.02) \times 10^{-3}$	[3]
Δm_d	=	$(0.496 \pm 0.032) ps^{-1}$	[26]
m_t	=	$(174 \pm 10^{+13}_{-12})$ GeV	[27]
$\lvert V_{cb}\rvert$	=	0.0378 ± 0.0026	[28]
$\lvert V_{ub}\rvert/\lvert V_{cb}\rvert$	=	0.08 ± 0.02	[28]
B_K	=	0.825 ± 0.035	[29]
$\sqrt{B_d}\, f_{B_d}$	=	(180 ± 30) MeV	[30]

The resulting 1σ allowed contour emerging from the overlap of the three constraints coming from ϵ, $B_d - \bar{B}_d$ mixing and the ratio of $|V_{ub}|/|V_{cb}|$, shown in Fig.

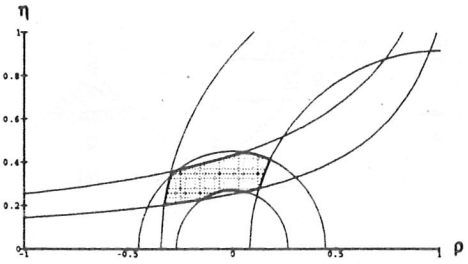

Figure 2: Constraints on the (ρ, η) plot

3, gives a roughly symmetric region around $\rho = 0$ within the ranges

$$0.2 \leq \eta \leq 0.5 \; ; \quad -0.4 \leq \rho \leq 0.4 \; .$$

As anticipated by our qualitative discussion this region implies that the CKM phase δ is large ($\rho = 0$ corresponds to $\delta = \pi/2$). One should note, however, that this analysis does not establish the CKM paradigm. Using only the B physics constraints one sees that in Fig. 2 there is also an overlap region for $\eta = 0$, which gives $\rho = -0.33 \pm 0.08$ [25]. So one can still imagine that ϵ is due to some other CP violating interaction, as in the superweak model [10], with the CKM phase δ being very small. As Wang and I [25] discussed, one may perhaps eliminate this possibility by improving the bounds on $B_s - \bar{B}_s$ mixing to $\Delta m_s \geq 10$ ps^{-1}. Since the present LEP bound from ALEPH is $\Delta m_s \geq 6$ ps^{-1} [31], this is not going to be easy. Much more promising, however, is to try to establish the correctedness of the CKM paradigm by looking at further tests of CP violation, both in the Kaon system and by meausuring CP-violating asymmetries in B-decays.

In principle, one can obtain quantitative tests of the CKM model purely with Kaon experiments. However, the needed experiments are very challenging, either due to the high precision required or due to the rarity of the processes to be studied. Furthermore, the analysis of these results is also theoretically very difficult, since it requires better estimates of hadronic matrix elements than what we have at present. A good example of both of these challenges is provided by ϵ'/ϵ. The present data on this ratio is inconclusive, with the result obtained at Fermilab [32]:

$$\mathrm{Re}\,\frac{\epsilon'}{\epsilon} = (7.4 \pm 5.2 \pm 2.9) \times 10^{-4} \quad [\mathrm{E731}] \; ,$$

being consistent with zero within the error, while the result of the NA31 experiment at CERN [33] giving a non-zero value to 3σ:

$$\mathrm{Re}\,\frac{\epsilon'}{\epsilon} = (23.0 \pm 3.6 \pm 5.4) \times 10^{-4} \quad [\mathrm{NA31}] \; .$$

Theoretically, the predictions for ϵ'/ϵ are dependent both on the value of the CKM matrix elements and, more importantly, on an estimate of certain hadronic matrix elements.

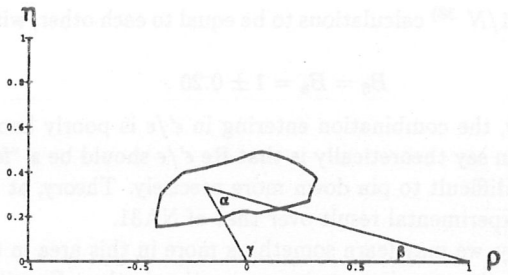

Figure 3: Allowed region in the $\rho - \eta$ plane. Also shown in the plot is a possible unitarity triangle.

2.1.1 *Prospects for meausuring* $\frac{\epsilon'}{\epsilon}$

There has been considerable activity recently to try to narrow down the expectations for ϵ'/ϵ in the Standard Model. To describe the theoretical status here, I find it useful to make use of an approximate formula for this ratio derived by Buras and Lautenbacher [34]. These authors express the real part of this ratio as the sum of two terms [6]

$$\mathrm{Re}\,\frac{\epsilon'}{\epsilon} \simeq 3.6 \times 10^{-3} A^2 \eta \left[B_6 - 0.175 \left(\frac{m_t^2}{M_W^2} \right)^{0.93} B_8 \right] .$$

Here B_6 and B_8 are quantities related to the matrix elements of the dominant gluonic and electroweak Penguin operators, respectively. The electroweak Penguin contribution is suppressed relative to the gluonic Penguin contribution by a factor of α/α_s. However, as remarked earlier, it does not suffer from the $\Delta I = 3/2$ suppression and so one gains back a factor of about 20. Furthermore, as Flynn and Randall [36] first noted, the contribution of these terms can become significant for large top mass because it grows approximately as m_t^2.

The result of the CKM analysis presented earlier brackets $A^2\eta$ in the range

$$0.12 \leq A^2\eta \leq 0.31 .$$

For $m_t = 175$ GeV the square bracket in the Buras-Lautenbacher formula reduces to $[B_6 - 0.75 B_8]$. Hence one can write the expectation from theory for ϵ'/ϵ as

$$4.3 \times 10^{-4}[B_6 - 0.75 B_8] \leq \mathrm{Re}\,\frac{\epsilon'}{\epsilon} \leq 11.2 \times 10^{-4}[B_6 - 0.75 B_8] .$$

Because the top mass is so large, the predicted value for ϵ'/ϵ depends rather crucially on **both** B_6 and B_8. These (normalized) matrix elements have been estimated by

[6] Because the difference between the $I = 0$ and $I = 2$ $\pi\pi$ phase shifts is also near 45° [35], to a good approximation $\epsilon'/\epsilon \simeq \mathrm{Re}\,\epsilon'/\epsilon$.

both lattice [37] and $1/N$ [38] calculations to be equal to each other, with an individual error of $\pm 20\%$:

$$B_6 = B_8 = 1 \pm 0.20 \, .$$

Thus, unfortunately, the combination entering in ϵ'/ϵ is poorly known. It appears that the best one can say theoretically is that Re ϵ'/ϵ should be a "few" times 10^{-4}, with a "few" being difficult to pin down more precisely. Theory, at any rate, seems to favor the E731 experimental result over that of NA31.

Fortunately, we may learn something more in this area in the near future. There are 3rd generation experiments in preparation both at Fermilab (KTeV) and CERN (NA48). These experiments should begin taking data in a year or so and are designed to reach statistical and systematic accuracy for ϵ'/ϵ at the level of 10^{-4}. The Frascati Φ factory DAPHNE, which should begin operations in 1997, in principle, can also provide interesting information for ϵ'/ϵ. At DAPHNE one will need an integrated luminosity of $\int \mathcal{L} \, dt = 10 \text{ fb}^{-1}$ to arrive at a statistical sensitivity for ϵ'/ϵ at the level of 10^{-4}. However, if this statistical sensitivity is reached, the systematic uncertainties will be quite different than those at KTeV and NA48, providing a very useful cross-check. It is important to remark that, irrespective of detailed theoretical predictions, the observation of a non-zero value for ϵ'/ϵ at a significant level would provide direct evidence for $\Delta S = 1$ CP violation and would rule out a superweak explanation for the observed CP violation in the neutral K sector.

2.2 Rare Kaon Decays

There are alternatives to the ϵ'/ϵ measurement which could reveal $\Delta S = 1$ (direct) CP violation. However, these alternatives involve daunting experiments [39], which are probably out of reach in the near term. Whether these experiments can (or will?) eventually be carried out is an open question. Nevertheless, it seems worthwhile here to try to outline some of the theoretical expectations for these meausurments.

2.2.1 K_S decays

CP Lear already, and DAPHNE soon, will enable a more thorough study of K_S decays by more efficient tagging. The decay $K_S \to 3\pi^o$ is CP-violating, while the $K_S \to \pi^+\pi^-\pi^o$ mode has both CP-conserving and CP-violating pieces. However, even in this case the CP-conserving piece is small and vanishes in the center of the Dalitz plot. Hence one can extract information about CP violation from $K_S \to 3\pi$ decays. The analogue K_S/K_L amplitude ratios to η_{+-} and η_{oo} for $K \to 3\pi$ have both $\Delta S = 1$ and $\Delta S = 2$ pieces:

$$\eta_{ooo} = \epsilon + \epsilon'_{ooo} \; ; \;\; \eta_{+-o} = \epsilon + \epsilon'_{+-o} \, .$$

However, in contrast to what obtains in the $K \to 2\pi$ case, here the $\Delta S = 1$ pieces can be larger. Cheng [40] gives estimates for ϵ'_{+-o}/ϵ and ϵ'_{ooo}/ϵ of $O(10^{-2})$, while others are more pessimistic [41]. Even so, there does not appear to be any realistic prospects in the near future to probe for $\Delta S = 1$ CP-violating amplitudes in $K_S \to 3\pi$. For

instance, at DAPHNE even with an integrated luminosity of 10 fb^{-1} one can only reach an accuracy for η_{+-o} and η_{ooo} of order 3×10^{-3}, which is at the level of ϵ not ϵ'.

2.2.2 *Asymmetries in charged K-decays*

CP violating effects involving charged Kaons can only be due to $\Delta S = 1$ transitions, since $K^+ \leftrightarrow K^-$ $\Delta S = 2$ mixing is forbidden by charge conservation. A typical CP-violating effect in charged Kaon decays necessitates a comparison between K^+ and K^- processes. However, a CP-violating asymmetry between these processes can occur only if there are at least two decay amplitudes involved and these amplitudes have **both** a relative weak CP-violating phase and a relative strong rescattering phase between each other. Thus the resulting asymmetry necessarily depends on strong dynamics.

To appreciate this fact, imagine writing the decay amplitude for K^+ decay to a final state f^+ as

$$A(K^+ \to f^+) = A_1 \, e^{i\delta_{W_1}} e^{i\delta_{S_1}} + A_2 \, e^{i\delta_{W_2}} e^{i\delta_{S_2}} \, .$$

Then the corresponding amplitude for the decay $K^- \to f^-$ is

$$A(K^- \to f^-) = A_1 \, e^{-i\delta_{W_1}} e^{i\delta_{S_1}} + A_2 \, e^{-i\delta_{W_2}} e^{i\delta_{S_2}} \, .$$

That is, the strong rescattering phases are the same but one complex conjugates the weak amplitudes. From the above, one sees that the rate asymmetry between these processes is

$$\begin{aligned} \mathcal{A}(f^+; f^-) &= \frac{\Gamma(K^+ \to f^+) - \Gamma(K^+ \to f^-)}{\Gamma(K^+ \to f^+) + \Gamma(K^- \to f^-)} \\ &= \frac{2A_1 A_2 \sin(\delta_{W_2} - \delta_{W_1}) \sin(\delta_{S_2} - \delta_{S_1})}{A_1^2 + A_2^2 + 2A_1 A_2 \cos(\delta_{W_2} - \delta_{W_1}) \cos(\delta_{S_2} - \delta_{S_1})} \, . \end{aligned}$$

Unfortunately, detailed calculations in the standard CKM paradigm for rate asymmetries and asymmetries in Dalitz plot parameters for various charged Kaon decays give quite tiny predictions. This can be qualitatively understood as follows. The ratio $A_2 \sin(\delta_{W_2} - \delta_{W_1})/A_1$ is typically that of a Penguin amplitude to a weak decay amplitude and so is of order ϵ'/ϵ. Furthermore, because of the small phase space for $K \to 3\pi$ decays, or because one is dealing with electromagnetic rescattering in $K \to \pi\pi\gamma$, the rescattering contribution suppress these asymmetries even more. Table 2 gives typical predictions, contrasting them to the expected reach of the Frascati Φ factory with $\int \mathcal{L} \, dt = 10$ fb^{-1}. For the $K \to 3\pi$ decays, Belkov *et al.* [42] give numbers at least a factor of 10 above those given in Table 2. However, these numbers are predicated on having very large rescattering phases which do not appear to be realistic [43]. One is lead to conclude that, if the CKM paradigm is correct, it is unlikely that one will see a CP-violating signal in charged Kaon decays.

Table 2: Predictions for Asymmetries in $K^{\pm}$ Decays

Asymmetry	Prediction	Φ Factory Reach
$\mathcal{A}(\pi^+\pi^+\pi^-;\pi^-\pi^-\pi^+)$	5×10^{-8} [44]	3×10^{-5}
$\mathcal{A}(\pi^+\pi^o\pi^o;\pi^-\pi^o\pi^o)$	2×10^{-7} [44]	5×10^{-5}
$\mathcal{A}_{\rm Dalitz}(\pi^+\pi^+\pi^-;\pi^-\pi^+\pi^+)$	2×10^{-6} [44]	3×10^{-4}
$\mathcal{A}_{\rm Dalitz}(\pi^+\pi^o\pi^o;\pi^-\pi^o\pi^o)$	1×10^{-6} [44]	2×10^{-4}
$\mathcal{A}(\pi^+\pi^o\gamma;\pi^-\pi^o\gamma)$	10^{-5} [45]	2×10^{-3}

2.2.3 $K_L \to \pi^o\ell^+\ell^-$; $K_L \to \pi^o\nu\bar{\nu}$

Perhaps more promising are decays of the K_L to π^o plus lepton pairs. If the lepton pair is charged, then the process has a CP conserving piece in which the decay proceeds via a 2γ intermediate state. Although there was some initial controversy [46], the rate for the process $K_L \to \pi^o\ell^+\ell^-$ arising from the CP-conserving 2γ transitiion is probably at, or below, the 10^{-12} level [47]:

$$B(K_L \to \pi^o\ell^+\ell^-)_{\rm CP\ cons.} = (0.3 - 1.2)\times10^{-12}.$$

Thus this contribution is just a small correction to the dominant CP-violating amplitude arising from an effective spin 1 virtual state, $K_L \to \pi^o J^*$. Since $\pi^o J^*$ is CP even, this part of the amplitude is CP-violating. It has two distinct pieces [48]: an indirect contribution from the CP even piece (ϵK_1) in the K_L state, and a direct $\Delta S = 1$ CP-violating piece coming from the K_2 part of K_L:

$$A(K_L \to \pi^o J^*) = \epsilon A(K_1 \to \pi^o J^*) + A(K_2 \to \pi^o J^*)\ .$$

To isolate the interesting direct CP contribution in this process requires understanding first the size of the indirect contribution. The amplitude $A(K_1 \to \pi^o J^*)$ could be determined absolutely if one had a measurement of the process $K_S \to \pi^o\ell^+\ell^-$. Since this is not at hand, at the moment one has to rely on various guesstimates. These give the following range for the indirect CP-violating branching ratio [49]

$$B(K_L \to \pi^o\ell^+\ell^-)^{\rm indirect}_{\rm CP\ violating} = (1.6 - 6)\times10^{-12}\ ,$$

where the smaller number is the estimate coming from chiral perturbation theory, while the other comes from relating $A(K_1 \to \pi^o J^*)$ to the analogous amplitude for charged K decays.

The calculation of the direct CP-violating contribution to the process $K_L \to \pi^o\ell^+\ell^-$, as a result of electroweak Penguin and box contributions and their gluonic corrections, is perhaps the one that is most reliably known. The branching ratio obtained by Buras, Lautenbacher, Misiak and Münz in their next to leading order calculation of this process [50] is

$$B(K_L \to \pi^o\ell^+\ell^-)^{\rm direct}_{\rm CP-violating} = (5 \pm 2)\times10^{-12}\ ,$$

where the error arises mostly from the imperfect knowledge of the CKM matrix.

Experimentally one has the following 90% C.L. for the two $K_L \to \pi^o \ell^+ \ell^-$ processes:

$$B(K_L \to \pi^o \mu^+ \mu^-) < 5.1 \times 10^{-9}$$
$$B(K_L \to \pi^o e^+ e^-) < 1.8 \times 10^{-9}$$

The first limit comes from the E799 experiment at Fermilab [51], while the second limit combines the bounds obtained by the E845 experiment at Brookhaven [52] and the E799 Fermilab experiment [53]. Forthcoming experiments at KEK and Fermilab should be able to improve these limits by at least an order of magnitude[7], if they can control the dangerous background arising from the decay $K_L \to \gamma\gamma e^+ e^-$ [54]. Even more distant experiments in the future may actually reach the level expected theoretically for the $K_L \to \pi^o e^+ e^-$ rate [55]. However, it will be difficult to unravel the direct CP-violating contribution from the indirect CP-violating contribution, unless the $K_S \to \pi^o e^+ e^-$ rate is also measured simultaneously.

In this respect, the process $K_L \to \pi^o \nu\bar{\nu}$ is very much cleaner. This process is purely CP-violating, since it has no 2γ contribution. Furthermore, it has a tiny indirect CP contribution, since this is of order ϵ times the already small $K^+ \to \pi^+ \nu\bar{\nu}$ amplitude [56]. Next to leading QCD calculations for the direct rate have been carried out by Buchalla and Buras [57], who give the following approximate formula for the branching ratio for this process

$$B(K_L \to \pi^o \nu\bar{\nu}) = 8.2 \times 10^{-11} A^4 \eta^2 \left(\frac{m_t}{M_W}\right)^{2.3} .$$

This value is very far below the present 90% C.L. obtained by the E799 experiment at Fermilab [58]

$$B(K_L \to \pi^o \nu\bar{\nu}) < 5.8 \times 10^{-5} .$$

KTeV should be able to lower this bound substantially, perhaps to the level of 10^{-8}, but this still leaves a long way to go!

2.2.4 $K^+ \to \pi^+ \nu\bar{\nu}$

The last process I would like to consider in this section is the charged Kaon analogue to the process just discussed. Although the decay $K^+ \to \pi^+ \nu\bar{\nu}$ is not CP violating, it is sensitive to $|V_{td}|^2 \simeq A^2\lambda^6[(1-\rho)^2 + \eta^2]$ and so, indirectly, it is sensitive to the CP violating CKM parameter η. For the CP violating decay $K_L \to \pi^o \nu\bar{\nu}$ the electroweak Penguin and box contributions are dominated by loops containing top quarks. Here, because one is not looking at the imaginary part, one cannot neglect altogether the contribution from charm quarks. If one could do so, the branching ratio formula for $K^+ \to \pi^+ \nu\bar{\nu}$ would be given by an analogous formula to that for $K_L \to \pi^o \nu\bar{\nu}$ but with $\eta^2 \to \eta^2 + (1-\rho)^2$.

[7] The goal of the KEK 162 experiment is to get to a BR of $O(10^{-10})$ for this mode, while KTeV hopes to push this BR down to 5×10^{-11}.

Because m_t is large, the $K^+ \to \pi^+ \nu\bar{\nu}$ branching ratio is not extremely sensitive to the contribution of the charm-quark loops [59]. Furthermore, when next to leading QCD corrections are computed the sensitivity of the result to the precise value of the charm-quark mass is reduced considerably [60]. Buras *et al.* [61] give the following approximate formula for the $K^+ \to \pi^+ \nu\bar{\nu}$ branching ratio

$$B(K^+ \to \pi^+ \nu\bar{\nu}) = 2 \times 10^{-11} A^4 \left[\eta^2 + \frac{2}{3}(\rho^e - \rho)^2 + \frac{1}{3}(\rho^\tau - \rho)^2\right] \left(\frac{m_t}{M_W}\right)^{2.3} .$$

In the above the parameters ρ^e and ρ^τ differ from unity because of the presence of the charm-quark contributions. Taking $m_t = 175$ GeV and $m_c(m_c) = 1.30 \pm 0.05$ GeV [62], Buras *et al.* [61] find that ρ^e and ρ^τ lie in the ranges

$$1.42 \leq \rho^e \leq 1.55 \; ; \;\; 1.27 \leq \rho^\tau \leq 1.38 \; .$$

Using the range of η and ρ determined by the CKM analysis discussed earlier gives about a 40% uncertainty for the $K^+ \to \pi^+ \nu\bar{\nu}$ branching ratio, leading to the expectation

$$B(K^+ \to \pi^+ \nu\bar{\nu}) = (1 \pm 0.4) \times 10^{-10} \; .$$

This number is to be compared to the best present limit coming from the E787 experiment at Brookhaven. Careful cuts must be made in the accepted π^+ range and momentum to avoid potentially dangerous backgrounds, like $K^+ \to \pi^+ \pi^o$ and $K^+ \to \mu^+ \pi^o \nu$. There is a new preliminary result for this branching ratio [63]

$$B(K^+ \to \pi^+ \nu\bar{\nu}) < 3 \times 10^{-9} \quad (90\% \text{ C.L.})$$

which updates the previously published result from the E787 collaboration [64]. This value is still about a factor of 30 from the interesting CKM model range, but there are hopes that one can get close to this sensitivity in the present run of this experiment.

2.3 The Promise of B-decay CP Violation

If the CKM paradigm is correct, the analysis of current constraints on the CKM matrix shows that the CP-violating phase δ is sizable. The reason why one has **small** CP-violating effects in the Kaon sector is solely due to the interfamily mixing suppression. In B_d and B_s decays one can involve all three generations directly and, in certain cases, one can obviate this supression altoghether [65]. Thus the study of CP violation in B-decays appears very promising.

To produce CP-violating effects, as usual, one has to have interference between two amplitudes that have different CP-violating phases. Because one is interested in looking for potentially large sources of CP violation in B-decays, it is important to identify where in the B system sizable phases may reside. Within the CKM paradigm there are two places where large phases appear. The first of these is

the relative phase between the $|B_d>$ and $|\bar{B}_d>$ states, which make up the neutral B mass eigenstates:

$$|B_{d\pm}> \simeq \frac{1}{\sqrt{2}}[(1+\epsilon_{B_d})|B_d> \pm (1-\epsilon_{B_d})|\bar{B}_d>] \ .$$

This $B_d - \bar{B}_d$ mixing phase arises from a box-graph similar to that of Fig. 1a. Here, however, this graph is dominated by the contribution of the top quark loop and one has that

$$\frac{(1-\epsilon_{B_d})}{(1+\epsilon_{B_d})} \simeq \frac{V_{td}}{V_{td}^*} = e^{-2i\beta} \ ,$$

where β is the phase of the td matrix element of the CKM matrix ($V_{td} = |V_{td}|e^{-i\beta}$). If the CKM phase δ is large so is, in general, β since

$$\tan\ \beta = \frac{\sigma \sin\ \delta}{1 - \sigma \cos\ \delta} = \frac{\eta}{1-\rho} \ .$$

The second place where a large phase appears is in any process involving, at the quark level, a $b \to u$ transition since $V_{ub} = |V_{ub}|e^{-i\delta}$ provides precisely a measure of the CKM phase.

The potentially large $B_d - \bar{B}_d$ CP-violating phase β is a prediction of the CKM paradigm which can be well tested, since this phase is unpolluted by strong interaction effects. This is also the case for the corresponding mixing phase arising from $B_s - \bar{B}_s$ mixing. However, in this case the CKM prediction is that this phase should vanish, since V_{ts} is approximately real. So for the case of B_s decays the relevant tests are null tests. At any rate, because of $B_d - \bar{B}_d$ mixing, a state $|B_{d\ \mathrm{phys}}(t)>$ which at $t = 0$ was a pure $|B_d>$ state, evolves in time into a superposition of $|B_d>$ and $|\bar{B}_d>$ states:

$$|B_{d\ \mathrm{phys}}(t)> = e^{-im_{B_d}t}e^{-\Gamma_{B_d}t/2}[\cos \Delta m_d t/2\ |B_d> + ie^{-2i\beta} \sin \Delta m_d t/2\ |\bar{B}_d>] \ .$$

A similar formula applies for B_s decays.

It is also possible to isolate cleanly the CP-violating phases appearing at the quark level by comparing the decays of B mesons into some definite final state f to the corresponding transition of $\bar{B}$ mesons to the charged-conjugate final state $\bar{f}$. If these transitions are dominated by a single quark decay amplitude [66], so that

$$A(B \to f) = a_f e^{i\delta_f}; \qquad A(\bar{B} \to \bar{f}) = a_f^* e^{i\delta_f} \ ,$$

where δ_f is a strong rescattering phase, then the ratio of these two amplitudes will be directly sensitive to the quark decay phase. In these circumstances, for decays involving $b \to u$ transitions, the ratio

$$\frac{A(\bar{B} \to \bar{f})}{A(B \to f)} \simeq \frac{A(b \to uq\bar{q}')}{A(\bar{b} \to \bar{u}\bar{q}q')} = \frac{V_{ub}}{V_{ub}^*} = e^{-2i\delta}$$

is a measure of the CP-violating phase δ. On the other hand, the corresponding ratio of amplitudes which involve a $b \to c$ transition at the quark level will contain no large CP-violating phase at all, since V_{cb} is real.

In view of the above considerations, the best way to study CP violation in neutral B-decays is through a comparison of the time evolution of decays of states "born" as a B_d (or a B_s) into final states f, which are CP self-conjugate [$\bar{f} = \pm f$], to the corresponding time evolution of states which were born as a $\bar{B}_d$ (or a $\bar{B}_s$) and decay to $\bar{f}$ [67]. A straightforward calculation gives for the time dependent rates for these processes the expressions:

$$\Gamma(B_{phys}(t) \to f) = \Gamma(B \to f) e^{-\Gamma_B t}[1 - \eta_f \lambda_f \sin \Delta m_B t]$$

$$\Gamma(\bar{B}_{phys}(t) \to \bar{f}) = \Gamma(B \to f) e^{-\Gamma_B t}[1 + \eta_f \lambda_f \sin \Delta m_B t]$$

In the above η_f characterizes the CP parity of the state f, with $\bar{f} = \eta_f f$ and $\eta_f = \pm 1$, while λ_f encapsulates the mixing and decay CP violation information for the process. For all decays $B \to f$ which are dominated by just **one** weak decay amplitude the parameter λ_f is free of strong interaction complications and takes one of four values, depending on whether one is dealing with a B_d or B_s decay and on whether the decay processes at the quark level involves a $b \to c$ or a $b \to u$ transition. In these circumstances λ_f meausures purely CKM information and one finds

$$\begin{aligned}
&\lambda_f = \sin 2\beta && [B_d \text{ decays; } b \to c \text{ transition}] \\
&\lambda_f = \sin 2(\beta + \delta) \equiv \sin 2\alpha && [B_d \text{ decays; } b \to u \text{ transition}] \\
&\lambda_f = 0 && [B_s \text{ decays; } b \to c \text{ transition}] \\
&\lambda_f = \sin 2\delta \equiv \sin 2\gamma && [B_s \text{ decays; } b \to u \text{ transition}] .
\end{aligned}$$

The angles α, β and γ entering in the above equations have a very nice geometrical interpretation [68]. They are the angles of the, so called, unitarity triangle in the $\rho - \eta$ plane, whose base is along the ρ-axis going from $\rho = 0$ to $\rho = 1$ and whose apex is the point (ρ, η). That this is the case can be easily deduced by considering the bd matrix element of the CKM unitarity equation ($V^\dagger V = 1$):

$$V_{ub}^* V_{ud} + V_{cb}^* V_{cd} + V_{tb}^* V_{td} = 0 .$$

To leading order in λ, the above equation reduces to

$$V_{ub}^* + V_{td} = A\lambda^3$$

which, upon dividing by $A\lambda^3$, is precisely the equation describing the unitarity triangle. One possible unitarity triangle, with the angles α, β and γ identified, is shown in Fig. 3.

Because our present knowledge of the CKM matrix still allows a considerable range for ρ and η, as shown in Fig. 3, there is considerable uncertainty on what to expect for $\sin 2\alpha$, $\sin 2\beta$ and $\sin 2\gamma$. Nevertheless, from an analysis of the allowed region in the $\rho - \eta$ plane, one can infer the allowed ranges for the unitarity triangle angles. In general, one finds that while both $\sin 2\alpha$ and $\sin 2\gamma$ can vanish, $\sin 2\beta$ is both **nonvanishing and large** [70]. This is illustrated in Fig. 4, taken from

my recent examination of this question with Wang [25], which plots the presently allowed region in the $\sin 2\alpha - \sin 2\beta$ plane. One sees from this figure that

$$0.23 \leq \sin 2\beta \leq 0.84 .$$

Thus, in contrast to CP violation phenomena in the Kaon system, for the B system within the CKM paradigm there are places where one expects to see large effects.

From the above discussion, it is clear that a particularly clean test of the CKM paradigm would be provided by the meausurement of $\sin 2\beta$, via the observation of a difference in the rates of specific B_d and $\bar{B}_d$ decays to CP self-conjugate states which involve a $b \to c$ transition. A favored mode to study is the decay $B_d \to \psi K_S$ along with its conjugate [71]. This decay has a largish branching ratio [3] and quite a distinct signature from the leptonic decay of the ψ. Furthermore, one can argue that this decay is quite clean theoretically. Recall that the identification of λ_f with one of the angles of the unitarity triangle required that the decay rate for the process $B \to f$ be dominated by a single decay amplitude. This, in general, is only approximately true. For instance, for the process in question, at the quark level both a $b \to c$ decay graph and a $b \to s$ Penguin graph contribute. However, although this decay involves more than one amplitude, both of these amplitudes have the same weak decay phase [72]. The amplitude involving the quark decay graph has no weak phase since it involves a $b \to c$ transition. This is also true for the $b \to s$ Penguin graph, since this graph is dominated by the top loop contribution which is dominantly real. Hence, effectively, the ratio of $A(\bar{B}_d \to \psi K_S)$ to $A(B_d \to \psi K_S)$ is, to a very good approximation, unity and $\lambda_{\psi K_S}$ indeed meausures $\sin 2\beta$.

Even though $\sin 2\beta$, at least in the CKM paradigm, is large, the meausurement of $\lambda_{\psi K_S}$ is far from trivial, since one must be able to determine whether the decaying state was born as a B_d or a $\bar{B}_d$ and one must have sufficient rate to detect the produced ψ though its small leptonic decay mode. Nevertheless, it is clear that future meausurements of this and allied decay modes (like $B_d \to \psi K^* \to \psi K_S \pi$ [73]) perhaps at HERA-B, but certainly at the B factories under construction at SLAC and KEK and eventually in hadron colliders, offers an excellent chance of verifying- or put into question- the CKM paradigm.

The prospects of meausuring the other two angles of the unitarity triangle, α and γ, and thus of checking the CKM prediction $\alpha + \beta + \gamma = \pi$, appear more difficult. These meausurments are, nevertheless, quite important. As Winstein [69] has pointed out, even if one were to meausure a large value for $\sin 2\beta$ this still does not totally exclude a superweak explanation. One could imagine a perverse superweak model which, somehow, contained a small $\Delta S = 2$ CP-violating mixing phase, of $O(\epsilon)$, but a large $\Delta B = 2$ CP-violating mixing phase, 2β. This model can be ruled out by meausuring the angle α independently since, as there are no decay phases, it predicts that $\sin 2\beta = \sin 2\alpha$. As Fig. 4 shows, this "superweak' prediction is not excluded by present day data. Thus, if by chance, future meausurements of α and β were to fall on the superweak line one would still need a measurement of γ

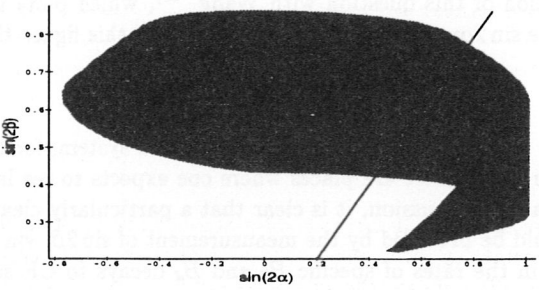

Figure 4: Plot of the allowed region in the $\sin 2\alpha - \sin 2\beta$ plane. The vertical line corresponds to the superweak prediction $\sin 2\alpha = \sin 2\beta$ [69].

to settle the issue [8].

Most likely, the decay mode $B_d \to \pi^+\pi^-$ is the process that is best suited to study the angle α [71]. However, the branching ratio for this mode is not yet totally in hand, but is probably quite small, of $O(10^{-5})$ [9]. This mode also may suffer some Penguin pollution, with estimates ranging from 1 % to 10 % in the amplitude [72]. The CLEO [74] indications that the branching ratio of $B_d \to \pi K$ is approximately the same as that for $B_d \to \pi\pi$ give one already some assurances that the Penguin amplitude in $B_d \to \pi^+\pi^-$ cannot dominate the process, since this amplitude is smaller by a factor of $|V_{td}|/|V_{ts}|$ compared to the $B_d \to \pi K$ amplitude. Furthermore, in principle, one can isolate the contribution of the Penguin graphs in the process $B_d \to \pi^+\pi^-$ by meausuring in addition the decays $B_d \to \pi^o\pi^o$ and $B^+ \to \pi^+\pi^o$ [75]. These extra meausurements allow for a complete isospin analysis of the amplitudes entering in these two body decays and an isolation of the relative rescattering phases. Similar techniques [76] may allow the extraction of the angle α in other decay modes, like $B_d \to \rho\pi$, which are not CP self-conjugate.

The determination of the angle γ is even more problematic. In principle, this angle can be determined by studying the time evolution of certain B_s decays. Here, perhaps, the best mode to study would be the decay $B_s \to \pi^o K_S$. However, at the asymmetric B factories now under construction, meausurements of B_s decays are unlikely. These colliders are optimized to operate at the $\Upsilon(4s)$ and running above the B_s production threshold will entail substantial loss of luminosity. Thus a determination of $\sin 2\gamma$ from B_s decays will have to await dedicated experiments at hadron colliders. One may, however, be able to determine γ, and thus the CKM phase δ, before that by utilizing different techniques. For instance, Gronau and

[8] In superweak models the angle 2γ is the phase associated with $B_s - \bar{B}_s$ mixing and does not necessarily vanish. However, in these models all B_s decays to CP self-conjugate states, irrespective of whether they involve a $b \to u$ or a $b \to c$ transition, should produce $\lambda_f = \gamma$.

[9] Recently, CLEO has observed a few B_d decays into pairs of light mesons and has been able to determine the branching ratio for the sum of the decay rates into both πK and $\pi\pi$ final states: $BR(B_d \to \pi K + \pi\pi) = (1.8 \pm 0.6 \pm 0.2) \times 10^{-5}$ [74].

Wyler [77], have shown that one could, in principle, extract γ by studying the charged B decays $B^{\pm} \to DK^{\pm}$ and their neutral counterparts, using isospinology to isolate the rescattering phases. It remains to be seen, however, whether this approach can really bear fruit in the presence of experimental errors.

3 Looking for new CP-violating phases

I would like to argue now a little more broadly about tests of CP violation. Obviously, it is very important to check whether the CKM paradigm is correct. Positive signals for $\epsilon'/\epsilon \neq 0$ will indicate the general validity of the CKM picture, since they require the presence of a $\Delta S = 1$ phase. However, given the large theoretical uncertainty on the value of this quantity, it is clear that values of ϵ'/ϵ consistent with zero at the 10^{-4} level cannot disprove this picture. In my view, it is likely that what will provide the crucial smoking gun for the CKM paradigm are searches for CP violation in the B system. The detection of the expected large asymmetry in $B_d \to \psi K_S$ decays is of paramount importance, with the meausurement of the other angles in the unitarity triangle and of rare Kaon decays providing eventually a more detailed picture. However, whether the CKM picture is (essentially) correct or not, it is also importat to mount experiments which may provide the first glimpse at **other** CP-violating phases, besides the CKM phase δ. Of course, if the CKM picture is incorrect then one knows that at least some of these new phases are superweak in nature, arising in the $\Delta S = 2$ (and, perhaps, in the $\Delta B = 2$) sectors. Even if the CKM paradigm is essentially correct, there may be other phases which produce small violations in the fermion mixing matrix but which are important elsewhere.

Indeed, there are good theoretical arguments for having further CP-violating phases, besides the CKM phase δ. For instance, to establish a matter-antimatter asymmetry in the Universe one needs to have processes which involve CP violation [6]. If the origin of this asymmetry comes from processes at the GUT scale, then, in general, the GUT interactions contain further CP-violating phases besides the CKM phase δ [78]. If this asymmetry is established at the electroweak scale [79], then most likely one again needs further phases, both because intrafamily suppression gives not enough CP violation in the CKM case to generate the asymmetry and because one needs to have more than one Higgs doublet [80]. Indeed this last point gives the fundamental reason why one should expect to have further CP-violating phases, besides the CKM phase δ. It is likely that the standard model is part of a larger theory. For instance, supersymmetric extensions of the SM have been much in vogue lately. Any such extensions will introduce further particles and couplings and thus, by the simple corollary mentioned in the Introduction, they will introduce new CP-violating phases.

The best place to look for non-CKM phases is in processes where CP violation within the CKM paradigm is either vanishing or very suppressed. One such example is provided by experiments aimed at measuring the electric dipole moments of the neutron or the electron, since electric dipole moments are predicted to be extremely small in the CKM model. Another example concerns measure-

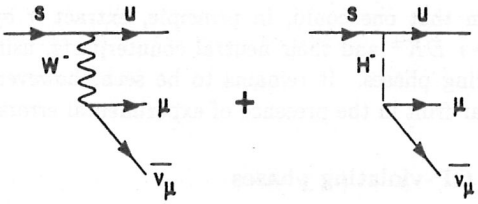

Figure 5: Graphs contributing to $\langle P_\perp^\mu \rangle$

ments of the transverse muon polarization $\langle P_\perp^\mu \rangle$ in $K_{\mu 3}$ decays, which vanishes in the CKM paradigm [81]. The transverse muon polarization measures a T-violating triple correlation [82]

$$\langle P_\perp^\mu \rangle \sim \langle \vec{s}_\mu \cdot (\vec{p}_\mu \times \vec{p}_\pi) \rangle \ .$$

In as much as one can produce such an effect also as a result of final state interactions (FSI) this is not a totally clean test for new CP-violating phases. With two charged particles in the final state, like for the decay $K_L \to \pi^- \mu^+ \nu_\mu$, one expects FSI to give typically $\langle P_\perp^\mu \rangle_{FSI} \sim \alpha/\pi \sim 10^{-3}$ [83]. However, for the process $K^+ \to \pi^o \mu^+ \nu_\mu$ with only one charged particle in the final state, the FSI effects should be much smaller. Indeed, Zhitnitski [84] estimates for this proceses that $\langle P_\perp^\mu \rangle_{FSI} \sim 10^{-6}$. So a $\langle P_\perp^\mu \rangle$ measurement in the $K^+ \to \pi^o \mu^+ \nu_\mu$ decay is a good place to test for additional CP-violating phases.

The transverse muon polarization $\langle P_\perp^\mu \rangle$ is particularly sensitive to scalar interactions and thus is a good probe of CP-violating phases arising from the Higgs sector [85]. One can write the effective $K_{\mu 3}$ amplitude [86] as

$$A = G_F \sin\theta_c f_+(q^2) \left\{ p_K^\mu \bar{\mu} \gamma_\mu (1-\gamma_5) \nu_\mu + f_S(q^2) m_\mu \bar{\mu} (1-\gamma_5) \nu_\mu \right\} \ .$$

Then

$$\langle P_\perp^\mu \rangle = \frac{m_\mu}{M_K} \mathrm{Im}\ f_S \left[\frac{|\vec{p}_\mu|}{E_\mu + |\vec{p}_\mu| n_\mu \cdot n_\nu - m_\mu^2/M_K} \right] \simeq 0.2\ \mathrm{Im}\ f_S \ .$$

Here $n_\nu (n_\nu)$ are unit vectors along the muon (neutrino) directions and the numerical value represents the expectation after doing an average over phase space [87].

Contributions to Im f_S can arise in multi-Higgs models (like the Weinberg 3-Higgs model [88]) from the charged Higgs exchange shown in Fig. 5, leading to [89]

$$\mathrm{Im}\ f_S \simeq \mathrm{Im}(\alpha^* \gamma) \frac{M_K^2}{M_{H^-}^2} \ .$$

Here $\alpha(\gamma)$ are constants associated with the charged Higgs coupling to quarks (leptons). Because a leptonic vertex is involved, one in general does not have a strong constraint on $\mathrm{Im}(\alpha^* \gamma)$. By examining possible non-standard contributions to the B semileptonic decay $B \to X \tau \nu_\tau$, Grossman [90] obtains

$$\mathrm{Im}(\alpha^* \gamma) < \frac{0.23\ M_{H^-}^2}{[\mathrm{GeV}]^2}$$

which yields a bound for $\langle P_\perp^\mu \rangle$ of $\langle P_\perp^\mu \rangle < 10^{-2}$. Amusingly, this is the same bound one infers from the most accurate measurement of $\langle P_\perp^\mu \rangle$ done at Brookhaven about a decade ago [91], which yielded

$$\langle P_\perp^\mu \rangle = (-3.1 \pm 5.3) \times 10^{-3} \, .$$

In specific models, however, the leptonic phases associated with charged Higgs couplings are correlated with the hadronic phases. In this case, one can obtain more specific restrictions on $\langle P_\perp^\mu \rangle$ due to the strong bounds on the neutron electric dipole moment. For instance, for the Weinberg 3 Higgs model, one relates $\mathrm{Im}(\alpha^* \gamma)$ to a similar product of couplings of the charged Higgs to quarks [89]:

$$\mathrm{Im}(\alpha^* \gamma) = \left(\frac{v_u}{v_e} \right)^2 \mathrm{Im}(\alpha^* \beta) \, ,$$

where v_u (v_e) are the VEV of the Higgs doublets which couples to up-like quarks (leptons). The strong bound on the neutron electric dipole moment [3] then gives the constraint

$$\mathrm{Im}(\alpha^* \beta) \leq \frac{4 \times 10^{-3} \, M_{\mathrm{H}^-}^2}{[\mathrm{GeV}]^2} \, .$$

If one assumes that $v_u \sim v_e$, this latter bound gives a strong constraint on $\langle P_\perp^\mu \rangle$ [$\langle P_\perp^\mu \rangle < 10^{-4}$]. However, this constraint is removed if $v_u / v_e \sim m_t / m_\tau$.

Similar results are obtained in the simplest supersymmetric extension of the SM. In this case, Im f_{S} arises from a complex phase associated with the gluino mass. Assuming all supersymmetric masses are of the same order, Christova and Fabbrichesi [92] arrive at the estimate

$$\mathrm{Im} \, f_{\mathrm{S}} \simeq \frac{M_{\mathrm{K}}^2}{m_{\tilde{g}}^2} \frac{\alpha_s}{12\pi} \sin \phi_{\mathrm{susy}} \, ,$$

where ϕ_{susy} is the gluino mass CP-violating phase. This phase, however, is strongly restricted by the neutron electric dipole moment. Typically, one finds [93]

$$\sin \phi_{\mathrm{susy}} \leq \frac{10^{-7} \, m_{\tilde{g}}^2}{[\mathrm{GeV}]^2}$$

leading to a negligible contribution for $\langle P_\perp^\mu \rangle$, below the level of $\langle P_\perp^\mu \rangle_{\mathrm{FSI}}$.

An experiment (E246) is presently underway at KEK aimed at improving the bound on $\langle P_\perp^\mu \rangle$ obtained earlier at Brookhaven. The sensitivity of E246 is such that one should be able to achieve an error $\delta \langle P_\perp^\mu \rangle \sim 5 \times 10^{-4}$ [87]. This level of precision is very interesting and, in some ways, it is comparable or better to d_n measurements for probing CP-violating phases from the scalar sector. This is the case, for instance, in the Weinberg model if v_u / v_e is large. At any rate, if a positive signal were to be found, it would be a clear indication for a non-CKM CP-violating phase. Furthermore, as Garisto [94] has pointed out, a positive signal at the level aimed by the E246 experiment would imply very large effects in the corresponding

decays in the B system involving τ-leptons (processes like $B^+ \to D^o \tau^+ \nu_\tau$), since one expects, roughly,

$$\langle P_\perp^\tau \rangle_B \sim \frac{M_B}{M_K} \frac{m_\tau}{m_\mu} \langle P_\perp^\mu \rangle_K \ .$$

Thus, in principle, a very interesting experimental cross-check could be done.

4 Concluding Remarks

I would like to conclude more or less in the way in which I started this review, by reemphasizing that even after thirty years from the discovery of CP violation this phenomena remains shrouded in mystery. However, there are some grounds for optimism. It is quite possible that before the year 2000 we shall know whether the CKM model provides the approximately correct description of CP violation. For instance, a convincing non zero determination of ϵ'/ϵ would exclude the superweak hypothesis, while a meausurement of $\sin 2\beta \sim O(1)$ would strongly favor the CKM explanation. Both of these experimental results could be on hand in this time frame.

A more detailed understanding of the full CKM structure, or a further understanding of CP violation if the CKM paradigm fails, will be more difficult. The meausurement of α is probably the simplest of the more difficult things to accomplish. A direct meausurement of the CKM phase δ, or equivalently the angle γ, by means of experiments in the B sector or through the study of rare K decays, is very challenging. So are attempts at finding non CKM phases, although experiments searching for these effects are to be encouraged since they would signal new physics beyond the Standard Model. Indeed, it is important also that other CP violation experiments where one expects very small effects in the Standard Model be pushed to their limits, as surprises may arise. A case in point is provided by searches for CP violation in charged K decays, or in K_S decays, to be carried out here at DAPHNE, where little is really known. It is unclear, however, whether all this experimental activity will be able to throw any light on the strong CP problem. Nevertheless, if we are to really understand CP violation, one day we will have to understand why $\bar{\theta} \simeq 0$.

Acknowledgments

Part of the material on CP violation in K-decays presented here is drawn from a talk I gave at the 23rd INS Symposium in Tokyo, Japan [95]. This work was supported in part by the Department of Energy under Grant No. FG03-91ER40662.

References

1. J. H. Christenson, J. W. Cronin, V. L. Fitch, and R. Turlay, Phys. Rev. Lett. **13**(1964) 138.

2. B. Pagels, to appear in the Proceedings of the 23rd INS Symposium, Tokyo, Japan, 1995.

3. Particle Data Group: L. Montanet *et al.*, Phys. Rev. **D50**(1994) 1173.

4. C. O. Dib and R. D. Peccei, Phys. Rev. **D46**(1992) 2265.

5. J. W. Cronin, Rev. Mod. Phys. **53**(1981) 373.

6. A. Sakharov, JETP Lett. **5**(1967) 24

7. T. D. Lee, Phys. Reports **9C**(1974) 148.

8. I. Kobzarev, L. Okun, and Y. Zeldovich, Phys. Lett. **50B**(1974) 340.

9. S. Barr, Phys. Rev. **D30**(1984) 1805; A. Nelson, Phys. Lett. **143B**(1934) 165. See also, R. D. Peccei, in **25 Years of CP Violation**, ed. J. Tran Than Van (Editions Frontiers, Gif-sur-Yvette, 1990).

10. L. Wolfenstein, Phys. Rev. Lett. **13**(1964) 562.

11. N. Cabibbo, Phys. Rev. Lett. **10**(1963) 531; M. Kobayashi and T. Maskawa, Prog. Theor. Phys. **49**(1973) 652.

12. C. G. Callan, R. Dashen and D. Gross, Phys. Lett. **63B**(1976) 334.

13. R. Jackiw and C. Rebbi, Phys. Rev. Lett. **37**(1976) 172.

14. N. V. Krasnikov, V. A. Rubakov and V. F. Tokarev, J. Phys **A12**(1979) L343. For a pedagogical discussion see also, A. A. Anselm and A. A. Johansen, Nucl. Phys. **B407**(1993) 652.

15. V. Baluni, Phys. Rev. **D19**(1979) 2227: R. Crewther, P. Di Vecchia, G. Veneziano and E. Witten, Phys. Lett. **88B**(1979) 123: **91B**(1980) 487 (E).

16. For a review, see, for example, R. D. Peccei in **CP Violation** ed. C. Jarlskog (World Scientific, Singapore, 1989).

17. R. D. Peccei and H. R. Quinn, Phys. Rev. Lett. **38**(1977) 1440; Phys. Rev. **D16**(1977) 1791.

18. S. Weinberg, Phys. Rev. Lett. **40**(1978) 223: F. Wilczek, Phys. Rev. Lett. **40**(1978) 271.

19. D. B. Kaplan and A. V. Manohar, Phys. Rev. lett. **56**(1986) 2004.

20. H. Leutwyler, Nucl. Phys. **B337**(1990) 108.

21. L. Wolfenstein, Phys. Rev. Lett. **51**(1983) 1945.

22. F. Gilman and M. Wise, Phys. Lett. B**83**(1979) 83; Phys. Rev. D**20**(1979) 83; B. Guberina and R. D. Peccei, Nucl. Phys. B**163**(1980) 289.

23. E. P. Shabalin, Sov. J. Nucl. Phys. **28**(1978) 75.

24. See, for example, Y. Nir in Proceedings of the 1992 SLAC Summer School (SLAC, Stanford, California, 1993).

25. R. D. Peccei and K. Wang, Phys. Lett. **B349**(1995) 220.

26. R. Forty, to appear in the Proceedings of the International Conference on High Energy Physics (ICHEP 94), Glasgow, Scotland, July 1994.

27. CDF Collaboration: F. Abe *et al.*, Phys. Rev. D**50** (1994) 2966.

28. S. Stone, Proceedings of the 1994 DPF Conference, Albuquerque, New Mexico, ed. Sally Seidel (World Scientific, Singapore, 1995).

29. S. Sharpe, Nucl. Phys. B (Proc. Suppl.)**34**(1994) 403.

30. This is a guesstimate of the value of this parameter coming from Lattice QCD calculations. For a compilation of the most recent results, see J. Shigemitsu, to appear in the Proceedings of the International Conference on High Energy Physics (ICHEP 94), Glasgow, Scotland, July 1994.

31. Y. B. Pan, to appear in the Proceedings of the International Conference on High Energy Physics (ICHEP 94), Glasgow, Scotland, July 1994.

32. E731 Collaboration: L. K. Gibbons *et al.*, Phys. Rev. Lett. **70**(1993) 1203.

33. NA31 Collaboration: G. D. Barr *et al.*, Phys. Lett. B**317** (1993) 1233.

34. A. J. Buras and M. E. Lautenbacher, Phys. Lett. B**318** (1993) 212. See also, A. J. Buras, in **Phenomenology of Unification from Present to Future**, ed. G. Diambrini-Palazzi *et al.* (World-Scientific, Singapore, 1994).

35. J. Gasser and U. G. Meissner, Phys. Lett. **B258**(1991) 219.

36. J. Flynn and L. Randall, Phys. Lett. B**216**(1989) 221; *ibid.* B**224**(1989) 221; Nucl. Phys. B**326**(1989) 3.

37. M. Ciuchini, E. Franco, G. Martinelli, and L. Reina, Phys. Lett. B**301**(1993) 263.

38. A. J. Buras, M. Jamin, and M. T. Lautenbacher, Nucl. Phys. B**408**(1993) 209.

39. For a review see, J. C. Ritchie and S. G. Wojcicki, Rev. Mod. Phys. **65**(1993) 113.

40. H. Y. Cheng, Phys. Rev. D**43**(1991) 1579.

41. J. F. Donoghue, B. R. Holstein, and G. Valencia, Phys. Rev. D**36**(1987) 798.

42. A. A. Belkov *et al.*, Phys. Lett. B**232**(1989) 118.

43. G. Isidori, L. Maiani and A. Pugliese, Nuc. Phys. B**381** (1992) 522.

44. These results come from the Ph.D. Thesis of F. Pettit (UCLA 1995). They are quite similar to those obtained by G. Isidori, L. Maiani, and A. Pugliese, Nucl. Phys. B**381**(1992) 522.

45. H. Y. Cheng, Phys. Lett. B**315**(1993) 170; Phys. Rev. D**49**(1994) 3771; N. Paver, Riazzudin, and F. Simeoni, Phys. Lett. B**316(1993)** 397. These papers supercede an earlier, more optimistic, estimate of C. O. Dib and R. D. Peccei, Phys. Lett. B**249** (1990) 325.

46. L. M. Seghal, Phys. Rev. D**38**(1988) 808; D**41**(1991) 161; T. Morozumi and H. Iwasaki, Prog. Theor. Phys. **82**(1989) 371.

47. A. G. Cohen, G. Ecker, and A. Pich, Phys. Lett. B**304** (1993) 347; see also G. D'Ambrosio *et al.*, CERN TH-7503, 1994.

48. C. O. Dib, I. Dunietz, and F. Gilman, Phys. Lett. B**218** (1989) 487; Phys. Rev. D**39**(1989) 2639.

49. See for example, B. Winstein and L. Wolfenstein, Rev. Mod. Phys. **65**(1993) 1113.

50. A. J. Buras, M. E. Lautenbacher, M. Misiak, and M. Münz, Nucl. Phys. **B423**(1994) 349.

51. E779 Collaboration: D. H. Harris *et al*, Phys. Rev. Lett. **71**(1993) 3914.

52. E845 Collaboration: K. E. Ohl *et al.*, Phys. Rev. Lett. **64** (1990) 2755.

53. E799 Collaboration: D. H. Harris *et al*, Phys. Rev. Lett. **71**(1993) 3918.

54. B. H. Greenlee, Phys. Rev. D**42**(1990) 3724.

55. B. Winstein, to appear in the Proceedings of the 23rd INS Symposium, Tokyo, Japan, 1995.

56. L. S. Littenberg, Phys. Rev. D**39**(1989) 3222.

57. G. Buchalla and A. J. Buras, Nucl. Phys. B**400**(1993) 225.

58. E799 Collaboration: M. Weaver, Phys. Rev. Lett. **72**(1994) 3758.

59. C. O. Dib, Phys. Lett. B**282**(1992) 201.

60. G. Buchalla and A. J. Buras, Nucl. Phys. B**412**(1994) 106.

61. A. J. Buras, M. E. Lautenbacher, and G. Ostermaier, Phys. Rev. **D50** (1994) 3433.

62. J. Gasser and H. Leutwyler, Phys. Rept. **87C**(1982) 77.

63. L. S. Littenberg, to appear in the Proceedings of the 23rd INS Symposium, Tokyo, Japan, 1995.

64. E787 Collaboration: M. S. Atiya, Phys. Rev. Lett. **70**(1993) 2521; Phys. Rev. **D48**(1993) R1.

65. A. Carter and A. I. Sanda, Phys. Lett. **45**(1980) 952; Phys. Rev. **D23**(1981) 1567; I. I. Bigi and A. I. Sanda, Nucl. Phys. **B193**(1981) 95; **B281**(1987) 41.

66. I. Dunietz and J. L. Rosner, Phys. Rev. **D34**(1986) 1404; Y. Azimov, V. A. Khoze and N. G. Uraltsev, Yad. Fyz. **45**(1987) 1412; D. Du, I. Dunietz and D. Wu, Phys. Rev. **D34**(1986) 3414.

67. For an early discussion see, for example, R. D. Peccei, in the Proceedings of the Workshop on the Experimental Program at UNK, Protvino, USSR, 1987. For a more detailed exposition see, for example, I. I. Bigi, V. A. Khoze, A. I. Sanda and N. G. Uraltsev in **CP Violation** ed. C. Jarlskog (World Scientific, Singapore, 1989).

68. For a discussion see, for example, C. Jarlskog in **CP Violation** ed. C. Jarlskog (World Scientific, Singapore, 1989).

69. B. Weinstein, Phys. Rev. Lett. **68**(1992) 1271.

70. There have been numerous analyses of the allowed values for the angles α, β and γ. Early studies can be found in P. Krawczyk *et al*, Nucl. Phys. **B307**(1988) 19; C. O. Dib *et al*, Phys. Rev. **D41**(1990) 1522; Y. Nir and H. R. Quinn, Phys. Rev. **D42**(1990) 1473.

71. For a discussion, see for example, Y. Nir and H. Quinn, in **B Decays**, ed. S. Stone (World Scientific, Singapore, 1992).

72. D. London and R. D. Peccei, Phys. Lett. **B223**(1989) 257; B. Grinstein, Phys. Lett. **B229**(1989) 280; M. Gronau, Phys. Rev. Lett. **63**(1989) 1451; Phys. Lett. **B300**(1993) 163.

73. B. Kayser, M. Kuroda, R. D. Peccei and A. I. Sanda, Phys. Lett. **B237**(1990) 508.

74. This meausurement is discussed in S. Playfer and S. Stone, HEPSY 95-01.

75. M. Gronau and D. London, Phys. Rev. Lett. **65**(1990) 3381.

76. H. R. Quinn and A. E. Snyder, Phys. Rev. **D48**(1993) 2139.

77. M. Gronau and D. Wyler, Phys. Lett. **B265**(1991) 172.

78. See for example, R. D. Peccei, in **25 Years of CP Violation**, ed. J. Tran Thanh Van (Editions Frontiers, Gif-sur-Yvette, 1990).

79. V. A. Kuzmin, V. A. Rubakov and M. E. Shaposnikov, Phys. Lett. **155B**(1985) 36; For a review, see for example, M. E. Shaposnikov, Physica Scripta, **T36**(1991) 183.

80. For a discussion, see for example, M. Dine, Nucl. Phys. B (Proc. Suppl.) **37A**(1994) 127.

81. M. Leurer, Phys. Rev. Lett. **62** (1989) 1967.

82. J. J. Sakurai, Phys. Rev. **109**(1958) 980.

83. G. S. Adkins, Phys. Rev. D**28**(1983) 2285.

84. A. R. Zhitnitski, Sov. J. Nucl. Phys. **31**(1980) 529.

85. P. Castoldi, J. M. Frere, and G. L. Kane, Phys. Rev. D**39**(1989) 2633.

86. G. Belanger and C. O. Geng, Phys. Rev. D**44**(1991) 2789.

87. Y. Kuno, Nucl. Phys. B (Proc. Suppl.) **37A**(1994) 87.

88. S. Weinberg, Phys. Rev. Lett. **37**(1976) 657.

89. R. Garisto and G. Kane, Phys. Rev. D**44**(1991) 2038; G. Belanger and C. O. Geng, Phys. Rev. D**44** (1991) 2789.

90. Y. Grossman, Nucl. Phys. B**426**(1994) 355.

91. S. R. Blatt *et al.*, Phys. Rev. D**27**(1983) 1056.

92. E. Christova and M. Fabbrichesi, Phys. Lett. B**315** (1993) 113.

93. M. Dugan, B. Grinstein, and L. Hall, Nucl. Phys. B**255** (1985) 413.

94. R. Garisto, Phys. Rev. D**51**(1995) 1107.

95. R. D. Peccei, to appear in the Proceedings of the 23rd INS Symposium, Tokyo, Japan, 1995.

EXPECTATIONS AND MEASUREMENTS OF CP VIOLATION IN THE D SYSTEM USING THE TAU/CHARM FACTORY FACILITY

P. Roudeau
Laboratoire de l'Accélérateur Linéaire, IN2P3-CNRS
et Université de Paris-Sud, 91405 Orsay, France

1 Introduction

During the past years a lot of attention has been devoted to the study of CP violation in K and B systems. In D hadron decays, the Standard Model predicts very small effects from CP violation. As a consequence precise measurements of the CP violating phase are not expected, as for B decays. However, the study of CP violation in D meson decays remains of great interest to observe direct CP violation, expected from the Standard Model, and to search for physics outside the Standard Model. In this respect the study of $D^0 - \bar{D}^0$ oscillations appears to be sensitive to new physics scenarios which are not detected in K or B decays only. More details on this subject can be found in the articles given in [1]. The most recent study on the measurement capabilities of a Tau/Charm factory to detect CP violation can be found in [2].
In section 2, $D^0 - \bar{D}^0$ oscillations are considered and CP violation in the D system is described in section 3. Finally section 4 gives an overview of the Tau/Charm factory project.

2 $D^0 - \bar{D}^0$ mixing

2.1 Theoretical expectations

$D^0 - \bar{D}^0$ mixing receives contributions from short and long distance processes (Fig. 1). Short distance box diagrams are expected to give an extremely small contribution to Δm_D, of the order of 5×10^{-9} eV [3]. This value has to be compared with the D^0 total

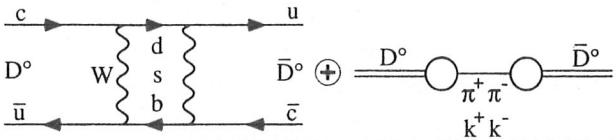

Figure 1: Short and long distance contributions to $D^0 - \bar{D}^0$ oscillations

width $\Gamma_D \sim 1.6 \times 10^{-3}$ eV. From evaluations done in 1986 [4] a large enhancement was foreseen on Δm_D from long distance contributions and values as high as 10^{-6} eV were quoted. Two recent analyses [5], done in the framework of HQET, have found that large cancellations should occur between the different contributing channels in long distance diagrams and they agree to conclude that $\Delta m_D \sim 1 - 4 \times 10^{-8}$ eV.

2.2 Experimental sensitivity

Experiments usually measure the ratio r_D between the probabilities to observe a $\bar{D}^0$ state when a D^0 has been initially produced.
Basically two situations have to be considered:

- Study of the proper time distribution for DCSD (Doubly Cabibbo Suppressed Decays) with D^0 mesons produced in jets. The presence of a D^0 or a $\bar{D}^0$ particle at production time is tagged by the decay $D^{*\pm} \rightarrow \overset{(-)}{D}{}^0 \pi^\pm$. If a D^0 has been tagged, the $K^+\pi^-$ final state can be obtained in two ways:
  - from $D^0 \rightarrow K^+\pi^-$ through a DCSD transition.
  - from $D^0 \rightarrow \bar{D}^0 \rightarrow K^+\pi^-$ through a Cabibbo favoured transition after oscillation of the D^0.

The proper time distribution is then expected to be:

$$P_{K^+\pi^-}(t) = e^{-t/\tau}\left[a + \frac{r_D}{2}\left(\frac{t}{\tau}\right)^2 + b\left(\frac{t}{\tau}\right)\right] \qquad (1)$$

The last term corresponds to the interference between the two mechanisms. Events from mixing appear as an excess at large decay time.
The present limit on $D^0 - \bar{D}^0$ oscillation has been obtained in this way by the E691 experiment: $r_D < 3 \times 10^{-3}$ [6]. Several experiments are planned at FNAL to improve

this limit.
At an asymmetric B factory, similar studies can be made and it is expected to reach $r_D \lesssim 5\ 10^{-5}$ with an integrated luminosity of 30 fb^{-1}.

• Study of specific final states in the decay $\psi(3.77) \to D^0\bar{D}^0$.
As an example, a final state like $K^-\pi^+K^-\pi^+$ is obtained only if one of the D^0 mesons has mixed, there is no contribution expected from DCSD because of Bose-Einstein statistics [7].
At higher center of mass energies where one produces $\psi(4.14) \to D^-D^{*+}$ the D^0 at production time can be tagged by reconstructing the D^-, and the D^0, at decay time, can be signed by a decay channel where no contamination from DCSD transition is expected (as semileptonic decays).
Including several channels a limit close to 10^{-5} can be expected at a Tau/Charm factory.
Table 1 summarizes theoretical expectations and experimental sensitivities for mixing:

Table 1: Expected experimental limits on $D^0 - \bar{D}^0$ mixing and theoretical prediction

	r_D
expt. (1994)	$< 3 \times 10^{-3}$
A.B.F	$< 5 \times 10^{-5}$
τ/c	$< 2 \times 10^{-5}$
Theory (Δm_D only)	$10^{-10} - 10^{-9}$

2.3 Perspectives on $D^0 - \bar{D}^0$ mixing

The ratio r_D can be expressed in terms of the mass and width differences of the $D^0_{1,2}$ physical states:

$$r_D \simeq \frac{1}{2}\left[\left(\frac{\Delta m_D}{\Gamma}\right)^2 + \left(\frac{\Delta\Gamma_D}{2\Gamma_D}\right)^2\right] \qquad (2)$$

There is a long way for experimentalists to reach the level predicted by the Standard Model. This extremely small value has also a great interest because it opens the possibility that phenomena coming from extensions of the Standard Model will show up. This has been recently investigated [1], and it appears that D decays can have a different sensitivity as compared to B and K systems. As an example a Minimal Supersymmetric Standard Model where the squark masses are not degenerate can give a large contribution to Δm_D reaching values close to the present experimental limit.

2.4 A word of caution

To be confident that $D^0 - \bar{D}^0$ mixing is a good opportunity to search for New Physics, it seems also that a closer look has to be given to the evaluation of $\Delta\Gamma_D$. The general belief is that its value should be similar to Δm_D but contributions from annihilation or Penguin diagrams can receive enhancements from non perturbative QCD origin and are not perhaps well enough evaluated at present.

3 CP violation in D mesons

Whereas, in the Standard Model, effects from CP violation are proportional to $A^2\lambda^6\eta$ (using the Wolfenstein notation for the CKM matrix), the total decay rates for K, D and B mesons are proportional to λ^2, 1 and λ^4, respectively. Thus the D system is not a priori a favoured place to search for effects from CP violation unless Cabibbo suppressed decays (proportional to λ^2) are envisaged for which one expects a level for CP violation similar to the one observed in the K system (typically $\sim 10^{-3}$).

3.1 Two mechanisms leading to CP violation[2)]

3.1.1 CP violation through mixing

A CP asymmetry can be obtained if a D^0 and a $\bar{D}^0$ can contribute to the same final state (f) and the corresponding asymmetry can be written:

$$\begin{aligned} A_{CP} &= \frac{\Gamma(\bar{D}^0 \to f,t) - \Gamma(D^0 \to f,t)}{\Gamma(\bar{D}^0 \to f,t) + \Gamma(D^0 \to f,t)} \\ &\simeq \frac{\Delta m_D}{\Gamma} I_m \frac{q}{p} \bar{\rho}_f \frac{t}{\tau_D} \simeq 10^{-8} \frac{t}{\tau_D} \end{aligned} \tag{3}$$

In the Standard Model this asymmetry is expected to be extremely small and provides a window through which New Physics may appear (it should appear through mixing too).

This is a very different situation as compared to the B system where A_{CP} is large and one can do nice measurements of the phase angles expected in the Standard Model. But, in that case, the opportunity to observe new physics will be a priori more difficult and has to be identified through measurement uncertainties of the large component expected from the Standard Model.

3.1.2 Direct CP violation

There is not yet any evidence for direct CP violation. It implies that the decay rate of a particle into a given final state is different from the decay rate of its anti-particle

into the conjugate final state. The CP violating asymmetry is defined as:

$$A_{CP} = \frac{\Gamma(D \to f) - \Gamma(\bar{D} \to \bar{f})}{\Gamma(D \to f) + \Gamma(\bar{D} \to \bar{f})} \tag{4}$$

Three conditions have to be fulfilled to produce a non-vanishing value for A_{CP}. This can be seen easily by considering that the final state (f) can be reached in two ways which correspond to two different weak and strong amplitudes, respectively:

$$\mathcal{A} = Ae^{i\delta_1} + Be^{i\delta_2} \quad (\delta_1 \text{ and } \delta_2 \text{ are two strong interaction phases}) \tag{5}$$

By CP transformation, δ_1 and δ_2 are unaffected whereas A and B are changed into their complex conjugates A* and B*:

$$\bar{\mathcal{A}} = A^* e^{i\delta_1} + B^* e^{i\delta_2} \tag{6}$$

If it is assumed, as usual, that one of the amplitudes dominates |A| >> |B| then

$$\mathrm{A}_{CP} \sim 2\frac{|\mathrm{B}|}{|\mathrm{A}|} sin(\varphi_A - \varphi_B) sin(\delta_1 - \delta_2) \tag{7}$$

where φ_A and φ_B are the two weak phases. A_{CP} has a measurable value if:

- the two weak phases are different,
- the two strong phases are also different,
- |B| is not negligible as compared to |A|.

3.2 Expectations for D hadrons[8)]

We consider, in the following, a specific example for charged D decays:

$$\mathrm{D}^+ \to \mathrm{K}^+ \bar{\mathrm{K}}^{*0} \tag{8}$$

The two contributing weak amplitudes are shown in figure 2 and their amplitudes, at the quark level, are respectively proportional to λ and λ^5, thus $\frac{|\mathrm{B}|}{|\mathrm{A}|}$ in formula (7) is of order $\lambda^4 \sim 10^{-3}$. QCD corrections have to be considered and are of perturbative and non-perturbative origins. Perturbative corrections tend to enhance, by about 2, the penguin contribution as compared to the leading order evaluation. Non-perturbative contributions depend on the final state. As an example when the $(u\bar{s})$ system is a pseudo-scalar meson, because of the (V - A) × V structure of the penguin term, it will be enhanced.

Finally, final state interactions have to be involved to generate the strong phase shift between the two processes. D hadrons sit in a mass region where one expects a

lot of resonances and the D decay branching fractions can be explained only if final state interactions are taken into account. A detailed model has been constructed which explains most of the measured decay rates [9] and has been applied to predict values for CP asymmetries in various channels. As an example, in the decay channel shown in figure 2, the penguin diagram is $\Delta V = 1/2$ whereas the Cabibbo suppressed transition contributes to $\Delta V = 1/2$ and $3/2$ amplitudes (in SU(3) symmetry, in addition to the I-spin, the U-and V-spins have to be considered: d and s quarks form a U-spin doublet, whereas u and s are members of a V-spin doublet).

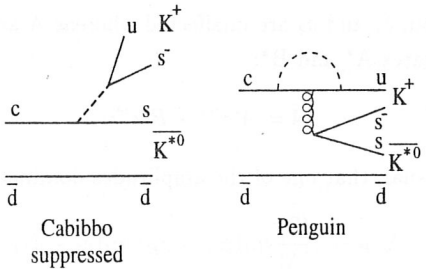

Figure 2: Two mechanisms contributing to $D^+ \to K^+\bar{K}^{*0}$.

Table 2 gives present expectations for a few D^+ decay channels [9]:

Table 2: Expected CP asymmetries in D^+ decays[9]

decay channel	BR(%)	$A_{CP}(\times 10^{-3})$
$D^+ \to \pi^+\pi^0$	0.2	0
$D^+ \to \pi^+\eta$	0.7	$-1.5 \pm .4$
$D^+ \to K^+\bar{K}^0$	0.7	$1 \pm .3$
$D^+ \to \rho^+\pi^0$	0.4 ?	$2.9 \pm .8$
$D^+ \to K^{*+}\bar{K}^0$	2 ?	$-0.9 \pm .3$
$D^+ \to \bar{K}^{*0}K^+$	0.4	$2.8 \pm .8$

3.3 Measurement of CP violation at a Tau/Charm factory

Two examples are considered in the following to illustrate the procedures which can be used at a Tau/Charm factory to observe direct CP violation [2].

3.3.1 *Direct CP violation in D^0 decays*

At the $\psi(4.14)$, the decays $D^+D^{*-}(\rightarrow \bar{D}^0\pi^-)$ and $D^-D^{*+} \rightarrow (D^0\pi^+)$ are a source of tagged D^0 and $\bar{D}^0$. D^0 decay final states like $\pi^+\pi^-$ and K^-K^+ have the same experimental acceptance and detection efficiency. Tagging efficiencies will be different for D^0 and $\bar{D}^0$ states because tracks from the (D^+, π^-) and (D^-, π^+) systems behave differently inside the detector. These differences have to be measured accurately and this will be possible with registered data by studying the behaviour of tagged final states having large branching fractions (as $D^+ \rightarrow K^-\pi^+\pi^+$) for which no CP asymmetry is expected.

3.3.2 *Direct CP violation in D^+ decays*

At the $\psi(3.77)$, the D^+D^- final state can be considered. The $D^\pm$ decay channels are self tagging modes. There is thus no need for an additional tag as compared to D^0 channels. As before, the main experimental problem comes from the precise control of differences in experimental detection for K^+ and K^- and also for π^+ and π^- at various momenta.
At the τCF, these controls can be obtained using the $K\pi\pi$ final state of the D^+ and also J/ψ decays which are sources of hadrons of different types.

3.4 Comparison with expectations for direct CP violation in K and B systems

The expected asymmetries for D hadrons are at a level of 10^{-3}, a similar value is expected in kaon decays. For Bs some channels can have asymmetries at the few 10^{-3} level but the corresponding branching fractions, which involve b$\rightarrow$ u transitions, are extremely small and Bs are perhaps not favoured also to get the needed strong phases because of their masses. D hadrons can thus be a very rich laboratory to look for direct CP violation if these effects are at the 10^{-3} level because a lot of different channels are expected to contribute which could be studied. In parallel, the detailed measurements of D^0, D^+ and D_s^+ decay modes, will constrain the model parameters. Some of these parameters can also be obtained by a precise spectroscopy of $q\bar{q}$ systems in the 2 GeV region which could be obtained by studying J/ψ decays.
For CP asymmetries at the 10^{-3} level the luminosity of 10^{33} cm^{-2} s^{-1} of the τCF collider is marginal and values of 3 - 4 10^{33} cm^{-2} s^{-1} must be considered.

4 The Tau/Charm factory project

At several places, in previous sections the name "Tau/Charm factory" (τCF) has been mentioned and, in the following, the main characteristics of this project will

be given which concern the machine, the detector and the physics. More details can be found in [10].

The energy domain covered by the machine is shown in figure 3. The high end of this range is fixed by the spectroscopy of charmed baryons whereas the low end is not yet well defined. It would be certainly important to have an overlap with the energy interval covered by DAFNE to ensure an accurate measurement of the $e^+ e^-$ annihilation cross-section into hadrons. This is an important issue to reduce present uncertainties in the evaluation of the electromagnetic coupling constant at the energy scale of the Z^0 mass ($\alpha(M_z)$). The luminosity will be maximum at $E_{CM} = 4$ GeV and the design of the machine has to be such that it will not decrease by an order of magnitude when considering the total covered energy range.

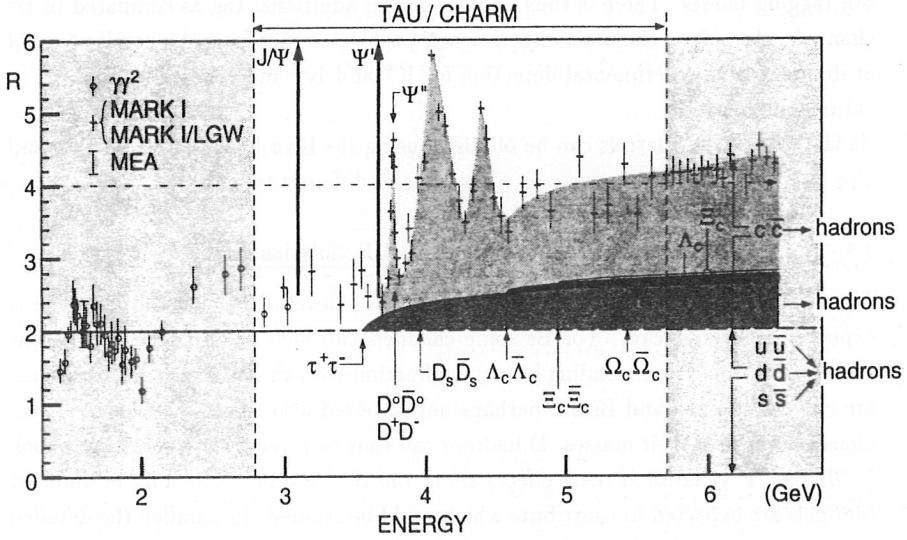

Figure 3: Energy domain of the τCF.

The physics program concerns three main areas: the spectroscopy of hadrons using J/ψ decays, Tau decays and Charm decays. In each area two main objectives will be pursued to:

- obtain accurate and reliable measurements of important quantities,
- explore new domains.

For this, it is necessary to register large statistics of events and to control systematic uncertainties so that they will not limit the precision of the measurements. The control of systematics is provided by the physics, in this energy domain:

- the J/ψ is an intense source of tagged hadrons ($\pi, K, \rho, \eta, K^0_s, K^0_L$) which can be used to monitor the detector performances

- the study of particles close to their production threshold provides unique kinematical and dynamical conditions which can be used to isolate background free signals.

To produce large events rates, a high luminosity collider has to be designed and several parameter lists have been already proposed [11] which give 10^{33} cm^{-2} s^{-1} luminosity with classic separation of the beams using electrostatic separators. Since several years the possibility has been also considered to have a very small dispersion of the center of mass energy (of the order of 100 KeV) to match the natural J/ψ width and so to get more efficient collisions to produce $J/\psi s$. The corresponding optical scheme, known as the monochromatization scheme has been designed. To reach higher luminosities, $3-4 \times 10^{33}$ cm^{-2} s^{-1}, beams crossing at angle have been proposed.

A recent study by Dubna and Orsay allows to switch from one optics to the other by changing only magnetic elements in the straight section [12].

The detector, proposed for this machine provides enormous improvements as compared to detectors working in this energy range in previous experiments as shown in table 3. In figure 4 a transverse section of the detector has been displayed. It shows

Table 3: Comparison between different detectors operating in the 3-4 GeV region concerning the angular acceptance and energy resolution (taken from R. Landua in "Journées sur les projets de la Physique Hadronique", 12-14 janvier 1995 - Super-Besse, France).

experiment	DM2	MARKIII	BES	EXACT
collider	DCI	SPEAR	BEPC	TCF
solid angle (% of 4π) for charged particles	80	70	76	90
solid angle for photons (% of 4π)	70	90	93	99
$\Delta P_T/P_T$(at 1 GeV/c)(%)	3.5	2.1	2.7	0.4
$\Delta E_\gamma/E_\gamma$ (at 1 GeV/c)(%)	20	17	24	2.2

the large solid angle coverage for charged particles and photons. If the precise measurement of charged tracks is obtained over 90 % of the solid angle, their detection is achieved, as for photons on 99 % of 4π srd. The high accuracy on photon energies are given by a C_s I crystal calorimeter. The detection of neutral hadrons, and the signature for muons is given by a finely segmented hadron calorimeter.

In the following, some highlights of the physics which can be done at the τCF are presented.

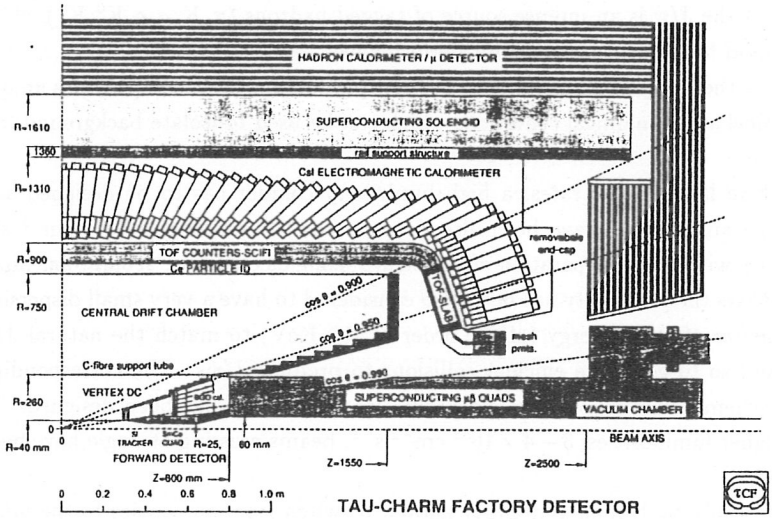

Figure 4: Transverse section of the τCF detector.

4.1 Light quark and gluon spectroscopy

In addition to precise measurements of the parameters of the transitions in the charmonium system, charmonium decays are an ideal laboratory to study hadron spectroscopy in the mass range between m_π and 3 GeV/c^2.

Expected statistics are given in Table 4 for one year of running (10 fb^{-1}), three orders of magnitude more data, as compared to present experiments, are envisaged.

The search for glueballs or hybrid states benefits from the properties of charmonium decays in which the c and $\bar{c}$ quarks annihilate and new constraints are made available as compared to similar studies made in $p\bar{p}$ annihilation and fixed targets experiments.

The initial state has well defined quantum numbers: those of the considered charmonium state.

The quark and glue content of a given produced resonance can be measured by looking at the production rate of this state in conjunction with a ϕ (s $\bar{s}$ content), ω ($u\bar{u}, d\bar{d}$ content) or a photon (g content). The measured fractions of π, K, η particles emitted in the final state can also be compared with expectations for pure glue

states. Finally the large solid angle covered by the detector allows to do partial wave analyses to assign the spin-parity quantum numbers to the studied state. The three orders of magnitude increase in statistics, as compared to previous experiments is really needed considering that these previous experiments, observe candidates at a rate of a few tens of events precluding any detailed analysis of the flavour content of the decay products and of the Dalitz plots.

Table 4: Expected statistics for one year running at the τCF (10 fb^{-1} as compared to present available statistics (taken from R. Landua in "Journées sur les projets de la Physique Hadronique", 12-14 janvier 1995 - Super-Besse, France).

	Present	τCF
J/ψ	20 M	10 000 M
ψ'		6 000
χ_0	<.1 M	540
χ_1	< .1 M	540
χ_2	< .1 M	480
η	.02 M	10
η'	.003 M	40

4.2 Charm physics

At the τCF charmed particles can be generated in pairs close to their production thresholds. This is a unique situation which has important nice features:

- the energy of each D hadron is equal to the beam energy and this constraint allows to reduce the combinatorial background when searching for exclusive final states.
- having completely reconstructed one of the charmed hadrons, one knows that the other is its anti-particle and one knows also its direction and momentum. This is a way to measure absolute branching fractions and to isolate very pure samples of decays with none or one missing particle (as leptonic and semileptonic decays for instance).

The properties of the detector will allow also the spectroscopy of final states containing neutral hadrons to be made properly. This is particularly important when considering charmed baryons where a lot of neutral baryons are expected to be produced in the final state.

The physics reach of the study of charmed hadron decays concerns not only the spectroscopy of these states but it is also a laboratory to study QCD at the frontier between perturbative and non perturbative regimes in precisely defined conditions.

4.2.1 *Charmed hadron spectroscopy*

The τCF will provide absolute branching fractions for all charmed hadrons which can be produced by the collider. The accuracy will be $\sim$ 1 % (or better) for D^0, D^+, D_s and Λ_c^+ and a few % for strange charmed baryons. For the first time we will be able to compare D hadron decays using the same absolute scale. The present relative uncertainty on D_s absolute branching fractions is of the order of 30 % (the one quoted in PDG94 is incorrect) and is 15 % for the Λ_c^+. The situation is better for D^0 (4 %) and for the D^+ (10 %). The τCF is the only place where absolute branching fractions for the D_s, Λ_c and strange charmed baryons can be obtained.
The other important issue is to measure the complete set of charmed hadron decay branching fractions to be able to extract the relative importance of the different quark diagrams and to study final state interactions. Fixed target experiments can register large statistics but on very specific channels with at most one neutral particle (π^0, K_s^0).
The τCF is also probably the only place where the absolute spectroscopy of D^{**} states can be achieved, especially for the anticipated broad states.

4.2.2 *Rare decays*

D branching fractions of the order of 10^{-4} or below will be considered in this category and thus this concerns a very large amount of possible final states. Only one example is given here relative to D radiative decays. Contrary to B radiative decays, for charm, these mechanisms are supposed to originate mainly from non-perturbative QCD contributions and not from short distance quark mechanisms [13].
It is thus of importance to measure these transitions for charm, to be able to control the remaining contributions from these non-perturbative mechanisms, in B decays because they are not calculable. In table 5 have been summarized some expected branching fractions [13] and the expected numbers of events, reconstructed in one year.

4.2.3 *Leptonic decays*

This is the first example where precise informations can be extracted on non-perturbative QCD.
The D leptonic branching fractions are given by the following expression:

$$B(D_q^+ \to \ell\nu_e) = \frac{G_F^2}{8\pi} m_D m_\ell^2 |V_{cq}|^2 \left(1 - \frac{m_\ell^2}{m_D^2}\right)^2 f_D^2 \tau_D, \qquad q = d, s \tag{9}$$

and, using $f_{D_s} = 230$ MeV and $f_{D^+}/f_{D_s} = 0.9$, the following values are expected: (Table 6). No signal is foreseen in $e\nu$ channels because of helicity conservation. All

these channels can be precisely measured ($\sigma f_D/f_D \sim 1\%$) at the τCF.

Other experiments which can contribute to this domain are emulsion experiments,

Table 5: Expected branching fractions and numbers of reconstructed candidates (10 fb^{-1}) for D meson radiative decays. The tagged (untagged) candidates are obtained with (without) reconstructing the other D meson.

Radiative decays			
	BR($\times 10^{-5}$)	♯ tagged	♯ un tagged
$D^0 \to \bar{K}^0\gamma$	7 - 12	120 - 210	960 - 1700
$\rho^0\gamma$	.1 - .5	6 - 30	50 - 240
$\omega^0\gamma$	.2	2	16
$\phi\gamma$	.1 - 3.4	1.3 - 45	10 - 360
$D^+ \to \rho^+\gamma$	2 - 6	12 - 36	170 - 510
$b_1^+\gamma$	3.5	12	170
$K^{*+}\gamma$	.1 - .3	1 - 3	14 - 40
$D_s^+ \to \rho^+\gamma$	6 - 38	5 - 30	60 - 360
$b_1^+\gamma$	6	3	36

Table 6: Leptonic decay branching fractions for charged D mesons.

	D_s	D^+
$\tau\nu$	2×10^{-2}	5×10^{-4}
$\mu\nu$	2×10^{-3}	2×10^{-4}
$e\nu$	10^{-5}	

BES and CLEO. It seems that they can go hardly below 10 % relative accuracy on f_{D_s} ($D_s \to \mu\nu$ channel) for several reasons: statistical limitations for the first two, importance of the background and of other contributing mechanisms for CLEO.

The accurate measurements obtained at the τCF on f_D and f_{D_s} will be of high importance:

- to give constraints on lattice QCD evaluation of these parameters,
- to measure directly the effect of different spectator quarks by comparing f_{D^+} and f_{D_s},
- to allow an accurate determination of $f_B(\sigma_{f_B}/f_B < 5\%)$ by extrapolating from the D to the B region, using lattice QCD.

This will be certainly, for a long time, the most precise determination of f_B.

4.2.4 Semileptonic decays:

As already demonstrated by MARKIII, using tagged events, background free semileptonic decays of D hadrons can be isolated. The production of D hadrons at rest gives

also a kinematical separation between $\pi\ell\nu$ and K$\ell\nu$ final states.
The τCF will provide a detailed measurement of the q^2 dependence of the form factors especially for D$\rightarrow V\ell\nu$ where three of them contribute and this for Cabibbo and non-Cabibbo suppressed decay channels. The understanding of the QCD dynamics in D semileptonic decays can be used to extract V_{bu} in B decays using B$\rightarrow \pi\ell\nu$ and $\rho\ell\nu$ final states [14].
The τCF is also the only place where the inclusive lepton energy distribution in semileptonic decays can be measured because the D momentum is precisely known. Because of the low expected background it is also possible to measure in an inclusive way the mass distribution of the hadronic system produced in these decays.
All these measurements are important bench marks for lattice QCD, QCD sum rules, heavy quark expansion and quark models.

4.3 Tau physics

The measurement accuracy on the values of several parameters of the Standard Model can be improved at the τCF:

- $m_\tau(\sigma(m_\tau) < 100$ KeV)
- m_{ν_τ} (a limit at the 1-2 MeV level is expected)
- leptonic branching fraction $(\sigma(BR_\ell)/BR_\ell \lesssim 10^{-3})$.

The large and uniform detection volume covered by the apparatus allows also original measurements as the determination of light quark masses from angular distributions of the 3π system in $\tau \rightarrow \nu_\tau 3\pi$ decays [15].
The extraction of the strong coupling constant $\alpha_s(m_\tau^2)$ can be extended at the τCF by measuring contributions of non-perturbative origin. The spectral functions for τ decays into even and odd numbers of pions and also with or without strangeness in the final state can be accurately measured as well.

5 Conclusions

The high luminosity of the τCF collider and the peculiar kinematical conditions of particle production close to their threshold give large statistics of very pure events samples. The presence of the J/ψ, in addition to the dedicated physics program that it provides, gives a powerful way to monitor the detector performances and then to control systematic uncertainties.
Accurate measurements of Standard Model parameters can be obtained at the τCF as $\alpha_s(m_\tau^2), \alpha_{em}(q^2), m_q(q = u, d, s, c), m_\tau, m_{\nu_\tau}$.
τ, D and Charmonium decays are ideal tools to study QCD in the non-perturbative regime and under precisely defined conditions. With τs one can measure $\alpha_s(m_\tau^2)$

and a lot of fundamental parameters entering into the chiral symmetry description of strong interactions. D decays are a laboratory to understand B decays and to correct the non-perturbative QCD contribution in their decays. In this way D hadrons will contribute in an important way to extract V_{bu} and to constrain other CKM matrix elements as V_{td} and V_{ts}. Finally charmonium decays are the ideal place to search for glueballs or hybrid states.

The program of physics which can be done at the τCF is complementary to the one expected at other machines.

- DAFNE covers a lower energy range
- B factories will benefit, as explained before, form the understanding of D decays which can be gained at the τCF
- LEP and high energy colliders need accurate measurements, and the absolute branching fraction of charmed hadron decays, to describe more precisely jet properties,
- fixed target experiments are the best place to measure D hadron lifetimes and to study their production mechanisms.

References

1. J.L. Hewett, SLAC-PUB-6695 and proceedings of "The Tau/Charm Factory in the Era of B factories and CESR", Stanford, August 15-16, 1994.

2. J.R. Fry and T. Ruf, proceedings of the "Third workshop on the Tau Charm Factory", Marbella, Spain, 1-6 June 1993, p. 387 (Editions Frontières)

3. H.Y. Cheng, Phys. Rev. **D26** (1982) 143
   L.L. Chau, Phys. Rep. **95 C** (1983) 1

4. L. Wolfenstein, Phys. Lett. **164 B** (1985) 170
   J.F. Donoghue, E. Golowich and B.R. Holstein, Phys. Rev. **D33** (1986) 179

5. H. Georgi, Phys. Lett. **B297** (1992) 353
   T. Ohl, G. Ricciardi and E.H. Simmons, Nucl. Phys. **B403** (1993) 605

6. Particle Data, Phys. Rev. **D50** (1994)

7. I. Bigi, SLAC report 343, June 1989, 169

8. I thank L. Oliver (LPTHE Orsay) for illuminating discussions on this subject

9. F. Buccella, M. Lusignoli, G. Mangano, G. Miele, A. Pugliese and P. Santorelli, Phys. Lett. **B302** (1993) 319 and ROMA preprint n^0 1070-1994, hep-ph/9411286

10. "Third Workshop on the Tau Charm Factory", Marbella, Spain, 1-6 June 1993 (Editions Frontières)

11. Y. Baconnier et al., CERN/AC/90-07
P. Beloshitsky, LAL/RT 92-09, Orsay (June 1992)
A. Faus-Golfe and J. Le Duff, LAL/TRT 93-07, Orsay (June 1993)
E.A. Perelstein et al., JINR Tau-Charm Factory study, proceedings of the XVth Int. Conf. on High Energy Accel. Hamburg, Germany, July 20-24, 1992, World Scientific Ed.

12. P. Beloshitsky, J. Le Duff, B. Mouton and E. Perelstein, LAL/RT/94-05

13. G. Burdman, E. Golowich, J.L. Hewett and S. Pakvasa, SLAC-PUB-95-6692

14. D. Scora and N. Isgur, CEBAF-TH-94-14 (and references therein)
As. Abada et al., Nucl. Phys. **B416** (1994) 675.

15. J. Stern, N.H. Fuchs and M. Knecht, proceedings of the "Third workshop on the Tau Charm Factory", Marbella, Spain, 1-6 June 1993, p. 197 (Editions Frontières).

DETERMINATION OF THE CKM MATRIX FROM B DECAYS

Ahmed Ali
DESY, Notkestrasse 85, 2000 Hamburg 52, (Germany)

(No written contribution arrived)

CP VIOLATION: MACHINE, EXPERIMENTS, THEORY

PARALLEL SESSION

K. Berkelman	CESR Status Report	167
R. Aleksan	BABAR: A New Detector for Studying CP Violation in the B System	177
T. Iijima	KEK B–Factory Project and BELLE Experiment	189
A. Schwarz	CP Violation at Hadronic Machines: HERAB	201
H.J. Lipkin	CP Violation for Pedestrians	203
G. Martinelli	A Theoretical Appraisal of ε'/ε	215
E.A. Paschos	CP Violation in the Time Evolution of the Decay $K^0 \to \pi^0 e^+e^-$	217
E.P. Shabalin	CP Violating Decay $\eta \to 2\pi$ in Different Theories of Breakdown of CP Symmetry	223

CESR STATUS REPORT

Karl Berkelman
Laboratory of Nuclear Studies, Cornell University

ABSTRACT

Besides extending the exploration of rare B decays and determination of CKM matrix elements, a symmetric energy e^+e^- collider like CESR can make a significant contribution to the observation and measurement of CP violation in B decays. The classic measurement of mixing-mediated $B^0\overline{B^0}$ aymmetries, previously thought to be the exclusive domain of asymmetric energy B factories, is possible at a symmetric collider, although at the price of about a factor of three in required luminosity. The symmetric collider can make the measurement of the angle γ, not accessible in the classic experiment, by observing B^+B^- rate asymmetries in decay modes such as $K\pi$ and DK. Such measurements require higher beam luminosity and improvements in particle detection. CESR and CLEO are now being upgraded to accomplish this.

1 – CESR

The Cornell Electron Storage Ring is a symmetric energy e^+e^- collider, operating since 1979 at center-of-mass energies between 9 and 12 GeV. The threshold for b quark production occurs in this energy range, and the $\Upsilon(4S)$ resonance just above $B\overline{B}$ threshold has been the ideal energy for studying the properties and interactions of the B_d and B_u mesons. At $E_{cm} = 10.58$ GeV the cross section for $e^+e^- \rightarrow \Upsilon(4S) \rightarrow B\overline{B}$ is 1.1 nb and the continuum background of non-b production is about 3 nb.

CESR boasts the world's highest colliding beam luminosity, up to $L_{pk} = 3.5 \times 10^{32}/\text{cm}^2\text{-s}$ and $\int L dt = 18\ \text{pb}^{-1}/\text{day}$. This is achieved by electrostatically separating the electron and positron orbits in a pretzel configuration, intersecting them at a ± 2 mrad crossing angle at the center of the CLEO detector. Presently,

there are 18 circulating bunches of 1.4×10^{10} particles per bunch in each beam. At the intersection point the depth of focus parameter is $\beta_v^* = 1.8$ cm, and the limiting beam-beam tune shift is $\xi_v = 0.033$. CESR can produce 20,000 B^+B^- and $B^0\overline{B^0}$ events per day.

2 – Status of B Meson Physics

In the years since the 1977 discovery of the first b quark states we have learned a considerable amount about the b, not only at CESR but also at DORIS, LEP, Fermilab, and elsewhere. Besides the charged and neutral B's we now have the B^*, B_s, B_s^*, and Λ_b. Both the Cabibbo favored $b \to c$ decay (e.g., $B \to D\ell\nu$, ..., $B \to D\pi$, ..., $B \to \phi K$, ...) and the suppressed $b \to u$ decay ($B \to \pi\ell\nu$, $B \to \pi\pi$) have been measured. Most recently, the rare effective neutral current $b \to s$ loop decays (penguins) have been seen by CLEO ($B \to K^*\gamma$, $B \to K\pi$).

In the Standard electroweak model the transitions between quark species are accomplished by the emission or absorption of the charged intermediate vector boson $W^\pm$. Each of the charge $\frac{2}{3}$ quarks $\hat{q}_i$ couples to each of the charge $-\frac{1}{3}$ quarks $\check{q}_j$ with a $\hat{q}_i\check{q}_jW$ vertex factor gV_{ij}, where the V_{ij} elements form a 3×3 unitary matrix called the CKM matrix. [1] For each matrix element the table shows the expression in terms of the four Wolfenstein parameters, [2] our present experimental knowledge of the absolute value (assuming the validity of the Standard Model but not requiring unitarity), and an example of the kind of process used for the measurement..

Cabibbo-Kobayashi-Maskawa Matrix Elements.

$V_{ud} = 1 - \lambda^2/2$	0.974 ± 0.0010	$n \to pe\overline{\nu}$	nuclear β decay
$V_{us} = \lambda$	0.2205 ± 0.0018	$K \to \pi\pi$	strange decay
$V_{cs} = -\lambda$	1.01 ± 0.18	$D \to K\pi$	charm decay
$V_{cd} = 1 - \lambda^2/2$	0.204 ± 0.017	$D \to \pi\pi$	no-s charm decay
$V_{cb} = A\lambda^2$	$0.040 \pm 0.002 \pm \mathit{0.002}$	$B \to De\nu$	b decay
$V_{ub} = A\lambda^3(\rho - i\eta)$	$0.0034 \pm 0.0002 \pm \mathit{0.0008}$	$B \to \pi e\nu$	charmless b decay
$V_{ts} = -A\lambda^2$	$0.037 \pm 0.006 \pm \mathit{0.008}$	$B \to K^*\gamma$	penguin decay
$V_{td} = A\lambda^3(1 - \rho - i\eta)$	$0.010 \pm 0.0004 \pm \mathit{0.003}$	$B^0 \leftrightarrow \overline{B^0}$	mixing

Our rather imperfect information of the ρ and η parameters is best specified in terms of the location of the apex of the triangle in the complex plane implied by the unitarity relation,

$$V_{td}V_{tb}^* + V_{cd}V_{cb}^* + V_{ud}V_{ub}^* = 0. \qquad (1)$$

The magnitude of CP violating effects will be proportional to the area of the triangle.

Since the poorly determined CKM elements are those involving the third generation (b and t quarks), there is plenty of work left to do in B physics. Improvements in the measurement of the listed B decay and mixing processes will help,

but it is probably more important to build up a wide base of B interaction data to better constrain the models that are responsible for the rather large theoretical uncertainties (in italics in the table) in the extraction of the CKM elements from the data. A symmetric energy e^+e^- collider is well suited for such measurements. What may not be so obvious is that a symmetric collider can also make a significant contribution to the measurement of CP violation in B decay.

3 – The Classic CP Violation Experiment: B^0 Decay with Mixing

In order to observe a CP violation in B meson decays we need to see an asymmetry arising from the interference of two amplitudes that have different weak phases. The $B^0 - \overline{B^0}$ mixing amplitude can provide the alternate decay route needed for interference. That is, a non-flavor-specific final state f^0 like ψK_S can be reached by either B^0 directly or after oscillating to $\overline{B^0}$. To know whether the produced meson was a B^0 or a $\overline{B^0}$ we rely on the fact that B mesons are produced in pairs of opposite flavor and tag the flavor of one B by observing the other decaying into a flavor-specific final state: $b \to \ell^- X$ versus $\bar{b} \to \ell^+ X$ or $b \to c \to s$ versus $\bar{b} \to \bar{c} \to \bar{s}$.

Since two neutral B's produced in an e^+e^- collision will oscillate to their antiparticles in a correlated way, we have to consider the joint time evolution of the $B_f B_{tag}$ pair: [3]

$$\frac{d^2N}{dt_f dt_{tag}} = \frac{N}{2\tau^2} e^{-t_f/\tau} e^{-t_{tag}/\tau} \left(1 - q \sin 2\phi \cdot \sin x_d \frac{t_f - t_{tag}}{\tau}\right), \qquad (2)$$

where N is the total number of measured tagged events, τ is the B^0 mean lifetime, $x_d = \Delta m \tau \approx 0.7$ is the mixing rate, and $q_{tag} = \pm 1$ is the sign of the charge of the tag.

The second term in the brackets contains the CP violating phase difference $\phi = \frac{1}{2}\phi_{M12} - \phi_f$, where ϕ_{M12} is the phase of the $(B^0\ \overline{B^0})$ mass matrix element M_{12} responsible for $B^0\overline{B^0}$ mixing, and ϕ_f depends on the quark transitions in the $B^0 \to f^0$ and $\overline{B^0} \to f^0$ decays. In the Standard Model M_{12} is proportional to $(V_{tb}V_{td}^*)^2$ From mixing data we know $|M_{12}|$, but ϕ_{M12} is not known experimentally. The Standard Model predicts $\phi_f = \arg(V_{cb}V_{cd}^*)$ for decay modes involving charm, such as ψK_S, and $\phi_f = \arg(V_{ub}V_{ud}^*)$ for charmless modes, like $\pi^+\pi^-$. If one can measure the CP violating asymmetry in one or several charm modes and in one or several charmless modes, one will then have direct measurements of two of the angles in the unitarity triangle. The third angle cannot be measured directly in neutral B decays.

The favored e^+e^- center-of-mass energy for the measurement is at the $\Upsilon(4S)$ resonance, because of the large cross section and the clean $B\overline{B}$ final state.

However, since the CP violating term in equation (2) is odd in $t_f - t_{tag}$, the corresponding overall rate asymmetry for $q = +1$ versus $q = -1$ vanishes identically. To see a CP violation one has to be sensitive to the asymmetry in the time dependent differential decay rates.

The favored technique [4] is to boost the $B\overline{B}$ system by colliding e^+ and e^- of different energies in order to make the decay time evolution observable. With enough luminosity, though, it is possible to make the measurement at a symmetric energy collider.

4 – The Classic Experiment at a Symmetric Collider

The mean decay length of B's from an $\Upsilon(4S)$ produced at rest is only

$$\gamma\beta c\tau = \sqrt{(M_{4S}/2m_B)^2 - 1} \times c\tau = 30\ \mu\text{m}.$$

The beams in CESR annihilate in a region of r.m.s size $\delta x \times \delta y \times \delta z = 600 \times 8 \times 18000\ \mu\text{m}^3$. In the vertical the annihilation point is tolerably well defined relative to the decay length and the vertex measurement resolution. The height $\overline{y}$ of the midpoint between the two measured decay vertices, y_f and y_{tag}, measures $t_f - t_{tag}$:

$$\overline{y} = \frac{y_f + y_{tag}}{2} = \frac{1}{2}\cos\chi \cdot \gamma\beta c(t_f - t_{tag}) + y_{beam}. \tag{3}$$

where χ is the angle between the momentum of the B_f and the upward y axis.

The mean value of $t_f - t_{tag}$ is obtained by integrating equation (2):

$$\langle t_f - t_{tag}\rangle = \frac{1}{N}\int\int (t_f - t_{tag})\frac{d^2N}{dt_f dt_{tag}}dt_f dt_{tag} = \frac{2x_d q\tau}{(1+x_d^2)^2}\sin 2\phi. \tag{4}$$

From equations (3) and (4) it is clear that whether $\overline{y}$ will tend to be above or below the beam line will depend on two signs, the charge of the tag q and the sign of $\cos\chi$, that is, whether the B that decays to ψK_S goes up or down. Combining the two signs and defining a parameter for each event,

$$k = q\frac{\cos\chi}{|\cos\chi|} = \pm 1, \tag{5}$$

we can subdivide the data set into two subclasses, depending on whether $k = +1$ or $k = -1$. If the two $\overline{y}$ means differ, CP is violated:

$$\langle\overline{y}\rangle_k = k\frac{9}{16}\frac{x_d}{(1+x_d^2)^2}\gamma\beta c\tau \sin 2\phi + y_0. \tag{6}$$

The measured difference $\Delta = \langle\overline{y}\rangle_{+1} - \langle\overline{y}\rangle_{-1}$ between the average $\overline{y}$ values for the two event subclasses will then be a direct measure of the CP violation parameter $\sin 2\phi$:

$$\sin 2\phi = \frac{8}{9}\frac{(1+x_d^2)^2}{x_d}\frac{\Delta}{\gamma\beta c\tau} = \frac{\Delta}{10.3\ \mu\text{m}}. \tag{7}$$

A $B \to \psi K_S$ Monte Carlo simulation based on the CLEO (phase 2) detector shows that the separation Δ between the weighted averages of the two distributions can be measured to an r.m.s. accuracy of

$$\delta\Delta = \frac{34\ \mu\text{m}}{\sqrt{N}}. \tag{8}$$

Combining this with equation (7) we can compute the r.m.s. accuracy in the measurement of $\sin 2\phi$ as a function of the number of measured tagged events:

$$\delta \sin 2\phi = 3.3/\sqrt{N}. \tag{9}$$

For the asymmetric B Factory the measurement sensitivity is given by $\delta \sin 2\phi = 2.0/\sqrt{N}$. That is, the penalty for not boosting the B's is a factor of about three in the number of events required.

This is the process for which the asymmetric energy B Factories were designed. However, taking advantage of good vertex resolution and small vertical beam size, a symmetric machine could make the same measurement, even at the $\Upsilon(4S)$, but it would require higher luminosities than the measurement with asymmetric energies. Only if the asymmetric machines were delayed in reaching high luminosities, or if non-standard physics made the effect anomalously large, would there be a chance for a symmetric collider to contribute significantly to this measurement.

5 – Other CP Violation Experiments

Although predictions of asymmetries at B Factories are generally based on the Standard Model for CP violation, non-standard mechanisms may actually be a more likely solution to the baryogenesis problem. Many theorists believe that the Kobayashi-Maskawa mechanism for CP violation is not sufficient to generate the observed baryon-antibaryon asymmetry in the universe or even to maintain an initial asymmetry through cool-down. [5]

Various extensions or alternatives to the Standard Model have been suggested. Such models characteristically involve hypothetical high mass particles, [6] such as fourth generation quarks, leptoquarks, squarks, gluinos, charged Higgs, charginos, right-handed W's, and so on. They have no effect on a tree diagram dominated B decay, such as $B \to \psi K_S$, but can contribute significantly to loop processes such as the box diagram in mixing. Any non-standard model would produce the predicted Standard Model results for the mixing mediated $B \to \psi K_S$ CP violation experiment, provided the phase of M_{12} were not significantly different from the value that one would (incorrectly) deduce from the already measured magnitude $|M_{12}|$ and the Standard Model box diagram. This reduces the likelihood that the

measurement of the time evolution in $B^0\overline{B^0}$ decays will produce any surprises. If we observe the expected asymmetries for $B \to \psi K_S$, we will still not be able to conclude that the Standard Model picture of CP violation is correct. Although a measurement of the asymmetry in $B \to \pi^+\pi^-$ could help, we will have to look for other kinds of CP violation in B decay, not involving $B^0 - \overline{B^0}$ mixing.

An important test of the Standard Model and a possible indicator of non-standard physics is the check to see if the three angles α, β, and γ in the unitarity triangle, as determined by CP violating asymmetries and the Standard Model, sum to π as they should if the Standard Kobayashi-Maskawa Model is correct. The angles α and β are measured in the mixing mediated neutral B asymmetries at the $\Upsilon(4S)$ resonance, but the third angle γ is not. Although γ can in principle be determined from CP violating asymmetries in B_s decays, such as $B_s \to \rho K_S$, a much more likely prospect is the measurement of the $B^+ \to K^+\pi^0$ versus $B^- \to K^-\pi^0$ decay rate asymmetry, which in the Standard Model is proportional to $\sin\gamma$.

It is likely then that in order to verify the Standard Model or to see new physics we will have to measure the untagged time-integrated B^+ versus B^- decay rate asymmetries arising from interference between two direct decay amplitudes, for instance between tree and loop decay diagrams. These searches can be carried out in any experiment in which B and $\overline{B}$ are produced in equal numbers. The CP violating asymmetry is observed simply by comparing the total numbers of observed B and $\overline{B}$ decays to the chosen mode. Tagging and decay length measurements are not needed. Many of the favorable modes are charmless modes, which do not suffer from the low detection efficiencies typical of charmed final states.

Although such measurements have not been favored, because of the dependence of the observable asymmetries on poorly known strong interaction amplitudes and phases in addition to the desired weak interaction dependences, recent work on the $B^\pm \to K^\pm\pi^0$ [7] and $B^\pm \to (D^0 \text{or} \overline{D^0})K^\pm$ [8] decays has shown that by combining measurements of closely related modes it may be possible to extract the weak parameters without prior knowledge of the strong parameters. Although the expected $B^+ \to K^+\pi^0$ versus $B^- \to K^-\pi^0$ rate asymmetry is expected to be $< 2\%$ in the Standard Model, there are other modes of the form $B \to (K \text{or} K^*) + (\rho, \omega, \text{or}\phi)$ for which similar arguments apply. but with different strong interaction magnitudes and phases. If the the interfering amplitudes are equal in magnitude and the strong interaction phase difference is 90°, the CP violating effect is enhanced by an order of magnitude relative to the effect in $B^\pm \to K^\pm\pi^0$.

Since non-standard models such as those involving charged Higgs can have enhanced CP violating effects relative to the Standard KM Model, one of them might turn out to be the key to the solution of the baryogenesis problem. Loop processes

in B decays, particularly the $b \to s$ penguin amplitude, may be our most sensitive probe of such physics. We will need to measure the branching ratios of as many such modes as we can, but even if they turn out to be as predicted by the Standard Model, it will be important to measure the CP violating $B^{\pm}$ rate asymmetries in those modes in which the loop diagram interferes with a tree diagram or where two loop diagrams with different quarks interfere.

6 – The CESR/CLEO Upgrade

The program for the study of CP violation in B decays to be carried out at a symmetric energy e^+e^- collider operating near the $B\overline{B}$ threshold includes the following goals:

1. improvement in the measurements relevant to the values of the KM matrix elements,

2. measurements of rates for B decay modes that are potential sources of CP violating asymmetries, such as ψK_S, $\pi\pi$, $K\pi$, DK, $D\overline{D}$, and related processes,

3. measurement of tagged decay time asymmetries in mixing mediated neutral B decays,

4. measurement of B^+ versus $B-$ decay rate asymmetries arising from interfering decay amplitudes.

Symmetric energy e^+e^- colliders are particularly well suited to the first two goals and have already made important contributions to our knowledge of V_{cb}, V_{ub}, V_{td}, and V_{ts} and to the study of rare loop processes in B decays. In seeking the third goal, a symmetric machine will suffer from a disadvantage relative to an asymmetric collider of the same luminosity, but a boosted $B\overline{B}$ frame has no advantage for the last goal, and may even have disadvantages.

Each of the elements of the program requires an order of magnitude increase in the size of the available B decay data set. The most straightforward way to raise CESR luminosity significantly is to increase the number of colliding beam bunches, keeping the charge per bunch at the tune shift limit. By introducing opposite displacements into the electron and positron beam orbits, including a crossing angle at the interaction point, we have over the past decade increased the number of bunches stored from the original one per beam to the present 18 per beam. Further increases up to 45 bunches are foreseen. As the total beam current is raised, the increased synchrotron radiation power requires that we upgrade the vacuum pumping and vacuum chamber hardware as well as the rf accelerating system. We have

recently successfully tested in CESR a radically new superconducting rf cavity design optimized for very high beam currents. Provided we can continue to deal with the increased synchrotron radiation power, there seems to be no physical obstacle to increasing the luminosity in the next four years by another factor of at least five, bringing CESR to the same level of luminosity proposed for the asymmetric B Factories. The conservative step-by-step approach, making use of experience gained along the way, may be more successful in achieving high luminosity than the attempt to do it all at once in the untried asymmetric energy configuration. Past projections of CESR luminosity have always been exceeded.

The search for rare B decay processes requires not only an increase in collider luminosity but also a significant upgrade in the selectivity of the detector. We have to improve the ability of the CLEO apparatus to distinguish the infrequent events of interest from the overwhelming bulk of less interesting events. The detector already represents the state of the art in resolution both in charged particle momentum and in electromagnetic calorimetry. Its weakness has always been in particle identification at momenta above about 1 GeV/c. For instance, although CLEO has seen a clear signal in the sum of $B^0 \to K^+\pi^-$ and $B^0 \to \pi^+\pi^-$, [9] it is at present not possible to distinguish unambiguously the two interesting decay modes. We are now embarked on a project to replace the tracking chambers of the CLEO detector with a new system, consisting of a four-layer silicon tracker followed by a cylindrical drift chamber, providing enough space to insert a ring imaging Cherenkov detector with a lithium fluoride radiator and a TEA photon converter. The combination of dE/dx measurements in the tracking chambers and Cherenkov imaging will provide better than four standard deviation separation of K's and π's over the full momentum range of B decays, that is, up to 2.4 GeV/c. Such a capability may be more difficult to achieve at an asymmetric collider, where the decay products can be boosted to more than 4 GeV/c.

In summary, most of the goals of the study of CP violation do not require asymmetric beam energies. Even the measurement of mixing mediated CP violation in neutral B decays, considered to be the exclusive domain of asymmetric B Factories, can be accomplished with a modest penalty in sensitivity by a symmetric machine like CESR. On the other hand, the simplicity of the symmetric energy configuration has advantages in making the achievement of high luminosity and good detector capabilities more straightforward and less risky. I am confident that CESR will be able to make a significant contribution to the observation and understanding of CP violation in B decay.

References

1. M. Kobayashi and T. Maskawa, Prog. Theor. Phys. **35**, 252 (1977); N. Cabibbo, Phys. Rev. Lett. **10**, 531 (1963).

2. L. Wolfenstein, Phys. Rev. Lett. **51**, 1945 (1984).

3. Much of the theory of CP violation in B decays was first developed by I. Bigi and A. Sanda. Their work is summarized in I. Bigi, V.A. Khoze, N.G. Uraltsev, and A. Sanda in *CP Violation*, ed. C. Jarlskog, World Scientific, Singapore, 1988, and preprint SLAC-PUB-4476 (1987). These include references to earlier work.

4. P. Oddone in *Proceedings of the UCLA Workshop on Linear Collider B-Factory Conceptual Design*, Los Angeles, 1987.

5. A.G. Cohen, D.B. Kaplan, and A.E. Nelson, Ann. Rev. Nucl. Part. Sci. **43**, 27 (1993); M. Dine, *Lepton And Photon Interactions*, ed. P. Drell and D. Rubin, AIP, 1993.

6. C.O. Dib, D. London, and Y. Nir, Modern Phys. **A6**, 1253 (1991); Y. Nir and H.R. Quinn, Ann. Rev. Nucl. Part. Sci. **42**, 211 (1992).

7. M. Gronau, J.L. Rosner, and D. London, Phys. Rev. Lett. **73**, 21 (1994); N.G. Deshpande and X.-G. He, Phys. Rev. Lett. **74**, 26 (1995).

8. M. Gronau and D. Wyler, Phys. Lett. **B265**, 172 (1991).

9. M. Battle et al. (CLEO), Phys. Rev. Lett. **71**, 3922 (1993).

BABAR: A NEW DETECTOR FOR STUDYING CP VIOLATION IN THE B SYSTEM

R. Aleksan[1]
DAPNIA/SPP, Centre d'Etudes Nucléaires, Saclay,
F-91191 Gif-sur-Yvette Cedex, France

ABSTRACT

A new detector for investigating the CP violation mechanism in the B meson system is being built and is scheduled to take data at PEP II, the asymmetric B Factory in construction at SLAC, at the end of this century. Its main characteristics are briefly overviewed in this paper. Its sensitivity for measuring CP violation in some selected B decays is also discussed, underlining the great potential of this detector to accomplish a comprehensive study of this phenomenon.

1 – Introduction

In order to explain why the observed universe is matter dominated, it is necessary to create a mechanism which allows one to distinguish matter from antimatter. This is accomplished together with a few other conditions by introducing the non-conservation of the CP symmetry in the theory describing the interactions between the particles at the early stage of the universe [1]. At the turn of the century, we should begin to understand the origin of the CP violation phenomenon observed 30 years ago by J.H. Christenson, J.W. Cronin, V.L. Fitch and R. Turlay [2] as *BABAR*, the new proposed detector at the PEP II asymmetric e^+e^- B Factory of SLAC, will record its first data at the $\Upsilon(4S)$ resonance where pairs of B mesons are produced. The expression "asymmetic B Factory" is used to designate a facility which has two beams with different energies in order to give a longitudinal boost to the center of mass system and which is able to deliver a very high luminosity ($\mathcal{L} \geq 3 \times 10^{33} cm^{-2} s^{-1}$).

The *BABAR* detector [3], a schematic view of which is shown in figure 1, has been designed by a large international collaboration consisting of about 480 physicists and engineers from 10 countries (Canada, China, France, Germany, Italy, Norway, Russia, Taiwan, UK and US). It will instrument the unique interaction region of PEP II and is scheduled to be operational by year 1999, about six months after the startup of the collider foreseen in the fall 1998.

[1] on behalf of the *BABAR* Collaboration

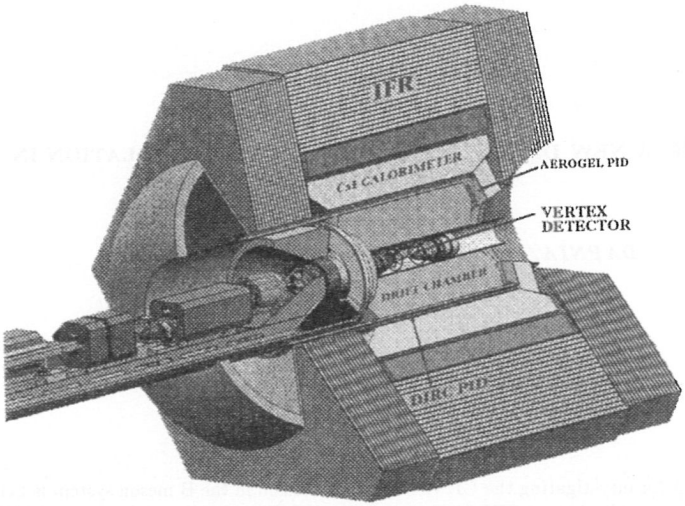

Figure 1: Schematic view of the *BABAR* detector

2 – CP violation in the B system

In the Standard Model (SM) of the fundamental interactions [SU(3)×SU(2)×U(1)], all CP non-conserving phenomena are induced through the interference of processes involving different "Weak" phases. These phases are generated by the mixing of the quark flavors via the charged weak currents, $W^{\pm}$, providing that a minimun of 3 fermion families exist. In this framework, the Cabibbo mixing 2×2 matrix [4] can be extented to a more general $n \times n$ matrix. If only 3 families of fermions exist as indicated by LEP data [5], only 3 mixing angles and one phase, δ, are necessary to describe the corresponding unitary 3×3 matrix as proposed by Kobayashi and Maskawa [6]. A useful approximation of the CKM matrix has been proposed by Wolfenstein [7].

$$V_{CKM} = \begin{pmatrix} V_{ud} & V_{us} & V_{ub} \\ V_{cd} & V_{cs} & V_{cb} \\ V_{td} & V_{ts} & V_{tb} \end{pmatrix} = \begin{pmatrix} 1-\frac{\lambda^2}{2} & \lambda & A\lambda^3(\rho - i\eta) \\ -\lambda & 1-\frac{\lambda^2}{2} & A\lambda^2 \\ A\lambda^3(1-\rho-i\eta) & -A\lambda^2 & 1 \end{pmatrix} + \mathcal{O}(\lambda^4) \quad (1)$$

Here, the parameter $\lambda = 0.2205$ is the sine of the Cabibbo angle while $A = 0.82 \pm 0.04$ is deduced from the measurements of V_{cb} [8] and ρ and η are in the range 0 to 1/2 [9]. From the various unitarity relations which can be derived, a particularly interesting one connects CKM elements related to B physics:

$$V_{ub}^{*} - \lambda V_{cb} + V_{td} \simeq 0 \quad (2)$$

This equation represents the so-called "unitarity triangle" in which the lengths of the sides are of the same order, see figure 2.

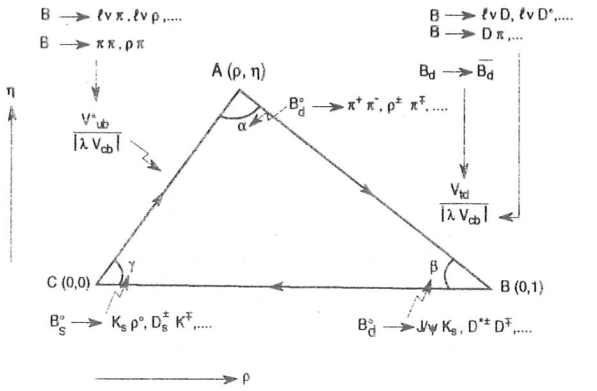

Figure 2: The unitarity triangle. Some B decay modes which are relevant for the sides and angles measurements are also indicated.

The ultimate goal of the *BABAR* detector is to observe CP violation in the B meson system in a large variety of modes. This systematic study should allow us to get either a comprehensive understanding of this phenomenon in the framework of the Standard Model or eventually explore a new domain. CP violation should manifest itself as a time dependent asymmetry in some B decays. A simple, although not exclusive, laboratory is provided by final states which are also CP eigenstates. The measured asymmetry is then directly related to the angle $\Phi = \alpha$, β or γ of the unitarity triangle as shown by the following equations.

$$Pr(\overset{(-)}{B^0} \to f_{CP}) = \frac{e^{-\Delta t/\tau}}{\tau}\left(1 \overset{(-)}{+} \eta_{CP} \sin 2\Phi \sin x_d \Delta t/\tau\right) \qquad (3)$$

where $x_d = (m_{B_1^o} - m_{B_2^o})\tau \simeq 0.735 \pm 0.045$ [9] and Δt is the decay time of the second B meson after the decay of the first one has occured. This quantity is derived through the measurement of the distance between both B decays using $\Delta t \simeq m_B \Delta z / E_B c$. In the formula above, B_1^o and B_2^o are the B_d^o mass eigenstates. Finally, η_{CP} (± 1) is the CP parity of the final state and m_B, E_B and τ are the B_d^o mass, energy and lifetime respectively.

Many B decay modes involving J/ψ and kaons, D-meson pairs and light meson pairs have been studied with detailed Monte Carlo to extract the parameters sin2β and sin2α which are directly connected to the value of the phase δ. The sensitivity to sin2β and sin2α are expected to be 0.059 and 0.09 respectively after 1 year of operation of *BABAR* at PEP II during which an integrated luminosity of 30 fb^{-1} is expected. Table 1 gives a summary of the modes which have been considered together with their "CP reach". Figure 3 shows how these errors compare with the present allowed region obtained by the measurement of the sides of the triangle. A significant improvement of the errors on the sides is also expected. constraining further the triangle and leading together with the angle measurements to a powerful consistency test of the SM in a yet

Final State	Br	Φ	$\delta(\sin 2\Phi)$
$J/\psi K^0_S$	0.5×10^{-3}	β	0.098
$J/\psi K^0_L$	0.5×10^{-3}	β	0.16
$J/\psi K^{*}$ [10]	1.6×10^{-3}	β	0.19
Sum J/ψ X		β	0.076
D^+D^-	6×10^{-4}	β	0.21
$D^{*+}D^{*-}$ [11]	7×10^{-4}	β	0.15
$D^{*\pm}D^{\mp}$ [11]	8×10^{-4}	β	0.15
Sum D D		β	0.095
Combined		β	0.059
$\pi^+\pi^-$	1.2×10^{-5}	α	0.20
$\rho\pi$ [12]	5.8×10^{-5}	α	0.11
$a_1\pi$ [12]	6×10^{-5}	α	0.24
Combined		α	0.09

Table 1: Expected errors on the measurement of $\sin 2\Phi$ from various channels with 30 fb^{-1}. The assumed branching fractions and the measured angle are also indicated.

very obscure sector of the theory.

3 – The *BABAR* detector

High performance and robust detectors are needed to accomplish this program successfully. The observation of CP asymmetries requires in particular:

- a precise measurement of the distance between the 2 B meson decays (of the order of 250 μm for beam energies of 9 GeV against 3.1 GeV as planned at SLAC)
- an efficient and relatively pure tagging of the flavor of the B which is not fully reconstructed. Electrons, muons and Kaons will be used for this purpose
- a large acceptance, a good efficiency and excellent particle identification for the modes which need to be fully reconstructed.
- a good momentum and energy resolution for the charged and neutral particles in order to reject the combinatorial background.

The *BABAR* detector has indeed been optimized [3] to fulfill the above criteria. It uses whenever possible well established technologies such as a silicon vertex detector [13], a central drift chamber, a Cesium Iodide Calorimeter [14] and Resistive Plate Chambers [15] for the intrumented flux return. Only the particle identification system uses new techniques since no currently used method is able to satisfy our required needs. The dimension, acceptance and the expected performances of the individual sub-detectors are summarized in the table 2.

In the following, we give a brief overview of the main features of the various subdetectors.

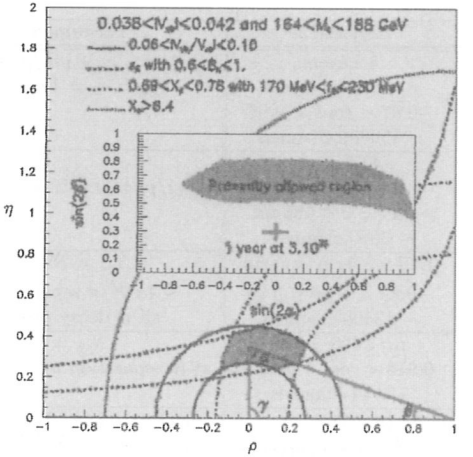

Figure 3: Present constraints of the unitarity triangle in the complex plane (ρ, η). The corresponding region for $\sin 2\beta$ versus $\sin 2\alpha$ is also shown.

3.1 The silicon vertex detector

The distance between both B decays (fig. 4) is measured by means of a double silicon vertex detector with strips running parallel and perpendicular to the beam direction. Five layers of silicon detector

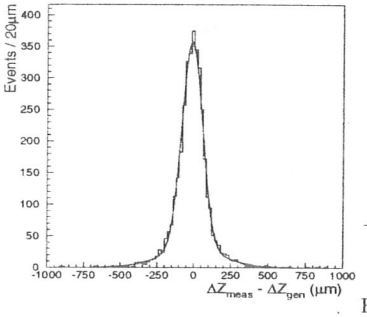

Figure 4: Resolution in Δz for $B^o \to \pi^+\pi^-$ with a primary lepton tag.

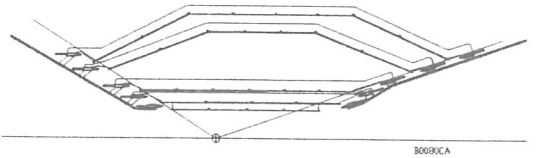

Figure 5: A view of the vertex detector in a plane containing the beam axis.

(fig. 5) at a radius extending from 3.2 to 14.4 cm from the interaction region are used for sufficient redundancy and to perform an efficient tracking of the soft pions over 91% of the solid angle. The total surface of silicon detector needed is about one m^2 with a longest strip dimension of about 24 cm. In order to minimize the multiple scattering, all the electronics is located outside of the acceptance of the detector by carrying the signals out by means of thin capton foils. This technique

Detector	Dimensions	Performance
Double-sided Silicon Strip detector	5 Layers $r = 3.2 - 14.4$ cm $-0.87 < \cos\theta < 0.96$ ~ 150000 channels	$\sigma_z = \sigma_{xy} = 50\,\mu\text{m}/p_t \oplus 15\,\mu\text{m}$ $\sigma_\phi = \sigma_\theta = 1.6\,\text{mr}/p_t$
Small Cell Drift Chamber	40 Layers $r = 22.5 - 80.0$ cm $-111 < z < 166$ cm ~ 7000 channels	$\sigma(p_t)/p_t = [0.21\% + 0.14\% \times p_t]$
DIRC Cherenkov light imaging PID	$1.75 \times 3.5\,\text{cm}^2$ quartz $-0.84 < \cos\theta < 0.90$ ~ 13400 channels	$N_{pe} = 20 - 50$ $\gtrsim 4\sigma$ K/π separation for all B decay products
Aerogel Threshold counter PID	n=1.006, 1.055 $0.916 < \cos\theta < 0.955$ ~ 140 channels	$N_{pe} = 10$ π/K separation up to 4.3 GeV/c
CsI(Tl) Calorimeter	$16 - 17.5\ X_0$ $\sim 4.8 \times 4.8$ cm crystals ~ 6800 channels	$\sigma_E/E = 1\%/E(\text{GeV})^{\frac{1}{4}} \oplus 1.2\%$ $\sigma_\theta = 3\,\text{mr}/\sqrt{E(\text{GeV})} \oplus 2\,\text{mr}$
Superconducting coil and segmented iron	IR=1.40 m L = 3.85 m	$B = 1.5$T
RPC instrumented flux return	16–17 Layers ~ 42000 channels	$\epsilon_\mu > 90\%$ for $p_\mu > 0.8$ GeV/c

Table 2: Summary of the main parameters of the *BABAR* detector (all angles are in the laboratory).

has already been tested succesfully.

3.2 The central drift chamber

Charged particle tracking is achieved in the central drift chamber with a total of 40 layers of axial and stereo wires . The inner and outer radii are 22.5 cm and 80 cm respectively. In order to ensure a very good single cell efficiency and low occupancy, a geometry with small cells (width $\simeq$ 1.8 cm) has been adopted. The momentum of the charged particles which are generated in B decays and reconstructed in the drift chamber is in the range 0.1-4.5 GeV/c. High resolution (fig. 6) is obtained by operating the chamber in a magnetic field of 1.5T generated by a superconducting solenoid. To improve further the momentum resolution, the multiple scattering is reduced by using a low Z gas [16, 17] such as He:i-C_4H_{10} 80:20. Cosmic tests with this type of gas have shown that excellent single cell resolution can be achieved ($\sigma \simeq 120 - 140\ \mu m$ on average) (fig. 7).

3.3 The particle identification system

Particle identification is one of the key elements of this detector. It is necessary to obtain a good effective tagging efficiency. Electron identification is done with the combination of the CsI calorimeter (see below) and the drift chamber. Muons are identified down to 0.5 GeV/c by instru-

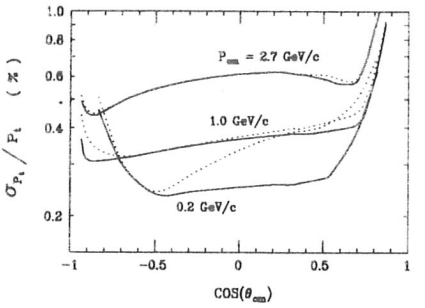

Figure 6: Transverse momentum resolution versus the center of mass angle. The dotted curve show the total momentum resolution (σ_p/p) assuming a 100 μm vertex constraint.

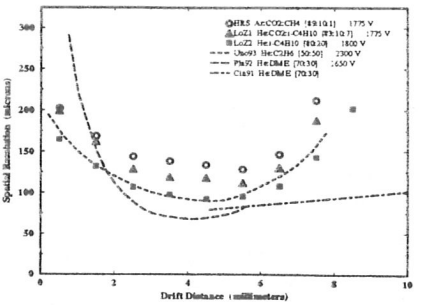

Figure 7: Single cell resolution for different gas mixture measured in a prototype chamber. Curves are the results of studies done elsewhere.

menting the flux return with 17 layers of Resistive Plate Chambers. This fine segmentation allows one in addition to identify K_L, increasing thus the sensitivity to $\sin(2\beta)$. Finally Kaon identification is achieved over 90% of the solid angle with dedicated detectors based on the observation of Čerenkov light. A novel technique (DIRC [18]) is used in the barrel region (fig. 8). It is based

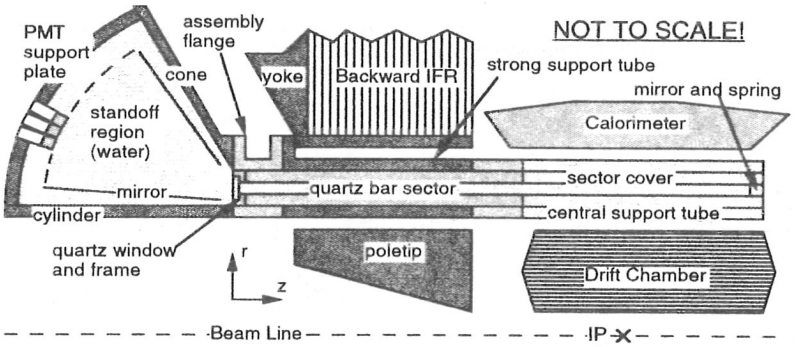

Figure 8: Schematic view of the DIRC (not to scale).

on the collection of Čerenkov light produced by the particle traversing quartz bars. The light is internally reflected in the 4.8 m long bars and detected outside of the flux return on an array of about 13000 phototubes allowing one to reconstruct the image of a truncated Čerenkov cone. A striking particularity of this device is the increase of the number of photoelectrons as the tracks are going toward the forward direction, giving a good π/K separation over the full acceptance of the detector for the most energetic particles produced in B decays such as in the reaction $B \to \pi^+\pi^-$ (fig. 9). Most recent beam tests at CERN [19] have confirmed the promising potential of such

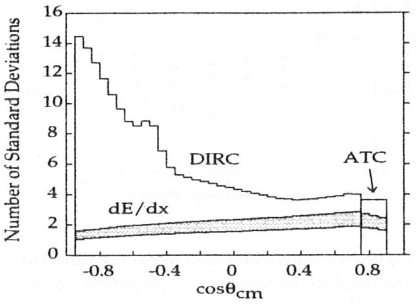

Figure 9: π/K separation for pions from $B \to \pi^+\pi^-$ as a function of the polar angle of the most energetic pion using DIRC and Aerogel. The shaded region shows the separation using dE/dx only.

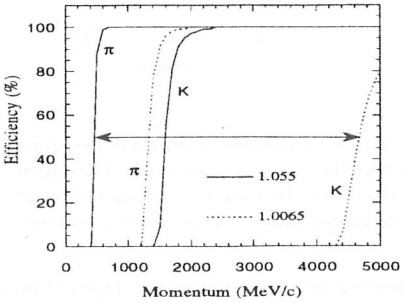

Figure 11: Threshold curve for pions and kaons as a function of momentum for the two aerogel index.

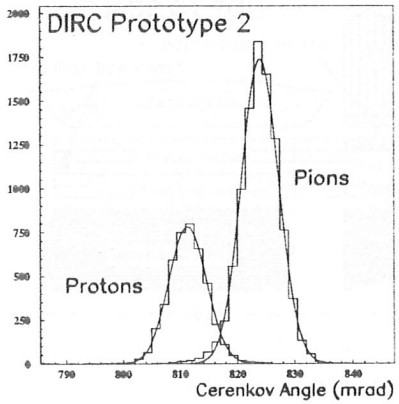

Figure 10: π/p separation at p=5.4 GeV/c (corresponding to π/K separation at 2.7 GeV/c) as obtained from a beam test using a detector equivalent to a quarter of the final device.

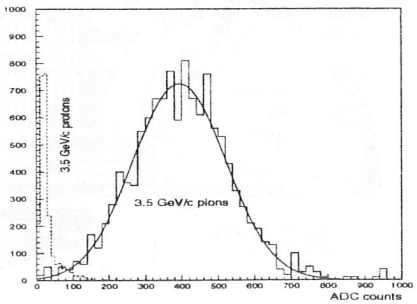

Figure 12: Responses of a prototype 1.0085 aerogel counter to 3.5 GeV/c pions (solid line) and the below threshold protons using a fine mesh tube in a 1.3T magnetic field.

a detector (fig. 10). In the forward region, the Kaon identification is performed using Aerogel Threshold Counters (ATC) with a combination of two different indices (n_1=1.0065 and n_2=1.055) (fig. 11) possibly readout by fine mesh photomultipliers or hybrid photodiodes. Beam test results have established the proof of principle of such a detector as can be seen from fig. 12.

3.4 The CsI calorimeter

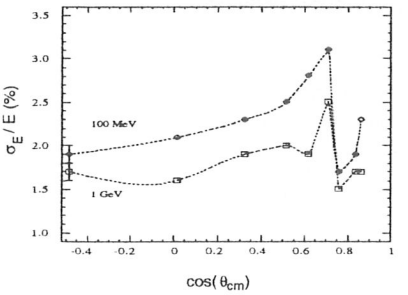

Figure 13: Single photon energy resolution as a function of the polar angle for $E_\gamma = 0.1$ and 1.0 GeV.

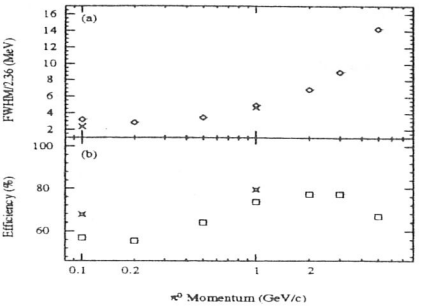

Figure 14: (a) Mass resolution and (b) efficiency for π^o generated at $\cos\theta_{cm} = 0^o$ vs the π^o energy. The crosses indicate the performance with no material in front of the calorimeter.

The average photon energy in generic B decays is about 200 MeV with a maximum energy above 4 GeV in some specific B decay modes. It is therefore mandatory to get a very low detection threshold ($\sim$ 20 MeV). Furthermore, excellent energy resolution over a large energy range is required to suppress the combinatorial background. These considerations have lead the collaboration to choose a calorimeter made of about 6800 CsI crystals read out by silicon photodiodes -presently the best calorimeter option. The depth of the crystals is gradually increased from 16.0 X_0 to 17.5 X_0 as one goes from the backward region to the forward end cap to match the boost of the particles. The expected performance of the calorimeter is briefly summarized in the figures 13 and 14. Such a device is operating very satisfactorily in the CLEO II detector.

3.5 The instrumented flux return

Finally, as mentioned above, 17 layers of Resistive Plate Chambers [20] are used to instrument the flux return. Such chambers offer an efficient, robust and economical way for optimizing the acceptance coverage as demonstrated by operating experiments [15]. In addition to providing a very effective muon detection (fig. 15), this system allows one to reconstruct K_L^o and therefore to study the CP asymmetry in the mode $B \to J/\psi K_L^0$ (fig. 16).

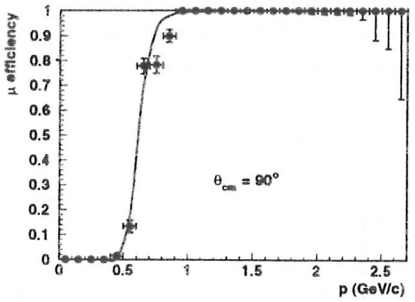

Figure 15: Efficiency for identifying muons with $\cos\theta_{cm} = 0$ as function of the muon momentum.

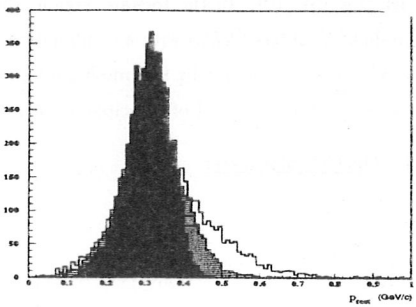

Figure 16: Reconstructed momentum of the B meson in the $\Upsilon(4S)$ rest frame for $B \to J/\psi K_L^0$ (dashed). The narrower distribution is due to the beam energy smearing while the broadest one shows the effect of removing the RPC layer inside the coil.

4 – Conclusion

The *BABAR* detector provides a very promising tool to explore in detail the CP violation mechanism. It will allow us to make a comprehensive study of this phenomenon about 35 years after its discovery, possibly leading us toward new directions in particle Physics.

References

1. A.D. Sakharov, Pis'ma Zh. Ekps. Teor. Fiz. **5** (1967) 32.

2. J.H. Christenson, J.W. Cronin, V.L. Fitch and R. Turlay, Phys. Rev. Lett. **13** (1964) 138.

3. *BABAR* Technical Design Report, SLAC-R-95-457, March, 1995.

4. N. Cabibbo, Phys. Rev. Lett. **10** (1963) 531.

5. B. Adeva et al, L3 Collaboration, Phys. Lett. B **231** (1989) 509;
   D. Decamp et al, ALEPH Collaboration,, Phys. Lett. B **231** (1989) 519;
   M.Z. Akrawy et al, OPAL Collaboration,, Phys. Lett. B **231** (1989) 530;
   P. Aarino et al, DELPHI Collaboration,, Phys. Lett. B **231** (1989) 539.

6. M. Kobayashi and T. Maskawa, Prog. Theor. Phys. **42** (1973) 652.

7. L. Wolfenstein, Phys. Rev. Lett. **51** (1983) 1945.

8. J.M. Gerard, Plenary talk at the High Energy Physics conference of European Physical Society, Brussels, 7/27-8/2. 1995.

9. R. Aleksan, Plenary talk at the High Energy Physics conference of European Physical Society, Brussels, 7/27-8/2, 1995.

10. B. Kayser, M. Kuroda, R.D. Peccei and A.I. Sanda, Phys. Lett. B **237** (1990) 508; I. Dunietz, H. Quinn, A. Snyder, W. Toky and H.J. Lipkin, SLAC-PUB-5270, November 1990.

11. R. Aleksan, A. Le Yaouanc, L. Oliver, O. Pene and J.C. Raynal, Phys. Lett. B **317** (1993) 173.

12. R. Aleksan, I. Dunietz, B. Kayser, F. Le Diberder, Nucl. Phys. B **361** (1991) 141.

13. see for example G.Batignani *et al.*, Nucl. Inst. and Meth. A **310** (1991) 160, Nucl. Inst. and Meth. A **320** (1992) 66.

14. Y. Kubota *et al.*, Nucl. Inst. and Meth. A **320** (1992) 66.

15. see for example A. Aloisio et al., Proceedings of the Sixth Pisa Meeting on Advanced Detectors, Isola d'Elba, Italy (1994), submitted to *Nucl. Instr. Methods.*

16. S.M. Playfer, R. Bernet, R. Eichler and B. Stampfli, Nucl. Inst. and Meth. A **315** (1992) 494.

17. A. Boyarski, D. Briggs and P. Burchat, Nucl. Inst. and Meth. A **323** (1992) 267.

18. P. Coyle *et al.*, Nucl. Inst. and Meth. A **343** (1994) 292.

19. G. Hamel de Monchenault and M. Zito, *BABAR* -DIRC note-1 ,July 1995.

20. R. Santonico and R. Cardarelli, Nucl. Inst. and Meth. A **187** (1981) 377, Nucl. Inst. and Meth. A **263** (1988) 20.

KEK B-FACTORY PROJECT AND THE BELLE EXPERIMENT

Toru Iijima
National Laboratory for High Energy Physics, Tsukuba 305, Japan

ABSTRACT

A B-factory project at KEK, referred to as "KEKB", began officially in 1994. An asymmetric double-ring collider of 3.5 GeV positrons and 8 GeV electrons, designed to provide a peak luminosity of 10^{34} cm^{-2}s^{-1}, is being constructed. The production and decay of B mesons at the $\Upsilon(4S)$ resonance will be studied with a detector named "BELLE". A definitive test of the standard model for the CP-violation mechanism will be performed. The current status of the KEKB project and the BELLE detector are presented.

1 Introduction

At KEK, a B-factory project "KEKB" is in progress. The project was approved by the government in 1994. The existing TRISTAN complex will be upgraded to a 3.5 GeV e^+ × 8 GeV e^- asymmetric collider to produce $B\overline{B}$ pairs on the $\Upsilon(4S)$ resonance in a moving CM frame. The collider is equipped with a single detector "BELLE", and B meson decays will be studied in detail. The primary goal of the experiment is to detect CP violating effects in B meson decays and to provide definitive information regarding the mechanism of CP violation. Moreover, detailed studies of the decay processes of B mesons, the heaviest flavor which can be easily obtained currently, may provide a first look at phenomena beyond the standard model.

In the BELLE experiment, the standard model prediction for the CP violation mechanism can be tested by determining the three angles and sides of the so-called "unitarity triangle", which is shown in Fig. 1. The sensitive decay modes for each angle and side are indicated in the figure. CP violation is represented by non-zero or non-180° values of the three internal angles, which can be measured through the CP violating asymmetry A_f. The asymmetry A_f is expressed as:

$$A_f = \frac{R(B^0 \to f) - R(\overline{B^0} \to f)}{R(B^0 \to f) + R(\overline{B^0} \to f)} = sin2\phi_{CP} \cdot sin(\Delta m \cdot \Delta t)\,. \qquad (1)$$

where Δm denotes the mass difference of two B^0 mass eigenstates and Δt the proper time difference of the B^0 and $\overline{B^0}$ decays. The angle ϕ_{CP} is the phase difference between the $B^0 - \overline{B^0}$ mixing amplitude and the $B^0 \to f$ decay amplitude, and is

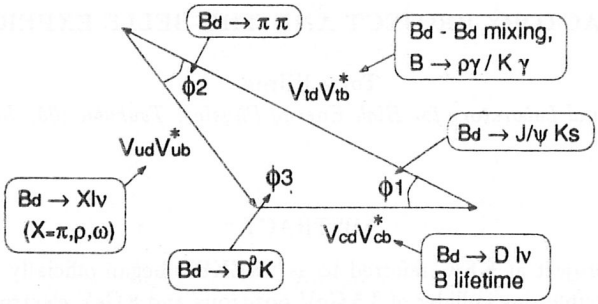

Figure 1: Unitarity triangle.

directly related to the internal angles ϕ_i. The two angles ϕ_1 and ϕ_2 are determined with this technique by using the decay modes, $B^0 \to J/\psi K_S$ ("gold-plated mode") and $B^0 \to \pi\pi$, respectively.

For these measurements, a high intensity source of B mesons is indispensable because the branching fractions for the decay modes of interest in CP violation are small, typically a few times 10^{-5}. In order to test the standard model by determining the three angles and sides of the unitarity triangle, a total integrated luminosity of 100 fb^{-1} is required. KEKB is designed to provide a peak luminosity of 10^{34} cm^{-2}s^{-1} to achieve this goal. Another key issue is the measurement of Δt in Eq.1. The asymmetry A_f vanishes if it is integrated over time. The 3.5 GeV e^+ × 8.0 GeV e^- asymmetric collider produces the $\Upsilon(4S)$'s in a moving CM frame, so that the decay length of B meson is stretched by a Lorentz boost with $\beta\gamma = 0.42$. The BELLE detector is designed to have a vertex resolution of $\Delta z \sim 80\,\mu$m, so that the time evolution of B decays can be tracked. In this paper, the KEKB accelerator and the BELLE experiment are reviewed and their present status are reported.

2 KEKB Accelerator

KEKB is a high luminosity, asymmetric electron-positron collider, which is optimized for studies of the production and decays of B mesons at $E_{CM} = 10.58$ GeV[1]. Fig. 2 shows a schematic layout of KEKB. Two rings, a high energy ring (HER) for 8 GeV electrons and a low energy ring (LER) for 3.5 GeV positrons, will be built side-by-side in the existing TRISTAN tunnel. Beams are injected from a linac and are collided at an interaction point (IP) in the Tsukuba experimental hall, where the BELLE detector will be installed. The present 2.5 GeV linac will be upgraded to 8 GeV, so that beams can be injected without intermediate acceleration. This

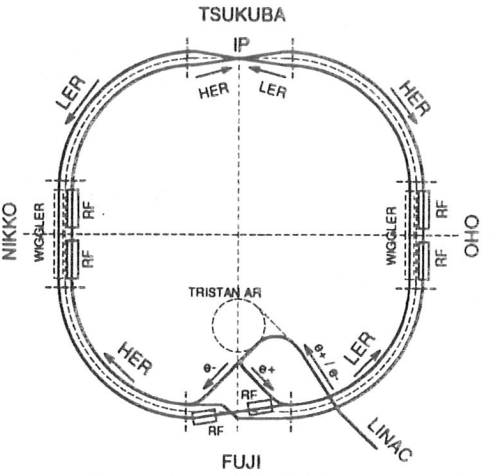

Figure 2: Schematic layout of KEKB.

will be achieved by increasing the number of accelerator structures from 160 to 240 units, by increasing the power and number of klystrons from 30 MW to 60 MW and from 40 to 60, respectively, and by using SLED (SLAC Energy Doubler) pulse compression cavities. The positron bunch intensity will also be increased by a factor of ~ 20, by raising the e^- beam energy at the e^+ production target from 200 MeV to 4.5 GeV.

In Table 1 are shown the major machine parameters of KEKB. The luminosity for flat beams is expressed in the following form in units of $\mathrm{cm^{-2}s^{-1}}$:

$$L = 2.2 \times 10^{34} \cdot \xi \cdot \frac{E \cdot I}{\beta_y^*}, \tag{2}$$

where ξ is the beam-beam tune shift, E the energy in GeV and I the current in Ampere and β_y^* is the vertical beta function at IP. Therefore, for the goal luminosity of $10^{34}\,\mathrm{cm^{-2}s^{-1}}$, the required beam intensities are $I = 1.1$ A for HER and $I = 2.6$ A for LER, with $\xi = 0.05$ and $\beta_y^* = 1cm$. This goal will be achieved in full-bunch operation, where every RF bucket is filled. In this case, approximately 5000 bunches will be stored in the ~ 3000 m circumference ring.

The most serious problem in storing large beam currents is longitudinal coupled-bunch-instability (CBI), which is excited in RF cavities in the accelerating mode. Both normal conducting and superconducting RF cavities are being considered as solutions. The normal conducting RF cavity, referred to as "ARES"

Table 1: machine parameters of KEKB.

Ring		LER	HER	
Energy	E	3.5	8.0	GeV
Luminosity	$\mathcal{L}$	1×10^{34}		$cm^{-2}s^{-1}$
Half crossing angle	θ_x	±11		mrad
Tune shifts	ξ_x/ξ_y	0.039/0.052		
Beta function at IP	β_x^*/β_y^*	0.33/0.01		m
Beam current	I	2.6	1.1	A
Bunch spacing	s_b	0.6		m
Particles/bunch	N	3.3×10^{10}	1.4×10^{10}	
Number of bunches / ring	N_B	5000		
Circumference	C	3016.26		m

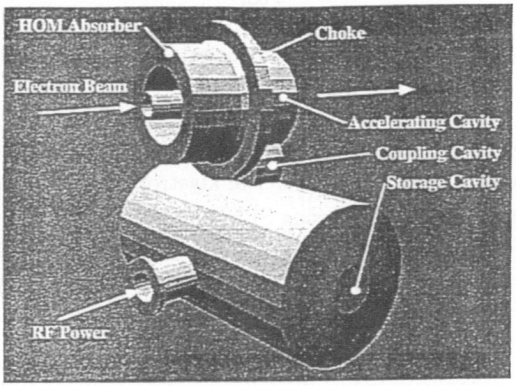

Figure 3: Schematic view of ARES.

(Accelerator Resonantly coupled with Energy Storage), is under development. The system consists of three cavities: an acceleration cavity, a coupling cavity and an energy storage cavity; as shown in Fig. 3. The total stored energy in the three-cavity system is significantly increased by the energy storage cavity, and thus the growth rate of CBI is reduced. The acceleration cavity has a damped structure, in which the higher order mode (HOM) field is absorbed by micro-wave absorbers. The superconducting RF cavity is characterized by a simple, large beam pipe and antenna-type input couplers. While the development of both technologies are in progress, ARES is expected to play a leading role in the initial phase. Both ARES and a superconducting cavity will be tested with a beam of up to 500 mA, stored in TRISTAN-AR, in 1996.

In full-bunch operation at KEKB, the bunch spacing is as short as 0.6 m. In order to avoid parasitic collisions of opposing beams, the two beams must be separated immediately before and after the collision. In the KEKB design, a finite crossing angle scheme has been chosen instead of the head-on collision scheme. The half crossing angle is 11 mrad. In this choice, large beam separation at the first parasitic collision point is obtained, and separation bend magnets are no longer necessary. This leads to a significant reduction of synchrotron radiation at the IP, which may cause background problems for detector operation. A risk is the possible luminosity reduction due to geometrical effects and excitation of synchro-betatron resonances. However, a recent simulation of beam-beam interactions has shown that, although some new resonances are excited, there are still regions of the tune diagram suitable for operation [1,2]. Moreover, a Crab crossing scheme is considered as a fall-back solution. In this technology, the head-to-tail orientations of opposing bunches are re-aligned by a special RF cavity (Crab cavity) and the beam-beam effects are made equivalent to those for head-on collisions. A superconducting Crab cavity has been developed in a joint KEK-Cornell collaboration. The R&D is in progress, aiming toward the fabrication of full scale Crab cavities in three years.

Dismantlement of the TRISTAN complex has already started, and machine commissioning will commence in the Fall of 1998.

3 BELLE Experiment

3.1 Overview

In order to carry out the above mentioned experiment for B meson decays, the detector must have the following attributes:

- A good vertex resolution is essential for measuring the proper time difference of Δt in Eq.(1). The goal is to measure Δt with a resolution better than $\tau/2$ (τ is the proper life time of the B meson), corresponding to a 95 μm position resolution along the beam direction.

- For charged particle tracking, detection of low-p_t tracks, such as π's from $B^0 \to D^{*+} l\nu \to D^0\pi^+ l\nu$, is important. A good momentum resolution is also important for reducing background contamination in the kinematical reconstruction of events. A typical example is the $B \to \pi^+\pi^-$ decay, sensitive to the angle ϕ_2, which must be separated from $B \to K^\pm\pi^\mp$.

- Particle identification is needed for tagging the flavor of the B mesons and for reconstructing exclusive B-meson final states. Flavor tagging uses the sign of the charged K mesons as well as the charged leptons. The detector must

be able to separate charged π's and K's in the momentum region from 0.2 to 1.5 GeV/c for flavor tagging, and up to 4 GeV/c for the measurement of exclusive modes, such as $B \to \pi^+\pi^-$.

- Electromagnetic calorimetry must be made with high efficiency and good energy resolution, including the low momentum region, because most of B decays have associated γ's.
- Detection of K_L's and μ's is important for some decay modes. In particular, for the ϕ_1 measurement, identification of K_L's are necessary for detecting $B^0 \to J/\psi K_L$ decays, and that of $\mu^\pm$ is necessary for reconstructing $J/\psi \to \mu^+\mu^-$.

The BELLE detector has been designed, taking into account these requirements. Fig. 4 shows the layout of the detector, which is configured around superconducting solenoid, that provides a 1.5 Tesla magnetic field, and its iron return yokes. Decay vertices of B mesons are reconstructed by a silicon vertex detector (SVD). Charged particle tracking is provided by a wire drift chamber (CDC), that extends to a radius of 90 cm. Particle identification is made by a Ćerenkov counter (PID) and time-of-flight counter (TOF) arrays, together with a dE/dx measurement in CDC. Electromagnetic showers are detected in a nine-thousand block array of CsI(Tℓ) crystals (CsI) located inside the solenoid coil. Muons and K_L mesons are identified by an array of detectors (KLM), interspersed in the iron return yoke of the magnet. Recently, a threshold aerogel Ćerenkov counter (ACC), the principle of which has been proven in beam tests, has been selected as the PID device, among possible technologies which included a fast-RICH and a DIRC (Detection of Internally Reflected Ćerenkov light) counter.

In order to realize the BELLE detector, an international collaboration of forty institutes from nine countries was formed in 1993. Following the submission of a Letter of Intent (LoI)[3], the collaboration submitted a Technical Design Report (TDR)[4] in December 1994. The experiment has been fully approved by the Lepton Collider Program Advisory Committee (LCPAC) of KEK. The performance and present status of each detector component are described in the following subsections.

3.2 Detector components

3.2.1 Vertex Detector (SVD)

Double-sided Silicon Strip Detectors (DSSD) with z strips (n-type strips) and $r-\phi$ strips (p-type strips) are used as the detector element. The readout of the z-strips is made via a Double Metal Layer (DML) structure. Fig. 5 shows the configuration of the SVD. Four DSSD layers are arranged in two superlayers, each having two

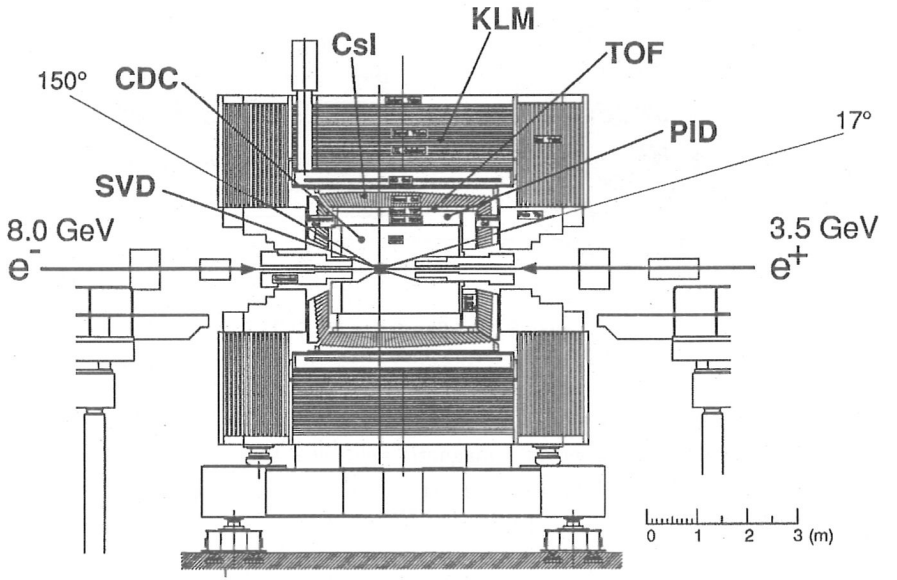

Figure 4: The BELLE detector.

DSSD sublayers with a 2 mm distance between them. The z-strip pitch is widened (as wide as 250 μm for elements in the forward edge) until the contribution to the vertex resolution from the detector position resolution becomes comparable to that from multiple scattering effects. A signal-to-noise ratio of more than 20 is expected with the presently designed readout electronics. The two-superlayer configuration is advantageous in reducing the noise hits, which is important for fast triggering. The expected vertex resolution is $\Delta z \sim 80\,\mu$m, and well satisfies our requirement.

3.2.2 Charged Particle Tracking (CDC)

A wire drift chamber (CDC) covers the radial region from 8 cm to 89 cm. The chamber consists of 52 layers of wires arranged in 13 superlayers, which are either coaxial or small-angle-stereo. For the inner three layers, signals are read out by cathode strips to provide the fast z-trigger information and good z-track extrapolation resolution back to the SVD. The use of a low-Z gas is essential for minimizing the material. The selected 50% He - 50% C_2H_6 gas mixture has a long radiation length (640 m), has a drift velocity that saturates at 4 cm/μs for a relatively low electric field and also has a good dE/dx resolution provided by the large ethane component.

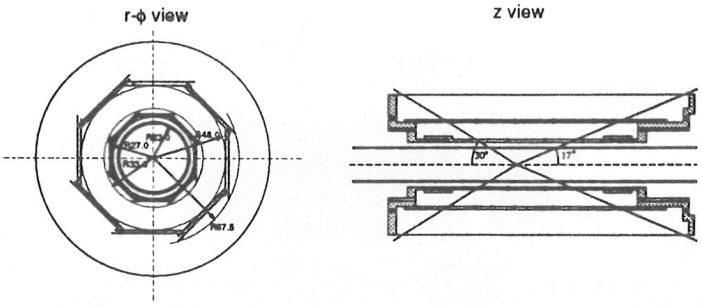

Figure 5: Configuration of SVD.

Fig. 6 shows the results of a beam test of a prototype chamber. A position resolution of 128 μm has been obtained in a magnetic field of 1 Tesla. The obtained dE/dx resolution is 10% with 10 layers sampling, which is extrapolated to 5% with more than 40 samplings in the real chamber.

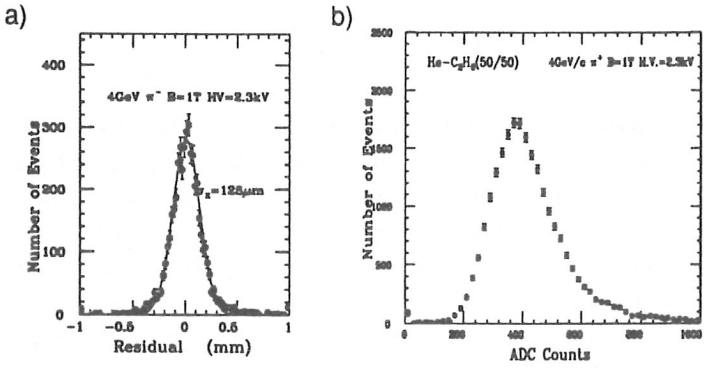

Figure 6: Beam test results of a CDC prototype chamber: a) position resolution and b) dE/dx distribution for 10 layers.

3.2.3 *Particle Identification (TOF and PID)*

The time-of-flight (TOF) counter array is used for π/K separation in the momentum region below 1.2 GeV/c. It is a 128-element array of 4 cm thick, 2.5 m long plastic scintillator bars, instrumented with a 2" diameter finemesh PMT on each end. The expected timing resolution is about 100 ps, while the typical flight path length from

the IP is 1.2 m. The covered momentum region is extended up to 3.6 GeV/c by aerogel Čerenkov counters ACC. The barrel ACC is a 960-element array, each having an approximately 12 $cm \times 12$ $cm \times 12$ cm aerogel radiator. The refractive index of the aerogel radiator is 1.010, 1.015 or 1.020 depending on the polar angle. Each detector module is instrumented with two finemesh PMT's, of which the diameters are 3", 2.5" and 2" for $n = 1.010, 1.015$ and 1.020 modules, respectively. The production of low index silica aerogels, with hydrophobic characteristics, has become possible at KEK. In Fig. 7 are shown the beam test results for an $n = 1.015$ ACC module. Fig. 7-a) shows the pulse height spectra for 3.5 GeV/c π^-'s and subthreshold 0.7 GeV/c π^-'s (dashed), while Fig. 7-b) shows the detection efficiencies for π's and K's as a function of the momentum. The endcap ACC is a 298-element array, each having an approximately 10 $cm \times 10$ $cm \times 10$ cm aerogel radiator and instrumented with one 3" diameter finemesh PMT. The refractive index is chosen to be $n = 1.030$, so that it also serves for the flavor tagging.

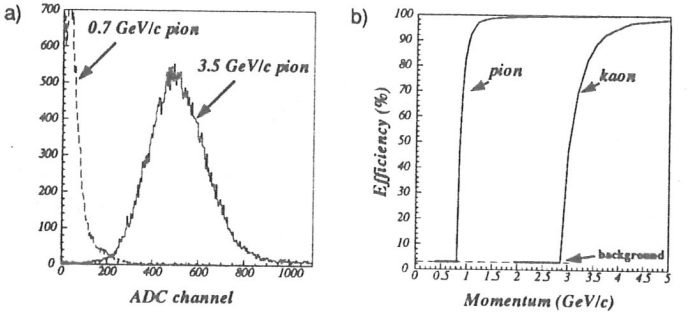

Figure 7: Beam test results of an $n = 1.015$ ACC prototype counter (see text).

3.2.4 *Electromagnetic Calorimetry (CsI)*

The electromagnetic calorimeter is composed of about 9000 CsI(Tℓ) crystals. The size of each CsI(Tℓ) crystal is determined so that approximately 80 % of the total energy deposited by a photon injected at the center is contained in the crystal. The length has been chosen to be 30 cm, corresponding to 16.2 X_0. Signals will be read out by two silicon photodiodes, attached to the end of each crystal block. The equivalent electronic noise is expected to be about 500 electrons per channel. Fig. 8 shows the energy resolution as measured with beam. With all the inner detectors included, a simulation predicts that the energy dependence of the energy resolution

is expressed in the form $\sigma/E = 0.73(\%)/\sqrt{E(GeV)} \oplus 2.1(\%)$. Production of crystals has already started.

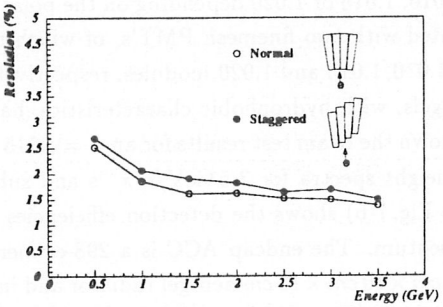

Figure 8: Energy resolution of CsI(Tℓ) as measured with beam.

3.2.5 K_L and Muon Detection (KLM)

The KLM detector consists of an octagonal barrel and two endcaps that are composed of a sandwich of fourteen 5 cm iron absorber plates and fifteen (fourteen) 4 cm instrumented gaps in the barrel (in each endcap). Resistive Plate Chambers (RPC's) have been selected as the device technology. Long-term stability tests are in progress using several resistive electrode materials such as ABS, bakelite and glass.

3.3 CP Reach

A Monte Carlo simulation has been performed to examine the capability of the BELLE detector for determining the angles and sides of the unitarity triangle. The expected accuracy in the measurement of three angles, with 100 fb^{-1} data and based on the present detector design, are summarized in Table 2. Details of the study can be found in Ref.3. Combining data from all the possible channels, the expected accuracy for the angle measurement is 0.06 for $sin\,2\phi_1$, 0.10 for $sin\,2\phi_2$ and 13° for ϕ_3. As for the three sides, the expected accuracy is $\sim$ 1% for $|V_{cb}|$ and $|V_{ub}|$ and 12 $\sim$ 25% for $|V_{td}/V_{ts}|$. The redundant measurements of the unitarity triangle to these accuracies will allow us to test the standard model.

4 Summary

In this paper, the current status of the KEKB accelerator and the BELLE experiment have been reviewed. The conversion of the TRISTAN complex to the KEKB

Table 2: Expected accuracy for the determination of three angles of the unitarity triangle.

Quantity	Decay mode	BR	Expected error
$sin(2\,\phi_1)$	$J/\psi\,K_S$	5.0×10^{-4}	0.08
	$J/\psi\,K_L$	5.0×10^{-4}	0.13
	$J/\psi\,K^{*0}$	1.6×10^{-3}	$0.17 \sim 0.46$
$sin(2\,\phi_2)$	$\pi^+\pi^-$	1.3×10^{-5}	0.17
	$\rho^\pm\pi^\mp$	6.0×10^{-5}	$0.11 \sim 0.24$
ϕ_3	$B^0 \to D^0\,K_S$	5.0×10^{-5}	$\leq 25°$
	$B^\pm \to D^0\,K^\pm$	3.5×10^{-4}	$\leq 15°$

accelerator has already started. The ultimate luminosity goal is $10^{34}\,\mathrm{cm}^{-2}\mathrm{s}^{-1}$. In order to overcome coupled-bunch-instabilities, which are the most serious problem for storing large beam currents, development of two types of RF cavities, a normal conducting cavity "ARES" and a superconducting cavity, is in progress. A finite crossing angle scheme with an 11 mrad half crossing angle has been chosen, which enables us to attempt high luminosity operation at an early stage.

The production and decay of B mesons will be studied in detail with the BELLE detector. Intensive R&D work is now in progress, and the detector design is near completion. Production of some detector components has already begun. The primary goal of the BELLE experiment is redundant measurement of the unitarity triangle. The standard model prediction for the CP violation will be tested with an integrated luminosity of more than 100 fb^{-1}.

We aim to start the KEKB accelerator commissioning in the Fall of 1998, at which time, the BELLE detector will already be installed in the beam line. Data taking is expected to commence in early 1999.

References

1. The KEKB Accelerator Technical Design Report, KEK (in press).

2. N.Toge and K.Hirata, KEK Preprint 94-160, 1994

3. The BELLE Collaboration, Letter of Intent for *A Study of CP Violation in B Meson Decays*, KEK Report 94-2, 1994.

4. The BELLE Collaboration, Technical Design Report for *A Study of CP Violation in B Meson Decays*, KEK Report 95-1, 1995.

CP VIOLATION AT HADRONIC MACHINES: HERAB

Andreas Schwarz
DESY, Notkestrasse 85, DESY, Notkestrasse 85, 2000 Hamburg 52, (Germany)

(No written contribution arrived)

CP VIOLATION FOR PEDESTRIANS

Harry J. Lipkin
Department of Particle Physics, Weizmann Institute of Science
Rehovot 76100, Israel
and
Raymond and Beverly Sackler Faculty of Exact Sciences
School of Physics and Astronomy, Tel Aviv University, Tel Aviv, Israel

ABSTRACT

The difficulties which prevented new CP violation effects from being found experimentally until now are discussed and a simple pedestrian guide is presented to the two approaches presently considered in kaon and B physics: CP violating charge asymmetries and neutral meson mixing.

1 – Introduction - two ways to see CP violation

Before 1964 the two kaon flavor eigenstates K^o and $\bar{K}^o$ carrying strangeness ± 1 were believed to be CP - conjugate and mixed by a CP-conserving weak interaction into mass eigenstates $|K_S\rangle$ and $|K_L\rangle$ which were also CP eigenstates with opposite eigenvalues. Very different lifetimes arise ($\tau_S = 9 \times 10^{-11}$ sec; $\tau_L = 5 \times 10^{-8}$sec) because the dominant 2π decay mode with largest phase space is allowed by CP only for K_S. $K_L \to 2\pi$ was a transition between CP-eigenstates with opposite eigenvalues and therefore forbidden.

So far the only experimental evidence for CP violation is the 1964 discovery [1] of $K_L \to 2\pi$ where the two mass eigenstates produced by neutral meson mixing both decay into the same CP eigenstate. This result is described by two parameters,

$$\eta_{+-} \equiv \frac{\langle \pi^+\pi^- | T | K_L \rangle}{\langle \pi^+\pi^- | T | K_S \rangle} \equiv \epsilon + \epsilon'; \qquad \eta_{oo} \equiv \frac{\langle \pi^o\pi^o | T | K_L \rangle}{\langle \pi^o\pi^o | T | K_S \rangle} \equiv \epsilon - 2\epsilon' \qquad (1.1)$$

Today $\epsilon \approx$ its 1964 value, ϵ' data are still inconclusive and there is no new evidence for CP violation. One might expect to observe similar phenomena in other systems and

also direct CP violation as charge asymmetries between decays of charge conjugate hadrons $H^{\pm} \to f^{\pm}$. Why is it so hard to find CP violation? How can B Physics help? Does CP lead beyond the standard model? We now present a pedestrian symmetry approach which exhibits the difficulties and future possibilities of these two types of CP-violation experiments, neutral meson mixing and direct charge asymmetry: what may work, what doesn't work and why.

2 – Charge asymmetries - Difficulties and possibilities

2.1 How CPT complicates detection of CP Violation

Can decays of K^+ and K^- be different? For decays to charge conjugate final states $|f^{\pm}\rangle$ described by the Fermi Golden Rule, CPT and hermiticity show there is no asymmetry,

$$W_{K^{\pm} \to f^{\pm}} \approx (2\pi/\hbar) |\left\langle f^{\pm} \right| H_{wk} \left| K^{\pm} \right\rangle|^2 \rho(E_f) \tag{2.1}$$

$$\frac{|\langle f^-| H_{wk} |K^-\rangle|}{|\langle f^+| H_{wk} |K^+\rangle|} = \frac{CPT |\langle f^-| H_{wk} |K^-\rangle|}{|\langle K^+| H_{wk}^{\dagger} |f^+\rangle^*|} = \frac{|\langle K^+| H_{wk} |f^+\rangle|}{|\langle K^+| H_{wk} |f^+\rangle^*|} = 1 \tag{2.2a}$$

CPT also requires equal total widths of K^+ and K^-. Since s-wave elastic $\pi^{\pm}\pi^o$ scatterings go into one another under CPT, $\sigma_{el,s}(\pi^+\pi^o) = \sigma_{el,s}(\pi^-\pi^o)$ is a very narrow Breit-Wigner resonance at the kaon mass with the same width for both charge states,

$$\Gamma_{tot}(K^+) = \Gamma_{tot}(K^-) \tag{2.2b}$$

Thus the following conditions are necessary for observation of charge-asymmetric decays:

1. Golden rule breaks down. This is exact first order perturbation theory and can only break down where higher order contributions are important. Second-order weak contributions are negligible; thus higher order strong contributions are needed.

2. Conspiracy of several decay modes. Total widths must be equal. Any asymmetry in the partial widths of a pair of conjugate modes must be compensated by opposite asymmetries in other modes.

For kaons all charge asymmetry effects should be small. All principal decays lead to approximate strong S-matrix eigenstates and the golden rule should be good. S-wave $\pi^{\pm}\pi^o$ is an exact eigenstate of strong S since no inelastic channels are open. The 3π final states are dominated by I=1 s-wave and thus all nearly proportional to the same strong-S eigenstate. The I=3 component is $\Delta I = 5/2$ and doubly suppressed by $\Delta I = 1/2$.

2.2 Beating CPT for Charge Asymmetries in $K \to 3\pi$

Here two isospin channels are open, I=1 and I=3 for the dominant partial wave where all pion pairs are in relative s waves. Although the I=3 amplitude is very much suppressed, it need not be zero. Therefore a small effect can be observed when these two different decay modes can conspire to give the same total width and final state rescattering can beat the Fermi golden rule via higher order transitions in strong interactions; e.g.

$$K^- \to \pi^-\pi^+\pi^- \to \pi^-\pi^o\pi^o; \qquad K^+ \to \pi^+\pi^-\pi^+ \to \pi^+\pi^o\pi^o \tag{2.3}$$

$$\frac{W_{K^+\to\pi^+\pi^o\pi^o}}{W_{K^-\to\pi^-\pi^o\pi^o}} = \frac{|S_{el}M(\pi^+\pi^o\pi^o) + S_{cex}M(\pi^+\pi^-\pi^+)|^2}{|S_{el}M(\pi^-\pi^o\pi^o) + S_{cex}M(\pi^-\pi^+\pi^-)|^2} \tag{2.4}$$

where $M(f^\pm) \equiv \langle f^\pm | H_{wk} | K^\pm \rangle$ and S_{el} and S_{cex} denote strong elastic and charge exchange scattering. A CP-violating asymmetry can arise in the subspace of $K \to 3\pi$ decays. The isospin eigenstates $(3\pi)_I$ are exact strong-S eigenstates. However, asymmetries can occur when final states are not strong eigenstates; e.g. $\pi^\pm\pi^o\pi^o$. Thus for I=1 and 3,

$$|A\{(K^+ \to (3\pi)_I^+\}| = |A\{K^- \to (3\pi)_I^-\}| \tag{2.5}$$

$$\Gamma_{tot}(K^+) = \sum_{I=1,3} \Gamma\{K^+ \to (3\pi)_I^+\} = \Gamma_{tot}(K^-) = \sum_{I=1,3} \Gamma\{K^- \to (3\pi)_I^-\} \tag{2.6}$$

$$A^\pm(f^\pm) \equiv A\{K^\pm \to f^\pm\} = \sum_{I=1,3} C_I^f |A\{K^\pm \to (3\pi)_I^\pm\}| \cdot e^{\pm iW_I} e^{iS_I} \tag{2.7}$$

where C_I^f denotes isospin Clebsch-Gordan coefficients, and we introduce a shortened notation $A^\pm(f^\pm)$ for $A\{K^\pm \to f^\pm\}$ Every isospin amplitude is written as the product of its magnitude, and weak and strong phase factors $e^{\pm iW_I}$ and e^{iS_I}. The weak CP-violating phase reverses sign under charge conjugation; the strong CP-conserving phase remains unchanged. Then I=3 - I=1 interference can produce charge asymmetry,

$$|A^+(\pi^+\pi^o\pi^o)|^2 - |A^-(\pi^-\pi^o\pi^o)|^2 = -4C_1^fC_3^f|A_1A_3|\sin(W_1 - W_3)\sin(S_1 - S_3) \tag{2.8a}$$

$$|A^+(\pi^+\pi^-\pi^+)|^2 - |A^-(\pi^+\pi^-\pi^-)|^2 = 4C_1^fC_3^f|A_1A_3|\sin(W_1 - W_3)\sin(S_1 - S_3) \tag{2.8b}$$

The asymmetries are seen to be equal and opposite for the two charge states, cancel in the total rates as expected from CPT and vanish unless *both* $W_1 \neq W_3$ *and* $S_1 \neq S_3$. The vanishing of the asymmetry when $S_3 = S_1$ is simply interpreted in view of eq. (2.4) since $S_3 = S_1$ implies no charge exchange, $S_{cex} = 0$. Thus the condition for observing an asymmetry is that at least two amplitudes arising from different strong eigenstates must contribute, and that they must have both different strong phases and different weak phases.

In kaon decays charge asymmetries are always small, since they arise from interference between one dominant amplitude and a much weaker amplitude. A ϕ factory can provide high intensity kaon beams where such small effects may be observed. In the 3π system there is also the possibility of interference between the dominant s-wave decay and other higher partial waves. These will average out over the total decay rates but might be observed as charge asymmetries in certain regions of the angular distributions. In B decays there are many open channels and many possibilities for interference between roughly equal amplitudes. These are discussed below.

3 – Symmetry analysis of neutral meson mixing

3.1 A Quasispin Description of Neutral Meson Mixing

We describe neutral meson mixing by a quasispin SU(2) picture with the two flavor eigenstates of the kaon system, K^o and $\bar{K}^o$ defined as eigenstates of σ_z with "spin up" and "spin down" respectively [2, 3, 4, 5],

$$\sigma_z |K^o\rangle = |K^o\rangle; \quad \sigma_z \left|\bar{K}^o\right\rangle = -\left|\bar{K}^o\right\rangle \tag{3.1}$$

Strong and electromagnetic interactions conserve quasispin. Weak interactions break quasispin. If CPT is conserved the mass eigenstates K_S and K_L are equal mixtures of K^o and $\bar{K}^o$. We can then choose phases and the direction of the quasispin x axis to make

$$|K_L\rangle = (1/\sqrt{2})(|K^o\rangle + \left|\bar{K}^o\right\rangle); \quad \sigma_x |K_L\rangle = |K_L\rangle; \quad \langle K_L|\sigma_z|K_L\rangle = \langle K_L|\sigma_y|K_L\rangle = 0 \tag{3.2}$$

If CP is conserved, K_S and K_L are eigenstates of both CP and σ_x. If CP is violated, K_S and K_L are not necessarily orthogonal and both can decay into the same CP eigenstate $|f\rangle$. However, an orthonormal basis of linear combinations of the two mass eigenstates can always be constructed to forbid a given decay mode $|f\rangle$ for one of the basis states,

$$\langle f| T \left|K_\nu^f\right\rangle = 0; \qquad \langle K_\mu^f \left|K_\nu^f\right\rangle = 0 \tag{3.3}$$

This can be seen explicitly by using eqs. (1.1)

$$|K_\nu^{oo}\rangle \equiv |K_L\rangle - \eta_{oo}|K_S\rangle; \quad \langle \pi^o\pi^o| T |K_\nu^{oo}\rangle = 0 \tag{3.4a}$$

$$\left|K_\nu^{\pm}\right\rangle \equiv |K_L\rangle - \eta_{+-}|K_S\rangle; \quad \left\langle \pi^+\pi^-\right| T \left|K_\nu^{\pm}\right\rangle = 0; \quad \langle \pi^o\pi^o| T \left|K_\nu^{\pm}\right\rangle = -3\epsilon' \langle \pi^o\pi^o| T |K_S\rangle \tag{3.4b}$$

The parameter ϵ' expresses the difference between the states $|K_\nu^\pm\rangle$ and $|K_\nu^{oo}\rangle$. A $|K_\nu^\pm\rangle$ beam should not decay to $\pi^+\pi^-$, while the decay $K_\nu^\pm \to \pi^o\pi^o$ is proportional to ϵ' and could be used in a null experiment to determine ϵ'.

The basis (3.3) determines a direction in quasispin space. If K_ν^f and K_μ^f are equal mixtures of K^o and $\bar{K}^o$, which often occurs when $|f\rangle$ is a CP eigenstate,

$$\left|K_\nu^f\right\rangle = (1/\sqrt{2})(e^{i\theta_f/2}\,|K^o\rangle + e^{-i\theta_f/2}\left|\bar{K}^o\right\rangle) = e^{i\sigma_z\theta_f/2}\,|K_L\rangle\,; \quad \left\langle K_\nu^f\right|\sigma_z\left|K_\nu^f\right\rangle = 0 \tag{3.5a}$$

$$\left|K_\mu^f\right\rangle = (1/\sqrt{2})(e^{i\theta_f/2}\,|K^o\rangle - e^{-i\theta_f/2}\left|\bar{K}^o\right\rangle) = -ie^{i\sigma_z(\theta_f+\pi)/2}\,|K_L\rangle\,; \quad \left\langle K_\mu^f\right|\sigma_z\left|K_\mu^f\right\rangle = 0 \tag{3.5b}$$

Then the state K_ν^f defines an axis in the $x-y$ plane at an angle θ_f away from the x axis. The values of θ_f for two different CP eigenstates are directly to the CP-violation parameters ϵ and ϵ'. . If they are the same for two eigenstates, like $\pi^+\pi^-$ and $\pi^o\pi^o$, $\epsilon' = 0$. If CP is conserved, $\theta_f = 0$ when f is a CP-eigenstate.

3.2 The use of the Einstein-Podolsky-Rosen effect in ϕ decays

The EPR effect provides a means for creating beams of particles in the state $\left|K_\nu^f\right\rangle$ defined by eq. (3.3).

The decay of the odd-parity ϕ vector meson at rest into an odd-parity state of two neutral kaons with momenta $\vec{k}$ and $-\vec{k}$ can be described both in the $(K^o;\bar{K}^o)$ and $(K_\mu^\pm;K_\nu^\pm)$ bases.

$$\phi \to K^o(\vec{k})\bar{K}^o(-\vec{k}) - K^o(-\vec{k})\bar{K}^o(\vec{k}) = K_\nu^\pm(\vec{k})K_\mu^\pm(-\vec{k}) - K_\mu^\pm(-\vec{k})K_\nu^\pm(\vec{k}) \tag{3.6}$$

If a decay $K_\mu^\pm \to \pi^+\pi^-$ is detected at $-\vec{k}$, the wave function collapses to make a $K_\nu^\pm$ beam at $\vec{k}$. This proposal [7], called "An experiment for the future" in 1968 is now being implemented at ϕ factories.

A similar approach to the B system, using the basis (3.3) and the odd-parity $\Upsilon(4S)$ as the B analog of the ϕ gives

$$\Upsilon(4S) \to B^o(\vec{k})\bar{B}^o(-\vec{k}) - B^o(-\vec{k})\bar{B}^o(\vec{k}) = B_\nu^f(\vec{k})B_\mu^f(-\vec{k}) - B_\mu^f(-\vec{k})B_\nu^f(\vec{k}) \tag{3.7}$$

The EPR effect is in common use in $\Upsilon(4S)$ B decay experiments [8, 5], noting that detecting a $B_\mu^f \to f$ at $-\vec{k}$ produces a B_ν^f beam at $\vec{k}$.

3.3 EPR in the K_L - K_S basis

In order to take into account the mass difference and decays of the mass eigenstates K_L and K_S it is convenient to write eq. (3.6) in the K_L - K_S basis. Although these

states are not orthogonal when CP is violated, they are linearly independent and can be used if proper account is taken of their non-orthogonality. Thus we can write:

$$\phi \to K_L(\vec{k})K_S(-\vec{k}) - K_L(-\vec{k})K_S(\vec{k}) \to \alpha(\vec{k})\beta(-\vec{k}) \tag{3.8}$$

where α and β denote final states resulting from kaon decay.

The transition matrix describing ϕ decay into two kaons which then decay into a state α with momentum $\vec{k}$ and a state β with momentum $-\vec{k}$ can be written

$$\left\langle \alpha(\vec{k})\beta(-\vec{k})\right| T \left|\phi\right\rangle = \left\langle \alpha\right| T \left|K_L\right\rangle \left\langle \beta\right| T \left|K_S\right\rangle - \left\langle \alpha\right| T \left|K_S\right\rangle \left\langle \beta\right| T \left|K_L\right\rangle \tag{3.9}$$

where $\langle\alpha| T |K_L\rangle$, $\langle\beta| T |K_L\rangle$, $\langle\alpha| T |K_S\rangle$ and $\langle\beta| T |K_S\rangle$ denote the transition matrix elements for the decays respectively $K_L \to \alpha$, $K_L \to \beta$, $K_S \to \alpha$ and $K_S \to \beta$ and there is no overall normalization. This can be rewritten

$$\left\langle \alpha(\vec{k})\beta(-\vec{k})\right| T \left|\phi\right\rangle = \left\langle \alpha\right| T \left|K_S\right\rangle \left\langle \beta\right| T \left|K_S\right\rangle (\eta_\alpha - \eta_\beta) \tag{3.10a}$$

where the parameter η_f is defined for any final state f as a generalization of eq. (1.1)

$$\eta_f = \frac{\langle f| T |K_L\rangle}{\langle f| T |K_S\rangle} \tag{3.10b}$$

We immediately obtain the result for the case $\alpha = \beta$

$$\left\langle \alpha(\vec{k})\alpha(-\vec{k})\right| T \left|\phi\right\rangle = 0 \tag{3.11a}$$

while for the case $\alpha = \pi^+\pi^-$ and $\beta = \pi^o\pi^o$

$$\left\langle \pi^+\pi^-(\vec{k}); \pi^o\pi^o(-\vec{k})\right| T \left|\phi\right\rangle = \left\langle \pi^+\pi^-\right| T \left|K_S\right\rangle \cdot \langle\pi^o\pi^o| T |K_S\rangle \cdot (\eta_\pm - \eta_{oo}) =$$

$$= 3\left\langle \pi^+\pi^-\right| T \left|K_S\right\rangle \cdot \langle\pi^o\pi^o| T |K_S\rangle \cdot \epsilon' \tag{3.11b}$$

3.4 Time and space dependence of correlated decays

These results are only valid in the vicinity of the point where the kaon pair is created. For the general case the difference in decay rates and masses of the two kaon eigenstates must be taken into account. A recent clarification [6] of the considerable confusion regarding this issue points out that measurements are always made in space and no times are explicitly measured. In particular the difference between transit times of K_L and K_S between source and detector not only are not measured but are prevented from being measured by the way the experiment is prepared and the uncertainty principle.

Kaon pairs produced by ϕ decay at a ϕ factory come from what is effectively a point source. The extension of the source must be small compared with the

distance between the source and detector if any oscillations in space are observed. This immediately introduces a crucial momentum uncertainty. It is therefore a good approximation to consider a wave function with the position of the source and the energies of the kaons sharply defined. The momenta of the kaons and their production and detection times are therefore not sharply defined. For this case the transition matrix element for two kaon decays observed in the mode α at a distance x_1 from the source and in the mode β at a distance x_2 is given by

$$\langle\alpha(x_1)\beta(x_2)|\,T\,|\phi\rangle = \langle\alpha|\,T\,|K_S\rangle\cdot\langle\beta|\,T\,|K_S\rangle\cdot$$

$$\cdot\left\{\eta_\alpha e^{-(\lambda_L x_1+\lambda_S x_2)/2}\cdot e^{i(p_L x_1+p_S x_2)} - \eta_\beta e^{-(\lambda_S x_1+\lambda_L x_2)/2}\cdot e^{i(p_S x_1+p_L x_2)}\right\} \qquad (3.12a)$$

where λ_L and λ_S are the decay lengths of K_L and K_S with the experimental energies and p_L and p_S are their momenta. Note that the two terms in eq. (3.12a) express the EPR "entanglement" correlations between kaons detected at two points x_1 and x_2. However, all the necessary information is in the transition matrix element (3.12a) and one need not worry about "collapses of wave functions" or any timing problems. One needs only to calculate the value of this matrix element for the particular states α and β detected in the experiment. The relation (3.12a) can be rewritten

$$\langle\alpha(x_1)\beta(x_2)|\,T\,|\phi\rangle = e^{-(\lambda_L+\lambda_S)(x_1+x_2)/4}\cdot e^{i(p_L+p_S)(x_1+x_2)/2}\cdot\langle\alpha|\,T\,|K_S\rangle\cdot\langle\beta|\,T\,|K_S\rangle\cdot$$

$$\cdot\left\{\eta_\alpha e^{-(\lambda_L-\lambda_S)(x_1-x_2)/4}\cdot e^{i(p_L-p_S)(x_1-x_2)/2} - \eta_\beta e^{(\lambda_L-\lambda_S)(x_1-x_2)/4}\cdot e^{-i(p_L-p_S)(x_1-x_2)/2}\right\} \qquad (3.12b)$$

The transition probabilities are proportional to the squares of the matrix elements,

$$|\,\langle\alpha(x_1)\beta(x_2)|\,T\,|\phi\rangle\,|^2 = e^{-(\lambda_L+\lambda_S)(x_1+x_2)/2}\cdot|\,\langle\alpha|\,T\,|K_S\rangle\cdot\langle\beta|\,T\,|K_S\rangle\,|^2\cdot$$

$$\cdot\left\{|\eta_\alpha|^2 e^{-(\lambda_L-\lambda_S)(x_1-x_2)/2} + |\eta_\beta|^2 e^{(\lambda_L-\lambda_S)(x_1-x_2)/2} - 2Re[\eta_\alpha\eta_\beta^*\cdot e^{i(p_L-p_S)(x_1-x_2)}]\right\} \qquad (3.13)$$

For the case where the same decay mode is observed at x_1 and x_2

$$|\,\langle\alpha(x_1)\alpha(x_2)|\,T\,|\phi\rangle\,|^2 = 2|\eta_\alpha|^2 e^{-(\lambda_L x_1+\lambda_S x_2)}\cdot|\,\langle\alpha|\,T\,|K_S\rangle\,|^4\cdot\{1-\cos[(p_L-p_S)(x_1-x_2)]\} \qquad (3.14a)$$

This vanishes as expected when $x_1 = x_2$. The case $\eta_\beta = -\eta_\alpha$ is also of interest. This includes the case where the two decay modes are those allowed respectively for K^o and $\bar{K}^o$; e.g. semileptonic decay modes.

$$|\,\langle\alpha(x_1)\beta(x_2)|\,T\,|\phi\rangle_{\eta_\beta=-\eta_\alpha}\,|^2 = e^{-(\lambda_L x_1+\lambda_S x_2)}\cdot|\,\langle\alpha|\,T\,|K_S\rangle\,|^4\{1+\cos[(p_L-p_S)(x_1-x_2)]\} \qquad (3.14b)$$

This is a maximum at $x_1 = x_2$, where the two-kaon state is the pair with opposite strangeness eigenvalues originally created.

4 – CP violation in B decays

4.1 How B and K physics differ

4.1.1 *Quasispin Symmetry Breaking by Mass and Lifetime Differences*

The lifetime difference is determined by phase space and independent of the standard model. The mass difference is determined by dynamical effects depending upon standard model. Lifetime symmetry breaking is dominant in the kaon system where a pure K_L state can be produced simply by waiting. Mass breaking is dominant in heavy quark mesons and can be described as a "magnetic field" in quasispin space.

4.1.2 *Good and bad news about the B-K difference*

1. No Dominant B Decay Mode

   No Lifetime Difference in B decays

   B-Mass Eigenstates Cannot be Separated by Waiting

2. Many B Decay Modes

   Rich Data - Small Branching Ratios $\approx 1\%$

   Final State Rescattering - Beats Golden Rule

   Conspiracies Beat CPT Restrictions

3. $B^o - \bar{B}^o$ Oscillations During Decay

   Time Dependence Confuses Measurements

   CP Violation Observable in Mixing Phases

4. Standard model requires active participation of 3 generations for CP violation

   All Dominant Hadronic B decays involve 3 Generations

   CP violation Observable in B Decays in Direct Diagrams $b \to c\bar{u}d$

   CP Violation in K and D decays only via diagrams with virtual t and b quarks

4.2 Beating CPT for Charge Asymmetries in B Physics

Can decays of B^+ and B^- be different? Here many more channels are open, different decay modes can conspire to give the same total width and final state rescattering can beat the Fermi golden rule via higher order transitions in strong interactions; e.g.

$$B^- \to \bar{K}^o\pi^- \to K^-\pi^o; \qquad B^+ \to K^o\pi^+ \to K^+\pi^o \tag{4.1}$$

$$\frac{W_{B^+\to K^+\pi^o}}{W_{B^-\to K^-\pi^o}} = \frac{|S_{el}M(K^+\pi^o) + S_{cex}M(K^o\pi^+)|^2}{|S_{el}M(K^-\pi^o) + S_{cex}M(\bar{K}^o\pi^-)|^2} \tag{4.2}$$

This has no simple counterpart in the kaon system. Here both $(K\pi)$ isospin eigenstates $I = 1/2$ and $I = 3/2$ are $\Delta I = 1$ and equally allowed.

A simplified model which considers only charge-exchange scattering and neglects final state scattering between $K\pi$ and other final states shows how a CP-violating asymmetry can arise. In this approximation the isospin eigenstates $(K\pi)_I$ are exact strong-S eigenstates. and asymmetries can occur in final states like $K^\pm\pi^o$, Thus for I=1/2 and 3/2,

$$|A\{(B^+ \to (K\pi)_I\}| = |A\{B^- \to (\bar{K}\pi)_I\}| \tag{4.3}$$

$$\Gamma_{tot}(B^+) = \sum_{I=\frac{1}{2},\frac{3}{2}} \Gamma\{B^+ \to (K\pi)_I\} = \Gamma_{tot}(B^-) = \sum_{I=\frac{1}{2},\frac{3}{2}} \Gamma\{B^- \to (\bar{K}\pi)_I\} \tag{4.4}$$

$$A\{B^\pm \to f^\pm\} = \sum_I C_I^f |A\{B^\pm \to (K\pi)_I\}| \cdot e^{\pm iW_I} e^{iS_I} \tag{4.5}$$

I=3/2 - 1/2 interference can produce charge asymmetry,

$$|A^+(K^+\pi^o)|^2 - |A^-(K^-\pi^o)|^2 = -4C_{\frac{1}{2}}^f C_{\frac{3}{2}}^f |A_{\frac{1}{2}}A_{\frac{3}{2}}| \sin(W_{\frac{1}{2}} - W_{\frac{3}{2}}) \sin(S_{\frac{1}{2}} - S_{\frac{3}{2}}) \tag{4.6a}$$

$$|A^+(K^o\pi^+)|^2 - |A^-(\bar{K}^o\pi^-)|^2 = 4C_{\frac{1}{2}}^f C_{\frac{3}{2}}^f |A_{\frac{1}{2}}A_{\frac{3}{2}}| \sin(W_{\frac{1}{2}} - W_{\frac{3}{2}}) \sin(S_{\frac{1}{2}} - S_{\frac{3}{2}}) \tag{4.6b}$$

Again as in eqs. (2.8) The asymmetries are seen to be equal and opposite for the two charge states, cancel in the total rates as expected from CPT and vanish unless *both* $W_{\frac{1}{2}} \neq W_{\frac{3}{2}}$ *and* $S_{\frac{1}{2}} \neq S_{\frac{3}{2}}$. The condition for observing an asymmetry is that at least two amplitudes arising from different strong eigenstates must contribute, and that they must have both different strong phases and different weak phases.

4.3 Charge asymmetry in standard model - Trees and penguins in $B \to K\pi$

In the standard model two diagrams with different weak phases contribute to $B \to K\pi$ decays via two different strong eigenstates and can produce a CP asymmetry [9, 10]. The tree diagram gives only $K^\pm\pi^o$; the penguin only I=1/2 $K\pi$.

$$B^+(\bar{b}u) \to_{(tree)} \to \bar{u} + W^+ + u \to \bar{u} + u + \bar{s} + u \to K^+ + \pi^o \tag{4.7a}$$

$$B^-(b\bar{u}) \to_{(tree)} \to u + W^- + \bar{u} \to u + \bar{u} + s + \bar{u} \to K^- + \pi^o \tag{4.7b}$$

$$B^+(\bar{b}u) \to_{(penguin)} \to \bar{t} + W^+ + u \to \bar{s} + u \to (K\pi)_{I=1/2} \tag{4.8a}$$

$$B^-(b\bar{u}) \to_{(penguin)} \to t + W^- + \bar{u} \to s + \bar{u} \to (\bar{K}\pi)_{I=1/2} \tag{4.8b}$$

The tree has two suppressed weak vertices, $b \to u$ and $s \to u$; the penguin has no such suppression is expected to be strong enough to compete with the tree and produce tree-penguin interference and CP violation.

4.4 EPR correlations in $\Upsilon(4S)$ decays

The EPR description used above for kaon decay correlations in ϕ decays can be used for B factories and the decay (3.7), with the added simplification that $\lambda_L \approx \lambda_S \equiv \lambda$.

$$|\langle\alpha(x_1)\beta(x_2)|T|\Upsilon(4S)\rangle|^2 = e^{-\lambda(x_1+x_2)} \cdot |\langle\alpha|T|B_S\rangle \cdot \langle\beta|T|B_S\rangle|^2 \cdot$$

$$\cdot\left\{|\eta_\alpha|^2 + |\eta_\beta|^2 - \eta_\alpha\eta_\beta^* \cdot e^{i(p_L-p_S)(x_1-x_2)} - \eta_\alpha^*\eta_\beta \cdot e^{-i(p_L-p_S)(x_1-x_2)}\right\} \qquad (4.9)$$

For the case where the same decay mode is observed at x_1 and x_2

$$|\langle\alpha(x_1)\alpha(x_2)|T|\Upsilon(4S)\rangle|^2 =$$

$$= 2|\eta_\alpha|^2 e^{-\lambda(x_1+x_2)} \cdot |\langle\alpha|T|B_S\rangle|^4 \cdot \{1 - \cos[(p_L - p_S)(x_1 - x_2)]\} \qquad (4.10a)$$

This describes the $B^o - \bar{B}^o$ oscillations in which the probability of observing the same state at both x_1 and x_2 oscillates as a function of $(x_1 - x_2)$ and vanishes at $(x_1 = x_2)$. The case $\eta_\beta = -\eta_\alpha$ here describes the $B^o - \bar{B}^o$ oscillations in which the probability of observing a B^o at x_1 and a $\bar{B}^o$ at x_2 oscillates with the opposite phase to the case of identical B's (4.10a),

$$|\langle\alpha(x_1)\beta(x_2)|T|\Upsilon(4S)\rangle_{\eta_\beta=-\eta_\alpha}|^2 =$$

$$= 2|\eta_\alpha|^2 e^{-\lambda(x_1+x_2)} \cdot |\langle\alpha|T|B_S\rangle|^4\{1 + \cos[(p_L - p_S)(x_1 - x_2)]\} \qquad (4.10b)$$

5 – Conclusion - the Lipkin approach to CP

In 1956, after a 100% parity violation [11] was found in a difficult experiment, a much simpler experiment [12] showed that beta rays were polarized, proving parity violation. Anyone who had started our experiment [12] at the same time as Ambler et al [11] would have obtained results first and discovered parity violation. But the community had been brainwashed by the theorists who insisted that parity violation violated the "standard model" of that time. They only considered sensitive experiments where a negative result could shoot down this crazy theory, not a simple experiment that could only detect a 100% effect.

Moral for CP : Don't be brainwashed by the standard model. It might even fail to explain CP and lead to new physics beyond. This would not challenge its validity in all other areas. Keep it in mind but try to use a more general approach. Data inadequate for testing standard model CP predictions will be available long before adequate data. These preliminary data can supply information useful for planning subsequent experiments. There may also be unexpected large effects. Look for easy experiments that even Lipkin can do - even if theorists say no.

Acknowledgements

This research is supported in part by grant no. I-0304-120.07/93 from the German-Israeli Foundation for Scientific Research and Development.

References

1. J.H. Christensen et al., Phys. Rev. Lett. **13**, 138 (1964).
2. T. D. Lee and C. S. Wu, Ann. Rev. Nuc. Sci. **16**, 511 (1966).
3. Harry J. Lipkin, Argonne preprint ANL-HEP-PR-88-66 Submitted to Nuclear Physics B (1988)
4. Harry J. Lipkin, Phys. Lett. **B219**, 474 (1989).
5. Harry J. Lipkin, In: "Developments in General Relativity, Astrophysics and Quantum Mechanics", A Jubilee Volume in Honour of Nathan Rosen, Jerusalem, Edited by F.Cooperstock, L.P. Horwitz and J. Rosen, Annals of the Israel Physical Society, **9**, 315 (1990).
6. Harry J. Lipkin, Physics Letters **B348**, 604 (1995).
7. Harry J. Lipkin, Phys. Rev. **176**, 1715 (1968).
8. I. I. Bigi and A. I Sanda, Nuc. Phys. **B281**, 41 (1987).
9. Yosef Nir and Helen Quinn Phys. Rev. Lett. **67**, 541 (1991).
10. Harry J. Lipkin, Yosef Nir, Helen R. Quinn and Arthur E. Snyder, Phys. Rev. **D44**, 1715 (1991).
11. E. Ambler et al., Phys. Rev. **105**, 1413 (1957).
12. A. de-Shalit et al., Phys. Rev. **107**, 1459 (1957).

A THEORETICAL APPRAISAL OF ε'/ε

Guido Martinelli
Università di Roma I - La Sapienza Dipartimento di Fisica
P.le A. Moro 5, I-00185–Roma (Italy)

(No written contribution arrived)

CP VIOLATION IN THE TIME EVOLUTION OF THE DECAY $K^0 \to \pi^0 e^+e^-$

Gerhard O. Koehler, Emmanuel A. Paschos
Institut fuer Physik, Universitaet Dortmund D–44221 Dortmund, Germany

ABSTRACT

We examine the possibility of extracting $\mathcal{CP}$-violating terms in the decay $K^0 \to \pi^0 e^+ e^-$ by studying the time evolution of a K^0 beam. We focus on the interference region and search for clear effects. We find that experiments which average over the electron and positron momenta can detect $\mathcal{CP}$ violation as an oscillation in the decay rate. The branching ratio is $(3-5) \times 10^{-12}$ and direct $\mathcal{CP}$ violation dominates over a wide range of the parameters.

The decay $K_L \to \pi^0 e^+ e^-$ provides a crucial test of the standard model. Its status was resently reviewed [1]. In an article to be published [2] the time evolution of a pure K^0 state is given in terms of the time development of the physical states K_L and K_S as follows

$$|K^0(t)> = \frac{1}{\sqrt{2}} \left[e^{-iX_L t}(\, |K_2> + \epsilon |K_1>) + e^{-iX_S t}(\, |K_1> + \epsilon |K_2>) \right]. \qquad (1)$$

The decay proceeds through two intermediate states, $K^0 \to \pi^0\gamma$ and $K^0 \to \pi^0\gamma\gamma$, with the single or two photons converting into electron positron pairs. The decaying kaon has spin 0, and angular momentum conservation demands the intermediate state $\pi^0\gamma$ to be in a p-wave. It follows, then, that the $\mathcal{CP}$ eigenvalue of $\pi^0\gamma$ is $(-1)_\pi (+1)_\gamma (-1)^{l=1} = +1$. Thus K_1 can decay through the $\pi^0\gamma$ channel in terms of $\mathcal{CP}$-conserving parts, whereas K_2 decays through the $\mathcal{CP}$-violating parts of the Hamiltonian. We denote these amplitudes as

$$A_1 = < \pi^0 e^+ e^- | \ \mathcal{H}_\gamma \ | K_1 > ; \qquad \mathcal{CP}\text{-conserving} \qquad (2)$$

$$B = < \pi^0 e^+ e^- | \ \mathcal{H}_\gamma \ | K_2 > ; \qquad \mathcal{CP}\text{-violating (direct) .} \qquad (3)$$

These would be the only two amplitudes if there were no higher order terms. In fact the decay of a K^0 can also proceed through the intermediate state $\pi^0\gamma\gamma$, which is

higher order in the electromagnetic coupling. This contribution to the decay width is not a priori negligible, because it has to be compared with $\mathcal{C}P$-violating terms which are suppressed. To be specific, the intermediate state of a pion and two photons has many partial waves so that both $\mathcal{C}P = +1$ and $\mathcal{C}P = -1$ states are allowed. The small $\mathcal{C}P$ violating amplitude we will ignore. Thus the decay $K_2 \to \pi^0\gamma\gamma \to \pi^0 e^+ e^-$ is $\mathcal{C}P$-conserving with the final state odd under the $\mathcal{C}P$ transformation. We define the relevant amplitude as

$$A_2 = < \pi^0 e^+ e^- |\ \mathcal{H}_{\gamma\gamma}\ | K_2 > ; \qquad \mathcal{C}P\text{-conserving.} \tag{4}$$

Next, we compute the time evolution of the decays dropping the term $\epsilon(B+A_2)$ in comparison to A_1 on several resons: i) B is small, being $\mathcal{C}P$-violating, ii) A_2 is small, being higher order in electromagnetism and iii) these two small terms are multiplied by the small parameter ϵ. Neglecting $\epsilon(B + A_2)$, the K_S decays are $\mathcal{C}P$-conserving. The K_L decays contain A_2, which is $\mathcal{C}P$-conserving, and the $\mathcal{C}P$-violating amplitudes B and ϵA_1. The amplitude B represents direct $\mathcal{C}P$ violation, whereas the violation in ϵA_1 arises through the mass matrix. Since both terms are very likely suppressed, it becomes necessary to consider the A_2 term.

$$\begin{aligned}
\frac{d\Gamma}{ds d\Delta}(t) &= \frac{1}{512\,\pi^3 m_K^3}\Big\{ e^{-\Gamma_L t}\left[|B^+ + A_2^+ + \epsilon A_1^+|^2 + |B^-|^2\right] + e^{-\Gamma_S t}\,|A_1^+|^2 \\
&\quad + e^{-\frac{\Gamma_L+\Gamma_S}{2}t}\, 2\, Re\Big[e^{-i\Delta m_K \cdot t}\,(B^+ + A_2^+ + \epsilon A_1^+)A_1^{+*}\Big]\Big\} \qquad (5) \\
&\quad \times \frac{1}{2}\left[\,\lambda(s, m_K^2, m_\pi^2) - \Delta^2\,\right]; \\
s &= (p_K - p_\pi)^2, \quad \Delta = (p_K - k_-)^2 - (p_K - k_+)^2 \qquad \text{and} \\
\lambda(s, m_K^2, m_\pi^2) &= s^2 + m_K^4 + m_\pi^4 - 2\,s\,m_K^2 - 2\,s\,m_\pi^2 - 2\,m_K^2 m_\pi^2.
\end{aligned}$$

with A_1^+, A_2^+, B^+ being vector amplitudes and B^- being the axial-vector. This expression shows three time intervals: decays for K_S-, K_L mesons and an interference region. The first two show the typical exponential behavior for the decays, and the interference has an oscillatory term as well. We point out an important property of the interference term. The A_2 amplitude is odd under the $\mathcal{C}P$ transformation and thus antisymmetric under the exchange of the electron and positron energies or momenta. This is born out by explicit calculation, with equation (15) being linear in Δ. The A_1^+ amplitude is even under exchange of the electron and positron momenta. Therefore the term $A_2^+ A_1^{+*}$ drops out in an experiment which symmetrizes over the electrons and positrons. The remaining interference terms in equation (5) are $\mathcal{C}P$-odd. Thus the presence of an oscillation in the interference region is a clear indication of $\mathcal{C}P$ violation.

The B-amplitude is calculated by means of an effective Hamiltonian for $\Delta S = 1$ semileptonic transitions derived by using the operator-product-expansion [3] Since the B-amplitude is $\mathcal{C}P$-violating, it involves the imaginary parts of the Wilson coefficients, and the dominant terms are [4]

$$\begin{aligned}
&Im(C_7)\, O_7, \quad \text{where} \quad O_7 = (\bar{s}_L\, \gamma_\mu\, d_L)\,(\bar{e}\,\gamma^\mu\, e) \\
&Im(C_8)\, O_8, \quad \text{where} \quad O_8 = (\bar{s}_L\, \gamma_\mu\, d_L)\,(\bar{e}\,\gamma^\mu\, \gamma_5 e).
\end{aligned} \tag{6}$$

The reduced matrix elements of the operators involve quark currents between hadronic states and can be related to K_{l3} decays through an isospin rotation [4]

$$B = \bar{u}(k_-)\not{p}_K\left[B^+ + B^-\gamma_5\right]v(k_+) \tag{7}$$

$$B^+ = i\frac{G_F}{\sqrt{2}}V_{ud}V_{us}^*\,\alpha\,2\sqrt{2}f_+(s)Im(C_7), \quad B^- = i\frac{G_F}{\sqrt{2}}V_{ud}V_{us}^*\,\alpha\,2\sqrt{2}f_+(s)Im(C_8).$$

Following the Kobayashi Maskawa parametrization for the quark mixing matrix we use for the coefficients the values [3]

$$Im(C_7) = -\frac{1}{V_{ud}V_{us}^*}\,\mathrm{Im}(V_{td}V_{ts}^*)\,0.74 \quad \text{and} \quad Im(C_8) = -\frac{1}{V_{ud}V_{us}^*}\,\mathrm{Im}(V_{td}V_{ts}^*)\,(-0.70) \tag{8}$$

with $m_t = 170$ GeV. The main uncertainty comes from the factor $Im(\lambda_t) = Im(V_{td}V_{ts}^*) = -s_1s_2s_3c_2sin\delta$ for which we will allow the range $(1.0 - 2.0) \times 10^{-4}$. Varying the parameters, we obtain the branching ratio

$$BR(K_L \to \pi^0e^+e^-)_{direct} = (2.4 - 9.7) \times 10^{-12}. \tag{9}$$

A calculation of the amplitude A_1 can be performed using chiral perturbation theory (χPT) as a low energy limit of QCD. We define A_1 through the equation

$$A_1 = <\pi^0\,e^+e^-|\mathcal{H}_\gamma|K_1> = \bar{u}(k_-)\,A_1^+\not{p}_K\,v(k_+), \tag{10}$$

$$A_1^+ = \frac{G_F}{\sqrt{2}}V_{ud}V_{us}^*\,g_8\,\frac{\alpha}{\pi}\,2\left[w_+ + \frac{1}{6}\,\ln\frac{m_\pi^2}{m_K^2} + 2\,\phi(s)\right]$$

where the loop-function $\phi(s)$can be found in [5]. The coupling constant of the octet of pseudoscalar mesons g_8 was found from the decay $K \to \pi\pi$ to be $g_8 = 5.1$. ω_+ was determined from a χ^2-analysis of the spectrum for the decay $K^+ \to \pi^+e^+e^-$, based on a calculation in χPT [5, 6] to be $w_+ = 0.89^{+0.24}_{-0.14}$. This yields a branching ratio for the decay

$$BR(K_L \to \pi^0e^+e^-) = 1.71 \times 10^{-15} - 1.14 \times 10^{-12} \tag{11}$$

if the decay occurs only through the CP-violating piece of the K^0-$\overline{K}_0$ mass-matrix.

Since the decay $K_L \to \pi^0e^+e^-$ via 2 γ's has not yet been observed it was suggested to study the intermediate decay $K_L \to \pi^0\gamma\gamma$, which has recently been observed, with the branching ratio [7]

$$BR(K_L \to \pi^0\gamma\gamma) = (1.7 \pm 0.3) \times 10^{-7}. \tag{12}$$

The amplitude for the decay $K_L \to \pi^0\gamma\gamma$ has been estimated by two different methods. One method uses a two-component model [8] including pion loops and vector meson intermediate states. The second method applies χPT [9] The two approaches differ in several respects, but for the amplitude which is dominant in our investigation they agree [2].

The amplitude for $K_L(p_K) \to \pi^0(p_\pi)\gamma(k)\gamma(k')$ has the general structure

$$M = \epsilon^\mu \epsilon^\nu \Big[F\,(k'_\mu k_\nu - g_{\mu\nu}\, k'\cdot k\,) + G\,(g_{\mu\nu}\, k\cdot p_K\, k'\cdot p_K + p_{K\mu}\, p_{K\nu}\, k'\cdot k - p_{K\mu}\, k_\nu\, k'\cdot p_K - k'_\mu\, p_{K\nu}\, k\cdot p_K\,)\Big]. \quad (13)$$

In the two-component model [10] the pion-loop diagrams contribute only through the F amplitude, whose contribution to A_2 is proportional to m_e and thus small. The vector meson pole diagram contributes to the amplitude $A_2^+(s,\Delta)$ defined by

$$A_2 = A(K_2 \to \pi^0 e^+ e^-)_{2\gamma} = \bar{u}(k_-)\, A_2^+ \not{p}_K\, v(k_+). \quad (14)$$

Defining $\beta = \sqrt{1-4m_e^2/s}$, the absorptive part of $A_2^+(s,\Delta)$ is

$$\mathrm{Im}\, A_2^+ = \frac{\alpha}{16}\frac{G_{eff}}{m_V^2}\frac{\Delta}{\beta}\left[\frac{2}{3} + \frac{2}{\beta^2} - \left(\frac{1}{\beta^2} - \beta^2\right)\frac{1}{\beta}\ln\frac{1+\beta}{1-\beta}\right]. \quad (15)$$

We notice that $\mathrm{Im}A_2^+$ is an odd function of Δ, as demanded by CP conservation. The coupling G_{eff}, appearing above, is chosen in such a way that it reproduces the branching ratio in equation (12). The dispersive part is calculated with the help of a dispersion relation [10]. Inserting the numerical values we obtain a branching ratio dominated by the vector meson coupling constant

$$Br(K_L \to \pi^0 e^+ e^-)_{2\gamma} = 1.66\times 10^{-12}\,(1+\rho) = 4.15\times 10^{-12} \quad (16)$$
$$\text{with } \rho = \Gamma_{disp}/\Gamma_{abs} = 1.5 \text{ and } G_{eff}\, m_K^2 = 0.15\times 10^{-7}.$$

With the amplitudes described so far and the general equation (5) we calculate the time evolution for the decay $K^0 \to \pi^0 e^+ e^-$. The results are shown in figures 1 and 2 . We notice three regions of physical interest.

1) The K_S-region, where the CP-conserving amplitude contributes to the decay width. A measurement in this region will determine parameters of the K_S-decay like ω_+.

2) The K_L-decay region in which the relevant amplitude is $|B + A_2 + \epsilon A_1|^2$. The interference term $Re(A_2 B^+ + \epsilon A_1 A_2)$ is odd in Δ and one could define an asymmetry in Δ in order to extract this term. The sum of the absolute values squared is even in Δ, and we will need precise measurements of the amplitudes in order to observe an excess of events.

3) More interesting is the interference region which has an oscillatory behavior. The term $A_2 A_1^+$ is a linear function in Δ and drops out when we average over the electron positron pair. The remaining terms BA_1^+ and $\epsilon|A_1|^2$ are both CP-violating. Thus the appearance of an oscillation in the interference region is evidence for CP violation.

A numerical investigation shows that the oscillation in the interference term is caused, as expected, by the CP violating terms and that the dominant contribution to the decay is CP violating [2]. Experiments which study K_L-decays for long times require a precise measurement of magnitudes in order to establish a CP-violating

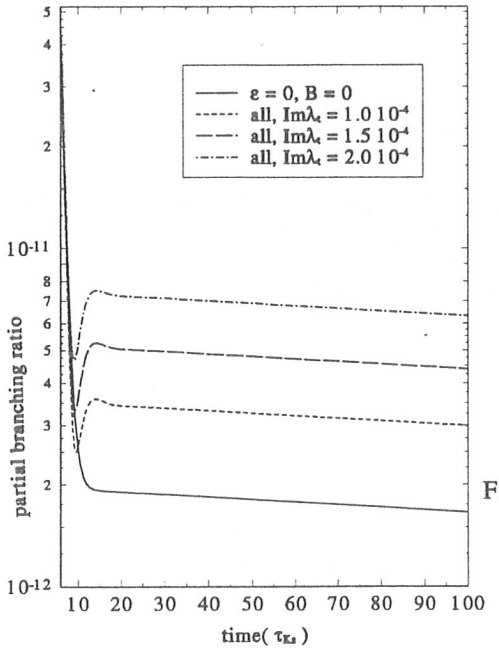

Figure 1: Time development of the decay
$\Gamma(K^0 \to \pi^0 e^+ e^-)/\Gamma(K^0 \to \text{all})$; $\omega_+ = 0.89$

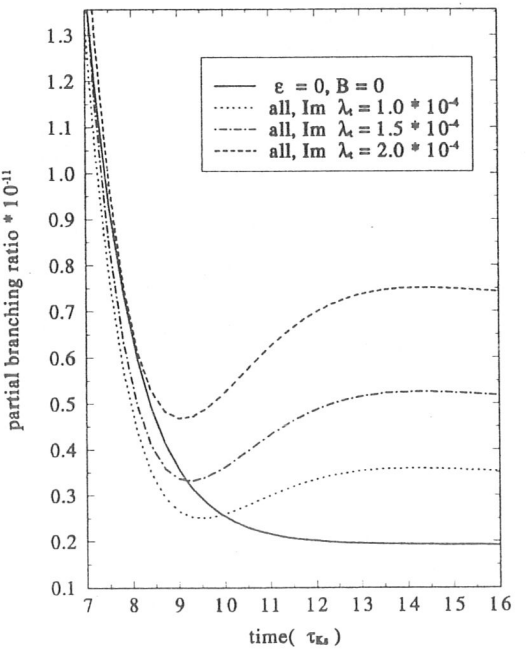

Figure 2: Same as in fig 1. but on linear scales.

signal. The branching ratio is in the range $(3-5)\times 10^{-12}$. In contrast to this situation, the oscillation in the interference region is unambiguous. We compared the magnitudes of the various terms and found that BA_1^+ dominates over $\epsilon|A_1|^2$. Only if we choose ω_+ at the upper bound ($\omega_+ = 1.13$) the two contributions are of comparable size. But the direct CP-violating term is still larger by $(6-113)\%$ for $\mathrm{Im}(\lambda_t) = (1.0-2.0)\times 10^{-4}$.

We conclude that an experiment searching for a branching ratio down to 10^{-12} and sensitive to the time development of the decay can observe CP violation as an oscillation in the interference region. The experiment does not require a measurement of the e^+e^- energy asymmetry. Several aspects of this article can be tested in Daphne. For instance one can search for the final states $\pi^0 e^+ e^{-0}$ in the short and long components of the Daphne beams. The rates for this decay are small, but any observation evan an CP conserving one is of interest.

Acknowledgements

We wish to thank BMBF, Bonn for financial support and the Science Project No. SCI-CT91-0729.

References

1. J.L. Rosner, in Proccedings of the DPF '94 Meeting, Albuquerque, New Mexico, 1994 (World Scientific, Singapore, in press); L.S. Littenberg, in Procceedings of the Workshop on CP Violation at Kaon Factory, Vancouver, 1989), p. 19.
2. G.O. Köhler and E.A. Paschos, DO-TH 94/16, accepted for publication in Phys. Rev. D (1995).
3. F.J. Gilman and M.B. Wise, Phys. Rev. D **21** (1980) 3150; C.O. Dib, I. Dunietz and F.J.Gilman, Phys. Rev. D **39** (1989) 2639; J.M. Flynn and L. Randall, Nucl. Phys. B **326**, (1989) 31; Erratum Nucl. Phys. B **334**, (1990) 580; A.J. Buras, M.E. Lautenbacher, M. Misiak and M. Münz, Nucl. Phys. B **423**, (1994) 349.
4. J.F. Donoghue, B.R. Holstein and G. Valencia, Phys. Rev. D **35** (1987) 2769.
5. G. Ecker, A. Pich and E. de Rafael, Nucl. Phys. B **291**, (1987) 692.
6. C. Alliegrot et al. , Phys. Rev. Lett. **68** (1992) 278.
7. G.D. Barr et al. , Phys. Lett. B **242**, (1990) 523; G.D. Barr et al. , Phys. Lett. B **284**, (1992) 440.
8. L.M. Sehgal, Phys. Rev. D **6**, (1972) 367; L.M. Sehgal, Phys. Rev. D **41**, (1990) 161.
9. G. Ecker, A. Pich and E. de Rafael, Phys. Lett. B **189** (1987) 363; A.G. Cohen, G. Ecker and A. Pich, Phys. Lett. B **304**, (1993) 347; G. Ecker, A. Pich and E. De Rafael, Phys. Lett. B **237**, (1990) 481.
10. L.M. Sehgal, Phys. Rev. D **38**, (1988) 808; P. Heiliger and L.M. Sehgal, Phys. Rev. D **47**, (1993) 4920.

CP VIOLATING DECAY $\eta \to 2\pi$ IN DIFFERENT THEORIES OF BREAKDOWN OF CP SYMMETRY

E.P. Shabalin
ITEP, Moscow, Russia

ABSTRACT

In the Standard Model (SM) of electroweak interaction with CP invariant strong interaction, the CP violating effects in flavour-conserving processes are expected to be very tiny and look beyond the experimental reach in the near decade(s).

If, however, both the Kobayashi-Maskawa mechanism and mechanism of spontaneous CP violation work, such a theory allows to have a picture of CP violation consistent with existing limits on parameters ε' and d_n and gives for the upper limit of the $\eta \to 2\pi$ rate a value one order larger than the upper limit for this rate originated by θ-term of QCD lagrangian.

1 Introduction

In order to clarify the nature of CP violation it is very important that in addition to studying flavour-changing processes also to look for CP effects in flavour-conserving transitions, such as $\eta \to 2\pi$ decay or interaction of baryons with electromagnetic field through their electric dipole moment. The reason is that predicting more or less the same picture of CP violation in strangeness-changing decays of $\{K^0, \bar{K}^0\}$ system, the different theories predict very different values for flavor-conserving processes, in particular, for CP violating $\eta \to 2\pi$ decay. The table 1 illustrates the situation.

Table 1.
Expected values of CP violating effects in flavour-changing and flavour-conserving processes originated by different sources of breakdown of CP symmetry.

Strangeness-changing processes	Flavour-conserving processes
Standard Model with CP invariant strong interaction [1]	
$\eta_{\pm} = \varepsilon + \varepsilon'$ $\eta_{00} = \varepsilon - 2\varepsilon'$ $\lvert\varepsilon'/\varepsilon\rvert^{th} \approx (3 \div 6)10^{-4}$ [3]	$d_n \leq 10^{-32} e$ cm [2] $R_{\eta 2\pi} = \frac{\Gamma(\eta \to 2\pi)}{\Gamma(\eta \to \text{all})} \leq 2 \cdot 10^{-27}$ [4]
Superweak interaction [5]	
$\eta_{\pm} = \eta_{00}$ $\varphi_{\pm} = \varphi_{00} = \varphi_{SW} \simeq 43.7^0$	Amplitudes $\sim g_{SW} G_F^2 \sin^2\theta_C$ In particular, $R_{\eta 2\pi} \approx 3 \cdot 10^{-49}$
Spontaneous CP violation in theory with natural flavour conservation [6]	
$\lvert\varepsilon'/\varepsilon\rvert^{th} \sim 5 \cdot 10^{-2}$ [7] versus $\lvert\varepsilon'/\varepsilon\rvert^{exp} = (1.5 \pm 0.8)10^{-3}$ [9]	$d_n^{th} \approx 10^{-24} e$ cm [8] versus $d_n^{exp} \leq 1.1 \cdot 10^{-25} e$ cm [9] $R_{\eta 2\pi} \gg R_{\eta 2\pi}$ (SM)
Strong CP violation due to θ-term in QCD [10]	
	$d_n \approx 2 \cdot 10^{-16} \lvert\theta\rvert e$ cm [11] $R_{\eta 2\pi} \approx 350 \cdot \theta^2 \leq 1.2 \cdot 10^{-16}$ [12] at $\theta \leq 6 \cdot 10^{-10}$ from d_n^{exp}

The Table 1 leads to conclusion that $\eta \to 2\pi$ decay will have a chance to be observed in future only in the case of breakdown of CP symmetry in strong interaction with magnitude of θ not far from the existent upper limit on this quantity. The other source of $R_{\eta 2\pi} \gg R_{\eta 2\pi}(SM)$ - the spontaneous CP violation in Higgs sector, seems to be excluded by experimental data. But the last conclusion relates to the situation when the spontaneous CP violation is the only source of breakdown of CP symmetry. If, instead, this mechanism works simultaneously with Kobayashi-Maskawa mechanism [13] of CP violation then the picture is changed in a considerable way. In such a theory, it turns to be possible to have [14]

$$\begin{aligned} &1) \quad \lvert\varepsilon'/\varepsilon\rvert = (\text{anyvalue}) \leq (1.5 \pm 0.8)10^{-3} \\ &2) \quad d_n^{th} \leq 0.1 d_n^{ex} \\ &3) \quad R_{\eta 2\pi} \leq 1.8 \cdot 10^{-15} \end{aligned} \tag{1}$$

The theory with two sources of CP violation could be especially useful, if the future experiments will confirm that $\varepsilon'_{exp} > \varepsilon'^{th}(SM)$.

Let's now turn to foundation of the results concerning $\eta \to 2\pi$ decay in different models of CP violation.

2 $\eta \to 2\pi$ in SM with CP invariant strong interaction

In SM, a violation of CP invariance occurs due to imaginary part of coupling constants. But Hermicity of the $\eta\pi\pi$ interaction does not allow a complex coupling constant for such a vertex if η meson and $(\pi\pi)$ system are the self-conjugate states. Therefore, $\eta \to 2\pi$ transition could take place only if η or $(\pi\pi)$ states have a small admixture of some non-self-conjugate states, for instance, $K^0(\bar{K}^0)$ or $(K\pi)$ respectively. In other words, $\eta \to 2\pi$ transition must be the two-step transition [2]

$$\eta \to \{K^0, \bar{K}^0\} \to 2\pi \ , \quad \text{or} \quad \eta \to \{K\pi, \bar{K}\pi\} \to 2\pi \tag{2}$$

and $\eta \to 2\pi$ transition becomes allowed if the phase Δ and δ of first-step and second-step transition, defined as

$$< K^0|\eta >= | < K^0|\eta > |e^{i\Delta} \quad \text{and} \quad < 2\pi|K^0 >= | < 2\pi|K^0 > |e^{-i\delta} \tag{3}$$

are different, that is, $\Delta \neq \delta$.

A calculation of the matrix elements in eqs. (3) can be performed using the effective non-leptonic lagrangian for $\Delta S = \pm 1$ transition given in ref. [15].

$$L(|\Delta S| = 1) = \sqrt{2} G_F \sin\theta_C \cos\theta_C \sum_{j=1}^{6} (c_j O_j + c_j^* O_j^\dagger) \tag{4}$$

where

$$\begin{aligned}
O_1 &= (\bar{s}_L\gamma_\mu d_L)(\bar{u}_L\gamma_\mu u_L) - (\bar{s}_L\gamma_\mu u_L)(\bar{u}_L\gamma_\mu d_L), \ (\{8_f\}, \ \Delta I = 1/2), \quad (5)\\
O_2 &= 2(\bar{s}_L\gamma_\mu d_L) \sum_{q=u,d,s} (\bar{q}_L\gamma_\mu q_L) - O_1, \ (\{8_f\}, \ \Delta I = 1/2),\\
O_3 &= O_2 - 5(\bar{s}_L\gamma_\mu d_L)(\bar{s}_L\gamma_\mu s_L), \ (\{27\}, \ \Delta I = 1/2),\\
O_4 &= (\bar{s}_L\gamma_\mu d_L)(\bar{u}_L\gamma_\mu d_L)(\bar{u}_L\gamma_\mu u_L) + (\bar{s}_L\gamma_\mu U_L)(\bar{u}_L\gamma_\mu d_L) -\\
&- (\bar{s}_L\gamma_\mu d_L)(\bar{d}_L\gamma_\mu d_L), \ (\{27\}, \ \Delta I = 3/2),
\end{aligned}$$

[2] The intermediate states with non-zero charm, or beauty give considerably smaller contribution to $\eta \to 2\pi$ transition.

$$O_5 = (\bar{s}_L\gamma_\mu\lambda^a d_L)(\sum_{q=u,d,s}\bar{q}_R\gamma_\mu\lambda^a q_R)(\{8\},\ \Delta I = 1/2),$$
$$O_6 = (\bar{s}_L\gamma_\mu d_L)(\sum_{q=u,d,s}\bar{q}_R\gamma_\mu q_R)(\{8\},\ \Delta I = 1/2).$$

The above set of operators is not sufficient for calculation of the ratio ε'/ε in $K_L \to 2\pi$ decay [3, 16] but, as it will be seen later, is quite sufficient for our purpose.

The diquark operators can be expressed through the physical mesonic field using the relations [17]

$$\bar{q}^j_L\gamma_\mu q^i_L = \frac{if_\pi^2}{4}\{(\partial_\mu V)V^+ - V(\partial_\mu V^+) - \frac{r}{\Lambda^2}[m(\partial_\mu V^+ - \partial_\mu V)]\}_{ij} \qquad (6)$$

$$\bar{q}^j_R q^k_L = -\frac{1}{4}f_\pi^2 r[V - \frac{1}{\Lambda^2}\partial^2 V]_{kj} \qquad (7)$$

where

$$V = exp(i\sqrt{2}\hat{\pi}/f_\pi)\ ,\ r = \frac{2m_\pi^2}{m_u + m_d}\ ,\ \Lambda \sim 1GeV\ ,\ f_\pi \approx 93MeV \qquad (8)$$

and

$$\hat{\pi} = \begin{pmatrix} \frac{\pi_0}{\sqrt{3}} + \frac{\pi_8}{\sqrt{6}} + \frac{\pi_3}{\sqrt{3}} & \pi^+ & K^+ \\ \pi^- & \frac{\pi_0}{\sqrt{3}} + \frac{\pi_8}{\sqrt{6}} - \frac{\pi_3}{\sqrt{2}} & K^0 \\ K^- & \bar{K}^0 & \frac{\pi_0}{\sqrt{3}} - 2\frac{\pi_8}{\sqrt{6}} \end{pmatrix} \qquad (9)$$

The result for $\eta \to 2\pi$ matrix element is

$$< \pi^+\pi^-|\eta >= 6.02 \cdot 10^{-15}\beta Rec_5\frac{Imc_5}{Rec_5}[-\sqrt{3}\sin\theta_P(c_1 + c_2) +$$

$$+ \frac{10\cos\theta_P + 2\sqrt{2}\sin\theta_P}{\sqrt{6}}c_3 + (\frac{2\sin\theta_P}{\sqrt{3}} + \frac{\cos\theta_P}{\sqrt{6}})c_4 e^{i(\delta_2 - \delta_0)}]GeV \qquad (10)$$

Using then the numerical values of c_i obtained in ref. [18] and [19] and estimate [20] giving $|Imc_5/Rec_5| = (1 \pm 0.4)|s_2 s_3 \sin\delta|$ and taking $\theta_P = -19,47^0$ we come to result

$$R_{+-} = \frac{\Gamma(\eta \to \pi^+\pi^-)}{\Gamma(\eta \to \text{all})} \leq (0.66^{+0.63}_{-0.32})10^{-27}\sin^2\delta \qquad (11)$$

where δ is the Kobayashi-Maskawa phase. The rate of $\eta \to \pi^0\pi^0$ is half as big.

As it follows from eq. (10), the amplitude of $\eta \to 2\pi$ decay is determined mainly by $\Delta I = 1/2$ part of intermediate $K \to 2\pi$ amplitude and for this

reason is not practically sensitive to corrections introducting by the operators corresponding to so-called electroweak penguin and box diagrams.

The result (11) does not leave a hope to observe this decay if the phase δ is the only source of CP violation. But importance of this result consists in possibility to affirm that the observation of such decay would be the evidence for other sources of CP violation, such as θ-term in QCD lagrangian, or spontaneous CP violation in Higgs sector of the theory.

3 $\eta \to 2\pi$ decay caused by CP violation in strong interaction

A complicated topological structure of QCD vacuum state originates CP violation described by θ-term

$$L^{\theta}_{QCD} = -\theta \frac{\alpha_s}{8\pi} G^a_{\mu\nu} \tilde{G}^a_{\mu\nu} \quad [10] \tag{12}$$

In chiral theory it performs into

$$L^{\theta}(\eta \to 2\pi) = -\theta \frac{m_\pi^2}{2\sqrt{2} f_\pi} \cdot \frac{\Delta m_P^2}{\Delta m_P^2 + \frac{3}{2} m_\pi^2} (\pi^+ \pi^- + \frac{\pi^{0^2}}{2})(\sqrt{2}\pi_0 + \pi_8) \tag{13}$$

demonstrating the direct dependence of the result on solution of $U(1)$ problem because Δm_P^2 is a difference between magnitudes of $(m^2_{\pi^0})^{phys}$ and $m^2_{\pi^0}$ following from Gell-Mann-Okubo mass relation. In eq. (13), $\pi^0 = \pi_3 \neq \pi_0$. At $\theta \leq 6 \cdot 10^{-10}$ (from the data on d_n) one gets

$$R^{\theta}_{\eta 2\pi} \leq 1.2 \cdot 10^{-16} \tag{14}$$

4 $\eta \to 2\pi$ decay in theory with Kobayashi-Maskawa and Weinberg mechanism of CP violation [6]

If the SM is complicated by extension of the Higgs sector up to three Higgs doublet, the additional source of CP violation appears – the spontaneous breakdown of CP symmetry in Higgs sector [6]. Then, in addition to diagrams in Fig. 1 contributing in Kobayashi-Maskawa scenario to CP violating parameter ε and ε' in $K \to 2\pi$ decay, the new set of diagrams shown in Figs.

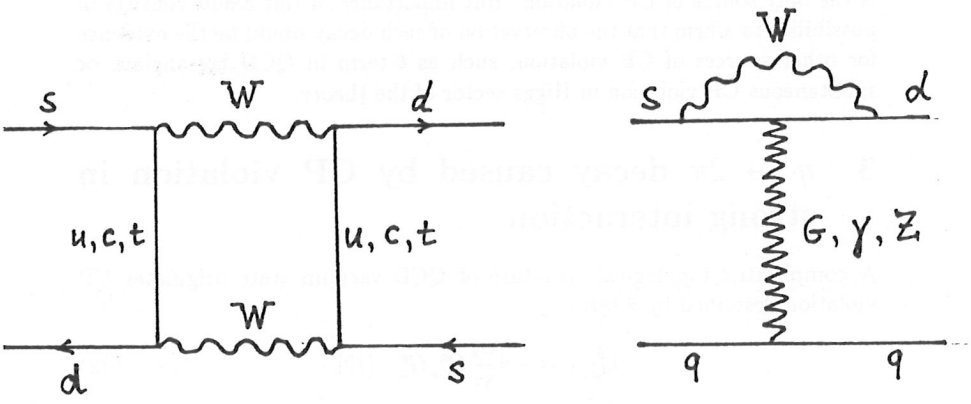

(a) (b)

Figure 1

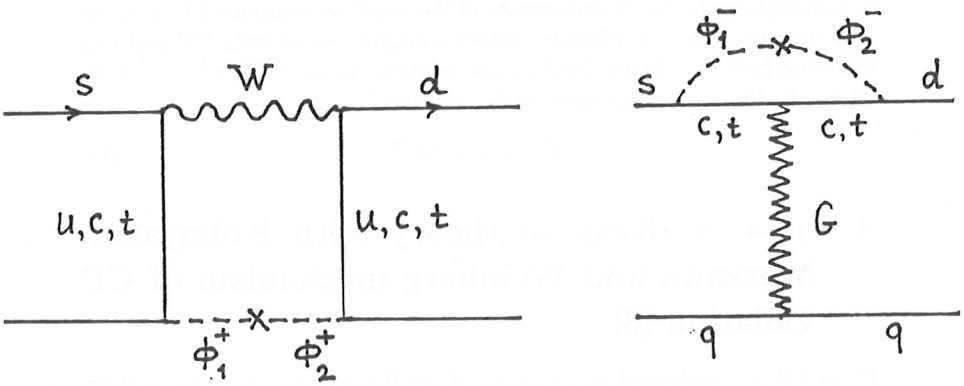

(a) (b)

Figure 2

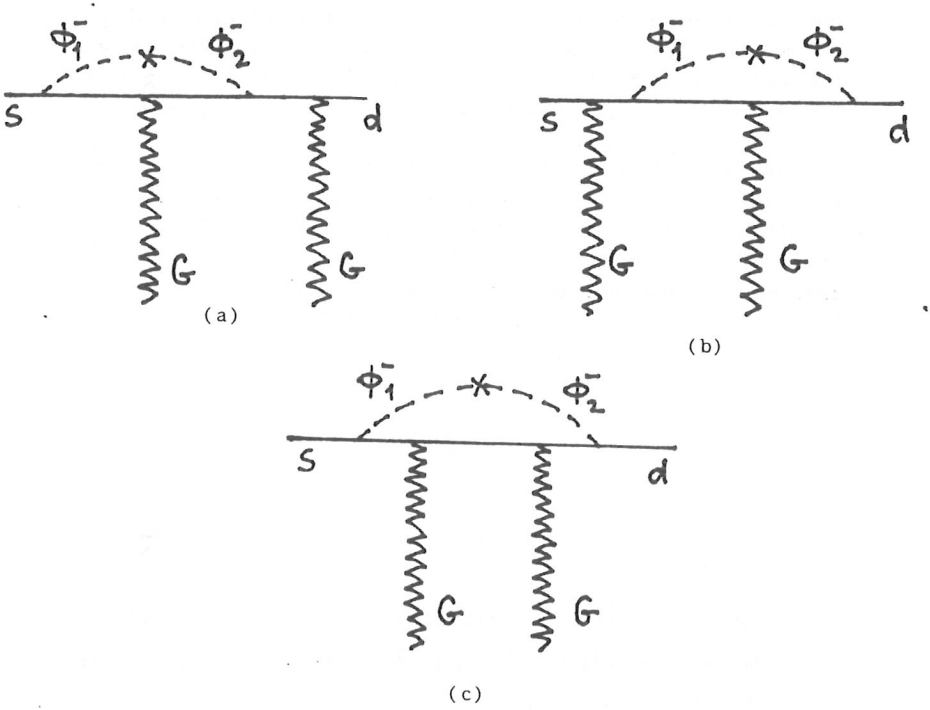

Figure 3

·2 and 3 give a contribution to these parameters originated by Weinberg mechanism of CP breakdown.

If this last source is considered as the only one, such a mechanism gives too large values for ε'/ε [7] and d_n [8] in comparison with experimental data. The cardinal solution of the problem consists in assumption that the KM mechanism works also and gives the main contribution to ε. Then the Weinberg mechanism can contribute considerably to ε' and can originate a large enough magnitude of $\eta \to 2\pi$ decay. But to estimate $R_{\eta 2\pi}$ one needs first to extract a value of unknown parameter ImA of the Weinberg theory from the data on ε'. The important new result in the analysis of the problem concerning ε' in Weinberg model consists in the observation [14] that the diagrams in Fig. 3 give by 5 times larger contribution into ε' than the diagram in Fig. 2b considered previously in literature [7]. The same set of diagram as in Fig. 3 originates the $\eta \to 2\pi$ transition and this allows to express $g_W^{eff}(\eta\pi\pi)$ through $\varepsilon'_W = \varepsilon'_{exp} - (\varepsilon')^{th}_{KM}$.

From the existing data $|\varepsilon'/\varepsilon|^{exp} = (1.5 \pm 0.8)10^{-3}$ and theoretical prediction $|\varepsilon'_{KM}/\varepsilon|^{th} \sim 3 \cdot 10^{-4}$ [3] one can conclude that $|\varepsilon'_W/\varepsilon| \leq 2 \cdot 10^{-3}$. Then calculating a contribution of diagrams in Fig. 2 and 3 into ε'_W and comparing it with the experimental limit on ε'_W one can extract the value of ImA. Inserting this value into diagrams like the ones in fig. 3 but conserving the flavour one can obtain for the coupling constant of effective interaction

$$L^{eff}(\eta \to 2\pi) = g_W \eta\pi\pi$$

the result

$$|g_W| \leq 3.6 \cdot 10^{-10} \cdot \left(\frac{-\sin\theta_P + \sqrt{2}\cos\theta_P}{\sqrt{3}}\right) GeV \tag{15}$$

At $\theta_P = -19.47^0$

$$R_{\eta 2\pi} \leq 1.8 \cdot 10^{-15} \tag{16}$$

5 Electric dipole moment of the neutron in theory with KM and Weinberg mechanisms of CP violation

Our estimate of ImA is

$$ImA = 7.1 \cdot 10^{-8}\left[\left(\ln\frac{m_H^2}{m_c^2} - 1\right)\left(1 + x\frac{V_{td}V_{st}}{V_{cd}V_{sc}}\right)\right]^{-1} \tag{17}$$

where

$$x = \frac{V_{ts}}{V_{cs}} \cdot \frac{m_t^2}{m_c^2} \cdot \frac{m_H^2}{m_t^2 - m_H^2}\left(1 - \frac{m_H^2}{m_t^2 - m_H^2}\ln\frac{m_t^2}{m_H^2}\right).$$

$$\cdot (\ln \frac{m_H^2}{m_c^2} - 1)^{-1} \tag{18}$$

Inserting this ImA into the formulae of ref. [8] one obtains

$$|D_n| \leq 0.11 \cdot 10^{-25} \left(\frac{1 + x \frac{V_{ts}^2}{V_{cs}^2}}{1 + x \frac{V_{td}}{V_{cd}} \frac{V_{ts}}{V_{ts}}} \right) e\text{cm} \tag{19}$$

In the above formulae, V_{ij} are the elements of K-M matrix taken at $\delta = 0$.

6 Conclusions

1. The minuteness of $R_{\eta 2\pi}$ in SM with CP invariant strong interaction presents a golden opportunity for manifestation of the other sources of CP violation.

2. Observation $R_{\eta 2\pi}$ at the level 10^{-16} would not be obligatory the evidence of CP violation due to θ-term in QCD lagrangian. The spontaneous CP violation in the Higgs sector could give also such a rate when it is accompanied by the Kobayashi-Maskawa mechanism of CP violation.

3. Observation $R_{\eta 2\pi}$ with a magnitude few times larger than $R_{\eta 2\pi}^{\theta}$ would be the evidence of CP violation in Higgs sector.

4. In $K_L \to 2\pi$ decays, it is possible, in principle, that the part ε'_{KM} is cancelled by ε'_W. Therefore, $\varepsilon' \to 0$ would not be inevitable the evidence of superweak CP violation.

5. Observation (at DAΦNE) $\varepsilon' > (\varepsilon')_{SM}^{th}$ would be the evidence of CP violation in Higgs sector!

7 Acknowledgments

This report was prepared during my stay in Lund Institute of Technology, Dept. of Math. Physics and I thank this Department for hospitality.

The main results concerning η decay were obtained in two joint works with Prof. C.Jarlskog (Refs. [4] and [14]) and I am very grateful to her for a fruitful collaboration.

This work was partially supported by the International Science Foundation under the grant No. 85000 and INTAS under the grant No. 94-3986.

References

[1] S.L.Glashow, Nucl. Phys. **22** (1961) 579
S.Weinberg, Phys. Rev. Lett. **19** (1967) 1264
A.Salam, in Elementary Particle Theory, Ed. N.Svartholm (Almqvist and Wiksell, 1968).

[2] E.Shabalin, Usp. Fiz. Nauk **139** (1983) 561 (Sov. Phys. Usp. **26(4)** (1983) 297).

[3] G.Buchalla, A.J.Buras and M.K.Harlander, Nucl. Phys. **B337** (1990) 313
M.Ciuchini, E.Franko, G.Martinelli and L.Reina, Phys. Lett. **B301** (1993) 263.

[4] C.Jarlskog and E.Shabalin, Preprint Lund-MPh-95/01.

[5] L.Wolfenstein, Phys. Rev. Lett. **13** (1964) 569.

[6] S.Weinberg, Phys. Rev. Lett. **37** (1976) 657.

[7] N.G.Deshpande, Phys. Rev. **D23** (1981) 654
A.I.Sanda, Phys. Rev. **D23** (1981) 2647.

[8] A.R.Zhitnitskii and I.B.Khriplovich, Yad. Fiz. **34** (1981) 167 [Sov. J.Nucl. Phys. **34** (1981) 95].

[9] Particle Data Group, Phys. Rev. **D50** (1994) 1173.

[10] G.t'Hooft, Phys. Rev. Lett. **37** (1976) 8.

[11] V.Baluni, Phys. Rev. **D19** (1979) 2227
R.J.Crewther *et al.*, Phys. Lett. **B88** (1979) 123
E.P.Shabalin, Yad, Fiz. **36** (1982) 981 [Sov. J. Nucl. Phys. **36** (1982) 575]
H.J.Schnitzer, Phys. Lett. **139B** (1984) 217.
L.J.Dixon *et al.*, Preprint SLAC-PUB-5344, 1990.

[12] R.J.Crewther *et al.*, Phys. Lett. **88B** (1979) 123
M.A.Shifman, A.I.Vainshtein and V.I.Zakharov, Nucl. Phys. **B166** (1980) 494
C.Jarlskog and E.Shabalin, this Report.

[13] M.Kobayashi and T.Maskawa, Prog. Theor. Phys. **49** (1973) 652.

[14] C.Jarlskog and E.Shabalin, Preprint Lund-MPh-95/05.

[15] A.I.Vainshtein, V.I.Zakharov and M.A.Shifman, JETP **72** (1977) 1275.

[16] J.M.Flynn, L.Randall, Phys. Lett. **B224** (1989) 221
E.A.Paschos and Y.L.Wu, Mod. Phys. Lett. **A6** (1991) 93.

[17] W.A.Bardeen, A.J.Buras and J.-M-Gerard, Nucl. Phys. **B293** (1987) 787.

[18] L.B.Okun, "Leptons and Quarks" (North-Holland Publ. Comp., 1982) p.p. 315-323.

[19] E.Shabalin, Nucl. Phys. **B409** (1993) 87.

[20] M.B.Voloshin, Preprint ITEP-22 (1981), unpublished.

QUANTUM MECHANICS AND TIME EVOLUTION OF THE $K\bar{K}$ SYSTEM

PARALLEL SESSION

Y.N. Srivastava	Real and Virtual Strange Processes	237
P.H. Eberhard	EPR Paradox and Tests of Quantum Mechanics at DAΦNE	247
L. Stodolski	EPR Effects without Collapse of the Wavefunction	267
N.E. Mavromatos	Experimental Tests of CPT Symmetry and Quantum Mechanics at CPLEAR	269
L. Khalfin	CP Violation Problem Beyond Approximate Lee–Ohme–Yang Theory	287
J. Bogdanowicz	On the Concept of the Life Time of Unstable Particles (The Φ Delayed Decay)	289

REAL AND VIRTUAL STRANGE PROCESSES

Y.N. Srivastava, A. Widom and E. Sassaroli
Physics Department, Northeastern University, Boston U.S.A
and
Physics Department & INFN, University of Perugia, Perugia, Italy

ABSTRACT

Following notions of quantum mechanics as interpreted by the Copenhagen School, we make a distinction between measurements involving one or two virtual K mesons. New predictions result for the period of K oscillations at the Φ factory.

1 Introduction

Our purpose is to discuss the insight that may be gained from Φ factory experiments ($\Phi \rightarrow K^o + \bar{K}^o$) concerning a central issue of quantum measurements; i.e. *What is virtual and what is real?* Before discussing our concrete predictions (i.e. numbers!) for the outcome of some Φ factory experiments, we wish first to discuss qualitatively that *not all* aspects of quantum measurements have simple agreed upon answers. Briefly, we have a great deal of sympathy with Einstein who lost the debate with Bohr. Known experiments do fit into Bohr's scheme and mere "thought experiments" get boring after a while. Einstein and Bohr did agree upon what the quantum mechanical scheme entailed, but disagreed on whether this scheme was the complete story [1, 2, 3].

A primary rule of the scheme is that all experimental data are classical. Suppose that experimental data are stored on (say) a computer disk. Now imagine that the magnetic grains on the disk were in superposition (an amplitude for "0" and an amplitude for "1" on all of the little magnetic bits in some big binary file). If the computer sends to the standard output the message "disk unreadable", then you know you have no data. Real data are "classical" to a sufficient degree of accuracy. (A few coherent quantum bits here or there might appear in an "error bar", but if you are really in quantum superposition, you have no data.) We call data *real.* The primary rule is that data are classical. The classical part of physics is essential

to quantum mechanics in the Bohr scheme. Superposition of amplitudes applies to those parts of the physical system that you *do not see.* There is no data on a quantum object interacting with the classical measurement apparatus. If you have data, then it is from the classical part of the physical system. What you do not see, i.e. the quantum part of the physical system, is what we call *virtual.* The apparatus is real, and the quantum object is virtual. According to the dictates of Bohr, a measurement is an interaction between a classical apparatus and a quantum object. That was decided by Bohr, Heisenberg, and other assorted friends of the Copenhagen School. That is the conventional scheme of things. We have reviewed all this because over the years many workers have distorted what others previously agreed constituted the quantum mechanical analysis of measurements. For example, we offer a $100.00 reward to the first reader who finds for us a manuscript with Bohr as an author which includes the so-called "collapse of the wave function" as a part of quantum mechanical theory.

Briefly, in the canonical "electron moves through two slits thought experiment" you get quantum interference when there are no data on which slit the electron passed through. The electron path is then "virtual". If data exist showing which slit the electron chooses, then electron is real and there is no interference. The electron is real when you see it and virtual when you do not see it.

Bohr found no problems. The outcome of an experiment depends on how you set up the real (classical) apparatus, and PLEASE do not ask for data from a virtual (quantum) object. JUST DO NOT ASK WHAT THE QUANTUM OBJECT IS DOING! If you get the data, then the object is *not quantum.* Do not ask because there will be no data! Einstein had some problems. He asked questions. Einstein looked at the moon and it was real. Einstein stopped looking. Then what? We think the moon is still real, but the contrary has been proposed by some perfectly competent physicists. So it is our *prejudice* that the moon is real! And we really do not care who looks at it.

2 What is Virtual and What is Real in Particle Physics?

In particle physics there are theoretical and experimental views of the matter. From the theoretical view we would take as "virtual" the somewhat technical but conventional definition of those processes in the "internal parts" of the Feynman diagrams. Consider the Feynman diagram in Fig.1. The "external legs" (solid lines) are real. In the laboratory they show up as data, e.g. particle tracks. You see them in an experiment. The dotted line is internal. That is a "virtual" particle. Bohr has warned us not ask about the virtual quantum process. You are not meant to know (dear reader) about the virtual. Do not ask! For example, there are two (Bohr) complimentary views: (i) four momentum space amplitudes and (ii) space-time amplitudes.

(i) In momentum space the "virtual particle" dotted line in Fig.1 has a nice four momentum label $P_{virtual}$. That seems simple enough. The only problem is

that

$$[P^2_{virtual} + (Mc)^2] \neq 0. \quad (possibly\ off\ mass\ shell). \tag{1a}$$

Virtual particles may not be on the "mass shell". Real particles are on the mass shell. Virtual particles are not real. Bohr warned us not to ask.

(ii) The space-time "virtual particle" in the words of Feynman "...does anything it likes...". It goes forward in time. It goes backward in time. It goes space-like. Any old speed said Feynman. Anything it likes,

$$x^2_{virtual} = r^2_{virtual} - c^2t^2_{virtual} > 0 \quad (possibly\ superluminal\ speed). \tag{1b}$$

STOP IT! Bohr dictates that if it is virtual, then do not ask. Virtual particles are not real. There will be no data.

(iii) But experimentalists tell us every day that there are data on virtual particles you do not actually see. Look again at the Feynman diagram of Fig.1. Suppose the external legs are measured tracks shown in postscript colors on an experimentalist's transparency (right after we see a small person standing next to a huge machine). *We do not see the dotted line.* The right tracks lead to a primary vertex and left tracks emerge from the secondary vertex. The dotted line is a particle that moved from the primary vertex to the secondary vertex. *Only nobody sees it!* It had no charge! It left no track! But we all know it was there. This, by our definition, is an *experimental virtual particle.* It moved from vertex to vertex and nobody saw it. We are not talking about the moon. We are talking about an elementary particle. If you do not see it, then it is virtual. But the experimentalists tell us that this virtual particle moved from the primary vertex y to the secondary vertex x along a classical path at constant (four velocity) v and on the mass shell,

$$x^\mu = y^\mu + v^\mu\tau, \quad (experimental\ virtual\ particle), \tag{2a}$$

$$P^2_{virtual} + (Mc)^2 = M^2(v^2 + c^2) = 0, \quad (experimental\ virtual\ particle). \tag{2b}$$

Comparing the experimentally employed Eqs.(2) to the exciting theoretical possibilities in Eqs.(1), we find that the experimentalist's virtual particle is rather dull and classical, i.e. *it looks real (not virtual) even if you do not see it.*

Bohr had all the answers. He threw in the correspondence principle along with the complimentarity of momentum space and space-time. Only Einstein was worried. The correspondence principle says that when the action of the particle is large on the scale of $\hbar$ the particle is classical *even if you do not look at it.* The particle going from the primary to the secondary vertex had to move so far that the action was very large compared with $\hbar$. The particle may do "anything it likes", but when the action is large it "likes" to be classical with overwhelming probability. To do otherwise would have such small probability as to be a miracle. Miracles can happen, but they are hard to duplicate. There are no good statistics on miracles.

The mathematics is that the propagator from vertex to vertex

$$[-\partial_\mu\partial^\mu + \kappa^2]D(x-y) = \delta(x-y), \quad \kappa = (Mc/\hbar), \tag{3}$$

has the Dirac-Feynman path integral representation

$$D(x-y)=\int_{z(0)=y}^{z(\tau)=x}\prod_{\tau}\left(\frac{\mathcal{D}p\mathcal{D}z}{2\pi\hbar}\right)exp\frac{i}{\hbar}\int_{y}^{x}[p_{\mu}dz^{\mu}-\mathcal{H}(p)d\tau], \tag{4}$$

where

$$\mathcal{H}(p)=\frac{1}{2M}[p^2+(Mc)^2]. \tag{5}$$

If the particle were classical, then the free particle Hamilton-Jacobi equation [4]

$$-\frac{\partial S}{\partial\tau}=\mathcal{H}\left(p=\frac{\partial S}{\partial x}\right), \tag{6a}$$

$$S(x-y,\tau)=-\frac{Mc^2}{2}\left(\tau-\frac{(x-y)^2}{c^2\tau}\right), \tag{6b}$$

would yield the classical experimental Eqs.(2) via the equations

$$-\frac{\partial S}{\partial\tau}=0,\quad S=-Mc\sqrt{-(x-y)^2},\quad M\frac{dx^{\mu}}{d\tau}=\partial^{\mu}S. \tag{6c}$$

The actual space-time propagator in the Schwinger "proper time" representation is given by

$$D(x-y)=\frac{M}{8\pi^2\hbar}\int_{0}^{\infty}\left(\frac{d\tau}{\tau^2}\right)exp\frac{i}{\hbar}S(x-y,\tau), \tag{7}$$

where the proper time τ internal to the particle need not be the laboratory proper time $\sqrt{-(x-y)^2/c^2}$ between the vertex events. The particle has all the proper time in the world to do what it likes; forward in time, backward in time, spacelike ... and so forth. But the Bohr correspondence principle tells us that when the action in Eq.(7) obeys $|S|>>\hbar$, then the stationary phase evaluation of the proper-time integral in Eq.(7) yields $\tau=\sqrt{-(x-y)^2/c^2}$ and what the particle then likes to do is to be classical. The experimentalist has every right to suppose that the "virtual particle" is classical even if nobody detects the path, and likewise for the moon. If Bohr's correspondence holds true, then all is right with this boring world. But when a particle shows up that exhibits virtual quantum interference, in *spite* of the correspondence principle, everybody says that this particle must be very strange.

3 The "$K^o\overline{K^o}$" Particle

The "$K^o\bar{K}^o$" virtual particle is not merely strange, it has some deep psychological problems. It cannot decide whether to exhibit itself as a K^o going forward in time or as $\bar{K}^o$ going backward in time. (The language is that of Stückelberg and Feynman.) If the dotted line in Fig.1 is "$K^o\bar{K}^o$" as a virtual particle, it will never be classical even for $|S|>>\hbar$ because *any decent free classical particle* (or classical anti-particle) will make up its mind once and for all which direction in time it wants to go and then it learns to live in psychological peace with its decision. Hence, the Bohr

correspondence principle works very well except for those cases where it does *not* work very well.

If a "$K^o\bar{K}^o$" T violating particle (we assume TCP=1) goes from a primary to a secondary vertex its inner turmoil refuses the classical limit of the Bohr correspondence principle and remains truly virtual, oscillating with quantum interference phase factors. Very good. Now the Bohr dictate is that we cannot ask what the "$K^o\bar{K}^o$" is doing. But it is really hard not to try and form a mental picture such as maybe the particle path is still classical but "wobbles" a little bit.

The mathematics is that the (two by two) non-Hermitian mass matrix of the "$K^o\bar{K}^o$" [4, 5, 6]

$$\mathcal{M} = M - i(\hbar\Gamma/2c^2), \tag{8}$$

produces the (two by two) "wobbly" propagator

$$\mathcal{D}(x-y) = \frac{\mathcal{M}}{8\pi^2\hbar}\int_0^\infty \left(\frac{d\tau}{\tau^2}\right) exp\frac{i\mathcal{M}}{2\hbar}[-c^2\tau + \frac{(x-y)^2}{\tau}]. \tag{9}$$

The Bohr correspondence principle tells us to evaluate the proper time integral by stationary phase yielding the particle proper time as the laboratory proper-time so that asymptotically the particle has the laboratory proper-time

$$\mathcal{D}(x-y) \sim e^{-i\mathcal{M}c^2\tau/\hbar}, \quad -c^2\tau^2 \approx (x-y)^2, \tag{10}$$

and we are allowed (if we choose) to think of the propagator Eqs.(9) and (10) as a proper time Schrödinger equation

$$i\hbar\frac{\partial}{\partial\tau}\begin{pmatrix} A_{K^o}(\tau) \\ A_{\overline{K}^o}(\tau) \end{pmatrix} = \mathcal{M}c^2\begin{pmatrix} A_{K^o}(\tau) \\ A_{\overline{K}^o}(\tau) \end{pmatrix}, \tag{11}$$

but we are not allowed to think of the "$K^o\bar{K}^o$" traveling from a primary vertex to a secondary vertex as real (i.e. classical). It is truly an experimental virtual particle. Typical of this kind of experiment is the CPLEAR project [7] where the Feynman diagram of a typical event is shown in Fig.2. The "$K^o\bar{K}^o$" is not observed (there is no track) and it is truly virtual because you cannot Bohr correspond when you need a Schrödinger equation. Bohr has warned us about getting data from a quantum object.

One notes that the four velocity of the "$K^o\bar{K}^o$" particle

$$v^\mu = \frac{(x^\mu - y^\mu)}{\tau}, \quad \tau = \sqrt{\frac{-(x-y)^2}{c^2}}, \tag{12}$$

is determined if we know the space-time positions of the vertex events in which the classical paths (legs of the Feynman diagrams) are located. That the "$K^o\bar{K}^o$" particle is still virtual is due to the fact that it has two possible ("long" or "short") four momenta

$$p_L = M_L v \quad or \quad p_S = M_S v, \tag{13}$$

so that a typical amplitude

$$A(\tau) = A_L e^{-\Gamma_L \tau/2} e^{-iM_L c^2 \tau/\hbar} + A_S e^{-\Gamma_S \tau/2} e^{-iM_S c^2 \tau/\hbar}, \tag{14}$$

has two "plane wave" fixed momentum states going from vertex y to vertex x, e.g. in Eqs.(12), (13) and (14)

$$exp(-iM_j c^2 \tau/\hbar) = exp(ip_j \cdot (x-y)/\hbar), \quad j = L \text{ or } S. \tag{15}$$

The notion that the single virtual "$K^o \bar{K}^o$" has no trouble making up its mind as to its velocity but becomes confused about what should be its momentum, due to its mass splitting $\Delta M = (M_L - M_S)$, is crucial to the conventional analysis of single $\mathcal{D}(x,y)$ propagator experiments (even when a regenerator is included as part of the propagator). While theoretically this seems all right, e.g. the value of ΔM found in CPLEAR should agree with ΔM in regenerator experiments [8], we still feel somewhat uncomfortable with the result.

If the single virtual (large spreading wave packet) "$K^o \bar{K}^o$" is in a superposition of two plane wave momentum states, as in Eqs.(14) and (15), and this particle scatters off other particles, should not some other particles also have trouble deciding in which momentum states *they are*? After all, no matter what the state of mind of each particle may be, there should be four momentum conservation. In other words, if an initial state is in a superposition of two different incoming four momenta (P_1 and P_2), i.e.

$$|\Psi> = c_1 |in, P_1> + c_2 |in, P_2>, \tag{16a}$$

and if the scattering operator conserves four momenta, i.e.

$$S|\Psi> = c_1 |out, P_1> + c_2 |out, P_2>, \tag{16a}$$

then shouldn't the outgoing particles (with the same amplitudes c_1 and c_2) also be in superposition? The confused particles would also be virtual, since Bohr dictates that those particles which leave tracks are real and classical and thereby do not maintain "superpositions". The superposition principle has to be relegated to the virtual processes that you do not observe, and don't ask what a virtual particle is doing because there will be no data!

Let us now proceed to "two propagator" experiments wherein there are at least two virtual particles. These include the proposed Φ factory experiments, and here momentum conservation has some unusual implications.

4 Two Propagator Experiments

Shown in Fig.3 (below) are typical Feynman diagrams of a previous two propagator experiment [9] (which involves a virtual Λ) as well as a virtual "$K^o \bar{K}^o$". Also shown is a typical two propagator Feynman diagram for a process anticipated at the Φ factory [10]. If the "$K^o \bar{K}^o$" internal propagators are forced to have a superposition

of two four momentum states, then we have predicted that even the Λ would be forced to be in a superposition of two momentum states. "Λ oscillations" [11] would be the result of such a superposition, born by a combination of the mass splitting $\Delta M = (M_L - M_S)$ and of momentum conservation at the $\bar{K}^o + p^+ \rightarrow \Lambda + \pi^+$ vertex. The inner turmoil of the "$K^o\bar{K}^o$" spreads to any other virtual particle connected to it in the Feynman diagram.

To see that a discussion of the real and the virtual is not trivial, consider the Φ factory two virtual K meson process. The total four momentum is determined by the real electron positron pair producing the Φ,

$$P_\Phi = p_{e+} + p_{e-} = p_{L,left} + p_{S,right} = p_{S,left} + p_{L,right}. \tag{17}$$

Now, from the two propagators you try to put together a simple two particle wave function (not quite a Schrödinger wavefunction because there are too many "times"),

$$\Psi_{simple}(\tau_{right}, \tau_{left}) = A_L(\tau_{right})A_S(\tau_{left}) - A_L(\tau_{left})A_S(\tau_{right}), \tag{18}$$

where

$$A_j(\tau) = e^{-\Gamma_j\tau/2}e^{-iM_jc^2\tau/\hbar} \quad (j = L \; or S). \tag{19}$$

But we find that the total momentum conservation Eq.(17) cannot be maintained by Eq.(18); e.g., see Eq.(15),

$$A_L(\tau_{right})A_S(\tau_{left}) \sim exp\frac{i}{\hbar}(p_L \cdot x_{right} + p_S \cdot x_{left}), \tag{20a}$$

$$A_L(\tau_{left})A_S(\tau_{right}) \sim exp\frac{i}{\hbar}(p_L \cdot x_{left} + p_S \cdot x_{right}), \tag{20b}$$

but the two plane waves in Ψ_{simple} will not conserve total momentum unless $p_L = p_S$ (*false!*). This ultimately violates the one velocity and two momenta inner turmoil Eq.(13), and would thereby afford an undue psychological relief to the mass difference induced $K^o\bar{K}^o$ oscillations. So, the simple wave function in Eq.(18) appears inadequate for describing the two propagator result, if conservation of total momentum is strictly applied [12].

What is needed for conservation of total momentum is precisely what is written in Eq.(17), which *actually describes conservation of momentum.* Only one needs more proper times in the amplitude, because you need more momenta in the plane waves

$$\Psi(\tau_{L,right}, \tau_{L,left}, \tau_{S,right}, \tau_{S,left}) =$$

$$A_L(\tau_{L,right})A_S(\tau_{S,left}) - A_L(\tau_{L,left})A_S(\tau_{S,right}). \tag{21}$$

What can we do with all of those times (don't ask!)? Here are the numbers we promised you (dear reader) in Sec.1. Actually it is one (singular) number but it is predicted to occur very often in the data.

When you absolute square amplitudes with a wave function that has two terms, e.g. Eq.(21), the cross terms give you interference. For the problem at hand the interference phase is given by

$$\theta = \frac{c^2}{\hbar}[M_L(\tau_{L,left} - \tau_{L,right}) - M_S(\tau_{S,left} - \tau_{S,right})]. \tag{22}$$

Defining averages and differences

$$\tau_i = (1/2)(\tau_{L,i} + \tau_{S,i}), \quad (i = left\ or\ right), \tag{23a}$$

$$\Delta\tau_i = \tau_{L,i} - \tau_{S,i}, \quad (i = left\ or\ right), \tag{23b}$$

$$\bar{M} = (1/2)(M_L + M_S), \quad \Delta M = (M_L - M_S), \tag{23c}$$

we find from Eqs.(22) and (23),

$$(\hbar\theta/c^2) = \bar{M}(\Delta\tau_{left} - \Delta\tau_{right}) + \Delta M(\tau_{left} - \tau_{right}). \tag{24}$$

The first term on the left hand side Eq.(24) would not be present if we employed Eq.(18). But again by conservation of momentum we find the two terms on the right hand side of Eq.(24) approximately equal, and thus the factor of two in our final result

$$\theta = 2(c^2\Delta M/\hbar)(\tau_{left} - \tau_{right}). \tag{25}$$

The factor of "2" in Eq.(25) is the central result of this work.

5 Conclusion

We are *emotional* about a factor of "2" because we believe it says something unexpected about what is virtual and what is real. Others are *very emotional* about it because they calculate the factor to be "1"!. But the nice thing about it, is that the answer will surely be found at the Φ factory, with the experimentalists as the final referees. In Italy, where Galileo taught us that experimental data are the final arbiters in a theoretical dispute, what else could happen?

References

1. A. Einstein in "Albert Einstein Philosopher Scientist", Library of Living Philosophers, edited by P. A. Schlipp, Open Court Publishing Co. Illinois(1970).

2. N. Bohr "Discussions with Einstein"in "Quantum Theory and Measurement", page 9, edited by J. A. Wheeler and W. H. Zurek, Princeton University Press(1983).

3. A. Fine, "The Shaky Game: Einstein Realism and the Quantum Theory", University of Chicago Press, Chicago (1986).

4. Y. Srivastava, A. Widom and E. Sassaroli, "Spatial Correlations in Two Neutral Kaon Decays", *Zeitschrift Für Physik C* **66** (1995) 601.

5. T. D. Lee, R. Oheme and C. N. Yang, *Phys Rev* **106** (1957) 340.

6. R. G. Sachs, *Ann. Phys.* **22**, (1963) 239.

7. R. Adler et al, *Phys. Lett B* **286** (1992) 188.

8. Review of Particle Properties, *Phys Rev D* (1994) 397.

9. U. Camerini et al, *Phys. Rev.* **128** (1962) 352.

10. The DAΦNE Physics Handbook, edited by L. Maiani, G. Pancheri and N. Paver, INFN Laboratori Nazionali di Frascati (1992).

11. Y. Srivastava, A. Widom and E. Sassaroli, *Phys. Lett. B* **344** (1995) 436.

12. E. Sassaroli, Y. Srivastava and A. Widom, "Lepton Oscillations", submitted for publication.

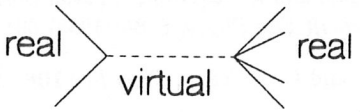

Figure 1: Real and Virtual

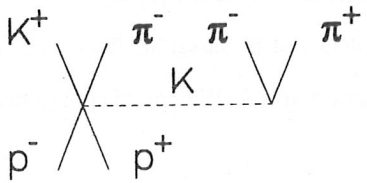

Figure 2: CPLEAR Event

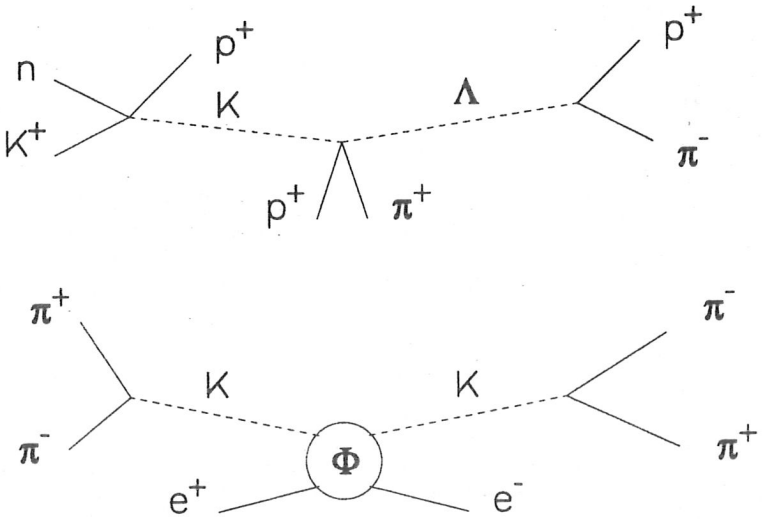

Figure 3: Examples of Two Propagator Events

EPR PARADOX AND TESTS OF QUANTUM MECHANICS AT DAΦNE

Philippe H. Eberhard
Lawrence Berkeley Laboratory
University of California, Berkeley, CA 94720

ABSTRACT

The two-neutral-kaon system produced by the decay of the ϕ-meson exhibits properties illustrating the EPR paradox. Some of these properties can be tested experimentally at Daϕne in what we call an "EPR-test". If the predictions of quantum mechanics are verified, the conclusion that can be drawn from such test is : if individual kaons *can* be described without hidden variables, there are non-local effects in kaon physics. Other tests may be considered, "Bell-tests", which can, in addition, show evidence for non-local effects in a large class of hidden-variables theories. However Bell-tests are more difficult experimentally.

Other tests of quantum mechanics can be performed at Daϕne, not directly linked to the EPR paradox, yet very meaningful because they test very fundamental aspects of the theory.

1 Introduction.

In 1935, Einstein, Podolsky, and Rosen (EPR) pointed out a property of the predictions of quantum mechanics, which was considered paradoxical by them at the time, [1], and still is by many physicists today, [2]. The property discovered by EPR implies that, in any attempt to describe what quantum systems really are, either there must be parameters that cannot be accounted for by the wave-function (e.g. hidden variables), or there are phenomena propagating faster than light. EPR preferred the explanation without faster-than-light effects. However, in 1964, Bell

*This work is supported in part by the Director, Office of Energy Research, Office of High Energy and Nuclear Physics, Division of High Energy Physics of the U.S. Department of Energy under Contract DE-AC03-76SF00098.

demonstrated that it is not possible to avoid these effects propagating faster than light in any attempt to describe the reality of quantum systems, *even if one uses hidden variables*, [3]. This is a consequence of certain predictions of quantum theory concerning certain experiments involving more than one particle.

Some physicists do not care about having a picture of what quantum systems are, [4], and, for them, the EPR-paradox may be of no interest. However, there are others, for whom that paradox is interesting, because it provides a unique insight on the real phenomena that lie behind the mathematical rules of our quantum mechanical predictions and are responsible for what is observed [5].

To prove that these faster-than-light effects are physical phenomena of nature, one can test some of these particular predictions of quantum theory that require these effects. That is the goal of *EPR-experiments*. To date, a wide range of predictions about relevant two-particle systems have been tested, [6], and, as a result, these faster-than-light effects are very likely to exist. However no experiment so far provides an absolute and unchallengeable proof, because they all have *loopholes*, [7]. In this paper, we describe how to gather evidence in kaon physics, using ϕ-factories.

To avoid confusion, we will call

- *EPR-tests* the experiments essentially checking the predictions of quantum mechanics needed to reproduce the EPR demonstration : i.e. there are faster-than-light effects if there are no hidden variables;

and

- *Bell-tests* the experiments checking the predictions needed to prove Bell's statement : i.e. there are faster-than-light effects even if there are hidden variables.

EPR-tests are easily done at Daϕne; Bell-tests are much harder experimentally and may require an asymmetric ϕ-factory, [8].

2 The Controversy.

2.1 The EPR Argument.

The quantum system that EPR considered, [1], is a system of two particles, which we label the left particle a and the right particle b. The measurements of the position x_a of the left particle corresponds to an operator X_a; of its momentum p_a to P_a; of the position x_b of the right particle to the operator X_b; and of the momentum p_b of the right particle to P_b. The operators X_b-X_a and P_b+P_a commute. Therefore there are states of that quantum system in which x_b-x_a is determined and equal to a known quantity Δx, while p_b+p_a is also determined and equal to another known quantity p_{total}. EPR gave an expression for the state-vector corresponding to such a state. If, after preparing a system in such a state, we measure x_a first and x_b later, quantum mechanics predicts that we will find

$$x_b = \Delta x + x_a \ . \tag{1}$$

If we measure p_a first and p_b later, we will find

$$p_b = p_{total} - p_a \ . \tag{2}$$

Then the EPR-argument is quite simple. After we measure x_a on the left particle, the system is in a quantum state where the position x_b of the right particle can be predicted with certainty if we decide to measure it. If, on the contrary, we measure p_a on the left, the system is in a state where the momentum p_b of that right particle can be predicted with certainty. Whether we perform the measurement of x_a or the measurement of p_a on the left particle a, we end up in two *different* situations, with different wave-functions for particle b on the right : after the measurement on a and before the one on b, we are either in

- case #1 where we have measured x_a, thus can predict the value of x_b but not of p_b;

or in

- case #2 where we have measured p_a, thus can predict p_b but not x_b.

These are indeed the predictions of quantum mechanics. The question is, in these two cases, what is different about particle b ? Is it the particle itself [1] or is it only our knowledge of it ?

If we assume that particle b on the right is different, we have to assume that a measurement on particle a is able to transform particle b,[2] at a distance. It has to happen before any measurement is made on b, i.e. within a time interval one may choose as small as we want. The effect has to propagate instantaneously from left to right, i.e. faster than light. According to the principle of relativity, for some observers in some fast moving Lorentz restframes, the modification of particle b occurs at a time prior to the time of the measurement on a on the left, which caused that modification. EPR discarded such a possibility and assumed, on the contrary, that what was different between case #1 and case #2 was only our knowledge of what is on the right side of the system. They supported the view that there were two "elements of reality" associated with particle b on the right: one corresponding to a unique value of x_b and one to an unique value p_b, as in hidden-variables theories. Both exist as characteristics of the particle; the measurement of x_a or of p_a on the left only reveals what the value of x_b or of p_b is.

Of course there is no wave-function capable of describing a particle with unique values for both x_b and p_b at the same time, therefore capable of describing what particle b is in reality. According to EPR, one needs more to describe a real particle than a wave-function. Quantum mechanics is "incomplete", [1)].

[1] of course if you care about what particle b is in reality,

[2] or, in more general terms, a feature of the quantum system correlated 100 % with the result of a measurement performed on the right,

2.2 Alternate Points of View.

There is still this other interpretation whereas particle b on the right is different in case #1 where x_a is measured on the left and in case #2 where p_a is. Then one has to accept that a measurement on the left particle can modify the particle on the right. According to Niels Bohr,

> "...Of course there is in a case like that just considered no question of a mechanical disturbance of the system under investigation during the last critical state of the measuring procedure. But, even at this stage, there is the question of *an influence on the very conditions which define the possible types of predictions...* Since these conditions constitute an inherent element of the description of any phenomenon to which the term 'physical reality' can be properly attached, we see that the argumentation of the mentioned authors (EPR) does not justify their conclusion that quantum-mechanical description is essentially incomplete. [9]

If we adopt that point of view, the measurement procedure on particle a on the left has an "influence" on the "physical reality" of particle b on the right; there is no evidence either for or against hidden variables but, instead, there is an "influence" that propagates faster than light.

Both EPR's and Bohr's points of view remained acceptable until Bell demonstrated that, if quantum systems obey quantum mechanics, one cannot describe what they are, even using hidden variables, without assuming the existence of influences propagating faster than light. Thus Bell resolved the controversy in Bohr's favor. To prove his point, Bell used another experiment than the EPR *gedanken* experiment described above. Such proof can be made also using the two-neutral-kaon system produced by the decay of the ϕ-meson. That is the proof that will be sketched in Sect. 4.

Quantum mechanics provides recipes to make predictions of what can be observed, [4], as *a car user's manual* tells you what the reaction of a car is when you press such or such button. Quantum mechanics does not describe the *engine under the hood* and how it works. This is unfortunately true whether one uses wave-function collapses or Feynman paths for the calculations, [10]. Not all physicists are satisfied with a *user's manual*, no matter how accurately it describes *the car behavior*. For these physicists, the mechanisms that make things happen are important and deserve being studied, [11]. Then the EPR-paradox is an opportunity to *look under the hood* and find out about the faster-than-light capability that these mechanisms are supposed to have.

3 An EPR-Test with Kaons.

3.1 Predictions of Quantum Mechanics.

The two-neutral-kaon system produced by ϕ-decay is in a C^- state, [12]. The state-vector at birth is

$$\propto \quad K_L K_S - K_S K_L \ , \tag{3}$$

where K_L (K_S) refers to the state of a long(short)-lived kaon; the first symbol, K_L (K_S) in the term $K_L K_S$ ($K_S K_L$) refers to the kaon labeled a on the left; and the second symbol, K_S (K_L), in the term $K_L K_S$ ($K_S K_L$) refers to kaon labeled b on the right. Let Δm be the $K_L - K_S$ mass difference and Γ_L, (Γ_S) the total decay rates of the K_L (K_S) meson. Consider a particular decay mode and assume there is a decay amplitude $\mathcal{A}_L$ ($\mathcal{A}_S$) for K_L (K_S) to decay this way. The probability for the left kaon a of decaying via this mode at time t_a in its proper restframe and the right kaon b of decaying via the same mode at time t_b in its own restframe, per unit of times of t_a and t_b, is

$$\frac{\partial^2 p}{\partial t_a \partial t_b} \propto \left| \mathcal{A}_L \mathcal{A}_S \left(e^{-\frac{\Gamma_L}{2} t_a} e^{-(\frac{\Gamma_S}{2} + i\Delta m) t_b} - e^{-(\frac{\Gamma_S}{2} + i\Delta m) t_a} e^{-\frac{\Gamma_L}{2} t_b} \right) \right|^2 \tag{4}$$

$$\propto f_L(t_a) f_S(t_b) + f_S(t_a) f_L(t_b) - 2\, f_{cos}(t_a) f_{cos}(t_b) - 2\, f_{sin}(t_a) f_{sin}(t_b) \ ; \tag{5}$$

where

$$f_L(t) = e^{-\Gamma_L t} \ , \tag{6}$$

$$f_S(t) = e^{-\Gamma_S t} \ , \tag{7}$$

$$f_{cos}(t) = e^{-\frac{\Gamma_S + \Gamma_L}{2} t} \cos(\Delta m\, t) \ , \tag{8}$$

$$f_{sin}(t) = e^{-\frac{\Gamma_S + \Gamma_L}{2} t} \sin(\Delta m\, t) \ . \tag{9}$$

Let us use the general form of any joint probability distribution for any kaon pair decaying into the same or via different decay modes on the left and on the right :

$$\begin{aligned} \frac{\partial^2 p}{\partial t_a \partial t_b} = & \left(C_{LL} f_L(t_a) + C_{SL} f_S(t_a) + 2C_{cos,L} f_{cos}(t_a) + 2C_{sin,L} f_{sin}(t_a) \right) f_L(t_b) \\ + & \left(C_{LS} f_L(t_a) + C_{SS} f_S(t_a) + 2C_{cos,S} f_{cos}(t_a) + 2C_{sin,S} f_{sin}(t_a) \right) f_S(t_b) \\ + & \ 2 \left(C_{L,cos} f_L(t_a) + C_{S,cos} f_S(t_a) + 2C_{cos,cos} f_{cos}(t_a) + 2C_{sin,cos} f_{sin}(t_a) \right) f_{cos}(t_b) \\ + & \ 2 \left(C_{L,sin} f_L(t_a) + C_{S,sin} f_S(t_a) + 2C_{cos,sin} f_{cos}(t_a) + 2C_{sin,sin} f_{sin}(t_a) \right) f_{sin}(t_b) \ . \end{aligned} \tag{10}$$

Eq. (10) involves 16 coefficients $C_{i,j}$ of 16 functions $f_i(t_a) f_j(t_b)$ of t_a and t_b, derived from the functions defined in Eqs. (6), (7), (8), and (9). The functions $f_i(t_a) f_j(t_b)$ of t_a and t_b are all different from one another. Therefore all of the coefficients

$C_{i,j}$ can be determined unambiguously from the predicted or from the measured distribution $\frac{\partial^2 p}{\partial t_a \partial t_b}$. Quantum mechanics predicts Eq. (5), thus coefficients

$$C_{LS} = C_{SL} = -C_{cos,cos} = -C_{sin,sin} = > 0 \,, \tag{11}$$

$$all\ other\ C_{i,j} = 0 \,. \tag{12}$$

3.2 Local Models of "Reality".

The probability of Eqs. (4) and (5) has been computed using the two-kaon system state-vector, i.e. a mathematical entity describing the pair of kaons and what we know about it without specifying which quantity is a characteristic of kaon a, which one is a characteristic of kaon b, and which one just describes what we know about the real parameters of the system.

In a model describing what the system is, there are parameters attributed to the system and, for those parameters, probability distributions corresponding to what we know. These parameters are supposed to have real values, which we may not know, independent of what any observer knows. That independence from an observer is associated, in day to day life, with the idea of *reality*, [13]. That is why those parameters are said to be parameters describing the *reality of the system*. Each set k of values of these *real* parameters is associated with a statistical weight w_k, indicating how probable that set of parameters is, given our knowledge of the situation. The probabilities of given outcomes of observations are obtained by averaging the probabilities associated with each set of parameters over all possible sets, weighting each set k with the weight w_k.

If the model is *local*, each *real* parameter is given a location. For the two-kaon system under consideration, there are parameters attached to kaon a and parameters attached to kaon b, evolving independently from what happens to the other kaon of the pair. The initial values of these parameters are set before the two kaons part; they may vary from one pair of kaons to the next. Correlations between observations made on kaon a and on kaon b result from correlations between initial values of the parameters attached to a and b in the same set.

In a local model where there are no hidden variables, the set of *real* parameters consists of two wave-functions, ψ_a^k and ψ_b^k, associated with kaon a and kaon b, respectively. Each wave-function is a two-component wave-function, as in one-kaon quantum mechanics, and it determines all probabilities of observations made on that kaon, including all decay rates, associated with the set k. We define the coefficients α_L^k, α_S^k, β_L^k, and β_S^k such that, following the decay of the ϕ-meson, the wave-functions of the pair of kaons are

$$\psi_a^k = \alpha_L^k K_L + \alpha_S^k K_S \,, \tag{13}$$

$$\psi_b^k = \beta_L^k K_L + \beta_S^k K_S \,. \tag{14}$$

3.3 The EPR-Inequality.

In this local model, let us consider any joint decay-time distribution of kaon a and kaon b via the same or into different modes. The joint probability distribution for particle a (b) on the left (right) to decay into final states corresponding to decay amplitudes $\mathcal{A}_L$ ($\mathcal{B}_L$) if the kaon is a K_L and $\mathcal{A}_S$ ($\mathcal{B}_S$) if the kaon is a K_S :

$$\frac{\partial^2 p}{\partial t_a \partial t_b} = \sum_k w_k \left| \mathcal{A}_L \alpha_L^k e^{-\frac{\Gamma_L}{2} t_a} + \mathcal{A}_S \alpha_S^k e^{-(\frac{\Gamma_S}{2} + i\Delta m) t_a} \right|^2 \times \left| \mathcal{B}_L \beta_L^k e^{-\frac{\Gamma_L}{2} t_b} + \mathcal{B}_S \beta_S^k e^{-(\frac{\Gamma_S}{2} + i\Delta m) t_b} \right|^2 . \quad (15)$$

In our local model, the distribution $\frac{\partial^2 p}{\partial t_a \partial t_b}$ is still of the form of Eq. (10), but the coefficients $C_{i,j}$ are functions of the w_k, α_L^k, α_S^k, β_L^k, β_S^k, $\mathcal{A}_L$, and $\mathcal{A}_S$, $\mathcal{B}_L$, and $\mathcal{B}_S$. In particular,

$$C_{LL} = \sum_k w_k \left| \mathcal{A}_L \alpha_L^k \right|^2 \left| \mathcal{B}_L \beta_L^k \right|^2 , \quad (16)$$

$$C_{SS} = \sum_k w_k \left| \mathcal{A}_S \alpha_S^k \right|^2 \left| \mathcal{B}_S \beta_S^k \right|^2 , \quad (17)$$

$$C_{cos,cos} = \sum_k w_k \ \Re\left\{ \mathcal{A}_L^* \alpha_L^{k*} \mathcal{A}_S \alpha_S^k \right\} \ \Re\left\{ \mathcal{B}_L^* \beta_L^{k*} \mathcal{B}_S \beta_S^k \right\} , \quad (18)$$

$$C_{sin,sin} = \sum_k w_k \ \Im\left\{ \mathcal{A}_L^* \alpha_L^{k*} \mathcal{A}_S \alpha_S^k \right\} \ \Im\left\{ \mathcal{B}_L^* \beta_L^{k*} \mathcal{B}_S \beta_S^k \right\} . \quad (19)$$

Applying Schwartz inequality to the sequences $\sqrt{w_k} \mathcal{A}_L \alpha_L^k \mathcal{B}_L \beta_L^k$ and $\sqrt{w_k} \mathcal{A}_S \alpha_S^k \mathcal{B}_L \beta_S^k$; one obtains the following relation between the coefficients :

$$C_{cos,cos}^{\ 2} + C_{sin,sin}^{\ 2} \leq C_{LL} \ C_{SS} . \quad (20)$$

Note that this inequality holds also if the decays are degenerate [3]. It applies also if the two decay modes are the same on the left and on the right, i.e. if $\mathcal{A}_L = \mathcal{B}_L$ and $\mathcal{A}_S = \mathcal{B}_S$. However, if the two modes are the same, the coefficients corresponding to the predictions of quantum mechanics, $C_{cos,cos}$ and $C_{sin,sin}$ of Eq. (11) are not zero, while C_{LL} and C_{SS} given by Eq. (12) are zero. The predicted coefficients violate Ineq. (20). Therefore these quantum mechanical predictions cannot be accounted for by any local model describing kaons with a two-component wave-function only. One needs either non-locality or additional parameters. That is the result obtained by EPR, [1], using their own *gedanken* experiment (see Sect. 2).

The coefficients C_{ij} can also be determined experimentally from a fit of expression (10) to the measured joint decay distribution $\frac{\partial^2 p}{\partial t_a \partial t_b}$. If that distribution $\frac{\partial^2 p}{\partial t_a \partial t_b}$ can be explained using a local model without hidden variables, Ineq. (20) will hold. On the contrary, if the experimentally determined values of $C_{cos,cos}$,

[3] i.e. if their rates are the sum of the rates computed with two amplitudes $\mathcal{A}_L$, two amplitudes $\mathcal{A}_S$, two amplitudes $\mathcal{B}_L$, and two amplitudes $\mathcal{B}_S$

$C_{sin,sin}$, C_{LL}, and C_{SS} are consistent with the predictions of quantum mechanics of Eqs. (11) and (12), these coefficients will violate Ineq. (20), ruling out locality without hidden variables.[4]

Ineq. (20) is used here to test locality without hidden variables, i.e. to make *EPR-tests*; the role of that inequality here is similar to the one of Bell inequalities in *Bell-tests*, which show non-locality with hidden variables. By analogy, we give Ineq. (20) the appellation "EPR-inequality".

3.4 Non-Locality or Hidden Variables.

As an example of *non-local* model *without hidden variables* that reproduces the predictions of quantum mechanics, let us consider a description sometimes used for computing decay distributions of kaons produced by ϕ-meson decay. At birth, the system is a mixture of : either a pair where the wave-function of kaon a is $\psi_a^1 = K_L$ on the left and the one of kaon b is $\psi_b^1 = K_S$ on the right; or a pair where, for kaon a, $\psi_a^2 = K_S$ and, for kaon b, $\psi_b^2 = K_L$. The decay rates of each kaon are those predicted by its wave-function but, as soon as one kaon decays via a particular mode, the wave-function of the second kaon *collapses* immediately into a state orthogonal to the amplitude of that mode. That model reproduces all the predictions computed with the two-body state-vector; it describes the kaons as a two-component wave-function; but the *collapse* of the wave-function of the second kaon depends on the decay mode of the first kaon, at some distance. The model implies a *non-local* influence.

Of course, to reproduce the predictions, all that is needed is that the collapse of the wave-function of the second kaon occurs after the first kaon has decayed but before the second one does. With the slow moving kaons produced by ϕ-decay, there is often enough time between the two decay times t_a and t_b for light to propagate from the location of one kaon decay to the location of the other. For these events there is a non-local influence but not necessarily faster-than-light. The only events requiring a faster-than-light influence are those for which, in the laboratory, the distance between the two kaons at the times of their decay is larger than the difference between their decay times multiplied by the velocity of light c. In terms of proper times, t_a and t_b, this condition reads

$$\frac{|t_b - t_a|}{t_b + t_a} < \frac{\textit{kaon velocity in the } \phi\textit{-rest frame}}{c} \approx 0.21 \ . \qquad (21)$$

To prove experimentally the faster-than-light character of that non-locality without hidden variables, the coefficients $C_{cos,cos}$, $C_{sin,sin}$, C_{LL}, and C_{SS} to be introduced into Ineq. (20) should be determined in a fitting procedure of expression (10) restricted to events satisfying Ineq. (21). The other events prove some form of non-locality, but not the faster-than-light aspect of it.

To illustrate that, if *hidden variables* are used, not all local descriptions of two-kaon systems are ruled out by our EPR-test, let us construct a model *with hidden*

[4] of course assuming sufficient statistical accuracy.

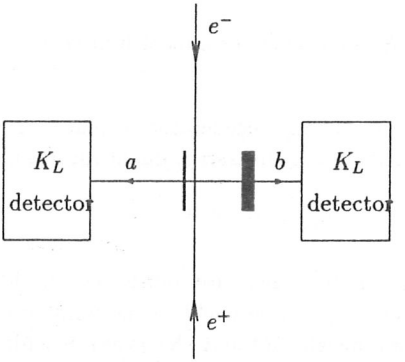

Figure 1: **Experimental Layout for a Bell-test with Kaons**, seen from above. *Kaons a and b traverse different regenerators of different thicknesses at different distances from the interaction point. Both regenerators are removable.*

variables that reproduces the predictions of quantum mechanics for this particular experiment, but that is *local.* In this model each kaon carries *elements of reality* determining its future time and mode of decay, but created at the time the ϕ-meson decays. These elements of reality correspond to hidden variables whose values get set randomly according to probability distributions predicted by quantum mechanics for the times and the modes of decays. At the time of the ϕ-decay, the two kaons are still together and there is no need for non-local effects to correlate the values taken by these hidden variables. Subsequently, the kaons carry these elements of reality along with them and decay at the times and via the modes dictated by the hidden variables, i.e. at preset times and via preset modes whose statistical distributions necessarily agree with the predictions of quantum mechanics.

For a Bell-test which excludes local models based on hidden variables of this type, i.e. on variables set at the time of the ϕ-meson decay, we need experimental features that cannot be included in the kaon description and can only come as a *surprise* for the kaon. We need *external* parameters which depend on an experimenter's decision, in principle unknown to the kaons when the ϕ-meson decays, for instance a measurement apparatus or a piece of material on a kaon path. The Bell-test described hereafter makes use of regenerators precisely because the presence of a regenerator depends on an experimenter's decision.

4 A Bell-Test with Kaons.

4.1 Setups.

An experimental layout for a Bell-test is sketched on Fig. 1. Kaons a and b from a ϕ-factory are emitted in opposite direction; kaon a on the left toward a thin regenerator nearby and kaon b toward a thicker one located farther away from the intersection point. Behind each regenerator, there is a neutral-particle detector located far enough to detect only kaons emerging as K_L's and with an angular resolution good enough to reject K_L's regenerated incoherently. The test consists of

measuring the number n_{LL} of $K_L K_L$ events per unit of luminosity in four different setups :

- n^0_{LL}, in setup 0, i.e. without any regenerator in place; in this setup, the number n^0_{SS} of $K_S K_S$ events is also measured; quantum mechanics predicts

$$n^0_{LL} = n^0_{SS} = 0 \; ; \tag{22}$$

- n^a_{LL}, in setup a, i.e. with only the regenerator on the left on the path of kaon a; quantum mechanics predicts n^a_{LL} to be equal to the number of kaons a born K_S (i.e. belonging to a pair initially of the $K_S K_L$ type), reaching regenerator a and coherently regenerated into K_L;

- n^b_{LL}, in setup b, i.e. with the regenerator only on the right on the path of kaon b; quantum mechanics predicts n^b_{LL} to be equal to the number of kaons b reaching regenerator b and regenerated into K_L;

- n^{ab}_{LL}, in setup ab, i.e. with the two regenerators in place; quantum mechanics predicts $K_L K_L$ events due to the two coherent regeneration processes in regenerators a and b and an interference phenomenon between them; the contribution of the $K_S \to K_L$ regeneration in regenerator a is smaller than in setup a because, to produce a $K_L K_L$ event in setup ab, kaon b has also to survive as a K_L when traversing regenerator b; this happens only a fraction p^b_{thru} of the time; similarly the contribution of the regeneration in regenerator b is reduced by the factor p^a_{thru} with respect to setup b :

$$n^{ab}_{LL} = n^a_{LL} p^b_{thru} + n^b_{LL} p^a_{thru} + n^{int}_{LL} \; , \tag{23}$$

  where n^{int}_{LL} is the interference term between the regeneration process in regenerator a and the one in regenerator b.

If regenerator b is farther away from the intersection point than regenerator a, the interference term n^{int}_{LL} can be made positive because of the effect of the $K_L - K_S$ mass difference. That interference term can even be made large enough to overcompensate the reduction due to the absorption factors p^a_{thru} and p^b_{thru} in Ineq. (23). Then,

$$n^{ab}_{LL} > n^a_{LL} + n^b_{LL} \; . \tag{24}$$

These conditions are adequate for a Bell-test.

4.2 A Bell-Type Argument.

In order to simplify the argument, let us neglect the non-orthogonality of K_L's and K_S's and assume that each kaon that decays can be identified unambiguously as a K_L or a K_S by its decay mode or time, in contrast with the EPR-test of Sect. 3 where the average number of K_L and of K_S was just estimated statistically. There

are only three possibilities to observe a kaon : decaying as a K_L; or decaying as a K_S; or interacting in a regenerator.

To reproduce the predictions of quantum mechanics, according to which there are only K_LK_S and K_SK_L events in setup 0, a local model must describe the kaon pairs at birth as a mixture of: pairs where kaon a is earmarked to decay as a K_L and kaon b as a K_S; and pairs where it is the other way around.[5] Any other possibility where one kaon has both a chance to decay as a K_L and a chance to decay as a K_S would produce K_LK_L or K_SK_S events in setup 0.

In a local model, kaon pairs earmarked K_LK_S at birth can contribute to K_LK_L events in setup ab only if kaon b is regenerated from K_S into K_L in the regenerator on the right, and if kaon a remains a K_L. Then, since kaon b evolves independently of what lies in the path of kaon a, one sees that these pairs produce K_LK_L events in setup b too. Similarly, pairs born K_SK_L contribute to K_LK_L events in setup ab only if they contribute to K_LK_L events in setup a too. If there are only K_LK_S and K_SK_L events in setup 0, a local model requires

$$n_{LL}^{ab} \leq n_{LL}^{a} + n_{LL}^{b} \ , \tag{25}$$

in contradiction with Ineq. (24). Ineq. (25) is true for any local model of kaons whether or not it uses hidden variables. Therefore a prediction of quantum mechanics leading to Ineq. (24) cannot be explained unless there is some non-local phenomenon involved.

In an experimental test, n_{LL}^{0} and n_{SS}^{0} will not be measured equal to zero in setup 0 but only, at best, consistent with zero. One should then take into account the possibility of having small amounts of K_LK_L and K_SK_S pairs in setup 0. Still assuming that kaons are earmarked as K_L or K_S before they decay,[6] one can see that, in a local model, pairs of K_LK_L events in setup 0 correspond to K_LK_L events in setup ab only if both kaons remain K_L's as they traverse the regenerators. These pairs correspond to K_LK_L events in setups a and in setup b too. These pairs reinforce Ineq. (25). On the contrary, pairs seen as K_SK_S in setup 0 correspond to events of type K_LK_L in setup ab if both kaons are regenerated into K_L in the regenerators. They will not correspond to K_LK_L events in either setup a or b. K_SK_S pairs in setup 0 must be taken into account and Ineq. (25) has to be generalized into :

$$n_{LL}^{ab} \leq n_{LL}^{a} + n_{LL}^{b} + n_{SS}^{0} \ . \tag{26}$$

Ineq. (26) is a form of Bell inequality, equivalent to the one of Ref. [14].

4.3 Practical Considerations.

Unfortunately, the decay mode and the decay time of a kaon cannot always identify that kaon as a K_L or a K_S unambiguously. An analysis has been made of the

[5] Of course this earmarking could be done either by a simple K_L or K_S wave-function, or it can be done using a hidden variable.

[6] The argument can be made without this assumption too, [15].

consequence of that ambiguity in Ref. [15]. The conclusion is that, if the results of the test confirm the predictions of quantum mechanics, not all local hidden-variables theories are ruled out, but only a large class of them. There are *loopholes*, in this Bell-test, as in all experiments performed so far, [7]. However, the Bell-test of this section is different because it deals with kaon physics and, in kaon physics, it is more general than the EPR-test of Sect. 3.

To make the Bell-test above a feasible experiment, we need a substantial amount of coherent regeneration. At Daϕne, kaon momenta are small and correspond to very small regeneration amplitudes, [16]. Chances to conduct such a test would be better at an asymmetric ϕ-factory, [8], because kaon momenta could be made larger. The best energy combination for the e^- and the e^+ beams is around 1.6 GeV against 160 MeV, which produces kaons of approximately 0.7 GeV/c, [17]. Copper is a good choice for the regenerator material. Measuring all thicknesses and distances along the kaon paths, regenerator a (b) should be about 5 mm (6 cm) thick and regenerator b located 17 cm farther from the intersection point than regenerator a. Let η_0 be the probability that a K_S does not decay over a distance equal to the distance of regenerator a to the intersection point,[7] and N the number of neutral kaon pairs produced.

$$For \quad N \times \eta_0 = 10^8 \ , \qquad n^a_{LL} = 4560 \ , \tag{27}$$

$$n^b_{LL} = 2190 \ , \tag{28}$$

$$n^{ab}_{LL} = 8570 \ . \tag{29}$$

These numbers violate Ineq. (26). In principle, they make a Bell-test possible, but the experiment is difficult. Yet the conditions here are probably more favorable than at Daϕne.

5 Summary and Conclusions.

Certain predictions of quantum mechanics cannot be explained in any model of what quantum systems are *in reality* without assuming that there are non-local influences. For two-kaon systems produced by ϕ-decay, the prediction for the joint distribution for the two kaons decaying into the same modes are given by Eqs. (11) and (12). These predictions require non-locality if hidden variables are assumed not to exist. This non-locality can be demonstrated experimentally at Daϕne by performing the EPR-test of Sect. 3. If the data used for the test is restricted to events where Ineq. (21) is satisfied, the faster-than-light character of that non-locality can be demonstrated too.

Of course, if the result of the test agrees with quantum mechanics, there are local hidden-variable models that are also eliminated by our EPR-test, in particular the one-particle "pilot-wave" model, where each particle is described by a wave and

[7] that distance cannot be known unless we know the machine design,

a point-like singularity [8], [18]. However it is easy to construct other local models with hidden variables that are not ruled out by our EPR-test, such as the one described in Sect. 3.4.

A Bell-test, i.e. a test able to eliminate a large class of local hidden-variables theories can be designed, relying on the $K_S \to K_L$ regeneration phenomenon, (see Sect. 4). That test has loopholes, but is more powerful than the EPR-test of Sect. 3, because it is harder to construct local theories that survive a result in accordance with quantum mechanics, [19]. Unfortunately the test is more difficult experimentally and may be feasible only at an asymmetric ϕ-factory, [17].

The difference between an EPR-test and a Bell-test is how large a domain of hidden-variables theories is excluded if the predictions of quantum mechanics are verified. To cover as large a domain as possible, other tests can be conceived, such as the one described in the Appendix, in Ref. [17], and those mentioned in Refs. [20].

In kaon physics, Daϕne provides other opportunities to perform tests of quantum mechanics, not so tightly coupled with the EPR-paradox. Some of them have been suggested in Ref. [21]. They check very fundamental aspects of the theory and, may be, also explore possible effects induced by Planck-mass physics at our energy scale, [22].

I am taking this opportunity to thank the organizers of this workshop for inviting me, in particular Profs. G. Pancheri and N. Paver, with whom I had quite a few interesting discussions.

[8]This model can reproduce all the predictions of one-particle quantum mechanics without involving "wave-functions" collapses. Thus it does not imply faster-than-light effects.

References

1. A. Einstein, B. Podolsky and N. Rosen, Phys. Rev. **47** (1935) 777 .

2. For instance: B. D'Espagnat, in *Quantum Theory and Pictures of Reality*, W. Schommers, ed., Springer Verlag, Heidelberg (1989) 130 .

3. J.S. Bell, Physics **1** (1964) 195 .

4. For a more precise description of this point of view, see for instance M. Jammer, in *The Philosophy of Quantum Mechanics*, Wiley, New York (1974) ; or E.P. Wigner in *Quantum Theory and Measurement*, Princeton University Press, Princeton, NJ (1983) .

5. For instance: D. Bohm and B. Hiley, Found. Phys. **5** (1975) 93 ; G.C. Ghirardi, A. Rimini and T. Weber, Phys. Rev. **D 34** (1986) 470 ; G.C. Ghirardi, P. Pearle, and A. Rimini, Phys. Rev. **D 42** (1990) 78 .

6. S.J. Freedman and J.F. Clauser, Phys. Rev. Lett. **28** (1972) 938 ; J.F. Clauser, Phys. Rev. Lett. **37** (1976) 1223 ; E.S. Fry and R.C. Thompson, Phys. Rev. Lett. **37** (1976) 465 ; A. Aspect, P. Grangier, and G. Roger, Phys. Rev. Lett. **47** (1981) 460 ; ibid. **49** (1982) 91 ; A. Aspect, J. Dalibard, G. Roger, Phys. Rev. Lett. **49** (1982) 1804 .

7. N.D. Mermin, "The EPR experiment – thoughts about the 'Loophole,' " *New Techniques and Ideas in Quantum Measurement Theory*, edited by D.M. Greenberger (New York Academy of Science, New York, 1986) pp. 422-428 .

8. Such a factory was proposed, for instance, by C. Rubbia, *A $\Phi \rightarrow K_L + K_S$ Factory using the Trieste Synchrotron Light Source* ST/M-88/4, Sincrotrone Trieste, 34012 Trieste .

9. N. Bohr, Phys. Rev. **48** (1935) 696 .

10. L. Stodolsky, at this workshop, advocated using Feynman's paths as a mode to compute the probabilities.

11. J.S. Bell, *Speakable and Unspeakable in Quantum Mechanics*, Cambridge University Press, Cambridge (1987) .

12. Particle Data Group, *Review of Particle Properties*, Phys. Rev. **D 45** (1992) p. II.7 .

13. J. Piaget, *La Construction du Réel chez l'Enfant* (Delachaux et Niestlé, Neuchâtel, Switzerland, 1950) .

14. J.F. Clauser and M.A. Horne, Phys. Rev. **D10** (1974) 526 .

15. P.H. Eberhard, *Testing the Non-Locality of Quantum Theory in Two-Kaon Systems.* LBL-32100, LBL, Berkeley (1992), in Nucl. Phys. **B** 398 (1993) 155 .

16. R. Baldini and A. Michetti, private communication, (1993) .

17. P.H. Eberhard and F. Uchiyama, Nucl. Instr. and Meth. in Phys, Res. **A** 350 (1994) 144 .

18. L. DeBroglie, Ann. Phys. **3** (1925) 22 .

19. For instances, models inspired by F. Selleri, Ann. N.Y. Acad. Sci. 480 (1986) 518 .

20. For instance: M. Roos, University of Helsinki, preprint HU-TFT-80-5, (1980) ; F. Selleri, Lett. Nuovo Cim. **36** (1983) 521 ; D. Cocolicchio, Found. Phys. Lett. **3** (1990) 359 ; D. Home and F. Selleri, J. Phys. **A 24** (1991) L1073 ; O. Piccioni, *Proceeding of the Workshop on Physics and Detectors for Daφne*, G. Pancheri, ed., Frascati (1991) 279 ; I.I. Bigi, Nucl. Phys. **B** (Proc. Suppl.) **24 A** (1991) 24 ; P. Privatera and F. Selleri, Phys. Lett. **B 296** (1992) 261. See also criticism in: G.C. Ghirardi, R. Grassi, and T. Weber, *Proceeding of the Workshop on Physics and Detectors for Daφne*, G. Pancheri, ed., Frascati (1991) 261 .

21. P.H. Eberhard, in *The Second Daφne Physics Handbook*, L Maiani, G. Pancheri, and N. Paver, eds., Frascati (1995), 99 .

22. N. Mavromatos, Report at this workshop, and references within.

APPENDIX : Testing Bell's inequality at DAΦNE

Antonio Di Domenico
Dipartimento di Fisica, Universitá "La Sapienza" & INFN Sezione di Roma, Rome, Italy.

Bell's theorem [1] states that a generic local realistic hidden-variables theory cannot reproduce all statistical predictions of quantum mechanics.

Let us consider, as usual, a pair of spin 1/2 particles in the singlet state moving in opposite directions:

$$|i\rangle = \frac{1}{\sqrt{2}}\{|A\uparrow(\vec{p})\rangle|A\downarrow(-\vec{p})\rangle - |A\downarrow(\vec{p})\rangle|A\uparrow(-\vec{p})\rangle\} \tag{30}$$

where the state $|A\uparrow(\vec{p})\rangle$ represents a particle moving in the $\vec{p}$ direction with the spin *up* along the $\vec{a}$ direction. Let us consider three different axes $\vec{a}$, $\vec{b}$, $\vec{c}$ and the corresponding spin projection operators $A = \vec{\sigma}\cdot\vec{a}$, $B = \vec{\sigma}\cdot\vec{b}$ and $C = \vec{\sigma}\cdot\vec{c}$. Let us assume that we perform a measurement of A, B or C on the particle moving in the $\vec{p}$ direction, and a measurement of A, B or C on the other particle moving in the opposite direction. It can be shown that, according to local realism, the following inequality can be derived [1, 2]:

$$\begin{aligned} P[A\uparrow(\vec{p}); B\uparrow(-\vec{p})] \;\leq\; & P[A\uparrow(\vec{p}); C\uparrow(-\vec{p})] + P[C\uparrow(\vec{p}); B\uparrow(-\vec{p})] + \\ & + P[C\downarrow(\vec{p}); C\downarrow(-\vec{p})] \end{aligned} \tag{31}$$

where $P[A\uparrow(\vec{p}); B\uparrow(-\vec{p})]$ is the probability of finding A=+1 (spin up) for the particle moving in the $\vec{p}$ direction, and B=+1 (spin up) for the particle moving in the opposite direction.

Inequality (31) is generally referred as Bell's inequality and holds for a generic local realistic hidden-variables theory. For some axes choices, quantum mechanical predictions violate the above inequality, showing the incompatibility of the quantum theory with either the thesis of realism or that of locality [1].

The experimental tests of inequality (31), referred as Bell-tests in the introduction of this contribution, have been performed essentially with photons in atomic-cascade experiments yielding results in excellent agreement with quantum mechanics [3]. However the validity of any experimental test of inequality (31) relies on some other *ad hoc* additional assumptions, although reasonable ones, than local realism. Here a possible test of inequality (31) at a ϕ-factory using neutral kaons and requiring somewhat different and slightly more restrictive additional assumptions than ones made in atomic-cascade experiments is discussed [4]. Whether it can be considered a Bell-test or an EPR-test will be shortly discussed at the end of this Appendix.

At a ϕ-factory a coherent neutral kaon state is produced in ϕ decays:

$$|i\rangle = \frac{1}{\sqrt{2}}\{|K^0(\vec{p})\rangle|\overline{K^0}(-\vec{p})\rangle - |\overline{K^0}(\vec{p})\rangle|K^0(-\vec{p})\rangle\} \tag{32}$$

A *quasispin* picture can be introduced such that the strangeness eigenstates $|K^0\rangle$ and $|\overline{K^0}\rangle$ are regarded as a quasispin doublet and called quasispin *up* and *down* along the z direction. Then CP eigenstates $|K_1\rangle \propto \left\{|K^0\rangle + |\overline{K^0}\rangle\right\}$ and $|K_2\rangle \propto \left\{|K^0\rangle - |\overline{K^0}\rangle\right\}$ are quasispin eigenstates *up* and *down* along the x axis. Let us also consider the quasispin eigenstates along a third generic direction x' and call them $|K_\alpha\rangle \propto \{|K_1\rangle - \eta^*|K_2\rangle\}$ and $|K_\beta\rangle \propto \{|K_2\rangle + \eta|K_1\rangle\}$ where η is a complex parameter that determines the x' direction. It is worth reminding that the physical states, i.e. Hamiltonian eigenstates, $|K_S\rangle \propto \{|K_1\rangle + \epsilon|K_2\rangle\}$ and $|K_L\rangle \propto \{|K_2\rangle + \epsilon|K_1\rangle\}$ where ϵ is the usual CP violation parameter, are non-orthogonal because of CP violation[9]. In the following $|\eta|$ is chosen of about the same order of $|\epsilon|$, so that terms of the order $O(|\eta|^2) \sim O(|\epsilon|^2) \sim 10^{-6}$ can always be neglected, while terms $O(|\eta|) \sim O(|\epsilon|) \sim 10^{-3}$ are retained.

In complete analogy to the spin case, a Bell's inequality can be written for the state (32), where spin projections along the $\vec{a}$, $\vec{b}$, $\vec{c}$ axes are substituted by quasispin projections along, for instance, the x', z, x axes (disregard, for the moment, any technical complication about quasispin measurement):

$$P[K_\alpha(\vec{p},t);K^0(-\vec{p},t)] \leq P[K_\alpha(\vec{p},t);K_1(-\vec{p},t)] + P[K_1(\vec{p},t);K^0(-\vec{p},t)] + \\ + P[K_2(\vec{p},t);K_2(-\vec{p},t)] \qquad (33)$$

Compared to inequality (31), inequality (33) shows an explicit dependence on time. This does not constitute a difficulty. However here, for simplicity, only the case in which both quasispins are measured at equal times is considered. The more general case of measurements at different times is treated elsewhere [4].

Inequality (33) holds for local realistic hidden-variables theories. For some η values it is violated by quantum mechanical predictions. However in order to perform an experimental test of inequality (33) the following additional assumptions have to be made:

(i) *the decay process is a local random process, namely decay rates are time-independent quantities, e.g.* $\Gamma(K^0 \to \pi^-\ell^+\nu) = const$;

(iia) *quantum mechanical predictions for single kaon state propagation in matter and in vacuum are valid, in particular those related to the four probabilities* $P[K_{\alpha,\beta}(0) \Rightarrow K_{1,2}(\Delta t)]$ *of finding a* $K_{1,2}$ *state at time* Δt *from an initial* $K_{\alpha,\beta}$ *state at time* $t = 0$;

(iib) *the four probabilities* $P[K_{\alpha,\beta}(0) \Rightarrow K_{1,2}(\Delta t);\lambda]$ *do not depend on* λ, *for any*

[9]Here CPT invariance is assumed for simplicity, even if it is not a necessary assumption

hidden variable λ [10] ; (iii) *the* $\Delta S = \Delta Q$ *rule holds* [11] .

The above assumptions are quite reasonable and allow us to identify the quasispin states necessary to perform measurements of probability distribution in inequality (33). In fact, as a consequence of assumptions (i) and (iii), $|K^0\rangle$, $|\overline{K^0}\rangle$, $|K_1\rangle$ and $|K_2\rangle$ could be identified by detecting special kaon decay channels, namely $K^0 \to \pi^-\ell^+\nu$, $\overline{K^0} \to \pi^+\ell^-\overline{\nu}$, $K_1 \to \pi^+\pi^-, \pi^0\pi^0$ and $K_2 \to \pi^0\pi^0\pi^0$ [12].

The $|K_\alpha\rangle$ state can be identified (a) by means of a regenerator or, more conveniently, (b) by time evolution in vacuum of the state itself. Here only method (b) will be considered (see Ref. [4]) for method (a)). This method is based on the fact that, as quasispin is not conserved, it *oscillates* in time. A suitable parameter $\eta = \eta(\Delta t)$ can be chosen such that, after a certain time Δt, a $|K_\beta\rangle$ is rotated into a pure $|K_2\rangle$ state, i.e. $P[K_\beta(0) \Rightarrow K_1(\Delta t)] = 0$, and a $K_1 \to \pi\pi$ decay at time $t + \Delta t$ unambiguously identifies the presence of a $|K_\alpha\rangle$ state at time t. It can be shown that additional assumptions (iia) and (iib) are necessary for the validity of this method [4]. Then, the following relation (and similar ones) holds:

$$P[K_1(\vec{p}, t + \Delta t); K^0(-\vec{p}, t)] = \kappa P[K_\alpha(\vec{p}, t); K^0(-\vec{p}, t)] \tag{34}$$

where $\kappa = P[K_\alpha(0) \Rightarrow K_1(\Delta t)] = e^{-\Gamma_S \Delta t}$, and the l.h.s. probability is measurable.

In order to test inequality (33) at a ϕ-factory a two step measurement can be performed:

Step(I): first, one should verify that the following relations hold, as predicted by quantum mechanics:

$$P[K_\alpha(\vec{p}, t); K_1(-\vec{p}, t)] \ll\sim |\Re(\eta)| e^{-\Gamma t}/2 \tag{35}$$

$$P[K_2(\vec{p}, t); K_2(-\vec{p}, t)] \ll\sim |\Re(\eta)| e^{-\Gamma t}/2 \tag{36}$$

[10] This assumption is quite reasonable because, as shown in the following, the η parameter can be chosen such that:

$$\begin{aligned}
P[K_\alpha(0) \Rightarrow K_1(\Delta t)] &= \int_\Lambda P[K_\alpha(0) \Rightarrow K_1(\Delta t); \lambda] \rho^\alpha(\lambda) d\lambda = e^{-\Gamma_S \Delta t} \\
P[K_\alpha(0) \Rightarrow K_2(\Delta t)] &= \int_\Lambda P[K_\alpha(0) \Rightarrow K_2(\Delta t); \lambda] \rho^\alpha(\lambda) d\lambda = 0 \\
P[K_\beta(0) \Rightarrow K_1(\Delta t)] &= \int_\Lambda P[K_\beta(0) \Rightarrow K_1(\Delta t); \lambda] \rho^\beta(\lambda) d\lambda = 0 \\
P[K_\beta(0) \Rightarrow K_2(\Delta t)] &= \int_\Lambda P[K_\beta(0) \Rightarrow K_2(\Delta t); \lambda] \rho^\beta(\lambda) d\lambda = e^{-\Gamma_L \Delta t}
\end{aligned}$$

where $\rho^{\alpha,\beta}(\lambda)$ are the λ distribution functions for the case of one-kaon state, and such that $\int_\Lambda \rho^{\alpha,\beta}(\lambda) d\lambda = 1$. This means that $P[K_\alpha(0) \Rightarrow K_2(\Delta t); \lambda]$ and $P[K_\beta(0) \Rightarrow K_1(\Delta t); \lambda]$ should vanish for $\rho^{\alpha,\beta}(\lambda) > 0$. Then, $P[K_{\alpha,\beta}(0) \Rightarrow K_{1,2}(\Delta t); \lambda]$ do not depend on λ, at least in the λ domain in which $\rho^{\alpha,\beta}(\lambda) > 0$. Even if this domain could be different, in general, from that corresponding to the two-kaons state produced in ϕ decay, it is reasonable to assume that the above probabilities do not depend on λ even in the case of two-kaons state.

[11] Experimentally $r = \frac{A(K^0 \to \pi^+\ell^-\overline{\nu})}{A(K^0 \to \pi^-\ell^+\nu)} \leq 2 \cdot 10^{-2}$. Here it is necessary that $r \leq 10^{-4}$, whereas the Standard Model prediction is $r = 10^{-6} \div 10^{-7}$.

[12] Apart from a negligible direct CP violation effect, neutral kaon decays into $\pi^+\pi^-$ or $\pi^0\pi^0$ are allowed for $|K_1\rangle$ and forbidden for $|K_2\rangle$, while the opposite happens for decays into $\pi^0\pi^0\pi^0$.

with $\Gamma = \Gamma_S + \Gamma_L$. Relation (35) can be easily experimentally verified, as shown elsewhere [4]. Verification of relation (36) is much more difficult because it corresponds to a suppressed decay rate measurement. However this verification should be still possible at a high-luminosity ϕ-factory like DAΦNE. Alternatively, one could avoid the experimental verification of relation (36) making the following additional assumption:

(iv) *the singlet state perfect anti-correlation holds,*

that makes $P[K_2(\vec{p},t);K_2(-\vec{p},t)] = 0$, even if it reduces the validity of the test to a less general class of hidden-variables theories.

Step(II): let us consider the quantity:

$$\Sigma = \frac{P[K_\alpha(\vec{p},t);K^0(-\vec{p},t)]/P[K_\alpha(\vec{p},t);\overline{K^0}(-\vec{p},t)]}{P[K_1(\vec{p},t);K^0(-\vec{p},t)]/P[K_1(\vec{p},t);\overline{K^0}(-\vec{p},t)]} \tag{37}$$

If step (I) measurements (and similar ones[13]) do not exhibit any deviation from quantum mechanical predictions, it can be easily shown [4] that a family of inequality of the form (33) can be reduced to the equality:

$$\Sigma = 1 \tag{38}$$

while the corresponding quantum mechanical prediction is $\Sigma_{QM} = 1 + 4\Re(\eta)$, independent on time t, and violating (38) by the quantity $4\Re(\eta)$.

From an experimental point of view, it is convenient to measure Σ through the relation:

$$\Sigma(\Delta t) = \frac{N[\pi\pi(\vec{p},t+\Delta t);\pi^-\ell^+\nu(-\vec{p},t)]/N[\pi\pi(\vec{p},t+\Delta t);\pi^+\ell^-\overline{\nu}(-\vec{p},t)]}{N[\pi\pi(\vec{p},t);\pi^-\ell^+\nu(-\vec{p},t)]/N[\pi\pi(\vec{p},t);\pi^+\ell^-\overline{\nu}(-\vec{p},t)]} \tag{39}$$

where $N[f_1(\vec{p},t');f_2(-\vec{p},t'')]$ is the measured decay rate into f_1 and f_2 channels at times t' and t'', respectively.

At DAΦNE, assuming an integrated luminosity $L \sim 10^4\ pb^{-1}$, a statistical error $\Delta\Sigma/\Sigma$ smaller than 0.1 % can be obtained, whereas the quantity $|4\Re(\eta)|$ is of the order of 1% in the case of $\Delta t = 1\ \tau_S$, with τ_S the K_S lifetime. Hence the statistical precision achievable at DAΦNE seems adequate to reveal Bell's inequality

[13]Other relations of the kind (35,36) should be verified, in particular one involving the probability $P[K_\beta(\vec{p},t);K_\beta(-\vec{p},t)]$ not directly measurable. However it can be rewritten as:

$$\begin{aligned} P[K_\beta(\vec{p},t);K_\beta(-\vec{p},t)] = {} & P[K_\alpha(\vec{p},t);K_\alpha(-\vec{p},t)] + P_{TOT} \\ & -P[K_\alpha(\vec{p},t);K_1(-\vec{p},t)] - P[K_\alpha(\vec{p},t);K_2(-\vec{p},t)] \\ & -P[K_1(\vec{p},t);K_\alpha(-\vec{p},t)] - P[K_2(\vec{p},t);K_\alpha(-\vec{p},t)] \end{aligned}$$

with

$$\begin{aligned} P_{TOT} = {} & P[K_1(\vec{p},t);K_1(-\vec{p},t)] + P[K_1(\vec{p},t);K_2(-\vec{p},t)] \\ & +P[K_2(\vec{p},t);K_1(-\vec{p},t)] + P[K_2(\vec{p},t);K_2(-\vec{p},t)] \end{aligned}$$

where terms at r.h.s. are all measurable probabilities.

violations. However the systematics should be carefully investigated. A general purpose detector like KLOE might successfully perform such a measurement.

As said in Sect. 5, the difference between an EPR-test and a Bell-test resides in the size of the domain of local hidden-variables theories excluded if the predictions of quantum theory are verified. Obviously, there is some arbitrariness in the definitions of these two kind of tests. The test suggested in this Appendix does not involve an experimental condition that depends on an experimentalist's decision; thus a hidden variable model of the type described in Sect. 3.4 can never be excluded. That restriction is the reason why additional assumption (i) has been introduced. However it is the author's belief that hypothesis (i) is so reasonable that the test suggested here should still be called a Bell-test rather than an EPR-test. In any case, it is worth noting that, as discussed elsewhere (see Appendix B in Ref. [4]), if method (a) were used to identify $|K_\alpha\rangle$ states, instead of method (b), the experimenter's decision could be still introduced to some extent in the test, even if, in this case, a slightly modified experimental set-up would be required than the one foreseen for KLOE at DAΦNE.

I would like to express my gratitude to Prof. P.H. Eberhard for fruitful suggestions and very stimulating and clarifying discussions on the subject. I am very grateful to Profs R. Baldini and G.C. Ghirardi for useful discussions and for their interest and help.

References

1. for a review see: J.Bell, Speakable and unspeakable in quantum mechanics, Cambridge University Press, 1987 and also J.F. Clauser and A. Shimony, Rep.Prog.Phys.**41** (1978) 1881

2. see also E.P. Wigner, Am.J.Phys. **38** (1970) 1005

3. for one of the most significant atomic-cascade experiments see A.Aspect et al., Phys.Rev.Lett. **49** (1982) 1804

4. A. Di Domenico, Nucl.Phys. **B450** (1995) 293

EPR EFFECTS WITHOUT COLLAPSE OF THE WAVEFUNCTION

Leo Stodolski
Max-Planck Institut fuer Physik
Postfach 40 12 12, Föhringer Ring 6, D–W–8000 München 40 (Germany)

(No written contribution arrived)

EXPERIMENTAL TESTS OF CPT SYMMETRY AND QUANTUM MECHANICS AT CPLEAR

N. E. Mavromatos [a] *
Laboratoire de Phys. Thèorique ENSLAPP (URA 14-36 du CNRS, associèe à l' E.N.S de Lyon, et au LAPP (IN2P3-CNRS) d'Annecy-le-Vieux), Chemin de Bellevue, BP 110, F-74941 Annecy-le-Vieux Cedex, France

and

T. Ruf *
CERN PPE Division, 1211 Geneva 23, Switzerland

ABSTRACT

We review a phenomenological parametrization of an open quantum-mechanical formalism for CPT violation in the neutral kaon system, and constrain the parameters using fits to recent CPLEAR data.

*For the Collaboration: John Ellis[(b)], Jorge L. Lopez[(c)], N. E. Mavromatos, D. V. Nanopoulos[(c)]

and

the CPLEAR Collaboration†

R. Adler[2], T. Alhalel[2], A. Angelopoulos[1], A. Apostolakis[1], E. Aslanides[11], G. Backenstoss[2], C.P. Bee[2], O. Behnke[17], A. Benelli[9], V. Bertin[11], F. Blanc[7,13], P. Bloch[4], Ch. Bula[13], P. Carlson[15], M. Carroll[9] J. Carvalho[5], E. Cawley[9], S. Charalambous[16], M. Chardalas[16], G. Chardin[14], M.B. Chertok[3], A. Cody[9], M. Danielsson[15], S. Dedoussis[16], M. Dejardin[14], J. Derre[14], J. Duclos[14], A. Ealet[11], B. Eckart[2], C. Eleftheriadis[16], I. Evangelou[8], L. Faravel[7], P. Fassnacht[11], J.L. Faure[14], C. Felder[2], R. Ferreira-Marques[5], W. Fetscher[17], M. Fidecaro[4], A Filipčič[10], D. Francis[3], J. Fry[9], E. Gabathuler[9], R. Gamet[9], D. Garreta[14], H.-J. Gerber[17], A. Go[15], C. Guyot[14], A. Haselden[9], P.J. Hayman[9], F. Henry-Couannier[11], R.W. Hollander[6], E. Hubert[11], K. Jon-And[15], P.-R. Kettle[13], C. Kochowski[14], P. Kokkas[2], R. Kreuger[6], R. Le Gac[11], F. Leimgruber[2], A. Liolios[16], E. Machado[5], I. Mandic'[10], N. Manthos[8], G. Marel[14], M. Mikuž[10], J. Miller[3], F. Montanet[11], T. Nakada[13], A. Onofre[5], B. Pagels[17], I. Papadopoulos[16], P. Pavlopoulos[2], J. Pinto da Cunha[5], A. Policarpo[5], G. Polivka[2], R. Rickenbach[2], B.L. Roberts[3], E. Rozaki[1], T. Ruf[4], L. Sakeliou[1], P. Sanders[9], C. Santoni[2], K. Sarigiannis[1], M. Schäfer[17], L.A. Schaller[7], A. Schopper[4], P. Schune[14], A. Soares[14], L. Tauscher[2], C. Thibault[12], F. Touchard[11], C. Touramanis[4], F. Triantis[8], E. Van Beveren[5], C.W.E. Van Eijk[6], G. Varner[3], S. Vlachos[2], P. Weber[17], O. Wigger[13], M. Wolter[17], C. Yeche[14], D. Zavrtanik[10] and D. Zimmerman[3]

(a) On leave from P.P.A.R.C. Advanced Fellowship, Dept. of Physics (Theoretical Physics), University of Oxford, 1 Keble Road, Oxford OX1 3NP, U.K.
((b) CERN Theory Division, 1211 Geneva 23, Switzerland
((c) Center for Theoretical Physics, Department of Physics, Texas A\&M Univ., College Station, TX 77843-4242, USA, and Astroparticle Physics Group, Houston Advanced Research Center (HARC), The Mitchell Campus, The Woodlands, TX 77381, USA
† The CPLEAR Collaboration: [1]Univ. of Athens, [2]Univ. of Basel, [3]Boston Univ., [4]CERN, [5]LIP and Univ. of Coimbra, [6]Delft Univ. of Technology, [7]Univ. of Fribourg, [8]Univ. of Ioannina, [9]Univ. of Liverpool, [10]J. Stefan Inst. and Phys. Dep., Univ. of Ljubljana, [11]CPPM, IN2P3-CNRS et Université d'Aix-Marseille II, [12]CSNSM, IN2P3-CNRS, Orsay, [13]Paul-Scherrer-InstitutPSI), [14]CEA, DSM/DAPNIA, CE-Saclay, [15]KTH Stockholm, [16]Univ. of Thessaloniki, [17]ETH-IPP Zürich

1 Introduction and Summary

The neutral kaon system provides one of the most sensitive laboratories for testing quantum mechanics at the microscopic level and for testing discrete symmetries [1]. It is the only place where an experimental violation of CP has yet been seen [2], and it provides the strongest constraint on CPT violation, via an upper bound on the difference between the K^0 and the $\overline{K}^0$ masses in the context of quantum mechanics [3]. CPT symmetry is a property of quantum field theory which follows from locality, causality and Lorentz invariance [4]. It is therefore particulary important to look for CPT violation, which, if observed, would require us to revise one or more of these fundamental principles. In particular, the possibility of CPT violation has been raised in the context of quantum gravity [5], as a result of a possible modification of conventional quantum field theory.

A framework for analyzing this possibility is provided by the formulation [6] of open quantum-mechanical systems which are coupled to an unobserved environment. This would induce a loss of quantum coherence in the observed system, which should be described by a density matrix ρ that obeys a modified quantum Liouville equation

$$\dot{\rho} = i[\rho, H] + \not{\delta} H\rho \tag{1}$$

where the extra term $\propto \not{\delta} H$ may be conjectured to arise from quantum-gravitational effects and have a magnitude which is at most $\mathcal{O}(m_K^2/M_{Pl})$, where $M_{Pl} = 1.2 \times 10^{19}$ GeV is the gravitational mass scale obtained from Newton's constant: $M_{Pl} = G_N^{-\frac{1}{2}}$. An equation of the form (1) is supported by one interpretation of string theory [7], but could have more general applicability.

In the case of the neutral kaon system, the open-system equation (1) introduces [6] three CPT-violating parameters α, β, γ if energy and strangeness conservation are assumed, in addition to the CPT-violating parameters $\delta m = m_{K^0} - m_{\overline{K}^0}$ and $\delta\Gamma = \Gamma_{K^0} - \Gamma_{\overline{K}^0}$ that can be discussed in the conventional quantum-mechanical framework. Here we use recent CPLEAR data on tagged kaon decays [8, 9] into 2π final states, together with information on $|\eta_{+-}|$ and the semileptonic decay asymmetry, to obtain bounds on these CPT-violating parameters. A more detailed account appears elsewhere [10, 11].

2 Formalism and relevant observables

In this section we first review aspects of the modifications (1) of quantum mechanics believed to be induced by quantum gravity [6], as argued specifically in the context of a non-critical string analysis [7]. This provides a specific form for the modification (1) of the quantum Liouville equation for the temporal evolution of the density matrix of observable matter [7]

$$\frac{\partial}{\partial t}\rho = i[\rho, H] + \delta\not{H}\rho \qquad ; \qquad \delta\not{H} \equiv i\dot{g}^i G_{ij}[g^j, \rho] \tag{2}$$

where the the g^i are generic field-theory couplings on the string world sheet, and G_{ij} is a metric on the space of these couplings. The extra term $\delta\!\!\!/\!\!\!/$ in (2) is such that the time evolution has the following basic properties:

(i) The total probability is *conserved* in time

$$\frac{\partial}{\partial t} Tr\,\rho = 0 \tag{3}$$

(ii) The energy E is *conserved on the average*

$$\frac{\partial}{\partial t} Tr\,(E\rho) = 0 \tag{4}$$

as a result of the *renormalizability* of the world-sheet σ-model describing string propagation in a string space-time foam background.

(iii) The von Neumann entropy $S \equiv -k_B Tr\,\rho \ln \rho$ increases *monotonically with time*

$$\frac{\partial}{\partial t} S \geq 0 \tag{5}$$

which vanishes only if one restricts one's attention to critical (conformal) strings, in which case there is no arrow of time [7]. However, we argue that quantum fluctuations in the background space time should be treated by including non-critical (Liouville) strings [12, 13], in which case (5) becomes a strict inequality. This latter property also implies that the statistical entropy $S_{st} \equiv Tr\,\rho^2$ is also monotonically increasing with time, pure states evolve into mixed ones and there is an arrow of time in this picture [7].

(iv) Correspondingly, the superscattering matrix $\$$, which is defined by its action on asymptotic density matrices

$$\rho_{out} = \$\,\rho_{in} \tag{6}$$

cannot be factorised into the usual product of the Heisenberg scattering matrix and its hermitian conjugate

$$\$ \neq SS^\dagger \quad ; \quad S = e^{-iHt} \tag{7}$$

with H the Hamiltonian operator of the system. In particular this property implies that $\$$ has no inverse, which is also expected from the property (iii).

(v) The absence of an inverse for $\$$ implies that *strong* CPT invariance of the low-energy subsystem is lost, according to the general analysis of [5, 7].

It should be stressed that, although for the purposes of the present work we keep the microscopic origin of the quantum-mechanics-violating terms unspecified, it is only in the non-critical string model of Ref. [7] - and the associated approach to

the nature of time - that a concrete microscopic model guaranteeing the properties (i)-(v) has so far emerged naturally. Moreover, it is worth pointing out that within the non-critical-string framework, we expect that the string σ-model coordinates g^i obey renormalization-group equations of the general form

$$\dot{g}^i = \beta^i M_{Pl} \qquad : \qquad |\beta^i| = \mathcal{O}\left(\frac{E^2}{M_{Pl}^2}\right) \tag{8}$$

where the dot denotes differentiation with respect to the target time, measured in string (M_{Pl}^{-1}) units, and E is a typical energy scale in the observable matter system. Since G_{ij} and g^i are themselves dimensionless numbers of order unity, we expect that

$$|\delta \not{H}| = \mathcal{O}\left(\frac{E^2}{M_{Pl}}\right) \tag{9}$$

in general. However, it should be emphasized that there are expected to be system-dependent numerical factors that depend on the underlying string model, and that $|\delta \not{H}|$ might be suppressed by further (E/M_{Pl})-dependent factors, or even vanish. Nevertheless, (9) gives us an order of magnitude to aim for in the neutral kaon system, namely $\mathcal{O}((\Lambda_{QCD} \text{ or } m_s)^2/M_{Pl}) \sim 10^{-19}$ GeV.

In the formalism of Ref. [6], the extra (non-Hamiltonian) term in the Liouville equation for ρ can be parametrized by a 4×4 matrix $\delta \not{H}_{\alpha\beta}$, where the indices $\alpha, \beta, \ldots$ enumerate the Hermitian σ-matrices $\sigma_{0,1,2,3}$, which we represent in the $K_{1,2}$ basis. We refer the reader to the literature [6, 14] for details of this description, noting here the following forms for the neutral kaon Hamiltonian

$$H = \begin{pmatrix} M - \frac{i}{2}\Gamma - ReM_{12} + \frac{i}{2}Re\Gamma_{12} & \frac{1}{2}\delta m - \frac{i}{4}\delta\Gamma - iImM_{12} - \frac{1}{2}Im\Gamma_{12} \\ \frac{1}{2}\delta m - \frac{i}{4}\delta\Gamma + iImM_{12} - \frac{1}{2}Im\Gamma_{12} & M - \frac{i}{2}\Gamma + ReM_{12} - \frac{i}{2}Re\Gamma_{12} \end{pmatrix} \tag{10}$$

in the $K_{1,2}$ basis, or

$$H_{\alpha\beta} = \begin{pmatrix} -\Gamma & -\frac{1}{2}\delta\Gamma & -Im\Gamma_{12} & -Re\Gamma_{12} \\ -\frac{1}{2}\delta\Gamma & -\Gamma & -2ReM_{12} & -2ImM_{12} \\ -Im\Gamma_{12} & 2ReM_{12} & -\Gamma & -\delta m \\ -Re\Gamma_{12} & -2ImM_{12} & \delta m & -\Gamma \end{pmatrix} \tag{11}$$

in the σ-matrix basis. As discussed in Ref. [6], we assume that the dominant violations of quantum mechanics conserve strangeness, so that $\delta \not{H}_{1\beta} = 0$, and that $\delta \not{H}_{0\beta} = 0$ so as to conserve probability. Since $\delta \not{H}_{\alpha\beta}$ is a symmetric matrix, it follows that also $\delta \not{H}_{\alpha 0} = \delta \not{H}_{\alpha 1} = 0$. Thus, we arrive at the general parametrization

$$\delta \not{H}_{\alpha\beta} = \begin{pmatrix} 0 & 0 & 0 & 0 \\ 0 & 0 & 0 & 0 \\ 0 & 0 & -2\alpha & -2\beta \\ 0 & 0 & -2\beta & -2\gamma \end{pmatrix} \tag{12}$$

where, as a result of the positivity of the hermitian density matrix ρ [6]

$$\alpha, \gamma > 0, \qquad \alpha\gamma > \beta^2 \, . \tag{13}$$

We recall [14] that the CPT transformation can be expressed as a linear combination of $\sigma_{2,3}$ in the $K_{1,2}$ basis : $CPT = \sigma_3 \cos\theta + \sigma_2 \sin\theta$ for some choice of phase θ. It is apparent that none of the non-zero terms $\propto \alpha, \beta, \gamma$ in $\delta\not{H}_{\alpha\beta}$ (12) commutes with the CPT transformation. In other words, each of the three parameters α, β, γ violates CPT, leading to a richer phenomenology than in conventional quantum mechanics. This is because the symmetric $\delta\not{H}$ matrix has three parameters in its bottom right-hand 2×2 submatrix, whereas the H matrix appearing in the time evolution within quantum mechanics [15] has only one complex CPT-violating parameter δ,

$$\delta = -\frac{1}{2}\frac{\frac{1}{2}\delta\Gamma + i\delta m}{\frac{1}{2}|\Delta\Gamma| + i\Delta m} \tag{14}$$

where δm and $\delta\Gamma$ violate CPT, but do not induce any mixing in the time evolution of pure state vectors [15, 14]. The parameters $\Delta m = M_L - M_S$ and $|\Delta\Gamma| = \Gamma_S - \Gamma_L$ are the usual differences between mass and decay widths, respectively, of K_L and K_S states. For more details we refer the reader to the literature [14]. The above results imply that the experimental constraints [3] on CPT violation have to be rethought. There are essential differences between quantum-mechanical CPT violation [15] and the non-quantum-mechanical CPT violation induced by the effective parameters α, β, γ [6, 14].

Useful observables are associated with the decays of neutral kaons to 2π or 3π final states, or semileptonic decays to $\pi l\nu$. In the density-matrix formalism introduced above, their values are given [6] by expressions of the form

$$< O_i >= Tr(O_i\rho) \tag{15}$$

where the observables O_i are represented by 2×2 hermitian matrices. For future use, we give their expressions in the $K_{1,2}$ basis

$$O_{2\pi} = \begin{pmatrix} 0 & 0 \\ 0 & 1 \end{pmatrix}, \qquad O_{3\pi} \propto \begin{pmatrix} 1 & 0 \\ 0 & 0 \end{pmatrix}, \tag{16}$$

$$O_{\pi^- l^+ \nu} = \begin{pmatrix} 1 & 1 \\ 1 & 1 \end{pmatrix}, \qquad O_{\pi^+ l^- \bar{\nu}} = \begin{pmatrix} 1 & -1 \\ -1 & 1 \end{pmatrix}. \tag{17}$$

which constitute a complete hermitian set. In this formalism, pure K^0 or $\overline{\mathrm{K}}^0$ states, such as the ones used as initial conditions in the CPLEAR experiment [8, 9] are described by the following density matrices

$$\rho_{\mathrm{K}^0} = \frac{1}{2}\begin{pmatrix} 1 & 1 \\ 1 & 1 \end{pmatrix}, \qquad \rho_{\overline{\mathrm{K}}^0} = \frac{1}{2}\begin{pmatrix} 1 & -1 \\ -1 & 1 \end{pmatrix}. \tag{18}$$

We note the similarity of the above density matrices (18) to the semileptonic decay observables in (17), which is due to the strange quark (s) content of the kaon $\mathrm{K}^0 \ni \bar{s} \to \bar{u}l^+\bar{\nu}$, $\overline{\mathrm{K}}^0 \ni s \to ul^-\nu$, and our assumption of the validity of the $\Delta S = \Delta Q$ rule.

Below, we shall apply the above formalism to compute [10] the time evolution of certain experimentally-observed quantities that are of relevance to the

CPLEAR experiment [8,9]. These are asymmetries associated with decays of an initial K^0 beam as compared to corresponding decays of an initial $\overline{K}^0$ beam

$$A(t) = \frac{R(\overline{K}^0{}_{t=0} \to \bar{f}) - R(K^0{}_{t=0} \to f)}{R(\overline{K}^0{}_{t=0} \to \bar{f}) + R(K^0{}_{t=0} \to f)} , \tag{19}$$

where $R(K^0 \to f) \equiv Tr\,[O_f \rho(t)]$, denotes the decay rate into the final state f, given that one starts from a pure K^0 at $t = 0$, whose density matrix is given in (18), and $R(\overline{K}^0 \to \bar{f}) \equiv Tr\,[O_{\bar{f}} \bar{\rho}(t)]$ denotes the decay rate into the conjugate state $\bar{f}$, given that one starts from a pure $\overline{K}^0$ at $t = 0$.

To determine the temporal evolution of the above observables, which is crucial for experimental fits, it is necessary to know the equations of motion for the components of ρ in the $K_{1,2}$ basis. These are [6,14][1]

$$\dot{\rho}_{11} = -\Gamma_L \rho_{11} + \gamma \rho_{22} - 2Re\,[(ImM_{12} - i\beta)\rho_{12}] , \tag{20}$$

$$\dot{\rho}_{12} = -(\Gamma + i\Delta m)\rho_{12} - 2i\alpha Im\,\rho_{12} + (ImM_{12} - i\beta)(\rho_{11} - \rho_{22}) , \tag{21}$$

$$\dot{\rho}_{22} = -\Gamma_S \rho_{22} + \gamma \rho_{11} + 2Re\,[(ImM_{12} - i\beta)\rho_{12}] , \tag{22}$$

where ρ represents either $\Delta\rho$ or $\Sigma\rho$, defined by the initial conditions

$$\Delta\rho(0) = \begin{pmatrix} 0 & -1 \\ -1 & 0 \end{pmatrix} , \qquad \Sigma\rho(0) = \begin{pmatrix} 1 & 0 \\ 0 & 1 \end{pmatrix} . \tag{23}$$

corresponding to the difference between (sum of) initially-pure K^0 and $\overline{K}^0$ states. In these equations, $\Gamma_L = (5.17 \times 10^{-8}\, s)^{-1}$ and $\Gamma_S = (0.8922 \times 10^{-10}\, s)^{-1}$ are the inverse K_L and K_S lifetimes, $\Gamma \equiv (\Gamma_S + \Gamma_L)/2$, $|\Delta\Gamma| \equiv \Gamma_S - \Gamma_L = (7.364 \pm 0.016) \times 10^{-15}$ GeV, and $\Delta m = 530.0 \times 10^7\, s^{-1} = 3.489 \times 10^{-15}$ GeV is the $K_L - K_S$ mass difference. Also, the CP impurity parameter ϵ is given by

$$\epsilon = \frac{ImM_{12}}{\frac{1}{2}|\Delta\Gamma| + i\Delta m} , \tag{24}$$

which leads to the relations

$$Im\,M_{12} = \tfrac{1}{2}\frac{|\Delta\Gamma||\epsilon|}{\cos\phi}, \quad \epsilon = |\epsilon| e^{-i\phi} \quad : \quad \tan\phi = \frac{\Delta m}{\frac{1}{2}|\Delta\Gamma|}, \tag{25}$$

with $|\epsilon| \approx 2.2 \times 10^{-3}$ and $\phi \approx 45°$ the "superweak" phase.

These equations are to be compared with the corresponding quantum-mechanical equations of Ref. [15,14]. The parameters δm and β play similar roles, although they appear with different relative signs in different places, because of the symmetry of $\delta\not{H}$ as opposed to the antisymmetry of the quantum-mechanical evolution matrix H. These differences are important for the asymptotic limits of the density matrix, and its impurity. A pure state will remain pure as long as

[1] Since we neglect ϵ' effects and assume the validity of the $\Delta S = \Delta Q$ rule, in what follows we also consistently neglect $Im\,\Gamma_{12}$ [10].

$Tr\,\rho^2 = (Tr\,\rho)^2$ [6]. In the case of 2×2 matrices $Tr\,\rho^2 = (Tr\,\rho)^2 - 2\det\rho$, and therefore the purity condition is equivalently expressed as $\det\rho = 0$. The existence of the $\delta\!\!\!/$ term (12) obviously violates this condition, thereby leading to mixed states.

To make a consistent phenomenological study of the various quantities discussed above, it is essential to solve the coupled system of equations (20) to (22) for intermediate times. This requires approximations in order to get analytic results [16]. Writing

$$\rho_{ij}(t) = \rho_{ij}^{(0)}(t) + \rho_{ij}^{(1)}(t) + \rho_{ij}^{(2)}(t) + \cdots \tag{26}$$

where $\rho_{ij}^{(n)}(t)$ is proportional to $\widehat{\alpha}^{p_\alpha}\widehat{\beta}^{p_\beta}\widehat{\gamma}^{p_\gamma}|\epsilon|^{p_\epsilon}$, with $p_\alpha + p_\beta + p_\gamma + p_\epsilon = n$, one can obtain a set of differential equations at each order in perturbation theory.

At order n the differential equations are of the form

$$\frac{d}{dt}\left[e^{At}\rho_{ij}^{(n)}(t)\right] = e^{At}\sum_{i'j'}{}'\rho_{i'j'}^{(n-1)}(t) \tag{27}$$

which can be integrated straightforwardly in terms of the known functions at the $(n-1)$-th order, and the initial condition $\rho_{ij}^{(n)}(0) = 0$, for $n \geq 1$, *i.e.*,

$$\rho_{ij}^{(n)}(t) = e^{-At}\int_0^t dt'\, e^{At'}\sum_{i'j'}{}'\rho_{i'j'}^{(n-1)}(t')\ . \tag{28}$$

Following this straightforward (but tedious) procedure we can obtain the expressions for $\Delta\rho$ at any desired order.

3 Analytical results

We now proceed to give explicit expressions for the temporal evolution of the asymmetries $A_{2\pi}$, $A_{3\pi}$, A_T, A_{CPT}, and $A_{\Delta m}$ that are the possible objects of experimental study, in particular by the CPLEAR collaboration [8, 9]. A more detailed account of these results is given in ref. [10)2].

3.1 $A_{2\pi}$

The formula for this asymmetry, as obtained by applying the formalism of section 2, assumes the form

$$A_{2\pi} = \frac{Tr\,[O_{2\pi}\bar{\rho}(t)] - Tr\,[O_{2\pi}\rho(t)]}{Tr\,[O_{2\pi}\bar{\rho}(t)] + Tr\,[O_{2\pi}\rho(t)]} \equiv \frac{Tr\,[O_{2\pi}\Delta\rho(t)]}{Tr\,[O_{2\pi}\sum\rho(t)]}\ , \tag{29}$$

where the observable $O_{2\pi}$ is given in (17), and the $\Delta\rho$ and $\sum\rho$ density matrix elements are given as above (23). The result for the asymmetry, to second order in

[2] See also ref. [17].

the small parameters, can be written most concisely as

$$A_{2\pi}(t) = \Big\{ 2|\epsilon|\cos\phi + 4\hat{\beta}\sin\phi\cos\phi - 8\hat{\alpha}\sin\phi\cos\phi(|\epsilon|\sin\phi - 2\hat{\beta}\cos^2\phi) - 2\sqrt{|\epsilon|^2 + 4\hat{\beta}^2\cos^2\phi}\; e^{\frac{1}{2}(\Gamma_S-\Gamma_L)t}\left[\cos(\Delta m t - \phi - \delta\phi) + \frac{2\hat{\alpha}}{\tan\phi}X_\alpha\right]\Big\} / \Big\{1 + e^{(\Gamma_S-\Gamma_L)t}\left[\hat{\gamma} + |\epsilon|^2 - 4\hat{\beta}^2\cos^2\phi - 4\hat{\beta}|\epsilon|\sin\phi\right]\Big\} \quad (30)$$

where $\hat{\alpha}, \hat{\beta}, \hat{\gamma}$ are scaled variables $a/\Delta\Gamma$,$\beta/\Delta\Gamma$, $\gamma/\Delta\Gamma$, and $X_\alpha \equiv \cos\delta\phi\sin(\Delta m t - \phi) - \frac{1}{2}|\Delta\Gamma|t\tan\phi\cos(\Delta m t - \phi - \delta\phi) + \sin\phi\cos(\Delta m t - 2\phi - \delta\phi)$.

The above expression should be compared with the usual case (*i.e.*, $\hat{\alpha} = \hat{\beta} = \hat{\gamma} = 0$)

$$A_{2\pi}(t) = \frac{2|\epsilon|\cos\phi - 2|\epsilon|\, e^{\frac{1}{2}(\Gamma_S-\Gamma_L)t}\cos(\Delta m t - \phi)}{1 + e^{(\Gamma_S-\Gamma_L)t}\,|\epsilon|^2} \quad (31)$$

One can readily see whether CP violation can in fact vanish, its effects mimicked by non-quantum-mechanical CPT violation. Setting $|\epsilon| = 0$ one needs to reproduce the interference pattern and also the denominator. To reproduce the overall coefficient of the interference pattern requires $2\hat{\beta}\cos\phi = \pm|\epsilon|$. The denominator (neglecting $\hat{\gamma}$) becomes $-4\hat{\beta}^2\cos^2\phi \to -|\epsilon|^2$ and we have the wrong sign. Another problem is that $\delta\phi \to -sgn(\hat{\beta})\frac{\pi}{2}$ and the interference pattern is shifted significantly. This means that the effects seen in the neutral kaon system, and conventionally interpreted as CP violation, indeed cannot be due to the CPT violation.

3.2 $A_{3\pi}$

Analogously, the formula for the 3π asymmetry, to first order in the small parameters, is given by

$$A_{3\pi}(t) = \frac{\left[2|\epsilon|\cos\phi - 4\hat{\beta}\sin\phi\cos\phi\right] - 2e^{-\frac{1}{2}(\Gamma_S-\Gamma_L)t}\left[Re\eta_{3\pi}\cos\Delta m t - Im\eta_{3\pi}\sin\Delta m t\right]}{1 + \hat{\gamma} - \hat{\gamma}e^{-(\Gamma_S-\Gamma_L)t}}, \quad (32)$$

with

$$Re\eta_{3\pi} = |\epsilon|\cos\phi - 2\hat{\beta}\sin\phi\cos\phi, \quad Im\eta_{3\pi} = |\epsilon|\sin\phi + 2\hat{\beta}\cos^2\phi\,. \quad (33)$$

In the CPLEAR experiment, the time-dependent decay asymmetry into $\pi^0\pi^+\pi^-$ is measured [8, 9], and the data is fit to obtain the best values for $Re\eta_{3\pi}$ and $Im\eta_{3\pi}$.

3.3 A_T

In the CPT-violating case, to first order in the small parameters, one finds the following time-dependent expression for this asymmetry

$$A_T = \frac{4|\epsilon|}{\cos\delta\phi}$$

$$\left\{ \frac{e^{-\Gamma_L t}\cos(\phi-\delta\phi)+e^{-\Gamma_S t}\cos(\phi+\delta\phi)-2e^{-\Gamma t}\cos(\Delta m t-\delta\phi)\cos\phi}{e^{-\Gamma_L t}(1+2\widehat{\gamma})+e^{-\Gamma_S t}(1-2\widehat{\gamma})-2e^{-\Gamma t}[\cos\Delta m t+\frac{2\widehat{\alpha}}{\tan\phi}(\sin\Delta m t-\Delta m t\cos\Delta m t)]} \right\} \tag{34}$$

where we have defined

$$\tan\delta\phi = -\frac{2\widehat{\beta}\cos\phi}{|\epsilon|} + \ldots , \tag{35}$$

with the ... denoting higher order corrections [10]. The expression (34) aymptotes to

$$A_T \to \frac{4|\epsilon|\cos(\phi-\delta\phi)}{\cos\delta\phi(1+2\widehat{\gamma})} = \frac{4|\epsilon|\cos\phi - 8\widehat{\beta}\sin\phi\cos\phi}{1+2\widehat{\gamma}} . \tag{36}$$

3.4 A_{CPT}

Following the discussion in section 2, the formula for this observable, as defined by the CPLEAR Collaboration [9], is given by Eq. (19) with $f = \pi^- l^+ \nu$ and $\bar{f} = \pi^+ l^- \bar{\nu}$. To first order, in both the CPT-conserving and CPT-violating cases, we find

$$A_{CPT} = 0 . \tag{37}$$

We point out that this result is a quite distinctive signature of the modifications of the quantum mechanics proposed in Ref. [6, 14], since in the case of quantum-mechanical violation of CPT symmetry [15] there is a non-trivial change in A_{CPT}, proportional to the CPT-violating parameters δm and $\delta\Gamma$. Indeed, we obtain [10] the following first-order asymptotic result

$$A_{CPT}^{QM} \to 4\sin\phi\cos\phi\,\widehat{\delta m} + 2\cos^2\phi\,\widehat{\delta\Gamma} , \tag{38}$$

written in terms of the scaled variables. Part of the reason for this difference is the different role played by δm as compared to the β parameter in the formalism of Ref. [6], as discussed in detail in Ref. [14]. In particular, there are important sign differences between the ways that δm and β appear in the two formalisms, that cause the suppression to second order of any quantum-mechanical-violating effects in A_{CPT}, as opposed to the conventional quantum mechanics case.

3.5 $A_{\Delta m}$

Following Ref. [8], one can define $A_{\Delta m}$ as

$$A_{\Delta m} = \frac{R(\mathrm{K}^0\to\pi^+) + R(\overline{\mathrm{K}}^0\to\pi^-) - R(\overline{\mathrm{K}}^0\to\pi^+) - R(\mathrm{K}^0\to\pi^-)}{R(\mathrm{K}^0\to\pi^+) + R(\overline{\mathrm{K}}^0\to\pi^-) + R(\overline{\mathrm{K}}^0\to\pi^+) + R(\mathrm{K}^0\to\pi^-)} \tag{39}$$

in an obvious short-hand notation for the final states of the semileptonic decays, where only the pion content is shown explicitly. In the formalism of section 2, this expression becomes in the quantum-mechanics-violating case to first order

$$A_{\Delta m} = -\frac{2e^{-\Gamma t}\left[\cos\Delta m t + \frac{2\widehat{\alpha}}{\tan\phi}(\sin\Delta m t - \Delta m t\cos\Delta m t)\right]}{e^{-\Gamma_L t}(1+2\widehat{\gamma}) + e^{-\Gamma_S t}(1-2\widehat{\gamma})} \tag{40}$$

Since $\widehat{\gamma}$ is negligible, this observable provides an *exclusive* test of $\widehat{\alpha}$.

4 Regeneration

Regeneration involves the coherent scattering of a K^0 or $\overline{K}^0$ off a nuclear target, which we assume can be described using the normal framework of quantum field theory and quantum mechanics. Thus we describe it by an effective Hamiltonian which takes the form

$$\Delta H = \begin{pmatrix} T+\overline{T} & T-\overline{T} \\ T-\overline{T} & T+\overline{T} \end{pmatrix} \tag{41}$$

in the $K_{1,2}$ basis, where

$$T = \frac{2\pi N}{m_K}\mathcal{M}\,, \qquad \overline{T} = \frac{2\pi N}{m_K}\overline{\mathcal{M}} \tag{42}$$

with $\mathcal{M} = \langle K^0|A|K^0\rangle$ the forward K^0-nucleus scattering amplitude (and analogously for $\overline{\mathcal{M}}$), and N is the nuclear regenerator density. The regenerator effects ΔH can in principle be included as a contribution to H in the density matrix equation:

$$\partial_t \rho = -i[H,\rho] + i\delta\not{H}\rho \tag{43}$$

where $\delta\not{H}$ represents the possible CPT- and QM-violating term. However we note that the regenerator provides an 'environment' that induces an effective CPT violation within quantum mechanics, due to the inequivalent scattering of K^0 and $\overline{K}^0$ by the regenerator material.

It may be adequate as a first approximation to treat the regenerator as very thin, in which case we may use the impulse approximation, and the regenerator changes ρ by an amount

$$\delta\rho = -i[\Delta\mathcal{H},\rho] \tag{44}$$

where

$$\Delta\mathcal{H} = \int dt \Delta H \tag{45}$$

Writing

$$\rho = \begin{pmatrix} \rho_{11} & \rho_{12}^* \\ \rho_{12} & \rho_{22} \end{pmatrix}\,, \tag{46}$$

in this approximation we obtain

$$\delta\rho = -i\Delta T \begin{pmatrix} 2iIm\rho_{12} & -\rho_{11}+\rho_{22} \\ \rho_{11}-\rho_{22} & -2iIm\rho_{12} \end{pmatrix}\,, \tag{47}$$

where

$$\Delta T \equiv \int dt (T-\overline{T})\,. \tag{48}$$

This change in ρ enables the possible CPT- and QM-violating terms in (43) to be probed in a new way, as we now discuss in a special case.

Consider the idealization that the neutral K beam is already in a K_L state

$$\rho = \rho_L \approx \begin{pmatrix} 1 & \epsilon^*+B^* \\ \epsilon+B & |\epsilon|^2+C \end{pmatrix} \tag{49}$$

where

$$B = -i2\widehat{\beta}\cos\phi\, e^{-i\phi} \quad ; \quad C = \widehat{\gamma} - 4\widehat{\beta}^2\cos^2\phi - 4\widehat{\beta}|\epsilon|\sin\phi \tag{50}$$

Substituting Eqs. (49,50) into Eq. (47), we find that in the joint large-t and impulse approximations

$$\rho + \delta\rho = \begin{pmatrix} 1 + 2\Delta T Im(\epsilon + B) & \epsilon^* + B^* + i(1 - |\epsilon|^2 - C)\Delta T \\ \epsilon + B - i(1 - |\epsilon|^2 - C)\Delta T & |\epsilon|^2 + C - 2\Delta T Im(\epsilon + B) \end{pmatrix} . \tag{51}$$

We see that the usual semileptonic decay asymmetry observable

$$O_{\pi^- l^+ \nu} - O_{\pi^+ l^- \bar{\nu}} = \begin{pmatrix} 0 & 2 \\ 2 & 0 \end{pmatrix} \quad , \tag{52}$$

which measures $Re(\epsilon + B)$ in the case without the regenerator, receives no contribution from the regenerator (*i.e.*, ΔT cancels out in the sum of the off-diagonal elements). On the other hand, there is a new contribution to the value of $R_{2\pi} = R(K_L \to 2\pi) \propto Tr[O_{2\pi}\rho] = \rho_{22}$, namely

$$R_{2\pi} = |\epsilon|^2 + \widehat{\gamma} - 4\widehat{\beta}^2\cos^2\phi - 4\widehat{\beta}|\epsilon|\sin\phi - 2\Delta T Im(\epsilon + B) . \tag{53}$$

The quantity $Im(\epsilon + B)$ was not accessible directly to the observable $R_{2\pi}$ in the absence of a regenerator. Theoretically, the phases of ϵ and B (50) are fixed, *i.e.*,

$$Im(\epsilon + B) = -|\epsilon|\frac{\sin(\phi - \delta\phi)}{\cos\delta\phi} = -|\epsilon|\sin\phi - 2\widehat{\beta}\sin\phi\cos\phi . \tag{54}$$

Nevertheless, this phase prediction should be checked, so the regenerator makes a useful addition to the physics programme.

The above analysis is oversimplified, since the impulse approximation may not be sufficiently precise, and the neutral K beam is not exactly in a K_L state. However, it may serve to illustrate the physics interest of measurements using a regenerator [10]. We note that measurements with different thicknesses of regenerator should have a distinctive dependence $\Delta R_{2\pi} \propto \Delta T$, which is a nice signature. Moreover, the cylindrical geometry of the CPLEAR detector provides such different measurements "for free" at different planar angles.

5 CPLEAR Bounds on CPT-Violating Parameters

5.1 Description of the CPLEAR Experiment

The CPLEAR experiment [8, 19] is designed to determine CP and T violation in the neutral kaon system by measuring time-dependent decay rate asymmetries of CP and T conjugate processes. Initially-pure K^0 and $\overline{K}^0$ states are produced concurrently in the annihilation channels $(p\overline{p})_{rest} \to K^0 K^- \pi^+$ and $(p\overline{p})_{rest} \to \overline{K}^0 K^+ \pi^-$, each one with a branching ratio of $\approx 0.2\%$. The strangeness of the neutral kaon is tagged by the charge sign of the accompanying kaon. In *Fig. 1* the decay rates for K^0 and $\overline{K}^0$

measured by our experiment are shown separately, demonstrating the CP violation effect.

A detailed description of the experiment can be found elsewhere [20], and only a few important items are mentioned here. The high rate of 200 MeV/c antiprotons (10^6 $\bar{p}$/s) is delivered by the LEAR machine at CERN. The antiprotons are stopped inside a gaseous hydrogen target of 16 bar pressure. A cylindrical detector is placed inside a solenoid of 1 m radius, 3.6 m length, providing a magnetic field of 0.44 T. The charged tracking system consists of two proportional chambers, six drift chambers and two layers of streamer tubes. Fast kaon identification is provided by a threshold Čerenkov counter sandwiched between two scintillators. An electromagnetic calorimeter made of 18 layers of Pb converters and streamer tubes is used for photon detection and electron identification. An efficient and fast on-line data reduction is achieved with a multi-level trigger system based on custom-made hardwired processors.

Kinematical constraints (energy-momentum conservation, K^0 mass) and geometrical constraints (K^0 flight direction and vertex separation) are used in the analysis to suppress the background from unwanted K^0 decay channels and the background from $p\bar{p}$ annihilation events. In addition they improve the lifetime resolution.

Knowing the initial strangeness of the neutral kaon, we are able to calculate time-dependent CP-violating decay-rate asymmetries:

$$A_{+-}(t) = \frac{N_{\overline{K}^0 \to \pi^+\pi^-}(t) - \alpha N_{K^0 \to \pi^+\pi^-}(t)}{N_{\overline{K}^0 \to \pi^+\pi^-}(t) + \alpha N_{K^0 \to \pi^+\pi^-}(t)} \qquad (55)$$

All the acceptances common for K^0 and $\overline{K}^0$ cancel, thus reducing systematic uncertainties. The normalization factor α is proportional to the tagging efficiency of $\overline{K}^0$ relative to $K^0$and is determined experimentally from the data together with the CP-violation parameters.

5.2 Description of the fit

The results presented here are preliminary, and based on the CPLEAR data collected up to middle of 1994. The analysis based on standard quantum mechanics is presented in [19].

The measured rates $N_{\overline{K}^0 \to \pi^+\pi^-}(t)$ and $N_{K^0 \to \pi^+\pi^-}(t)$ have been corrected for regeneration. The residual background contribution, mainly from semileptonic decays, is extracted from a Monte Carlo simulation and taken into account in the fit. A systematic study of the effect of lifetime resolution and the regeneration correction is in preparation.

We use the formalism for $K^0 \to \pi^+\pi^-, \overline{K}^0 \to \pi^+\pi^-$ decays presented in section 3.1. In addition we require the following constraints to be fulfilled:

- $|\eta_{+-}|^2 = \hat{\gamma}^2 + |\varepsilon|^2 \dfrac{\cos(\varphi - 2\delta\varphi)}{\cos(\varphi)\cos^2(\delta\varphi)}$,where $|\eta_{+-}|$ is the CP-violation parameter

measured in K_L decays to $\pi^+\pi^-$, taken from the Particle Data Group [3], and $\tan(\delta\varphi) = -\dfrac{2\hat{\beta}\cos(\varphi)}{\varepsilon}$,

- $\delta_L = 2\varepsilon \cdot \cos(\varphi) - 4\hat{\beta}\cos(\varphi)\sin(\varphi)$, where δ_L is the semileptonic asymmetry measured in K_L decays, taken from the Particle Data Group [3],
- $\Delta m = (530.02 \pm 1.63) \cdot 10^7 \hbar s^{-1}$, is the average of the experiments listed in ref. [21].

Fitting the CP asymmetry shown in fig. 2 together with the above constraints, we obtain the following result for the CP- and CPT-violation parameters:

$$\begin{aligned} \varepsilon &= (2.257 \pm 0.011) \times 10^{-3} \\ \hat{\alpha} &= (-4.1 \pm 8.5) \times 10^{-3} \\ \hat{\beta} &= (-1.4 \pm 4.6) \times 10^{-5} \\ \hat{\gamma} &= (-0.3 \pm 3.3) \times 10^{-7} \end{aligned} \tag{56}$$

The χ^2 of the fit is 0.8/dof.

Limits for $\hat{\alpha}$, $\hat{\beta}$ and $\hat{\gamma}$ are calculated by taking into account only the physical region, i.e., by imposing the positivity constraints $\hat{\alpha}$, $\hat{\gamma} > 0$ and $\hat{\alpha} \cdot \hat{\gamma} > \hat{\beta}^2$. Integrating over the other two parameters we derive the following 90% confidence level upper limits:

$$\begin{aligned} \hat{\alpha} &< 4.2 \times 10^{-3} \\ |\hat{\beta}| &< 2.1 \times 10^{-5} \\ \hat{\gamma} &< 2.9 \times 10^{-7} \end{aligned} \tag{57}$$

5.3 Remark on the $K_S - K_L$ mass difference

In all experiments which have measured Δm so far, standard quantum mechanics has been assumed. The CPLEAR collaboration has started to make a common fit of the semileptonic asymmetry $A_{\Delta m}$ and the two-pion asymmetry A_{+-}, keeping Δm as a free parameter. These results will be published soon.

6 Theoretical Comment on two-particle decay correlations

Alternative interesting tests of quantum mechanics and CPT symmetry can be devised by exploiting initial-state correlations due to the production of a pair of neutral kaons in a pure quantum-mechanical state, e.g., via $e^+e^- \to \phi \to K^0\overline{K}^0$. In this case, the initial state may be represented by [18]

$$|k\ ;\ -k\rangle = \tfrac{1}{\sqrt{2}}\left[\left|K^0(k)\ ;\ \overline{K}^0(-k)\right\rangle - \left|\overline{K}^0(k)\ ;\ K^0(-k)\right\rangle\right] \tag{58}$$

At subsequent times $t = t_1$ for particle 1 and $t = t_2$ for particle 2, the joint probability amplitude is given in conventional quantum mechanics by

$$|k,\ t_1\ ;\ -k,\ t_2\rangle \equiv e^{-iH(k)t_1}e^{-iH(-k)t_2}\,|k\ ;\ -k\rangle \tag{59}$$

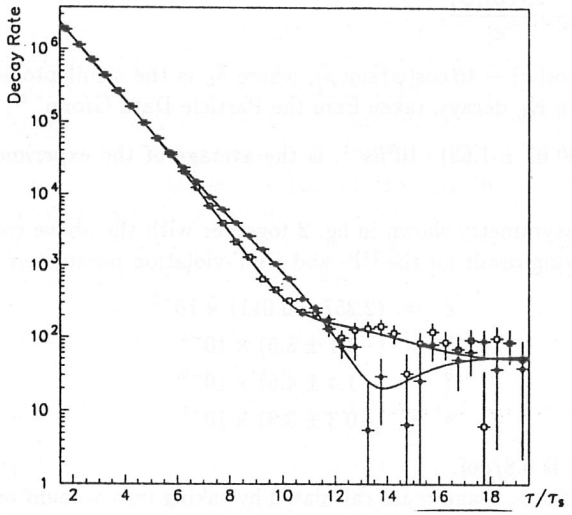

Figure 1: Acceptance-corrected decay rate of $\overline{K}^0$ (117) and K^0 (□). Lines are the expected rates when the Particle Data Group [3] values are used.

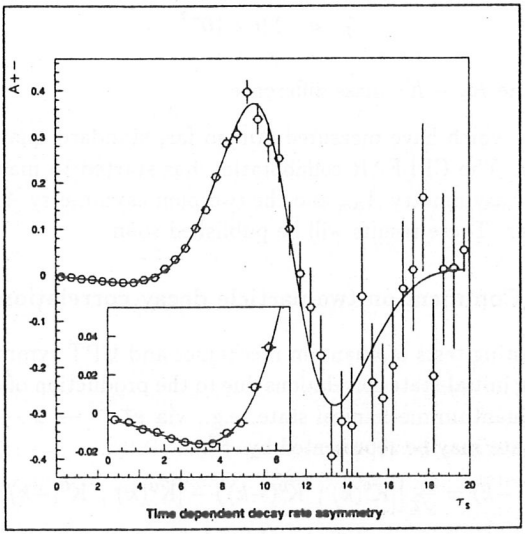

Figure 2: Decay-rate asymmetry as function of the decay eigentime. The line shows the result of the best fit.

Thus the temporal evolution of the two-particle state is completely determined by the one-particle variables (OPV) contained in H.

Tests of quantum mechanics and CPT symmetry in ϕ decays [22] have recently been discussed [17] in a conjectured extension of the formalism of [6,14], in which the density matrix of the two-particle system was hypothesized to be described completely in terms of such one-particle variables (OPV): H and (α, β, γ). It was pointed out that this OPV hypothesis had several striking consequences, including apparent violations of energy conservation and angular momentum.

As we have discussed above, the only known theoretical framework in which the EHNS equation has been derived is that of a non-critical string approach to string theory, in which (i) energy is conserved in the mean as a consequence of the renormalizability of the world-sheet σ-model, but (ii) angular momentum is not necessarily conserved, as this is not guaranteed by renormalizability and is not conserved in some toy backgrounds [23], though we cannot exclude the possibility that it may be conserved in some particular backgrounds. Therefore, we are not concerned that [17] find angular momentum non-conservation in their hypothesized OPV approach, but the absence of energy conservation in their approach leads us to the conclusion that irreducible two-particle parameters must be introduced into the evolution of the two-particle density matrix. The appearance of such non-local parameters does not concern us, as the string is intrinsically non-local in target space, and this fact plays a key role in our model calculations of contributions to $\delta\not{H}$. The justification and parametrization of such irreducible two-particle effects goes beyond the scope of these talks, and we plan to study this subject in more detail in due course.

7 Conclusions

We have discussed in these talks approximate expressions for a complete set of neutral kaon decay observables $(\pi\pi, 3\pi, \pi^{\pm} l^{\mp} \nu)$, which can be used to constrain the parameters α, β, γ characterising CPT violation in a formalism motivated by ideas about quantum gravity and string theory, that incorporates a possible microscopic loss of quantum coherence by treating the neutral kaon as an open quantum-mechanical system [6,7,14,10]. Detailed fits to recent CPLEAR experimental data on 2π decays have been reported based on our formulae [11]. These may be used to obtain indicative upper bounds

$$|\alpha| \lesssim 3.1 \times 10^{-17}\,\mathrm{GeV},\ |\beta| \lesssim 1.5 \times 10^{-19}\,\mathrm{GeV},\ |\gamma| \lesssim 2.1 \times 10^{-21}\,\mathrm{GeV} \qquad (60)$$

which are comparable with the order of magnitude $\sim 10^{-19}$ GeV which theory indicates [7] might be attained by such CPT- and quantum-mechanics-violating parameters.

We have not presented explicit expressions for the case where the deviation $\epsilon'/\epsilon \lesssim 10^{-3}$ from pure superweak CP violation is non-negligible, but our methods can easily be extended to this case. They can also be used to obtain more complete

expressions for experiments with a regenerator, if desired. Details of the extension of the formalism of ref. [6] to correlated $K^0\overline{K}^0$ systems produced in ϕ decay, as at DAϕNE [22], involves the introduction of two-particle variables, which lies beyond the scope of this paper.

We close by reiterating that the neutral kaon system is the best microscopic laboratory for testing quantum mechanics and CPT symmetry. We believe that violations of these two fundamental principles, if present at all, are likely to be linked, and have proposed a formalism that can be used to explore systematically this hypothesis, which is motivated by ideas about quantum gravity and string theory. Our understanding of these difficult issues is so incomplete that we cannot calculate the sensitivity which would be required to reveal modifications of quantum mechanics or a violation of CPT. Hence we cannot promise success in any experimental search for such phenomena. However, we believe that both the theoretical and experimental communities should be open to their possible appearance.

Acknowledgments

We would like to thank P. Eberhard for useful discussions. The work of N.E.M. has been supported by a European Union Research Fellowship, Proposal Nr. ERB4001GT922259, and that of D.V.N. has been supported in part by DOE grant DE-FG05-91-ER-40633. N.E.M. thanks D. Cocolicchio, G. Pancheri, N. Paver and other members of the DAΦNE working groups for their interest in this work.

References

1. J.S. Bell and J. Steinberger, proc. 1965 Oxford Intern. Conf. on Elementary Particles (Oxford 1966) , p. 165.

2. J.H. Christenson, J.W. Cronin, V.L. Fitch and R. Turlay, Phys. Rev. Lett. 13 (1964) , 138.

3. *Review of Particle Properties*, Particle Data Group, Phys. Rev. D50 (1994), 1173.

4. G. Lüders, Ann. Phys. (NY) 2 (1957), 1.

5. R. Wald, Phys. Rev. D21 (1980), 2742 ;
   D.N. Page, Gen. Rel. Grav. 14 (1982), 299 ;

6. J. Ellis, J.S. Hagelin, D.V. Nanopoulos and M. Srednicki, Nucl. Phys. B241 (1984), 381.

7. J. Ellis, N.E. Mavromatos and D.V. Nanopoulos, Phys. Lett. B293 (1992), 37;
   J. Ellis, N.E. Mavromatos and D.V. Nanopoulos, preprint CERN-TH.7195/94, ENS-LAPP-A-463/94, ACT-5/94, CTP-TAMU-13/94, lectures presented (by

J.E. and N.E.M.) at the *Erice Summer School of Sub-Nuclear Physics, 31st Course: From Supersymmetry to the Origin of Space-Time*, Ettore Majorana Centre, Erice, July 4-12, 1993, hepth 9403133, to be published in the proceedings;

For a pedagogical review of this approach see: D.V. Nanopoulos, Riv. Nuov. Cim. Vol. 17, No. 10 (1994), 1.

8. The CPLEAR Collaboration, in Proceedings of the XXVI International Conference on High Energy Physics, ed. by J. R. Sanford (AIP Conference Proceedings No. 272), p. 510.

9. The CPLEAR collaboration, *Measurement of the CP violation parameter* η_{+-} *using tagged* K^0 *and* $\overline{K}^0$, submitted to Phys. Lett. B.

10. J. Ellis, J.L. Lopez, N.E. Mavromatos and D.V. Nanopoulos, CERN, ENS-LAPP and Texas A & M Univ. preprint, ACT-06/95, CERN-TH.95-99, ENS-LAPP-A-521/95, CTP-TAMU-16/95 (1995), hep-ph 9505340.

11. The CPLEAR Collaboration and J. Ellis, J. L. Lopez, N.E. Mavromatos, D.V. Nanopoulos, in preparation.

12. I. Antoniadis, C. Bachas, J. Ellis and D.V. Nanopoulos, Phys. Lett. **B211** (1988), 393; Nucl. Phys. **B328** (1989), 117; Phys. Lett. **B257** (1991), 278.

13. F. David, Mod. Phys. Lett. **A3** (1988), 1651;

J. Distler and H. Kawai, Nucl. Phys. **B321** (1989), 509;

N.E. Mavromatos and J.L. Miramontes, Mod. Phys. Lett. **A4** (1989), 1847.

14. J. Ellis, N. E. Mavromatos and D.V. Nanopoulos, Phys. Lett. B **293** (1992) 142 and CERN-TH.6755/92.

15. C.D. Buchanan, R. Cousins, C. O. Dib, R.D. Peccei and J. Quackenbush, Phys. Rev. D **45** (1992) 4088; C.O. Dib and R.D. Peccei, Phys. Rev. D **46** (1992) 2265.

16. J. L. Lopez in *Recent Advances in the Superworld*, Proceedings of the HARC Workshop, The Woodlands, April 14-16, 1993, edited by J. L. Lopez and D. V. Nanopoulos (World Scientific, Singapore 1994), p. 272.

17. P. Huet and M. Peskin, Nucl. Phys. B **434** (1995) 3.

18. H. Lipkin, Phys. Lett. B **219** (1988) 474.

19. P. Pavlopoulos, these proceedings.

20. The CPLEAR Collaboration, *The CPLEAR detector at CERN*, in preparation.

21. Geweniger et al., Phys.Lett. B52(1974) 108;
Gjesdal et al., Phys.Lett. B52(1974) 113;
L.K. Gibbons et al., Phys.Rev.Lett. 70(1993) 1199;
B. Schwingenheuer et al., EFI 94-60, submitted for publication.
The CPLEAR Collaboration, *New measurement of the* K_S-K_L *mass difference by using semileptonic decays of tagged neutral kaons*, in preparation.

22. *Daφne Physics Handbook*, edited by L. Maiani, L. Pancheri and N. Paver (INFN, Frascati, 1992).

23. J. Ellis, N. E. Mavromatos and D.V. Nanopoulos, Proc. *'First International Conference on Phenomenology of Unification from Present to Future'*, Rome, 'La Sapienza' University, March 22-26 1994, p. 187 (World Sci.); preprint CERN-TH.7269/94, CTP-TAMU 26/94, ENSLAPP-A-474/94, hep-th/9405196.

CP VIOLATION PROBLEM BEYOND APPROXIMATE LEE–OHME–YANG THEORY

Leonid K. Halfin

Steklov Mathematical Institute Russian Academy of Sciences
Fontanka 27, RU-19101, St. Petersburg (Russia)

(No written contribution arrived)

ON THE CONCEPT OF THE LIFE TIME OF UNSTABLE PARTICLES (THE Φ DELAYED DECAY)

Jerzy Bogdanowicz
Soltan Institute for Nuclear Studies, Hoza 69, 00-681 Warsaw (Poland)

(No written contribution arrived)

HYPERNUCLEI AND K–N INTERACTIONS

PLENARY SESSION

A. Zenoni	Status Report on FINUDA	293
A. Gal	Hypernuclei: A Theoretical Review	315
B.R. Holstein	Weak Hypernuclear Decay	333
T. Yamazaki	Present Status of Hypernuclear Studies	347
C. Guaraldo	How to Solve at DAΦNE The "Kaonic Hydrogen Puzzle"	349
A. Olin	KN Scattering at DAΦNE ?	379

FINUDA STATUS REPORT

Aldo Zenoni
Dipartimento di Chimica e Fisica per i Materiali
Via Valotti 9, 25133 Brescia (Italy)
on behalf of the FINUDA Collaboration*

ABSTRACT

The FINUDA experiment, a large acceptance, high resolution spectrometer dedicated to hypernuclear physics is in construction at LNF's DAΦNE. Motivations, physics goals and expected performances of the apparatus are illustrated.

1 – The FINUDA experiment

FINUDA [1] is the second experiment approved for installation on DAΦNE [2], the Frascati ϕ factory, now being built at the Laboratori Nazionali di Frascati of INFN.

*M. Agnello[a], P. Amaudruz[l], G. Beer[l], M. Bertani[b], S. Bianco[b], E. Botta[c], T. Bressani[c], L. Busso[d], D. Calvo[c], P. Camerini[e], C. Cattaneo[f], L. Celano[g], N. Colonna[g], M. Corradini[h], G. D'Erasmo[g], A. Donzella[h], F.L. Fabbri[b], A. Feliciello[c], A. Filippi[i], V. Filippini[f], E.M. Fiore[g], L. Fiore[g], P. Gianotti[b], M. Giardoni[b], D.R. Gill[l], N. Grion[e], C. Guaraldo[b], F. Iazzi[a], A. Lanaro[b], L. Lee[l], E. Lodi Rizzini[h], V. Lucherini[b], S. Marcello[c], G. Marciano[f], G.M. Marshall[l], B. Minetti[a], N. Mirfakhrai[n], P. Montagna[f], O. Morra[d], A.A. Nozdrin[l], A. Olin[l], A. Pantaleo[g], V. Paticchio[g], E. Rossetto[c], A. Rotondi[f], R. Rui[e], P. Salvini[f], S. Sarwar[b], A. Sharma[c], G. Smith[l], L. Venturelli[h], S. Yen[l] and A. Zenoni[m]. [a]Dipartimento di Fisica del Politecnico di Torino and INFN, Sez. di Torino, I-10125 Torino, Italy; [b]INFN, Laboratori Nazionali di Frascati, I-00044 Frascati, Italy; [c]Dipartimento di Fisica Sperimentale, Univ. di Torino and INFN, Sez. di Torino, I-10125 Torino, Italy; [d]Istituto di Fisica Generale, Univ. di Torino and INFN, Sez. di Torino, I-10125 Torino, Italy; [e]Dipartimento di Fisica, Univ. di Trieste and INFN, Sez. di Trieste, I-34127 Trieste, Italy; [f]Dipartimento di Fisica Nucleare e Teorica, Univ. di Pavia and INFN, Sez. di Pavia, I-27100 Pavia, Italy; [g]Dipartimento di Fisica, Univ. di Bari and INFN, Sez. di Bari, I-70126 Bari, Italy; [h]Dipartimento di Chimica e Fisica per i Materiali, Univ. di Brescia and INFN, Sez. di Torino, I-25133 Brescia, Italy; [i]Dipartimento di Fisica Nucleare e Teorica, Univ. di Pavia and INFN, Sez. di Torino, I-27100 Pavia, Italy; [l]TRIUMF, 4004 Wesbrok Mall, Vancouver, BC, V6T 2A3, Canada; [m]Dipartimento di Chimica e Fisica per i Materiali, Univ. di Brescia and INFN, Sez. di Pavia, I-25133 Brescia, Italy; [n] Shahid Beheshty Univ. Dept of Phys, 19834 Teheran, Iran; [o] INFN, Sez. di Torino - Laboratorio Tecnologico, I-10125 Torino, Italy

Table 1: ϕ meson decay modes.

Decay mode	B.R.(%)	$p_{Max}(MeV/c)$
K^+K^-	49	127
$K^0_S K^0_L$	34	110
$\rho\pi$	13	132
$\pi^+\pi^-\pi^0$	2	462
$\eta\gamma$	1.3	362
others	~ 1	

DAΦNE will run in 1997 at the center of mass energy of the ϕ meson, with an initial luminosity of $\mathcal{L} = 10^{32} cm^{-2} s^{-1}$ and a final design luminosity one order of magnitude larger.

At its top luminosity DAΦNE will produce $\sim$ 5000 ϕ mesons per second, providing a unique source of monochromatic, collinear, quantum defined and tagged pairs of neutral and charged kaons (see Tab. 1). The neutral kaon decay mode will supply an abundant rate of $K^0_S K^0_L$ systems to the KLOE [3] experiment, where this unique possibility will be exploited for a measurement of $\Re(\epsilon'/\epsilon)$ to $\sim 10^{-4}$ and of other CP violating parameters in the $\overline{K}K$ system. Besides, the most frequent ϕ decay mode in K^+K^-, will provide beams of low energy (16.0 MeV), monochromatic, background free K^+ and K^- to the FINUDA experiment.

FI.NU.DA. (standing for *FIsica NUcleare a DAΦNE*) constitutes a unique example of an experiment of nuclear physics, which is traditionally a fixed target physics, carried out at a collider. The leading physical idea [4] is to exploit the low energy K^- beam from ϕ decay, tagged by the opposite K^+, for studies of high resolution Λ-hypernucleus spectroscopy with K^- at rest. The main reaction studied is the following :

$$K^-_{stop} + {}^A Z \rightarrow {}^A_\Lambda Z + \pi^- \tag{1}$$

where the low energy K^-, stopping inside the target material, gives origin, with a certain probability, to the formation of a hypernucleus and the isotropic emission of a prompt π^-. The spectrum of the emitted π^- will provide the energies and the excitation strengths of the hypernuclear levels. The following, delayed decay of the hypernucleus, which is mainly in non-mesonic modes for all but the lightest nuclei,

$${}^A_\Lambda Z \rightarrow^{(A-2)} Z + n + n \tag{2}$$

$${}^A_\Lambda Z \rightarrow^{(A-2)} (Z-1) + n + p \tag{3}$$

can be studied as well.

This approach looks very sound when expected counting rates and energy resolutions, which are the basic performances of the experiment, are compared with

those obtained or foreseen at fixed target machines. On the other side, the inconvenience for a fixed target experiment working at a collider, is a reduced flexibility in maintenance, nuclear target handling, variation of the magnetic field, etc.

2 – Production of Λ-hypernuclei

The merits of using the low energy K^- from ϕ decays for hypernuclear spectroscopy studies, can be better illustrated by reminding, briefly, how hypernuclei can be produced.

The most natural way of producing hypernuclei and study the hypernuclear spectra, is to make a beam of particles carrying strangeness (s quark) collide upon a nucleus. The physical process that has been commonly considered, is the "strangeness exchange" reaction

$$K^- + {}^A Z \rightarrow {}^A_\Lambda Z + \pi^- \tag{4}$$

where, in the elementary process, the K^- transforms a struck neutron into a Λ and emits a π^-. The energy spectrum of the π^- can be directly related to the hypernuclear energy levels. The reaction kinematics has the specific features that, with the π^- detected at 0^0, there is, in the laboratory frame, a "magic" value of the K^- momentum (531 MeV/c) for which the Λ hyperon is produced at rest. Practically, in that case, one neutron is replaced with a Λ so gently that the wave function of the nuclear system remains essentially unchanged (hence the name of "substitutional reaction" for the process).

The largest amount of hypernuclear spectroscopy data has been produced so far at BNL and KEK and in the past, also at CERN, by means of this type of reaction. However, the process is not appropriate for exciting low lying Λ hypernuclear states in heavy nuclei. Indeed in that case, the neutron has, in general, a high angular momentum, thus entailing large Δl reactions when the Λ sits in low lying orbits.

Another technique exploits "associated production" processes, where a $\bar{s}s$ pair is created inside the nucleus; typical processes are $(\pi^+, K^+), (\gamma, K^+), (p, K^+)$. Here a s-quark is transferred to a nucleon yielding a hyperon, whereas the antiquark $\bar{s}$ becomes a constituent of the K^+. Recently, the reaction

$$\pi^+ + {}^A Z \rightarrow {}^A_\Lambda Z + K^+ \tag{5}$$

at the cross section peak momentum of 1.05 GeV/c, was proved to be efficient for producing Λ-hypernuclei at BNL AGS. Since the elementary process is endothermic, a relatively large momentum ($\sim$ 350 MeV/c) is transferred to the Λ hyperon, always

for forward detection of the K^+. For this reason the reaction is suitable for exciting high spin hypernuclear states and, accordingly, well adapted to unfolding the shell structure of heavier nuclei since the Λ can populate the low lying hypernuclear levels. The process is complementary to the "strangeness exchange" one and, though the cross sections are lower by at least two orders of magnitude than those for the process (4), this drawback is overcompensate by the larger intensities of the available π^+ beams.

A way of combining the advantages of both the previous methods is to use beams of stopping K^-, which allow high production rates and a large number of hypernuclear final states to be obtained at the same time. The relevant process is

$$K^-_{stop} + {}^A Z \rightarrow {}^A_\Lambda Z + \pi^- \qquad (6)$$

where the stopping kaon forms a kaonic atom, is adsorbed at the nuclear surface and, with a certain probability, forms an hypernuclear state. The spectrum of the resulting π^-, which is emitted isotropically, gives the intensities and the energies of the hypernuclear levels.

The momentum transferred to the produced Λ-hyperon is of the same order of magnitude (250 MeV/c) than the one typical of π^+ induced associated production (5), therefore several hypernuclear levels may be excited. At the same time the production rates for defined hypernuclear final states are still quite high : 10^{-3}/stopped K^-. This technique has been used very efficiently at KEK, where an impressive bulk of high quality data has been produced [5].

Hypernucleus production processes induced by relativistic ions and antiprotons are neglected for simplicity; suffice to say that this latter technique has been employed at the LEAR of CERN to measure the lifetime of heavy hypernuclei in the mass range A $\sim$ 200, by studying the delayed fission following $\bar{p}$ annihilation at rest [6].

2.1 Advantages of K^-_{stop} for hypernuclear spectroscopy at DAΦNE

The advantages of using K^- at rest from ϕ decay for high resolution hypernuclear spectroscopy, become clear when the main features of the different production techniques are compared.

When K^- or π^+ beams in flight are used for "strangeness exchange" or "associated production" reactions, in order to obtain acceptable counting rates, thick targets of the order of several g/cm^2, must be employed. The target thickness limits the momentum resolution on the produced π^- or K^+, due to the uncertainty in the interaction point and the fluctuations in direction and energy lost in the target

material. Moreover, a limited angular acceptance is in general available, in such experiments, for detection of hypernuclear decay products.

The same problem occurs in experiments with K^- at stop. In fact, at proton machines, where kaons are emitted from an external production target, the distance between the source of the particles and the experimental area must be at least $10 \div 15$ m, for radiation safety requirements. Kaons of less than $400 \div 450$ MeV/c cannot obviously survive to such a distance in number suitable for an intense beam. For this reason high energy kaon beams have to be degraded to rest, with a moderator placed just in front of the target. The moderator introduces a large uncertainty in the momenta of the outgoing particles, due to the energy straggling. In this case too, thick targets are needed in order to obtain acceptable counting rates. The error introduced in the momentum of the emitted particles, due to the uncertainty of the interaction point, renders often useless the high resolution of the spectrometers coupled to such stopping devices.

On the contrary, the low energy and monochromatic K^- coming from the ϕ decay in DAΦNE, can be stopped in a material thickness of less than 100 mg/cm^2. Therefore, very thin targets (300 mg/cm^2) can be employed and the K^- can be stopped very close to the target surface. Consequently, outgoing π^- do not cross any significant amount of target and do not undergo any momentum degradation. This feature may provide unprecedented momentum resolution for hypernuclear spectroscopy, when thin targets are coupled to the best magnetic spectrometers that can be designed.

Moreover, a large solid angle of acceptance (typical of detectors at intersecting beam machines) can be available for the detection, with the same apparatus, both of the π^- from hypernucleus formation and of the hypernucleus decay products. This large acceptance constitutes a further advantage, compared to spectrometers built at fixed target machines. Finally, differently from fixed targets experiments, the direction of the K^- can be efficiently tagged by the direction of the K^+ and viceversa.

The only inconveniences of the K^- beam provided by the ϕ decays are the low intensity (216 K^-/s at $\mathcal{L} = 10^{32} cm^{-2} s^{-1}$ luminosity), if compared to extracted kaon beams ($\sim 10^4$ K^-/s), and its lack of collimation.

2.2 FINUDA performances, comparison with other experiments

In spite of the limitation in K^- beam intensity and poorness of collimation, the expected performances of the FINUDA apparatus in terms of momentum resolution, expected counting rates and detection of non-mesonic hypernuclear decays, result competitive not only with those obtained by existing experiments, but also with

Table 2: Performances of hypernuclear physics experiments.

Experiment	Resolution (FWHM)	Rate (event/hour)	Non-mesonic decays
BNL [7] $(K^-, \pi^-), (\pi^+, K^+)$	$\sim 1\ MeV$	$1 \div 5$	YES
KEK [8] (π^+, K^+)	$\sim 2\ MeV$	$1 \div 5$	?
CEBAF [9] (proposed) (e, e', K^+)	$\sim 200\ KeV$	5	NO
BNL [10] (proposed) (K^-_{stop}, π^0)	$< 1\ MeV$	60	??? thick target
FINUDA $\mathcal{L} = 10^{32} cm^{-2} s^{-1}$	$\sim 700\ KeV$	80 per state at 10^{-3}	6 ev/hour (n + p) 1 ev/hour (n + n)

those foreseen for proposed apparatuses at fixed target machines.

In Tab. 2 the main expected performances of FINUDA are compared with those of existing and proposed experiments. The FINUDA apparatus appears very competitive also with the new initiative on hypernuclear physics that will be proposed at BNL AGS, to study the (K^-, π^0) reaction with K^- at rest [10]. It is interesting to remark that the rates foreseen for the two experiments are similar, but for opposite experimental reasons: in the AGS case the flux of stopped K^- is $2 \cdot 10^4 s^{-1}$ and the solid angle of the spectrometer is $\sim 20\ msr$; for FINUDA the flux is two orders of magnitude lower, but the spectrometer solid angle is two orders of magnitude larger. The AGS choice of considering neutral pions is probably dictated by the need of using thick targets to obtain high stopping rates, which worsens the resolution of emerging charged particles. Additionally, it badly affects, owing to multiple scattering and absorbtion effects, the possible detection of $\sim 80\ MeV$ protons from hypernucleus non-mesonic decay.

The large counting rates that may be obtained by FINUDA at the initial luminosity of $\mathcal{L} = 10^{32} cm^{-2} s^{-1}$, offer the possibility to study hypernuclear states produced with capture rates of 10^{-3} rather easily, and to detect states produced with capture rates of 10^{-4}. Moreover, thanks to the thin thickness of the target, a specific technique for background suppression [11], based on the detection of correlated protons, can be applied in FINUDA and makes possible to attain the sensitivity needed for the detection of states with capture rates down to 10^{-5}.

Finally, FINUDA has also the advantage of profitting of an increase of luminosity up to a factor 10, at the top performances of the machine, which is not the case for the other fixed target experiments.

3 – The FINUDA apparatus

The FINUDA apparatus has been designed with the aim of exploiting, at best, the unique possibilities offered by the DAΦNE low energy K^- beam. Detailed descriptions of the apparatus and of the status of the single subdetectors can be found in the FINUDA proposal [1], in a Technical Report [12], which is to appear shortly, and in the 1995 Report on DAΦNE Physics and Detectors [13]. Here only a short description of the main features of the apparatus will be given.

FINUDA is a magnetic spectrometer with cylindrical geometry, optimized in order to have a large solid angle, optimal momentum resolution and good triggering capabilities. Geometrical acceptance is approximately $135^0 \geq \theta \geq 45^0$ (θ being the polar angle relative to the z-axis), naturally rejecting e^+e^- background from Bhabha scattering.

In Fig. 1 the interaction/target region is shown; immediately around the beam pipe a barrel of thin scintillators (TOFINO) is placed, with the aim of detecting and triggering on the crossing of the highly ionizing K^+K^- pairs that emerge from the interaction region. The K^+K^- angular distribution follows a $sin^2\theta$ law.

The position of the K^- trajectory immediately before the very thin target (1.5 mm of carbon is a typical thickness), is measured by an octagonal array of silicon microstrips (ISIM), with very high spatial resolution ($\sigma \sim$ 30-50 μm). Additionally, the same detectors can provide particle identification by ionization energy loss. The position of the interaction point inside the target can be reconstructed with high accuracy (250 μm), basing on this very precise position measurement. The minimum amount of material placed along the path of the kaons, is determined by the requirement that the low energy, monochromatic K^- can be stopped as close as possible to the external surface of the target.

Finally, an external array of ten silicon microstrips (OSIM) constitutes the most internal detector of the magnetic spectrometer. It measures, close to the target and with high spatial resolution, the crossing points of the charged tracks coming from the hypernucleus formation and decay.

The interaction/target region is surrounded by a large magnetic spectrometer formed by four arrays of detectors immersed in a very homogeneous magnetic field of 1.1 *Tesla* (See Fig. 2). The external silicon microstrip modules (OSIM), two arrays of planar low mass drift chambers (LMDC) and a system of longitudinal (along the beam axis) and stereo (inclined by 13^0) straw tubes (ST) provide the measurement of four points along the trajectories of the tracks emerging from the target. The tracking volume of the spectrometer is immersed in He atmosphere, in order to minimize the distortion of the particle trajectories originated by multiple scattering. For the same reason, the drift chambers are equipped with very thin

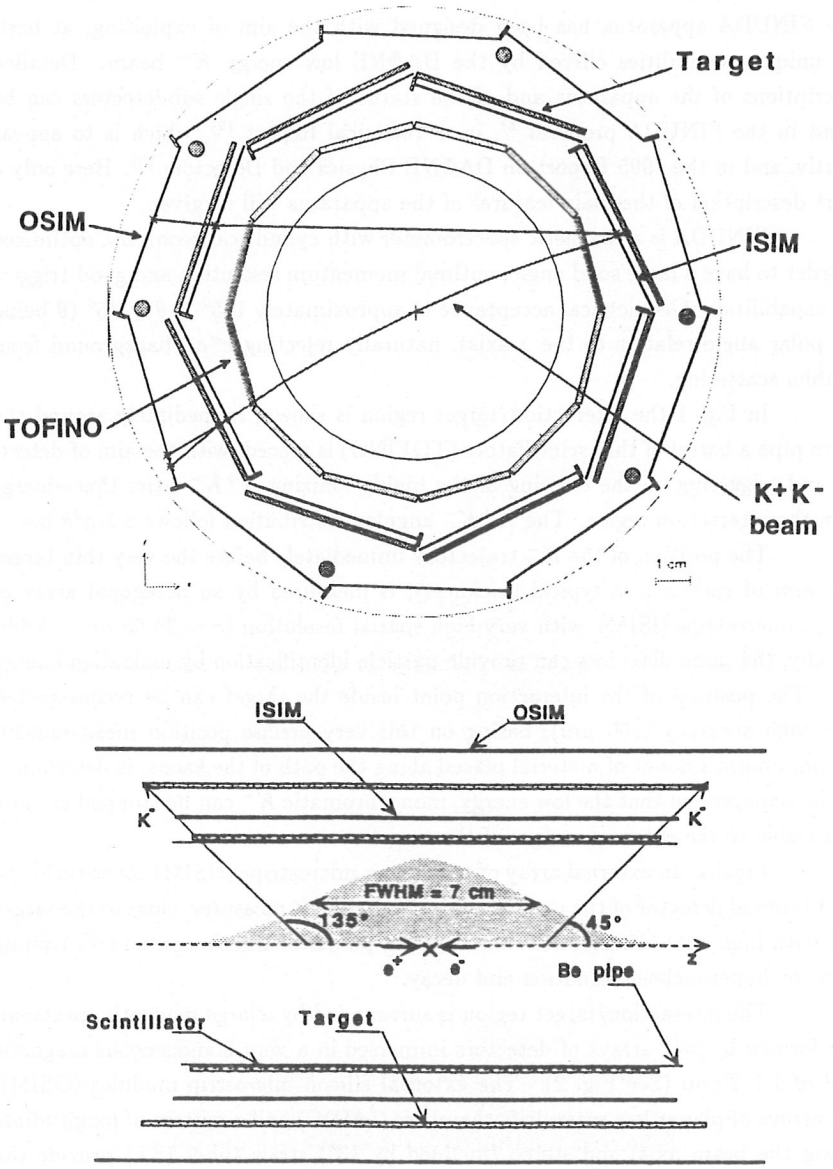

Figure 1: Internal detector region.

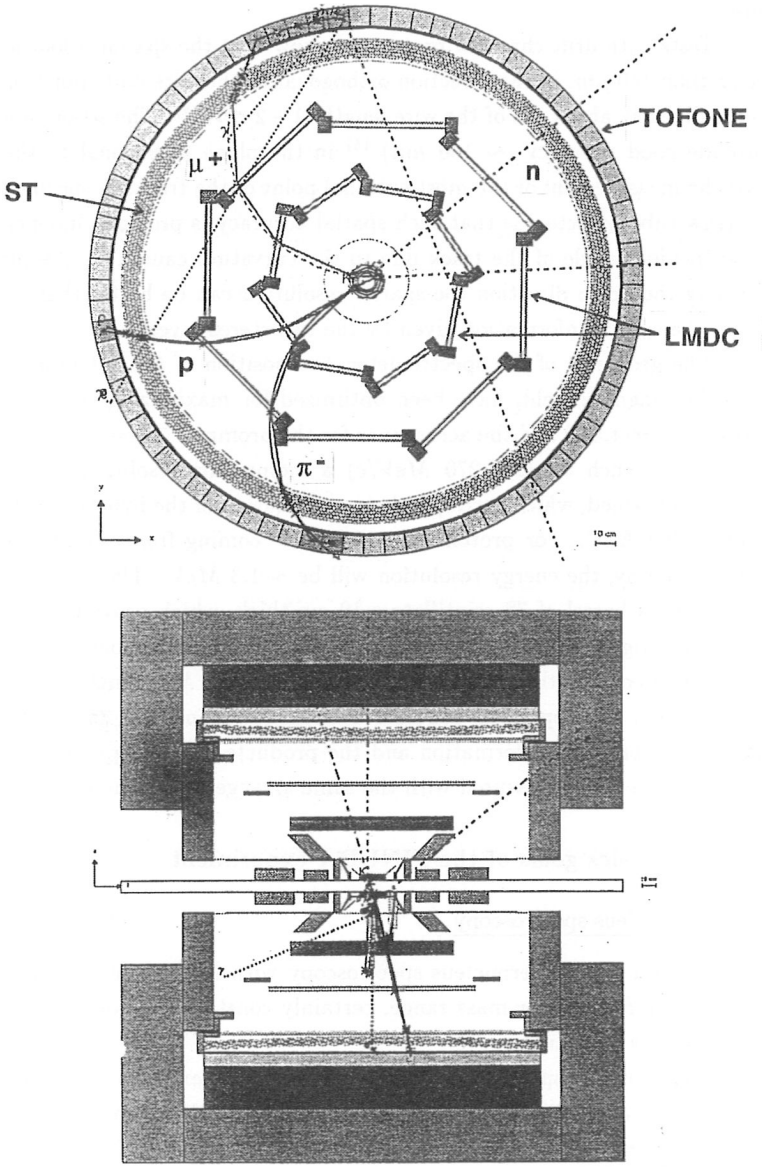

Figure 2: Cross sections of the FINUDA spectrometer. A typical hypernucleus formation event is shown.

mylar windows (6 and 12 μm) and are operated with a $He - iC_4H_{10}(70/30)$ gas mixture.

Tests with drift chamber prototypes show that the spatial resolutions can be better than 150 μm, in the direction orthogonal to the wire and, along the wire, by charge division, about 1% of the wire length ($1 \div 2\ cm$) [14]. The straw tube array can provide good accuracy ($\sim$ 100 μm) [15] in the plane orthogonal to the beam axis, for the measurement of the most external point of the track. A specific feature of the straw tube detectors is that such spatial accuracy is provided independently from the incident angle of the track due to the curvature caused by the magnetic field. Along the beam direction the spatial resolution can be better than 1.0 mm, thanks to the spatial information given by the two stereo layers.

The geometry of the spectrometer, the position of the detectors and the value of the magnetic field, have been optimized for maximizing the momentum resolution (see Sect.5.1) and the acceptance for the prompt π^- from Λ-hypernucleus formation. For such π^- (250-270 MeV/c) a momentum resolution of less than 0.3% can be obtained, which corresponds to a resolution of the hypernuclear energy levels of $\sim$ 700 KeV. For protons of $\sim$ 80 MeV coming from the hypernucleus non-mesonic decay, the energy resolution will be $\sim$ 1.3 MeV. The spectrometer is surrounded by a barrel of 72 scintillators 10 cm thick, which provides a fast logic signal for the trigger and allows neutrons coming from non-mesonic hypernuclear decay, to be detected with $\sim$ 15% efficiency and about 10 MeV energy resolution.

Finally, the apparatus provides a large acceptance ($\sim 2\pi$) both for π^- coming from hypernucleus formation and the products of the hypernucleus decay, which are detected and measured with the same arrangement of detectors.

4 – Main physics goals of the FINUDA experiment

4.1 Λ-hypernucleus spectroscopy

A large program of Λ-hypernucleus spectroscopy with high energy resolution, extended over the full nuclear mass range, certainly constitutes a top priority of the FINUDA physics program.

Hypernuclear spectroscopy can offer important experimental information both for nuclear and particle physics. From the nuclear physics point of view, a Λ hyperon imbedded inside a nucleus is expected to behave as a distinguishable baryon, not affected by Pauli blocking. Moreover, it is seen to experience an interaction with the nucleons appreciably weaker then the N-N force and a negligible spin-orbit central potential. The latter features of the Λ-N interaction are related, to a substantial extent, to the zero isospin of the Λ, which prevents the latter from

exchanging an isovector meson like the π or the ρ with a nucleon and determines a lack of strong tensor components in the interaction [16].

The relative weakness of the Λ-N interaction entails that the shell structure is not disrupted by the insertion of the Λ into a nucleus and the lack of Pauli blocking allows all the single particle states to be populated by a Λ. In the hypernuclear ground state, the Λ resides in the $1s$ shell and can explore very deeply the nuclear structure.

Fig. 3 shows, for a Λ-hypernucleus, what was never seen for an ordinary nucleus. The excitation spectrum [17] of ${}^{89}_{\Lambda}Y$ provides the best example of the validity of the single particle model, without the difficulty linked to the Pauli exclusion principle and to the pairing interactions, as it occurs in ordinary nuclei. In the spectrum, s,p,d,f and g Λ-orbitals are clearly seen and the validity of the concept of shell model is demonstrated in a striking way, not just in the valence region but deep within the nuclear interior. In non-strange nuclei a single particle deeply bound hole-state is so fragmented with excitation energy, to be essentially unobservable. The spectrum of Fig. 3 has been obtained with a resolution of 2.6 MeV FWHM and only the major shells are resolved. With better resolution more details, due to the spin splitting of different states, might appear.

From the particle physics side Λ hypernuclei are interesting since they may permit to obtain, in an indirect way, information on the Λ-N interaction in the low momentum region, where direct scattering experiments cannot be done, owing to the short lifetime of the Λ-hyperon. More interesting is the unique possibility offered by Λ-hypernuclei for testing a new approach to the description of nuclear matter. In fact, with the scarce energy resolution so far accessible to the experiments, the Λ seems to remain as a composite particle well distinguishable inside the nucleus. However, it is possible that high resolution experiments may reveal effects due to the partial deconfinement of the Λ in the nuclear matter.

At present, the knowledge about the hypernucleus phenomenology is very limited, both by the quality of the available experimental data and by the large gaps of ignorance in the chart of known Λ-hypernuclides (see Fig. 4 [18]). FINUDA can perform a large scientific program of high resolution hypernuclear spectroscopy on all nuclides that can be machined in solid targets and for which an acceptable formation rate is measured. The completion of this program could constitute a formidable step forward in the understanding of the main hypernuclear physics problems: from the origin of the nuclear spin-orbit force, the short range correlations, the possible new symmetries in many body spectroscopy and the rôle of flavour symmetry, to the hyperon-nucleon interaction and the rôle of strangeness in strong interaction, as well as the possible modifications of the baryon properties in the nuclear environment.

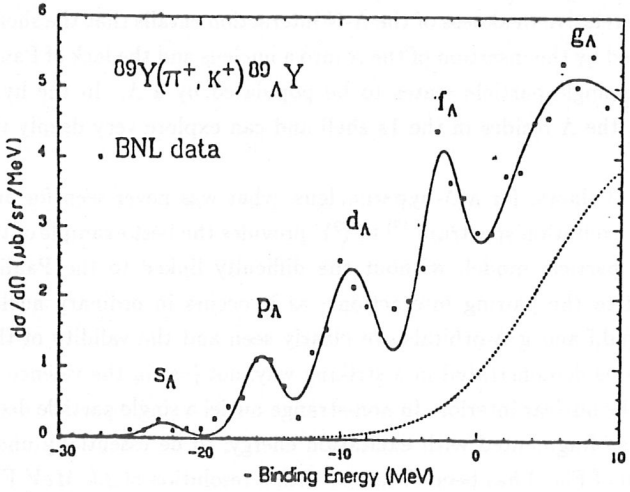

Figure 3: The excitation spectrum for the $^{89}Y(\pi^+, K^+)^{89}_{\Lambda}Y$ reaction at 1.05 GeV/c and $\theta_K = 10^0$.

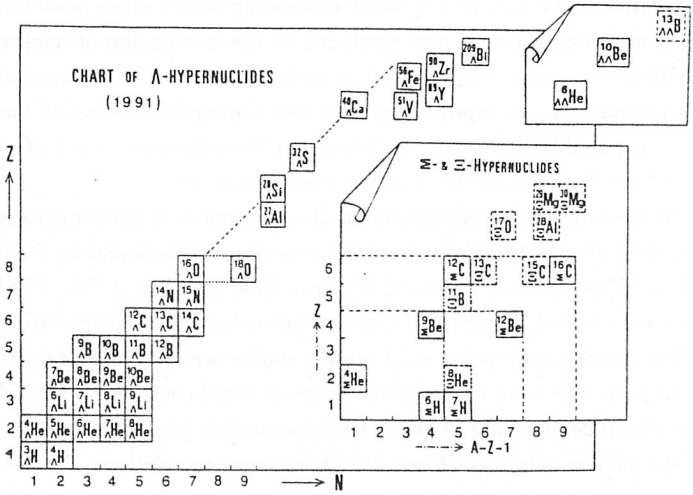

Figure 4: Chart of Λ-hypernuclides.

4.2 Non-mesonic decay of Λ-hypernuclei, $\Delta I = \frac{1}{2}$ rule.

The decay of hypernuclei, in particular the study of the non-mesonic ones and of the validity of the well-known $\Delta I = \frac{1}{2}$ rule, are probably the most important subjects that the FINUDA experiment will be able to investigate, both in term of physical interest and experimental feasibility.

The free Λ decays into two mesonic modes

$$\Lambda \to p + \pi^-(\sim 64\%) \quad and \quad \Lambda \to n + \pi^0(\sim 36\%) \tag{7}$$

with a lifetime $\tau_\Lambda = (2.36 \pm 0.02) \cdot 10^{-10} sec.$ The decay may occur, in principle, with isospin change $\Delta I = \frac{1}{2}$ or $\frac{3}{2}$. However, the experimental decay branching ratios of the Λ and other hyperons, imply a dominance of a factor 20 of the $\frac{1}{2}$ component over the $\frac{3}{2}$ one.

The origin of this empirical rule is not understood in a fundamental way. Several authors have added strong interaction corrections to the simple W exchange diagram, including both soft gluon radiative corrections and penguin diagrams [19]. In particular the penguin diagram is emphasized because of its $\Delta I = \frac{1}{2}$ character.

The situation described above for the weak decay of the free Λ-hyperon changes dramatically when the Λ is imbedded in the nuclear medium. The binding energy of the Λ-hyperon in the ground state increases linearly with A, reaching the saturation value of 25 MeV for heavy hypernuclei. Hence the phase space for the mesonic decay is greatly reduced ($p_{nucleon} \sim 100\ MeV/c$). Consequently, in all but the lightest nuclei, the mesonic decay mode is strongly inhibited by Pauli principle and the non-mesonic decay modes are dominant,

$$\Lambda + p \to n + p \tag{8}$$

$$\Lambda + n \to n + n \tag{9}$$

since they are not affected by Pauli blocking ($p_{nucleon} \sim 417\ MeV/c$).

The study of the weak decay of a Λ-hypernucleus aims to the understanding of the stability of the hypernuclear system and of the influence of the nuclear medium on the Λ itself. Moreover, through the study of the weak non-mesonic decays, which probe the high momentum and parity conserving part of the weak interaction, one can gain insight into the fundamental aspects of the pertinent four-Fermion, strangeness-changing weak-interaction process. Such weak process is masked by the strong interaction in non-strange N-N interactions. In particular, it has been recently suggested [20], after the analysis of some decay channels of *s*-shell hypernuclei, that the $\Delta I = \frac{1}{2}$ rule may be strongly violated in non-mesonic decay. So, precise measurement of the relative branching ratios for the non-mesonic

channels (8) and (9), could provide information about the structure of the weak hamiltonian, in particular the relative importance of the $\Delta I = \frac{1}{2}$ and $\Delta I = \frac{3}{2}$ amplitudes.

Notwithstanding the considerable interest of this subject, experimental data are scarce and not precise [21]. This is due to the tremendous difficulty in producing abundantly Λ-hypernuclei in their ground state and detecting the products of their decay. Extremely hard is to study the non-mesonic decay (9) for which two fast neutrons have to be detected and related to the hypernuclear ground state.

The FINUDA apparatus seems ideal for the study of non-mesonic decays. In fact, the very transparent structure of the detector and the extremely thin thickness of the target, allow the products of the hypernucleus decay to be efficiently detected. Moreover, the large solid angle of acceptance for both π^- from hypernucleus formation and decay products, provides quite high counting rates and allows the coincidence between the hypernucleus decay and the related hypernuclear ground state to be easily established.

However, the energy resolutions on protons (1.3 MeV) and neutrons (10 MeV) in the FINUDA apparatus will not allow, in general, the identification of the final nuclear states ${}^{A-2}(Z-1)$ and ${}^{A-2}Z$. In these inclusive measurements, an averaging over the final states of the weak decays $\Lambda + N \rightarrow N + N$ will be inherently present, and a possible violation of the $\Delta I = \frac{1}{2}$ rule could be inferred only by a systematic study of the ratio of the BR's, for the two non-mesonic channels, as a function of the mass number.

It has been suggested [22] that the use of a ${}^6Li$ target offers the possibility of performing an exclusive measurement of one of the non-mesonic decay modes of ${}^6_\Lambda He$

$$K^-_{stop} + {}^6Li \rightarrow \pi^0 + {}^6_\Lambda He \rightarrow {}^4He + (n+n) \tag{10}$$

The ${}^6_\Lambda He$ hypernucleus will stop in matter before decaying and, when it decays into the $(n+n)$ mode, it may result in the ${}^4He$ nucleus. The very large particle emission threshold of ${}^4He$ (19.8 MeV) allows the FINUDA apparatus to recognize the exclusive process by kinematic constraints, in spite of the limited energy resolution on the $(n+n)$ mode (14 MeV). In FINUDA such channel may be easily triggered by requesting two opposite slabs hit on the external scintillator barrel.

5 – FINUDA performances

5.1 Momentum resolution

The momentum resolution of the apparatus is its most crucial feature. In fact, the resolution on the momentum of the π^- emitted in the hypernucleus formation

is directly connected to the resolution on hypernuclear energy levels. For a π^- of 270 MeV/c, an uncertainty of 0.1% in momentum corresponds to an energy resolution of 240 KeV on the hypernuclear levels. Hence, to fulfill the physical expectations, FINUDA must feature not more than 0.3% in momentum resolution, which corresponds to $\sim$ 700 KeV in energy.

Factors affecting the momentum resolution are : the size of the spectrometer, the value of the magnetic field, the spatial resolution of the detectors and the multiple scattering along the particle path. To fulfill the requested performances, low mass detectors with high spatial resolutions have been adopted; in particular the requirement of low mass is particularly stringent on the detectors located along the particle trajectory and can be partially released for the detectors measuring the initial and final points of the tracks. Moreover, the tracking volume is immersed in helium atmosphere to minimize the effect of the multiple scattering.

Thanks to the transparency of the tracking volume, the average radiation length of the spectrometer amounts to 170,000 cm, to be compared with 540,000 cm for pure helium and 34,000 cm for air. The design spatial resolution of the detectors (see Sect.3) are reasonable extrapolations of the present technology and have been largely met in tests performed on prototypes. Finally, concerning the size of the spectrometer and the value of the magnetic field, they have been optimized with a compromise between minimum value of the magnetic field (1.1 $Tesla$), to minimize the effects on circulating beams, and minimum size of the spectrometer ($\sim$ 100 cm), to minimize costs.

An evaluation of the momentum resolution for pions with the standard formulae [23], shows that the requested performances are largely met in the FINUDA apparatus. In Fig. 5 the calculated behaviour of the momentum resolution for pions versus pion momentum, is shown for two values of the θ polar angle. It is worth remarking that, in the interesting range of momenta, the momentum resolution is dominated by the multiple scattering, which makes less crucial, for the performances of the apparatus, a possible worsening of the detector spatial resolutions.

Extensive simulations were carried out, with a Monte Carlo program, with populations of tracks of different particles emerging from the target; the results confirm the expectations. The momentum resolutions are evaluated to be 0.28% for π^- of 270 MeV/c, 0.79% for protons of 417 MeV/c and 0.24% for μ^+ of 236 MeV/c. As mentioned in Sect.3, the thin thickness of the target allows the high momentum resolution of the spectrometer to be fully exploited. In any case, a correction of the pion momentum for the energy lost in the target can be efficiently applied, since both the K^- interaction point and the exit point of the π^- from the target, can be reconstructed within an uncertainty of some hundreds of microns.

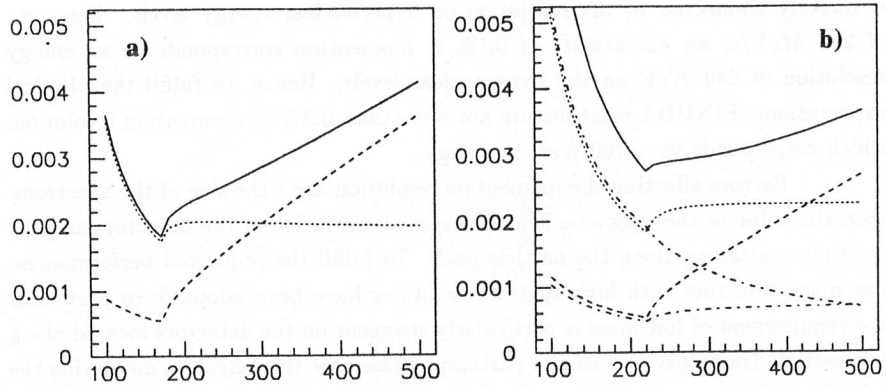

Figure 5: Momentum resolution ($\frac{\Delta p}{p}$ FWHM) for pions versus pion momentum. a) $\theta = 90^0$, b) $\theta = 50^0$. Dashed line: contribution from helix fit; dotted line: contribution from multiple scattering in helix fit; dotted-dashed lines : contributions from linear fit and multiple scattering in linear fit.

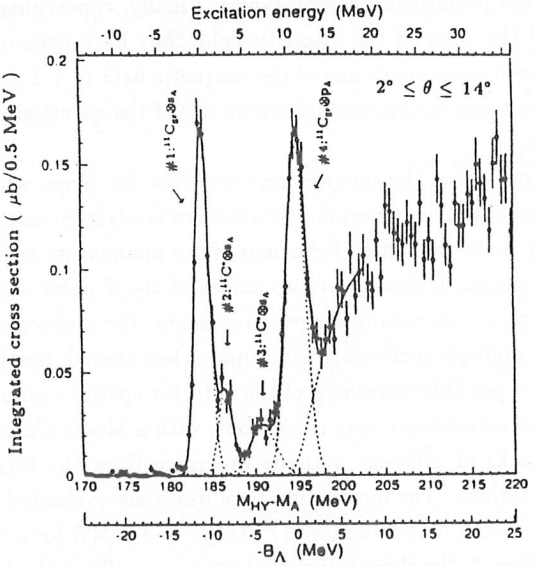

Figure 6: Excitation spectrum of ${}^{12}_{\Lambda}C$ obtained in the (π^+, K^+) reaction at 1060 MeV/c with the SKS spectrometer.

5.2 Trigger efficiency and rejection

The aim of the trigger logic of the FINUDA apparatus is to select hypernuclear events out of the background ones. In hypernuclear events the ϕ decays into K^+K^-, the K^- stops in the target, forms an hypernucleus and emits a prompt π^-. To be useful for high resolution spectroscopy the π^- must cross the full spectrometer and, therefore, must produce hits on one or more slabs of the external scintillator barrel at the end of its trajectory. Background events are Bhabha scattering and other decays of the ϕ as reported in Table 1.

Bhabha events are naturally reduced by the geometrical acceptance covered by the TOFINO scintillator array $135^0 \geq \theta \geq 45^0$. To select the ϕ decay into K^+K^- the trigger requirements exploit the back to back topology of the K^+K^- pairs and their large specific energy loss. In fact, low energy kaons from ϕ decay have a $dE/dx \sim 22\ MeV/cm$ against $dE/dx \sim 2\ MeV/cm$ for minimum ionizing particles from background reactions. Owing to the large difference in specific energy loss, the latter condition results the most powerful one. Additionally, a coincidence in the external barrel of scintillators within 10 ns is requested, to select prompt pions crossing the spectrometer against μ^+ coming from the delayed K^+ decay.

Table 3 shows typical triggering efficiency for hypernuclear events and residual background contamination calculated by Monte Carlo simulation. The counting rates are computed at a luminosity of $\mathcal{L} = 10^{32} cm^{-2} s^{-1}$. The efficiency of the trigger for hypernuclear events is very high and is limited essentially by the geometrical acceptance of the spectrometer. The background events are efficiently rejected and only the K^- interactions without formation of a hypernucleus produce an appreciable rate. For these events the fast coincidence is, in general, provided by a fast μ^+.

Accounting for the percentage of triggered events where the π^- is measured with high resolution ("forward" pions, not crossing the interaction region before entering the spectrometer) and assuming a chamber transparency of about 80%, the trigger rate of $8 \cdot 10^{-2}$ Hz expected at $\mathcal{L} = 10^{32} cm^{-2} s^{-1}$ luminosity provides about 80 *event/hour* useful for high resolution hypernuclear spectroscopy.

5.3 FINUDA performances in hypernuclear spectroscopy

Given the performances illustrated above for the resolution of the spectrometer and the trigger efficiency, it is possible to use Monte Carlo simulated events to estimate the resolution on hypernuclear levels in presence of a physical background. As an example, Fig. 6 shows a recent measurement of the spectrum of ${}^{12}_{\Lambda}C$ observed with the (π^+, K^+) reaction in flight [24] with an energy resolution of 2 MeV. The ground state of ${}^{12}_{\Lambda}C$ and its excited state at $\sim 10\ MeV$ are clearly seen; moreover two small

Table 3: Trigger efficiency and rejection. Counting rates.

Efficiency for hypernucleus formation events	
Tofino back-to-back × Energy threshold	81%
Tofone Prompt coincidence	46%
TRIGGER	39%
TRIGGER with π^- with 4 hits	29%
TRIGGER with high resolution "forward" π^-	13%
Rejection powers	
Bhabha	$< 10^{-2}$%
$\phi \to K_S K_L$	$3 \cdot 10^{-2}$%
$\phi \to \rho\pi$	$4 \cdot 10^{-2}$%
$\phi \to \pi^+\pi^-\pi^0$	10^{-2}%
K^- interaction without hypernucleus formation	7%
Trigger rates at $\mathcal{L} = 10^{32} cm^{-2} s^{-1}$	**Hz**
Hypernucleus formation ($10^{-3}/K^-_{stop}$ capture rate)	$8 \cdot 10^{-2}$
Bhabha	$< 4 \cdot 10^{-2}$
$\phi \to K_S K_L$	$5 \cdot 10^{-2}$
$\phi \to \rho\pi$	$2 \cdot 10^{-2}$
$\phi \to \pi^+\pi^-\pi^0$	10^{-3}
K^- interaction without hypernucleus formation	15

peaks at $\sim 2.6\ MeV$ and $\sim 6.8\ MeV$ excitation energy appear, corresponding to core excited states of ${}^{12}_{\Lambda}C$.

The same spectrum of states has been injected in the FINUDA apparatus by a Monte Carlo simulation. In the injected spectrum, which is seen in Fig. 7 a), the four peaks were generated as monochromatic lines over a background typical of K^-_{stop} experiments [5] on ${}^{12}C$, with intensities corresponding to the standard capture rate of $10^{-3}/K^-_{stop}$ for the ground state line. In the quoted K^-_{stop} experiment [5], the typical energy resolution is about 3 MeV and the signal/background ratio is around $\frac{1}{1}$; for FINUDA the same ratio might be expected to be of the order of $\frac{4}{1}$ or better.

The simulated spectrum was then processed through the full chain of simulation and reconstruction programs, where the effects of both the trigger efficiency (see Sect.5.2) and the Pattern Recognition efficiency (which has been estimated to be greater than 95%) are accounted for. The results of the procedure are seen in Fig. 7 b)-f). In Fig. 7 b) the raw reconstructed spectrum is shown; the cut in momentum at 180 MeV/c is due to the limit in acceptance of the spectrometer. The peaks appear enlarged by the contamination of "backward" pions, which emerge from the target in the direction of the beam pipe and cross the materials of the in-

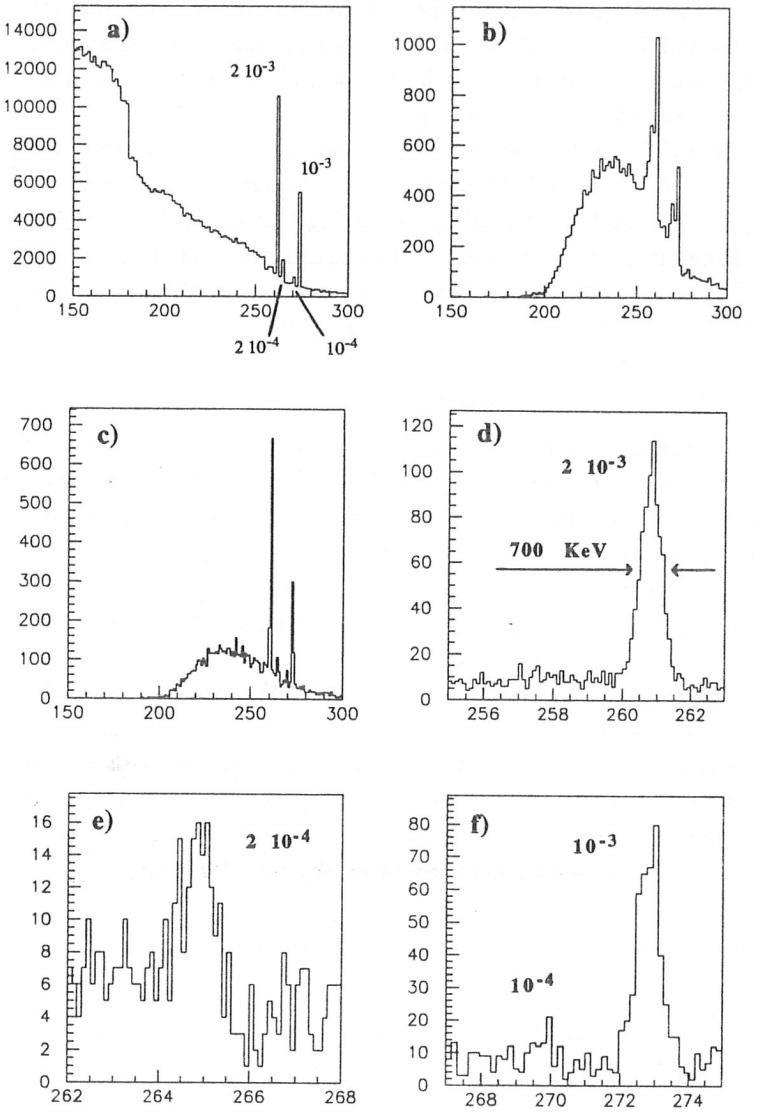

Figure 7: a) Spectrum injected in the Monte Carlo. b) Raw reconstructed spectrum. c) Reconstructed spectrum for "forward" pions, corrected for target crossing. d),e),f) Magnified views of the reconstructed peaks. (Momentum in MeV/c in abscissa)

teraction region before entering the spectrometer. In Fig. 7 c) only "forward" pions are selected and the correction to the momentum for target crossing is applied. The four peaks appear very clearly over the background, thanks to the optimal energy resolution foreseen for the FINUDA apparatus.

In Fig. 7 d),e),f) magnified views of the reconstructed spectrum are shown; The peaks at 10^{-3} are clearly identified over the background, whereas the peaks at 10^{-4} begin to be visible. It is worth remarking that the spectrum of Fig. 6 has been obtained in at least one week of data taking; the peak at 10^{-3} intensity in Fig. 7 f) contains $\sim$ 450 events that can be cumulated by FINUDA in 6 hours at $\mathcal{L} = 10^{32} cm^{-2} s^{-1}$ and in less than 1 hour at $\mathcal{L} = 10^{33} cm^{-2} s^{-1}$.

5.4 Hypernucleus lifetime measurement

In FINUDA the hypernucleus lifetime can be directly measured from the difference between the hit time of the prompt π^- on Tofone (or Tofino) and the hit time of the proton, which is delayed by the hypernucleus lifetime. The hit times have to be corrected for the time of flight of the particles, which give little contribution to the time uncertainty since momenta and trajectories are very accurately measured. This technique has been already adopted with success at BNL [25] and KEK [26].

Assuming a time resolution of $\sim$ 500 ps FWHM for the FINUDA Time of Flight system, a Monte Carlo simulation has shown that, thanks to the large acceptance of the FINUDA apparatus for the hypernucleus decay products, the lifetime of a hypernucleus can be reconstructed with 10% statistical error with $\sim$ 2000 events reconstructed in the hypernucleus ground state peak. Assuming a capture rate of 10^{-3} for the ground state, this number of events can be obtained, with the FINUDA apparatus, in 1 day of data taking at $\mathcal{L} = 10^{32} cm^{-2} s^{-1}$ luminosity.

6 – Milestones of the hypernuclear physics program

FINUDA will be installed in the second half of 1996 in DAΦNE and will be ready to perform its large program of hypernuclear physics at the starting time of the machine. The main physics priorities of the experimental program can be briefly summarized as follows.

- The first item will be the re-measurement of the excitation spectrum (with resolution $< 1\ MeV$), decay modes and lifetime of the ${}^{12}_{\Lambda}C$ nucleus, which is one of the hypernuclei most extensively studied.

- High statistic study of the production, decay and lifetime of the p-shell hypernuclei ${}^{7}_{\Lambda}Li$, ${}^{9}_{\Lambda}Be$, ${}^{10}_{\Lambda}B$. ${}^{6}_{\Lambda}He$ will be studied too using a ${}^{6}Li$ target.

- High statistic survey of the production of hypernuclei of higher mass, with targets of ^{27}Al, ^{51}V, ^{133}Cs, ^{165}Ho and ^{209}Bi.

It is worth remarking that, for all targets, a survey of the low momentum π^- spectra will be obtained, in parasitic way, for the events where the fast coincidence on Tofone is given by a μ^+ or π^+ coming from K^+ decay. In these events the π^- from the stopping K^- is detected by the spectrometer over the full spectrum. Negative pions of momentum less than 180 MeV/c don't reach the straw tube array owing to their curvature; nevertheless they can be reconstructed as well, although with lower quality and worse momentum resolution.

References

1. The Finuda Collaboration, FINUDA a detector for Nuclear Physics at DAΦNE, LNF Preprint LNF-93/021(IR), (1993)

2. G. Vignola in Workshop on Physics and Detectors for DAΦNE, Frascati, April 9-12, 1991; ed. G. Pancheri, (INFN-LNF, 1991) p.11

3. The KLOE Collaboration, KLOE a General Purpose Detector for DAΦNE, Rep. LNF-92/019(IR), (1992)

4. T. Bressani in Workshop on Physics and Detectors for DAΦNE, Frascati, April 9-12, 1991; ed. G. Pancheri (INFN-LNF, 1991) p.475.
   T. Bressani in Common Problems and Ideas of Modern Physics; eds. T. Bressani, B. Minetti and A. Zenoni (World Scientific, Singapore, 1992) p.211

5. T. Yamazaki et al., Nuovo Cim. **102A** 695(1989)

6. J.P. Bocquet et al., Phys. Lett. **B182** 146(1986)
   J.P. Bocquet et al., Phys. Lett. **B192** 312(1987)

7. P.H. Pile in Proc. LAMPF Workshop on (π, K) Physics, Los Alamos, NM 1990; eds. B.F. Gibson, W.R. Gibbs, M.B. Johnson, AIP (New York 1991) p.77

8. T. Nagae in Proc. of 23rd International Symposium on Nuclear and Particle Physics with Meson Beams in the 1 GeV/c Region, Tokyo, March 15-18 (1995)

9. E.V.Hungerford in Proc. LAMPF Workshop on (π, K) Physics, Los Alamos, NM 1990; eds. B.F.Gibson, W.R. Gibbs, M.B. Johnson, AIP (New York 1991) p.224

10. H.A Thiessen and J.C. Peng, AGS PROPOSAL Investigation of Light Hypernuclei Using the (K^-_{stop}, π^0) Reaction, October 3, (1994)

11. H. Tamura et al., Phys. Lett. **B160** 32(1985)

12. The FINUDA Collaboration, FINUDA Technical Report, FINUDA Note 09/LNF/PUB/95, to be published as a LNF Preprint

13. The FINUDA Collaboration, Status of the FINUDA Experiment, The Second Dafne Physics Handbook, eds. L.Maiani, G.Pancheri, N.Paver, published by S.I.S. Laboratori Nazionali di Frascati (1995)

14. M. Agnello et al., Performance of a large area drift chamber operating with $He - iC_4H_{10}$ mixture, to appear in Nucl. Instr. Meth. A (1995)

15. L. Benussi et al, High performance tracking with long straw tubes using dymethyl ether, Frascati Preprint LNF-94/047(IR) 1994, to appear on Nucl. Inst. Meth. A (1995)
L. Benussi et al., Test beam results and gas system for the straw tube detector, FINUDA Note 18/BC/ST/95 (1995)

16. A. Molinari and H. Feshbach, Hypernuclear Physics, The Second Dafne Physics Handbook, eds. L.Maiani, G.Pancheri, N.Paver, published by S.I.S. Laboratori Nazionali di Frascati (1995)

17. R.E. Chrien in Proc. LAMPF Workshop on (π, K) Physics, Los Alamos, NM 1990; eds. B.F. Gibson, W.R. Gibbs, M.B. Johnson, AIP (New York 1991) p.28

18. H. Bandō, T. Motoba and J. Žofka, Strangeness Nuclear Physics, Perspective of Meson Science, eds. T. Yamazaki, K. Nakai, K. Nagamine, North Holland (1992)

19. P.D. Barnes, Nucl. Phys. **A479** 89c(1988)

20. R.A. Schumacher, Nucl. Phys. **A547** 143c(1992)

21. J. Cohen, Prog. Par. Nucl. Phys. **25** 139(1990)

22. T. Bressani, Non mesonic decay of hypernuclei and the $\Delta I = \frac{1}{2}$ rule, The Second Dafne Physics Handbook, eds. L.Maiani, G.Pancheri, N.Paver, published by S.I.S. Laboratori Nazionali di Frascati (1995)

23. R.L. Gluckstern, Nucl. Instr. Meth. **24** 381(1963)

24. T. Hasegawa et al., Phys. Rev. Lett. **74** 224(1995)

25. J.J Szymanski et al., Phys. Rev. **C43** 849(1991)

26. H. Outa et al., Nucl. Phys. **A547** 109c(1992)

HYPERNUCLEI: A THEORETICAL REVIEW

Avraham Gal
Racah Institute of Physics, The Hebrew University, Jerusalem 91904, Israel

ABSTRACT

Issues of topical interest in strangeness nuclear physics are highlighted. These include the spin dependence of the effective ΛN interaction and the nature of the $\Lambda N \to NN$ nonmesonic weak decay in Λ hypernuclei; the density dependence of the Σ nuclear potential, as suggested by reanalyzing the Σ^- atomic data, and its implications for Σ hypernuclei; the interplay for strangeness $S = -2$ between Ξ hypernuclei and $\Lambda\Lambda$ hypernuclei; and the extrapolation to arbitrarily strange nuclei, $S \to -\infty$, composed of $p, n, \Lambda, \Xi^-, \Xi^0$ baryons.

1 – Introduction

Strangeness is an important element of hadronic physics. The study of hypernuclei provides some unique evidence on the elementary properties of baryon-baryon (BB) interactions in the strange sector, for example the four fermion $\Lambda N \to NN$ weak decay process for $S = -1$ hypernuclei, and whether or not it satisfies the $\Delta I = 1/2$ rule; or the strength of the ΞN and $\Lambda\Lambda$ interactions and their coupling, which is relevant to the binding or non binding of the $(uuddss)$ six-quark H dibaryon, as manifested in $S = -2$ hypernuclei. This makes it possible to partially constrain the freedom incurred in the application of QCD motivated models such as the quark model or one boson exchange SU(3) models, to study the intersections of these seemingly different approaches, and to look for immediate consequences such as how to extrapolate to multiple strangeness all the way down to strange matter, and to identify the relevant degrees of freedom.

For a general reference on hypernuclear physics, the latest HYP94 Proceedings [1] is useful. In this talk I will overview issues in strangeness nuclear physics as follows:

(i) the spin dependence of the effective ΛN interaction where my remarks will focus on prospects offered by doing the $(K^-, \pi^0\gamma)$ reaction, using the LAMPF neutral meson spectrometer at the AGS, but I will also comment on the ΛN configuration mixing components likely to be involved in explaining the ${}^{12}_{\Lambda}$C core-excited spectrum measured recently at KEK in the (π^+, K^+) reaction [2];

(ii) the nature of the $\Lambda N \to NN$ weak decay in Λ hypernuclei, currently explored at BNL and KEK;

(iii) the density dependence of the Σ nuclear optical potential which fitting to the Σ^- atomic data implies. Such a phenomenologically comprehensive analysis [3] suggests the presence of a repulsive component in the nuclear surface region which could even spread to the interior, thus preventing single particle Σ hypernuclear states from being bound except, perhaps, in very light systems;

(iv) aspects of $S = -2$ hypernuclear physics as highlighted by studying the decay widths arising from strong Λ and nucleon emission in Ξ-nucleus configurations due to $\Lambda\Lambda$ admixtures in Ξ states [4], [5]. These states could then be viewed as doorway states into daughter $\Lambda\Lambda$ and Λ hypernuclear states. The underlying mixing mechanism, due to $\Xi N \leftrightarrow \Lambda\Lambda$ coupling, will also induce some Ξ components into low lying $S = -2$ states, dominantly of $\Lambda\Lambda$ character, leading to an enhanced production cross section in the (K^-, K^+) reaction in flight via the excitation of the small Ξ components of the wavefunction in the first-order $K^-p \to K^+\Xi^-$ process;

and finally (v) the challenging prospects for extending $S = -1, -2$ hypernuclear structure into multi strangeness by realizing [6] that, for as large values of $|S|$ as desired, strong-interaction stable multi-strange nuclei composed of $\{p, n, \Lambda, \Xi^-, \Xi^0\}$ baryons exist, with $A = O(|S|)$ and with a very small electric charge fraction $Q/A = O(A^{-2/3})$. These objects are bound by about 20 MeV per baryon and decay dominantly by $\Delta S = 1$ nonmesonic weak interactions with lifetimes estimated to be of order 10^{-10} sec or somewhat shorter. The lightest of these species, where a Ξ hyperon is brought to stability against the strong decay $\Xi N \to \Lambda\Lambda$ is ${}_{\Xi^0\Lambda\Lambda}{}^{7}$He.

2 – Spin dependence in Λ hypernuclei

The spin dependence of the ΛN interaction has not been well determined to date. The low energy spin averaged cross section data are largely insensitive to it, and this shortcoming is reflected in fitted OBE ΛN interaction potentials which can accommodate an arbitrarily wide range of spin dependence [7]. There are several forms in which the ΛN spin dependence may effectively show up in Λ hypernuclei.

Here we discuss two of these: (i) a spin-orbit $\vec{\ell}_\Lambda \cdot \vec{s}_\Lambda$ term, and (ii) a spin-spin $\vec{s}_N \cdot \vec{s}_\Lambda$ term.

2.1 spin orbit.

The only direct limit on the Λ spin-orbit splitting was set from a measurement [8] of the reaction $^{13}C(K^-,\pi^-)\,^{13}_{\Lambda}C$ at $p_K = 800$ MeV/c, involving the $\Delta L = 0$ transition to $p_{1/2}(\Lambda)$ at $\theta_\pi \approx 0°$ and the $\Delta L = 2$ transition to $p_{3/2}(\Lambda)$ at $\theta_\pi \sim 15°$: $\varepsilon_\Lambda(\ell s) \equiv \varepsilon_\Lambda(p_{1/2}) - \varepsilon_\Lambda(p_{3/2}) < 0.4 \pm 0.4$ MeV. A somewhat better, although indirect limit has been determined from the observation [9] of just one hypernuclear γ ray in $^{9}_{\Lambda}$Be:

$$\varepsilon_\Lambda(\ell s) < 0.25 \text{ MeV} \quad , \qquad [\varepsilon_N(\ell s) \sim 4 - 6 \text{ MeV}] \tag{1}$$

where in parentheses the corresponding value of the nucleon spin-orbit splitting is shown. The smallness of the Λ spin-orbit with respect to that for a nucleon arises naturally in relativistic mean field models [10]. Whereas the depth of the hyperon-nucleus central potential is given approximately by $V_c \approx U_s + U_v$, with $U_s < 0$ and $U_v > 0$ due to scalar and vector mean fields, respectively, the spin-orbit potential $V_{LS}\vec{\ell}\cdot\vec{s}$ is given approximately by

$$V_{LS} \approx \frac{1}{2m^2 r}\frac{d}{dr}\left[(U_V - U_S) + 2\frac{f}{g}U_V\right] \approx \frac{1 + f/g}{m^2 r}U_V' \quad , \tag{2}$$

where f/g is the tensor to vector ratio of vector field couplings. On the r.h.s. we approximated $U_s \approx -U_v$ as following from the smallness of V_c with respect to the hyperon mass m. The quark model limits for f/g are 0 for N and -1 for Λ, and hence $V_{LS}(\Lambda)$ vanishes in this limit. More realistic OBE estimates [11] give a nonzero value, $V_{LS}(\Lambda)/V_{LS}(N) \sim 0.2$. An accurate determination of ε_Λ is due from the measurements [12] of $E1$ γ rays expected to deexcite the p_j spin-orbit doublet levels of $^{13}_{\Lambda}$C mentioned above. Another set of related measurements could be done by populating $^{12}_{\Lambda}$B $p(\Lambda)$ particle-stable levels via the reaction $^{12}C(K^-,\pi^0)^{12}_{\Lambda}B$ and looking for γ rays [13]. These will shed light on several other ΛN spin dependence parameters.

2.2 spin-spin.

The only direct measurement of a spin-spin splitting was done in the isodoublet $^{4}_{\Lambda}$He - $^{4}_{\Lambda}$H by observing [14] the $M1$ γ rays $1^+ \to 0^+$ of about $\Delta_s \approx 1$ MeV between the levels based on the core nucleus. It is not clear to what extent [15] the spin-spin splittings for $s(\Lambda)$ in the p shell are related to Δ_s by applying shell model considerations [16], [17].

Several searches [9], [18] for γ rays between levels split dominantly by the spin-spin ΛN interaction (notably in ${}^{7}_{\Lambda}$Li and ${}^{10}_{\Lambda}$B) have been unsuccessful. A promising candidate hypernucleus would be ${}^{9}_{\Lambda}$Li. The g.s. doublet $M1$ transition $5/2 \rightarrow 3/2$ could be looked for at CEBAF by populating the spin-flip $5/2^+$ level in the reaction [19] ^{9}Be(e, eK^+)${}^{9}_{\Lambda}$Li. The (K^-, π^0) reaction, although not expected to populate this level, will lead to a normal detection rate for the above $M1$ transition by populating the $5/2^+$ level indirectly, through a cascade γ ray from the higher $3/2^{+*}$ level [13]. In fact, a spin-flip γ ray will follow such a cascade even if the order of g.s. doublet levels is inverted with respect to that expected.

2.3 intershell configuration mixing.

The ${}^{12}_{\Lambda}$C spectrum measured recently in the (π^+, K^+) reaction at KEK [2] shows in addition to the known $s(\Lambda)\times{}^{11}$C 1^- ground state and $p(\Lambda)\times{}^{11}$C 2^+ states at 10.7 MeV also two new excitations, at 2.6 ± 0.2 MeV and at 6.9 ± 0.4 MeV. In this excitation range, a natural assignment consists of $s(\Lambda)\times{}^{11}$C $(J_c = 1/2^-, 3/2^-)1^-$ core-excited states where the former state is presumed to arise dominantly from $s(\Lambda)\times{}^{11}$C $(1/2^-$; 2.00 MeV), but the latter state is spaced away too far from the location expected for the next negative-parity core excited $s(\Lambda)\times{}^{11}$C $(3/2^-$; 4.80 MeV) state. Here we conjecture [20] that the 6.9 MeV ${}^{12}_{\Lambda}$C excitation is populated via $p(\Lambda)\times{}^{11}$C 2^+ admixtures into the dominant $s(\Lambda)\times{}^{11}$C $(J_c = 5/2^+, 3/2^+)$ 2^+ core-excited states, where the positive-parity ^{11}C core states lie at 6.90 and 7.50 MeV respectively. The intershell mixing mechanism involves ΛN interaction matrix elements of the type $< s(\Lambda)d(N)|V(\Lambda N)|p(\Lambda)p(N) >$, in addition to the constraint imposed by the conservation of CM motion. The same mixing mechanism is also responsible for proton emission from the $p(\Lambda)\times{}^{11}$C configuration [21] into low-lying states of ${}^{11}_{\Lambda}$B [22]. A careful combined analysis of these two problems should yield valuable information on the configuration mixing properties of the ΛN interaction.

3 – The $\Lambda N \rightarrow NN$ weak interaction

The weak-interaction nonmesonic decay process $\Lambda N \rightarrow NN$ has attracted considerable interest, particularly since a combined analysis [23] of all existing data for $A = 4, 5$ hypernuclei indicated that the $\Delta I = 1/2$ rule might be badly broken. If confirmed, this would be the first example of such a breakdown in nonleptonic weak interactions. However, the data collected so far, including the recently measured [24] partial decay rates $\Gamma_n = \Gamma(\Lambda n \rightarrow nn)$ and $\Gamma_p = \Gamma(\Lambda p \rightarrow np)$, for ${}^{4}_{\Lambda}$He produced in ^{4}He(K^-, π^-), do not provide a direct test. In due course it will become possible to measure the corresponding rates for ${}^{4}_{\Lambda}$H, produced in ^{4}He(K^-, π^0). The $\Delta I = 1/2$

rule predicts

$$\Gamma_n\left({}^{4}_{\Lambda}\mathrm{He}\right)/\Gamma_p\left({}^{4}_{\Lambda}\mathrm{H}\right) = 2 \tag{3}$$

for transitions which, owing to $J^\pi = 0^+$ for these hypernuclei, originate from ${}^1S_0$ ΛN states: ${}^1S_0 \to {}^1S_0 + {}^3P_0$. These transitions, which are relatively insignificant within OBE calculations [25], assume substantial strengths once evaluated by quark induced diagrams, and the corresponding calculations [26] suggest a strong departure from the $\Delta I = 1/2$ rule eq. (3).

By measuring the neutron stimulated rates in both ${}^{4}_{\Lambda}$He and ${}^{4}_{\Lambda}$H, it is possible to isolate the contribution due to the ${}^3S_1 \to {}^3P_1$ parity violating amplitude:

$$3\Gamma_n({}^3S_1 \to {}^3P_1) = 2\Gamma_n({}^{4}_{\Lambda}\mathrm{H}) - \Gamma_n({}^{4}_{\Lambda}\mathrm{He}) \quad . \tag{4}$$

Note that this expression does not require the $\Delta I = 1/2$ rule to be satisfied. The same $\to {}^3P_1$ amplitude also gives rise to a weak-decay asymmetry (measured [27] at KEK) $W(\theta) = 1 + A\cos\theta$ with $A \sim$ Re $[{}^3P_1({}^3S_1 + {}^3D_1)^*]$, where $\to {}^3S_1, {}^3D_1$ are the parity conserving amplitudes interfering with $\to {}^3P_1$ for initial ${}^3S_1$ ΛN states.

4 – Density dependence of the Σ nuclear potential

Σ hypernuclei largely remain *terra incognita*. There are lingering doubts about the extraction of peaks in past $(K^-, \pi^\pm)$ experiments for $A \geq 6$ and whether or not such peaks represent excitations involving relatively narrow Σ single particle bound states [28]. Most of the experimental effort in the past seven years has been devoted to a study of light Σ hypernuclear systems accessible in $(K^-, \pi^\pm)$ reactions on He targets [29]. The only positive signal, established both in capture at rest at KEK and in flight at BNL, is a $I = 1/2$ ${}^1S_0$ bound state of ${}^{4}_{\Sigma}$He. This came as a surprise since the width expected for this state was sizable, but in fact Harada *et al.* [30] had predicted a relatively narrow bound state of this kind owing to the presence of an inner repulsive component for $V_\Sigma(r)$ which pushes the wavefunction out, thus reducing the anticipated width. Batty *et al.* [3] have recently reanalyzed the full data set of Σ^- atoms: level shifts, widths and yields, in order to constrain the density dependence of $V_\Sigma(r)$. By introducing a phenomenological density dependence of the form

$$V_\Sigma(r) \sim [b_0 + B_0\,(\rho(r)/\rho(0))^\alpha]\,\rho(r) \quad , \qquad \alpha > 0 \quad . \tag{5}$$

and fitting the parameters b_0, B_0 and α to the data, greatly improved fits to the data are obtained. The complex parameter b_0 may be identified with the spin-averaged $\Sigma^- N$ scattering length. For the best-fit isoscalar potentials, Re V_Σ is attractive at low densities outside the nucleus, changing into repulsion in the nuclear surface region, as shown in fig. 1. The precise magnitude and shape of the repulsive component within the nucleus is not determined by the atomic data. It is interesting to note that such density dependent potentials do not produce bound states, and this conclusion is in agreement with the recent experimental search for Σ hypernuclear peaks at BNL [31].

Recently, it was shown by Mares *et al.* [32] that by treating the Σ-nucleus interaction potential in the framework of Dirac Phenomenology, with scalar (σ) and vector (ω, ρ) meson mean fields, and fitting its parameters to the relatively accurate Σ^- atom shift and width data in Si and in Pb, the obtained potential fits very well the whole body of data on Σ^- atoms. This potential, which is generally attractive far outside the nucleus, becomes repulsive at the nuclear surface and remains so in most of the acceptable fits. The recent Pb data [33] are particularly important in pinning down the isovector component of the potential which is sizable and which, for Σ^-, acts against nuclear binding in core nuclei with $N - Z > 0$, countering the attractive Coulomb interaction. On the other hand, for very light nuclear cores and perhaps only for $A = 4$ hypernuclei, this isovector component (Lane term) generates binding of Σ^+ configurations. In summary, all of these recent theoretical studies [3], [32] support the presence of a substantial repulsive component in the Σ-nucleus potential which to a various degree excludes Σ-nuclear binding, except perhaps for very special cases such as ${}^4_\Sigma$He [29], [30].

5 – Strangeness = −2 physics

Comparatively little is known about $S = -2$ systems. There are only three candidates [34] for $\Lambda\Lambda$ hypernuclei based on events seen in emulsion experiments with K^- beams, and their binding energies are consistent with a strongly attractive $\Lambda\Lambda$ interaction in the ${}^1S_0$ channel [35]. There are also a few other events attributed to the formation of Ξ hypernuclei [36], but convincing evidence is still lacking. Active experimental programs are underway at KEK and at BNL to study the double strangeness exchange reaction (K^-, K^+) on nuclear targets, following a first stage of searching for the H dibaryon. A spectrum measured [37] at KEK for incident momentum 1.65 GeV/c on Cu, for example, and K^+ observed in the forward direction is shown in fig. 2. The peak about $p(K^+) = 1.1$ GeV/c is due to the quasifree process $K^- p \to K^+ \Xi^-$. Similar data have been published [37] for several other nuclear targets, from C to Pb. The relatively low intensity of this K^- beam at present

is insufficient for identifying possible structure in the Ξ hypernuclear bound state region. In emulsion target the Ξ^- track is often traced down to a stopping point where it is captured by a nucleus, dominantly from an atomic state; however, Ξ^- capture at rest is *not* a promising way to produce Ξ hypernuclei. For $\Lambda\Lambda$ hypernuclei, it will lead mostly to excited, particle-unstable $\Lambda\Lambda$ configurations, except for very light species, with branching rates typically given by 1% or less [39]. Capture at rest could be a useful way to produce the *lightest* possibly bound $\Lambda\Lambda$ hypernuclei, such as

$$\Xi^- + {}^6\mathrm{Li} \rightarrow {}^{\;\;6}_{\Lambda\Lambda}\mathrm{He} + n \quad , \quad {}^{\;\;5}_{\Lambda\Lambda}\mathrm{H} + d \quad , \quad {}^{\;\;4}_{\Lambda\Lambda}\mathrm{H} + t \quad . \tag{6}$$

The rate calculated [39] for ${}^{\;\;6}_{\Lambda\Lambda}\mathrm{He}$ is relatively high, ~3%, but the neutron signal detection efficiency could be disturbingly low due to background low-energy neutrons from π^- absorption in the target. The lightest bound ${}^{\;\;4}_{\Lambda\Lambda}\mathrm{H}$ could also be produced in $\Xi^- + {}^4\mathrm{He} \rightarrow {}^{\;\;4}_{\Lambda\Lambda}\mathrm{H} + n$ [40]. Experiment 885 at the AGS is looking for similar reactions in a ${}^{12}\mathrm{C}$ target [41].

A potentially more general, and perhaps promising procedure for producing $S = -2$ bound nuclear systems is to use the (K^-, K^+) reaction in flight which is assumed to proceed via the underlying one-step process $K^- p \rightarrow K^+ \Xi^-$. Recently, Dover, Gal and Millener [5] have considered the mixing of Ξ hypernuclear states, produced via K^- induced reactions on p-shell nuclear targets, with $\Lambda\Lambda$ hypernuclear states. They pointed out that Ξ admixtures into the low-lying $\Lambda\Lambda$ states introduce an amplitude for populating $\Lambda\Lambda$ hypernuclear states in a one-step direct reaction process. This amplitude could conceivably be considerably larger than, and possibly interfere constructively with, the rather small amplitude for two-step production of two Λ's via, for example, the $(K^-, \pi^0)(\pi^0, K^+)$ process [42]. On the other hand, it is the $\Lambda\Lambda$ admixtures in the Ξ state which give the state its decay width into single Λ, nucleon and other channels.

The energies of the most important Ξ^- and $\Lambda\Lambda$ weak-coupling basis states and the relevant decay channels are given in fig. 3 for the specific case of a ${}^{12}\mathrm{C}$ target, with the energies measured with respect to the ${}^{\;\;12}_{\Lambda\Lambda}\mathrm{Be}$ ground state which is bound with respect to the $\Lambda + \Lambda$ threshold by $B_{\Lambda\Lambda}$ where

$$B_{\Lambda\Lambda} = 2B_\Lambda({}^{11}_{\Lambda}\mathrm{Be}) + \Delta B_{\Lambda\Lambda} \quad . \tag{7}$$

$\Delta B_{\Lambda\Lambda}$ is the interaction energy of a pair of Λ particles in the ${}^1S_0$ state and is around 4.5 MeV for the three known examples of $\Lambda\Lambda$ hypernuclei [34], [35]. The ${}^{11}\mathrm{B} + \Xi^-$ threshold is a further $28.3 - S_p({}^{11}\mathrm{B}) = 17.1$ MeV above the ${}^{10}\mathrm{Be} + \Lambda + \Lambda$ threshold. The binding energy of the 0s (0p) Ξ^- state is about 10.7 (1.5) MeV for the Ξ^- nucleus potential of Dover and Gal [36], which has a Woods-Saxon form with a well

depth of 24 MeV for $r_0 = 1.1$ fm and $a = 0.65$ fm. In the weak-coupling limit, the (K^-, K^+) reaction will populate the Ξ^- states in proportion to the proton pickup spectroscopic factor relating the target and core states. For no spin-flip, the 0s states will have spin-parity 1^- and two 0p 2^+ states will be most strongly produced, with equal cross sections in the weak-coupling limit. In practice, the 2^+ states will be mixed and separated by about an MeV depending on the ΞN interaction strength and the Ξ spin-orbit splitting, which is of the same order as the expected widths of the states.

The $\Lambda\Lambda$ admixtures into the Ξ state, by conversion on a $0s$- or $0p$-shell proton, give rise to decay amplitudes into the single-baryon escape channels shown at the left of fig. 3. The lowest threshold is for neutron emission, as will generally be the case since the transformation of two protons from the p-shell target nucleus leaves a neutron-rich $A-2$ core for the $\Lambda\Lambda$ hypernucleus. The $\Lambda\Lambda$ states which are most important for $\Xi^- p \rightarrow \Lambda\Lambda$ conversion from the $0s$ Ξ^- hypernuclear ground state are shown at the right in fig. 3. In the case of $0s0p \rightarrow 0s0p$ $\Xi^- p \rightarrow \Lambda\Lambda$ conversion, the $0p$ proton parentage of the ^{11}B ground state is spread over four ^{10}Be levels, and the energy denominators, ΔE_p in fig. 3, for perturbative estimate of the admixtures then range from $\sim$22 to $\sim$12 MeV. Similarly, the energy separation ΔE_s between the $^{12}_{\Xi}$Be $0s$ state and the centroid of the s^2_Λ configurations based on the $0s$ proton hole strength in ^{11}B is given by

$$\Delta E_s = 28.3 + B_{\Lambda\Lambda} - S_s(^{11}\mathrm{B}) - B_{\Xi^-} \simeq 10 \text{ MeV} \qquad (8)$$

The width estimates are obtained by concentrating the $0s$ hole strength at its centroid energy and making a perturbative calculation of the admixture of the $\Lambda\Lambda$ state based on this pure $0s$-hole state.

For the Ξ hypernuclear ground state Millener *et al.* [5] find a p-wave neutron emission width of order 0.6 MeV and a similar p-wave Λ emission width. The large p-wave neutron width is at odds with the calculation of ref. [4]. It leads to decays entirely into $s_\Lambda p_\Lambda$ states in $^{11}_{\Lambda\Lambda}$Be which are expected then to decay electromagnetically into the s^2_Λ configuration and finally into the s^2_Λ ground state. The direct formation of the s^2_Λ configuration proceeds slower, associated with a smaller $(s-d)$ neutron width of about 0.15 MeV, while the authors of ref. [4] calculate it to be as much as four times bigger. For the 2^+ Ξ hypernuclear states, Millener *et al.* [5] find a neutron emission width of about 1.1 MeV and Λ emission width of about twice that much. These, and in particular the neutron width, are considerably larger than those calculated in ref. [4]. The largest contribution to the width is for decays into p^2_Λ states. We therefore conclude that if the (K^-, K^+) reaction could be applied with a resolution of $\sim$2 MeV, there should exist Ξ hypernuclear states

sufficiently narrow for study, particularly aiming at the detection of their dominant neutron decay modes which would lead to identifiable $\Lambda\Lambda$ hypernuclear states in the daughter hypernucleus.

Another interesting feature of the K^+ momentum spectrum [37] shown in fig. 2 is the presence of a low momentum broad peak centered around 600 MeV/c. The $(K^-,\ K^+)$ cross section residing in the low momentum peak is far greater than that anticipated on the basis of second order strong processes, for instance $K^-p \to \pi^0\Lambda$ followed by $\pi^0 p \to K^+\Lambda$. This peak was interpreted by Gobbi *et al.* [38] as due to the one-step production and decay sequences

$$K^- + p \to M + \Lambda \quad , \qquad M \to K^+ + K^- \tag{9}$$

taking place on a proton embedded in a nuclear target. Here the meson M is a scalar $[f_0(975)$ or $a_0(980)]$ or a vector $[\varphi(1020)]$. This hypothesis was shown [38] to be approximately consistent with the shape of the K^+ spectrum, its integrated cross section and the A^α dependence observed for the (K^-, K^+) cross section on targets of mass number A. The production of the a_0 and f_0 mesons is estimated to contribute about one half of the K^+ peak at low momentum. A rapid energy dependence of the low momentum component of the (K^-, K^+) cross section in the region $p_{K^-} = 1.4 - 2$ GeV/c is predicted as one passes through the free space thresholds for the $K^-p \to M\Lambda$ reactions. Nuclear Fermi motion lowers the effective threshold for φ production to about $1.35 - 1.4$ GeV/c. The rapid p_{K^-} dependence of the $(K^-,\ K^+)$ cross section in the region of low K^+ momentum is a principal signature of the $K^-p \to M\Lambda$ mechanism. This merits an experimental test. The A dependence of the separate meson contributions will be instrumental in determining the MN cross section in the medium and thus test models in which the mesons M are more appropriately described by a quasi-molecular structure than by a quark-antiquark structure.

Lastly, we comment on the search for strange dibaryons. These are color-singlet configurations of six quarks, which for the lowest states possible are all in a $0s_q$ state, that cannot be separated asymptotically into two ordinary baryons. However, 20% of the wavefunction admits such a separation, and it is this coupling between the inner region $(r < r_0)$ where quark variables prevail and the outer region $(r > r_0)$ where baryonic variables prevail which is missing from early treatments of exotics via $6q$ bags. Lomon and collaborators [43] have used the R-matrix method to connect smoothly between the two regions. A key point in their work is the choice of $r_0 \sim 1.1$ fm, compared to $r_{eq} \sim 1.3$ fm, where r_{eq} is the appropriate equilibrium radius of the MIT $6q$ bag; in fact, it can be shown that $r_0 < r_{eq}$ must hold, and this means that unless the contribution from the outer region is overwhelmingly

attractive, the R-matrix calculation will give higher masses than the pure bag calculation. For $S = -2$, the lowest mass dibaryon predicted [43] is the H, a flavor-singlet 0^+ configuration [44] which in the SU(3) limit admits asymptotically the (20%) BB combination

$$\left(\sqrt{1/8}\right)\Lambda\Lambda + \left(\sqrt{1/2}\right)\Xi N + \left(\sqrt{3/8}\right)\Sigma\Sigma \quad . \tag{10}$$

Dover and Feshbach [45] argued on general grounds that the BB interaction is repulsive for eq. (10). The calculation by Lomon [43] places the H about 120-150 MeV above the $\Lambda\Lambda$ threshold, rather than the previously expected bound state. For $S = -1$, no stable dibaryons are predicted either. A check on Lomon's methodology is that for $S = 0$ it closely reproduces the $^1S_0$ dibaryon signal at $M = 2.735$ GeV ($\Gamma = 17$ MeV) recently observed at Saturne in the angular dependence of pp elastic scattering spin correlation [46].

6 – Strange hadronic matter

It has been speculated [47] that states of quark matter ("strangelets") with large strangeness per baryon ($|S|/A \sim 1$) might be even more stable at $\rho \sim 2\rho_0$ than normal nuclei. The existence of stable strangelets could have significant ramifications in astrophysics and for relativistic heavy-ion collisions. A number of experiments are underway to search for such multi-strange objects. Strangelets are objects in which the u, d, s quarks (in approximately equal numbers) are confined to a single large bag, where the parameters of the bag (radius, pressure) were extrapolated [48] from those fitted to a single baryon ($A = 1$). As mentioned in the last section, such an extrapolation apparently fails already for $A = 2$. It is inconceivable that for as low densities as $\rho \sim 2\rho_0$ (with respect to $\rho \sim 5\rho_0$ for which chiral symmetry may be restored, at $T = 0$) the coupling to hadronic degrees of freedom could be disregarded.

Recently, Schaffner *et al.* [6] considered bound states of nucleons (p, n) and hyperons (Λ, Ξ^-, Ξ^0) where the binding arises from attractive mean fields. In this case, the strange quarks are localized within individual hyperons which are assumed to retain their identity in the bound system. By using an extension of the relativistic mean field (RMF) theory, the existence of a broad class of multiply strange nuclei is predicted, with density $\rho \sim 2\rho_0$, strangeness fraction $f_s = |S|/A \sim 1$ and charge fraction $f_q = Q/A \sim 0$, comparable to the properties of hypothesized strange quark matter. The extension of the RMF to $S \neq 0$ systems is constrained by the known properties of $S = 0, -1, -2$ nuclear and hypernuclear systems. The binding energy calculated, between 12 to 22 MeV per baryon, depends on the model used for

the unknown hyperon-hyperon interactions, the lower limit holding for the case in which these interactions are ignored. The upper limit obtains for hyperon-hyperon interaction strengths as extrapolated from the Nijmegen model D, and normalized to the strength of the $\Lambda\Lambda$ interaction as determined from the few $\Lambda\Lambda$ hypernuclear binding energies known to date [34]. It was found that the existence of strong-interaction stable strange hadronic matter (SHM) is assured over a wide range of choices for the coupling constants.

The key point missed by all past works which have studied multi-Λ hypernuclei is that, beyond some number of Λ's (already for $|S|/A < 0.2$), the following instability occurs:

$$\Lambda + \Lambda \rightarrow \Xi^- + p \quad , \qquad \Xi^0 + n \quad . \tag{11}$$

Because of binding effects, reaction (11) can induce a strong decay of the many-body system, even though the reverse reactions $\Xi N \rightarrow \Lambda\Lambda$ proceed with sizable energy release of about 25 MeV in free space. Therefore, SHM necessarily includes a mixture of Λ's and Ξ's, such that the decays of eq. (11) are Pauli blocked in both directions. We note that SHM remains stable against strong interactions in the bulk limit ($A \rightarrow \infty$), owing to the tendency of Ξ^-'s and protons to occupy similar orbits so as to minimize the total Coulomb repulsion.

In fig. 4, baryon-emission stability domains for multi-strange nuclei with $A = 100$ are given in the (f_s, f_q) plane. These domains were calculated [49] by applying generalized Bethe-Weizsäcker formulae [50], assuming that there is a minimum number (here 8) of baryons of each species for which the underlying Fermi gas considerations still hold. Such formulae reproduce fairly well the binding energies calculated in the RMF model. The main domain (roughly parallelogram), representing SHM, is centered about $f_s \sim 1, f_q \sim 0$. The other domains stand for subclasses of SHM such as multi-Λ hypernuclei ($\{p, n, \Lambda\}$), or purely hyperonic nuclei ($\{\Xi^0, \Xi^-, \Lambda\}$) which require strong hyperon-hyperon forces for binding. These separate domains are disconnected from each other, the area between them corresponding to cases where for at least one of the species the number of constituents is smaller than the minimum chosen. Only for multi-Λ hypernuclei does one know from realistic microscopic calculations that its domain evolves continuously as function of f_s and f_q from ordinary nuclei, represented here by a portion of the f_q axis.

SHM is always unstable to weak decays. The associated lifetimes could be shorter than the 10^{-10} sec normal scale for hyperons. Most of the searches reported until now could not have detected such short lived objects. As far as laboratory production, it appears unthinkable at present to produce medium-heavy to heavy species in relativistic heavy-ion collisions. The lightest species ${}_{\Xi^0\Lambda\Lambda}{}^{7}\mathrm{He}$ could become accessible [51] in due course.

References

1. Nucl. Phys. **A585** (1995).
2. T. Hasegawa *et al.*, Phys. Rev. Lett. **74**, 224 (1995).
3. C.J. Batty, E. Friedman and A. Gal, Phys. Lett. **B335**, 273 (1994); Prog. Theor. Phys. Suppl. **117**, 227 (1994).
4. K. Ikeda, T. Fukuda, T. Motoba, M. Takahashi and Y. Yamamoto, Prog. Theor. Phys. **91**, 747 (1994); Y. Yamamoto, T. Motoba, T. Fukuda, M. Takahashi and K. Ikeda, Prog. Theor. Phys. Suppl. **117**, 281 (1994); M. Takahashi, Y. Yamamoto, T. Motoba and K. Ikeda, Phys. Rev. **C51**, 2196 (1995).
5. C.B. Dover, A. Gal and D.J. Millener, Nucl. Phys. **A572**, 85 (1994); D.J. Millener, C.B. Dover and A. Gal, Prog. Theor. Phys. Suppl. **117**, 307 (1994).
6. J. Schaffner, C.B. Dover, A. Gal, C. Greiner and H. Stöcker, Phys. Rev. Lett. **71**, 1328 (1993); Ann. Phys. **235**, 35 (1994).
7. Y. Yamamoto, A. Reuber, H. Himeno, S. Nagata and T. Motoba, Czech J. Phys. **42**, 1249 (1992); T. Motoba and Y. Yamamoto, in Ref. [1] p. 29c.
8. M. May *et al.*, Phys. Rev. Lett. **47**, 1106 (1981).
9. M. May *et al.*, Phys. Rev. Lett. **51**, 2085 (1983).
10. B.K. Jennings, Phys. Lett. **B246**, 325 (1990).
11. C.B. Dover and A. Gal, Prog. Part. Nucl. Phys. **12**, 171 (1984).
12. M. May, private communication.
13. R.H. Dalitz and A. Gal, Ann. Phys. **116**, 167 (1978).
14. A. Bamberger *et al.*, Nucl. Phys. **B60**, 1 (1973); M. Bedjidian *et al.*, Phys. Lett. **83B**, 252 (1979); **94B**, 480 (1980).
15. B.F. Gibson, Phys. Rev. **C49**, R1768 (1994).
16. D.J. Millener, A. Gal, C.B. Dover and R.H. Dalitz, Phys. Rev. **C31**, 499 (1985).
17. V.N. Fetisov, L. Majling, J. Zofka and R.A. Eramzhyan, Z. Phys. **A339**, 399 (1991).

18. R.E. Chrien *et al.*, Phys. Rev. **C41**, 1062 (1990).

19. C.B. Dover and D.J. Millener, in: Modern Topics in Electron Scattering, Eds. B.-Frois and I. Sick, World Scientific (Singapore, 1991) p. 608.

20. D.J. Millener, A. Gal and C.B. Dover (in preparation).

21. R.H. Dalitz, D.H. Davis and D.N. Tovee, Nucl. Phys. **A450**, 311c (1986).

22. A. Gal, Phys. Rev. **C28**, 2186 (1983).

23. R.A. Schumacher, Nucl. Phys. **A547**, 143c (1992).

24. R.A. Schumacher for the BNL E788 Collaboration, in: Properties and Interactions of Hyperons, Eds. B.F. Gibson, P.D. Barnes and K. Nakai, World Scientific (Singapore, 1994) p. 85.

25. B.R. Holstein, these Proceedings.

26. M. Oka, T. Inoue and S. Takeuchi, in: Properties and Interactions of Hyperons, Eds. B.F. Gibson, P.D. Barnes and K. Nakai, World Scientific (Singapore, 1994) p. 119; K. Maltman and M. Shmatikov, Phys. Lett. **B331**, 1 (1994), and in Ref. [1] p. 343c.

27. S. Ajimura *et al.*, Phys. Lett. **B282**, 293 (1992); T. Kishimoto *et al.*, in Ref. [1] p. 205c.

28. C.B. Dover, D.J. Millener and A. Gal, Phys. Rep. **184**, 1 (1989).

29. R.S. Hayano *et al.*, Phys. Lett. **B231**, 355 (1989); R.S. Hayano, Nucl. Phys. **A547**, 151c (1992); M. Barakat and E.V. Hungerford, *ibid.*, 157c.

30. T. Hararda, S. Shinmura, Y. Akaishi and H. Tanaka, Nucl. Phys. **A507**, 715 (1990); T. Harada and Y. Akaishi, Phys. Lett. **B234**, 455 (1990); **B262**, 205 (1991).

31. R. Sawafta for the BNL E887 Collaboration, in Ref. [1] p. 103c, and in these Proceedings.

32. J. Mares, E. Friedman, A. Gal and B.K. Jennings, submitted for publication.

33. R.J. Powers *et al.*, Phys. Rev. **C47**, 1263 (1993).

34. M. Danysz *et al.*, Nucl. Phys. **49**, 121 (1963); D.J. Prowse, Phys. Rev. Lett. **17**, 782 (1966); S. Aoki *et al.*, Prog. Theor. Phys. **85**, 1287 (1991).

35. R.H. Dalitz *et al.*, Proc. R. Soc. London **A246**, 1 (1989); C.B. Dover, D.J. Millener, A. Gal and D.H. Davis, Phys. Rev. **C44**, 1905 (1991); Y. Yamamoto, H. Takaki and K. Ikeda, Prog. Theor. Phys. **86**, 867 (1991); H. Himeno, T. Sakuda, S. Nagata and Y. Yamamoto, *ibid.* **89**, 109 (1993).

36. C.B. Dover and A. Gal, Ann. Phys. **146**, 309 (1983).

37. T. Iijima *et al.*, Nucl. Phys. **A546**, 588 (1992).

38. C. Gobbi, C.B. Dover and A. Gal, Phys. Rev. **C50**, 1594 (1994).

39. D. Zhu, C.B. Dover, A. Gal and M. May, Phys. Rev. Lett. **67**, 2268 (1991).

40. I. Kumagai-Fuse, T. Koike and Y. Akaishi, in Ref. [1] p. 367c.

41. G.B. Franklin, in Ref. [1] p. 83c.

42. A.J. Baltz, C.B. Dover and D.J. Millener, Phys. Lett. **123B**, 9 (1983).

43. E.L. Lomon, in: High-Energy Spin Physics, Minneapolis, 1988, AIP Conf. Proc. **187**, Ed. K.J. Heller (NY, 1989) p. 630; W.R. Greenberg and E.L. Lomon, Phys. Rev. **D47**, 2703 (1993); E.L. Lomon, in: Workshop on Future Directions in Particle and Nuclear Physics at Multi-GeV Hadron Beam Facilities, BNL, March 1993, Ed. D.F. Geesaman, BNL 52389 (1993).

44. R.L. Jaffe, Phys. Rev. Lett. **38**, 195 (1977); 617(E).

45. C.B. Dover and H. Feshbach, Ann. Phys. **198**, 321 (1990).

46. J. Ball *et al.*, Phys. Lett. **B320**, 206 (1994).

47. E. Witten, Phys. Rev. **D30**, 272 (1984).

48. E. Farhi and R.L. Jaffe, Phys. Rev. **D30**, 2379 (1984); **32**, 2452 (1985).

49. S. Balberg, A. Gal and J. Schaffner, Prog. Theor. Phys. Suppl. **117**, 325 (1994).

50. C.B. Dover and A. Gal, Nucl. Phys. **A560**, 559 (1993).

51. A.J. Baltz, C.B. Dover, S.H. Kahana, Y. Pang, T.J. Schlagel, E. Schnedermann, Phys. Lett. **B325**, 7 (1994).

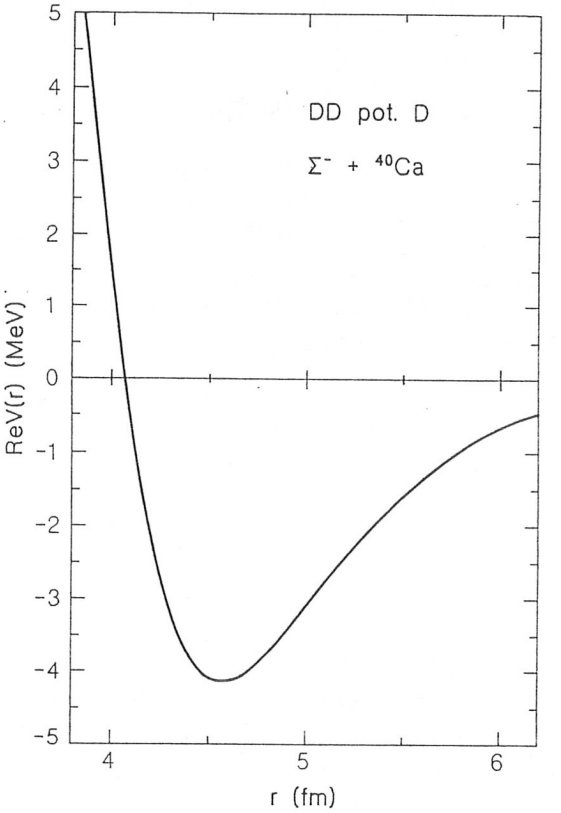

Figure 1: Re $V_\Sigma(r)$ at the nuclear surface as fitted [3] to the Σ^- atom data.

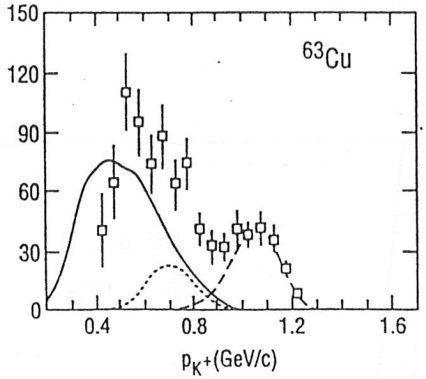

Figure 2: The spectrum of forward K^+ in the (K^-, K^+) reaction [37] at 1.65 GeV/c on Cu. The curves show (from right to left) the calculated contributions [38] due to Ξ, Ξ^* and mesons of hidden strangeness.

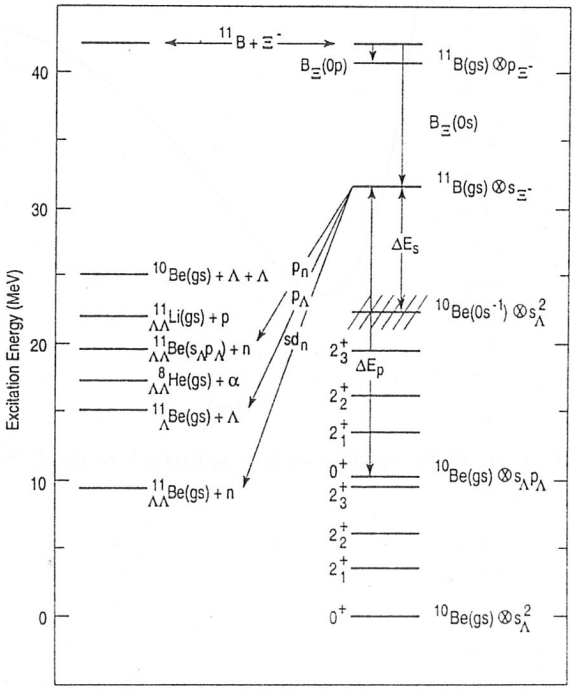

Figure 3: Energy spectrum and decay thresholds for Ξ and $\Lambda\Lambda$ hypernuclear configurations for the case of a ^{12}C target [5].

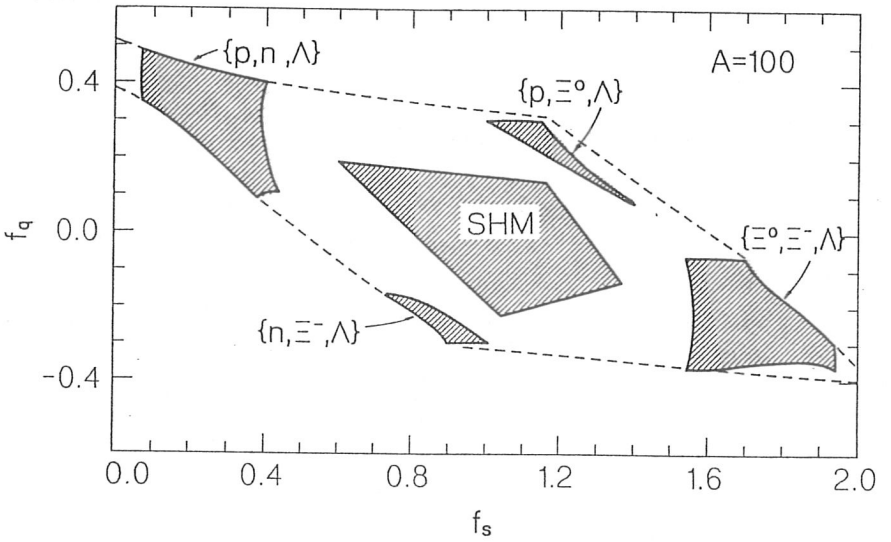

Figure 4: Baryon emission stability domains calculated by using the generalized Bethe-Weizsäcker formula [49], [50] for multi-strange nuclei with $A = 100$.

WEAK HYPERNUCLEAR DECAY

Barry R. Holstein
Department of Physics and Astronomy
University of Massachusetts
Amherst, MA 01003
and
Institute for Nuclear Theory
Department of Physics, NK-12
University of Washington
Seattle, WA 98195

ABSTRACT

Because of Pauli suppression effects the $N\pi$ decay mode of the free Λ is not of importance in hypernuclei with $A \geq 10$. Rather the decay of such hypernuclei proceeds via the nucleon-stimulated mode $\Lambda N \to NN$, analysis of which presents a considerable theoretical challenge and about which there exists only a limited amount of experimental information. Herein we confront existing data with various theoretical analyses which have been developed.

1 – Introduction to Hypernuclear Decay

The properties of the lambda hyperon are familiar to all of us. Having a mass of 1116 MeV, zero isospin and unit negative strangeness, it decays nearly 100% of the time via the nonleptonic mode $\Lambda \to N\pi$ and details can be found in the particle data tables [1]

$$\Gamma_\Lambda = \frac{1}{263\text{ps}} \qquad \text{B.R.}\,\Lambda \to \begin{cases} p\pi^- & 64.1\% \\ n\pi^0 & 35.7\% \end{cases} \tag{1}$$

The decay can be completely described in terms of an effective Lagrangian with two phenomenological parameters

$$\mathcal{H}_w = g_w \bar{N}(1 + \kappa\gamma_5)\boldsymbol{\tau} \cdot \boldsymbol{\phi}_\pi \Lambda \tag{2}$$

where $g_w = 2.35 \times 10^{-7}, \kappa = -6.7$ and Λ is defined to occupy the lower entry of a two component column spinor. The kinematics are such that for decay at rest the final state nucleon emerges with energy about 5 MeV, which means that the corresponding momentum is $p_N = \sqrt{2M_N E_N} \approx 100$ MeV.

Now, however, consider what happens if the Lambda is bound in a hypernucleus. [2] In this case, even neglecting binding energy effects, the 100 MeV

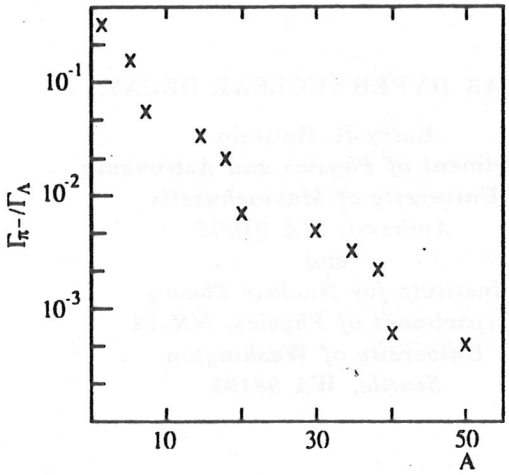

Figure 1: Calculated ratio of pionic hypernuclear decay to free lambda decay rate.

momentum of the outgoing nucleon is generally much less than the Fermi momentum of the nucleus so that the decay will be Pauli blocked. A very simple estimate of this effect can be generated within a simple Fermi gas model, wherein, neglecting any effects of binding energy or of wavefunction distortion, one finds

$$\frac{1}{\Gamma_\Lambda}\Gamma_\pi = 1 - \frac{1}{2}\sum_{nj\ell} N_{nj\ell}\langle nj\ell|j_\ell(k_\pi r)|1S_{\frac{1}{2}}\rangle \tag{3}$$

with $N_{nj\ell}$ being the occupation number for the indicated state. The result of this calculation reveals that the importance of such pionic decays rapidly falls as a function of nuclear mass—

$$\frac{1}{\Gamma_\Lambda}\Gamma_\pi \sim \begin{cases} A = 10 & A = 25 & \ldots \\ 1/20 & 1/120 & \ldots \end{cases} \tag{4}$$

However, while the existence of the nuclear medium suppresses the $N\pi$ mode, it also opens up a completely new possibility, that of the nucleon-stimulated decay—$\Lambda N \rightarrow NN$. Assuming that the energy is shared equally between the outgoing pair of nucleons one has then $E_N \simeq \frac{1}{2}(m_\Lambda - m_N) \approx 90MeV$. The corresponding momentum is $p_N \sim 400MeV$ and is well above the Fermi momentum, so that Pauli suppression is not relevant. According to the above arguments the importance of this nonmesonic (NM) mode compared to its mesonic counterpart should rapidly increase with A, and this expectation is fully borne out experimentally, as shown in Figure 1. A theory of hypernuclear weak decay then has basically nothing to do with the pionic mode favored by a free Λ and must deal with the much more complex $\Lambda N \rightarrow NN$ process. [3] The observables which can be measured experimentally and should be predicted by theoretical analysis include

	${}^{5}_{\Lambda}$He	${}^{11}_{\Lambda}$B	${}^{12}_{\Lambda}$C
$\frac{1}{\Gamma_\Lambda}\Gamma_{NM}$	0.41 ± 0.14	$1.25 \pm 0.16^*$	1.14 ± 0.20
$\Gamma_{NM}(p/n)$	1.07 ± 0.58	$0.96^{+0.8}_{-0.4}$	$0.75^{+1.5}_{-0.35}$

Table 1: Experimental BNL data for nonmesonic hyperon decay. *Note that we have scaled the experimental number to account to exclude the pionic decay component.

i) the overall decay rate Γ_{NM};

ii) the ratio of proton-stimulated ($\Lambda p \to np$) to neutron-stimulated ($\Lambda n \to nn$) decay—$\Gamma^p_{NM}/\Gamma^n_{NM} \equiv \Gamma_{NM}(p/n)$;

iii) the ratio of parity-violating to parity-conserving decay—

$$\Gamma^{PV}_{NM}/\Gamma^{PC}_{NM} \equiv \Gamma_{NM}(PV/PC)$$

—which is measured, *e.g.*, via the proton asymmetry in polarized hypernuclear decay

iv) final state n,p decay spectra;

v) *etc.*

The present experimental situation is somewhat limited. Most of the early experiments in the field employed bubble chamber or emulsion techniques. It was therefore relatively straightforward to determine the ratio of the decay rates of the two modes, but much more difficult to measure the absolute rates. This changed when an early Berkeley measurement on ${}^{16}_{\Lambda}$O yielded the value [4]

$$\frac{\Gamma({}^{16}_{\Lambda}\mathrm{O})}{\Gamma_\Lambda} = 3 \pm 1 \tag{5}$$

However, this was still a very low statistics experiment with sizable background contamination. Recently a CMU-BNL-UNM-Houston-Texas-Vassar collaboration undertook a series of direct timing—fast counting—hypernuclear lifetime measurements yielding the results summarized in table 1. [5] In addition, there exist a number of older emulsion measurements in light ($A \leq 5$) hypernuclei, details of which can be found in a recent review article. [6] However, the only experimental numbers for heavy systems are obtained from delayed fission measurements on hypernuclei produced in $\bar{p}$-nucleus collisons and are of limited statistical precision [7]

$$\Gamma({}^{238}_{\Lambda}\mathrm{U}) = (1.0^{+1.0}_{-0.5}) \times 10^{-10}\mathrm{sec.} \qquad \Gamma({}^{209}_{\Lambda}\mathrm{Bi}) = (2.5^{+2.5}_{-1.0}) \times 10^{-10}\mathrm{sec.} \tag{6}$$

The problem of dealing with a weak two-body interaction within the nucleus has been faced previously in the context of nuclear parity violation, and one can

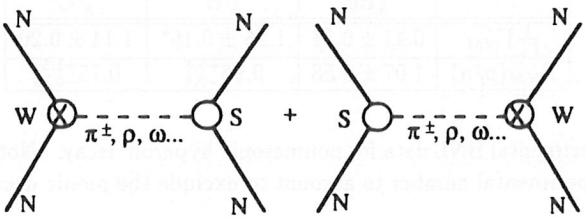

Figure 2: Meson exchange picture of nuclear parity violation.

build on what has been learned therein. [8] Specifically, the weak interaction at the quark level is shortranged, involving W,Z-exchange. However, because of the hard core repulsion the effective NN effects are modelled in terms of long-range one-meson exchange interaction, just as in the case of the conventional strong nucleon-nucleon interaction, [9] but now with one vertex being weak and parity-violating while the second is strong and parity-conserving. The exchanged mesons are the lightest ones—$\pi^{\pm}, \rho, \omega$—associated with the longest range. (Exchange of neutral spinless mesons is forbidden by Barton's theorem. [10])

A similar picture of hypernuclear decay can then be constructed, but with important differences. While the basic meson-exchange diagrams appear as before, the weak vertices must now include both parity-conserving *and* parity-violating components, and the list of exchanged mesons must be expanded to include both neutral spinless objects (π^0, η^0) as well as strange mesons (K, K^*), as first pointed out by Adams. [11] Thus the problem is considerably more challenging than the corresponding and already difficult issue of nuclear parity violation.

One of the significant problems in such a calculation involves the evaluation of the various weak amplitudes. Indeed, the only weak couplings which are completely model-independent are those involving pion emission, which are given in Eqn. 2. In view of this, a number of calculations have included *only* this longest range component. Even in this simplified case, however, there is considerable model-dependence, as the results are strongly sensitive to the short-ranged correlation function assumed for the nucleon-nucleon interaction, as will be seen. Below we shall review previous theoretical work in this area and detail our own program, which involves a systematic quark model- (symmetry-) based evaluation of weak mesonic couplings to be used in hypernuclear decay calculations.

Transition	Operator
${}^1S_0 \to {}^1S_0(I=1)$	$\frac{1}{4}a(q^2)(1-\sigma_\Lambda\cdot\sigma_N)$
${}^1S_0 \to {}^3P_0(I=1)$	$\frac{1}{8}b(q^2)(\sigma_\Lambda-\sigma_N)\cdot\hat{q}(1-\sigma_\Lambda\cdot\sigma_N)$
${}^3S_1 \to {}^3S_1(I=0)$	$\frac{1}{4}c(q^2)(3+\sigma\cdot\sigma_N)$
${}^3S_1 \to {}^3D_1(I=0)$	$\frac{3}{2\sqrt{2}}d(q^2)(\sigma_\Lambda\cdot\hat{q}\sigma_N\cdot\hat{q}-\frac{1}{3}\sigma_\Lambda\cdot\sigma_N)$
${}^3S_1 \to {}^1P_1(I=0)$	$\frac{\sqrt{3}}{8}e(q^2)(\sigma_\Lambda-\sigma_N)\cdot\hat{q}(3+\sigma_\Lambda\cdot\sigma_N)$
${}^3S_1 \to {}^3P_1(I=1)$	$\frac{\sqrt{6}}{4}f(q^2)(\sigma_\Lambda+\sigma_N)\cdot\hat{q}$

Table 2: Transition operators of allowed $\Lambda N \to NN$ transitions from relative S-states. Here $\mathbf{q}$ specifies the relative momentum of the outgoing nucleons while σ_Λ, σ_N operate on the $\Lambda N, NN$ vertices respectively.

2 – Hypernuclear Decay in Nuclear Matter

As discussed above one of the significant problems in the calculation of hypernuclear decay involves the evaluation of the various weak NNM vertices. Indeed, the only weak couplings which are completely model-independent are those involving pion emission, which are given in Eqn. 2. In view of this, a number of calculations have included *only* this longest range component. Even here there is considerable model-dependence, however, as the results are strongly sensitive to the short-ranged correlation function assumed for the nucleon-nucleon interaction. As a warm-up to a realistic calculation then we can begin with a pion-exchange-only calculation in "nuclear matter" (*i.e* a simple Fermi gas model with $N_n = N_p$ and $P_f \sim 270$ MeV) with and without nucleon-nucleon correlation effects. Here the $\Lambda - N$ relative momentum is very soft so that only ${}^1S_0$ and ${}^3S_1$ initial states are assumed to be involved. Then

$$\begin{aligned}\Gamma_{NM} &= \frac{1}{(2\pi)^5}\int d^3k_1 \int d^3k_2 \int_0^{k_F} d^3k_i \delta^4(p_i - p_f) \\ &\times \frac{1}{2}\sum_{spin} |\langle f|\mathcal{H}_w|i\rangle|^2 = \sum_{\alpha\beta}\Gamma_{NM}(\beta \leftarrow \alpha) \end{aligned} \tag{7}$$

We can break this down further by identifying effective transition operators for the various partial wave channels which contribute to the decay process —*cf.* Table 2—in terms of which we find for the total nonmesonic hypernuclear decay rate

$$\Gamma_{NM} = \frac{3}{8\pi\mu_{\Lambda N}^3}\int_0^{\mu_{\Lambda N}k_F} p^2 dp q m_N \left(|a|^2 + |b|^2 + |c|^2 + |d|^2 + |e|^2 + 3|f|^2\right) \tag{8}$$

where $\mu_{\Lambda N} = \frac{m_\Lambda}{m_\Lambda + m_N}$ arises from the switch from the nuclear rest frame to the ΛN center of mass frame and p,q are related by

$$q^2 = m_N(m_\Lambda - m_N) + \frac{p^2}{2\mu_{\Lambda N}} \tag{9}$$

	Adams [11]	McK-Gib [12]	Oset-Sal [13]	UMass [14]
$\frac{1}{\Gamma_\Lambda}\Gamma_{NM}$(no corr.)	0.51	4.13	4.3	3.84
$\frac{1}{\Gamma_\Lambda}\Gamma_{NM}$(corr.)	0.06	2.31	2.1	1.82

Table 3: Non-mesonic hypernuclear decay rates calculated by various groups using pion-exchange only in "nuclear matter."

	Adams [11]	McK-Gib [12]	Oset-Sal [13]	UMass [14]
$\Gamma_{NM}(p/n)$ (no corr.)	19.4	-	-	11.2
$\Gamma_{NM}(p/n)$ (corr.)	2.8	-	-	16.6

Table 4: Proton to neutron stimulated decay ratios for pion-only exchange in "nuclear matter."

The results obtained by various groups are displayed in Table 3.

Obviously there is basic agreement except for the pioneering calculation of Adams. [11] The problems with his calculation were two—Adams used an incorrect value of the weak coupling constant g_w as well as too-strong a tensor correlation, both of which tended to reduce the calculated rate. When these are corrected the corresponding numbers are found to be 3.5 (no correlations) and 1.7 (with correlations) and are in basic agreement with other predictions. From this initial calculation then we learn that the basic nonmesonic decay rate is indeed anticipated to be of the same order as that for the free Λ *and* the important role played by correlations.

A second quantity of interest which emerges from such a calculation is the p/n stimulated decay ratio, given by

$$\Gamma_{NM}(p/n) = \frac{\int_0^{\mu_{\Lambda N} k_F} p^2 dpq(|a|^2 + |b|^2 + 3|c|^2 + 3|d|^2 + 3|e|^2 + 3|f|^2)}{\int_0^{\mu_\Lambda k_F} p^2 dpq(2|a|^2 + 2|b|^2 + 6|f|^2)} \tag{10}$$

and which has been calculated by two of the groups, yielding the results shown in Table 4. An interesting feature here is that the numbers come out so large—proton stimulated decay is predicted to predominate over its neutron stimulated counterpart by nearly an order of magnitude. The reason for this is easy to see. In a pion-exchange-only scenario the effective weak interaction is of the form

$$\mathcal{H}_w \sim g\bar{N}\tau N \cdot \bar{N}\tau\Lambda \tag{11}$$

Then $\Lambda n \to nn \sim g$ but $\Lambda p \to np \sim (-1 - (\sqrt{2})^2)g = -3g$ since both charged and neutral pion exchange are involved. In this naive picture then we have $\Gamma_{NM}(p/n) \sim 9$, in rough agreement with the numbers given in Table 4.

Armed now with theoretical expectations, we can ask what does experiment say? The only reasonably precise results obtained for nuclei with $A > 4$ are those

	McK-Gib [12] $\pi+\rho$	McK-Gib [12] $\pi-\rho$	Nard. [15]
$\frac{1}{\Gamma_\Lambda}\Gamma_{NM}$	3.52	0.72	0.7

Table 5: Nonmesonic decay rates in nuclear matter in pi plus rho exchange models

measured at BNL on ${}^{5}_{\Lambda}$He, ${}^{12}_{\Lambda}$C and ${}^{11}_{\Lambda}$B, which are summarized in Table 1. We observe that the measured nonmesonic decay rate is about a factor of two lower than that predicted in Table 3 while the p/n stimulation ratio differs by at least an order of magnitude from that given in Table 4. The problem may be, of course, associated with the difference between the nuclear matter within which the calculations were performed and the finite nuclear systems which were examined experimentally. Or it could be due to the omission of the many shorter range exchanged mesons in the theoretical estimate. (Or *both!*)

Before undertaking the difficult problem of finite nuclear calculations, it is useful to first examine the inclusion of additional exchanged mesons in our calculations. As mentioned above, a primary difficulty in this approach is that none of the required weak couplings can be measured experimentally. Thus the use of some sort of model is required, and the significance of any theoretical predictions will be no better than the validity of the model. One early attempt by McKellar and Gibson, for example, included only the rho and evaluated the rho couplings using both SU(6) symmetry methods as well as the well known but flawed factorization approach. [12] Well aware of the limitations of this method, they allowed an arbitrary phase between the rho and pi amplitudes and they renormalized the factorization calculation by a factor of $1/\sin\theta_c\cos\theta_c$ in order to account for the $\Delta I = \frac{1}{2}$ enhancement. Obviously this is only a rough estimate then and this is only for the rho meson exchange contribution! A similar approach was attempted by Nardulli, who calculated the parity conserving rho amplitude in a simple pole model and the parity violating piece in a simple quark picture. [15] Results of these calculations are shown in Table 5

To my knowledge, the only comprehensive calculation which has been undertaken to date is that of our group at UMass. In the case of the parity violating interaction we employed a variant of the (broken) $SU(6)_w$ symmetry calculations which were employed successfully by Desplanques, Donoghue and Holstein to calculate the various weak NNM couplings in the case of nuclear parity violation. [8] In this approach there exist three (in principle unknown) reduced matrix elements which, when multiplied by the relevant generalized "Clebsch-Gordan" coefficients, relate all such parity-violating amplitudes. Two of these are determined empirically in terms of experimental hyperon decay data, while the third is given by a factorization calculation. While the success of this approach in the case of nuclear parity violation is not without question, [16] this procedure provides a plausible and unambiguous approach to the problem.

More difficult is the determination of the parity-conserving weak couplings.

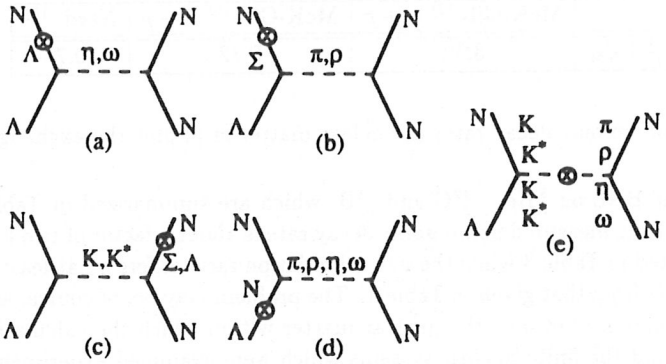

Figure 3: Pole diagrams used in evaluation of weak parity-conserving $\Lambda N \to NN$ couplings.

In this case we employ a pole model using the diagrams shown in Figure 3. What is needed here are the weak parity-conserving amplitudes for $\Lambda - N$ and $\Sigma - N$ transitions, which we determine via the current algebra (chiral symmetry) relations

$$\begin{aligned} \lim_{q_\pi \to 0} \langle \pi^0 n | \mathcal{H}_w^{(-)} | \Lambda \rangle &= \frac{-i}{F_\pi} \langle n | [F_{\pi^0}^5, \mathcal{H}_w^{(-)}] | \Lambda \rangle = \frac{i}{2F_\pi} \langle n | \mathcal{H}_w^{(=)} | \Lambda \rangle \\ \lim_{q_\pi \to 0} \langle \pi^0 p | \mathcal{H}_w^{(-)} | \Sigma^+ \rangle &= \frac{-i}{F_\pi} \langle p | [F_{\pi^0}^5, \mathcal{H}_w^{(-)} | \Sigma^+ \rangle = \frac{i}{2F_\pi} \langle p | \mathcal{H}_w^{(-)} | \Sigma^+ \rangle \end{aligned} \tag{12}$$

and the weak $K - \pi$ coupling which is similarly given in terms of the experimental $K\pi\pi$ decay amplitude

$$A_{K\pi} = -iF_\pi \frac{k \cdot q}{m_K^2 - m_\pi^2} \langle \pi^0 \pi^0 | \mathcal{H}_w | K^0 \rangle_{physical} \tag{13}$$

Again this procedure has well documented flaws. [17] However, in the present context it is reasonable successful and for a first generation calculation, we consider it to provide a reasonable estimate for the parity conserving weak couplings.

Combining with the various strong meson couplings we can now substitute into the diagrams shown in Figure 3 to generate the many effective parity conserving two-body operators which can be used to evaluate the nonmesonic decay amplitudes. Details of these procedures are given in ref. 10. Using the resultant two-body operators one can then generate the various predictions for nonmesonic decay in nuclear matter. Results are summarized in table 6, where we specifically identify the contributions from various channels.

The results are very intriguing. The overall decay rate is reduced somewhat from its pion-exchange-only value, in agreement with the experimental results. More

	π (no corr.)	π (corr.)	$\pi+\rho$	π,ρ,η ω,K,K^*
$^1S_0 \to {}^1S_0$	.010	.000	.001	.001
$^1S_0 \to {}^3P_0$	.156	.037	.052	.018
$^3S_1 \to {}^3P_1$	.312	.117	.113	.456
$^3S_1 \to {}^1P_1$	.468	.128	.100	.110
$^3S_1 \to {}^3S_1$	.010	.789	.589	.202
$^3S_1 \to {}^3D_1$	2.93	.751	.693	.444
Total	3.89	1.82	1.55	1.23

Table 6: Decay rates for various combinations of meson exchange in nuclear matter.

	$\Gamma_{NM}(PV/PC)$	$\Gamma_{NM}(p/n)$
π (no corr.)	0.14	11.2
π (with corr.)	0.18	16.6
$\pi+\rho$	0.21	13.1
$\pi,\rho,\omega,\eta,K,K^*$	0.90	2.9

Table 7: The parity violating to parity conserving and p to n ratios for hypernuclear decay in "nuclear matter."

striking is the modification of the p/n ratio and in the ratio of parity violating to parity conserving decay, defined as

$$\Gamma_{NM}(PV/PC) = \frac{\int_0^{\mu_{\Lambda N}} p^2 dpq(|b|^2+|e|^2+|f|^2)}{\int_0^{\mu_{\Lambda N}} p^2 dpq(|a|^2+|c|^2+3|d|^2)} \tag{14}$$

values of which are shown in Table 7. We observe that inclusion of additonal exchanges plays a major role in reducing the p/n ratio from its pion-only-exchange value. The resulting value of 2.9 is still somewhat larger than the experimental values shown in Table 1 but clearly indicate the presence of non-pion exhange components.

The reason that kaon exchange in particular can play such a major role can be seen from a simple argument due to Gibson [18] who pointed out that since the final NN system can have either I=0 or I=1, the effective kaon exchange interaction can be written as

$$\begin{aligned}\mathcal{L}_{eff} &= A_0(\bar{p}p+\bar{n}n)\bar{n}\Lambda + A_1(2\bar{n}p\bar{p}\Lambda - (\bar{p}p-\bar{n}n)\bar{n}\Lambda) \\ &\sim (A_0-3A_1)\bar{p}p\bar{n}\Lambda + (A_0+A_1)\bar{n}n\bar{n}\Lambda \end{aligned} \tag{15}$$

where the second line is obtained via a Fierz transformation. Since for parity violating kaon exchange we have $A_0 \sim 6A_1$ we find [18]

$$\Gamma_{NM}(p/n) = \left(\frac{A_0-3A_1}{A_0+A_1}\right)^2 \sim 1/5 \tag{16}$$

	π-no corr.	π-corr.	all exch.
α	-0.078	-0.192	-0.443

Table 8: Proton asymmetry coefficient in various scenarios.

which clearly indicates the importance of inclusion of non-pion-exchange components in predicting the p/n ratio.

A second strong indication of the presence of non-pion-exchange can be seen from Table 7 in that the rate of parity violating to parity conserving transitions is substantially enhanced by the inclusion of kaon and vector meson exchange as compared to the simple pion-exchange-only calculation. We can further quantify this effect by calculating explicitly the angular distribution of the emitted proton in the $\Lambda p \to np$ transition (there can be no asymmetry for the corresponding $\Lambda n \to nn$ case due to the identity of the final state neutrons), yielding

$$W_p(\theta) \sim 1 + \alpha P_\Lambda \cos\theta \tag{17}$$

where

$$\alpha = \frac{\int_0^{\mu_{\Lambda N} k_F} p^2 dpq \frac{\sqrt{3}}{2} Re f^*(\sqrt{2}c + d)}{\int_0^{\mu_{\Lambda N} k_F} p^2 dpq \frac{1}{4}(|a|^2 + |b|^2 + 3|c|^2 + 3|d|^2 + 3|e|^2 + 3|f|^2} \tag{18}$$

is the asymmetry parameter. Results of a numerical evaluation are shown in Table 8 so that again inclusion of non-pion-exchange components has a significant effect, increasing the expected $\Lambda p \to np$ asymmetry by more than a factor of two. This prediction of a substantial asymmetry is consistent with preliminary results obtained for p-shell nuclei at KEK. [19]

3 – Hypernuclear Decay in Finite Nuclei

Although the nuclear matter calculations are of great interest in identifying basic properties of the decay process, true confrontation with experiment requires calculations involving the finite nuclei on which the measurements are conducted. Of course, such calculations are considerably more challenging than their nuclear matter counterparts and require Λ shell model considerations as well as non-S-wave capture. Nevertheless a number of groups have taken up the challenge. For the case of the nonmesonic decay of ${}^{12}_{\Lambda}\mathrm{C}$ the results are summarized in Table 9. In comparing with the experimental results given in Table 1, we see that the UMass calculation is certainly satisfactory, but the discrepancy between the UMass and TRIUMF work is disturbing and needs to be rectified before either is to be believed.

A second nucleus on which there has been a good deal of work, both experimentally and theoretically, is ${}^{5}_{\Lambda}\mathrm{He}$, which is summarized in Table 10. Here again what is important is not so much the agreement of disagreement with experiment but rather the discrepancies *between* the various calculations which need to be clarified before any significant confrontation between theory and experiment is possible.

	Oset-Sal [13]	TRIUMF [20]	UMass [14]
$\frac{1}{\Gamma_\Lambda}\Gamma_{NM}$ π (no corr.)		1.6	3.4
π (corr.)	1.5	2.0	0.5
$\pi + K$ [20]; $\pi, \eta, \rho\omega, K, K^*$ [14]		1.2	0.2
$\Gamma_{NM}(p/n)\pi$ (no corr.)		5.0	4.6
π (corr.)		5.0	5.0
$\pi + K$ [20]; $\pi, \eta, \rho, \omega, K, K^*$ [14]		4.0	1.2
$\Gamma_{NM}(PV/PC)\pi$ (no corr.)		0.4	0.1
π (corr.)		0.5	0.1
$\pi + K$ [20]; $\pi, \eta, \rho, \omega, K, K^*$ [14]		0.3	0.8

Table 9: Calculated properties of nonmesonic hypernuclear decay of ${}^{12}_{\Lambda}$C.

	Oset-Sal [13]	TRIUMF [20]	TTB [21]	UMass [14]
$\frac{1}{\Gamma_\Lambda}\Gamma_{NM}\pi$(no corr.)		1.0	0.5	1.6
π(corr.)	1.15	0.25	0.144	0.9
$\pi + K$ [20]; $\pi, \eta, \rho, \omega, K, K^*$ [14]		0.22		0.5
$\Gamma_{NM}(p/n)\pi$ (no corr.)		5.0		15
π (corr.)		4.8		19
$\pi + K$ [20]; $\pi, \eta, \rho, \omega, K, K^*$ [14]		5.4		2.1

Table 10: Calculated properties of the nonmesonic decay of ${}^{5}_{\Lambda}$He.

Before leaving this section, it is important to raise an additional issue which needs to be resolved before reliable theoretical calculations are possible—that of the $\Delta I = \frac{1}{2}$ rule. [22] Certainly in any venue in which it has been tested—nonleptonic kaon decay—$K \to 2\pi, 3\pi$, hyperon decay—$B \to B'\pi$, $\Delta I = \frac{1}{2}$ components of the decay amplitude are found to be a factor of twenty or so larger than their $\Delta I = \frac{3}{2}$ counterparts. Thus it has been natural in theoretical analysis of nonmesonic hypernuclear decay to make this same assumption. (Indeed without it the already large number of unknown parameters in the weak vertices expands by a factor of two.) However, recently Schumacher has raised a serious question about the correctness of this assumption, which if verified will have serious implications about the direction of future theoretical analyses. [23] The point is that by use of very light hypernuclear systems one can isolate the isospin structure of the weak transition. Specifically, using a simple delta function interaction model of the hypernuclear weak decay process, as first written down by Block and Dalitz in 1963 [24], one determines

$$
\begin{aligned}
{}^{4}_{\Lambda}\mathrm{He} : \gamma_4 = \Gamma_{NM}(n/p) &= \frac{2R_{n0}}{3R_{p1} + R_{p0}} \\
{}^{5}_{\Lambda}\mathrm{He} : \gamma_5 = \Gamma_{NM}(n/p) &= \frac{3R_{n1} + R_{n0}}{3R_{p1} + R_{p0}} \\
\gamma = \Gamma_{NM}({}^{4}_{\Lambda}\mathrm{He})/\Gamma_{NM}({}^{4}_{\Lambda}\mathrm{H}) &= \frac{3R_{p1} + R_{p0} + 2R_{n0}}{3R_{n1} + R_{n0} + 2R_{p0}}
\end{aligned}
\tag{19}
$$

where here R_{Nj} indicates the rate for N-stimulated hypernuclear decay from an initial configuration having spin j. One can then isolate the ratio R_{n0}/R_{p0} by taking the algebraic combination

$$
\frac{R_{n0}}{R_{p0}} = \frac{\gamma\gamma_4}{1 + \gamma_4 - \gamma\gamma_5} \tag{20}
$$

and from the experimental values [25]

$$
\gamma_4 = 0.27 \pm 0.14, \qquad \gamma_5 = 0.93 \pm 0.55, \qquad \gamma = 0.73^{+0.71}_{-0.22} \tag{21}
$$

we determine

$$
\frac{R_{n0}}{R_{p0}} = \frac{0.20^{+0.22}_{-0.12}}{0.59^{+0.80}_{-0.47}} \tag{22}
$$

in possible conflict with the $\Delta I = \frac{1}{2}$ rule prediction—$R_{n0}/R_{p0} = 2$.[1] If confirmed by further theoretical and experimental analysis this would obviously have important ramifications for hypernuclear predictions. However, recent work at KEK has indicated that the correct value for γ should be nearer to unity than to the value 0.73 used above in which case the ratio is considerably increased and there may be no longer any indication of $\Delta I = \frac{1}{2}$ rule violation. [26]

[1] Note that final state nn or np configurations which arise from initial ${}^1S_0$ states are of necessity I=1.

4 – Conclusions

We have given a brief overview of the field of weak hypernuclear physics. Because of limited experimental data and of the difficulty of doing reliable theory, the present situation is quite unsatisfactory. Although there is very rough qualitative agreement between theoretical expectations and experimental measurements, it is not clear whether discrepancies which do exist are due to experimental uncertainties, to theoretical insufficiencies, or both. On the theoretical side, what is needed are reliable calculations on finite hypernuclei (preferably by more than one group) which clearly indicate what signals should be sought in the data. The issue associated with the validity of the $\Delta I = \frac{1}{2}$ rule must be clarified. In addition there have been recent speculations about the importance of two-nucleon stimulated decay [27] (which could account for as much as 15% of the decay amplitude according so some estimates) and of the importance of direct quark (*i.e.* non-meson-exchange) mechanisms, [28] which deserve further study in order to eliminate the vexing double counting problems which arise when both direct quark and meson exchange components are included. On the experimental side, we require an extensive and reliable data base developed in a variety of nuclei in order to confirm or refute the predicted patterns. Clearly the strong program of hypernuclear physics at DAΦNE will provide a major step in this direction.

Acknowledgements

The above research was supported in part by the National Science Foundation and by the Department of Energy. It is also a pleasure to acknowledge the warm hospitality shown by our hosts at DAΦNE.

References

1. Part. Data Group, Phys. Rev. **D50**, 1221 (1994).
2. W. Cheston and H. Primakoff, Phys. Rev. **92**, 1537 (1953).
3. A comprehensive review of such processes is given by J. Cohen, Prog. Part. Nucl. Phys. **25**, 139 (1990); see also B.R. Holstein, *Weak Interactions in Nuclei*, Princeton Univ. Press, Princeton (1989), Ch. 5.
4. K.J. Nield et. al., Phys. Rev. **C13**, 1263 (1976).
5. R. Grace et al., Phys. Rev. Lett. **55**, 1055 (1985); P.D. Barnes, Nucl. Phys. **A450**, 43c (1986).
6. A comprehensive review of such processes is given by J. Cohen, Prog. Part. Nucl. Phys. **25**, 139 (1990); see also B.R. Holstein, *Weak Interactions in Nuclei*, Princeton Univ. Press, Princeton (1989), Ch. 5.
7. J.P. Bocquet et al., Phys. Lett. **B182**, 146 (1986) and **B192**, 312 (1987); S. Polikanov et al., Nucl. Phys. **A478**, 805c (1988).

8. B. Desplanques, J.F. Donoghue and B.R. Holstein, Ann. Phys. (NY) **124**, 449 (1980).

9. See, e.g., M.M. Nagels et al., Phys. Rev. **D12**, 744 (1975) and **D15**, 2547(1977).

10. G. Barton, Nuovo Cimento **19**, 512 (1961).

11. J.B. Adams, Phys. Lett. **22**, 463 (1966); Phys. Rev. **156**, 1611 (1967).

12. B.H.J. McKellar and B.F. Gibson, Phys. Rev. **C30**, 322 (1984).

13. E. Oset and L.L. Salcedo, Nucl. Phys. **A443**, 704 (1985) and **A450**, 371c (1986).

14. J.F. Dubach, Nucl. Phys. **A450**, 71c (1986); also, in Proc. Int. Symp. on Weak and Electromagnetic Int. in Nuclei (WEIN), ed. H.V. Klapdor, Springer-Verlag (1986); J.F. Dubach et al., UMass preprint (1995).

15. G. Nardulli, Phys. Rev. **C38**, 832 (1988).

16. E.G. Adelberger and W. Haxton, Ann. Rev. Nucl. Part. Sci. **35**, 501 (1985).

17. E. Golowich, J.F. Donoghue and B.R. Holstein, Phys. Rept. **131**, 319 (1986).

18. B.F. Gibson, Nuovo Cim. **102A**, 367 (1989).

19. T. Kishimoto, *Properties and Interactions of Hyperons*, ed. B.F. Gibson, P.D. Barnes and K. Nakai, World Scientific, New York (1994).

20. A. Ramos et al., Phys. Lett. **B264**, 233 (1991); Nucl. Phys. **A544**, 703 (1992) and **A547**, 103c (1992).

21. K. Takeuchi, H. Takaki and H. Bando, Prog. Theo. Phys. **73**, 841 (1985); H. Bando, Prog. Theo. Phys. Suppl. **81**, 181 (1985).

22. See, *e.g.*, E. Golowich, J.F. Donoghue and B.R. Holstein, *Dynamics of the Standard Model*, Cambridge Univ. Press, New York (1992), Ch. VIII.

23. R.A. Schumacher, Nucl. Phys. **A547**, 143c (1992).

24. M.M. Block and R.H. Dalitz, Phys. Rev. Lett. **11**, 96 (1963).

25. V.J. Zeps and G.B. Franklin, to be published in Proc. INS Symposium #23, Tokyo (1995).

26. H. Outa, private communication.

27. M. Ericson, Nucl. Phys. **A547**, 127c (1992); M. Shmatikov, Phys. Lett. **B337**, 48 (1994).

28. See, e.g., C.Y. Cheung, D.P. Heddle and L.S. Kisslinger, Phys. Rev. **C27**, 335 (1983); D.P. Heddle and L.S. Kisslinger, Phys. Rev. **C23**, 608 (1986); K. Maltman and M. Shmatikov, Phys. Lett. **B331**,1 (1994); T. Inoue, S. Takeuchi and M. Ota, Tokyo Inst. Tech. preprint TIT/HEP-279/NP (1995).

PRESENT STATUS OF HYPERNUCLEAR STUDIES

Toshimitsu Yamazaki
INS Tokyo University, 3-2-1 Midori-cho, Tanashi-shi, Tokyo 188 (Japan)

(No written contribution arrived)

HOW TO SOLVE AT $DA\Phi NE$ THE "KAONIC HYDROGEN PUZZLE"

C. Guaraldo, V. Lucherini, C. Petrascu*
Laboratori Nazionali di Frascati dell'INFN, Frascati, Italy

* On leave of absence from IFA, Bucharest, Romania

ABSTRACT

The feasibility of an X-ray measurement at $DA\Phi NE$ on kaonic hydrogen for the definitive determination of the energy level shift and width due to the $\overline{K}N$ strong interaction, is demonstrated. The "kaon beam" from the ϕ's produced in e^+e^- collisions; a hydrogen target of moderate density, in order to reduce Stark mixing effects; a Charge-Coupled Device (CCD) as soft X-rays detector, are the main elements of the proposal.

Preface

" The most *important experiment* to be carried out in low energy K-meson physics today is the *definitive* determination of the energy level shifts in the K^-p and K^-d atoms, because of their direct connection with the physics of $\overline{K}N$ interaction and their complete independence from all other kinds of measurements which bear on this interaction".

R.H.Dalitz
Proc. Int. Conf. on "Hypernuclear and Kaon Physics", Heidelberg 1982.

also cited by

C.J. Batty
Proc. Int. Conf. on "Intense Hadron Facilities and Antiproton Physics", Torino 1990.

1 - Introduction

In this paper the proposal of a new experiment of an X–ray measurement on the kaonic hydrogen atom using the $DA\Phi NE$ e^+e^- collider is presented. The proposal is based on the use of the "kaon beam" coming from the decay of the ϕ's produced in $DA\Phi NE$; an X–ray detector constituted by Charge-Coupled Device (CCD); a hydrogen target of moderate density, in order to reduce Stark mixing effects.

In Chapter 2 the case of exotics atoms and the kaon–nucleon interaction is reviewed and the importance of an X–ray measurement on kaonic hydrogen with good statistics, low background and good resolution is underlined. Chapter 3 describes the proposed experimental set-up. In Chapter 4 principle and performance of CCD are recalled. In Chapter 5 the results of an atomic cascade calculation which gives the yield of the transition to be measured in kaonic hydrogen are presented. Chapter 6 contains a description of the simulation program. We have developed an original new version of the CERN code GEANT3 (version 3.21), which is accurate down to 1 KeV. Using this code, an evaluation of all the sources of background has been performed – a crucial point for this measurement – and is described in detail in the Chapter. Chapter 7 gives the conclusions which center on the full feasibility of the experiment.

2 - Exotic atoms and the kaon–nucleon interaction

2.1 - Formation of an exotic atom

An "exotic atom" is formed when an incident negatively charged particle such as a muon, a pion, a K-meson, an antiproton or a Σ-hyperon, is stopped in a target and captured into a high atomic Bohr orbit around the nucleus, replacing one of the outer electrons and giving rise to a highly excited atom. The particle then cascades down through its own series of atomic levels, initially by Auger transitions, in which orbital electrons are ejected and in the later stages of the cascade by emission of X-rays. Finally, in the case of hadronic atoms, at some final n-value, nuclear absorption by the nucleus dominates, all hadrons reaching the level are captured and the X-ray series terminates.

The strong interaction causes a shifting of the energy of the lowest atomic level from its purely electromagnetic value, whilst the absorption reduces the lifetime of the state and so X-ray transitions to this final atomic level are broadened. Precise measurements of the X-ray energy spectrum then allow the energy shift (ϵ) and width (Γ) associated with this final level to be determined. As the atomic number and size of the nucleus increase, the absorption occurs from higher n–values. For example, in kaonic hydrogen transitions to n=1 states (K series) have been observed; in light nuclei such as He, Li, Be, etc. the transitions terminate at n=2, whereas in heavy nuclei such as Pb or U the X-ray series finishes at n=7.

In order to determine the energy shift ε, the electromagnetic energy of the unshifted line must first be calculated. This is usually obtained by solving the Klein-Gordon wave equation using the Coulomb potential obtained from a realistic nuclear charge distribution. Other corrections can be calculated using second–order perturbation theory and include first and higher order vacuum polarization, electron screening, relativistic corrections to the reduced mass approximation, nuclear polarization and the Lamb shift. Depending on the energy of the level to be calculated and on the magnitude of the various corrections, the electromagnetic energy can usually be calculated to an accuracy of a few electron volts.

The energy shift (ε) and width (Γ) of the $1s$ level in kaonic hydrogen, measured from the $2p$ - $1s$ X–ray transition, can be related in a fairly model independent way to the real and imaginary part of the complex s-wave K^-p scattering length a_{K^-p}: to first order in $\mu\alpha\, a_{K^-p}$

$$\varepsilon + \frac{i}{2}\Gamma = 2\alpha^3\mu^2\, a_{K^-p} = 412\, a_{K^-p}\, eV fm^{-1}$$

with μ reduced mass, α fine structure constant. This expression is known as the Deser-Trueman formula [1].

As far as experiments are concerned, collisional effects in the atomic cascade due to Stark mixing and external Auger transitions are important and the yield of X–rays decreases with increasing target density. This is a particular problem for kaonic hydrogen experiments, where high density targets are required to reduce the path of the kaon and hence the probability of kaon decay during the processes of stopping, atomic capture and atomic cascade. A compromise between number of stopped kaons in a reasonable volume and yield of $2p$ - $1s$ X–rays has to be carefully looked by varying the density of a gaseous target through its pressure and temperature parameters.

2.2 - The kaon–nucleon interaction at low energies

The $\overline{K}N$ interaction at low energies has *rich, complex dynamical aspects*, which are *neither simple nor well understood.* Not simple, since the K^-p and $\overline{K}^0n$ channels are coupled by charge exchange and, furthermore, are strongly coupled to several πY channels ($Y = \Lambda, \Sigma$) open at the K^-p threshold (1432 MeV total energy in the centre of mass):

$$K^-p \rightarrow K^-p$$
$$K^-p \rightarrow \overline{K}^0n - 5\, MeV$$
$$K^-p \rightarrow \pi\Sigma + 100\, MeV$$
$$K^-p \rightarrow \pi^0\Lambda + 180\, MeV$$

Moreover, this energy region is dominated by the presence of the s-wave $\Lambda(1405)$ resonance, a strangeness -1, $I = 0$ resonance which decays only to $\Sigma\pi$.

This resonance also couples strongly to the $\overline{K}N$ system, but does not decay to it since it is some 30 MeV below the $\overline{K}N$ threshold.

Resonances occur also in other partial waves above (the $\Lambda(1520)$ in d-wave) and below (the $\Sigma(1385)$ in p-wave) threshold.

Experimental data are available for:

a) the K^-p cross sections for the elastic and inelastic processes;

b) the three branching ratios for the K^-p absorption at rest [2]:

$$\gamma = \lim_{k\to 0} \frac{\sigma(K^-p \to \pi^+\Sigma^-)}{\sigma(K^-p \to \pi^-\Sigma^+)} = 2.36 \pm 0.04$$

$$R_c = \lim_{k\to 0} \frac{\sigma(K^-p \to charged\ particle)}{\sigma(K^-p \to all\ final\ states)} = 0.664 \pm 0.011$$

$$R_n = \lim_{k\to 0} \frac{\sigma(K^-p \to \pi^0\Lambda)}{\sigma(K^-p \to all\ neutral\ states)} = 0.189 \pm 0.015$$

c) the $\pi\Sigma$ invariant mass distribution below the K^-p threshold, which exibits the $\Lambda(1405)$ resonance;

d) the $1s$ level shift of the K^-p atom determined through X-ray measurements.

2.2.1 The scattering data

The data for a)–c), with varying degrees of accuracy, became available in the 1950s through the 1970s. The data on a) were (and still are) available only for about 1440 MeV and above in the center of mass energy of the K^-p system.

Analyses have usually been made by using a K-matrix formulation with the assumption that its matrix elements are smooth functions of energy, thus allowing extrapolation down to threshold and below to describe the multichannel problem. A constant scattering length approach was used in early analyses, equivalent to neglecting the variation in the final state momentum. Energy dependences were then allowed in subsequent zero-range and finite-range K-matrix analyses and in some cases waves higher than s-wave were included, so as to exploit also high energy data. The constraint to the K-matrix analysis that the $\pi\Sigma$ mass spectrum obtained from the $\pi^-p \to \pi\Sigma K$ reaction should be fitted simultaneously with data above threshold was added, in order to better determine the parameters of the $\Lambda(1405)$. Dispersion relations turned out to give powerful constraints on the analysis of low energy K^-p data.

No particular disharmony was noticed among data. The $\overline{K}N$ scattering lengths were determined in this way [4)÷ 5)].

The K^-p scattering length a_{K^-p} is deduced by the isospin average:

$$a_{K^-p} = \frac{1}{2}(a_0 + a_1)$$

where a_0 and a_1 are the scattering lengths for the channels I=0, 1. In Table 1 results of $\overline{K}N$ scattering analyses are reported. Common distintive feature of the measured scattering lengths, obtained by considering cross sections, branching ratios at threshold and $\pi\Sigma$ invariant mass distribution, is the *negative value of the real part of* a_{K^-p}:

$$Re\, a_{K^-p} < 0$$

Table 1

S-wave $\overline{K}N$ scattering lengths (fm)

Reference	I = 0		I = 1	
	a_0	b_0	a_1	b_1
Sakitt *et al.* (1965)	- 1.63±0.07	0.51±0.05	- 0.19±0.08	0.44±0.04
Kim *et al.* (1967)	- 1.67±0.04	0.71±0.04	- 0.07±0.06	0.68±0.03
von Hippel *et al.* (1968)	- 1.65±0.04	0.73±0.02	- 0.13±0.02	0.51±0.03
Martin & Ross (1970)	- 1.74±0.04	0.70±0.01	- 0.05±0.04	0.63±0.06
Martin *et al.* (1981)	- 1.70±0.07	0.68±0.04	0.37±0.09	0.60±0.07

This means, from the Deser-Trueman formula, and the Warsaw convention [8], that the *energy shift* due to the strong interaction turns out *negative*:

$$\epsilon < 0$$

i.e. the strong interaction is *repulsive* and shifts the electromagnetic level to a *less bound energy*. Hadronic shifts and widths obtained from the scattering lengths given by the analyses of scattering data [4)÷5)] are reported in Table 2.

In addition to the data a)–c) there are data on the Coulomb–nuclear interference in the K^-p scattering at higher energies, i.e., for E≥1500 MeV. When extrapolated to low energies, also these data were found to be consistent with $Re\, a_{K^-p} < 0$ [9].

2.2.2 The "kaonic hydrogen puzzle"

The three published X-ray experiments have all used liquid hydrogen targets and one or more Si(Li) detectors to measure X-ray transitions. Davies *et al.* [10] observed

a 2σ peak at 6.52±0.06 KeV, which they attributed to the $2p$ - $1s$ X-ray. Izycki *et al.* [11] observed a weak pattern of 3 lines at 6.96±0.09, 7.99±0.07 and 8.64±0.10 KeV with significance 2σ, 3σ and 2σ, which they assigned to the $2p$, $3p$ and $4p$ - $1s$ transistions. On the other hand Bird *et al.* [12] saw a similar series of three lines with significance σ, 3σ and 0.5 σ.

It is difficult to interpret and reconcile the X-ray spectra measured by these three experiments. For example, in the experiment of Davies *et al.* [10] the single peak only shows up clearly in the spectrum where the background has been reduced by selecting a particular time region of pulses from the detector. Izycki *et al.* [11] claim a very large detector acceptance by using a target which is not much larger than the beam size and with the detectors very close to the beam. Finally, the X-ray lines measured by Bird *et al.* [12] were only observed in the first part of the experimental run. In the later stages of the experiment only a rather smooth spectrum was measured.

Table 2

The energy shift ΔE_{1S} and width Γ_{1S} of the K^-p 1S state as obtained from kaonic hydrogen X-ray measurements and scattering analyses

Method	Experiment	ΔE_{1S} (eV)	Γ_{1S} (eV)
Kaonic hydrogen X-ray measurements	Davies *et al.* (1979)	$+40 \pm 60$	$0\ ^{+230}_{-0}$
	Izycki *et al.* (1980)	$+370 \pm 80$	560 ± 80
	Bird *et al.* (1983)	$+193 \pm 60$	$80\ ^{+220}_{-80}$
K^-p *scattering analyses*	Sakitt *et al.* (1965)	-375 ± 21	396 ± 25
	Kim *et al.* (1967)	-358 ± 16	568 ± 25
	von Hippel *et al.* (1968)	-367 ± 8	511 ± 16
	Martin & Ross (1970)	-367 ± 12	544 ± 25
	Martin *et al.* (1981)	-272 ± 21	527 ± 33

The measured values are generally inconsistent with each other at least as far as the magnitude of the strong interaction shift ε is concerned, *however they are all in agreement about the sign of* ε:

$$\varepsilon > 0\,,$$

as reported in Table 2. This means that the hadron interaction of the kaon shifts the atomic level to a more bound energy, in direct contradiction with the repulsive strong interaction found from scattering data analyses. It follows, from the Deser–Trueman formula, that X-rays emitted in transitions to the $1s$ level of kaonic hydrogen give a *positive sign for the real part of the scattering length*

$$Re\, a_{K^-p} > 0$$

whilst the real part of the $K^- p$ scattering length obtained from K–matrix analyses of scattering data turns out negative.

The striking discrepancy between scattering data and X-ray measurements, apparent in Table 2, is often referred to as the *"kaonic hydrogen puzzle"*.

2.2.3 Corrections to scattering length

There are two principal corrections to the isospin average formula for the scattering length. The first takes into account the threshold difference between the $\overline{K}p$ and $\overline{K}^0 n$ channels, the second considers the Coulomb correction.

Threshold effects for zero range interaction [13] and for finite range interaction [14] give a marked change in the value of the scattering length, the real part increasing by about 50% and the imaginary part by 20%. Inclusion of Coulomb corrections to the threshold corrected values, using either the Dalitz [15] or the Wycech [16] approach, gives similar results.

Higher order terms to the Deser-Trueman formula were also considered by Trueman [1] and by Stepien–Rudzka and Wycech [16]. To second order, the effect on ε is seen to be small, whilst the values of Γ are typically increased by 10%.

2.3 - The importance of an X-ray measurement on kaonic hydrogen

We discuss now the scientific meaning of an X–ray measurement on kaonic hydrogen.

X–rays given off in transitions to the $1s$ level of kaonic hydrogen show that the nuclear interaction of the kaon is of attractive nature and therefore gives rise to a more bound system [10)÷ 12]. This is a puzzle, in that the hadronic shift is in a direction opposite to that calculated [17)÷ 19] with the use of the analyses of low-energy $\overline{K}N$ experiments [4)÷ 5), 20)÷ 26]. It is also opposite to the shift observed in heavier kaonic atoms [8], in which again the interaction turns out repulsive. Unraveling this puzzle is therefore crucial for an understanding of the kaon–nucleon interaction. Moreover, since for the kaon-proton system at threshold the energy region is dominated by the presence of the $\Lambda(1405)$ resonance, the structure of this object can be investigated. Indeed, whether the $\Lambda(1405)$ is composite ($\overline{K}N$ bound state or $\Sigma\pi$ resonance) or is elementary (three–quark state) or is a $\overline{K}N$ bound state with an admixture of three quark–state is controversial [27)÷ 31].

In the simplest analysis, the atomic level shift and width are related to scattering data via the proportionality expressed by the Deser–Trueman formula [1]. Since corrections to the formula found in exact calculations [18), 19), 32] are large, but not large enough to reverse the sign of ε, the problem must be with either experiments or the behaviour of the scattering amplitude around threshold. As we have seen, corrections to the scattering length substantially do not change the value

obtained analyzing the scattering data, hence attention has to be paid to X-ray measurements. Here the situation is actually confused on the experimental point of view.

The quality of the existing X-ray data has been already discussed: high background, which is not surprising since this is typical of a hadron beam which has to be degraded; large statistical errors; suspected systematic errors; inconsistencies among the results. However, the X-ray data agree at least on one point – that $Re\, a_{K^-p}$ is positive, so a discrepancy with scattering data exists.

To confirm this result, mainly as far as sign is concerned, but giving also a precise determination of the magnitude of shift and width, is the reason why a new experiment,with high resolution, good background rejection and high statistics, is badly needed. Once more, it is useful to recall that X-ray results represent the *only* direct experimental evidence on the near-zero-energy $\overline{K}N$ interaction. Hence, the strong statement of Dalitz, that we reported in the First Preface, according to which *the most important experiment to be carried out in low energy K-meson physics today is the definitive determination of the energy level shift in the K^-p and K^-d atoms.*

The M- and K-matrix analyses extrapolate scattering data (cross sections and amplitudes determined by Coulomb-nuclear interference) measured at higher energies down to threshold and below. The X-ray experiment calls this extrapolation into question. For a nearly attractive interaction, $Re\, f_{K^-p}$ starts out positive at threshold and reverses sign each time the strength of the interaction increases to the point where it supports another subthreshold bound state (see fig. 1). Accordingly, *the sign and magnitude of Re f deduced from the shift in kaonic hydrogen are related to the existence and nature of subthreshold states.*

Thus the puzzle centers on the energy dependence of the scattering amplitude $f_{K^-p}(E)$ in the region from the Coulomb bound state (8 KeV below threshold) to the low end of the scattering data (5 MeV above threshold). Note these energy differences: here lies the capability of a better investigation and understanding of the $\overline{K}N$ interaction diplayed by X-ray measurements, which do not need any extrapolation to zero–energy.

Along this line, several attempts to reconcile scattering data and energy shift measurements have been made so far: see for instance [34)÷ 42)]. We shall give two significant examples, chosen in order to show the role played by the $\Lambda(1405)$ and also that of quark degrees of freedom in the $\overline{K}N$ interaction.

The Kumar and Nogami model [41)] assumes that there is an "elementary" baryon Λ_0, which has the same quantum numbers as $\Lambda(1405)$ and a mass near the K^-p threshold (1432 MeV). The Λ_0 could be a three–quark state which is as elementary as the nucleon. The Λ_0 is a "bare" particle which can not be observed directly, but it causes the observed resonance $\Lambda(1405)$. The relevant fact is that

the presence of Λ_0 *leads to a rapid variation of the* K^-p *scattering length around threshold* such that the apparent contradiction between the atomic level shift and the scattering data could be avoided. More specifically, Kumar and Nogami assumed that the K^-p amplitude f_{K^-p} is dominated by the I=0 component and in the model the $\overline{K}N$ isosinglet amplitude f_0 satisfies the following conditions:

i) $Re\, f_o \simeq 0$ at threshold,

ii) $Re\, f_o$ vanishes at E=1405 MeV, *implying an unstable bound state* $\overline{K}N$ (see fig.1.1).

From the model, $a_{K^-p} \geq 0$, which is consistent with the atomic data. However, the model is not complete, since it does not attempt to fit all available data, such as the branching ratios at threshold [2].

The Tanaka and Suzuki model [42] assumes directly a central hypothesis consistent with the atomic data, i.e. $Re\, a_{K^-p} > 0$ at threshold. All the four "categories" of experimental data a)÷d) are fitted without the need of an "elementary" three–quark state such as the Λ_0. Therefore, the $\Lambda(1405)$ is simply a two–body composite system and one is led to ask whether or not the $\Lambda(1405)$ is a $\overline{K}N$ bound state rather than a $\pi\Sigma$ resonance. It is of course conceivable that the $\overline{K}N$ and $\pi\Sigma$ channels are coupled so strongly that there is no clear answer to this question. However, the model provides some insight into this aspect. Indeed the $Re\, f_{K^-p}$ is positive around threshold but the real part of the I=0 component of the amplitude, $Re\, f_o$, vanishes and changes its sign below the $\overline{K}N$ threshold. This implies that there is an unstable bound state of $\overline{K}$ and N in the isosinglet state. In this sense, $\Lambda(1405)$ is an unstable bound state of $\overline{K}$ and N.

Summarizing, good data (in terms of statistics, low background, good resolution) from kaonic hydrogen X–ray measurements will allow:

- understanding the antikaon–nucleon interaction, in particular by definitively solving the "kaonic hydrogen puzzle";
- understanding the nature of the $\Lambda(1405)$ and therefore testing also the prediction of the quark model;
- clarifying the behaviour with energy around threshold of the scattering amplitude f_{K^-p};

and, moreover,

- studying the influence of quark configurations on the spectrum of hadronic atoms;
- understanding astrophysical implications, like kaon–condensation in dense neutron star matter [40].

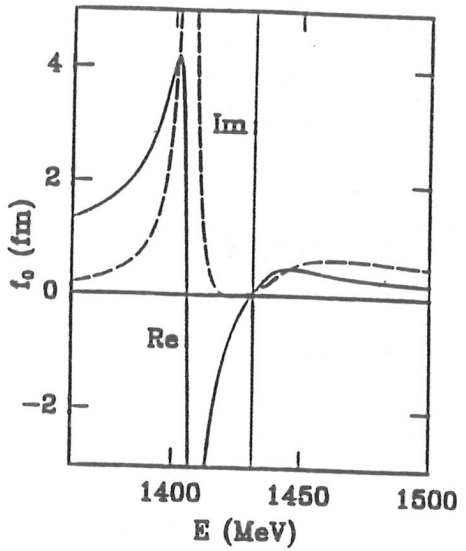

Figure 1: The $\overline{K}N$ isosinglet amplitude f_0 versus the total c.m. energy. The solid and dashed lines represent the real and imaginary part, respectively, of the amplitude. The vertical line shows the $\overline{K}p$ threshold (1432 MeV)

References

1. S. Deser *et al.*, Phys. Rev. **96** (1954) 774;
   T.L. Trueman, Nucl. Phys. **26** (1961) 57;
   A. Deloff, Phys. Rev. **C13** (1976) 730.

2. D.N. Tovee *et al.*, Nucl. Phys. **B33** (1971) 493;
   R.J. Nowak *et al.*, Nucl. Phys. **B139** (1978) 61;
   J. K. Kim, Columbia University Report, Nevis **149** (1966).

3. M. Sakitt *et al.*, Phys. Rev. **B139** (1965) 719.

4. J.K. Kim, Ph.D. Thesis Columbia University, Nevis **149** (1966);
   J.K. Kim, Phys. Rev. Lett. **19** (1967) 1074.

5. F.von Hippel and J.K. Kim, Phys Rev. Lett. **20** (1968) 1303.

6. A.D. Martin and G.G. Ross, Nucl. Phys. **B16** (1970) 479.

7. A.D. Martin, Nucl. Phys. **B179** (1981) 33.

8. C.J. Batty, Nukleonika **25** (1980) 545.

9. P. Baillon *et al.*, Nucl. Phys. **B105** (1976) 365.

10. J.D. Davies *et al.*, Phys. Lett. **B83** (1979) 55.

11. M. Izycki *et al.*, Z. Phys. **A297** (1980) 11.

12. P.M. Bird *et al.*, Nucl. Phys. **A404** (1983) 482.

13. R.H. Dalitz and S.F. Tuan, Ann. Phys. **10** (1960) 307.

14. C.J. Batty and A. Gal, Il Nuovo Cimento **102A** (1989) 255.

15. R.H. Dalitz and S.F. Tuan, Ann. Phys. **10** (1960) 307;
A. Deloff and J. Law, Phys. Rev. **C20** (1979) 1597.

16. W. Stepien-Rudzka and S. Wycech, Nukleonika **22** (1977) 929.

17. R. C. Barrett, J. Phys. **G9** (1983) 355.

18. R. H. Landau, Phys. Rev **C 28** (1983) 1324;
R.H. Landau and B. Cheng, Phys. Rev. **C 33** (1986) 734.

19. J. Thaler, J. Phys. **G10** (1984) 1037.

20. W. E. Humphrey and R. R. Ross, Phys. Rev. **127** (1962) 1305.

21. W. Kittel, G. Otter and I. Wacek, Phys. Lett. **21** (1966) 349.

22. T.S. Mast *et al.*, Phys. Rev. **D11** (1975) 3078.

23. T.S. Mast *et al.*, Phys. Rev. **D14** (1976) 13.

24. R.O. Bangerter *et al.*, Phys. Rev. **D23** (1981) 1484.

25. J. Ciborowski *et al.*, J. Phys. **G8** (1982) 13.

26. D. Evans *et al.*, J. Phys. **G9** (1983) 885.

27. R.H. Dalitz and J.G. McGinley, in *Low and Intermediate Energy Kaon-Nucleon Physics*, edited by E. Ferrari and G. Violini (Reidel, Boston, 1981), p. 97.

28. S. Capstick and N. Isgur, in *Hadron Spectroscopy-1985*, edited by S. Oneda, AIP Conference Proceedings No. 132 (American Institute of Physics, New York, 1985), p. 267.

29. E. A. Veit, B. K. Jennings, A. W. Thomas and R. C. Barrett, Phys. Rev. **D 31** (1985) 1033.

30. B. K. Jennings, Phys. Lett. **176 B** (1986) 229.

31. K. Maltman and N. Isgur, Phys. Rev. **D 34** (1986) 1372.

32. H.H. Brouwer, J.W. de Maag and L.P. Kok, Z. Phys. **A 318** (1984) 1.

33. K.S. Kumar *et al.*, Z. Phys. **A304** (1982) 301.

34. B.O. Kerbikov, Pis'ma Zh. Eksp. Teor. Fiz. **37** (1983) 118.

35. B.O. Kerbikov, Yad. Fiz. **41** (1985) 725.

36. J. Schnick and R.H. Landau, Phys. Rev. Lett. **58** (1987) 1719.

37. P. Y. Fink *et al.*, Phys. Rev. **C41** (1990) 2720.

38. G. He and R. M. Landau, Phy. Rev. **C48** (1993) 3047.

39. E. Friedman, A. Gal and C. J. Batty, Phys. Lett. **B308** (1993) 6.

40. C.–H. Lee *et al.*, Phys. Lett. **B326** (1994) 14.

41. K.S. Kumar and Y. Nogami, Phys. Rev. **D21** (1980) 1834.

42. K.Tanaka and A. Suzuki, Phys. Rev. **C45** (1992) 2068.

3 - The experimental set-up

3.1 - The principle of the experiment

The principle of the proposed experiment is very simple: the low momentum negative kaons produced by decay of ϕ's, created by e^+e^- collisions in the interaction point of one of the straight sections of DAΦNE, leave the beam pipe through a thin window, are degraded in energy down to few MeV, enter a hydrogen target placed few centimeters above the pipe and are there stopped. A fraction of kaons is captured in an outer orbit of the hydrogen atom, thus forming an exotic atom. The kaon then cascades down through its own series of bound atomic states until it reaches a level where the short-range strong interaction acts on the particle causing its absorption.

Measuring, with a suitable soft X-ray detector, such as a Charge–Coupled Device (CCD), the last X-ray transition (the $2p$–$1s$ in kaonic hydrogen), allows one to obtain the shift of the $1s$ level caused by the $\bar{K}N$ strong interaction.

3.2 The overall set-up

The DEAR experimental set-up has been designed taking into account the characteristics of the DAΦNE "kaon beam": low momentum (127 MeV/c), K^- emitted with a $sin(\theta)^2$ law (where θ is the angle measured respect to the beam pipe axis), all around the pipe.

The target has been placed at $\theta = 90°$, and the degrader, window thickness, and target density have been selected in order to optimize, on one hand the number of stopped kaons, and on the other the detected X-rays. Moreover, the set-up has to allow the use of very thin windows between the target volume containing gaseous hydrogen and the CCD detectors, described in Chapter 3, which are located

all around the cylindrical target, in order to reach a high transmission efficiency of the soft X-rays.

In fig. 2 the main components of the set-up are indicated: the beryllium cylindrical window, through which the K^-s, produced by the ϕ decays, leave the DAΦNE pipe; the vacuum box, containing the cylindrical target cell, with cooled and pressurized hydrogen inside, and outside the CCDs.

The selection of the hydrogen density has been optimized taking into consideration the number of stopped kaons, the eventual decrease of the X-ray yield due to Stark mixing with an increase in density, the K^- life time (which is a relevant parameter due to the K^- low momentum), and the thicknesses of different windows interposed through the K^- path. The optimum choice is a hydrogen pressure 3 atm and a temperature 25 K, obtained using a liquid helium cryogenic system. The resulting target density is $3.6 \cdot 10^{-3} g/cm^3$. As described in Chapter 5, the expected yield of K_α X-rays per stopped kaon in these conditions turns out to be about 3%.

Having fixed the target density, the overall dimensions of the set-up together with the window thicknesses were determined using the Monte Carlo simulation code described in Chapter 6.

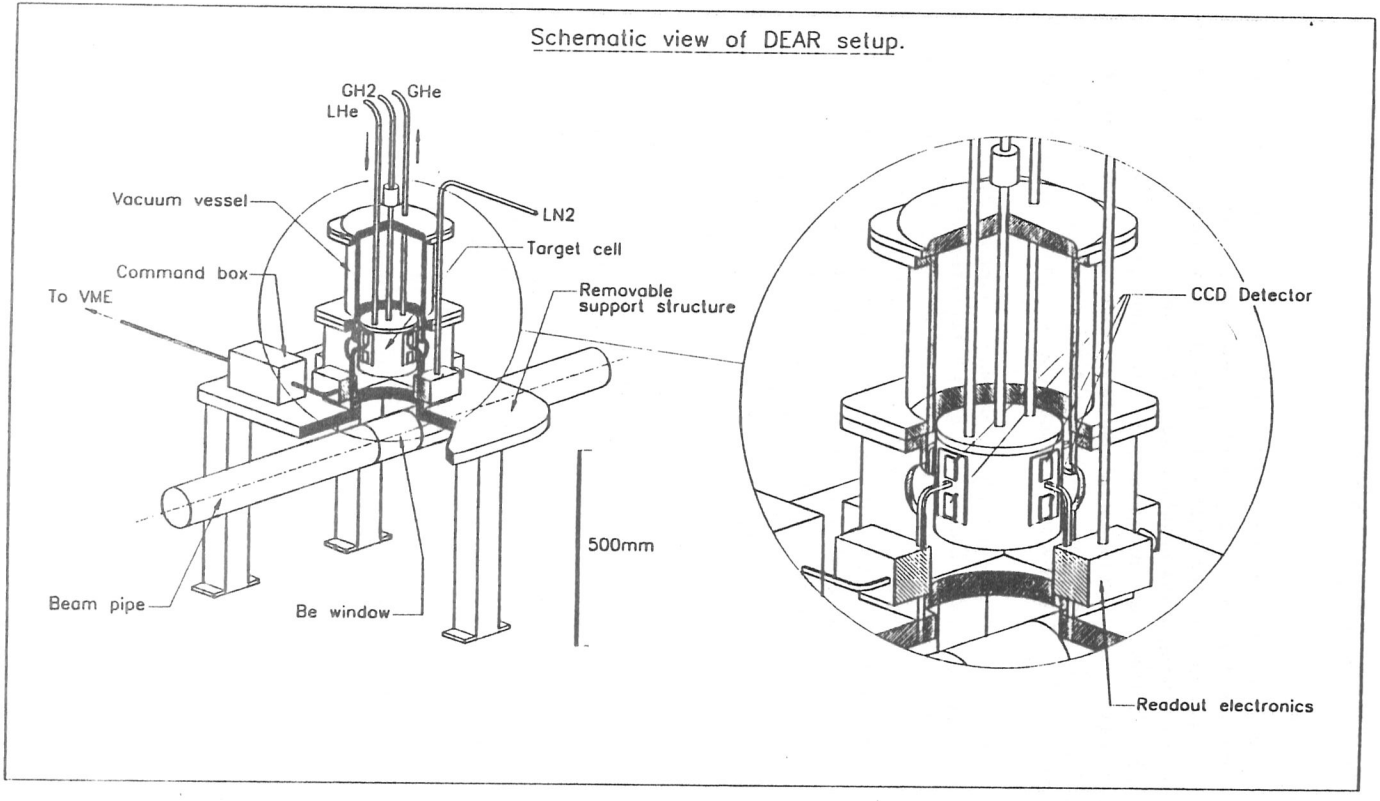

Figure 2: Schematic view of the DEAR experimental set-up

4 - CCDs (Charge-Coupled Devices)

4.1 Introduction

CCDs are solid state detectors with a pixel structure [1)÷ 4)]. The separation of the columns is done with a channel stop (NPN diode structure) between each column. The rows are separated by potential wells which are produced by an array of electrodes mounted on top of the depletion layer. Three electrodes are needed for one pixel. When a CCD is in accumulation mode, a positive voltage is applied to two of them and a negative voltage to the third. For the readout, the accumulated electrons are shifted to a special readout line at the end of the columns, electrode by electrode, by applying three AC voltages with the proper phases to the electrodes of the pixels.

Although CCDs were initially developed for detecting light and mainly to be used in video cameras, they are also very good X-ray detectors in the energy range from 1 keV (limited by the thickness of the electrodes) to 12 KeV (limited by the depletion depth). This leads to applications in X-ray spectrometry, as here in this proposal, or in X-ray astronomy. More generally, sophisticated X-ray versus particle discrimination might also prove useful in future X-ray satellite missions with CCD detectors, since X-rays will have to be cleanly separated from all other cosmic rays [5)]. A different application is the position measurement of charged particle tracks. However, for high energy physics applications the CCDs are usually too slow; silicon strip detectors are used instead [4)].

The good two dimensional spatial resolution of the CCDs (22.5 μm × 22.5 μm) turns out to be crucial to extract the weak signal out of the large background, which is one of the characteristics of the kaonic hydrogen experiments. In most cases X-rays produce single-pixel events, whereas the tracks of charged particles produce cluster events with more than one hit pixel (see fig. 3). The usual way to distinguish X-rays from background (mainly charged particles and higher energy gamma rays) is to require that none of the 8 surrounding pixels have a charge that is considerably above the noise level. If all eight surrounding pixels are below this limit, the event is considered an X-ray. A total background discrimination (except for X-ray background) can be achieved by applying other tests, e.g. on the mean value or on the standard deviation of the energy of the eight neighboring pixels [6)÷ 8)].

4.2 Performance

4.2.1 Measured energy resolution (in beam)

In beam measured energy resolution (FWHM) is given in the table below:

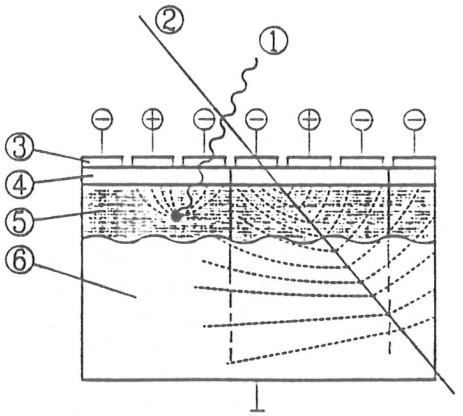

Figure 3: Particle detection in a CCD: (1)X-ray, (2)charged particle track, (3)electrodes, (4)insulator, (5)depletion layer and (6) bulk material. A pixel covers 3 electrodes. The depletion layer is 6 μm for normal CCDs and 30 μm for deep depleted CCDs. All our CCDs are deep depleted. The bulk material is approximately 1 mm thick. The dotted lines correspond to possible e^- migration.

X-ray energy $[KeV]$	energy resolution (FWHM) $[eV]$
2	$\leq$ 120
3	140 - 150
6	$\approx$ 170
8	$\approx$ 190

The energy resolution depends slightly on the CCD exposure time. The resolution values are better than those of other comparable detectors.

The energy resolution of a CCD is given by:

$$\Delta E\,(FWHM) \;=\; 2.355 \times \omega(N^2 + \frac{FE}{\omega})^{1/2}(eV)$$

with

E = X-ray energy
F = Fano factor $\approx$ 0.12
ω = conversion energy for an electron-hole pair in Si = 3.68 eV
2.355 = r.m.s. $\rightarrow$ FWHM conversion factor
N = r.m.s. transfer and readout noise.

As an example, the number of electron - hole pairs created by a 6 KeV X-ray is 6 KeV/3.68 eV which is about 1600.

4.2.2 Background rejection

The CCD background rejection capabilities are very powerful, even though our CCDs cannot be triggered. In fact CCDs have a much better signal/background ratio than Si(Li) detectors, which are triggered. This may be somewhat surprising. One has to keep in mind that in the environment of an accelerator a lot of the background is event correlated and triggering is therefore less effective. With CCDs, however, background (except soft X-rays) can be completely eliminated. As said in the introduction, this is based on the fact that, in most cases, an X-ray in the 1 - 10 KeV energy region deposits its energy in a single pixel of 22.5 μm $\times$ 22.5 μm. Charged particles, gammas and neutrons, on the other hand, are split into several pixels. Background, for example at the πE5 beam line at PSI, fills, on the average, 5.5 pixels and the most probable hit is 4 pixels. Since a pixel has 8 neighbors, a **good X-ray event is a single pixel hit surrounded by 8 pixels which are part of the noise.** In a very high background environment, the 8 pixels surrounding an X-ray event have to be examined statistically to make sure that they are part of the noise peak [6]. The intrinsic CCD noise is $\approx$ 200 eV.

Why does a soft X-ray hit mostly only 1 pixel and charged particles hit several? The interactions are different. Soft X-ray interaction is by photoelectric effect which is localized in space within the depletion layer, whereas charged particles loose energy by ionization everywhere in the silicon (see fig. 3). The electrons of the electron - hole pairs created in the silicon cannot escape if they are in the potential well of the depletion zone of the pixel. However, in the border regions of a pixel, and especially in the bulk material, these electrons can move almost freely. This movement is enhanced by a suitable voltage applied to the bulk. Since, for topological reasons, all charged particles will at some time cross pixel borders, they can be eliminated. Of course some X-rays in the border regions will also be eliminated, but, by chance, the pixel size is just right for a good soft X-ray detection efficiency, as needed in the kaonic hydrogen experiment.

4.2.3 CCD size and readout time

The number of pixels per CCD is 770 $\times$ 1152 $\approx$ 887000. The CCD surface is $\approx$ 17 $\times$ 26 mm^2 $\approx$ 4.5 cm^2. The two halfs of each CCD are read out simultaneously. Today, up to four CCDs can be read out at the same time. This will be increased to the 8 CCDs necessary for the experiment. The transfer and readout time per pixel is 64 μs. The total readout time of the system (= 1/2 CCD readout time) is 64 μs $\times$ 444000 $\approx$ 28 s. Accumulation of data continues during the readout. The pixel readout time could be reduced to 20 μs at the expense of a 30 % loss in energy resolution, according to recent measurements performed at Neuchâtel.

The CCD collection time should not be too long, so that the same 8 pixel cluster which defines a good X-ray event is not hit twice. To be safe, *the number of hit pixels should not exceed $\approx$ 5 %, corresponding to approximately 4000 - 5000 background events per 1/2 CCD.* Based on Monte-Carlo calculations presented in

Chapter 6, the safety limit on DAΦNE is reached after 50 min of data taking. Taking a factor of safety of 10, the CCD exposure time at DAΦNE can be of 5 min, which is very comfortable.

4.2.4 CCD detector efficiency

The total X-ray detection efficiency is a product of the intrinsic CCD efficiency, and the X-ray transmission through the different windows and through the hydrogen gas in the target. The CCD efficiency for a 6 KeV X-ray is around 60%.

4.2.5 Data acquisition and on-line analysis

Since there are no triggers, fast coincidences, interrupts, etc., data acquisition is very simple. Events are collected into the CCDs for a finite time and are then read out. The long exposure time allows for a full on-line analysis.

It is therefore possible, for example, to see and print out a kaonic hydrogen X-ray energy spectrum with sophisticated background cuts, any time during the experiment.

References

1. J.D.E. Beynon and D.R. Lamb, *Charge-coupled devices and their applications,* Mc-Graw Hill (London) 1980.

2. W.S. Boyle and G.E. Smith, *Charge-coupled semiconductor device*, Bell Syst. Tech. Journal **49** (1970) 587.

3. R.L. Rodgers, *Charge-coupled imager for 525-line television*, Digest of IEEE Intercon, March 1974, Session 2.

4. G. Charpak and F. Sauli, Ann. Rev. Nucl. Part. Sci. **34** (1984) 285.

5. J.L. Culhane, Nucl. Instr. and Meth. **A310** (1991) 1.

6. D. Sigg, Nucl. Instr. and Meth. **A345** (1994) 107.

7. EEV (English Electric Valve), Waterhouse Lane, Chelmsford, Essex, CM1 2QU, England.

8. J.-P. Egger, D. Chatellard and E. Jeannet, *Progress in soft X-ray detection: The case of exotic hydrogen*, Particle World **3** (1993) 139;
G. Fiorucci *et al.*, Nucl. Instr. and Meth. **A 292** (1990) 141;
D. Varidel *et al.*, Nucl. Instr. and Meth. **A 292** (1990) 147.

5 - Kaonic X-ray intensities

The intensity distribution of the K^-p X-rays is calculated by assuming that the atomic capture occurs at n=25 and with angular momentum l distributed statistically. Then the radiative transition rates are calculated to give the probability of observing a particular transition in the cascade.

For neutral exotic atoms such as $\pi^- p$, K^-p, $\bar{p}p$, collisional Stark mixing introduces an important density dependence to the X-ray yields. The strong electric fields seen in atomic collisions induce $nl \rightarrow nl \pm 1$ transitions. These are calculated using the model of Borie and Leon [1]. In the model, the strength of the Stark effect is adjusted by two parameters: the Stark mixing coefficient (k_{STK}) and the kinetic energy of kaonic hydrogen atom when it is formed (T). The parameters $k_{STK} = 1.88$ and T=1 eV give a good description of the π^-p and $\bar{p}p$ intensities.

Also required for this calculation are the strong interaction shifts and widths of the levels. Only the $1s$ and $2p$ values are significant; we estimate these from kaonic atom systematics [2]. The strength of the absorption from the ns levels are calculated by scaling the $1s$ absorption according to the ratio of the density of the Coulomb wave functions at the nucleus. A similar scaling from the $2p$ level absorption is used for the absorption from the np levels. As a consequence, if the $2p$ width is large, the intensity of the K_α and K_β lines will be reduced. In Table 3 are given the expected X-ray yields for the configuration, together with some variations of these parameters in order to estimate the sensitivity of the result.

Table 3: Calculated X-ray intensities for kaonic hydrogen

P (atm)	k_{STK}	T (eV)	Δ_{1s} (eV)	Γ_{1s} (eV)	Γ_{2p} (meV)	K_α (%)	K_β (%)	$K_{>\beta}$ (%)	L_α (%)	L_β (%)	L_γ (%)	L_∞ (%)
36	1.88	1	-100	400	.1	4.5	2.6	8.2	2.3	2.8	1.9	0.8
36	1.88	1	-100	400	.5	1.4	1.0	5.8	1.0	1.7	1.6	0.7
10	1.88	1	-100	400	.1	7.3	3.3	12.5	3.6	3.0	3.5	2.3
36	1.88	1	-100	200	.1	4.1	2.2	7.3	2.0	2.5	1.7	0.7
36	1.88	.3	-100	400	.1	6.4	3.7	11.3	3.3	4.0	2.7	1.0

References

1. E. Borie and M. Leon, Phys. Rev. **A21** (1980) 1460.
2. C.J. Batty, Nucl. Phys. **A372** (1981) 418.

6 - The simulation program

6.1 Introduction

The simulation of the proposed experimental set-up and its physics performance was done with a Monte Carlo program in the framework provided by the CERN simulation package GEANT3 [1], using the version 3.21 of the code.

The Monte Carlo program was mainly finalized to simulate the physical processes involved, in order to optimize the experimental set-up as far as geometry (dimensions, materials, etc.) and performance (counting rate, background contamination) are concerned. All the relevant physical volumes of the apparatus, the detector structure, as well as the mechanical walls and supports interposed in the particle paths were modelled with appropriate level of detail. Also the relevant elements of the DAΦNE interacting region (pipe geometry and structure, Be window dimensions and thickness) were included in the Monte Carlo.

The program generates the primary ϕ-mesons produced by the e^+e^- collisions, taking into account the electron and positron energy spread and the beam dimensions in the crossing point, according to the parameters expected for DAΦNE. The generated ϕ's are then allowed to decay in all their relevant final states, according to the corresponding branching ratios:

$$\begin{aligned} \phi \rightarrow \quad & K_s^0 + K_L^0 \quad (34.4\%) \\ \rightarrow \quad & K^+ + K^- \quad (49.1\%) \\ \rightarrow \quad & \rho + \pi \quad (12.9\%) \\ \rightarrow \quad & \pi^+ + \pi^- + \pi^0 \quad (2.40\%) \end{aligned}$$

The decay particles are then transported through the materials of the experimental set-up, allowing them, apart from the processes of energy loss and multiple scattering, to decay or interact both electromagnetically (e.m.), eventually generating e.m. showers, and hadronically. When a K^- is stopped in the target, its hadronic interaction at rest with the proton is switched on using *dedicated routines*, according to the following reactions:

$$\begin{aligned} K^- + p \rightarrow \quad & \Lambda + \pi^0 \quad (7.5\%) \\ \rightarrow \quad & \Sigma^+ + \pi^- \quad (19.6\%) \\ \rightarrow \quad & \Sigma^- + \pi^+ \quad (46.7\%) \\ \rightarrow \quad & \Sigma^0 + \pi^0 \quad (26.1\%) \end{aligned}$$

and for other materials the corresponding reactions on a neutron.

Moreover, an X-ray photon of 6.5 KeV is also generated when the stopping point is inside the target, to simulate the emission of X-rays from the formation of

kaonic-hydrogen.

Finally, all particles which hit the CCD detectors are recorded, in order to extract all the relevant information: type of particle, deposited energy, momentum spectrum, and so on.

6.2 The Monte Carlo program

The performance of the experimental set-up, both regarding the counting rate of "signal" photons (6.5 KeV), emitted after the formation of kaonic-hydrogen, and the signal to background ratio, where background photons are soft (less than 10 KeV) X-rays, depends critically on the *reliability of the code at very low energies.* In particular, *the behaviour of photons, electrons and positrons must be accurate below the minimum low energy cut-off (10 KeV) of the standard GEANT package.*

For energies below few tens of KeV the photoelectric process is the most relevant one. We have verified that the interaction cross sections used in the GEANT program remain accurate at very low photon energies, i.e. also photons below 10 KeV are correctly propagated through materials.

Electrons and positrons can generate photons by the bremssthralung process. This process has the well known "infrared" catastrophe, and hence could potentially produce hazardous (less than 10 KeV) X-rays. In the GEANT package, the bremsstrahlung process is treated in three different routines: GBRELE,GBREME and GBRSGE, which all are based on the bremsstrahlung cross section values tabulated in the paper of S.M. Seltzer and M.J. Berger [2)], for all materials and for electron energies from 1 KeV up to 10 GeV. In all the mentioned routines a fundamental role is played by the parameter k_c, which is the low energy cut-off. It is the photon energy below which the bremsstrahlung process is treated only as a continuous energy loss of the electron (positron), to be summed up to the ionization energy loss (routine GBRELE). Above k_c, the bremsstrahlung photon is generated according to the energy/angular distribution of the bremsstrahlung process by the routine GBREME. To calculate the total cross section of bremsstrahlung, for an electron (positron) of kinetic energy T, travelling in a given material, for emission of a photon with any energy above k_c and below T, the routine GBRSGE is used in GEANT.

We have verified, for different materials, electron kinetic and photon cut-off k_c energies, that the values calculated in the GEANT routines GBRELE and GBREME are accurate down to 1 KeV by comparing their calculated values with the corresponding ones reported in the tabulation given in the paper of S.M. Seltzer and M.J. Berger [2)].

On the other hand, the total cross section values calculated by the GEANT routine GBRSGE are unreliable when the cut-off parameter k_c is put below 10 KeV.

To recover the expected logarithmic increase of the cross section as a function of the electron energy T also when k_c is less than 10 KeV, *we modified the GBRSGE routine, for k_c below 10 KeV, in such a way that the total bremsstrahlung cross section values σ follow the law:*

$$\sigma = \alpha(k_c) + \beta(k_c)\log(T)$$

The values of the parameters $\alpha(k_c)$ and $\beta(k_c)$ were obtained from a fit of the cross section values above k_c=10 KeV. We estimate that this approximation is not worse than the 10-15% error quoted for the GEANT code between 10 KeV and 1 MeV.

6.3 Physics performance

Using the Monte Carlo code, the physical performance of the proposed experimental apparatus has been calculated, and is summarized in the following paragraphs.

6.3.1 Kaon stopping points

The bidimensional distribution of the kaon stopping points si shown in fig. 4. The pipe, the Al vacuum box, the target cell and the windows are clearly seen, together with the target volume.

The selected geometry allows stopping inside the cryogenic hydrogen target of a 3.4% fraction of all the charged kaons produced from ϕ's decay.

6.3.2 Momentum spectra

The momentum distribution of all hitting the CCD detectors has been calculated. As an example, in fig. 5 the momentum distribution of positive pions is shown.

As it is seen, the peaks in the π^+ spectrum at 182 MeV/c, due to the reaction $K^-p \rightarrow \Sigma^-\pi^+$ and the one at 205 MeV/c, due to the decay $K^+ \rightarrow \pi^+\pi^0$ are all clearly reproduced.

6.3.3 Counting rate

In the experimental set-up described in Chapter 2, the number of 6.5 KeV obtained X–rays, deriving from kaonic-hydrogen formation, which hit the 8 CCD detectors is 765 for 1100000 generated ϕ's. The measured CCD efficiency for 6 KeV photons is about 60% (well reproduced by our Monte Carlo, which gives, for the $30\mu m$ depletion layer of the CCD used in the simulation, a "physical" efficiency of 65%). Supposing a yield of 3% for 6.5 KeV K_α X–rays from kaonic-hydrogen (from the cascade calculation reported in Chapter 5 with the selected conditions of pressure and temperature (hence density) of the hydrogen target) and a DAΦNE luminosity

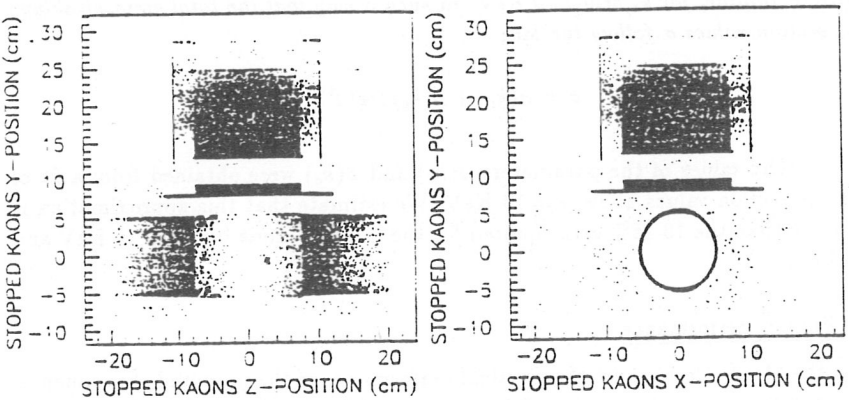

Figure 4: Bidimensional distribution of the kaon stopping points. In a) is shown the y versus z distribution for any x, and in b) the y versus x distribution for any z. It should be remembered that K^-s from ϕ decays are not a directional beam, but are emitted in the whole solid angle.

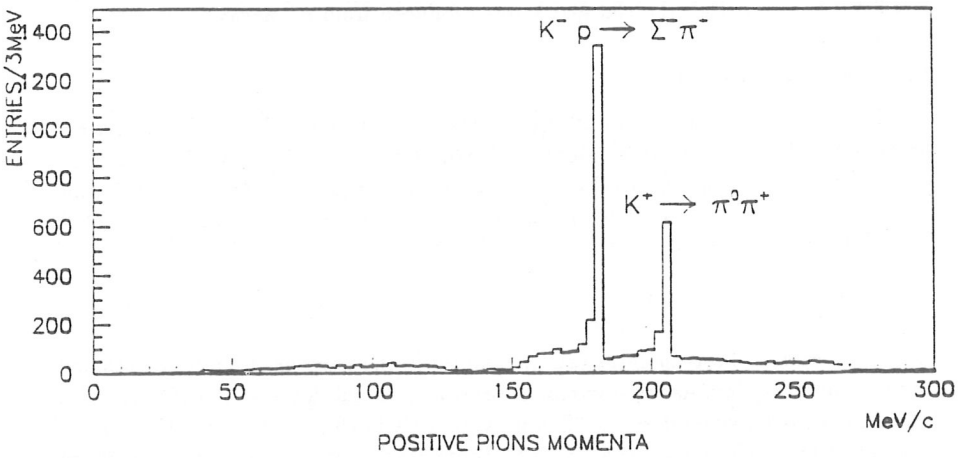

Figure 5: Momentum distribution of positive pions that hit the CCDs. The peak from the reaction $K^-p \rightarrow \Sigma^-\pi^+$ at 182 MeV/c and the peak from the decay $K^+ \rightarrow \pi^0\pi^+$ at 205 MeV/c are clearly seen.

of $10^{32} s^{-1} cm^{-2}$, the expected counting rate is about *20 X-rays per hour*. Due to the CCD resolution at this X-ray energy (about 150 eV), these 20 X-rays in one hour are expected to be spread out, within $\pm 2\sigma$, in 4 channels of 100 eV width around 6.5 KeV, if we assume an intrinsic width $\Gamma_{1s} = 200$ eV ($\Gamma_{tot} = 250$ eV $\sigma \simeq 100\, eV$). If $\Gamma_{1s} = 400$ eV ($\Gamma_{tot} = 420$ eV $\sigma \simeq 180$ eV), the signal is spread over 4 channels, within $\pm$ 1.2 σ, or over 7 channels, within $\pm$ 2 σ.

6.3.4 Background evaluation

The background on CCDs can be divided in two categories: the first affects the operational conditions of a CCD causing its "blindness", i.e., it is connected to the maximum number of pixels which can be involved in a CCD avoiding "double hits" (in the sense explained in Chapter 3). This background is directly given by the number of ionizing particles which hit the surface of a CCD (or, better, half a CCD, since the readout takes into account half a CCD). The second category of background is represented by the hits of soft X-rays (below 10 KeV) which affect signal identification and peak resolution.

The background particles can have, in turn, two origins: particles generated by the hadronic interaction of the stopped K^- ("hadronic background"), and "machine background" generated by the electrons and positrons lost from the primary beams circulating in $DA\Phi NE$. This last type of background has two main sources: primary particles lost by the Touschek effect and primary particles lost by beam-gas interaction (Coulomb scattering and bremsstrahlung on the residual gas inside the pipe).

Hadronic background As noted, each stopped K^- has a hadronic interaction at rest with the protons of the target and with the protons and neutrons of the target materials (walls, windows, etc.). As a result of these interactions, "hadronic" particles are produced which can hit the CCDs, depositing energy in them, or, as for the case of photons coming from π^0s decay, initiating an e.m. shower which can produce soft X-rays hitting the CCDs. With the Monte Carlo program, we generated 1100000 ϕ's, corresponding to 42 *min* of beam time at a luminosity of $10^{32} s^{-1} cm^{-2}$ and obtained 10190 ionizing hits on CCDs and 5 X-rays below 10 KeV.

The 10190 ionizing hits on CCDs in 42 *min* correspond to a blindness of 4.07 $part.s^{-1}$ on 8 CCDs (overall surface $\cong 36\ cm^2$), equivalent to 0.113 $part.cm^{-2} s^{-1}$, which means 0.25 $part.s^{-1}$ on 1/2 CCD.

The 5 X-rays below 10 KeV on CCDs in 42 *min* correspond to 0.07 background photons per channel of 100 eV per hour, which means 0.28 X–rays/h over 4 channels. This is equivalent to a background level of $\simeq$ 1.4% and to a signal/background ratio of about 71:1. This *low hadronic soft X-ray background on the CCDs* can be explained by their very thin depletion layer ($30\mu m$), which pre-

vents electrons or positrons to radiate inside the CCD. On the contrary, the usual Si detectors used in previous experiments on kaonic hydrogen (see Chapter 2), were affected by a very high hadronic background of soft X-rays. This was due to the large thickness (few mm), used in order to obtain 100% detection efficiency, which caused the detector itself to act as radiator for electrons and positrons.

Machine background

a) Background from Touschek effect The Touschek background was studied with the dedicated Monte Carlo program in the following configurations:

a.1. DAY-ONE configuration for a KLOE-type section, with the following parameters [3]:

- no central quadrupole;
- aperture of the first quadrupole of 43 mm
- scraper aperture of 9 σ_x
- 915 lost particles per second per beam per bunch
- $8.9 \cdot 10^{10}$ particles per bunch.

In this configuration the lost particles (electrons and positrons) are hitting the pipe with an angle of about 12.5 mrad, in the radial plane, having a distribution along the z-axis (beam-line) spread between (-75, -45) cm and (45,75) cm with respect to the impact point [3].

Using our Monte Carlo program the background coming from the Touschek effect was studied in the following way: 1 million electrons hitting the pipe with an angle of 12.5 mrad in the radial plane, in the region: (-75, -45) cm, (upstream), and having an uniform distribution along the z-axis were simulated. Their interaction (showers) with all the materials present in the experimental set-up were considered, the showers and all the particles created being followed down to 1 KeV, and all the particles hitting the CCD's being recorded.

The rate of lost particles under the conditions of $10^{32} s^{-1} cm^{-2}$ luminosity, corresponding to 30 bunches, is about 55 kHz, which means that the 1 million generated events correspond to a real time of about 18 seconds.

The following numerical results for the operational regime of CCD's (blindness of CCD's) were obtained:

- a total number of 1950 particles depositing energy in the 8 CCD's were obtained, which means:

- Number of particles/s over 8 CCD's = 108 part/s in 8 CCD's
- Number of particles/cm^2/s = 3.0 part/cm^2/s
- Number of particles/s over 1/2 CCD = 6.6 part/s over 1/2 CCD

a.2. DAY-ONE configuration for a KLOE-type section, with the optics parameters as follows:

- no central quadrupole
- aperture of the first pair of quadrupoles (low-beta) of 53 mm
- scraper aperture of 10 σ_x

In this configuration, the number of positive energy lost particles (those for which the relative energy change due to Touschek effect is positive) is zero, whereas for the negative energy lost particles (those for which the relative energy change due to Touschek effect is negative) the loss is 140 lost particles/s/beam/bunch. These particles are lost at 2.2 m from the interaction point (downstream). Since the lost particles are hitting the pipe far away downstream, their contribution can be considered negligible.

b) Background from beam-gas interaction As a starting point for the evaluation of the Coulomb scattering and beam-gas bremsstrahlung background the KLOE note by E. Gero [4] was used. In the report a study of this kind of background was done, with specific reference to the KLOE configuration. In this study the following conditions were considered: average vacuum of $4 \cdot 10^{-10}$ torr and 120 bunches circulating.

From the Gero tables [4], the rates of lost particles hitting the pipe in the region (-46,-10)cm from the interaction point (our region of interest) are:

- Rate of lost particles (charged) coming from Coulomb scattering at large angles: 6 KHz
- Rate of lost particles (charged) coming from Coulomb scattering at small and very small angles: 0 KHz
- Rate of lost particles (charged + photons) coming from hard beam-gas bremsstrahlung: 6.2 KHz
- Rate of lost particles (charged + photons) coming from soft beam-gas bremsstrahlung: 0.7 KHz
- Rate of lost particles (charged + photons) coming from very soft beam-gas bremsstrahlung: 0.8 KHz.

The previous rates take into account reduction of the rates resulting from introducing a scraper before the splitter (Appendix C of [4]). The total rate of Coulomb and beam-gas bremsstrahlung background turns out 13.7 KHz.

In our Monte Carlo program we simulated these effects by generating 6.5 million electrons uniformly hitting the pipe between 10 and 46 cm upstream the interaction point, with an angle distributed between 0.667 and 6 mrad. The resultant secondary particles were followed in the experimental set-up, down to an energy of 1 KeV and all the particles arriving at the CCDs were registered.

We were considering the following two regimes:

1. The luminosity of $10^{32} s^{-1} cm^{-2}$ (30 bunches) and a vacuum of $4 \cdot 10^{-10}$ torr, a situation in which the total rate of loss of particles via Coulomb scattering and beam-gas bremsstrahlung is 13.7/4 KHz = 3.4 KHz. The 6.5 million lost particles generated correspond then to a time of about 1900 seconds. The results are the following:

• Operational limit of CCD's (blindness of CCD's)

The total number of particles depositing energy in the CCD's is 10240, which means:

- Number of particles/s on 8 CCD's = 4.96 part/s
- Number of particles/cm^2/s = 0.14 part/cm^2/s
- Number of particles/s over 1/2 CCD = 0.30 part/s over 1/2 CCD

• X-ray background

A total number of 28 X-rays, with energy below 10 KeV, depositing their energy in the CCD's, were registered in 1900 seconds. This means that we have 0.28 X-rays/channel in 1900 seconds (channel bin 100 eV), or 0.5 X-rays/channel in one hour. Since our signal coming from kaonic hydrogen in one hour is about 20 X-rays, spread over 4 channels, the Coulomb and beam-gas bremsstrahlung X-rays integrated background is about 2 X-rays in one hour in 4 channels. This is equivalent to a 9% X-ray background with respect to the overall number of X-rays in the energy region and to a signal/background ratio of 10:1.

2. If one considers that the vacuum may not be optimal ($4 \cdot 10^{-10}$ torr) at the end of the commissioning, it is realistic to consider a more pessimistic evaluation, taking, for instance, the values of lost particles for the full luminosity of 120 bunches, instead of the figures for 30 bunches.

Under these conditions, which can be assumed as a realistic evaluation, we have seen that the rate of Coulomb scattering and beam-gas bremsstrahlung lost particles is 13.7 KHz, and the 6.5 million lost particles generated correspond to a time of about 480 seconds. The results of the Monte Carlo simulation are:

• Operational limit of CCD's (blindness of CCD's)

The total number of particles depositing energy in the CCD's is 10240 in 475 seconds, which means:

- Number of particles/s over 8 CCD's = 20 part/s
- Number of particles/cm^2/s = 0.56 part/cm^2/s
- Number of particles/s over 1/2 CCD = 1.2 part/s over 1/2 CCD

• X–ray background

A total number of 28 X-rays with energy below 10 KeV, depositing their energy in the CCD's, were obtained in 480 seconds. This means that we have 0.28 X-rays per channel in 480 seconds (channel bin 100 eV), or about 2 X-rays per channel in one hour. Since our signal in one hour is about 20 X-rays, spread over 4 channels, the Coulomb and beam-gas bremsstrahlung X-ray integrated background for 4 channels is about 8 X-rays in one hour. This is equivalent to a 29% X-ray background with respect to the overall number of X-rays in the energy region and to a signal/background ratio of 2.5:1.

6.4 Summary

In conclusion, the Monte Carlo simulation program gives the following results, for a DAΦNE luminosity of $10^{32} cm^{-2} s^{-1}$:

- *K_α 6.5 KeV X-ray rate: about 20/hour*
- *Soft X-ray hadronic background: about 0.28/hour*
- *Soft X-ray machine background: about 8/hour*
  (worst case: bad vacuum conditions during the commissioning phase)
- *Hits depositing energy over half a CCD:*
  - *hadronic: about 15 part/min*
  - *machine: about 72 part/min*

References

1. R. Brun, F. Bruyant, M. Maire, A.C. McPherson and P. Zanarini, GEANT3, CERN Report DD/EE/84-1 (1987) 1.
2. M.Seltzer and M.J.Berger, Nucl. Instr. and Meth. **B12** (1985) 95.
3. S.Guiducci, *Background evaluation in DAΦNE*, addendum to DAΦNE Technical Note **IR-6** (1995).
4. E.Gero, *Beam-gas background calculation for DAΦNE*, KLOE Note **102** (1994).

7 - Conclusion

We have proposed a new experiment to be performed at $DA\Phi NE$ on kaonic hydrogen and demonstrated its full feasibility. The "winning" elements of the proposal are basically the following:

- the unique features, in terms of low momentum, high purity, monochromaticy, which characterize the "kaon beam" produced in the $DA\Phi NE$ collider from ϕ's decay;
- the performance of Charge-Coupled Device (CCD) detector, in terms of resolution and, above all, as background rejection capability, which make this device the best detector for soft X-ray measurements in the background of an accelerator;
- the use of a hydrogen target of moderate density (a cryogenic gaseous pressurized target), in order to reduce Stark mixing effects.

In order to simulate the experimental set-up and its physics performance, we have developed a new version of the CERN code GEANT3 (version 3.21), which is accurate down to 1 KeV. Using this code we have performed a careful evaluation of all the sources of background –both coming from hadron interaction of kaons and as result of the cascades initiated from the particles lost from the circulating beams – which is a crucial point for this measurement.

With the Monte Carlo we have also evaluated the expected rate of the K_α X-rays, which turned out very promising and such to obtain, in 3 hours of data taking, the same statistics collected in all the previous X-ray measurements on kaonic hydrogen.

Acknowledgements

We wish to thank the Director of Frascati Laboratories, Prof. E. Iarocci, for the continuous encouragement and the useful discussions.

We are very grateful to the Director of $DA\Phi NE$ Machine Project, Dr. G. Vignola and to Dr. S. Guiducci for the helpful discussions and their support by providing us essential information on the $DA\Phi NE$ performance.

We acknowledge Dr. F. Nichitiu for his essential role played at the birth of the Proposal, bringing to our attention the fascinating case of the kaonic hydrogen puzzle.

Finally, we acknowledge Mrs. D. Pierluigi who made the editing of the Proposal with skilfulness and patience.

KN SCATTERING AT DAΦNE ?

Art Olin
TRIUMF, 4004 Wesbrook Mall, Vancouver, BC, Canada,olin@triumf.ca

ABSTRACT

Existing measurements of the KN and $\overline{K}$N scattering lengths suffer from large uncertainties, particularly in the I=0 channel. The low energy kaons from ϕ decay available at DAΦNE can be used to improve this situation. Three experimental approaches are discussed:

- A solid hydrogen target and silicon calorimeter surrounding the collision point. This would also use the magnet and tracking detectors of the FINUDA experiment.
- A hydrogen TPC is proposed as an active target in the magnetic field of the FINUDA magnet.
- The FINUDA detector with a CH_2 target could be used to measure an important cross-section.

1 – Motivation

The DAΦNE collider will produce a source of monoenegetic 16 MeV kaons from ϕ decay, and sophisticated targets and detectors may be made to work well inside a kaon decay length. This affords a unique experimental opportunity to study low energy kaon nucleon interactions. In this paper I will discuss some possible target and detector designs that could be appropriate for this environment.

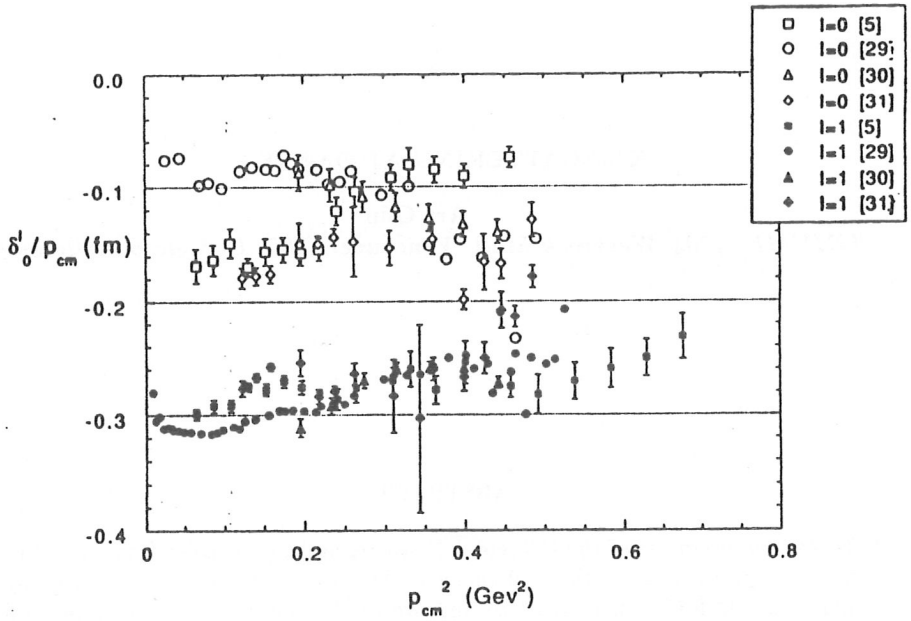

Figure 1:

Elastic K^+N scattering is an interesting system in which to study non-resonant nuclear forces. The K^+ contains a valence u quark and $\bar{s}$ antiquark, and so cannot annihilate with the u and d valence quarks of which nucleons are composed in the naive quark model, so excitation of baryon resonances is excluded. this system is further simplified by the absence of one pion exchange. In the $\overline{K}$N system, on the other hand, there is a rich structure due to the excitation of resonances, particularly the subthreshold $\Lambda(1405)$.

Hadronic scattering lengths play an important role in our understanding of non-perturbative QCD. These observables, though nontrivial, can be calculated with current techniques. Calculations have been carried out using the cloudy bag model [1, 2], and the non-relativistic quark model [3]. Lattice gauge techniques have also been used to calculate non-resonant scattering lengths [4]; these techniques could be applied to the KN system. In the cloudy bag model, the KN scattering lengths depend only on the contact part of the interaction, and the I = 0 isospin component is 0 as a consequence of chiral SU(3) symmetry. Higher quality data would help determine the extent to which chiral models are applicable to kaonic systems. In the quark model formalism, the dominant process is one gluon exchange, and the ratio of I=0 to I=1 scattering lengths depends on the shape of the quark wavefunctions.

There is at present substantial interest in the strangeness content of the nucleon. This has arisen because of several experimental results which can be explained theoretically by the inclusion of a significant admixture of strange quarks in the nucleon wavefunctions. The best known are the long-standing problem of the $\pi N\sigma$-term [5] and the recent studies of the proton spin structure function [6]. The resolution of the question of whether the nucleon contains strange quarks is of fundamental importance because it relates to our understanding of QCD at the confinement scale. It has been suggested by Jaffe and Korpa [7] that new data and an improved theoretical analysis of the $KN\sigma$-term is important for the resolution of this problem. Extraction of the $KN\sigma$-terms from the presently available experimental data cannot provide an adequate test because at present the experimental errors are much too large [8].

There is also considerable interest in the nature of the $\Lambda(1405)$. In quark models it is nearly impossible to simultaneously fit both the $\Lambda(1405)$ and the $\Lambda(1520)$. Thus it is significant that in the cloudy bag model [1, 2] the $\Lambda(1405)$ is a $\overline{K}$N quasi-bound state arising from $\overline{K}$N $\Sigma\pi$ coupled channel potentials while the $\Lambda(1520)$ remains a nearly pure quark state [2]. Studies of the $\Lambda(1405)$are complicated because it is half way between the $\overline{K}$N and $\Sigma\pi$ thresholds. Its structure is far from a pure Breit-Wigner resonance and ref. [2] suggests that there are two poles in the complex plane rather then the one naively expected. High quality data for both the $\overline{K}$N$\rightarrow\overline{K}$N and $\overline{K}$N $\rightarrow \Sigma\pi$ reactions close to the $\overline{K}$N threshold would help clarify the nature of the $\Lambda(1405)$.

The experimental data on the KN and $\overline{K}$N scattering lengths is limited. It comes from bubble chamber measurements carried out using 100-300 MeV K's, so the low energy points are from reactions observed at the ends of long tracks. The technique proposed here will be very different in terms of systematic errors. It can be seen from Fig 1 (taken from Barnes *et al.* [3]), that, despite the large errors. the experiments give conflicting results. The accessible reactions are (K^+ p, K^+ p), (K^0_L p, K^+ n), (K^0_L p,K^0_S p), (K^0_L p,K^0_L p), and, using a deuterium target, (K^+ n,K^+n). These measurements will pin down the poorly known KN I=0 scattering length. Also the measured K^-p scattering length, to be determined from (K^- p, K^- p), is incompatible with the energy shift of the K^-p atomic Xray.

2 – FINUDA for the KN measurements

The FINUDA detector has already been described in some detail at this meeting. It can be used to provide neutron detection and also tagging for the various reactions

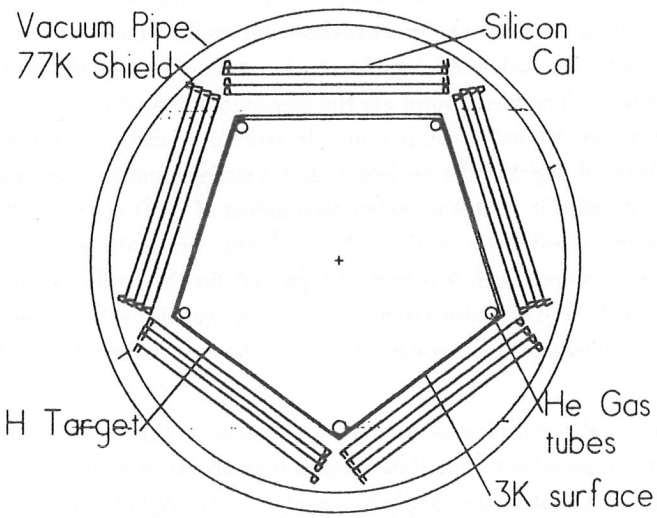

Figure 2: Schematic arrangement of the solid hydrogen target and Si calorimeter. The view is along the beam direction with the collision region in the center.

involved. In particular, it can provide a charge tag for K's which scatter and subsequently decay. From the $K^0_S \to \pi\pi$ decay one can tag an associated K^0_L. In this way the outer tracking chambers and TOFONE provide very useful information, and it seems efficient to incorporate them in the design of a KN scattering experiment. The targets and detectors described in the next sections will be placed inside the FINUDA magnet and tracking chambers.

3 – A Solid Hydrogen Target for DAΦNE

For the KN measurements a solid hydrogen target could be incorporated near the collision point as shown in Fig 2. The innermost pentagonal section of beam pipe is attached to pipes carrying He gas and cooled to 3°K. A solid hydrogen or deuterium layer, about 0.5 mm thick, will be condensed onto the outer surface of this pipe. A differential pressure valve system will be required to limit the pressure difference allowed across the inner pipe.

The task of maintaining a 20cm long solid hydrogen target at 3°K in the envi-

ronment of a collider interaction region poses some unusual problems. Our proposed solution [9] is to cool with a flow-through pumped He cryostat capable of providing 2W of cooling power at 3°K. The target will be surrounded by a shield clamped to 77°K cooled by liquid nitrogen. The shield is extended for 50cm along the beam line in order to limit the radiative heat load on the target. A conceptual layout is shown in Fig 3. Note that the hydrogen is to be frozen on to the outside of very thin foils attached to the cooling pipes. These will be Be or Al depending on our construction experience with prototypes. These foils will not be exposed to a substantial pressure differential, but can provide a measure of isolation from the collider vacuum. The heat loads considered on the target are thermal radiation along the beam pipe, heating by currents induced by the collider beam, and heating from the incident synchrotron radiation.

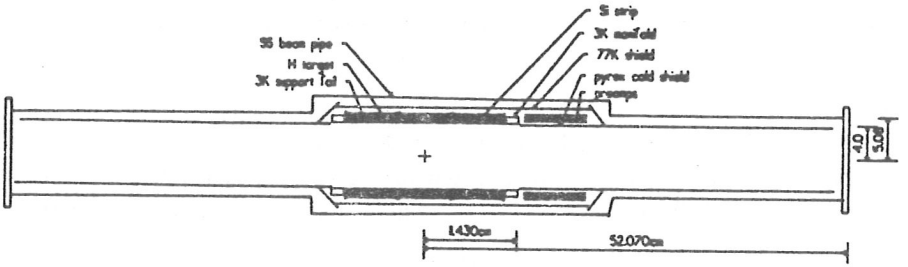

Figure 3: Schematic arrangement of the solid hydrogen target and associated beam line viewed from above.

The image-current heating is a well-studied problem in the engineering of RF cavities [10]. For the DAΦNE situation of 5A beams the effective frequency is 6GHz. For the highest quality copper at room temperature, we calculate a heat load of 1W, which would present a clear problem. At 77°K it is 500mW. We propose to cover the inside surface of the target support foils with 1 μm of Nb which will be superconducting. Using measured surface resistivities in superconducting RF cavities, a heat load of only 0.4 mW is then expected. The cold section of the beam pipe making the transition to 77°K will be constructed of pyrex glass to avoid the problem of image current heating.

The intensity of the synchrotron radiation on the hydrogen target has been calculated using formulas from a handbook used to design synchrotron radiation beams [11]. The peak photon energy is 33eV, and the total radiated power is 3.4KW. The hydrogen target subtends an angle of 0.3 mrad, resulting in a heat load of about

measurement, while the remaining three layers are 500 μm to ensure that all the recoils stop in the calorimeter, while most of the unscattered kaons pass through. The inner detector has 2-coordinate readout, but a pixel size of 1 mm^2 is all that is necessary to ensure that the recoils fall on separate pixels. For the outer three detectors only single sided readout is required. A measurement of the opening angle of the pions from K^0_S decay to 1° will determine the K^0_S energy to approximately 1 MeV.

The Si calorimeter would operate at 77°K. It could be constructed of ladders of planar detectors 64x64 mm^2 forming a pentagon. Cooling of the detectors would be mainly through their radiation to the surrounding cryostat. A set of trigger scintillators is placed just outside the vacuum region. Surrounding this are the components of the FINUDA spectrometer for hypernuclear measurements; for the KN work their function is to determine the charge of the kaons from the charges of the decay particles.

A simulation program using GEANT routines and incorporating generally the apparatus just described has been used to investigate and optimize the detector characteristics. This consists of an event generator producing kaon pairs, an optional routine to force a chosen reaction in the hydrogen or deuterium target, and then

100mW. The heat deposited on the pyrex shield is not considered to be a problem because of the high cooling power at 77°K.

The heat load from infrared radiation along the beam pipe is estimated to be 60 mW from the 77°K pipe and 40mW from the 300°K pipe, for a total of about 100mW. This could be further improved by recessing the target by 1 mm in order to reduce its solid angle to the radiation.

4 – A Silicon Calorimeter for KN recoils

The target region is surrounded by a silicon microstrip calorimeter consisting of four layers of silicon microstrip detectors whose purpose is to measure the energy and $\frac{dE}{dx}$ of the scattered particles. The first layer is rather thin - 150 μm- for the $\frac{dE}{dx}$ some analysis code to look at energy deposit patterns in the silicon detectors, cell occupancies, coincidence efficiencies, and angular and energy resolution.

The (K^+ p, K^+ p) interaction has a rather clear signature consisting of both energy and energy loss measurements in the silicon calorimeter, together with a tag of one of the K-decay particles to identify the charge of that vertex. The requirement that the proton exit the 0.5mm H target eliminates the 0°-30° region which includes the interesting Coulomb interference effects. The scattering angle would be computed from the energies deposited by the scattered particles in the calorimeter. The hit position of the tagging kaon then gives redundant information. All this information is independent of multiple scattering in the silicon, thus allowing a good determination of the acceptance. Fig 4 shows a set of simulation calculations of detector response to this reaction. From the scatterplot of energy deposited against scattering angle one may gauge the the uncertainty in scattering angle introduced by energy loss in the target, and also the angular acceptance. A comparison of Fig 4d with 4c shows the effect of the additional energy from kaon decays deposited in the same pixels as the kaon track. It appears that this effect is reasonably small, but may impose a systematic limit on our calculation of the acceptance. Of course, no such additional energy is produced by the scattered proton. Good K - p discrimination is found using ΔE vs E scatterplots for particles traversing more than one silicon wafer. Even when cuts are imposed requiring coincidence kaons and protons both with particle ID and with energies summing to 16 MeV a respectable acceptance remains. The optimum analysis technique will require enough information to uniquely identify the event while having an accurately calculable acceptance.

For the (K^- p, K^-p) events the K^- will usually be captured in the Si calorimeter rather than decaying. The additional energy deposited from the capture products will cause events to be lost due to the sum energy cut, thus reducing the acceptance. Again this can be recovered by relaxing the energy cut on the kaon track and obtaining the scattering angle from the proton.

The signature of the (K^0_L p, K^+ n) reaction consists of the K^0_S decay vertex, K^+ in the Si calorimeter, and a neutron with the correct time of flight and angle. In this case a clear identification of the K^+ might prove sufficient, which would improve our efficiency. The redundant neutron scattering angle and TOF information allows one to distinguish the direct reaction neutrons from neutrons and photons produced in other processes. This will also be important for (K^+ n, K^+ n) measurements using a deuterium target.

With Daphne producing 1000 ϕ /s, (20% of the nominal rate) and typical

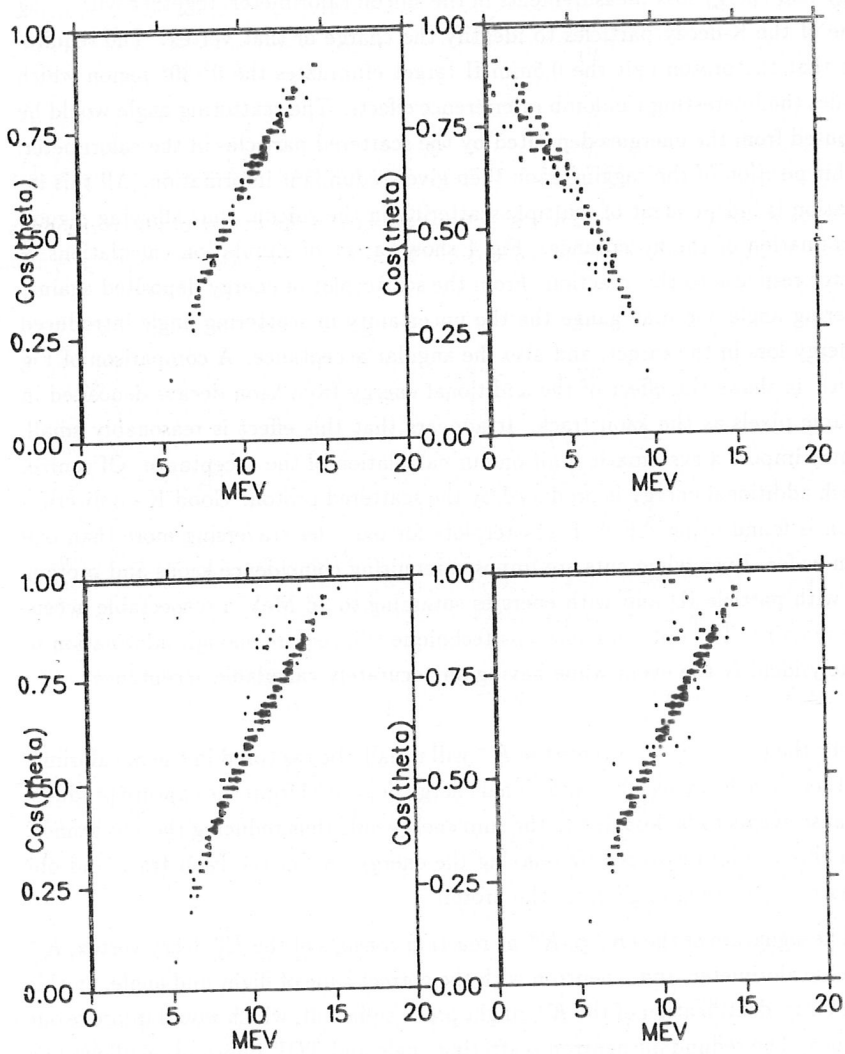

Figure 4: a) K^+ with p in coincidence, particle id, and sum energy cut.
b) Proton, same cuts as a).
c) K^+ deposited energy without proton coincidence requirement. d) as c) but including the additional energy from K^+ decays.

Table 1: Calculated detector acceptances (%)

Reaction	Meson	Baryon	Coinc +ID	Energy sum
K^+ p $\rightarrow K^+$ p	49	55	40	25
K^0_L p $\rightarrow K^+$ n	43	14	14	7
K^- p $\rightarrow K^-$ p	42	53	37	23
K^+n $\rightarrow K^+$n	60	58	13	11

KNcross sections of 20 mb, an interaction rate in the the target of about 0.1 hz is expected. The calculated acceptances for the various event signatures are given in Table 2.

Target thickness and uniformity is an important consideration in this experiment. We prepared hydrogen layers at TRIUMF on a cold backing with five implanted ^{241}Am spot sources in order to study the target uniformity. The α's were detected using a silicon counter. By introducing the hydrogen into the vacuum volume at a distance and a pressure of 5×10^{-4} torr and with the surface temperature at 4°K, layers uniform within the measurement accuracy of 5% were obtained. The energies of the unscattered charged kaons provide an excellent monitor of the hydrogen layer thickness during the run.

5 – A Hydrogen TPC as an Active Target/Detector

An alternative worth considering is a hydrogen TPC. While it is known that hydrogen gas is problematic as a wire chaber gas, it has successfully been used in a TPC by a Fermilab $\gamma + p \rightarrow X + p$ measurement [12]. In this case, as in KN scattering, the emphasis was on the tracking of heavily ionizing particles, namely protons of energy 10 MeV to 50 MeV. The Fermilab TPC was 45cm diameter and 75cm long and operated at 15 bar in a field of 0.1 T. A resolution of 200 μm was achieved for minimum ionizing particles.

For KN we are studying via simulations a TPC with rather similar properties:

- Size 50cm diameter ,25cm length enclosing a Be beam pipe of 10cm diameter
- Pressure 1 bar and operating at 40°K
- Axial magnetic field of 1.1 T.

The higher dE/dx of our very slow particles will compensate the higher H_2 density used in the Fermilab experiment, so we anticipate that comparable or better

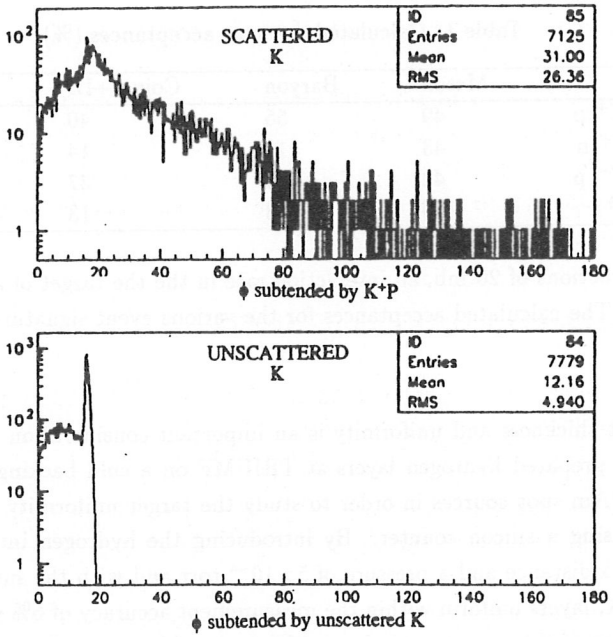

Figure 5:

resolution will be obtained for this detector. This is not critical since the track lengths are typically many centimeters. Drift time for the electrons is 25 μm, so event rates of a few kiloherz can be handled. In contrast to the Si calorimeter, this detector would have advantages in cost, acceptance, and uniformity. For a 1 Khz ϕ production rate a reaction with 20 mb an event rate of 0.05 hz is predicted.

A very nice feature of this detector is the ability to have an efficient trigger for KN scattering events. Unscattered K^+ travel radially and their tracks projected onto the endcap would subtend an angle ϕ of 16°. In figure 5 we compare these track ϕ values for KP scattering events with the unscattered tracks. Clearly this can form the basis for a very simple and specific trigger if a radial readout scheme for the endcap is implemented. A prescaled two particle prompt trigger would be used to monitor the incident flux.

With the lower gas density, it is possible that the TPC will not be able to track minimum ionizing particles. This is important, for example, for reactions involving a K^0_S tag. In that case, the tracking capability of the FINUDA chambers would be needed in addition to the TPC. Otherwise only the neutron detectors and magnet would be required.

Systematic errors in this approach will come from the accuracy and efficiency

of identifying the desired reaction within a fiducial volume. The relevant factors, position resolution and particle identification, seem to be under good control, so very precise data seems possible. The excellent position resolution will allow measurements of small angle scattering, well into the Coulomb interference region which is sensitive to the sign of the phase shifts. Thus this approach looks very promising, and the next steps to be taken are simulations of the acceptance for various reactions and a closer look at the technical design.

6 – KN measurements with the FINUDA detector

One of the reactions which can determine the I=0 scattering length is $K^0_L p \rightarrow K^+ n$. Direct measurements from bubble chamber days are $\sigma = 1.6 \pm 0.7$ mb at 0-600 MeV/c [13], and $\sigma = 9.6 \pm 1.8$ mb at 600 MeV/c [14].

Let us consider the signature for this reaction occuring in a CH_2 target in its normal position in the FINUDA detector.This event would have a simple signature:

- A reconstructed K^0_S.
- A single charged K^+ track through OSIM, the outer silicon tracker.
- No corresponding ISIM hit.
- A neutron with correct angle and TOF in TOFONE, the outer thick scintillator barrel.

Since the TOF will give a very accurate value for the neutron energy, the energy resolution for the K^+ is not of great importance, and thus rather thick CH_2 targets can be utilized.

To trigger on such events we could require:

- Two prompt hits in ISIM (from K^0_S decay).
- Hit in TOFONE with delay appropriate for a 2 MeV-15 MeV neutron.
- A delayed hit 5ns < t < 20ns in TOFONE (from the K^+.)

Again, simulation studies are needed to estimate the rates and achievable precision.

Acknowledgements

The simulation calculations have been carried out together with Guiseppi Tagliente of the University of Bari, who has been visiting TRIUMF this year supported by an Italian Government Fellowship. I also thank Dave Gill, George Beer, Byron Jennings, Ted Barnes, and Toshio Numao for valuable discussions.

References

1. E.A. Veit, A.W. Thomas, and B.K. Jennings, Phys. Rev. D31(1985) 2242.
2. G.H. He and R.H. Landau, University of Oregon Preprint OSU-THK-1003.
3. T. Barnes and E.S. Swanson, Phys. Rev. C49(1994) 1166.
4. R. Gupta, A. Patel, and S.R. Sharpe, Nucl. Phys. B383(1992) 309.
5. T.P. Cheng and R. Dashen, Phys. Rev. Lett. 26(1971) 33; C.A. Dominguez and P. Langacker, Phys. Rev. D24(1981) 1905.
6. J. Ashman *et al.*, Phys. Lett. B206(1988) 364 and Nucl. Phys. B328(1989) 1.
7. R.L. Jaffe and C.L. Korpa, Comments Nucl. Part. Phys. 17 (1987) 163.
8. P.M. Gensini, in Workshop on Physics and Detectors for Daphne, ed G. Pancheri (INFN-LNF 1991) 453.
9. This design has been prepared in conjunction with Calvin Winter of Quantum Technologies, Inc.
10. H. Piel, Superconducting Cavities, from Superconductivity in Particle Accelerators, CERN 89-04.
11. J. B. Murphy, Synchrotron Light Source Data Book, from Physics of Particle Accelerators, AIP Conf. Proc. 249 (1992).
12. T.J. Chapin, R.L. Cool, K. Goulanos, J.P. Silverman, G.R. Snow, H. Sticker, and S.N. White, Nucl. Inst. and Methods 197 (1982) 305.
13. G.W. Meisner and F.S. Crawford, Phys. Rev. D3(1971) 2553.
14. J.C.M. Armitage et al, Nucl. Phys. B123(1977) 11.

HYPERNUCLEI AND K–N INTERACTIONS

PARALLEL SESSION

A. Molinari	About the Decay of the Λ in a Nucleus	393
A. Ramos	One–And Two–Nucleon Induced Λ Decay	405
R. Alzetta	Non Leptonic Λ Weak Decays in Light to Medium Hypernuclei	415
R. Sawafta	Σ Hypernuclei	427
B. Saghai	Low Energy K^-–Proton Interactions	435
T. Barnes	KN Scattering in the Nonrelativistic Quark Model	445
R.C. Barrett	Relativistic Equations for Kaon–Nucleus Interactions	459
M. Iwasaki	Measurement of Kaonic Hydrogen X–Rays at KEK	461

ABOUT THE DECAY OF THE Λ IN A NUCLEUS

W.M. Alberico, M.B. Barbaro and A. Molinari

Dipartimento di Fisica Teorica dell'Università di Torino and
Istituto Nazionale di Fisica Nucleare, Sezione di Torino
Via P. Giuria 1, I–10125 Torino, Italy

Abstract

A few aspects of the Λ mesonic and non-mesonic decay in nuclei are shortly addressed.

1 The mesonic decay of the Λ

In the following we shortly deal with the decay of the Λ inside a nucleus.

In free space the decay of the Λ into a pion and a nucleon is characterized by a long lifetime ($\tau_\Lambda = 2.63 \times 10^{-10}$ s) because it stems from the weak interaction and its occurrence goes together with a change of strangeness. Yet in a nucleus, at variance with the neutron, the Λ remains unstable.

Indeed in the former case the neutron-proton mass difference of 1.26 MeV should be compared with about 8 MeV of binding energy: hence the general stability of the neutron inside a nucleus and, as a consequence, of the nucleus itself. On the contrary in the case of the Λ one has

$$m_\Lambda - (m_N + m_\pi) \sim 40\ MeV \tag{1}$$

which is substantially larger than the Λ binding energy in a nucleus [1]: hence the instability of an hypernucleus.

However one would like to know how nuclear structure affects τ_Λ. If one sticks to a pure mesonic decay, namely

$$\Lambda \to p + \pi^- \tag{2}$$

or

$$\Lambda \to n + \pi^0 \,. \tag{3}$$

then it is easily recognized that when the Λ is at rest the energy E_N and the momentum p_N of the emitted nucleon are given by

$$E_N = \frac{p_N^2}{2m_N} \simeq \frac{(m_\Lambda - m_N)^2 - m_\pi^2}{2m_\Lambda} \sim 5\ MeV \tag{4}$$

and

$$p_N = \sqrt{2m_N E_N} \simeq 100\ MeV/c \tag{5}$$

respectively. Hence, conceiving the nucleus as a Fermi liquid with a Fermi momentum in the range $220 \leq k_F \leq 270\ MeV/c$, it turns out that the Λ decay is Pauli blocked, which is indeed what happens already for quite low mass number, starting, say, from $A \simeq 15$ or even less.

A detailed calculation of the pionic Λ decay in a nucleus has been recently performed by Oset and Nieves [3]. Their findings are displayed in Fig.1.

The following is worth noticing in their results:

i) the width for the processes (2) and (3) is indeed reduced by orders of magnitude with respect to the free space and the reduction grows with the mass number A, as expected;

ii) when the distorsion of the outgoing pion is accounted for by letting the latter to move in an optical potential, then the reduction is somewhat tempered, but of course it remains very substantial;

iii) finally of much relevance is that for ^{41}Ca the width for decaying in the uncharged channel (3) becomes even larger than the one for decaying in the charged channel (2), thus possibly indicating a violation of the $\Delta I = 1/2$ rule.

2 The $\Delta I = 1/2$ rule

A remarkable empirical finding in the Λ decay relates to a selection rule holding in isospace. It is indeed found that the decay of the isospin zero ($I = 0$) Λ leads overwhelmingly to a pion and a nucleon coupled to an isospin $I = 1/2$ rather than to an $I = 3/2$ state. The consequences, easy to work out, of this selection rule on the decay width are

$$\Gamma(\Lambda \to n\pi^0) = \frac{1}{2}\Gamma(\Lambda \to p\pi^-) \tag{6}$$

or

$$\frac{\Gamma(\Lambda \to charged\ hadrons)}{\Gamma(\Lambda \to all\ hadrons)} = \frac{2}{3} \tag{7}$$

and are found to hold to within a few percent. Yet violations occur and indeed one has just been quoted above for the mesonic channel. Further ones are expected to occur in the non-mesonic channel.

Furthermore, the theoretical foundation of the rule remains still now rather obscure.

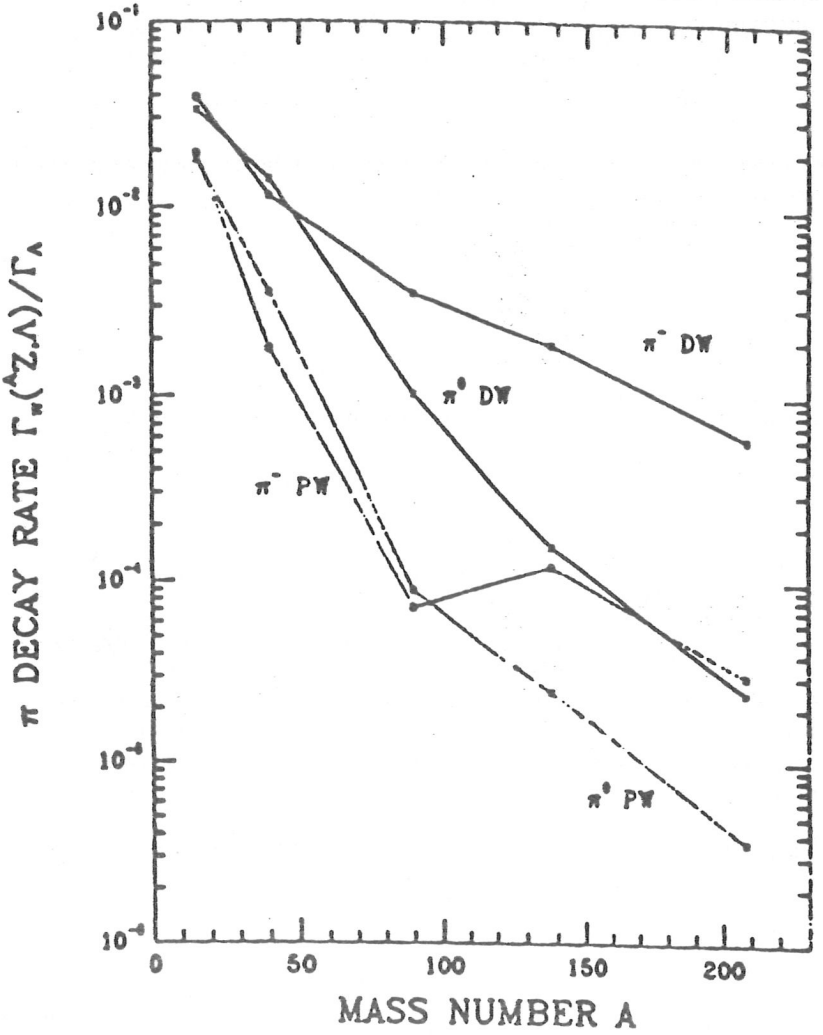

Figure 1: The mesonic width Γ_π versus the free one as calculated by Oset and Nieves [2].

3 Non-mesonic decay of the Λ: one nucleon induced process

An alternative route for the decay of the Λ in a nucleus was first conjectured by Block and Dalitz as long ago as 1963 [4]. It may be referred to as the *one nucleon induced decay.* Indeed it corresponds to the occurrence of the process

$$\Lambda + N \rightarrow N + N \,. \tag{8}$$

Assuming the energy to be equally shared by the two outgoing nucleons one has for the energy of a nucleon

$$E_N \simeq \frac{m_\Lambda - m_N}{2} \sim 89 \; MeV \,. \tag{9}$$

Hence

$$p_N = \sqrt{2 m_N E_N} \simeq 400 \; MeV/c \gg k_F \,. \tag{10}$$

This channel of decay thus escapes the blocking induced by the Pauli principle and indeed the experimental finding for the ratio of the widths associated with the non-mesonic decay Γ_{nm} versus the mesonic one Γ_π yields

$$\frac{\Gamma_{nm}}{\Gamma_\pi} \gg 1 \tag{11}$$

already for $A \gtrsim 8 \div 10$.

An interesting calculation of the non-mesonic one nucleon induced decay has been performed by Ramos and Bennhold [2] in the hypernucleus ${}^{12}_{\Lambda}C$. These authors assume a weak meson-exchange interaction (namely having one strong and one weak vertex) carried by $\pi, \eta, K, \rho, \omega$ and K^* and also address the question of the nature of the partner nucleon assisting the decay (namely whether it is a proton or a neutron). Their results [2] deserve two comments:

i) concerning the width it appears that, when all the above mentioned mesons carrying the interaction are brought into the game, one obtains a value essentially identical to the one obtained with the pion alone, which is however still somewhat lower than the experimental value ($\Gamma_{nm}/\Gamma_{free} = 0.87$ to be compared with the experimental value $\Gamma_{exp}/\Gamma_{free} = 1.14 \pm 0.20$);

ii) concerning the ratio Γ_n/Γ_p, where the width Γ_n relates to the non-mesonic Λ decay with a neutron partner whereas Γ_p has a proton partner, the theoretical prediction with the pion alone is 0.19, whereas with the full interaction it grows to 0.3, still a long way from the experimental value $1.33^{+1.12}_{-0.81}$.

Of significance is that only the lower bound of the experimental value appears to overlap with the predictions of the $\Delta I = 1/2$ rule, eventually indicating a violation of the latter.

For a better appreciation of the related physics it is worth now to briefly review how the Λ decay width is actually calculated. The basic formula is of course

$$\Gamma_\Lambda = -2Im\ \Sigma_\Lambda\ , \tag{12}$$

Σ_Λ being the Λ self-energy. Diagrammatically the process is illustrated in Fig.2, where the free and the *in medium* decay are displayed.

In the free case clearly the free pion propagator

$$\mathcal{D}_0(q,\omega) = \frac{1}{\omega^2 - q^2 - \omega_q^2}\ , \tag{13}$$

where

$$\omega_q = \sqrt{q^2 + m_\pi^2}\ , \tag{14}$$

should be used in calculating the Λ self-energy. One thus gets

$$\Gamma_\Lambda = \frac{3}{\pi}\int_0^\infty dq q^2 \left(s_\pi^2 + \frac{p_\pi^2}{m_\pi^2}q^2\right)\frac{\delta(\omega - \omega_q)}{2\omega_q} \tag{15}$$

where both the s and the p waves of the emitted pion are permitted owing to the parity non-conservation (actually the s piece violates the parity, the p one conserves it). To get the experimental value of the free Λ decay one uses the values

$$s_\pi = 2.34^{-7}\ ,\ \ p_\pi = 1.17 \times 10^{-7}\ . \tag{16}$$

The mesonic decay in the nucleus requires instead the π propagator in the medium, which reads

$$\mathcal{D}(q,\omega) = \frac{1}{\omega^2 - q^2 - \omega_q^2 - q^2\Pi(q,\omega)}\ , \tag{17}$$

$\Pi(q,\omega)$ being the so-called polarization propagator.

In order to describe the one nucleon induced Λ decay, $\Pi(q,\omega)$ should embody the particle-hole (ph) excitations of the system. For nuclear matter these cover the dashed region of Fig.3 and how they enter into the non-mesonic decay channel is illustrated by the diagram displayed in Fig.4a.

It is clear that only a far off-shell pion can excite ph states since the curve corresponding to the energy available for the emitted pion, namely

$$\omega = \Delta m - \frac{q^2}{2m_N} \tag{18}$$

with $\Delta m = m_\Lambda - m_N$, overlaps with the allowed ph zone only for pions far from the on-shell line (and also from the pionic branch in nuclear matter).

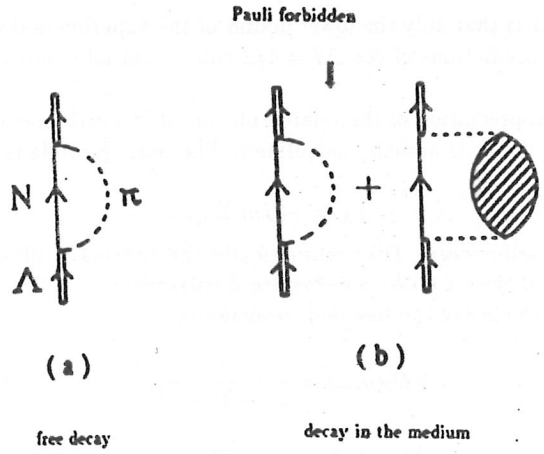

Figure 2: The Λ self-energy Σ in free space (a) and in the medium (b). The content of the dashed bubble is largely dictated by the degree of off-shellness of the pion.

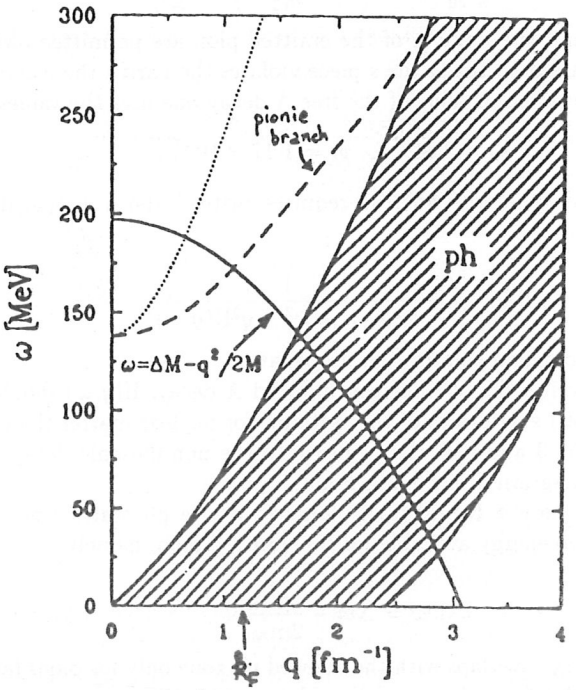

Figure 3: The excitation spectrum of nuclear matter. Dashed region: the p-h excitations. Also shown: the pionic branch in the vacuum and in the medium ($k_F = 1.2fm^{-1}$) and the Δ-excitation.

Even when the difference in the potential energy felt by a Λ and a nucleon inside nuclear matter in taken into account in (18),

$$\omega = \omega_m = \Delta m + (V_\Lambda - V_N) - \frac{q^2}{2m_N} , \tag{19}$$

the above conclusion is not going to be much changed.

Naturally pions emitted from the weak vertex can be far off-shell and thus the one nucleon induced process opens an important door for the Λ decay in a nucleus, as in fact the previously quoted calculation of Ramos and Bennhold [2] indicates.

Additional support comes from the approach to the same problem followed by Alberico *et al.* [5]. These authors use the RPA expression for the polarization propagator, namely

$$q^2\Pi_{ph}(q,\omega) = \frac{q^2\Pi^0(q,\omega)}{1 - g'(q)\Pi^0(q,\omega)} \tag{20}$$

$\Pi^0(q,\omega)$ being the bare ph propagator, which however, unlike in ref. [2], also includes the Δ resonance, namely

$$\Pi^0 = \Pi_0^N + \Pi_0^\Delta . \tag{21}$$

For the short range repulsion the Landau and Migdal type phenomenological expression [6]

$$g'(q) = \Gamma_\pi^2(q,\omega)\frac{1}{3}\frac{q^2 + q_c^2}{q^2 + q_c^2 + m_\pi^2} + C_\rho\Gamma_\rho^2\frac{2}{3}\frac{q^2 + q_c^2}{q^2 + q_c^2 + m_\rho^2} , \tag{22}$$

with $q_c = 600$ MeV, is utilized.

It is worth pointing out that $g'(q)$ couples the weak vertex not only to pionic modes, but also, via the parity conserving piece (p-wave), to the transverse (ρ-like) modes. The above takes care of the strong vertex where the virtual pion is absorbed.

Concerning the weak vertex, where the virtual pion is emitted, Alberico *et al.* [5] deduce the following expressions

$$V^{(s)}(q,\omega) = q^2\mathcal{D}_0(q,\omega) - q^2\tilde{\mathcal{D}}_0(q,\omega) \tag{23}$$

$$V^{(p,L)}(q,\omega) = g'_\Lambda + q^2\mathcal{D}_0(q,\omega) - \frac{2}{3}q^2\tilde{\mathcal{D}}_0(q,\omega) \tag{24}$$

$$V^{(p,T)}(q,\omega) = g'_\Lambda + \frac{1}{3}q^2\tilde{\mathcal{D}}_0(q,\omega) \tag{25}$$

where g'_Λ is taken just as a parameter (positive) simply because at present it cannot be computed and $\tilde{\mathcal{D}}_0(q,\omega)$ is the free pion propagator with q^2 replaced by $q^2 + q_c^2$.

The above vertices should then be inserted into the formula, easily derived from (15).

$$\Gamma^{(s)} = -\frac{3}{\pi^2} s_\pi^2 \int_{k_F}^{q_{max}} dq \left[V^{(s)}(q,\omega)\right]^2 Im\ \Pi_L(q,\omega)\ |_{\omega=\omega_m}\ , \tag{26}$$

to get the s-wave decay width, and into

$$\Gamma^{(p,\sigma)} = -\frac{3}{\pi^2}\frac{p_\pi^2}{m_\pi^2} \int_{k_F}^{q_{max}} dq \left[V^{(p,\sigma)}(q,\omega)\right]^2 Im\ \Pi_\sigma(q,\omega)\ |_{\omega=\omega_m}\ , \tag{27}$$

to get the p-wave one (ω_m is given by (19)). In the above total Pauli blocking has been assumed (the lower limit of integration is indeed k_F, the upper one being $q_{max} = \sqrt{2m_N(\Delta m + V_\Lambda - V_M)}$, as it is straightforward to verify) and the index σ refers to both the longitudinal (L) and transverse (T) channel, respectively.

The obtained results for the one-nucleon induced Λ decay are displayed in the first four row of Table 1 for a variety of choices for the parameter g'_Λ, which of course affect only the parity-conserving p-channel.

g'_Λ	0	0.1	0.2	0.3	0.4	0.5
$R_1^{(s)}$	0.36	0.36	0.36	0.36	0.36	0.36
$R_1^{(p,L)}$	1.02	0.69	0.42	0.22	0.091	0.024
$R_1^{(p,T)}$	0.008	0.012	0.096	0.26	0.51	0.83
R_1	1.39	1.06	0.88	0.84	0.96	1.22
$R_2^{(s)}$	0.40	0.40	0.40	0.40	0.40	0.40
$R_2^{(p,L)}$	0.40	0.31	0.24	0.18	0.12	0.079
$R_2^{(p,T)}$	0.0002	0.0009	0.005	0.013	0.025	0.040
R_2	0.79	0.71	0.64	0.59	0.54	0.52
$R = R_1 + R_2$	2.18	1.77	1.52	1.43	1.50	1.74

Table 1. Various contributions to the ratio R between the Λ decay widths in RPA-correlated nuclear matter and in the vacuum for different values of g'_A [5]. The second, third and fourth rows give the s-wave, the longitudinal and transverse p-wave and the total contribution respectively for the one-nucleon induced Λ decay. The same quantities for the two-nucleon induced Λ decay are quoted in the next four rows. In the final row the global ratio is displayed.

Note that for $g'_\Lambda = 0.3 \div 0.4$ the quoted nuclear matter result is essentially in accord with the previously reported one of ref.[2], obtained with a sophisticated interaction in an hypernucleus as light as ${}^{12}_{\Lambda}C$. On the other hand Ramos, Oset and Salcedo [8] obtain for a variety of nuclei (see Table 2) results substantially larger than those of Table 1, which might be due to the fact that the calculations in ref.[8] is done in finite nuclei in a local density approximation and with experimental single particle energies (but ignoring the Δ contribution).

	Γ_π	Γ_{1p1h}	Γ_{2p2h}
${}^{12}_{\Lambda}C$	0.31	1.45	0.27
${}^{16}_{\Lambda}O$	0.24	1.54	0.29
${}^{20}_{\Lambda}Ne$	0.14	1.60	0.32
${}^{40}_{\Lambda}Ca$	0.03	1.76	0.32
${}^{56}_{\Lambda}Fe$	0.01	1.82	0.32
${}^{89}_{\Lambda}Y$	-	1.88	0.31
${}^{100}_{\Lambda}Ru$	-	1.89	0.31
${}^{208}_{\Lambda}Pb$	-	1.93	0.30

Table 2. Hypernuclear decay widths according to [8]. Γ_π is the mesonic width, Γ_{1p1h} is the width for the decay (one-nucleon induced) into a two-nucleon final state whereas Γ_{2p2h} (two-nucleon induced) relates to a final state with three nucleons.

4 Non-mesonic decay of the Λ: two nucleons induced process

Alberico *et al.* [5] conjectured in 1990 that an alternative non-mesonic decay channel for the Λ in a nucleus could be offered by letting the pion to be absorbed by a correlated pair of nucleons (or to excite a 2p-2h state), as illustrated in Fig.4b.

This process goes in parallel to the related absorption of a real photon of, say, 100 MeV of energy, whose occurrence on a single nucleon in a nucleus can hardly meet the requirements of energy and momentum conservation.

A glance at Fig.3 is sufficient for concluding that pions emitted close to the mass shell preferentially select this channel to be absorbed, thus allowing the Λ to decay.

One has to realize that, in the medium, the pion dispersion relation corresponding to the pionic branch of Fig.3 would intercept (19) (with $V_\Lambda - V_N = 20\ MeV$) still in the Pauli blocked region, namely at $q \simeq 1.09\ fm^{-1}$. However the pionic branch in the medium has a width associated precisely with the 2p-2h excitations above referred to and, owing to this width, the decaying Λ can escape the constraints arising from the Pauli principle.

Indeed in the energy domain $\omega \simeq m_\pi$ the pionic branch decays via 2p-2h emission and thus overlaps with the parabola (19) also *outside the Pauli blocked domain.* Obviously the Λ decay in this instance results in a 3p-2h final state, as shown in Fig.4b.

The pioneering calculation of this process carried out in ref.[5] assumed

$$Im\ \Pi^*_{2p-2h} \neq 0 \quad \text{only when} \quad Im\ \Pi_{ph} = 0\ , \tag{28}$$

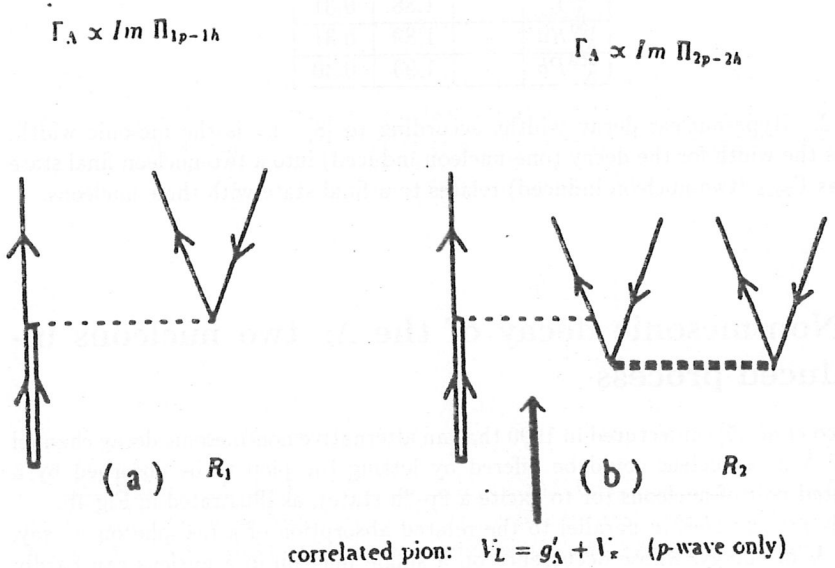

Figure 4: Schematic representation of the Λ decay: in the case a) the decay is driven by the coupling with a p-h excitation; in the case b) the decay is driven by the coupling with a 2p-2h excitation.

i.e. the complicated physics associated with the interference between 2p-2h and 1p-1h excitations is ignored: accordingly the 2p-2h contribution to the Λ decay in nuclear matter was restricted to the range

$$k_F \leq q \leq 1.65\ fm^{-1}\ . \tag{29}$$

In addition the following parametrization

$$\Pi^*_{2p-2h} = -4\pi\rho^2\mathcal{C}^0 \tag{30}$$

for the irreducible part of the polarization propagator was adopted, $\rho = 2k_F^3/3\pi^2$ being the nuclear matter density. The experimental information from quasi-elastic electron scattering (e, e') and from the mesic atoms suggests the value

$$Im\ \mathcal{C}^0 \simeq 0.18\ m_\pi^{-6} \tag{31}$$

for the imaginary part and

$$Re\ \mathcal{C}^0 \simeq 0.40\ m_\pi^{-6} \tag{32}$$

for the real part.

Utilizing these inputs one then writes for the polarization propagator

$$q^2\Pi(q,\omega) = \frac{q^2\left[\Pi^0(q,\omega) + 4\pi\rho^2\mathcal{C}^0\right]}{1 - g'(q)\left[\Pi^0(q,\omega) + 4\pi\rho^2\mathcal{C}^0\right]} \tag{33}$$

with $\Pi^0(q,\omega)$ and $g'(q)$ given by (21) and (22).

The results obtained with this approach, admittedly crude, are quoted in Table 1 and indeed point to a sizable width for the Λ decay associated with $2p-2h$ excitations.

Ramos, Oset and Salcedo [8] revisited the subject with a more refined calculation. In particular they took

$$\Pi^*_{2p-2h}(q,\omega) = -4\pi q^2\mathcal{C}_0^*\rho^2 \tag{34}$$

with

$$\mathcal{C}_0^*\rho^2 = (0.105 + i0.096)\ m_\pi^{-6}\ , \tag{35}$$

whose imaginary and real part are about half and a quarter, respectively, of (33).

In addition the calculation of Ramos *et al.* has been performed in finite nuclei via the local density approximation, but again ignoring the Δ excitation. Yet their results, while of course smaller, are not much at odd with the one of Table 1 and confirm, anyway, the importance of this channel for the decay of the Λ in a nucleus.

Of particular significance are the implications of the two-nucleon induced Λ decay for the ratio Γ_n/Γ_p, a subject which is currently much explored and likely to provide interesting clues on the validity of the $\Delta I = 1/2$ rule.

References

[1] A. Molinari and H. Feshbach, The Second Daphne Physics Handbook, Vol. II, (1995) 713, Ed. L. Maiani, G. Pancheri and N. Paver

[2] A. Ramos and C. Bennhold, Nucl.Phys. **A585** (1995) 375c

[3] E. Oset and J. Nieves, Nucl.Phys. **A585** (1995) 351c

[4] M.M. Block and R.H. Dalitz, Phys.Rev.Lett **11** (1963) 93

[5] W.M. Alberico, A. De Pace, M. Ericson and A. Molinari, Phys. Lett. **B??** (1991) 134

[6] E. Oset, H. Toki and W. Weise, Phys.Rep. **83** (1982) 281

[7] J. Dubach, Nucl.Phys. **A450** (1986)71c

[8] A. Ramos, E. Oset and L.L. Salcedo, Nucl.Phys. **A585** (1995)129c

ONE- AND TWO-NUCLEON INDUCED Λ DECAY

A. Ramos, A. Parreño
Dept. ECM, Facultat de Física, Diagonal 647, 08028 Barcelona, Spain
C. Bennhold
Dept. of Physics, The George Washington University, Washington DC 20052, USA
E. Oset
Dept. de Física Teórica, Universidad de Valencia, 46100 Burjassot, Spain
L.L. Salcedo
Dept. de Física Moderna, Universidad de Granada, 18071 Granada, Spain

ABSTRACT

The one- and two-nucleon induced mechanisms in the weak decay of Λ hypernuclei are studied. It is found that, in the ρ-meson contribution to the $\Lambda N \to NN$ decay, the central transitions, ignored in previous studies, are more important than the tensor ones and must be included. A complete meson-exchange $\Lambda N \to NN$ potential leaves the one-nucleon induced rate unchanged with respect to π-exchange results, while the neutron to proton induced ratio, Γ_n/Γ_p, is slightly smaller, differing even more from the experimental value. The two-nucleon induced $\Lambda NN \to NNN$ channel is about 15% of the total decay rate. Contrary to what was expected, including the two-nucleon mechanism in the reanalysis of the ${}^{12}_{\Lambda}$C data increases the experimental Γ_n/Γ_p ratio, which is in further disagreement with the existing theories.

1 – Introduction

When stable against particle emission, Λ-hypernuclei decay mainly through weak decay processes which do not involve leptons and may provide useful information in understanding the effective QCD corrections to the basic weak interaction. A free Λ-hyperon has a lifetime of 260 picoseconds and decays basically into a pion and a nucleon ($\Lambda \to p\pi^-$ ($\sim 64\%$), $\Lambda \to n\pi^0$ ($\sim 36\%$)), with a final momentum of about 100 MeV/c. When the Λ is embedded in the nuclear medium, this mesonic process is highly Pauli blocked and, even if a proper medium renormalization of the pion can increase the rate up to two orders of magnitude [1, 2, 3], this channel amounts to only 5% of the total decay width in ${}^{16}_{\Lambda}$O and less than 1‰ in ${}^{208}_{\Lambda}$Pb. Therefore, medium to heavy hypernuclei decay mainly through the nonmesonic channels, which have received increased experimental attention in the last few years [4, 5, 6, 7].

Traditionally, the nonmesonic decay of Λ-hypernuclei has been assumed to proceed via the $\Lambda N \to NN$ reaction. One of the present challenges for the theoretical models trying to describe this decay channel is to reproduce the experimental neutron to proton induced decay ratio, Γ_n/Γ_p, which is close to one, albeit with very large experimental error bars. The Λ mass excess (176 MeV) is now invested in kinetic energy in the final state and the nucleons emerge with a momentum of about 400 MeV/c. As a result, this process is not Pauli blocked and is not sensitive to the nuclear structure details making it a very suitable channel to investigate the weak decay mechanism. The large momentum exchanged also indicates that short range correlations in the initial state can be quite important. Being a short range process it may also receive contributions from heavier mesons. All these effects are analyzed in Sect. 2.

Another interesting channel, first investigated in Ref. [8] and reanalyzed in Ref. [9] in connection to its implications to the neutron to proton induced ratio, is the two-body induced process $\Lambda NN \to NNN$, where the pion emitted in the weak vertex is absorbed by a pair of nucleons which are correlated through the strong force. Results for this decay channel are given in Sect. 3.

2 – The one-nucleon induced decay $\Lambda N \to NN$

The nonmesonic $\Lambda N \to NN$ decay rate is given by [10]

$$\Gamma_{nm}^{(1)} = \int \frac{d^3P}{(2\pi)^3} \int \frac{d^3k}{(2\pi)^3} \overline{\sum} (2\pi)\delta(M_H - E_R - E_1 - E_2) \mid \mathcal{M} \mid^2 \qquad (1)$$

where $\mathcal{M} = \langle \psi_R; \mathbf{P}\mathbf{k}\, S\, M_S\, T\, M_T | \hat{O}_{\Lambda N \to NN} |_\Lambda A \rangle$ is the hypernuclear transition amplitude and M_H, E_R, E_1 and E_2 the mass of the hypernucleus, energy of the residual $(A-2)$-particle system, and total asymptotic energies of the emitted nucleons, respectively. A transformation to the center of mass ($\mathbf{P}$) and relative momentum ($\mathbf{k}$) of the two outgoing nucleons is implied in Eq. (1). The hypernuclear wavefunction is described in a mean field approach and the Λ is assumed to couple to the ground state of the nuclear $(A-1)$ core. The Λ and nucleon are described with harmonic oscillator wavefunctions with appropriate parameters, $b_\Lambda = 1.87$ fm and $b_N = 1.64$ fm, adjusted to the experimental separation energies and the ^{12}C charge form factor.

At the kinematic conditions of the (π^+, K^+) reaction carried out at KEK, the hypernucleus is created with a substantial amount of polarization in the ground state. Due to the interference between the parity conserving and parity violating amplitudes, the distribution of the emitted protons in the weak decay will show an

angular asymmetry with respect to the polarization axis given by

$$\mathcal{A}(\chi) = P_y A_y(\chi) = P_y \frac{3}{J+1} \frac{Tr(\mathcal{M}\hat{S}_y\mathcal{M}^\dagger)}{Tr(\mathcal{M}\mathcal{M}^\dagger)} = P_y \frac{3}{J+1} \frac{\sum\limits_{M_i} \sigma(M_i) M_i}{\sum\limits_{M_i} \sigma(M_i)} \cos\chi \qquad (2)$$

where P_y is the hypernuclear polarization perpendicular to the (π^+, K^+) reaction plane, A_y the asymmetry parameter characteristic of the weak decay process and $\sigma(M_i)$ the intensity of protons for a spin projection of the hypernucleus M_i.

2.1 The π and ρ mechanisms

The transition $\Lambda N \to NN$ involves a weak and a strong vertex. While there exist several strong meson-exchange potentials which, through fits to NN scattering data, provide information on the different strong NN-meson vertices, only the pion vertex is known experimentally in the weak sector

$$\mathcal{H}_{\Lambda N\pi} = iG_F m_\pi^2 \overline{\psi}_N (A + B\gamma_5)\boldsymbol{\tau}\boldsymbol{\phi}_\pi \psi_\Lambda \ , \qquad (3)$$

where $G_F m_\pi^2 = 2.21 \times 10^{-7}$ is the weak coupling constant. The empirical constants $A = 1.05$ and $B = -7.15$, adjusted to the observables of the free Λ decay, determine the strength of the parity violating and parity conserving amplitudes, respectively.

In order to avoid the complications present in introducing a short-range correlation function in a relativistic matrix element [11], we use a nonrelativistic transition potential, which, in the case of pion exchange, reads

$$V_\pi(\mathbf{q}) = -G_F m_\pi^2 \frac{g_{\pi NN}}{2M} \left(A + \frac{B}{2\overline{M}}\boldsymbol{\sigma}_1\mathbf{q}\right) \frac{\boldsymbol{\sigma}_2\mathbf{q}}{\mathbf{q}^2 + m_\pi^2} (\boldsymbol{\tau}_1\boldsymbol{\tau}_2) \qquad (4)$$

Introducing the oerator $S_{12}(\hat{\mathbf{q}}) = 3\boldsymbol{\sigma}_1\hat{\mathbf{q}}\boldsymbol{\sigma}_2\hat{\mathbf{q}} - \boldsymbol{\sigma}_1\boldsymbol{\sigma}_2$, the parity conserving potential can be divided into a central and a tensor contribution. For the weak and strong $\Lambda N\rho$ vertices we take [12]

$$\mathcal{H}^w_{\Lambda N\rho} = G_F m_\pi^2 \overline{\Psi}_N \left(\alpha\gamma^\mu - \beta i \frac{\sigma^{\mu\nu}q_\nu}{2\overline{M}} + \varepsilon\gamma^\mu\gamma_5\right) \boldsymbol{\tau}\boldsymbol{\rho}_\mu \Psi_\Lambda \qquad (5)$$

$$\mathcal{H}^s_{\Lambda N\rho} = \overline{\Psi}_N \left(F_1\gamma^\mu + i\frac{F_2}{2M}\sigma^{\mu\nu}q_\nu\right) \boldsymbol{\tau}\boldsymbol{\rho}_\mu \Psi_N \ , \qquad (6)$$

respectively, where the four momentum transfer q is directed towards the strong vertex. The strong $NN\rho$ couplings are taken from the Nijmegen interaction [13] while we employ the methods of Ref. [14], based on $SU(6)_w$ symmetry, to obtain the weak $\Lambda N\rho$ coupling constants $\alpha = -3.80$, $\beta = -6.77$ and $\varepsilon = 1.09$. The ρ-meson

Table 1: π and ρ exchange contribution to the $\Lambda N \to NN$ decay rate of ${}^{12}_{\Lambda}$C

	π	ρ	$\pi+\rho$
C (SI)	—	0.033	0.033
C (SD)	0.004	0.023	0.008
C (Total)	0.004	0.079	0.054
T	0.645	0.023	0.423
PV	0.354	1.7×10^{-4}	0.360
$\Gamma^{(1)}_{nm}$	1.003	0.103	0.836
Γ_n/Γ_p	0.134	0.026	0.157

transition potential is given by

$$V_\rho(\mathbf{q}) = G_F m_\pi^2 \left(F_1 \alpha - \frac{(\alpha+\beta)(F_1+F_2)}{4M\bar{M}} (\boldsymbol{\sigma}_1 \times \mathbf{q})(\boldsymbol{\sigma}_2 \times \mathbf{q}) + i \frac{\varepsilon(F_1+F_2)}{2M} (\boldsymbol{\sigma}_1 \times \boldsymbol{\sigma}_2)\mathbf{q} \right) \frac{1}{\mathbf{q}^2 + {m_\rho}^2} (\boldsymbol{\tau}_1 \boldsymbol{\tau}_2) \, . \quad (7)$$

Using the relation $(\boldsymbol{\sigma}_1 \times \hat{\mathbf{q}})(\boldsymbol{\sigma}_2 \times \hat{\mathbf{q}}) = (\boldsymbol{\sigma}_1 \boldsymbol{\sigma}_2) - (\boldsymbol{\sigma}_1 \hat{\mathbf{q}})(\boldsymbol{\sigma}_2 \hat{\mathbf{q}})$ the ρ-potential can be decomposed into a spin independent (SI), a spin dependent (SD), a tensor (T) and a parity violating (PV) piece. A monopole form factor $F(\mathbf{q}^2) = (\Lambda_c^2 - m^2)/(\Lambda_c^2 + \mathbf{q}^2)$, with m being the meson mass, is used at each vertex. We take the cut-off values of the Jülich YN interaction [15], ($\Lambda_\pi = 1.3$ GeV, $\Lambda_\rho = 1.4$ GeV), since the Nijmegen model distinguishes form factors only in terms of the transition channel. To account for the ΛN correlations, which are absent in the independent particle model, we include a correlation function

$$f(r) = \left(1 - \mathrm{e}^{-r^2/a^2}\right)^n + b r^2 \mathrm{e}^{-r^2/c^2} \, , \quad (8)$$

where the values $a = 0.5$, $b = 0.25$, $c = 1.28$ and $n = 2$ provide a good approximation to the results obtained from microscopic G-matrix calculations in finite hypernuclei [16] using the Nijmegen YN interactions. Final state interactions are taken into account via an average NN correlation function in the final state, for which we take $f_{\mathrm{FSI}}(r) = 1 - j_0(q_c r)$, with $q_c = 3.93$ fm^{-1}.

The nonmesonic decay rate of ${}^{12}_{\Lambda}$C is given, in units of the free lambda decay rate, in Table 1 for the π, ρ, and combined $\pi+\rho$ mechanisms. Since both the $\Lambda N\pi$- and the $\Lambda N\rho$-couplings are obtained within the same model, there is no sign ambiguity. First, we observe that the central contribution of the ρ-potential is the largest one, in contrast to the π case, which is dominated by the tensor transition. A number of theoretical studies in recent years have investigated the contribution of the ρ-meson to the $\Lambda N \to NN$ process [12, 17, 18]. Due to the different models employed

for the weak $\Lambda N\rho$-vertex these calculations have yielded widely varying results. However, all works until now that have studied the ρ-meson exchange diagram have only included the tensor part of the parity-conserving ρ-exchange term. This was in part motivated by the observation that the central potential of the π-exchange term gives only a negligible contribution. We find that the central part of the ρ-exchange is not only nonnegligible but is in fact larger than its tensor interaction. This can be traced to the fact that the ρ-exchange diagram has a much shorter range than the π-exchange potential, and that the ρ-tensor potential is much suppressed by the relative $L = 2$ motion of the nucleons in the final state [19]. Our findings are independent of the particular model that is used for the weak $\Lambda N\rho$-vertex. From Table 1 we observe that there is a destructive interference between the two mesons, leading to a 17% reduction of the rate calculated with π-exchange only. The neutron to proton induced ratio, on the other hand, is increased by about 20%, from the value 0.13 for π-exchange only to 0.16 when the ρ is also included. While this is nowhere near an increase that would be needed to explain experimental data [4, 6, 20], it is clearly a reflection of the fact that the tensor interaction of the ρ-exchange is not as dominant as it is in the π case.

2.2 The full one-meson-exchange weak potential

In this subsection we explore the effect of including also the contribution of the η, K, ω and K^* mesons in the decay of ${}^{12}_{\Lambda}$C. Although the structure of the potentials is the same as that of the π (for η and K) and the ρ (for ω and K^*) mesons, the isospin factors can be quite different and this could alter the neutron to proton induced ratio. Our results for the $\Lambda N \rightarrow NN$ nonmesonic rate, the neutron to proton induced decay ratio and the proton asymmetry are shown in Table 2. We observe that the interferences between the different mesons conspire to give a rate which is only 5% larger than that for pion exchange alone. The neutron to proton induced ratio is, as expected, more sensitive to the isospin structure of the exchanged mesons. However, the final result is smaller than that for pion exchange alone and the discrepancy with the experimental result is even larger. Note that the reduction comes essentially from K-exchange which, in the neutron induced channel, interferes destructively with the pion amplitude. To confirm this effect, it is imperative to develop other models for the weak vertices. We note that our results differ from the nuclear matter calculation of Ref. [21] even though we use the same model for the weak vertices. The proton asymmetry is also quite sensitive to the different mesons exchanged. To compare with experiment, the asymmetry parameter A_y, characteristic of the weak decay, is multiplied by the hypernuclear polarization P_y, which must be estimated from a theoretical calculation. We have taken the value

Table 2: Weak decay observables for $^{12}_{\Lambda}$C

	$\Gamma^{(1)}_{nm}$	Γ_n/Γ_p	$\mathcal{A}(0^\circ)$
π	1.003	0.134	−0.038
$+\eta$	0.955	0.202	−0.046
$+K$	1.098	0.029	−0.021
$+\rho$	0.919	0.029	−0.014
$+\omega$	0.935	0.039	−0.021
$+K^*$	1.047	0.079	0.012
EXP:	1.14 ± 0.20 [4]	$1.33^{+1.12}_{-0.81}$ [4]	-0.01 ± 0.10 [5]
	$0.93 \pm 0.17 \pm 0.01$ [6]	$1.74 \pm 0.54^{+0.23}_{-0.94}$ [6]	
		0.70 ± 0.30 [20]	
		0.52 ± 0.16 [20]	

$P_y = -0.21$ obtained in Ref. [22]. The present level of uncertainty in the experiment prevents using the asymmetry as an observable that could differenciate between different models for the weak vertices, although an improved measurement of the decay of $^{5}_{\Lambda}$He at KEK [23] may bring some light into this issue. Moreover, due to the fact that the asymmetry parameter of the mesonic decay of $^{5}_{\Lambda}$He is almost equal to that of the free Λ [24], by measuring the asymmetry of the mesonic channel this experiment will also provide an experimental determination of the hypernuclear polarization.

3 – The two-nucleon induced decay $\Lambda NN \to NNN$

In view of the large value of the two-nucleon induced channel $\Lambda NN \to NNN$ obtained in a nuclear matter calculation [8] and the speculation that it could bring the experimental neutron to proton induced ratio in closer agreement with the theoretical estimates, we carried out a detailed study of this mechanism and have extended it to finite nuclei using a local density approximation. The main idea is to evaluate the Λ decay width in nuclear matter through the Λ self-energy, Σ, and the relationship $\Gamma = -2\mathrm{Im}\,\Sigma$ [8, 9]. The essential point is that, to account for the new 3N emission channel, the pion emitted in the weak $\Lambda N\pi$ vertex is allowed to couple to $2p2h$ excited states, apart from the conventional ph and Δh excitations [1]. Therefore, the pion self-energy reads

$$\Pi^* = \Pi^*_{1p1h} + \Pi^*_{\Delta h} + \Pi^*_{2p2h} \,. \tag{9}$$

In this way, the original pion strength spreads out as a consequence of the pionic absorption width due to the coupling to $2p2h$ components, and part of this strength overcomes the Pauli blocking giving rise to a genuine $3N$ emission channel. In our

Table 3: Hypernuclear decay widths

	Γ_m	$\Gamma^{(1)}_{nm}$	$\Gamma^{(2)}_{nm}$
${}^{12}_{\Lambda}$C	0.31	1.45	0.27
${}^{16}_{\Lambda}$O	0.24	1.54	0.29
${}^{20}_{\Lambda}$Ne	0.14	1.60	0.32
${}^{40}_{\Lambda}$Ca	0.03	1.76	0.32
${}^{56}_{\Lambda}$Fe	0.01	1.82	0.32
${}^{89}_{\Lambda}$Y	—	1.88	0.31
${}^{100}_{\Lambda}$Ru	—	1.89	0.31
${}^{208}_{\Lambda}$Pb	—	1.93	0.30

reanalysis we use

$$\Pi^*_{2p2h}(q_0 = m_\pi, \mathbf{q} \simeq 0, \rho) = -4\pi \mathbf{q}^2 \mathcal{C}^*_0 \rho^2 \ , \tag{10}$$

with $\mathcal{C}^*_0 = (0.105 + i0.096) m_\pi^{-6}$, obtained from a recent empirical analysis of pionic atoms [25] and consistent with our input for the lowest order self-energy. Note that $\mathrm{Im}\,\mathcal{C}^*_0$ is about one half of the one used in Ref. [3], while $\mathrm{Re}\,\mathcal{C}^*_0$ is about four times smaller. We have extended $\Pi^*_{2p2h}(q^0, \mathbf{q})$ to new kinematical regions away from pionic atoms, by taking the imaginary part proportional to the available phase space of $2p2h$ excitations at $(q^0, \mathbf{q})$ and density ρ, and leaving the real part constant.

Our results in finite hypernuclei are shown in Table 3, where the different contributions to the total width (mesonic, one-body induced and two-body induced) are given separately in units of the free Λ decay width. We find that $\Gamma^{(2)}_{nm}/\Gamma_\Lambda$ is about 0.3, rather stable as a function of the mass number. The different result for $\Gamma^{(1)}_{nm}$ with respect to that shown in Table 2 for π-exchange is a consequence of the local density approximation and a slightly more localized Λ wavefunction used here.

3.1 Reanalysis of the neutron to proton ratio Γ_n/Γ_p

Even if $\Gamma^{(2)}_{nm}$ is at most 20% of the nonmesonic width, the existence of this channel has important repercussions with regard to the number of neutrons and protons emitted in the Λ decay process, information which is used to determine the ratio of neutron to proton induced Λ decay Γ_n/Γ_p. It is clear that in view of the new results one cannot associate all n or p emerging from the experiment to the primary $\Lambda n \to nn$ or $\Lambda p \to np$ reactions and hence a reanalysis of the experimental data is

needed. Taking into account the way the experiment was done, one may derive [10]

$$\frac{\Gamma_n}{\Gamma_p} = \left(\frac{\Gamma_n^{exp}}{\Gamma_p^{exp}}\right) \frac{1 - \frac{1}{2}\left(\frac{\Gamma_p^{exp}}{\Gamma_n^{exp}} + 1\right)\frac{\Gamma_{nm}^{(2)}}{\Gamma_{nm}^{exp}}}{1 - \left(\frac{\Gamma_n^{exp}}{\Gamma_p^{exp}} + 1\right)\frac{\Gamma_{nm}^{(2)}}{\Gamma_{nm}^{exp}}} , \tag{11}$$

written in terms of the rate Γ_{nm}^{exp} and the ratio $\Gamma_n^{exp}/\Gamma_p^{exp}$ obtained in Ref. [4]. Ignoring the two body induced mechanism one obtains, in $^{12}_{\Lambda}$C, $\Gamma_n^{exp}/\Gamma_p^{exp} = (N_n/N_p - 1)/2 = 0.75$ [4], whereas final state interaction corrections modify this ratio up to a value $\Gamma_n^{exp}/\Gamma_p^{exp} = 1.04$. Taking our theoretical estimate of $\Gamma_{nm}^{(2)} = 0.27\Gamma_\Lambda$ and the value $\Gamma_{nm}^{exp} = 1.14\Gamma_\Lambda$ [4], Eq. (11) gives $\Gamma_n/\Gamma_p = 1.54$, which represents a 50% increase with respect to the value without the two body induced decay process, contrary to the naive expectation. This ratio is in strong disagreement with the values provided by theoretical models based on the one pion exchange mechanism [1, 14, 10], which typically range between 0.1 and 0.2. We note that the ratio 1.54 has large error bars, coming, among other sources, from the experimental uncertainties in the values of N_p and N_n. Therefore, improved experiments with reduced uncertainties are necessary in order to make the corrections coming from by the $2p2h$ channel more noticeable.

4 – Conclusions

The $\Lambda N \to NN$ decay has been investigated in a nonrelativistic meson exchange-model which includes short range correlations, form factors and final state interactions. We have found that the largest contribution of the ρ-meson is the central one and must be included, in contrast to previous calculations which only considered the tensor transitions. As a result, the Γ_n/Γ_p ratio increases with respect to the value obtained with the π-exchange models but not sufficiently to explain the experimental data. However, the full meson exchange potential, which relies on an $SU(6)_w$ model to obtain the weak couplings, predicts an even smaller ratio, thereby increasing the discrepancy with experiment. This is due mainly to the K-meson which, in the neutron induced channel, interferes destructively with the dominant π-contribution. This ratio cannot be increased much more by the other mesons because their significance is smaller due to their larger masses. To confirm or refute these findings, it is imperative to develop alternative models for the weak vertices. The proton asymmetry is very sensitive to the different mesons exchanged. This is an indication that this observable could be used to discriminate between different theoretical models, as soon as new data with reduced statistical errors are available [23].

The two-nucleon mechanism $\Lambda NN \to NNN$ has been investigated in nuclear matter and extended to finite nuclei using a local density approximation. This

decay mode amounts to 15% of the total decay rate in medium to heavy hypernuclei and cannot be disregarded in the analysis of the experimental data. The consideration of this channel is essential in extracting the Γ_n/Γ_p ratio. From existing data in ${}^{12}_{\Lambda}$C we have shown that, contrary to the previous belief, the reanalyzed ratio increases by about 50% and it moves further away from the present theoretical estimates.

Our study clearly indicates that it is necessary to invest further theoretical efforts to understand the dynamics of the weak Λ decay, either by keeping the one-meson exchange picture and developing other models for the coupling constants at the weak vertices, or by going beyond the conventional picture and incorporating quark degrees of freedom into the problem [26, 27]. One should keep in mind, however, that such models will have to be able to reproduce the experimentally measured free hyperon decays. On the experimental side, it is important to obtain as many high accuracy data as possible. The efforts at KEK, with an improved measurement of the ${}^{5}_{\Lambda}$He decay, and the advent of the hypernuclear physics program (FINUDA) at DAΦNE represent excellent opportunities for obtaining valuable information which will shed some light onto the still unresolved problems of the weak decay of Λ hypernuclei.

Acknowledgements

This work has been partially supported by DGICYT contracts PB92-0761, PB92-0927 and AEN 93-1205 (Spain), and by US-DOE Grant no. DE-FG02-95-ER40907. A.P. acknowledges support from a doctoral fellowship of the Ministerio de Educación y Ciencia (Spain).

References

1. E. Oset and L.L Salcedo, Nucl. Phys. **A443**, 704 (1985).

2. K. Itonaga, T. Motoba and H. Bando, Z. Phys. **A330**, 209 (1988); T. Motoba, K. Itonaga and H. Bando, Nucl. Phys. **A489**, 683 (1988).

3. J. Nieves and E. Oset, Phys. Rev. C **47**, 1478 (1993).

4. J.J. Szymanski *et al*, Phys. Rev. C **43**, 849 (1991).

5. S. Ajimura *et al*, Phys. Lett. **B282**, 293 (1992).

6. H. Noumi *et al*, KEK preprint 95-10 (1995).

7. A. Zenoni with the FINUDA collaboration, these proceedings.

8. W.M. Alberico, A. De Pace, M. Ericson and A. Molinari, Phys. Lett. **B256**, 134 (1991).

9. A. Ramos, E. Oset and L.L Salcedo, Phys. Rev. C **50**, 2314 (1994).

10. A. Ramos, E. van Meijgaard, C. Bennhold and B.K. Jennings, Nucl. Phys. **A544**, 703 (1992).

11. A. Parreño, A. Ramos, C. Bennhold, and D. Halderson, in *Dynamical Features of Nuclei and Finite Fermi Systems*, X. Viñas, M. Pi and A. Ramos, eds., (World Scientific, Singapore, 1994) 318; A. Parreño, A. Ramos, and E. Oset, Phys. Rev. C **51**, 2477 (1995).

12. B.H.J. McKellar and B.F. Gibson, Phys. Rev. C **30**, 322 (1984).

13. M.N. Nagels, T.A. Rijken, and J.J. de Swart, Phys. Rev. D **15**, 2547 (1977); P.M.M. Maessen, Th. A. Rijken and J.J. de Swart, Phys. Rev. C **40**, 2226 (1989).

14. J.F. Dubach, Nucl. Phys. **A450**, 71c (1986); L. de la Torre, Ph.D. Thesis, Univ. of Massachusetts (1982)

15. B. Holzenkamp, K. Holinde, and J. Speth, Nucl. Phys. **A500**, 485 (1989).

16. D. Halderson, Phys. Rev. C **48**, 581 (1993).

17. K. Takeuchi, H. Takaki, and H. Bandō, Prog. Theor. Phys. **73**, 841 (1985).

18. G. Nardulli, Phys. Rev. C **38**, 832 (1988).

19. A. Parreño, A. Ramos, and C. Bennhold, Phys. Rev. C (submitted).

20. A. Montwill *et al*, Nucl. Phys. **A234**, 413 (1974).

21. B. Holstein, these proceedings.

22. K. Itonaga, T. Motoba, O. Richter and M. Sotona, Phys. Rev. C **49**, 1045 (1994).

23. T. Kishimoto, Nucl. Phys. **A585**, 205c (1995).

24. T. Motoba and K. Itonaga, Nucl. Phys. **A577**, 293c (1994).

25. O. Meirav, E. Friedman, R.R. Johnson, R. Olszewski and P. Weber, Phys. Rev. C **40**, 843 (1989).

26. K. Maltman and M. Shmatikov, Phys. Lett. **B331**, 1 (1994).

27. T. Inoue, S. Takeuchi and M. Oka, Nucl. Phys. A (in press).

NON-LEPTONIC Λ WEAK DECAYS IN LIGHT TO MEDIUM HYPERNUCLEI

R. Alzetta and G. Liberti
Dipartimento di Fisica, Università della Calabria
INFN Cosenza, I-87030 Arcavacata di Rende (CS), Italy
G. Preparata
Dipartimento di Fisica, Università di Milano
INFN Sezione di Milano, via G. Celoria 16, I-20133 Milano, Italy

ABSTRACT

We have calculated the lifetimes of Λ-hypernuclei in the region of mass numbers $9 \leq A \leq 50$ in the framework of the "Coherent Nucleus" theory founded in 1990 by one of us (G.P.).

1 – The Coherent Nucleus

The modern theoretical nuclear physics paradigm is based upon the following pillars: short-range two-body interaction (realistic or OBEP, TPEP, ...) *plus* Hartree-Fock equations *plus* many-body techniques. In other words:

1. a realistic model for the nucleus is postulated (the Shell Model long-range correlations);

2. the matematical Hartree-Fock self-consistency produces, starting from the short-range N-N forces, the shell model single particle levels and wave functions;

3. the usual many-body techniques are finally employed for the calculations of the nuclear structure and dynamics.

Apparently the Nuclear Physics community is not concerned about this keen contrast between the long-range correlations implied by the shell-model and the short-range N-N forces, a contrast which unsettled Hans Bethe [1] forty years ago. "Shell model works and that's enough" is still the leit-motiv.

Five years ago the existence of nuclear structure itself was discovered to be based on the collective, laser-like dynamics associated with the coherent interaction of the N-Δ-π system [2]. The densely packed nucleons inside the nucleus oscillate in phase with a π-field extending over *coherence domains* of the size of $4 \div 5$ fm. The number of nucleons packed inside a coherence domain is $A_{CD} \simeq 50$.

This coherent N-body dynamics has the effect of lowering by $\sim$ 60 MeV (the mass-gap of the nucleons inside the nucleus) the ground state of the nucleus, and of reducing, by approximately 50%, the original frequency

$$\omega_0 = m_\Delta - m_N \simeq 292 \text{ MeV} \tag{1}$$

(the coherent pions are off mass-shell), thus producing the cavity which traps the π-coherent field inside the nucleus. The coherent process is just below the threshold of "strong superradiance": the system develops no runaway and the π-field is weak but highly coherent.

The phenomenology of the spectrum and properties of Λ-hypernuclei shows that the Λ-hyperon within the nucleus behaves rather like the nucleons themselves, beying arranged in typical shell model levels associated with a potential $V_\Lambda \simeq 30$ MeV which displays no significant spin-orbit splitting. The hypernuclear potential calculated in the framework of the Coherent Nucleus theory [3] successfully meets the established phenomenology.

2 – The Lifetime Problem

The two main channels of hypernuclear Λ weak decay are the mesonic branch and the non-mesonic branch, corresponding, in our Coherent Hypernucleus theory, to the incoerent and the coherent part respectively of the decay mechanism.

In the mesonic decay process, the Λ decays non-leptonically into a N-π state, independently of the rest of the π's and the N/Δ's of the nucleus. Such process in large hypernuclei is highly suppressed by phase space and Pauli-blocking. In the Coherent Hypernucleus view of the non-mesonic decay process, the *Lambda* is converted into a nucleon inside the π^c-condensate. Therefore the rate of the

non-mesonic decay process is essentially determined by the weak non-leptonic conversion amplitude of a Λ into a nucleon in the coherent π-field.
The generally accepted picture of Nuclear Physics pictures the non-mesonic decay channel as mediated by the transition amplitudes [4]

$$\begin{array}{c} \Lambda + N \rightarrow N + N \\ \Lambda + N + N \rightarrow N + N + N \end{array} \tag{2}$$

When the weak coupling costants $g_{\Lambda NM}$, where M stands for any one-meson (π,ρ,ω,...) exchange, are introduced, surprisingly one finds in some non-mesonic decays severe discrepancies just with the so far universally valid ΔI=1/2 rule of weak non-leptonic interactions. [5]
But how can Nuclear Physics, with its modest energy scale ($\sim$ 10 MeV), influence the weak amplitude scale ($\sim$ 1 GeV) ? Our approach is free from such oddity.
In tab.1 the relevant experimental data are shown, where τ denotes the lifetime in (10^{-10} sec.),

$$n = \frac{\Gamma^n_{nm}}{\Gamma^n_{nm} + \Gamma^p_{nm}}, \tag{3}$$

$$Q^- = \frac{\Gamma^n_{nm} + \Gamma^p_{nm}}{\Gamma^{\pi^-}_m}, \tag{4}$$

where $\Gamma^{\pi^-}_m$ is the mesonic $\Lambda \rightarrow p\pi^-$ decay width and $\Gamma^{n(p)}_{nm}$ is the non-mesonic decay width of the Λ particle with final conversion $\Lambda \rightarrow n\pi^0(p\pi^-)$ respectively. Note that if the ΔI=1/2 rule is not violated, then n=1/3 and

$$Q^- = \frac{3}{2}\frac{\Gamma^{tot}_{nm}}{\Gamma^{tot}_m} \tag{5}$$

The measurements of these two quantities that will be produced by FINUDA [26] shall provide a decisive test for the ΔI=1/2 rule in hypernuclear decay.
The total non leptonic decay width is therefore given by

$$\Gamma_{tot} = \Gamma^{\pi^-}_m + \Gamma^{\pi^0}_m + \Gamma^n_{nm} + \Gamma^p_{nm}. \tag{6}$$

We recall that the free decay is mainly mesonic, whose channels are

$$\Lambda \rightarrow \begin{cases} p\pi^- & (64\%) \\ n\pi^0 & (36\%) \end{cases} \tag{7}$$

and its free decay width is $\Gamma_\Lambda \simeq 2.5 \times 10^{-12}$ MeV, corresponding to a lifetime $\tau_\Lambda \simeq 2.6 \times 10^{-10}$ sec.

Table 1: Lifetimes and decay rates of Λ-hypernuclei.

${}^{A}_{\Lambda}Z$	$\tau(10^{-10})$sec	Q^-	n	Ref.
${}^{3}_{\Lambda}H$	$2.85^{+1.27}_{-1.05}$			6)
	$2.64^{+0.84}_{-0.51}$			7)
	$1.28^{+0.35}_{-0.26}$			8)
	$2.46^{+0.62}_{-0.61}$			7)
${}^{4}_{\Lambda}H$	$2.68^{+1.66}_{-1.07}$			6)
	$1.94^{+0.24}_{-0.26}$			9)
		0.26 ± 0.13		10)
${}^{4}_{\Lambda}He$	$2.28^{+2.33}_{-1.29}$			6)
		0.52 ± 0.10	0.3 ± 0.1	10)
${}^{5}_{\Lambda}He$	$2.51^{+1.90}_{-0.73}$			6)
	$2.74^{+0.60}_{-0.50}$			8)
		1.21 ± 0.19		11)
		1.3 ± 0.1		12)
	2.56 ± 0.21	$1.03^{+0.34}_{-0.72}$	0.49 ± 0.14	16)
${}^{8}_{\Lambda}Li$		2.55 ± 0.66		13)
${}^{9}_{\Lambda}Be$		4.3 ± 1.1		14)
	2.01 ± 0.30			15)
${}^{11}_{\Lambda}B$	1.92 ± 0.22		$0.51^{+0.11}_{-0.15}$	16)
$A \geq 10$			$0.68^{+0.04}_{-0.03}$	17)
${}^{12}_{\Lambda}C$	2.11 ± 0.31	22^{+43}_{-12}	$0.57^{+0.14}_{-0.23}$	16)
$40 \leq A \leq 100$		100-200	0.6-0.9	18)
"Heavy"			0.85	19)
$A \geq 40$			0.9	20)
${}^{209}_{\Lambda}Bi$	$2.5^{+2.5}_{-1.0}$			21)
${}^{238}_{\Lambda}U$	$1.0^{+1.0}_{-0.5}$			21)
	1.25 ± 0.15			22)

3 – The Mesonic Decay

In our calculations the basic Λ-N-π vertex is introduced through the effective interaction hamiltonian:

$$\langle N\pi|H_w|\Lambda\rangle = C g_w \bar{u}_N(p_N)\,(1+\lambda\gamma_5)\,u_\Lambda(k_\Lambda) \tag{8}$$

with

$$C = \begin{cases} \sqrt{2} & \Lambda \to p\pi^- \\ -1 & \Lambda \to n\pi^0 \end{cases} \tag{9}$$

and $g_w = 2.35 \times 10^{-7}$, $\lambda = -6.9$, as one derives from the free decay.
Let the initial state be the 1s ground state for the Λ in a potential well with depth $V_\Lambda \simeq 25 \div 30$ MeV and wave function

$$\psi_\Lambda(\vec{x},t) = \sqrt{\frac{\pi}{2R_A^3}}\, j_0(k_\Lambda r) e^{-iE_\Lambda t} \tag{10}$$

where $R_A = 1.2A^{1/3}$ is the nuclear radius, $k_\Lambda = \pi/R_A$ is the Λ-momentum inside the Hypernucleus and $E_\Lambda = m_\Lambda - V_\Lambda + \frac{1}{2m_\Lambda}\left(\frac{\pi}{R_A}\right)^2$ its energy. The Λ-wave function above corresponds to the "infinite" square-well function.
In fig.1 we show the comparison among the experimental s-shell Λ-binding energies [23], B_Λ, and the calculated B_Λ, both for finite and "infinite" square well.
A straightforward calculation yields:

$$\Gamma_m(\Lambda \to N\pi) = \int \frac{d^3p}{(2\pi)^3}\theta(|\vec{p}| - p_F) \int \frac{d^3q}{(2\pi)^3} 2\pi\delta(E_\Lambda - E_N - E_\pi)\,|F(\vec{q},\vec{p})|^2 \tag{11}$$

where the "form factor" $F(\vec{q},\vec{p})$ is given by

$$F(\vec{q},\vec{p}) = g_w(q)\frac{1}{(2E_\pi)^{1/2}} \int d^3x \psi_\Lambda(\vec{x}) e^{-i(\vec{q}+\vec{p})\cdot\vec{x}} \tag{12}$$

and

$$|g_w(q)|^2 = g_w^2\left(1 + \frac{\lambda^2 q^2}{4m_N m_\Lambda}\right) \tag{13}$$

The N-energy is $E_N = m_N - V_N + \frac{p^2}{2m_N}$ ($V_N \simeq 50 \div 60$ MeV, is the standard nuclear depth) and the π-energy is $E_\pi = \sqrt{\vec{q}^2 + m_\pi^2}$. p_F is the Fermi momentum, reduced both by finite-size effects [24] and by the reduced nucleon density inside the nucleus, coming from the Coherent Nucleus theory [2]. This last reduction factor is 0.82, which is the nucleon percentage inside the nucleus.
In fig.2 we show our predictions for $\Gamma_m(A)/\Gamma_\Lambda$ [25]. These predictions are insensitive to small variations of the nuclear depth.

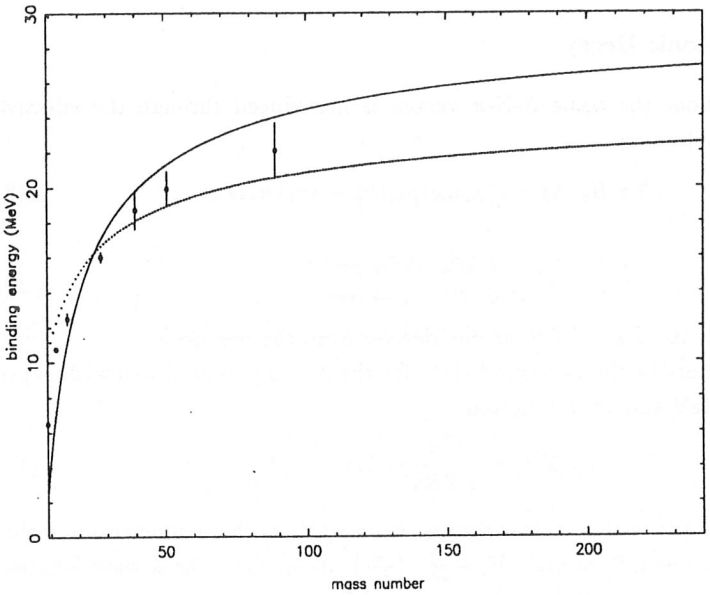

Figure 1: s-shell Λ-binding energies , B_Λ, as a function of mass number A. Full line: "infinite" square well $V_\Lambda = 30$ MeV; dotted line: finite square well $V_\Lambda = 25$ MeV.

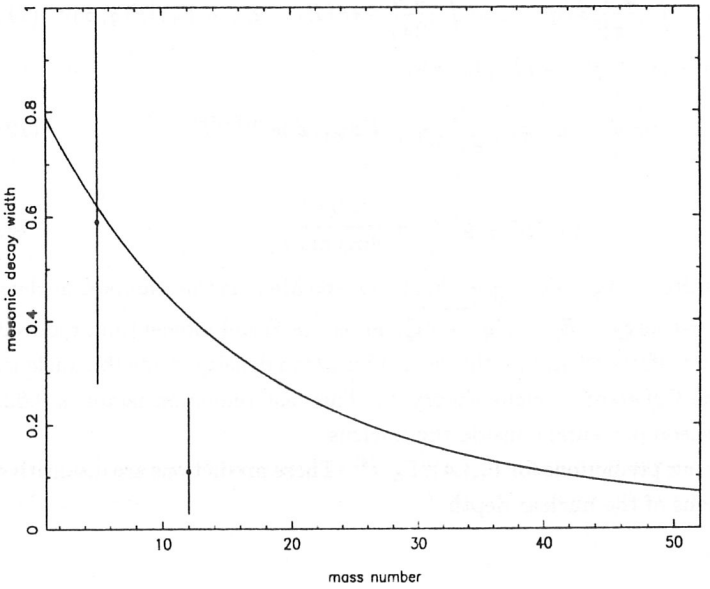

Figure 2: Mesonic decay width $\Gamma_m(A)/\Gamma_\Lambda$, for $V_N = 50$ MeV.

4 – The Non-Mesonic Decay

The non-mesonic mechanism involves a weak Λ-π-N vertex which couples the baryons to the π^c-condensate emerging from the coherent nuclear dynamics. The transition element is

$$\langle N\pi^c | \int dt H_w(t) | \Lambda \rangle \tag{14}$$

The Λ-wave function is the same as before. The wave-function of the emitted nucleon can be well approximated by a plane-wave function. In fact, the crossing time T_c, inside the nucleus, of the nucleon created in the Λ decay is slightly larger than the relaxation time of the coherent dynamics

$$T_{rel} = \frac{2\pi}{\omega_0} \simeq 1.4 \times 10^{-23} \text{ sec}, \tag{15}$$

i.e. the time of the nuclear relaxation into the coherent ground state with an energy gain per nucleon

$$\frac{\Delta E}{A} \simeq -60 \text{ MeV}. \tag{16}$$

Thus the nucleon has time enough to put itself in coherence with the other nucleons, so as to feel the nuclear potential V_N, but it does not dwell inside the nucleus, its energy belonging to the continuos spectrum. Its wave-function is therefore:

$$\psi_N(\vec{x}, t) = \frac{1}{\sqrt{V_A}} e^{i(\vec{p}\cdot\vec{x} - E_N t)} \tag{17}$$

The coherent π^c-field, emerging from the coherence mechanism is essentially a (p-wave) spherical Bessel function of first order $j_1(qr)$, corrected to take into account the π-finite size effects. Its radial dependence is show in fig.3.
After having collected all the main ingredients for the transition matrix elements of the non-mesonic decay, the calculation of the non-mesonic decay width Γ_{nm} proceeds in the standard way and yields:

$$\Gamma_{nm}(A) = \frac{(4\pi)^5}{36} g_w^2 \alpha^2 \frac{p}{\omega_0} m_N A G_A^2(p) \tag{18}$$

where

$$\alpha^2 = \sum_k \vec{\alpha}_k^2 = (0.29)^2 \tag{19}$$

and $\vec{\alpha}_k$ is the p-wave amplitude of the π^c-field with isospin component k, with its average value derived from the Coherence Equations [2]. Moreover, $p^2 = 2m_N\Delta(A)$,

is the square of the outgoing-nucleon momentum where $\Delta(A) = m_\Lambda - m_N - \omega_R - V_\Lambda + V_N + \frac{\pi^2}{2m_\Lambda R_A^2}$. The frequency ω_R is the reduced pion frequency.
Finally $G_A^2(p)$ is a collection of three terms containing integrals over products of spherical Bessel functions, which we have calculated numerically. In fig.4 the plot is shown of $\Gamma_{nm}/\Gamma_\Lambda$ as a function of A. In fig.5 the plot is shown of the relative lifetime

$$\frac{\tau(A)}{\tau_\Lambda} = \frac{\Gamma_\Lambda}{\Gamma_m + \Gamma_{nm}} \tag{20}$$

as a function of A, together with the few experimental data (for ${}^{9}_{\Lambda}$Be, ${}^{10}_{\Lambda}$B and ${}^{12}_{\Lambda}$C) present in the literature, for two values of V_N, the nuclear potential depth.
We await impatiently the results on Λ-hypernuclear decays that FINUDA [26] experiment will produce at Frascati on the DAΦNE machine.

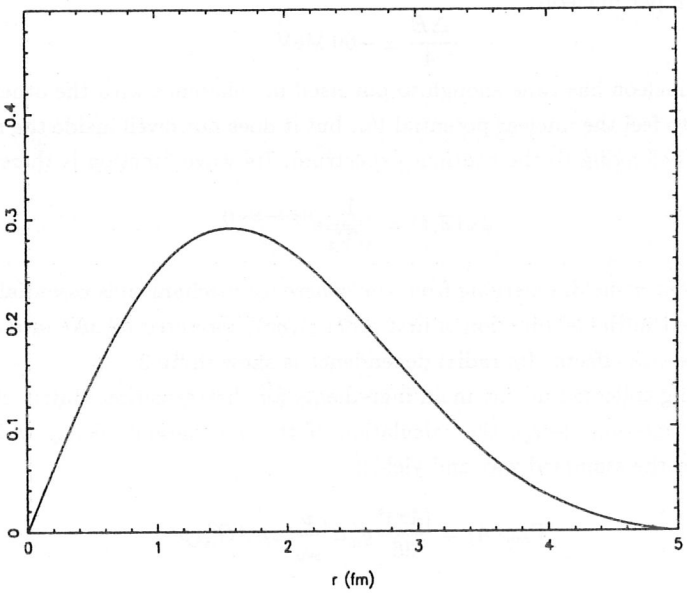

Figure 3: π^c-field radial dependence.

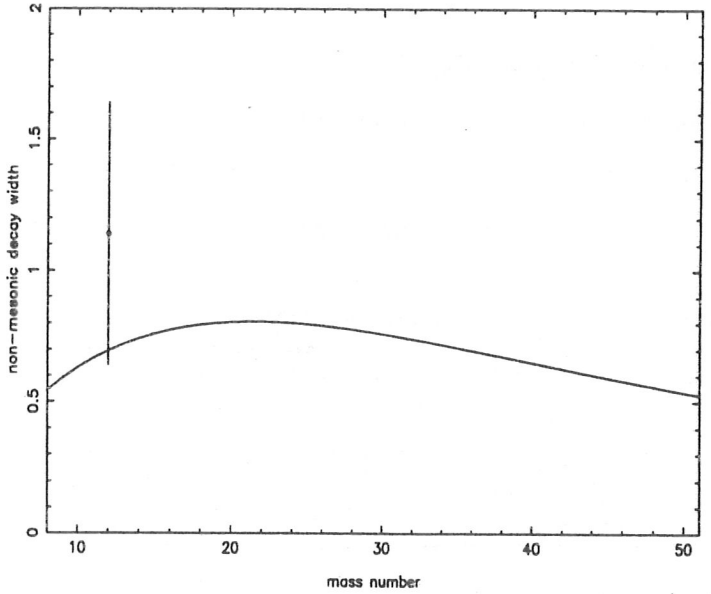

Figure 4: Non-mesonic decay width $\Gamma_{nm}(A)/\Gamma_\Lambda$, for $V_N = 50$ MeV.

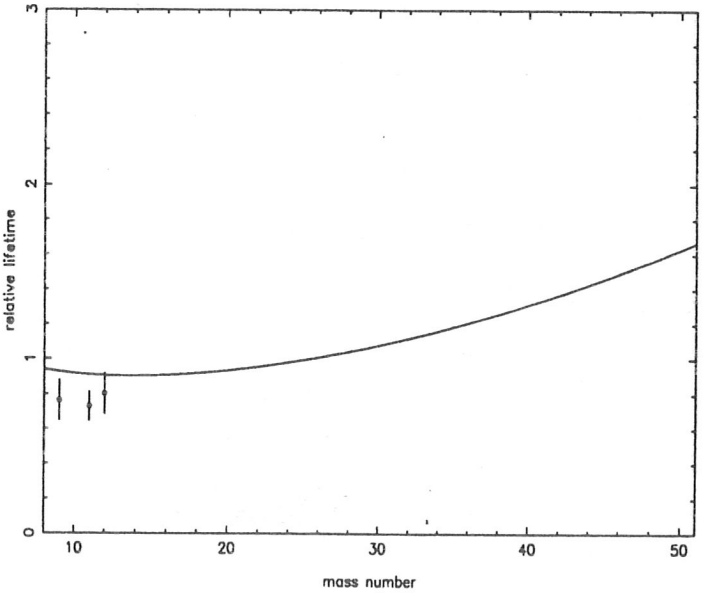

Figure 5: Relative Λ-lifetime $\tau(A)/\tau_\Lambda$ for $V_N = 50$ MeV.

References

1. H. Bethe, Phys. Rev. **103**, 1352 (1956).
2. G. Preparata, Nuovo Cim. **103A**, 1213 (1990).
3. G. Preparata and P.G. Ratcliffe, Nuovo Cim. **106A**, 685 (1993).
4. W.M. Alberico, A. De Pace, M. Ericson and A. Molinari, Phys. Lett. **B256**, 134 (1991).
5. R.A. Schumacher, Nucl. Phys. **A547**, 143c (1992).
6. R.E. Philips and J. Schneps, Phys. Rev. **D1**, 66 (1970).
7. G. Keyes et al., Nucl. Phys. **B67**, 269 (1973).
8. G. Bohm et al., Nucl. Phys. **B16**, 46 (1970).
9. H. Outa et al., Nucl. Phys. **A547**, 109c (1992).
10. M.M. Block et al., Nuovo Cim. **28**, 229 (1963).
11. H.G. Miller et al., Phys. Rev. **167**, 922 (1968).
12. G. Coremans et al., Nucl. Phys. **B16**, 209 (1970).
13. K.N. Chaudhari et al., Proc. Indian Acad Sci. **69A**, 78 (1969).
14. A. Montwill et al., Nucl. Phys. **A234**, 413 (1974).
15. R. Grace et al., Phys. Rev. Lett. **55**, 1055 (1985).
16. J.J. Szymanski et al., Phys. Rev. C **43**, 849 (1991).
17. K.L. Mangotra et al., Nuovo Cim. **13A**, 826 (1973).
18. J.P. Lagnaux et al., Nucl. Phys. **60**, 97 (1964).
19. S.N. Ganguli and M.S. Swami, Proc. Indian Acad Sci. **66A**, 77 (1967).
20. J. Cuevas et al., Nucl. Phys. **B1**, 411 (1967).
21. J.P. Bocquet et al., Phys. Lett. **B182**, 146 (1986); **B192**, 312 (1987).
22. T. Bressani, private communication.

23. P.H. Pile et al., Phys. Rev. Lett. **C20**, 2585 (1991).

24. C. Mahaux, P.F. Bortignon, R.A. Broglia and C.H. Dasso, Phys. Rep. **120**, 1 (1985).

25. R. Alzetta, G. Liberti, M. Gibilisco and G. Preparata, Mod. Phys. Lett. **A8**, 2335 (1993).

26. A. Zenoni et al., these proceedings.

Σ HYPERNUCLEI

Reyad Sawafta *
Brookhaven National Laboratory
Upton, New York, USA 11973

ABSTRACT

This paper aims at clearing up the status of narrow Σ hypernuclear states, which is a long-standing problem. Hypernuclear mass spectra for in-flight $(K^-, \pi^\pm)$ reactions from ^{1}H , ^{2}H , ^{6}Li and ^{9}Be have been measured. Preliminary results based on analysis of the $(K^-, \pi^\pm)$ spectra from ^{9}Be and ^{6}Li are discussed.

1 – INTRODUCTION

The Σ hypernuclear problem has been the subject of intense experimental and theoretical debate for more than 15 years. It was first stimulated by an observation of two narrow peaks in ^{9}Be (K^-, π^-) reaction at 720 MeV/c by the Saclay-Heidelberg group [1]. The widths of the peaks were unexpectedly narrow ($\Gamma \leq 8$ MeV), and they appeared above the Σ binding threshold. The width of Σ in nuclei was believed to be around $\Gamma \sim 25$ MeV due to the strong decay $\Sigma N \rightarrow \Lambda N$ conversion process in the nuclear medium.

Intensive theoretical and experimental investigation to explain why narrow Σ hypernuclear states could exist were initiated. The theoretical efforts are well summarized in recent review articles [2, 3, 4]. These attribute the reason for narrow widths of Σ hypernuclei to a combination of Pauli suppression, dispersion effects and the spin-isospin selectivity of the $\Sigma N \rightarrow \Lambda N$ process and the polarization of

*Representing the E887 Collaboration: K. Baker, M.Barakat, S. Bart, R.E. Chrien, W. Franklin, T. Fukuda, K. Gross, R.S. Hayano, K. Hicks, E.V. Hungerford, B. Mays, R. Michael, T. Nagae, W. Naing, I. Omata, S. Wissink, R. Sawafta, Y. Shimizu, L.Q. Tang, I.J. Zhu.

the nuclear medium by the interactions responsible for the $\Sigma N \rightarrow \Lambda N$ conversion. Experimentally, several groups at CERN [5, 6], BNL [7], and KEK [8] reported similar structures above the Σ binding threshold in early 1980s. The statistical significance, however, was limited due to poor statistics of the data. On the other hand, narrow peaks have not been observed in some reaction modes [9, 10, 11].

We review the experimental picture outlined above in some detail. The possible existence of Σ hypernuclei was first suggested by the Saclay-Heidelberg Collaboration (K^-, π^-) experiment at CERN on a ^{9}Be target at $p_K = 720$ MeV/c [1]. These data provided the first evidence for Σ hypernuclei with narrow structure. This experiment found two narrow ($\Gamma < 8$ MeV) peaks above the Σ binding threshold in the (K^-, π^-), separated by about 12 MeV, quite similar to what is observed in the Λ hypernuclear spectra for that target. Those peaks were assigned to $^{9}_{\Sigma^0}$Be. On the other hand no structure is evident in the (K^-, π^+) on the same target [9]. These peaks were attributed as low spin substitutional states reflecting the shell structure of the ^{9}Be hypernucleus as in the case of Λ hypernuclear states for the same target.

Peaks ($\Gamma < 5 - 10$ MeV) above the Σ binding threshold were further reported by low-statistics studies on p-shell nuclei at CERN [5, 6], at BNL [7] and KEK [8]. Structure below threshold was reported by subsequent studies on ^{4}He by stopped and in-flight (K^-, π^-) at KEK [12] and at BNL [13], respectively. No evidence of any narrow structure was observed on the same target in the (K^-, π^+) reaction or in the ^{3}He $(K^-, \pi^\pm)$ reactions [14]. Another experiment [16] has been approved and is scheduled to run at the AGS in 1996 to verify the structure below threshold in ^{4}He using the in-flight (K^-, π^-) reaction.

Despite these efforts, the Σ-nucleus interaction is not well understood. Experimental data have been taken on different targets at different momenta and at different conditions. These data suffer from poor resolution and insufficient statistics. Contradictions among the different sets of data often resulted more in clouding the issues than clarifying them. This can be demonstrated by quoting the different values that were extracted for the strength of Σ - spin-orbit interaction based on the p-shell data mentioned above, values of 5 MeV and 12 MeV were extracted from the CERN and KEK data [5, 6, 8], respectively.

This unsatisfactory situation strongly called for high statistics experiments to search for Σ hypernuclear states both above and below threshold. So, we have repeated some of these measurements [15] with sufficient statistics and reasonable energy resolution, to investigate systematically whether Σ hypernuclear states exist below or above threshold, or structures inconsistent with quasi-free production exist in light hypernuclei.

2 – EXPERIMENT

Hypernuclear mass spectra for in-flight $(K^-, \pi^\pm)$ reactions for ^{1}H , ^{2}H , ^{6}Li and ^{9}Be have been measured. The experiment was performed with K^- beam at the Low Energy Separated Beamline (LESB-II) at the Brookhaven National Laboratory Alternating Gradient Synchrotron (AGS). The incoming K^- beam and the outgoing pion trajectories are traced by the Moby-Dick spectrometer. The targets studied are polyethylene, lithium-6 deuteride, lithium-6, and beryllium-9, they are all solid and self supporting targets about 3 gm/cm^2 thick. The solid angle acceptance of the spectrometer is 18 msr, and the typical overall spectrometer efficiency after various off-line cuts is known to be about 60%.

For the $(K^-, \pi^\pm)$ reactions, the momentum transfer q is zero for an incident kaon momentum of about 300 MeV/c leading to Σ production. The formation of low spin "substitutional" states of the hypernucleus is favored at forward angles. The beam momentum for this experiment was selected at 600 MeV/c to balance the requirements of low momentum transfer against the beam intensity and the cross section. The outgoing pion momentum corresponding to the Σ hypernuclear region is about 480 MeV/c. The beam was tuned to optimize the K to π ratio, the singles rate in the beam counters and the beam phase space at the target. We obtained about 5.0×10^4 K^- per 5.0×10^{12} protons in an AGS beam spill of 1.2 seconds duration every 3 seconds and the K to π ratio was about 1:15.

The identification of the incoming K^- is carried out by the time-of-flight (TOF) along the LESB-II beam line. Further rejection of π^- contamination is done with the use of a Čerenkov counter of the total reflection type. The outgoing π^- is identified by a time-of-flight measurement in the pion spectrometer. The spectrometer is set at 4 degrees to the incoming beam axis. This makes it possible to determine the reaction vertex by extrapolating the kaon track and the pion track, with a resolution of about 0.5 cm along the beam direction. The vertex information can then be used to reject background events originating outside the target.

Based on GEANT simulations, misidentified muons and electrons resulting from three-body kaon in-flight decays result in a significant background around the Σ hypernuclear region. We have also implemented a range counter (filter) at the end of the spectrometer to discriminate between pions and muons. Muons are rejected with this filter, which is composed of an iron block 25.4 cm-thick and a scintillation counter. It works on the principle that the π's undergo strong interactions, but the μ's do not. Both the pion three-body kaon decays in flight which have an end-point at $p_\pi \sim 425$ MeV/c, and the (K^-, π^-) Λ quasi-free continuum have only a small effect on the the Σ quasi-free region. The two-body kaon decays at this momentum and angle lead to π^- and μ^- products with momenta outside the acceptance of the

spectrometer. All of the contributing backgrounds can be significantly reduced by using a combination of the range detector, time of flight, various off-line cuts and the barrel. The thickness of the iron block is adjusted to stop most of the pions ($\geq$95%) and detect muons in high efficiency ($\geq$90%) based on Monte Carlo simulations using GEANT.

The energy calibration of the spectrometer is quite important in the present experiment. The mass and cross section scales are calibrated against the Σ^- and Σ^+ masses by measuring the $K^-p \rightarrow \Sigma^+\pi^-$ and $K^-p \rightarrow \Sigma^-\pi^+$ reactions with a CH_2 target. The excitation energy scale is known to about 1 MeV.

3 – RESULTS

We have measured in-flight $(K^-, \pi^\pm)$ spectra for ^{1}H , ^{2}H , ^{6}Li and ^{9}Be at $p_K = 600$ MeV/c. Preliminary analysis of the $(K^-, \pi^\pm)$ spectra from ^{9}Be and ^{6}Li has been completed. The preliminary ^{9}Be $(K^-, \pi^\pm)$ spectra with acceptance correction are shown in Fig.1. The data are normalized to 1.0×10^9 K^- and the total K^- flux is about 4.8×10^9 and 3.3×10^9, for the (K^-, π^-) and (K^-, π^+) spectra, respectively. The zero mark on the missing mass scale represents the Σ^+ threshold production in the (K^-, π^-) reaction. The Σ -bound state peaks should appear to the left of this mark, and it is clear that there are no such peaks in either spectra. Note that there is a broad maximum in the continuum region of the ^{9}Be (K^-, π^-) spectrum, but not in the ^{9}Be (K^-, π^+) spectrum. Preliminary analysis of the ^{6}Li $(K^-, \pi^\pm)$ spectra also does not indicate any apparent structures.

As was mentioned earlier, the (K^-, π^-) experiment on a ^{9}Be target at $p_K = 720$ MeV/c reported two narrow ($\Gamma < 8$ MeV) peaks above the Σ binding threshold in the (K^-, π^-) , separated by about 12 MeV, quite similar to what is observed in the Λ hypernuclear spectra for that target. Those peaks were assigned as $^9_{\Sigma 0}$Be, while no structure was evident in the (K^-, π^+) on the same target. The (K^-, π^-) data is superimposed on our data in Fig. 1.

Our work confirms the two peaks in the Λ hypernuclear spectra in the ^{9}Be target similar to what was observed by the Saclay-Heidelberg Collaboration. We found no evidence however for a similar structure in the Σ hypernuclear spectra on the same target with 10 times better statistics than the previous data.

The observed spectra from both charge states can be explained by the nuclear structure of the target, and the Σ quasi-free production. If we subtract the normalized and acceptance corrected (K^-, π^-) and (K^-, π^+) spectra, the resulting spectrum shows a peak-like structure sitting on an exponential background presumably coming from the Λ qausi-free tail that can be produced only via the (K^-, π^-) reaction. The position is estimated to be 8.5 MeV, and the width is about

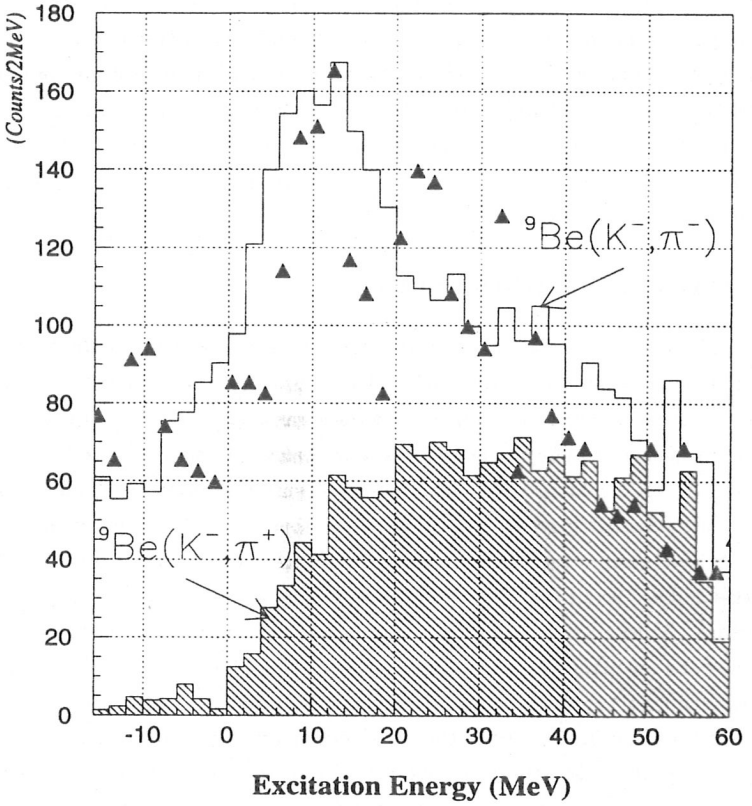

Figure 1: Preliminary (K^-, π^-) and the (K^-, π^+) (shaded) hypernuclear mass spectra for the ^{9}Be $(K^-, \pi^\pm)$ reactions taken in E887. The triangles are the old ^{9}Be (K^-, π^-) data from the Saclay-Heidelberg collaboration.

18 MeV (FWHM). The width and position of this structure provides important information on the nature of the ΣN interaction. The binding energies are 1.67 and 16.89 MeV, for a neutron and proton in ^{9}Be , respectively. In the (K^-, π^-) reaction one can produce either a Σ^o or a Σ^+ from a neutron or a proton, respectively, and at 600 MeV/c, the Σ^o production is an order of magnitude larger than that of Σ^+ . On the other hand, only Σ^- can be produced in the (K^-, π^+) reaction on a proton. Hence, a comparison of the (K^-, π^-) and (K^-, π^+) reactions at this momentum is virtually a direct comparison of Σ production from neutrons and protons, respectively. Since we see a structure in the (K^-, π^-) spectrum only, it is attributed at least *partially* to Σ^o quasi-free production on the loosely bound neutron in the $P_{3/2}$ shell of ^{9}Be . Detailed theoretical calculations are needed in order to have a quantitative description and interpretation of the new data.

4 – SUMMARY AND CONCLUSION

We have measured $(K^-, \pi^\pm)$ spectra from ^{1}H , ^{2}H , ^{6}Li and ^{9}Be at $p_K = 600$ MeV/c with reasonable energy resolution and with at least ten times the statistics reported in the previous measurements. The purpose of these measurements is to investigate systematically whether Σ hypernuclear states exist below or above Σ threshold.

The ^{9}Be $(K^-, \pi^\pm)$ spectra from these measurement greatly changed the experimental situation with regard to the narrow structures above the Σ binding threshold. We have obtained spectra with almost 10 times better statistics [15] than the Saclay-Heidelberg group [1], and our data show no evidence of any of the putative structure. A detailed comparison of the two data sets makes clear that the earlier claims have an inadequate statistical foundation. The ^{6}Li $(K^-, \pi^\pm)$ spectra also show no such structures. By implication, we can exclude all previously claimed examples of such narrow structures in the unbound energy region, since they are all statistically weaker than the ^{9}Be data. We can also assert that theoretical conclusions based on the previous data base are not valid because of statistical limitations.

The observed $(K^-, \pi^\pm)$ spectra from ^{9}Be can be explained *partially* by the nuclear structure of the target, and the Σ quasi-free production. The observed broad maximum in the ^{9}Be (K^-, π^-) spectrum is attributed to Σ^o quasi-free production on the loosely bound neutron in the $P_{3/2}$ shell of ^{9}Be . More detailed analysis of the new data combined with new and reliable theoretical calculations should provide useful information on the Σ -nucleon interaction.

We interpret our data to indicate that there are no narrow unbound Σ excitations. It remains an open question on whether bound Σ states exist; in particular if the reported structure in ^{4}He is a bound system; this will hopefully be clarified by experiment 905 [16] which will run during the next AGS running cycle in 1996. If

not confirmed, it might lead to an end of Σ hypernuclear spectroscopy after 15 years of long debate. On the other hand, its confirmation would enable the imposition of strong constraints on Σ-nucleon interaction models.

Acknowledgments

The author is grateful to Drs. C.B. Dover. A. Gal and D.J. Millener for helpful and stimulating discussions. This work was performed under the auspices of the U. S. Department of Energy and the National Science Foundation.

References

1. R. Bertini *et al.*, Phys. Lett. 90B (1980) 375.
2. C.B. Dover *et al.*, Physics Reports 184 (1989) 1.
3. Bando *et al.*, International Journal of Modern Physics 5 (1990) 4021.
4. E. Oset *et al.*, Physics Reports 188 (1990) 79.
5. R. Bertini *et al.*, Phys. Lett. 136B (1984) 29.
6. R. Bertini *et al.*, Phys. Lett. 158B (1985) 19.
7. H. Piekarz *et al.*, Phys. Lett. 110B (1982) 428.
8. T. Yamazaki *et al.*, Phys. Rev. Lett. 54 (1985) 102.
9. H. Kneiss, doctoral dissertation, Univ. of Heidelberg (1983), unpublished.
10. M. Iwasaki, doctoral dissertation, Univ. of Tokyo (1987), unpublished.
11. L.G. Tang *et al.*, Phys. Rev. C 38, (1988) 846.
12. R.S. Hayano *et al.*, Phys. Lett. 231B (1989) 355.
13. R.S. Hayano *et al.*, Nucl. Phys. A547 (1992) 151c.
14. M. Barakat *et al.*,
15. R. Sawafta, Nucl. Phys. A547 (1995) 103c.
16. T. Nagae *et al.*, AGS Experiment 905.

LOW ENERGY K^-–PROTON INTERACTIONS

Bijan Saghai

Service de Physique Nucléaire, CEA/DSM/DPNIA
Centre d'Études de Saclay, F–91191 Gif–sur–Yvette, France

Peter B. Siegel

California State Polytechnic University, Pomona CA 91768, USA

Abstract

A general coupled-channel formalism using a particle basis is presented, and applied succesfully to all the low energy $K^- - p$ process except the *1s* atomic level shift. The effect of the initial state interactions on the $K^- - p$ radiative capture branching ratios are found to be quite sizable.

1 Introduction

The interest in the K^--proton interactions is multifold[1], mainly due to two facts.

i) The $\Lambda(1405)$ resonance lies just below the $K^- - p$ threshold at 1432 MeV and offers an appropriate means to study the nature of this resonance. In the literature the $\Lambda(1405)$ is considered as an s-channel resonance [2] or as a quasi-bound $(K - N, \Sigma\pi)$ state [3]. In the quark-model approaches, this hyperon is considered as a pure q^3 state [4], a quasi-bound $\overline{K}$N state [5] or still as a hybrid $(q^3+q^4\overline{q}...)$ state [6]. A number of potential model fits to the scattering data incorporate the $\Lambda(1405)$ as a quasi-bound $(K - N, \Sigma\pi)$ resonance [7-10]. Very recent approaches treat this hyperon as an "elementary" field [11] or as a quasi-bound state [12] using chiral perturbation theory, or consider it as composed by an SU(2) soliton and a kaon bound in a S-wave [13].

ii) Even at low energies the K^- can scatter off the proton not only elastically but also go through inelastic reactions.

Investigating the K^--proton system, implies hence studying *simultaneously* the following eight channels:

$K^- p \to K^- p$, $\overline{K^0} - n$, $\Sigma^+\pi^-$, $\Sigma^0\pi^0$, $\Sigma^-\pi^+$, $\Lambda\pi^0$, $\Lambda\,\gamma$, $\Sigma\,\gamma$.

Besides, the amplitudes of the two radiative capture reactions can be related, *via* the crossing symmetry, to those of the strangeness photoproduction $\gamma p \to K^+\Lambda(K^+\Sigma^0)$. Much effort has been done experimentally and theoretically to understand this system. Close to the threshold (*i.e.* $p_K \leq 200 MeV/c$), there are roughly 70 total cross section data points [14]for the six strong interaction scattering process. In addition, threshold branching ratios have been measured with high accuracy: [15, 16]:

$$\gamma = \Gamma(K^-p \to \pi^+\Sigma^-)/\Gamma(K^-p \to \pi^-\Sigma^+) = 2.36 \pm .04,$$

$$R_c = \Gamma(K^-p \to \textit{charged particles})/\Gamma(K^-p \to \textit{all}) = .664 \pm .011,$$

$$R_n = \Gamma(K^-p \to \pi^0\Lambda)/\Gamma(K^-p \to \textit{ all neutral states}) = .189 \pm .015,$$

$$R_{\Lambda\gamma} = \Gamma(K^-p \to \Lambda\gamma)/\Gamma(K^-p \to \textit{all}) = .86 \pm .07 \pm .09 \times 10^{-3}\ ,$$

$$R_{\Sigma\gamma} = \Gamma(K^-p \to \Sigma^0\gamma)/\Gamma(K^-p \to \textit{all}) = 1.44 \pm .20 \pm .11 \times 10^{-3}.$$

Hence the existing data put tight constraints on the threshold amplitudes and potential coupling strengths. However, at present there is no comprehensive analysis which includes *both* the hadronic and electromagnetic branching ratios of the K^-p system.

In this contribution, we investigate all the low energy data within a *single model* using known coupling strengths and minimal SU(3) symmetry breaking for relevant vertices in the electromagnetic channels and emphasize the importance of the initial state interactions on the radiative capture branching ratios.

2 General Formalism

To study a coupled-channel system consisting of n hadronic channels and one electromagnetic channel, we assume that the interaction between channels can be represented for each partial wave l by real potentials of the form $V^l_{ij}(\sqrt{s}, k_i, k_j)$ with $\sqrt{s}$

the total energy and k_i the momentum of channel i in the center-of-mass frame. We also assume that the transition matrix element for each partial wave from channel i to channel j can be derived from a coupled-channel Lippmann-Schwinger equation:

$$T_{ij}(\sqrt{s}, k_i, k_j) = V_{ij}(\sqrt{s}, k_i, k_j) + \sum_m \int V_{im}(\sqrt{s}, k_i, q) G_m(\sqrt{s}, q) T_{mj}(\sqrt{s}, q, k_j) q^2 dq,$$

where $G_i(\sqrt{s}, q)$ is the propagator for channel i. The index l is suppressed since we are dealing only with the $l = 0$ partial wave.

Neglecting the back coupling of the photon channels, due to the weakness of the electromagnetic couplings, the T-matrix for radiative capture is the same as above with j replaced by γ and $m \neq \gamma$.

Since $\sqrt{s}$ and k_γ are fixed in the integral, we obtain for the T-matrix [10]:

$$T_{i\gamma}(\sqrt{(s)}, k_i, k_\gamma) = \sum_{m \neq \gamma} M_{im}(\sqrt{s}) V_{m\gamma}(\sqrt{s}, k_m, k_\gamma),$$

with the matrix M_{im} defined as

$$M_{im} \equiv \delta_{im} + \int V_{i,m}(\sqrt{s}, k_i, q) G_m(\sqrt{s}, q) v_{m\gamma}(q) q^2 dq + \sum_{n \neq \gamma} \int \int V_{in}(\sqrt{s}, k_i, q') \times$$

$$G_n(\sqrt{s}, q') V_{nm}(\sqrt{s}, q', q) G_m(\sqrt{s}, q) v_{m\gamma}(q) q'^2 dq' q^2 dq + \cdots.$$

The state m is the last hadronic one before the photon is produced. Since all the on-shell momenta are determined from $\sqrt{s}$ we have

$$T_{i\gamma}(\sqrt{s}) = \sum_{m \neq \gamma} M_{im}(\sqrt{s}) V_{m\gamma}(\sqrt{s}).$$

This convenient form for the transition matrix to the photon channels, separates out the strong part from the electromagnetic part of the interaction. The matrix M is determined entirely from the hadronic interactions. In the absence of channel-coupling M is the unit matrix. *Any deviation from unity is related to the initial state interactions.* For the strong channels we use separable potentials:

$$V^I_{ij}(k, k') = (g^2/4\pi) C^I_{ij} b^I_{ij} v_i(k) v_j(k'),$$

where the C^I_{ij} are determined from $SU(3)$-symmetry. The b^I_{ij} are "breaking parameters" which are allowed to vary from unity by $\pm 50\%$. The $v_i(k)$ are form factors,

taken here to be equal to $\alpha_i^2/(\alpha_i^2+k^2)$ as well as for the hadronic vertex (*i.e.* half off-shell part) of the electromagnetic amplitude, and g is an overall strength constant. These potentials are used in a coupled-channel Lippmann-Schwinger equation with a non-relativistic propagator.

For the radiative capture channels, we can write:

$$F_{K^-p\to\Lambda\gamma(\Sigma^0\gamma)} = \sum A_m(\sqrt{s}) f_{m\to\Lambda\gamma(\Sigma^0\gamma)},$$

where the f_m's are the amplitudes to go from the hadronic channel m to the appropriate photon channel. These amplitudes are derivable from Feynman diagrams representing the leading order contributions to the photoproduction process and include "extended Born" terms: the Λ and the Σ^0 exchange , and the vector meson exchange terms (K^*, ρ). The quantities A_m are unitless complex numbers, and contain all the information about the initial state interactions for radiative capture. Generally the sum over m is restricted to states which have charged hadrons. For the $K^- - p$ process the problem is greatly simplified, since there are only 3 channels which have charged hadrons: $\pi^+\Sigma^-$, $\pi^-\Sigma^+$ and K^-p. To a very good approximation, the A_m's are the same for both the $\Lambda\gamma$ and the $\Sigma^0\gamma$ channels.

3 Results and Discussion

Using the above formalism, two different separable potentials were considered: one guided by $SU(3)$ for the relative channel couplings [10] which fits all the low energy data [13-15] except the *1s* atomic-level shift [17], and one from Ref. [9] which fits all the low energy data including the scattering length from the *1s* atomic-level shift. Values for the A_m at the K^-p threshold for each fit are given in Table 1.

The resonance at an energy of 1405 MeV was also fitted and produced [10] as a $K - N(\Sigma\pi)$ bound state resonance.

To get an acceptable fit to all the data and determine the range of the A_m, we let the b_{ij}^I vary from 0.5 to 1.5. The A_i are a measure of how much the initial state interactions enhance the single scattering amplitude. As mentionned above, in the K^-p radiative decay calculation, only A_1, A_3, and A_5 contribute: $F_{K^-p\to\Lambda\gamma} = A_1 f_{\Sigma^-\pi^+\to\Lambda\gamma} + A_3 f_{\Sigma^+\pi^-\to\Lambda\gamma} + A_5 f_{K^-p\to\Lambda\gamma}$. In the absence of initial state interactions, $A_1 = A_3 = 0$ and $A_5 = 1$. As can be seen in Table I, the magnitude of A_1, A_3, and A_5 are between 0.8 and 1.3. Hence , cancellations amoung the various amplitudes can make the radiative capture probability very sensitive to the initial state interactions.

Table 1: The A_i values for two different strong potentials.

A_i	Potential with $SU(3)$-Symmetry [10]	Tanaka & Suzuki Potential [9]
A_1	+ 1.20 + 0.52 i	+ 1.49 − 0.28 i
A_2	− 1.02 − 0.14 i	− 1.10 + 0.52 i
A_3	+ 0.83 − 0.23 i	+ 0.71 − 0.75 i
A_4	− 0.16 − 0.34 i	− 0.30 − 0.39 i
A_5	− 0.15 + 1.06 i	+ 2.01 + 2.55 i
A_6	+ 1.18 − 0.41 i	+ 2.08 − 1.12 i

The important problem of include the appropriate isospin breaking effects due to the mass differences of the particles was handeled by using the correct relativistic momenta and reduced energies in the propagator. The effects are very important in calculating the threshold branching ratios, where the Coulomb potential can be neglected [18] when calculating the branching ratios.

To calculate the observables, we need to determine the values of the free parameters by least-squares fitting procedure to the data. The search was done using MINUIT code [19] on 13 parameters: the three ranges for the strong channels, the six breaking factors for the strong channels b^I_{ij}, and the four strong vertex coupling constants $g_{Kp\Lambda}$, $g_{Kp\Sigma}$, $g_{\pi\Sigma\Sigma}$, and $g_{\pi\Sigma\Lambda}$. We allowed the b^I_{ij} to vary ±50% from unity. Three of the 4 coupling constants, $g_{Kp\Sigma}$, $g_{\pi\Sigma\Sigma}$, and $g_{\pi\Sigma\Lambda}$ varied by ±50%, and the $g_{Kp\Lambda}$ coupling by ±20% from their SU(3) values respectively. Finally, The range parameters α were allowed to vary from 200 to 1000 MeV/c.

Our best fit values for the best known coupling constants are $g_{KN\Lambda}/\sqrt{4\pi} = -3.0$, and $g_{KN\Sigma}/\sqrt{4\pi} = 1.6$. Notice that their extracted values are in agreement with those obtained from strangeness photoproduction [20, 21] and hadronic sector [22, 23] analyses. The reduced χ^2 is 1.78.

3.1 Cross sections

In Fig. 1, we plot the total cross-section as a function kaon laboratory momentum P_{Lab}. The curves for each ratio correspond to the maximum allowed SU(3)-symmetry breaking as given above. The existing strong channels data are well reproduced. We have also studied in more details other breaking percentages and find [10] little sensitivity to the SU(3)-symmetry breaking effects in the domains studied here. Predictions for the two electromagnetic channels are also reported.

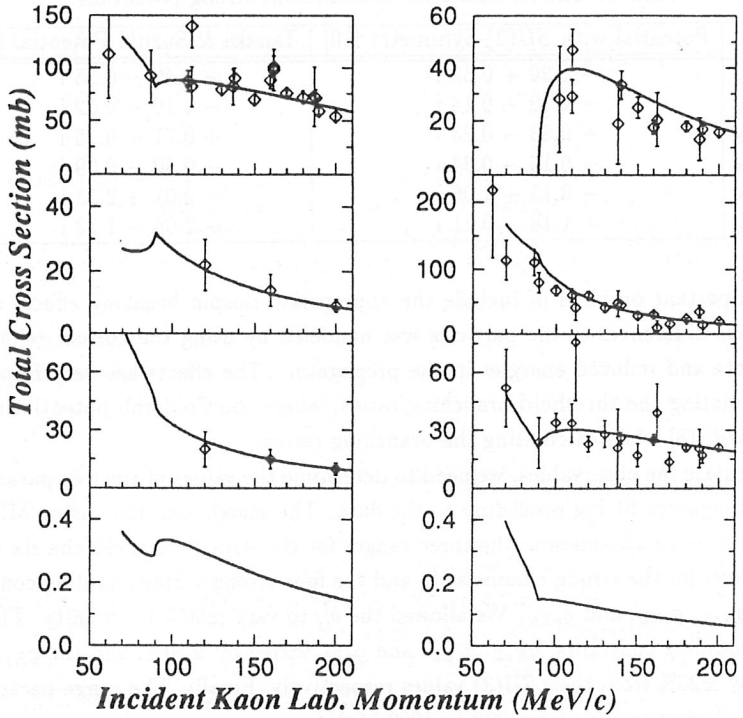

Figure 1: Total cross sections as a function of incident kaon momentum are compared with the available experimental data [14] for the six strong channels and the two electromagnetic channels: *a*) K^-p elastic scattering, *b*) $K^-p \to \overline{K^0}n$, *c*) $K^-p \to \pi^0\Lambda$, *d*) $K^-p \to \pi^+\Sigma^-$, *e*) $K^-p \to \pi^0\Sigma^0$, *f*) $K^-p \to \pi^-\Sigma^+$, *g*) $K^-p \to \Lambda\gamma$, and *h*) $K^-p \to \Sigma^0\gamma$.

3.2 Branching ratios

Tables 2 and 3 summarize threshold strong and electromagnetic branching ratios, respectively. Results of our calculation are in reasonable agreement with the data. The electromagnetic branching ratios deserve some comments.

The most striking feature comes from the drastical dependence of these branching ratios on the initial state interactions. The second row in Table 3 shows that if these interactions are switched off, the ratios $R_{\Lambda\gamma}$ and $R_{\Sigma\gamma}$ decrease by roughly a factor of 2 and more than one order of magnitude, respectively.

It is also interesting that at threshold $R_{\Lambda\gamma}$ is substantially less than $R_{\Sigma\gamma}$. Our recent

Table 2: K^-p threshold strong branching ratios

	γ	R_c	R_n
Present work	2.31	.661	.164
EXPERIMENT [15]	2.36 ± .04	.664 ± .011	.189 ± .015

Table 3: K^-p threshold radiative capture branching ratios. The final state interactions in the Tanaka & Suzuki Potential were included in this work.

Authors [Ref.]	$R_{\Lambda\gamma} \times 10^3$	$R_{\Sigma\gamma} \times 10^3$	Formalism
Present work	1.09	1.55	*coupled-channel* with FSI
Present work	0.56	0.12	*coupled-channel* without FSI
Zhong et al.[5]	1.90	2.30	*coupled-channel* with FSI
Tanaka & Suzuki[9]	17.5	3.29	*coupled-channel* with FSI
Workman & Fearing[24]	3.09	3.72	*Diagrammatic technique*
Williams et al.[25]	0.89	1.46	*Diagrammatic technique*
David et al.[21]	0.95	1.44	*Diagrammatic technique*
EXPERIMENT [16]	.86 ± .12	1.44 ± .20	

investigation [10] shows that this trend is general at energies below the $\overline{K^0}n$ threshold, while at higher energies the ratio $R_{\Lambda\gamma}$ becomes greater than $R_{\Sigma\gamma}$. Experimental data of these branching ratios at low energies with kaons in flight would help clarify the nature of the $\Lambda(1405)$.

The coupled channel calculation results by Zhong et al. [5] are too high roughly by a factor of 2, and our results using the Tanaka-Suzuki potential miss by far the data. Another approach, based on diagrammatic technique, has also been applied to this field. Williams et al. [25] obtain good agreement with the data, but their coupling constants disagree with the SU(3)-symmetry constraints. Workman-Fearing [24] and David et al. [21] respect the SU(3) values, and only the latter work produces results in agreement with the data.

3.3 Scattering length

The K^-p scattering length obtained from our best fit compares closely with the value from Ref. [21] . These real part, however, have the opposite sign compared to those extracted from the *1s* K^-p atomic level shift data [17], that we did not try to fit. The existing data on the *1s* atomic level shift suffer from lack of accuracy and even the values within quoted error bars seem questionable [26]. Nevertheless, from

Table 4: K^-p scattering length

Authors [Ref]	a_{K^-p} (fm)	*1s* atomic level shift
Present work	− 0.63 + 0.76 i	*not fitted*
Martin [22]	− 0.66 + 0.64 i	*not fitted*
Tanaka & Suzuki [9]	− 1.11 + 0.70 i	*not fitted*
Tanaka & Suzuki [9]	+ 0.34 + 0.77 i	*fitted*

these data it is generally infered that the scattering length has positive sign.
In trying to shed a light on this quest, we used the A_m obtained from the potential of Ref. [9] which fit all the hadronic low energy data and has the same sign for the scattering length as the atomic level shift data. We were able to reproduce their results using their non-relativistic potentials. From Table I we see that A_1 and A_3 do not differ too much from those obtained by our "SU(3) guided" potential. However, A_5 is much different in magnitude and its real part has the opposite sign. This desirable feature in reproducing the radiative capture branching ratios, is perhaps at the origin of the negative sign obtained for the scattering length.

4 Concluding remarks

We presented a coupled-channel formalism and reported the results of a comprehensive analysis of all the low energy K^-p data, except the *1s* atomic level shift. Results presented in this paper, reproduce well enough the existing strong and electromagnetic data from threshold up to $P_K^{lab} \approx 200$ MeV/c, with the relevant coupling constants close to their expected SU(3)-symmetry values. In all of the fits, the $\Lambda(1405)$ is produced as a bound $K - N(\Sigma\pi)$ resonance, and the initial state interactions are very important for the radiative capture branching ratios. Our predictions underline clearly the need for more experimental investigations, specially for the in flight branching ratios. One of the main motivations is of course clarifying the nature of the $\Lambda(1405)$ resonance. Another crucial quest concerns the scattering length. Our results tend to show that reproducing *simultaneously* the measured electromagnetic branching ratios and the scattering length can not be achieved with the present approches. New and accurate measurements of the kaonic atoms level shifts are hence highly desirable.

References

[1] *For a recent review see:* P.M. Gensini, Low-Energy Kaon-Nucleon Interactions and Scattering at DAϕNE, The Second DAϕNE Physics Handbook, ed. L.Maini et al., INFN, Frascati, 1995.

[2] T.A. DeGrand and L. Jaffe, Ann. Phys. (N.Y.) **100**, 425 (1976).

[3] R.H. Dalitz, S.F. Tuan, Ann. Phys. **10**, 307 (1960); R.H. Dalitz, T.-C. Wong, and G. Rajasekaran, Phys. Rev. **153**, 1617 (1967).

[4] M. Jones, R.H. Dalitz, R.R. Horgan, Nucl. Phys. **B129**, 45 (1977); J.D. Darewych, R. Koniuk and N. Isgur, Phys. Rev. **D32**, 1765 (1985).

[5] Y.S. Zhong, A. Thomas, B. Jennings, and R. Barrett, Phys. Rev. **D38**, 837 (1988).

[6] G. He and R.H. Landau, Phys. Rev. **C48**, 3047 (1993); M. Arima, S. Matsui, and K. Shimizu, Phys. Rev. **C49**, 2831 (1994).

[7] J. Schnick and R.H. Landau, Phys. Rev. Lett. **58**, 1719 (1987).

[8] P.B. Siegel and W. Weise, Phys. Rev. **C38**, 2221 (1988).

[9] K. Tanaka and A. Suzuki, Phys. Rev. **C45**, 2068 (1992)

[10] P.B. Siegel and B. Saghai, Phys. Rev. **C**, *in press.*

[11] C.H. Lee, G.E. Brown, D.P. Min, and M. Rho, Nucl. Phys. **A585**, 401 (1995); C.H. Lee, D.P. Min, and M. Rho, *The Role of* $\Lambda(1405)$ *in Kaon-Proton Interactions*, Saoul National University Preprint, SNUTP-95-060, (1995)..

[12] N. Kaiser, P.B. Siegel, and W. Weise, *Chiral Dynamics and the Low Energy Kaon-Nucleon Interactions*, Munich University preprint, TUM/T39-95-5 (1995).

[13] C.L. Schat, N. Scoccola, and C. Gobbi, Nucl. Phys. **A585**, 627 (1995).

[14] J. Ciborowski et al., J. Phys. **G 8**, 13 (1982); D. Evans et al., J. Phys. **G 9**, 885 (1983); W.E. Humphrey and R.R. Ross, Phys. Rev. **127**, 1305 (1962); J.K. Kim, Columbia University Report, Nevis 149 (1966); M. Sakitt et al., Phys. Rev.**139**, 719 (1965).

[15] D.N. Tovee et al., Nucl. Phys. **B33**, 493 (1971); R.J. Nowak et al., Nucl. Phys. **B139**, 61 (1978).

[16] D.A. Whitehouse et al., Phys. Rev. Lett. **63**, 1352 (1989).

[17] J.D. Davies et al., Phys. Lett. **83B**, 55 (1979); M. Izycki et al., Z. Phys. **A297**, 11 (1980); P.M. Bird, A.S. Clough, and K.R. Parker, Nucl. Phys. **A404**, 482 (1983).

[18] P.B. Siegel, Z. Phys. **A 328**, 239 (1987).

[19] F. James, *MINUIT Functional Minimization and Error Analysis*, D506-Minuit, CERN (1994).

[20] R.A. Adelseck and B. Saghai, Phys. Rev. **C42**, 108 (1990).

[21] J.C. David, C. Fayard, G.H. Lamot, F. Piron, and B. Saghai, in *Proceedings of the 8th Symposium on Polarization Phenomena in Nuclear Physics*, Bloomington, September 15-22, 1994, Ed. S. Vigdor et al., AIP Proceedings, *in press.*

[22] A.D. Martin, Nucl. Phys. **B179**, 33 (1981).

[23] J. Antolin, Z. Phys. C **31**, 417 (1986); M. Bozoian, J.C. van Doremalen, and H.J. Weber, Phys. Lett. **122B**, 138 (1983); R. Timmermans, Th. Rijken, and J.J. de Swart, Phys. Lett. **257B**. 227 (1991).

[24] R.L. Workman and H.W. Fearing, Phys. Rev. **D37**, 3117 (1988).

[25] R. Williams, and C. Ji, S. Cotanch, Phys. Rev. **C46**, 1617 (1992).

[26] H.H. Brouwer, J.W. de Maag, and L.P. Kok, Z. Phys. **A318**, 199 (1984); C.J. Batty, Nucl. Phys. **A508**, 89c (1990).

KN SCATTERING IN THE NONRELATIVISTIC QUARK MODEL

T.Barnes
Theoretical Physics Group, Physics Division, Oak Ridge National Laboratory
Oak Ridge, TN 37831-6373, USA

ABSTRACT

KN scattering is of interest as a probe of nuclear structure and, more fundamentally, as a laboratory for the study of nonresonant hadron-hadron interactions. KN is a theoretically attractive channel because of its simplicity, having only $S = 1/2$, no one pion exchange contributions and no valence $q\bar{q}$ annihilation. It may therefore be useful for the study of short-ranged quark forces analogous to the NN repulsive core. Since there are two isospin states, comparison of two closely related amplitudes is possible. This contribution reviews the experimental status of S-wave KN scattering and related theoretical studies based on quark-gluon dynamics. The experimental low-energy S-wave phase shift is well established for I=1, but is not yet well determined for I=0. The ratio of I=0 to I=1 scattering lengths is an interesting number theoretically, and may discriminate between different scattering mechanisms. A measurement of these scattering lengths at DAPHNE would be a useful contribution to low energy hadron physics.

1 – KN scattering and the importance of being exotic

KN scattering is interesting because it is rather simple. In a more representative hadron-hadron scattering process such as $\pi^- P \to \rho^o N$ there are at least three important scattering mechanisms, s-channel resonance formation, t-channel meson exchange, and short-ranged quark forces from overlapping quark wavefunctions. With all three mechanisms present it is difficult to distinguish the individual contributions. In contrast, in flavor-exotic KN scattering the s-channel resonance diagrams are absent because the kaon's $\bar{s}$ antiquark cannot annihilate with the nucleon's nonstrange valence quarks. Similarly the most important t-channel exchange,

one pion exchange, is forbidden by angular quantum numbers; the lightest t-channel exchanges possible are the vector $q\bar{q}$ states, and these are suppressed by their higher masses. This implies that we may be able to see scattering due to quark-gluon interactions in KN without important complications from additional mechanisms.

In this contribution we first discuss the experimental status of KN scattering, following which we review theoretical studies of KN using quark and gluon degrees of freedom. Here we primarily consider the short-ranged S-waves, which are the relevant amplitudes for near-threshold studies at DAPHNE. Although the higher partial waves are very interesting and exhibit large spin-orbit forces and possibly exotic "Z^*" resonances, [1] they are beyond the range of invariant mass which will initially be accessible at DAPHNE.

2 – Experimental status of low energy KN S-wave scattering

We begin by reviewing the status of experimental KN scattering lengths (abstracted from Barnes and Swanson [2]). Since there are unresolved disagreements between analyses in the I=0 channel, we show all relatively recent (since 1980) single-energy S-wave phase shifts. These are Martin and Oades [3] (Aarhus and UC London, 1980); Watts *et al.* [4] (QMC and RAL, 1980); Hashimoto [5] (Kyoto and VPI, 1984); and Hyslop *et al.* [6] (VPI, 1992). The I=1 data set analysed by Arndt and Roper [7] (VPI, 1985) was incorporated in the 1992 VPI analysis. Fig.1 shows these experimental I=0 and I=1 S-wave phase shifts versus $P_{cm} = |\vec{P}_{cm}|$.

For I=1, the linear low energy behavior which determines the scattering length is evident in the data, and Hyslop *et al.* cite a fitted value of $a_{I=1}^{KN} = -0.33$ fm. Previous analyses (summarized by Dover and Walker [1] and Hyslop *et al.* [6]) have given values between $-0.28(6)$ fm [8] and -0.33 fm. [6, 9]

In contrast, the I=0 phase shift is not yet well determined experimentally; evidently it is negative and somewhat weaker than I=1, but there is considerable disagreement between analyses. Since an extrapolation of this poorly determined quantity to threshold is problematical, the value of the I=0 KN scattering length is not well established. Previous (favored) solutions for $a_{I=0}^{KN}$ up to 1982 are summarized in Table 2.3 of Dover and Walker, [1] and range between +0.02 fm and $-0.11^{+0.06}_{-0.04}$ fm. There appear to be two sets of low energy values in the data of Fig.1, a smaller phase shift from the Aarhus-UCL and QMC-RAL collaborations and a larger one from from the Kyoto-VPI and VPI analyses. Below $P_{cm} = 0.4$ Gev the Kyoto-VPI and VPI results are larger than Aarhus-UCL and QMC-RAL by about a factor of two. The VPI group [6] actually cite a scattering length of $a_{I=0}^{KN} = 0.0$ fm, although this requires rapid low energy variation below the first experimental point.

A more useful way to present the S-wave phase shift data is to show δ_0^I / P_{cm}

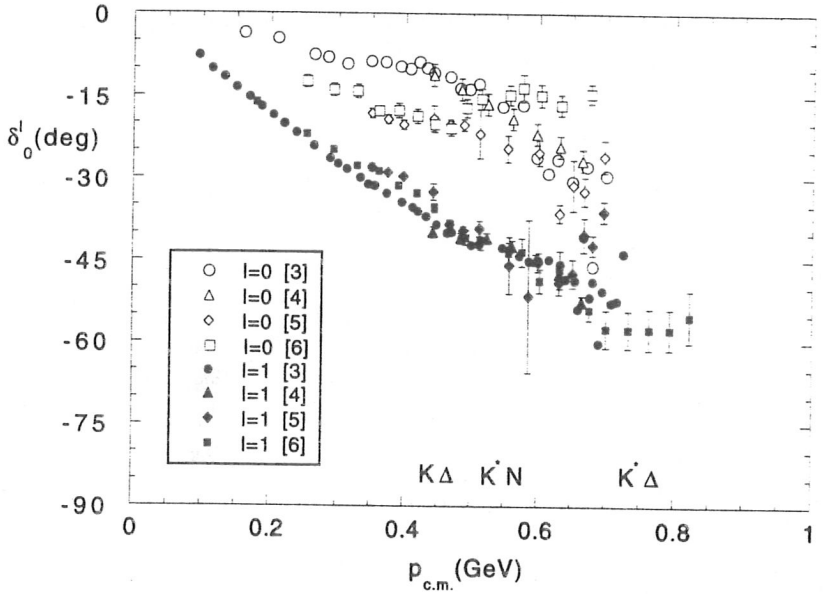

Figure 1: Recent experimental results for S-wave KN phase shifts. (Solid is I=1, open is I=0.)

versus P_{cm}^2; the intercept is the scattering length, and the slope at intercept determines the effective range. This is a "specific heat plot", motivated by the c/T versus T^2 plots of metal specific heats used to separate the Fermi-distribution term $\propto T$ from the phonon term $\propto T^3$. In Fig.2 we show the S-wave phase shifts in this manner; an I=1 scattering length of about $-0.31(1)$ fm is evident. Since the I=1 phase shift is close to linear for $P_{cm} < 0.4$ Gev ($k_{lab} < 0.7$ Gev), we assume that the I=0 phase shift is also approximately linear in P_{cm} for $P_{cm} < 0.4$ Gev. We can then read the I=0 scattering length from the intercept in Fig.2. A naive extrapolation to threshold leads to scattering lengths of about $-0.09(1)$ fm and $-0.17(2)$ fm respectively from the two sets of references. In summary, the experimental phase shifts shown in Fig.2 suggest to us scattering lengths of

$$\begin{aligned} a_{I=1}^{KN}(expt.) &= -0.31(1) \text{ fm} ; \\ a_{I=0}^{KN}(expt.)\Big|_{Aarhus-QMC-RAL-UCL} &= -0.09(1) \text{ fm} , \\ a_{I=0}^{KN}(expt.)\Big|_{Kyoto-VPI} &= -0.17(2) \text{ fm} . \end{aligned} \tag{1}$$

We emphasize that the I=0 values are our interpretation of the data in Fig.2, and the references cited quote smaller scattering lengths. Since the value of the I=0 scattering length is evidently controversial, an accurate determination should be a first priority at DAPHNE.

3 – Theoretical mechanisms of hadron-hadron scattering

3.1 Meson exchange or quark forces or both?

Two distinct mechanisms are widely assumed by theorists in models of hadron-hadron scattering. In the first approach one treats hadrons as fundamental fields with an effective Lagrangian, and assumes that the scattering mechanism is t-channel meson exchange and s-channel resonance formation, and perhaps higher-order virtual hadron processes. This implicitly assumes dominance of scattering by processes involving $q\bar{q}$ pair creation and annihilation. The second mechanism assumes that scattering (in the absence of s-channel resonances) is dominated by the quark-gluon interaction in overlapping hadron wavefunctions, rather than $q\bar{q}$ annihilation or pair production. The question of the range of validity of these two mechanisms is an open issue; certainly at large separations one pion exchange is dominant when allowed, but at separations below a characteristic hadron length scale the scattering should be best described in terms of quark and gluon degrees of freedom. [10]

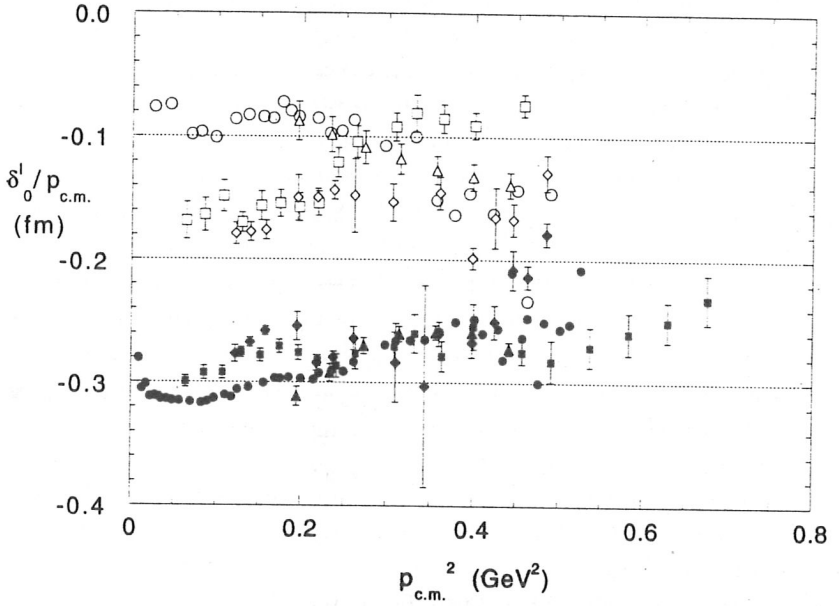

Figure 2: KN S-wave phase shifts plotted to show scattering lengths.

One should note that t-channel meson exchange and quark interchange are physically distinct processes, since they go through different intermediate states, here $q^5\bar{q}^2$ and $q^4\bar{q}$. This distinction makes it clear that both scattering mechanisms must be present, and our task is to determine the relative importance of each in a given reaction. This may require studies of nontrivial features such as spin-orbit effects in higher partial waves, which should be strongly mechanism-dependent. Isgur offers a confusion theorem [11] to the effect that it may prove difficult to distinguish higher-mass t-channel resonance exchange from quark-gluon forces (quark-interchange amplitudes in particular) because they have the same flavor flow in t-channel and both are short-ranged. Indeed, there is a danger than one type of model may effectively parametrize the other mechanism given sufficient degrees of freedom.

Scattering processes such as KN→KN which exclude one pion exchange and s-channel resonance formation may allow us to address the important theoretical issue of the relative importance of quark forces and meson exchange. Although this paper is concerned with the description of KN scattering at the quark-gluon level, we note in passing that several studies of KN scattering using effective hadron Lagrangians have appeared in the literature. [12] These typically find a positive or nearly zero I=0 KN scattering length, which is quite different from our quark model results. A measurement of $a_{I=0}^{KN}$ should allow a choice between these models.

The issue of the scattering mechanism has implications for nuclear physics as well. As an example, meson exchange models incorporate large contributions from t-channel vector meson exchange in KN scattering, and the Z-dependence of kaon-nucleus scattering [13] has been attributed to a decrease in mass of exchanged vectors within the nuclear medium. [14] If an improved understanding of the mechanism of KN scattering leads to the conclusion that vector exchange is actually unimportant, this would necessarily modify the interpretation of this effect.

3.2 KN scattering at the quark-gluon level

Nine theoretical studies of the KN interaction using quark and gluon degrees of freedom have been published to date. These references, their methods, and the topics studied are as follows:

1. I.Bender and H.G.Dosch, [15] resonating group; S-wave KN phase shifts (results only).

2. H.J.Pirner and B.Povh, [16] (comments); spin-orbit effects in KN versus NN.

3. I.Bender, H.G.Dosch, H.J.Pirner and H.G.Kruse, [17] resonating group; S-wave KN phase shifts (detailed calculation).

4. D.Mukhopadhyay and H.J.Pirner, [18] resonating group; P-wave KN amplitudes.

5. K.Maltman and S.Godfrey, [19] resonating group; possible Z^* resonances.

6. R.K.Campbell and D.Robson, [20] resonating group; S-wave KN phase shifts.

7. P.Bicudo and J.E.Ribeiro, [21] resonating group (improved method); S-wave KN phase shifts, comparison with previous references.

8. P.Ning, E.Zhao and P.Li, [22] resonating group; S- and P-wave KN phase shifts (discussion only, detailed publication in preparation).

9. T.Barnes and E.S.Swanson, [2] quark Born diagrams (OGE and constituent interchange); S-wave KN phase shifts, possible Z^* resonances.

The results of these calculations differ in detail and are occasionally in fundamental disagreement. We will summarize their results for KN and note which aspects of these papers are controversial.

The first extensive calculations of KN scattering were those of Bender *et al.*, [17] who used the lowest order QCD scattering process (one gluon exchange and constituent interchange) as the kernel in a variational resonating group calculation, with external SHO kaon and nucleon wavefunctions. This reference found a strongly repulsive interaction in I=1 KN and a weaker repulsion in I=0 KN, which gave S-wave phase shifts quite similar to the data. They concluded that the dominant contribution to an I=1 KN equivalent potential is the spin-spin hyperfine part of OGE; similar results have been reported for the NN repulsive core [23]. This supports the suggestion that KN and NN scattering are closely related.

Unfortunately, many aspects of the work of Bender *et al.* have not been reproduced in subsequent studies. Campbell and Robson [20] and find a small, negative I=0 phase shift but a large attractive contribution to the I=1 phase shift from the kinetic term, which is treated as an interaction in the resonating group formalism. They also find considerable sensitivity to the wavefunctions and to a local approximation to the resonating group equations. Bicudo and Ribeiro [21] used an improved resonating group approach which allowed a more direct determination of phase shifts, and tested previous results; on comparing with Bender *et al.* using the same interaction, they find a much stronger I=0 phase shift. In a similar comparison with Campbell and Robson, Bicudo and Ribeiro find a somewhat larger absolute scale for the KN phase shifts. This demonstrates the large systematic uncertainties which have accompanied resonating group studies of KN scattering amplitudes.

Another disturbing conclusion of the Bender *et al.* work is that I=1 KN scattering persists when the interaction is set to zero! (They find that the dominant

effect in I=1 KN scattering comes from the "normalization kernel" in the resonating group formalism.) This remarkable claim clearly requires further theoretical study; this no-interaction scattering may be an artifact of the resonating group approach, which can give spurious results when approximate external wavefunctions are used. [24]

There have also been studies of the higher KN partial waves, notably the P-waves. These are especially interesting because one of these flavor-exotic amplitudes ($\delta_{01} : I = 0, 2J = 1$) may show resonant phase motion. Pirner and Povh [16] noted however that a KN spin-orbit potential abstracted from a fitted NN one gives a good description of the four KN P-wave phase shifts ($I = 0, 1; 2J = 1, 3$), so the KN and NN spin-orbit interactions may actually have the same nonexotic origin. Mukhopadhyay and Pirner [18] subsequently found that OGE forces in a resonating group calculation fail to explain the δ_{01} KN phase shift, although the other three P-waves were close to experiment. Thus there may be a "spin-orbit problem" in the KN P-waves. This should be regarded as an unresoved issue, however, because a recent paper by Ning, Zhao and Li [22] states (without showing details) that these P-wave phase shifts can be described satisfactorily by an OGE interaction in a resonating group formalism.

3.3 KN phase shifts using quark Born diagrams

Evidently there is considerable systematic uncertainty in the hadron-hadron scattering amplitudes found using resonating group techniques, at least in KN. In a recent series of papers [2, 25, 26, 27] we have advocated a much simpler approach to hadron-hadron scattering at the quark-gluon level. We simply derive the lowest order scattering amplitude from a single interaction (usually OGE) between external hadron wavefunctions (from the nonrelativistic quark model), followed by constituent interchange to restore color singlet hadrons. We refer to these scattering diagrams as "quark Born diagrams". This method has been applied to I=2 $\pi\pi$ [25] and I=3/2 $K\pi$ [27] with excellent results. These reactions are similar to KN since they have no valence $q\bar{q}$ annihilation and one pion exchange is forbidden. Since the kernel is completely well defined we have no ambiguities in the calculation, and for realistic quark model parameters we can test the implicit assumption that a single interaction dominates the amplitude. Similar techniques have been applied to meson-meson scattering by Masud *et al.* [28] and by Blaschke *et al.* [29]

In the KN case the four independent quark Born diagrams are

D_1 =

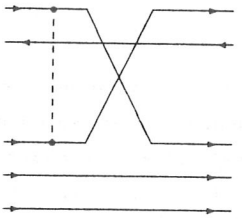

(2)

D_2 =

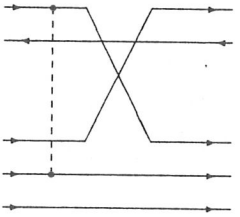

(3)

D_3 =

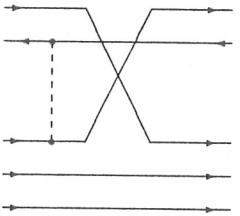

(4)

D_4 =

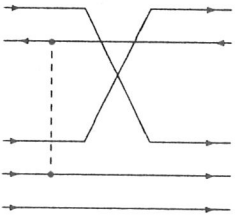

(5)

We assume hyperfine dominance of the KN scattering kernel as found by Bender *et al.* [17] and neglect the other OGE and confining terms, so our scattering Hamiltonian is

$$H_{scat} = \sum_{a,i<j} \left[-\frac{8\pi\alpha_s}{3m_i m_j}\,\delta(\vec{r}_{ij}) \right] \left[\vec{S}_i \cdot \vec{S}_j \right] \left[\mathcal{F}_i^a \cdot \mathcal{F}_j^a \right] . \tag{6}$$

The matrix element of this Hamiltonian between KN states consists of positive definite wavefunction-dependent overlap integrals (specific to each diagram) times a color-flavor-spin weight factor for each diagram. This weight factor is a channel-dependent group-theoretic number which is independent of the spatial wavefunctions. For the two KN isospins the weight factors which multiply diagrams $[D_1, D_2, D_3, D_4]$ are

$$[w_i]^{\rm KN}_{\rm I=0} = \left[0,\ \frac{1}{6},\ 0,\ \frac{1}{6} \right] \tag{7}$$

and

$$[w_i]^{\rm KN}_{\rm I=1} = \left[\frac{1}{3},\ \frac{1}{18},\ \frac{1}{3},\ \frac{1}{18} \right] . \tag{8}$$

Since the overlap integrals are all positive and are comparable near threshold, this tells us that both KN channels are repulsive (positive $\langle KN|H_I|KN\rangle$ matrix elements) and that I=1 dominates I=0.

Although we have general integral formulas for the scattering amplitudes for any spatial wavefunctions, it is interesting to specialize to SHO wavefunctions, since the matrix elements can be derived analytically and the wavefunction momentum scales α (baryons) and β (mesons) are known. The detailed derivation is given elsewhere; [2] here we simply cite the results for phase shifts and scattering lengths for the KN S-waves; these are

$$\delta_{I0}^{KN} = -\frac{4\alpha_s}{3m_q^2}\frac{P_{cm}E_K E_N}{(E_K+E_N)} \sum_{i=1}^{4} w_i\,\eta_i\,\exp(-A_i P_{cm}^2)\,i_0(B_i P_{cm}^2) \tag{9}$$

and

$$a_I^{KN} = -\frac{4\alpha_s}{3m_q^2}\frac{M_K M_N}{(M_K+M_N)} \sum_{i=1}^{4} w_i\,\eta_i\ . \tag{10}$$

The wavefunction-dependent quantities η_i, A_i and B_i are given by Barnes and Swanson. [2] One specifies the isospin state I=0 or I=1 through the choice of the diagram weights $\{w_i\}$. The final results for the scattering lengths are

$$a_{I=1}^{KN} = -\frac{4\alpha_s}{3m_q^2}\frac{M_K M_N}{(M_K+M_N)}$$

$$\cdot\left[\frac{1}{3} + \frac{1}{18}\left(\frac{12g}{7g+6}\right)^{3/2} + \frac{1}{3}\,\rho\left(\frac{6}{g+3}\right)^{3/2} + \frac{1}{18}\,\rho\left(\frac{12g}{(2g+3)(g+2)}\right)^{3/2} \right] \tag{11}$$

and

$$a_{I=0}^{KN} = -\frac{4\alpha_s}{3m_q^2}\frac{M_K M_N}{(M_K+M_N)}\left[\frac{1}{6}\left(\frac{12g}{7g+6}\right)^{3/2} + \frac{1}{6}\rho\left(\frac{12g}{(2g+3)(g+2)}\right)^{3/2}\right]. \quad (12)$$

These are functions of the three parameters α_s/m_q^2, $\rho = m_q/m_s$, $g = (\alpha/\beta)^2$ and the physical masses M_K and M_N. If we use a representative quark model parameter set $\alpha_s/m_q^2 = 0.6/(0.33)^2$ Gev^{-2}, $\rho = m_q/m_s = (0.33$ Gev $/0.55$ Gev$) = 0.6$, $\alpha = 0.4$ GeV and $\beta = 0.35$ GeV, we find scattering lengths of

$$a_{I=1}^{KN} = -0.35 \text{ fm} \quad (13)$$

and

$$a_{I=0}^{KN} = -0.12 \text{ fm} . \quad (14)$$

These compare well with experiment (1), although it is clearly important to improve the experimental I=0 number.

The ratio $a_{I=0}^{KN}/a_{I=1}^{KN}$ is especially interesting because the OGE strength α_s/m_q^2 and the physical hadron masses M_K and M_N cancel, leaving only $\rho = m_q/m_s$ and the relative length scale $g = (\alpha/\beta)^2$. Since α/β is near unity, the quark Born calculation leads to $a_{I=0}^{KN}/a_{I=1}^{KN} \approx +0.3$ (see Fig.3 of Barnes and Swanson [2]). Since t-channel meson exchange models usually predict this ratio to be negative or near zero, a measurement of $a_{I=0}^{KN}$ may allow experiment to distinguish between the two scattering mechanisms. A compilation of various predictions is given in Table 6-4 of Hyslop. [9]

Although we find very reasonable KN scattering lengths with conventional quark model parameters, when we compare the predicted S-wave phase shifts (9) (Fig.3, dashed line) with experiment well above threshold, it is clear that the predicted scattering is weaker than observed. A three-parameter fit to the full 1992 VPI I=0,1 energy independent S-wave data set [6] gives a very satisfactory description with $\alpha_s/m_q^2 = 0.59/(0.33)^2$ Gev^{-2} for the OGE interaction strength and nucleon and kaon scales $\alpha = 0.68$ GeV and $\beta = 0.43$ GeV (Fig.3, solid line). The largest change in the fit is the nucleon length scale α^{-1}, which is about 0.7 times conventional quark model values. This may imply that the usual single-Gaussian SHO wavefunctions with $\alpha \approx 0.4$ GeV are too smooth, which becomes apparent only as the momentum transfer is increased. This should be tested using more realistic Coulomb plus linear wavefunctions, which may have sufficient support at higher momentum scales to explain the observed S-wave phase shifts.

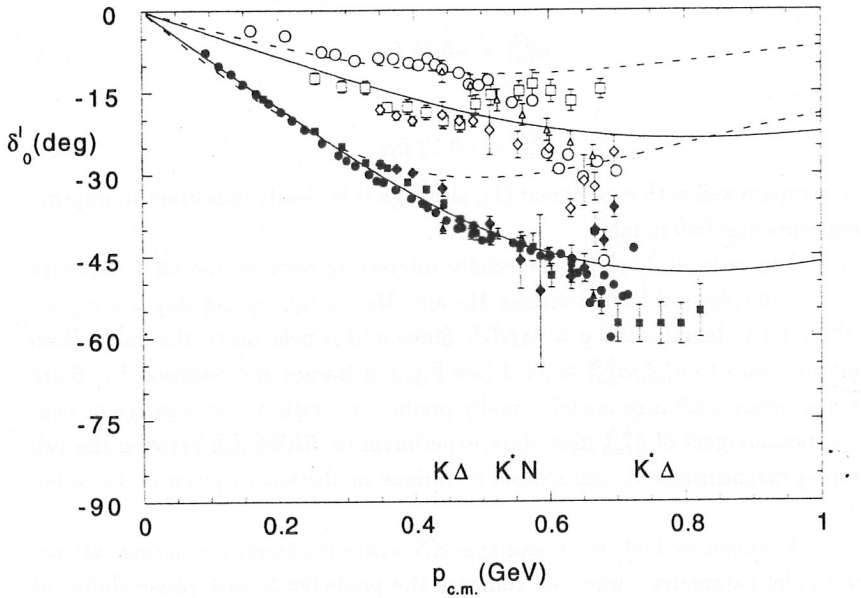

Figure 3: Quark Born diagram results for KN S-wave phase shifts compared to data. Dashed = conventional parameters, solid = fitted parameters.

Acknowledgements

I am grateful to the organisers of the DAPHNE'95 workshop for their kind invitation to present this contribution. I would also like to thank my colleagues E.S.Ackleh, A.Dzierba, A.Gal, H.Lipkin, A.Olin, G.Pancheri, R.Sawafta, J.Speth and E.S.Swanson for discussions of various issues relating to this material.

References

1. C.B.Dover and G.E.Walker, Phys. Rep. **89**, 1 (1982).
2. T.Barnes and E.S.Swanson, Phys. Rev. **C49**, 1166 (1994).
3. B.R.Martin and G.C.Oades, "KN Phase Shift Analysis Including Constraints from Fixed-t Analyticity". Unpublished report of results presented at the *IVth International Conference on Baryon Resonances "Baryon 1980"* (Toronto, 14-16 July 1980); see also G.C.Oades, in *Low and Intermediate Energy Kaon-Nucleon Physics* (1981), ed. E.Ferrari and G.Violini.
4. S.J.Watts *et al.*, Phys. Lett. **95B**, 323 (1980).
5. K.Hashimoto, Phys. Rev. **C29**, 1377 (1984).
6. J.S.Hyslop, R.A.Arndt, L.D.Roper and R.L.Workman, Phys. Rev. **D46**, 961 (1992).
7. R.A.Arndt and L.D.Roper, Phys. Rev. **D31**, 2230 (1985).
8. R.E.Cutkosky, H.R.Hicks, J.Sandusky, C.C.Shih, R.L.Kelly, R.C.Miller and A.Yokosawa, Nucl. Phys. **B102**, 139 (1976).
9. J.S.Hyslop, "An Analysis of K^+-Nucleon Scattering", Ph.D. thesis, Virginia Polytechnic Institute and State University (1990), report UMI-91-09407 (Aug. 1990).
10. N.Isgur, Acta Physica Austraica, Suppl. **XXVII**, 177 (1985).
11. N.Isgur, personal communication.
12. See for example A.C.Davis, W.N.Cottingham and J.W.Alcock, Nucl. Phys. **B111**, 233 (1976); J. Phys. **G4**, 323 (1978); R.Büttgen, K.Holinde and J.Speth, Phys. Lett. **163B**, 305 (1985); J.Cohen, Phys. Rev. **C39**, 2285 (1989).
13. D.Marlow *et al.*, Phys. Rev. **C25**, 2619 (1982); R. Weiss *et al.*, Phys. Rev. **C49**, 2569 (1994), and references cited therein.

14. G.E.Brown, C.B.Dover and W.Weise, Phys. Rev. Lett. **60**, 2723 (1988).

15. I.Bender and H.G.Dosch, Z. Phys. **C13**, 69 (1982).

16. H.J.Pirner and B.Povh, Phys. Lett. **114B**, 308 (1982).

17. I.Bender, H.G.Dosch, H.J.Pirner and H.G.Kruse, Nucl. Phys. **A414**, 359 (1984).

18. D.Mukhopadhyay and H.J.Pirner, Nucl. Phys. **A442**, 605 (1985).

19. K.Maltman and S.Godfrey, Nucl. Phys. **A452**, 669 (1986).

20. R.K.Campbell and D.Robson, Phys. Rev. **D36**, 2682 (1987).

21. P.Bicudo and J.E.Ribeiro, Z. Phys. **C38**, 453 (1988).

22. P.Ning, E.Zhao and P.Li, Euro. Phys. Lett. **21**, 897 (1993).

23. D.A.Liberman, Phys. Rev. **D16**, 1542 (1977); C.E.DeTar, Phys. Rev. **D17**, 302 (1977); *ibid.*, p.323; M.Oka and K.Yazaki, Phys. Lett. **90B**, 41 (1980); Prog. Theor. Phys. **66**, 556 (1981); *ibid.*, p.572; A.Fäßler, F.Fernandez, G.Lubeck and K.Shimizu, Phys. Lett. **112B** 201 (1982); K.Maltman and N.Isgur, Phys. Rev. Lett. **50**, 1827 (1983); M.Oka and C.J.Horowitz, Phys. Rev. **D31**, 2773 (1985); Y.Koike, Nucl.Phys. **A454**, 509 (1986); K.Shimizu, Rep. Prog. Phys. **52**, 1 (1989).

24. E.S.Swanson, personal communication.

25. T.Barnes and E.S.Swanson, Phys. Rev. **D46**, 131 (1992).

26. E.S.Swanson, Ann. Phys. (NY) **220**, 73 (1992).

27. T.Barnes, E.S.Swanson and J.Weinstein, Phys. Rev. **D46**, 4868 (1992).

28. B.Masud, J.Paton, A.M.Green and G.Q.Liu, Nucl. Phys. **A528**, 477 (1991); B.Masud, Phys. Rev. **D50**, 6783 (1994).

29. D.Blaschke and G.Ropke, Phys. Lett. **B299**, 332 (1993); K. Martins, D.Blaschke and E.Quack, Rostock/GSI report MPG-VT-UR-39-94 (Nov. 1994), hep-ph/9411302.

RELATIVISTIC EQUATIONS FOR KAON–NUCLEUS INTERACTIONS

Roger C. Barrett
Centre for Nuclear Physics Southern University of Surrey
GU2 5XH Guildford, Surrey, U.K.

(No written contribution arrived)

MEASUREMENT OF KAONIC HYDROGEN X-RAY AT KEK

M. Iwasaki, R.S. Hayano, T.M. Ito, S.N. Nakamura and T. Terada
Meson Sci. Lab. and Dept. of Phys., Univ. of Tokyo, Bunkyo, Tokyo 113, Japan
H. Outa
Inst. for Nucl. Study, Univ. of Tokyo, 3-2-1 Midori, Tanashi, Tokyo 188, Japan
T. Taniguchi and Y. Yamashita
KEK, 1-1 Oho, Tsukuba, Ibaraki 305, Japan
K. Bartlett, G.A. Beer, G. Mason and G. Trayling
Dept. of Phys. and Astro., Univ. of Victoria, POB3055, Victoria, Canada V8W3P6
D.R. Gill, A. Olin, M. Salomon and S. Yen
TRIUMF, 4004 Wesbrook Mall, Vancouver, B.C., Canada V6T2A3
L. Lee
Dept. of Phys., Univ. of Manitoba, Winnipeg, MB., Canada R3T2N2
R. Seki
Dept. of Phys. and Astro., California State Univ., Northridge, CA 91330, USA

ABSTRACT

The K^-p X rays measurement is one of the most fundamental studies of the $\overline{K}N$ interaction in the low energy region. Although three experiments have been performed previously, their results are not consistent with each other and none of them are significant in statistics. We have performed a measurement of K^-p X rays at KEK which adopts a new technique to improve the signal-to-noise ratio (S/N): specification of the final state of the K^-p reaction and using a gaseous hydrogen target (4 atm at 100 K).

1 – Introduction

The measurement of K^-p X rays probes the $\overline{K}N$ interaction in the lowest energy region. The energy shift and width of the kaonic hydrogen X rays due to the strong interaction gives us the information on the $\overline{K}N$ complex scattering length. Currently the experimental data [1, 2, 3] are quite puzzling, especially on its shift. The reported energy shifts are not consistent with each other and, furthermore, the sign of the shifts is opposite to that of the theoretical predictions[4–11] on the basis of the low energy scattering data (Fig. 1). While majority of the theoretical predictions insist on a negative (repulsive) shift, all experimental data report a positive (attractive) shift. It should be mentioned that the results of previous experiments are not statistically satisfactory as shown in Fig. 2.

This experiment is also important for other aspects, *i.e.*, it is deeply related with the puzzle of the $\Lambda(1405)$ [13]. The $\Lambda(1405)$ is a $J^P = \frac{1}{2}^-$ resonance [14, 15] and it is assigned to be a lowest $L = 1$ supermultiplet of the 3-quark system, paired with the $\Lambda(1520)$ $\frac{3}{2}^-$ [16]. If it is true, the question arises why the mass difference of this supermultiplet is as large as 100 MeV. Such a large mass difference between spin-orbit partners is unrealistic in

view of the well established N^* resonances as it is shown in the non-relativistic quark model [13]. Another assignment is that the $\Lambda(1405)$ is a $\overline{K}N$ bound state by the strong interaction [10]. To solve this $\Lambda(1405)$ puzzle, the knowledge of $\overline{K}N$ interaction in the low energy limit is indispensable.

This physics is also deeply related with the determination of the KN σ-term. With its possible large strength, the kaon condensation and possible existence of the light neutron stars has been discussed [17]. It is also important for the further understanding of the Σ-hypernuclear formation process [18]. To answer these questions, a precise and high-statistics experiment with better S/N is indispensable.

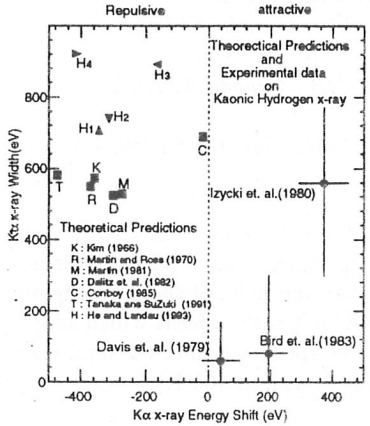

figure 1: The energy shift and width of K_α X ray of kaonic hydrogen atom.

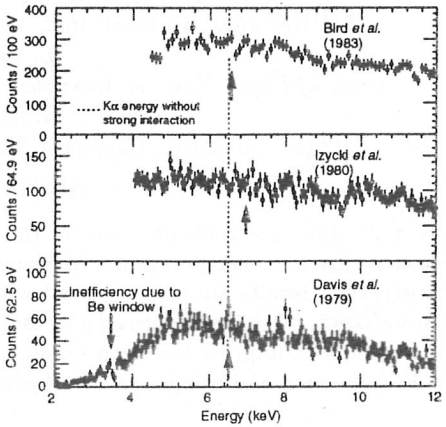

figure 2: Summary of the previous experimental data on the kaonic X ray. Arrows indicate the K_α position.

2 – Experimental Method

To obtain a conclusive result, we need to improve both statistics and the S/N as is shown in the results of the previous experiments. The experimental difficulties in the previous work may be summarized as follows;

- small solid angle of Si(Li) X-ray detector,
- the nuclear absorption of kaons from higher atomic states (Stark mixing),
- large background originating from high energy γ rays,
- large background from pion contamination in the kaon beam and
- large fraction of kaons stopped in materials around the target.

To overcome these difficulties, we designed our experiment according to the following criteria;

- mount 60 crystals of Si(Li) X-ray detector (200 mm^2) inside the hydrogen gas to achieve large acceptance and to avoid X-ray loss due to the window,
- use pressurized hydrogen gas at low temperature (100K) instead of liquid in order to reduce the Stark mixing effect
- specify the final state of the K^-p reaction to avoid main background source (γ ray), which produces a number of low energy X ray due to the bremsstrahlung by its converted electrons and
- observe the kaon stopping position to identify whether it stopped in the hydrogen.

2.1 Target density

The yield of kaonic hydrogen X ray has strong density dependence because of the kaon stopping density and the Stark effect. Because of the incident kaon beam momentum bite ($\Delta p/p = 8\%$), range straggling of the kaon is much larger than the hydrogen target thickness. Therefore, the kaon stopping yield increases linearly as the target density. On the contrary, the yield of kaonic hydrogen X ray per stopped kaon reduces when we increase the target density. The electric field of hydrogen atoms close to the K^-p atom mixes the different l-states so that the kaon can be absorbed from the highly excited atomic states before cascading down to the ground state. We optimize the target density based on the cascade calculation [19] and determined the hydrogen pressure to be 4 atm at the temperature of 100K. The detailed description of determination of our target density is given in a different paper [12].

2.2 Background sources

One of the main background source is produced by the contaminating particles in kaon beam such as pions and neutrons. We selected kaons efficiently by hardware trigger in order to get rig of those background by using Lucite Čerenkov counters. From the previous experimental data, it is known that we can reduce Si(Li) signal caused by the accidental background by order two compared to that of K^- absorption reaction [2] within the Si(Li) time resolution (about 1 μsec).

There are two other background sources, which are associated with K^- absorption reaction. One is the electronic X ray from ionization of the materials surrounding the target which gives monochromatic energy peak in the final X-ray energy spectrum. In particular, characteristic X ray from copper and iron are just in the region of interest. Therefore, we selected aluminum covered with thin teflon plate for the target vessel and its cryogenic system to avoid these problems. We have utilized, however, thin titanium foil for the purpose of in-beam calibration of the X-ray detector which have the characteristic X rays at 4.5 keV.

The other, which is more serious, arises from kaon decay and reaction products. When a kaon stops in the target gas, it is trapped in a hydrogen atom forming an exited state of a kaonic hydrogen atom. Then it cascades down by emitting the kaonic hydrogen X ray and finally reacts with the proton by the strong interaction. The X-ray spectrum has a large background due to the products of this interaction and also from the kaon free decay/reaction process which produce various particles including γ rays. The most crucial background source is the γ ray which, reacting with the materials surrounding the target, easily converts to a number of low energy X rays. Detailed study with the EGS4 simulation code shows that the low energy background is mainly produced by the bremsstrahlung of the electrons converted from high energy γ rays. It also indicates that the low energy background is quite large and it is consistent with the background level of previous experiments.

In order to remove the X-ray background originated from the high energy γ-rays, we selected the final state of the K^-p reactions in which no γ-ray is produced. The kaon decay/reaction products are listed in Table 1.

Table 1 : Branching ratio

Reaction	Produced particles	Branching ratio	Charged particle multiplicity (> 150 MeV/c)	γ multiplicity
		Free decay of K^-		
$\mu^-\nu$	$\mu^-\nu$	63.5 %	1	0
$\pi^-\pi^o$	$\pi^-2\gamma$	21.2 %	1	2
$\pi^-\pi^-\pi^+$	$\pi^-\pi^-\pi^+$	5.59 %	0	0
$e^-\pi^o\nu$	$e^-2\gamma$	4.82 %	1	2
$\mu^-\pi^o\nu$	$\mu^-2\gamma$	3.18 %	1	2
$\pi^-\pi^o\pi^o$	$\pi^-4\gamma$	1.73 %	0	4
		K^- p reaction		
$\Sigma^+\pi^-$	$\pi^-2\gamma$p	10 %	1	2
$\Sigma^+\pi^-$	$\pi^-\pi^+$n	10 %	2	0
$\Sigma^-\pi^+$	$\pi^+\pi^-$n	46 %	2	0
$\Sigma^o\pi^o$	$\pi^-3\gamma$p	18 %	0	3
$\Sigma^o\pi^o$	5γn	10 %	0	5
$\Lambda\pi^o$	$\pi^-2\gamma$p	4 %	0	2
$\Lambda\pi^o$	4γn	2 %	0	4

The branching ratios are taken from bubble chamber data [20]. We have omitted smaller branches (less than 0.1%) of π^- charge exchange and Panofsky gamma, which cannot produce two charged pions either.

2.3 Fiducial cut and konic hydrogen atom formation

From the table 1, it is seen that two branches without γ-ray emission can be selected by tagging on two charged pions with momenta larger than 150 MeV/c. The branching ratio

of those final states are fairly large (56 %) As it is shown in the table. Figure 3 exhibits the reason why we set the momentum threshold at 150 MeV/c. It shows the momentum distribution of $\pi^{\pm}$ created in the K^-p reactions.

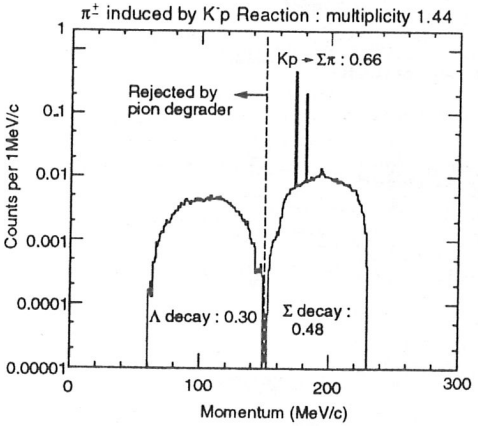

figure 3: Momentum distribution of $\pi^{\pm}$ created by K^-p reaction. Unfavorable π^-, produced by Λ decay, can be rejected by the degrader.

The mass deference between Σ and Λ separates the momentum distribution of their decay pion as shown in the Fig. 3. The pion associated with sigma production also located in the higher momentum side. Therefore if we select pion having momentum larger than 150 MeV/c, we can select both pion of the sigma production and the sigma decay at the same time. With this event selection, we can select the final states of the K^-p reaction which have no γ-ray production as a background source. As we have pointed out, the accidental background is not larger than 1 % of the whole background in the previous experiments so that this event selection provide us a good S/N with high efficiency.

In addition, this trigger condition gives the further advantage of allowing the determination of the kaon reaction position as a vertex by tracking both pion trajectories. This is very significant, because the rate of kaons stopping in the target vessel is 100 times higher than in the target gas. The kaons stopping in the target vessel do not contribute to the signal yield and moreover it may produce two pions together with nuclear γ rays, which can be a X-ray background source. We can easily reject those events by selecting out the vertex inside the target volume.

Although the fiducial cut within the target volume is quite important, we can not identify whether the kaon forms a kaonic hydrogen only from this information. It is more important to identify kaon whiçh forms kaonic hydrogen atom. It is known that the negatively-charged heavy particle is captured by an atom in quit short time after the particle stops in material. Therefore we can select the event in which a kaonic hydrogen atom is formed by identifying the stopped event. If the target density is low as the present case, the stopping power is quite small so that the time it takes the kaon to stop in the target is considerably long. The detailed description is given in section 3.

2.4 The experimental setup

Let us now describe more detail of the experiment at KEK K3 beamline. It is very important to maximize the kaon stopping density when we use a very low density

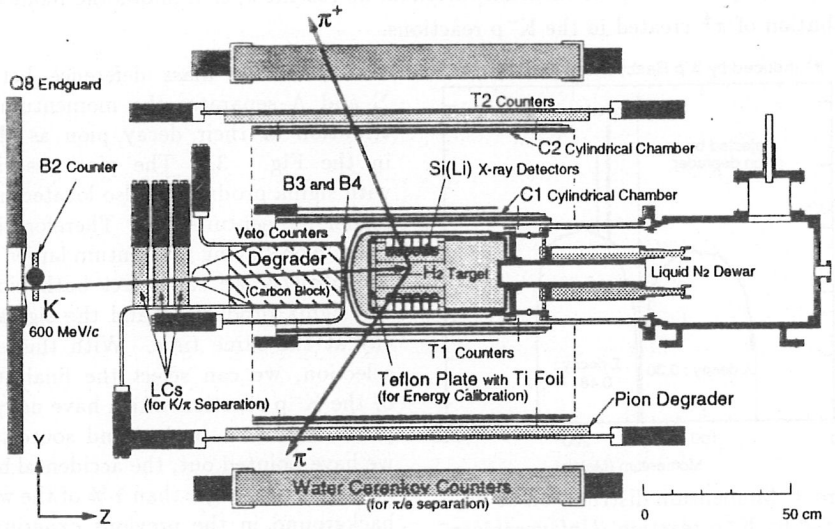

figure 4: The schematic view of the experimental setup.

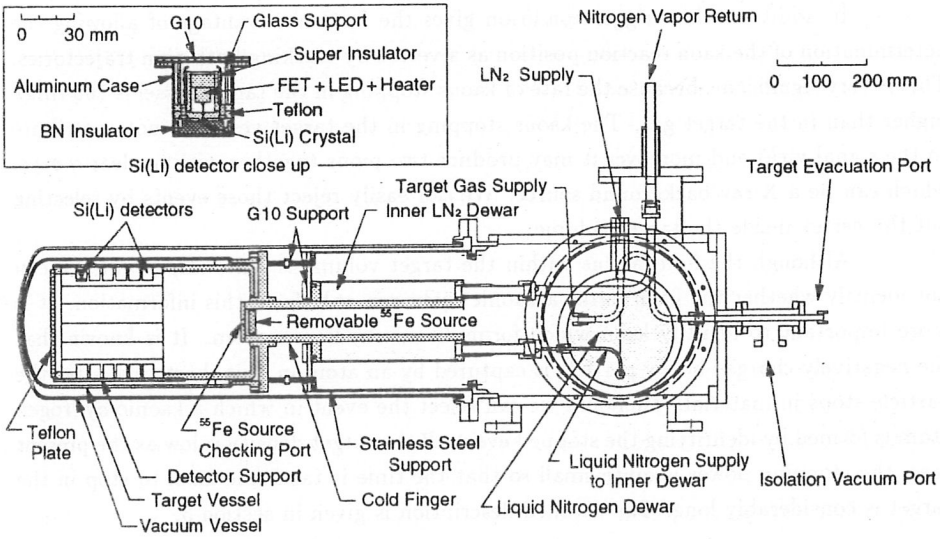

figure 5: Cryogenic target is operated at 4 atm, 100K. Sixty pieces of Si(Li) detectors are placed inside the hydrogen gas.

hydrogen gas target. We designed a wedge-shaped carbon degrader (monochrometer) and placed it at the momentum dispersive point of the kaon beam line in order to minimize the momentum bite. Kaons are identified by the time-of-flight (TOF) between two beam counters (B1 and B2) and pions are rejected by three lucite Čerenkov counters (Fig. 4). The K^- beam of 600 MeV/c is momentum-degraded by carbon blocks to stop it in the gas target. The events in which the kaons are lost in the degrader are vetoed by the pulse heights of the beam defining counters (B3 and B4) and veto counters surrounding the degrader.

The hydrogen target vessel is an aluminum cylinder of 290mmϕ × 540mm long (the effective volume inside the X-ray detector is 200mmϕ × 420mm long) (Fig. 5). Inside the gas target, we have placed an array of 60 optical feedback type Si(Li) X-ray detectors (each has 200 mm^2 effective area and is 5 mm thick) together with temperature-controlled FETs. The target is operated at 4 atm, 100K (a little higher than the liquid nitrogen temperature, because of the heating power for FETs).

The reasons for placing the Si(Li) crystals inside the hydrogen target are: i) to improve the Si(Li) crystals' solid angle which would be reduced by the support frame of the window foil and ii) to avoid the attenuation in the foil ($\sim$ 20% attenuation for 400μm). We checked the operation of the Si(Li) in the hydrogen atmosphere before the experiment and found that the Si(Li) detector can be operated stably under this condition at the same resolution as in vacuum when we control the FET's temperature.

To reduce the beam halo (pion) hit rate in each Si(Li) to less than 1 kHz and to maximize the detector solid angle, we located the Si(Li) detectors at 10 cm radius from the beam center (Fig. 5), where the beam intensity is $\sim$5 % of that of the beam center. The solid angle of the Si(Li) detectors is 6.7 % of the total solid angle, which is two orders of magnitude larger than the previous experiments. The shaping time of the Si(Li) signal is 10 μsec so that the dead time due to the pion-halo hit is about a few percent. The energy resolution of the Si(Li) detectors is checked under the beam condition with ^{55}Fe source and found to be 400 eV(FWHM) at 5.9 keV.

To track the two charged pions produced by the K^-p reaction, we use two cylindrical MWPCs and two layers of segmented pion trigger counters (T1 and T2). The effective length and anode plane radius are 740mm and 386mm for the inner chamber(C1), and 860mm and 978mm for outer chamber(C2), respectively. These chambers cover 70% of the total solid angle. Only those pions having momenta larger than 150 MeV/c are able to pass through the "pion degrader" (Fig. 4.) and make a hardware event trigger.

There are also a large number of fake triggers caused by high energy electrons, which could be easily misidentified as pions. These energetic electrons are mainly produced by γ-ray conversion. To reject them, we placed 70 mm thick water Čerenkov counters (WC) just behind the T2 counters (Fig. 4). Because the charged pions reduce

their energy in the pion degrader, the pulse height of electrons and pions are considerably different and we can separate these particles quite efficiently by the WC pulse height.

3 – Preliminary Analysis

We are now in the data analysis phase and not yet reached the final result. We report here the preliminary analysis procedure. To remove the fake event triggered by electrons, we made a contour plot of T2 counters vs WC pulse hight as shown in Fig. 6. In the higher pulse height region of WC counter, single and double electron hit caused by the Compton scattering and the pair creation are clearly shown. There are also some events which have lower pulse heights both in T2 and WC. The pulse height in T2 indicating that the particle which makes the event is not a charged one and it could be neutron. We selected two charged pion event by selecting the region as shown in the figure.

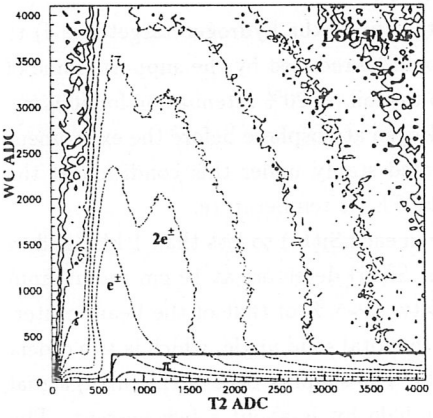

figure 6: The correlation of the pulse heights of Water Čerenkov and T2 counters. The solid line indicates the accepted event.

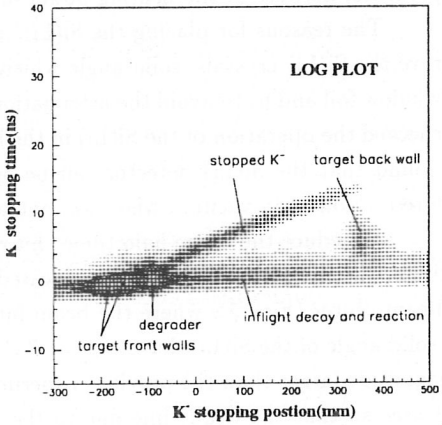

figure 7: The correlation between vertex position along the beam line (z) and the TOF between B2 and T2 counters.

A kaon forms a kaonic hydrogen atom when it stops. However, before it stops, it can decay or react with hydrogen in-flight. Those in-flight event can not be rejected by the target fiducial selection. To select the event in which a kaonic hydrogen atom is formed, we made a scatter plot of kaon stopping position along the beam axis and the TOF between beam trigger counter (B2) and pion counter (T2) as shown in figure 7. In the figure, it is shown that the stopped event is separated (delayed) from the in-flight event. This is because the target density is so low that the time it takes to stop a kaon in the target is long due to the small stopping power of the target while the in-flight event has shorter time due to its higher momentum when it react/decay. In the region of

the stopped event, there is a tail of in-flight event. To reduce such contamination, more detailed TOF analysis is needed (pion pass length correction etc.).

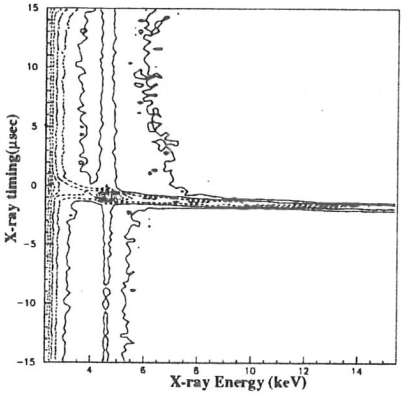

figure 8: The correlation between pulse hight and timing of Si(Li) detector.

In the X-ray experiment using highly contaminated kaon beam, X-ray signal timing is quite important for reducing the accidental background due to the contaminating particles. We observed Si(Li) X-ray timing relative to the kaon injection time. Because of the signal processing procedure, the X-ray timing has a correlation with its pulse hight as shown in Fig. 8. Two charged pion selection procedure is not applied in this figure, so the continuous X-ray locus induced by kaon reaction is clearly shown. All signals from Si(Li) have been overlaid in the figure. Therefore more detailed analysis is needed because each Si(Li) detector has its own energy-timing correlation.

4 – Conclusion

We selected events in which a kaon stops in the hydrogen target, forms a kaonic hydrogen atom and no γ ray produced in their absorption reaction.

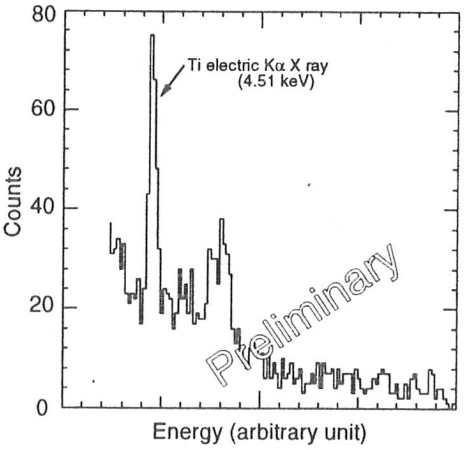

figure 9: The energy spectrum of kaonic hydrogen X ray.

As a preliminary result, we obtained the X-ray energy spectrum as shown in Fig. 9. In the figure, the energy scale is given in arbitrary unit, because our present analysis is not sophisticated in many aspects and more detailed analysis is required. The most clear peak in the energy spectrum is the titanium characteristic X-ray, which is the in-beam Si(Li) energy calibration peak. We will report a full account of our findings in forthcoming publications.

Acknowledgements

We would like to thank Dr. K. Yazaki for directing our interest to this field of the physics and Dr. K. Nakai for his support and the useful discussion. We appreciate the effort of JEOL staff, especially, Mr. M. Kuwata. With their great help, we succeeded in operating milti-channel Si(Li) detector in one cryostat under the hydrogen gas atmosphere. We are indebted to all the crew member of the KEK-PS, especially Dr. K.H. Tanaka and Dr. S.Ishimoto.

References

1. J.D. Davies *et al.*, Phys. Lett. **83B**, 55 (1979).
2. M. Izycki *et al.*, Z. Phys. **A297**, 11 (1980).
3. P.M. Bird *et al.*, Nucl. Phys. **A404**, 482 (1983).
4. J.K. Kim, Phys. Rev. Lett. **19**, 1074 (1967).
5. A.D. Martin and G. Ross, Nucl. Phys. **B16**, 479 (1970).
6. A.D. Martin, Nucl. Phys. **B179**, 33 (1981).
7. R.H. Dalitz *et al.*, Proceedings of the International Conference on Hypernuclear and Kaon Physics, Heidelberg, Germany 1982, MPIH-1982-V20.
8. J.E. Conboy *et al.*, J. Phys. G: Nucl. Phys. **12**, 1143 (1986).
9. K. Tanaka and A. Suzuki, Phys. Rev. **C45**, 2068 (1992).
10. M. Arima and K. Yazaki, Nucl. Phys. **A506**, 553 (1990).
11. G. He and R.H. Landau, Phys. Rev. **C48**, 3047 (1993).
12. M. Iwasaki *et al.*, Nucl. Phys. **A585**, 239c (1995).
13. N. Isgur and G. Karl, Phys. Rev. **D18**, 4187 (1978).
14. D.W. Thomas *et al.*, Nucl. Phys. **B58**, 15 (1973).
15. R.J. Hemingway, Nucl. Phys. **B253**, 742 (1985).
16. K.S. Kumar and Y. Nogami. Phys. Rev. **D21**, 1834 (1980).
17. G.E. Brown *et al.*, Nucl. Phys. **A567**, 937 (1994).
18. A. Matsuyama and K. Yazaki, Nucl. Phys. **A477** 673 (1988).
19. E. Borie and M. Leon, Phys. Rev. **A21**, 1460 (1980).
20. D.N. Tovee *et al.*, Nucl. Phys. **B33**, 493 (1971).

HADRONIC PHYSICS

PLENARY SESSION

J. Gasser	Prospects of Chiral Perturbation Theory	473
L. Montanet	Open Problems in Meson Spectroscopy, Which Should be Solved at DAΦNE	495
A. Courau	Two–Photon Physics at DAΦNE	505
G. Altarelli	The QED Running Coupling and DAΦNE	523
P. Spillantini	Experimental Search for Antimatter in the Universe	535
C. Rubbia	Matter Lifetime	537

PROSPECTS OF CHIRAL PERTURBATION THEORY

Jürg Gasser
Institut für Theoretische Physik der Universität Bern,
Sidlerstrasse 5, 3012 Bern, Switzerland

ABSTRACT

I review chiral perturbation theory and discuss a few open topics that are relevant for DAΦNE.

1 –Chiral Perturbation Theory [1)]

Chiral perturbation theory (CHPT) is a systematic method to analyse the low–energy structure of the Standard Model. In particular, it allows one to determine the low–energy behaviour of the Green functions built from quark currents, like the electromagnetic form factor of the mesons or the meson–meson scattering amplitudes. Matrix elements for semileptonic decays are calculable from quark current correlators as well, because the momenta of the external particles are small with respect to the W mass, and the weak interactions reduce to the current×current form in this case. For illustration, I note the following correspondence:

$$\langle 0|TA^i_\mu(x)V^{em}_\rho(y)A^j_\nu(z)|0\rangle \quad : \text{ electromagnetic form factor}$$

$$\langle 0|TA^i_\mu(x)A^k_\nu(y)A^l_\rho(z)A^m_\sigma(w)|0\rangle \quad : \ \pi\pi \text{ scattering amplitude}$$

$$\langle 0|TA^l_\mu(x)\bar{u}(y)\gamma_\nu s(y)A^m_\rho(z)|0\rangle \quad : \ K \to \pi e\nu \text{ decay}\,.$$

Here A^i_μ, V^{em}_ρ and Q denote the axial and the electromagnetic current and the charge matrix, respectively,

$$A^i_\mu \ = \ \bar{q}\gamma_\mu\gamma_5\frac{\lambda^i}{2}q \ \ , V^{em}_\mu = \bar{q}\gamma_\mu Q q \ , \tag{1}$$

$$Q = \frac{1}{3}\mathrm{diag}(2,-1,-1) \ , \tag{2}$$

where q collects the u, d and s quark fields,

$$q = \begin{pmatrix} u \\ d \\ s \end{pmatrix} \ . \tag{3}$$

It is very convenient to collect all Green functions in the generating functional whose properties may then be studied in a general manner. The construction goes as follows. One equips the QCD Lagrangian with external c-number fields v_μ, a_μ, s and p,

$$\mathcal{L} = \mathcal{L}^0_{QCD} + \bar{q}\gamma^\mu(v_\mu + \gamma_5 a_\mu)q - \bar{q}(s - i\gamma_5 p)q \ . \tag{4}$$

$\mathcal{L}^0_{QCD}$ is the Lagrangian with the masses of the three light quarks set to zero. The external fields v_μ, a_μ, s and p are hermitian 3×3 matrices in flavour space, and the quark mass matrix

$$\mathcal{M} = \mathrm{diag}(m_u, m_d, m_s) \tag{5}$$

is contained in the scalar field s. The generating functional is the logarithm of the vacuum transition amplitude,

$$e^{iZ[v,a,s,p]} = \langle 0 \ \mathrm{out}|0 \ \mathrm{in}\rangle \ , \tag{6}$$

and contains the external fields as arguments. Expanding Z in powers of v_μ, a_μ, s and p generates the connected Green functions of the quark currents. For example, the matrix element for $\pi\pi$ scattering is contained in the quartic term

$$\begin{aligned} Z \ = \ & \ldots + \frac{i^3}{4!}\int dx_1 dx_2 dx_3 dx_4 a^i_\mu(x_1) a^k_\nu(x_2) a^l_\rho(x_3) a^m_\sigma(x_4) \times \\ & \times \langle 0|T A^\mu_i(x_1) A^\nu_k(x_2) A^\rho_l(x_3) A^\sigma_m(x_4)|0\rangle + \ldots \ , \end{aligned} \tag{7}$$

with $a_\mu = a^b_\mu \frac{\lambda^b}{2}$.

Notice that the Lagrangian (4) is symmetric under local $SU(3)_L \times SU(3)_R$ transformations,

$$\begin{aligned} q \ & \rightarrow \ g_R \frac{1}{2}(1+\gamma_5)q + g_L \frac{1}{2}(1-\gamma_5)q \ , \\ g_{R,L} \ & \in \ SU(3)_{R,L} \ , \end{aligned} \tag{8}$$

provided the external fields are transformed accordingly,

$$\begin{aligned} r_\mu = v_\mu + a_\mu \ & \rightarrow \ g_R r_\mu g_R^\dagger + i g_R \partial_\mu g_R^\dagger \ , \\ l_\mu = v_\mu - a_\mu \ & \rightarrow \ g_L l_\mu g_L^\dagger + i g_L \partial_\mu g_L^\dagger \ , \\ s + ip \ & \rightarrow \ g_R(s+ip)g_L^\dagger \ . \end{aligned} \tag{9}$$

Here I consider only the case where the fields a_μ, v_μ are traceless,

$$\langle v_\mu \rangle = \langle a_\mu \rangle = 0 \ , \tag{10}$$

where $\langle A \rangle$ denotes the trace of the matrix A.

1.1 Effective low-energy theory

The generating functional admits an expansion in powers of external momenta and of quark masses [3, 4, 5]. This expansion is most conveniently carried out in an effective theory, where the quark and gluon fields of QCD are replaced by a set of pseudoscalar fields which describe the degrees of freedom of the Goldstone bosons π, K and η. On the level of this effective theory, the expansion amounts to a derivative expansion of the effective Lagrangian. Counting the quark mass as two powers of the momenta, the expansion starts at order $O(p^2)$ and is of the form

$$\mathcal{L}_{eff} = \mathcal{L}_2 + \mathcal{L}_4 + \mathcal{L}_6 + \dots \tag{11}$$

The effective Lagrangian generates the corresponding expansion of the generating functional,

$$Z = Z_2 + Z_4 + Z_6 + \dots \ . \tag{12}$$

This procedure to analyse the low-energy structure of the Green functions is called "chiral perturbation theory". If the effective Lagrangian is chosen properly, the resulting Green functions are identical to the ones in the Standard Model [3, 5].

To see how this works in detail, it is convenient to collect the pseudoscalar fields in a unitary 3×3 matrix,

$$U = \exp(i\sqrt{2}\Phi/F) \ , \qquad \Phi = \begin{pmatrix} \frac{\pi^0}{\sqrt{2}} + \frac{\eta_8}{\sqrt{6}} & \pi^+ & K^+ \\ \pi^- & -\frac{\pi^0}{\sqrt{2}} + \frac{\eta_8}{\sqrt{6}} & K^0 \\ K^- & \overline{K^0} & -\frac{2\eta_8}{\sqrt{6}} \end{pmatrix} \ . \tag{13}$$

The *leading-order term* in the low-energy expansion is then generated by the tree diagrams of the non-linear σ model coupled to the external fields v, a, s and p,

$$\mathcal{L}_2 = \frac{F^2}{4} \langle D_\mu U D^\mu U^\dagger + \chi U^\dagger + \chi^\dagger U \rangle \ , \tag{14}$$

where

$$D_\mu U = \partial_\mu U - i r_\mu U + i U l_\mu \ , \qquad \chi = 2B(s + ip) \ . \tag{15}$$

The effective Lagrangian contains only two parameters at this order in the energy expansion: the pion decay constant in the chiral limit, $F \simeq 93$ MeV, and B, which

is related to the quark condensate, $\langle 0|\bar{u}u|0\rangle = -F^2B[1 + O(m_{quark})]$. The constant B always appears multiplied by quark masses. At $O(p^2)$, the product Bm_{quark} can be expressed in terms of meson masses, e.g.,

$$M_{\pi^+}^2 = B(m_u + m_d) + O(m_{quark}^2) \ , \tag{16}$$

$$M_{K^+}^2 = B(m_u + m_s) + O(m_{quark}^2) \ . \tag{17}$$

The fields U, v, a, s and p that occur in the effective Lagrangian are subject to the following chiral counting rules [1],

$$\begin{aligned} U \quad &\sim \quad O(p^0) \ , \\ D_\mu U, v_\mu, a_\mu \quad &\sim \quad O(p) \ , \\ s, p \quad &\sim \quad O(p^2) \ . \end{aligned} \tag{18}$$

Therefore, the *leading-order* effective Lagrangian $\mathcal{L}_2$ is of order p^2. Furthermore, I note that $\mathcal{L}_2$ is invariant under the local transformation (9), provided the field U is transformed as

$$U \to g_R U g_L^\dagger \ . \tag{19}$$

The tree graphs generated by the Lagrangian (14) reproduce the soft pion theorems for mesons in a concise manner. To illustrate, I consider the matrix element for the process $\pi^+\pi^- \to \pi^0\pi^0$,

$$\begin{aligned} \langle \pi^0(p_3)\pi^0(p_4) \ \text{out}|\pi^+(p_2)\pi^-(p_1) \ \text{in}\rangle \ &= \\ i(2\pi)^4\delta^4(p_1 + p_2 - p_3 - p_4)T^{+-;00}(s,t) \ , \end{aligned} \tag{20}$$

where $s = (p_1 + p_2)^2, t = (p_3 - p_1)^2$ are the standard Mandelstam variables. There is only one diagram to evaluate. The result reads in the Condon-Shortley phase convention

$$T^{+-;00}(s,t) = \frac{-s + M^2}{F^2} + O(p^4) \ . \tag{21}$$

Here the symbol $O(p^4)$ collects terms of order $O(p^4, p^2 m_{quark}, m_{quark}^2)$. The result (21) is due to Weinberg [7] who used current algebra and PCAC to analyse the Ward identities for the four-point function of the axial current. The effective Lagrangian calculation is very simple - the result is the same.

At *next-to-leading order*, the generating functional consists of three terms [4] :

i) The one-loop graphs generated by the lowest-order Lagrangian $\mathcal{L}_2$.

ii) An explicit local action of order p^4.

[1] For a different counting see ref. [6].

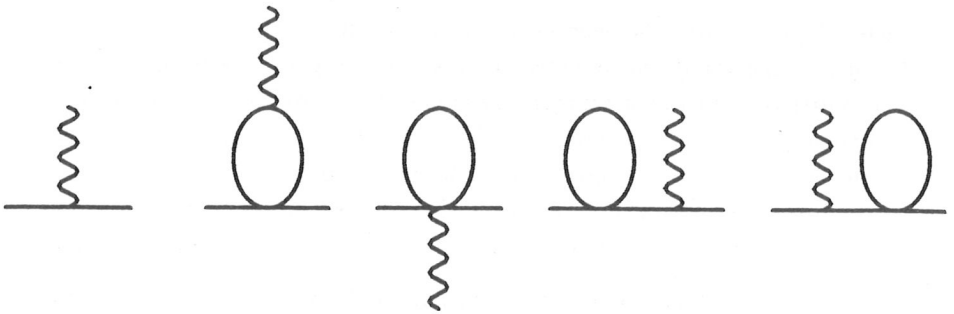

Figure 1: The tree and one–loop graphs, generated by $\mathcal{L}_2$, that contribute to the electromagnetic form factor of the charged pion. π, K and η are running in the loops. The wiggly line denotes the electromagnetic current.

iii) A contribution to account for the chiral anomaly.

I now briefly discuss the first two contributions.

1.2 One–loop graphs

For illustration, I consider the electromagnetic form factor F_V^π of the pion,

$$\langle \pi^+(p')|V_\mu^{em}(0)|\pi^+(p)\rangle = (p'+p)_\mu F_V^\pi(t) \;\; ; \;\; t=(p'-p)^2 \; . \tag{22}$$

Fig. 1 displays the relevant tree and one–loop graphs generated by $\mathcal{L}_2$.

The leading–order term (tree graph of $\mathcal{L}_2$) is trivial, because $eF_V^\pi(0)$ is the charge of the pion,

$$F_V^{\pi,tree} = 1 \; . \tag{23}$$

The one–loop graphs are ultraviolet divergent, and a regularization scheme is needed. Although the final result is independent of the regularization chosen, it is very convenient to use dimensional regularization for the following reason. In this scheme, the chiral symmetry of the effective theory is maintained, and only chiral symmetric counterterms are needed to cancel the divergences. Furthermore, because no new scale is introduced, the one–loop graphs are suppressed by two powers of the momenta relative to the tree diagrams [3]. The result for the electromagnetic form factor is

$$\begin{aligned} F_V^{\pi,one\ loop}(t) &= 2\phi(t,M_\pi;d)+\phi(t,M_K;d) \; , \\ \phi(t,M;d) &= -\frac{tM^{d-4}}{(4\pi)^{d/2}}\frac{\Gamma(2-\frac{d}{2})}{2F^2}\int_0^1 dx\; x(1-2x)\left[1-\frac{t}{M^2}x(1-x)\right]^{\frac{d-4}{2}} \; , \end{aligned} \tag{24}$$

where I have indicated the dependence of the loop functions ϕ on the dimension d of space–time. From this representation of ϕ it is explicitly seen that the loop contribution is of order p^2 and is therefore suppressed by two powers of the momenta with respect to the tree level result $F_V^{\pi,tree} = 1$. Notice that ϕ is independent of any renormalization scale μ by construction – the loop integrals only involve internal as well as external momenta and the masses of the pions and kaons. As long as d is not an integer, the result is finite. When $d \to 4$, the loop functions develop a pole,

$$\phi(t, M; d) \stackrel{d\to 4}{\to} -\frac{t}{96\pi^2 F^2 (d-4)} + O(1) \; . \tag{25}$$

An analogous result holds for all Green functions evaluated at next–to–leading order: as long as d is different from 4, the result is finite–ultraviolet singularities only show up when $d \to 4$. These singularities are cancelled by the contributions from the local action at order p^4 to which I now turn.

1.3 Local action at order p^4

To the loop diagrams discussed above, one has to add the tree diagrams from $\mathcal{L}_2 + \mathcal{L}_4$ with one vertex from $\mathcal{L}_4$ and any number of vertices from $\mathcal{L}_2$. The explicit form of $\mathcal{L}_4$ is [4]

$$\begin{aligned}
\mathcal{L}_4 \;=\; & L_1 \langle D_\mu U^\dagger D^\mu U\rangle^2 + L_2 \langle D_\mu U^\dagger D_\nu U\rangle \langle D^\mu U^\dagger D^\nu U\rangle \\
& + L_3 \langle D_\mu U^\dagger D^\mu U D_\nu U^\dagger D^\nu U\rangle + L_4 \langle D_\mu U^\dagger D^\mu U\rangle \langle \chi^\dagger U + \chi U^\dagger\rangle \\
& + L_5 \langle D_\mu U^\dagger D^\mu U (\chi^\dagger U + U^\dagger \chi)\rangle + L_6 \langle \chi^\dagger U + \chi U^\dagger\rangle^2 + L_7 \langle \chi^\dagger U - \chi U^\dagger\rangle^2 \\
& + L_8 \langle \chi^\dagger U \chi^\dagger U + \chi U^\dagger \chi U^\dagger\rangle - i L_9 \langle F_R^{\mu\nu} D_\mu U D_\nu U^\dagger + F_L^{\mu\nu} D_\mu U^\dagger D_\nu U\rangle \\
& + L_{10} \langle U^\dagger F_R^{\mu\nu} U F_{L\mu\nu}\rangle + L_{11} \langle F_{R\mu\nu} F_R^{\mu\nu} + F_{L\mu\nu} F_L^{\mu\nu}\rangle + L_{12} \langle \chi^\dagger \chi\rangle \; ,
\end{aligned} \tag{26}$$

where

$$\begin{aligned}
F_R^{\mu\nu} &= \partial^\mu r^\nu - \partial^\nu r^\mu - i[r^\mu, r^\nu] \; , \\
F_L^{\mu\nu} &= \partial^\mu l^\nu - \partial^\nu l^\mu - i[l^\mu, l^\nu] \; .
\end{aligned} \tag{27}$$

This is the most general Lagrangian of order p^4 that exhibits local gauge invariance in the form of Eqs. (9), (19) , Lorentz invariance, P and C. The equation of motion has furthermore been used to reduce the number of terms. The twelve new low–energy couplings (LECs) $L_1 \ldots, L_{12}$ are divergent (except L_3 and L_7). They absorb the divergences of the one–loop graphs. Consider for illustration again the electromagnetic form factor F_V^π. It receives a contribution from L_9,

$$F_V^{\pi,\mathcal{L}_4}(t) = \frac{2 L_9 t}{F^2} \; . \tag{28}$$

The sum $F_V^{\pi,one\ loop} + F_V^{\pi,\mathcal{L}_4}$ of the one–loop graphs and the counterterm contribution is finite, provided L_9 is appropriately tuned when $d \to 4$,

$$\begin{aligned} L_9 &= L_9^r(\mu) + \frac{\lambda(\mu)}{4} \ , \\ \lambda(\mu) &= (4\pi)^{-2}\mu^{d-4}\left\{\frac{1}{d-4} - \frac{1}{2}\left(\ln(4\pi) + \Gamma'(1) + 1\right)\right\} \ , \end{aligned} \tag{29}$$

where the renormalized coupling $L_9^r(\mu)$ is finite when $d \to 4$. Here I have introduced a renormalization scale μ. Although the coupling constant L_9 does not know about this scale,

$$\mu\frac{dL_9}{d\mu} = 0 \ , \tag{30}$$

the individual pieces in the splitting (29) do depend on it,

$$\mu\frac{d\lambda}{d\mu} = \frac{1}{16\pi^2} + O(d-4) \ , \ \mu\frac{dL_9^r}{d\mu} = -\frac{\mu}{4}\frac{d\lambda}{d\mu} \ . \tag{31}$$

Renormalization is now performed by writing

$$\phi(t, M; d) = \phi^{ren}(t, M, \mu; d) - \frac{t\lambda(\mu)}{6F^2} \ , \tag{32}$$

such that the complete expression for the form factor becomes

$$F_V^\pi(t) = 1 + 2\phi^{ren}(t, M_\pi, \mu; d) + \phi^{ren}(t, M_K, \mu; d) + \frac{2L_9^r t}{F^2} + O(p^4) \ . \tag{33}$$

F_V^π approaches a finite limit when $d \to 4$ and is scale independent by construction. For illustration, I display the renormalized loop integral [2] at $d = 4$,

$$\begin{aligned} \phi^{ren}(t, M, \mu; 4) &= \frac{t}{32\pi^2F^2}\int_0^1 dx\ x(1-2x)\log\left[1 - \frac{t}{M^2}x(1-x)\right] \\ &- \frac{t}{192\pi^2F^2}\left\{\log\frac{M^2}{\mu^2} + 1\right\} \ . \end{aligned} \tag{34}$$

Note that, as is required by unitarity, the function ϕ contains a branch point at $t = 4M^2$. The expression (34) is not expanded further in powers of t/M^2, because this would result in a Taylor series that is valid only in the range $|t| < 4M^2$. Stated differently, the momentum and quark expansion is performed at a fixed value of the ratio p^2/m_{quark}.

The same procedure carries over to all Green functions collected in the generating functional: they remain finite when $d \to 4$, provided the low–energy couplings L_i are appropriately tuned in this limit,

$$L_i = L_i^r(\mu) + \Gamma_i\lambda(\mu) \ . \tag{35}$$

[2] The combination $\phi^{ren}(t, M_\pi, \mu; 4) + \frac{2L_9^r t}{3F^2}$ is denoted by $H_{\pi\pi}$ in refs. [8, 9].

Table 1: Phenomenological values and source for the renormalized coupling constants $L_i^r(M_\rho)$. The quantities Γ_i in the fourth column determine the scale dependence of the $L_i^r(\mu)$ according to eq. (36). L_{11}^r and L_{12}^r are not directly accessible to experiment.

i	$L_i^r(M_\rho) \times 10^3$	source	Γ_i
1	0.4 ± 0.3	$K_{e4}, \pi\pi \to \pi\pi$	3/32
2	1.35 ± 0.3	$K_{e4}, \pi\pi \to \pi\pi$	3/16
3	-3.5 ± 1.1	$K_{e4}, \pi\pi \to \pi\pi$	0
4	-0.3 ± 0.5	Zweig rule	1/8
5	1.4 ± 0.5	$F_K : F_\pi$	3/8
6	-0.2 ± 0.3	Zweig rule	11/144
7	-0.4 ± 0.2	Gell-Mann–Okubo, L_5, L_8	0
8	0.9 ± 0.3	$M_{K^0} - M_{K^+}, L_5,$ $(2m_s - m_u - m_d) : (m_d - m_u)$	5/48
9	6.9 ± 0.7	$\langle r^2 \rangle_V^\pi$	1/4
10	-5.5 ± 0.7	$\pi \to e\nu\gamma$	$-1/4$
11			$-1/8$
12			5/24

The coefficients Γ_i have been evaluated in ref. [4] and are displayed in table 1. The couplings L_i are independent of the renormalization scale μ – therefore, the Green functions do not depend on it either. The scale dependence of the renormalized, finite couplings $L_i^r(\mu)$ is governed by the coefficients Γ_i,

$$L_i^r(\mu_2) = L_i^r(\mu_1) + \frac{\Gamma_i}{16\pi^2} \ln \frac{\mu_1}{\mu_2} \,. \tag{36}$$

The constants F, B, together with $L_1^r, \ldots, L_{10}^r$, completely determine the low–energy behaviour of pseudoscalar meson interactions to $O(p^4)$. L_{11}^r and L_{12}^r are contact terms that are not directly accessible to experiment.

1.4 Predictions

Once the low–energy couplings L_i^r are known (see section 3.1), the machinery set up above allows one to make predictions. As a simple example consider the charge radius of the electromagnetic form factor,

$$F_V^\pi(t) \;=\; 1 + \frac{1}{6}\langle r^2 \rangle_V^\pi t + O(t^2) \,. \tag{37}$$

The expression for $\langle r^2\rangle_V^\pi$ follows easily from Eqs. (33) and (34),

$$\langle r^2\rangle_V^\pi = \frac{12L_9^r}{F^2} - \frac{1}{32\pi^2F^2}\left\{2\log\frac{M_\pi^2}{\mu^2} + \log\frac{M_K^2}{\mu^2} + 3\right\} + O(m_{quark})\,. \tag{38}$$

Here, the symbol $O(m_{quark})$ stands for higher–order contributions which are not worked out here (two loops and beyond). Therefore, the constant L_9^r may be pinned down from the experimental value [10] $\langle r^2\rangle_V^\pi = 0.439 \pm 0.008$ fm^2. The same constant occurs [8, 9] in the slope λ_+ of the form factor $f_+^{K\pi}(t)$ measured in K_{e3}^0 decay [11],

$$\lambda_+ = 0.0286 \pm 0.0022\,. \tag{39}$$

Inserting $L_9^r = 6.9 \cdot 10^{-3}$ in the expression for λ_+ gives for the central value the postdiction

$$\lambda_+ = 0.031\,. \tag{40}$$

We see that the machine works properly. For a more thorough discussion of charge radii in the meson sector we refer the reader to refs. [8, 9]. Many more predictions have been worked out – for reviews see, e.g., ref. [12, 13]. The semileptonic decays which will be measured with high precision at DAΦNE provide the opportunity to expose the method to very thorough consistency checks.

1.5 CHPT as a Quantum Field Theory

The effective field theory discussed above belongs to the class of non-renormalizable Quantum Field Theories. Nevertheless, the Green functions evaluated within the framework of CHPT enjoy the good features of a renormalizable theory:

- They have the correct analytic and crossing symmetry properties.
- The corresponding S-matrix elements are unitary.

1.6 Further reviews

Many reviews of CHPT are available now [12, 13]–I refer the interested reader to these works for more details (anomaly, nonleptonic weak interactions, CHPT with baryons, generalized CHPT ...).

2 –Applications

CHPT is widely used today, and there are many applications: strong interaction processes, semileptonic and nonleptonic weak decays, heavy Higgs scenario, finite size effects in lattice calculations, Green functions at finite temperature, solid state

physics .... In my talk, I sketched among other things the predictions for elastic $\pi\pi$ scattering, K_{l3} form factors and $K \to 3\pi$ decays. Since an updated review of the relevance of CHPT for DAΦNE has become available recently in form of "The Second DAΦNE Physics Handbook" [2], I refer the reader to that reference for details. Reading that book, one becomes aware that DAΦNE is one of the few places where theory is ahead of experiment: there are many processes where CHPT has provided quite detailed predictions that await confirmation from the experimental side.

3 –Directions to go

I first mention a few topics–relevant for the physics at DAΦNE–that await a comprehensive treatment in the framework of CHPT. Then, I elaborate in some detail on isospin violations in the Standard Model.

3.1 Some open issues in CHPT

- *Low–energy constants*

  The drawback of the effective lagrangian approach to the low–energy analysis is the proliferation of new coupling constants that are not determined by symmetry considerations alone. The following methods for the determination of these couplings are discussed in the literature:

  - At order p^4 in the meson sector of QCD, the LECs have been pinned down from experimental data, and using large-N_c arguments. The result is shown in column 2 of table 1, where $L_1^r, \ldots, L_{10}^r$ are displayed at the scale $\mu = M_\rho$. The experimental information underlying these values is shown in column 3. L_1, L_2 and L_3 are taken from a recent overall fit to K_{e4} and $\pi\pi$ data [14], see also refs. [15, 16] and the section on K_{l4} decays in ref. [8]. $L_4, \ldots, L_{10}$ are taken from ref. [4]. For L_9 see also ref. [17]. The combination $L_9 + L_{10}$ has also been determined in ref. [18] from data on $\gamma\gamma \to \pi^+\pi^-$.
  - An interesting attempt to evaluate the low–energy constants L_i directly from the QCD-lagrangian has been undertaken in ref. [19]. The authors demonstrate the feasibility of extracting LECs from the lattice. More work is needed, however, to obtain reliable results.
  - Historically, the first method to understand the size of LECs consisted in evaluating the contribution from ρ–meson exchange to the generating functional [4]. For later developments of this approach, see refs. [20, 21].
  - The sum-rule method allows one to represent the low–energy constants in terms of integrals over spectral functions that may be saturated with

low-lying resonances [4, 22].

- The authors of ref. [23] explore the constraints on LECs imposed by positivity of the QCD measure.
- Various versions of the Nambu–Jona–Lasinio model have been used to estimate the low–energy couplings [24].

On the other hand, the algebraic structure of the various contributions to the effective lagrangian of the Standard Model has been determined to the following accuracy [25, 4, 26, 27, 31, 28, 29, 30) , 32, 33, 34]:

–QCD :			
Goldstone bosons :	$O(p^{M_G})$	, $0 \leq M_G \leq 6$	, $SU(3)$
meson-baryon interactions :	$O(p^{M_B})$	, $0 \leq M_B \leq 3$	, $SU(2)$
–nonleptonic weak interactions, mesons :	$O(p^{M_W})$	, $0 \leq M_W \leq 4$	, $SU(3)$
–electromagnetic interactions, mesons :	$O(e^2 p^{M_E})$	, $0 \leq M_E \leq 2$	, $SU(3)$

The constants at order $(M_G, M_B, M_W, M_E) = (6, 3, 4, 2)$ are not fully known. New ideas to determine them are obviously welcome.

- *Higher order calculations*

DaΦNE will provide an unprecedented amount of precise data on low–energy hadronic processes. In order to confront these data with the predictions of CHPT, it may be necessary in some cases to go beyond the next-to-leading order prediction – an example is provided by the phase shift difference $\delta_{I=0}^{J=0} - \delta_1^1$ of the elastic $\pi\pi$ scattering amplitude. That quantity can be measured in the threshold region in K_{l4} decays [35]. Another example is the $\eta \to 3\pi$ decay amplitude, that receives a substantial correction at one-loop order [36], such that a precise determination of the quark mass ratio $(m_d^2 - m_u^2)/m_s^2$ from this decay makes it necessary to estimate the contributions from yet higher orders [37, 38].

As far as I am aware, two methods have been used up to now to estimate higher order corrections: The first one consists in a brute force calculation of the Feynmangraphs. The case of elastic $\pi\pi$ scattering is relatively simple, because the corresponding two-loop diagrams generate Lorentz invariant functions that depend essentially on one kinematic variable only [39], as a result of which the graphs may be expressed in terms of elementary functions [40]. It has been demonstrated [41, 42] in the case of the processes $\gamma\gamma \to \pi\pi$ and $\eta \to \pi^0\gamma\gamma$, that the numerical evaluation of two-loop graphs in CHPT is technically feasible also in the general case (even if the graphs contain cuts in two variables or have anomalous thresholds).

The second possibility makes use of the analytic properties of the scattering amplitudes. One writes dispersion relations that incorporate unitarity to all orders in the chiral expansion [43, 37, 38, 14]. The idea is to suppress the contributions from high energies by writing sufficiently often subtracted amplitudes. The subtraction constants are then evaluated in the framework of CHPT–preferably in a kinematical point where higher order corrections play a minor role (e.g. near Adler zeros) [44, 38].

These techniques await applications in many cases.

- *Isospin breaking*

The precision of the data expected at DAΦNE requires in some cases the consideration of isospin breaking effects. In the Standard Model, these are generated by the quark mass difference $m_d - m_u$ and by the electromagnetic interaction. Effects from the *quark mass difference* in the meson sector are included in the effective lagrangians (14),(26) through the quark mass matrix χ. A corresponding complete discussion in the case where baryons are included is missing, although steps in this direction have been done [45, 46, 47, 34]. On the other hand, neither for mesons nor for baryons have isospin violations due to *virtual photon contributions* been investigated in a complete manner. Yet, several isospin violating effects have been worked out in the framework of the effective lagrangian technique [48, 47, 32, 33, 49], and the general structure of the terms of order $O(e^2p^2)$ in the meson sector has been determined [32, 33]. The evaluation of the corrections to the elastic $\pi\pi$ scattering amplitude at order $O(e^2p^2)$ is underway [50]. To extract the $\pi\pi$ scattering amplitude from K_{l4} decays with high precision from forthcoming data at DAΦNE, one must include leptons in the effective chiral lagrangian [51]. This procedure will bring earlier calculations [52] of electromagnetic effects in these decays into agreement with the present theoretical picture of the weak interactions.

I discuss below in more detail the issue at leading order in the low–energy expansion.

- *CHPT with baryons*

CHPT has its origin in the meson-nucleon system [53]. Ironically, these interactions are difficult to treat on the same level of accuracy as the mesonic sector–the corresponding order $O(p^4)$ calculation of the pion-nucleon scattering amplitude has not yet been accomplished, although several important steps in this direction have been done [54, 34, 28]. The reason for this situation is the following. The presence of the nucleon mass that stays finite in the chiral limit,

complicates the chiral counting. In the relativistic formulation of the meson-baryon system, the correspondence between the loop and the chiral expansion (valid in the meson sector) is lost: at a given order in the chiral expansion, an arbitrary number of loops may contribute [27]. To avoid this headache, Heavy Baryon CHPT (HBCHPT) has been formulated [54]. By shifting the dependence of the nucleon mass from the propagator to the vertices of the effective lagrangian, HBCHPT generates a systematic low–energy expansion.

Presumably, it will take still quite some time until a complete description of the pion-nucleon amplitude at order $O(p^4)$ becomes available. (At order $O(p^3)$, it is known since many years [27]). On the other hand, at least this accuracy will be necessary for a satisfactory description of the pion-nucleon system–whether it also suffices is an open question. Whether HBCHPT can be extended to $SU(3)$ in a meaningful manner (in order to provide e.g. precise predictions for FINUDA) remains to be seen as well.

For further details, in particular for photon induced processes, I refer the reader to reference [34]. Reading these reviews, it is clear that many applications in the baryon sector await (patient) loop calculators.

3.2 Isospin violations at leading order

Here, I elaborate on isospin violations at leading order in the electromagnetic coupling. To include virtual photons in the mesonic sector, the electromagnetic field A_μ is made dynamical by including in the effective lagrangian the appropriate kinetic term $-1/4 F_{\mu\nu}F^{\mu\nu}$. Furthermore, one uses minimal coupling,

$$v_\mu \to v_\mu - eQA_\mu \ , Q = \frac{1}{3}\mathrm{diag}(2,-1,-1) \ , \tag{41}$$

in the lagrangians (14) and (26). CHPT then automatically generates diagrams with real and virtual photons. However, there are additional contributions, not generated by this procedure. Indeed, according to the rules of CHPT, one has to include in the effective lagrangian all terms with the correct transformation properties. Now, consider as an example the exchange of a $J^{PC} = 1^{++}$ axial vector meson between two vertices that emit any number of Goldstone mesons and one photon[3]. After integration over the photon, these graphs generate, at low energies, new contributions to the Green functions, that are not taken into account by the minimal interaction introduced above. The structure of these terms is reproduced by inclusion of

$$\mathcal{L}_{e^2p^0} = e^2 C \langle QUQU^\dagger \rangle \tag{42}$$

[3]The relevant chiral invariant coupling generating these graphs may be found in ref. [20], eq. (3.15b).

in the effective lagrangian. Here, C is a low-energy constant, on the same footing as $F, B, L_1, \ldots, L_{10}, \ldots$. (This procedure generates additional contributions of a similar structure–they contain, however, also derivatives and/or quark mass insertions. I omit them here, because they are of higher order in the low-energy expansion.) In conclusion, the leading effective lagrangian (14) becomes in the presence of virtual photon corrections [55, 20, 47]

$$\mathcal{L}_{eff}^{leading} = \mathcal{L}_2 - \frac{1}{4} F_{\mu\nu} F^{\mu\nu} + e^2 C \langle Q U Q U^\dagger \rangle \ , \tag{43}$$

where $\mathcal{L}_2$ contains now the photon field through minimal coupling.

Remark: Instead of considering the exchange of axial vector mesons, one may introduce spurion fields for the charge operator and consider the effect of virtual photons directly in the underlying lagrangian. The result [55, 47] for the leading order effective lagrangian is again eq. (43).

3.2.1 *The spectrum at leading order*

Expanding the U-matrix in powers of the meson field ϕ and keeping only terms of order ϕ^2, one may read off from $\mathcal{L}_{eff}^{leading}$ the meson masses at leading order,

$$\begin{aligned} M_{\pi^\pm}^2 &= 2B\hat{m} + \delta M^2 \\ M_{K^\pm}^2 &= B(m_s + m_u) + \delta M^2 \\ M_{\pi^0}^2 &= 2B\hat{m} \\ M_{K^0}^2 &= M_{\bar{K}^0}^2 = B(m_s + m_d) \\ M_\eta^2 &= \frac{B}{3}(4m_s + 2\hat{m}) \end{aligned} \tag{44}$$

with

$$\delta M^2 = \frac{2e^2 C}{F^2} \ . \tag{45}$$

It is explicitly seen that isospin violating effects occur via the quark mass difference $m_d - m_u$ and via the low-energy coupling C. In accordance with Dashen's theorem [56], the lowest order electromagnetic lagrangian $\mathcal{L}_{e^2p^0}$ contributes an equal amount to the squared masses of $\pi^\pm, K^\pm$. On the other hand, it does not contribute to the masses of the neutral mesons, nor does it generate $\pi^0 - \eta$ mixing or $\eta \to 3\pi$ decays. Since the contribution of the up and down quark mass difference to $M_{\pi^\pm}^2 - M_{\pi^0}^2$ is tiny [45, 4], one may evaluate at this order in the low-energy expansion the constant C from the experimental mass difference of the pions, with the result

$$C = 6 \cdot 10^{-5} \mathrm{GeV}^4 \ . \tag{46}$$

3.2.2 *Elastic $\pi\pi$ scattering*

As a further application of the effective lagrangian $\mathcal{L}_{e^2p^0}$, I consider elastic $\pi\pi$ scattering in the framework of chiral $SU(2)_R \times SU(2)_L \times U(1)_V$. In the exponential parametrization

$$U = \exp i\phi/F \ , \ \phi = \begin{pmatrix} \pi^0 & \sqrt{2}\pi^+ \\ \sqrt{2}\pi^- & -\pi^0 \end{pmatrix} \ , \tag{47}$$

one has

$$\begin{aligned} \mathcal{L}_{e^2p^0} &= e^2C\langle Q^2\rangle - \delta M^2\pi^+\pi^- \\ &\quad + \frac{\delta M^2}{3F^2}(\pi^0\pi^0\pi^+\pi^- + 2\pi^+\pi^-\pi^+\pi^-) + O(\pi^6) \ . \end{aligned} \tag{48}$$

Consider now the amplitude for $\pi^+\pi^- \to \pi^0\pi^0$ scattering,

$$T^{c0}: \ \pi^+(p_1)\pi^-(p_2) \to \pi^0(p_3)\pi^0(p_4) \ . \tag{49}$$

At leading order, I find (Condon-Shortley phase convention)

$$\begin{aligned} T^{c0} &= \overbrace{\frac{-s+M^2}{F^2} + \frac{2\delta M^2}{3F^2}}^{\mathcal{L}_2} - \overbrace{\frac{2\delta M^2}{3F^2}}^{\mathcal{L}_{e^2p^0}} \\ &= \frac{-s+M^2}{F^2} \ , \end{aligned} \tag{50}$$

where $s = (p_1+p_2)^2$ is the usual Mandelstam variable. [Below, I will also use $t = (p_1-p_3)^2, u = (p_1-p_4)^2$.] The amplitude has therefore the same algebraic structure as in pure QCD–the two contributions proportional to δM^2 cancel[4]. This cancellation also occurs at the lagrangian level: instead of the exponential parametrization of the U–matrix, I take

$$\begin{aligned} U &= \sigma\mathbf{1} + i\varphi/F \ ; \ \sigma = \sqrt{1-\varphi^2/F^2} \ , \\ \varphi &= \begin{pmatrix} \pi^0 & \sqrt{2}\pi^+ \\ \sqrt{2}\pi^- & -\pi^0 \end{pmatrix} . \end{aligned} \tag{51}$$

In this case, the expansion of the electromagnetic part of the lagrangian stops at the terms quadratic in the fields,

$$\mathcal{L}_{e^2p^0} = e^2C\langle Q^2\rangle - \delta M^2\pi^+\pi^- \ . \tag{52}$$

[4]This statement depends on the variables chosen. On has also $T^{c0} = (-t-u+3M^2+2\delta M^2)/F^2$– in this decomposition, the electromagnetic corrections do show up. The effective lagrangian formulation unravels the variables in which the amplitude remains unchanged.

This decomposition makes it obvious that the only effect of $\mathcal{L}_{e^2p^0}$ is a mass shift for the charged pion. The $\pi\pi$ scattering amplitude

$$T^{ik;lm} \; : \; \pi^i(p_1)\pi^k(p_2) \to \pi^l(p_3)\pi^m(p_4) \tag{53}$$

becomes

$$T^{ik;lm} = \delta^{ik}\delta^{lm}A(s) + \delta^{il}\delta^{km}A(t) + \delta^{im}\delta^{kl}A(u) + O(e^2p^2, p^4) \; , \tag{54}$$

where

$$A(s) = \frac{s - M^2}{F^2} \; , \tag{55}$$

and where one–photon exchange (Coulomb–scattering) is not included (these contributions are of order $O(e^2)$). Therefore, the lagrangian $\mathcal{L}_{e^2p^0}$ does not affect the elastic $\pi\pi$ scattering amplitude at leading order [57].

3.2.3 *Power counting*

I add a comment about counting of chiral dimensions. Consider again the scattering amplitude T^{c0}. The Mandelstam variable s may be written as

$$s = (p_1 + p_2)^2 = 4(M_{\pi^+}^2 + \mathbf{p}_{\pi^+}^2) = 4(M_{\pi^0}^2 + \mathbf{p}_{\pi^0}^2) \; . \tag{56}$$

Above, we have counted M_{π^0} and $\mathbf{p}_{\pi^0}$ as quantities of order $O(p)$. If we assign chiral dimension zero to the electric charge, the momentum of the charged pion contains a piece of order $O(1)$ according to eq. (56)–electromagnetic interactions turn upside down the chiral counting. This situation is similar to the one in relativistic baryon CHPT, where the nucleon mass is a quantity of order $O(1)$. There, the remedy is heavy baryon chiral perturbation theory [54]. Here, we may simply count [32] the electric charge as a quantity of order $O(p)$ and the electromagnetic field as order $O(1)$. Then $\mathcal{L}_{eff}^{leading}$ is of order $O(p^2)$ (the kinetic term for the electromagnetic field carries two derivatives), and there is consistent chiral counting in the loop expansion [32]. In particular, the momentum of the charged pion is now also a quantity of order $O(p)$.

3.2.4 *Lifetime of pionium*

The experimental observation of $\pi^+\pi^-$–atoms (pionium) has recently been reported in ref. [58], and a proposal has been submitted [59] to measure the lifetime τ of the pionium ground state with 10% precision, using the 24 GeV/c beam at the Proton Synchrotron. This lifetime is related to the S–wave scattering length matrix A (evaluated at the $\pi^+\pi^-$ threshold) by [60, 61]

$$|K^{c0}| = \frac{0.30838(4)}{\sqrt{2\tau}} \; , \tag{57}$$

where τ (K^{c0}) is in units of 10^{-15} sec (fermi), and

$$A^{-1} = \begin{pmatrix} K^{cc} & K^{c0} \\ K^{c0} & K^{00} \end{pmatrix}^{-1} - i \begin{pmatrix} 0 & 0 \\ 0 & q_0 \end{pmatrix} . \tag{58}$$

The matrix elements K^{cc}, K^{c0}, K^{00} are real, and q_0 denotes the modulus of the centre of mass momentum of the neutral pions. [5]

In the absence of electromagnetic corrections and at $m_u = m_d$, K^{c0} is simply related to the $I = 0$ and $I = 2$ S–wave $\pi\pi$ scattering lengths [60, 61],

$$K^{c0}_{\{m_u=m_d, e=0\}} = \frac{1}{3}(a_2 - a_0) . \tag{59}$$

According to eqs. (57) and (59), a 10% measurement of the lifetime τ allows one to determine the combination $a_0 - a_2$ of S–wave scattering lengths at the 5% level and thus to confront the prediction of CHPT [63, 4, 40] with the data. For this, one must however first evaluate the isospin violating corrections to the relation eq. (59). In ref. [61, 62], potential models have been used for this purpose. The result depends on the details of the potentials used,

$$K^{c0}/K^{c0}_{\{m_u=m_d, e=0\}} = 1.027 \ldots 1.046 . \qquad \text{[potential models]} \tag{60}$$

About 94% of this correction is due to the mass difference between the neutral and the charged pion [61, 62]. I wish to show now that this part of the correction is very easy to evaluate with the effective lagrangian technique [64]. First, I recall that the quark mass difference $m_d - m_u$ generates only tiny effects in the pion mass spectrum and does not affect the elastic $\pi\pi$ scattering amplitude even at next-to-leading order, see ref. [45, 4]. I ignore therefore these effects altogether and concentrate on the contributions from electromagnetic interactions. Secondly, I use the fact that the quantity K^{c0} is related to the $\pi^+\pi^- \to \pi^0\pi^0$ matrix element $T^{+-;00}$ by

$$K^{c0} = \frac{1}{32\pi M_{\pi^+}} \mathrm{Re} T^{+-;00}(s = 4M^2_{\pi^+}) + O(p^5) . \tag{61}$$

At leading order in CHPT, and in the absence of electromagnetic interactions, one has therefore

$$K^{c0}_{\{m_u=m_d, e=0\}} = -3M_{\pi^0}/(32\pi F^2) \tag{62}$$

according to eq. (21). To incorporate mass effects from the electromagnetic interactions, I use eq. (50) and find

$$\begin{aligned} K^{c0}/K^{c0}_{\{m_u=m_d, e=0\}} &= \frac{M_{\pi^0}}{M_{\pi^+}} \frac{4M^2_{\pi^+} - M^2_{\pi^0}}{3M^2_{\pi^0}} \\ &= 1.056 . \qquad \text{[CHPT, leading order]} \end{aligned} \tag{63}$$

[5] Our normalization differs from the one in ref. [61], $K^{c0} = K_{\mathrm{oc}}$(Moor et al.)$/\sqrt{2}$.

CHPT thus confirms the sign and the size of the correction found in potential models [61, 62]. Work to understand in detail the small difference between the results eq. (60) and eq. (63) is in progress [64].

Acknowledgments

It is a pleasure to thank the organizers for the very interesting meeting and for the most enjoyable working atmosphere. Furthermore, I thank G. Colangelo and D. Toublan for useful discussions, and G. Colangelo for reading the manuscript.

References

1. The material in this section is essentially taken from J. Bijnens, G. Ecker and J. Gasser, Chiral perturbation theory, in ref. [2], p. 125.

2. The Second DAΦNE Physics Handbook (L. Maiani, G. Pancheri and N. Paver, eds.), INFN, Frascati, 1995.

3. S. Weinberg, Physica 96A (1979) 327.

4. J. Gasser and H. Leutwyler, Ann. Phys. 158 (1984) 142; Nucl. Phys. B250 (1985) 465.

5. H. Leutwyler, Ann. Phys. (N.Y.) 235 (1994) 165.

6. N.H. Fuchs, H. Sazdjian and J. Stern, Phys. Lett. B269 (1991) 183;
J. Stern, H. Sazdjian and N.H. Fuchs, Phys. Rev. D47 (1993) 3814;
M. Knecht and J. Stern, in ref. [2], p. 169.

7. S. Weinberg, Phys. Rev. Lett. 17 (1966) 616.

8. J. Bijnens et al., in ref. [2], p. 313.

9. J. Gasser and H. Leutwyler, Nucl. Phys. B250 (1985) 517.

10. S.R. Amendolia et al., Nucl. Phys. B277 (1986) 168. The literature on the subject may be traced fom this reference.

11. Review of Particle Properties, Phys. Rev. D50 (1994) vol. 3, part II.

12. H. Leutwyler, Foundations and Scope of Chiral Perturbation Theory, in ref. [13], p.14; Principles of Chiral Perturbation Theory, Lectures given at the Workshop

"Hadron 94", Gramado, RS, Brasil, BUTP-94/13 (hep-ph/9406283); Nonperturbative methods, Proc. of the XXVI Int. Conference on High Energy Physics, Dallas, 1992, Ed. J.R. Sanford, American Inst. Phys. (New York, 1993); Chiral effective Lagrangians, Lecture Notes in Physics, vol. 396, Eds. H. Mitter and H. Gausterer, Springer–Verlag (Berlin, 1991);
G. Ecker, Chiral Perturbation Theory, Prog. Part. Nucl. Phys. 35 (1995) 1; Chiral perturbation theory, in: Quantitative Particle Physics: Cargèse 1992, Eds. M. Lévy et al., Plenum Publ. Co. (New York, 1993) ;
U.-G. Meißner, Baryon chiral perturbation theory a.d. 1994. Lectures given at the " Indian Summer School on Electron Scattering off Nucleons and Nuclei", Prague. Preprint TK 94 17 (hep-ph/9411300); Recent developments in chiral perturbation theory, Rep. Prog. Phys. 56 (1993) 903; Proc. of the "Workshop on Effective Field Theories of the Standard Model", Dobogókö, Hungary, 1991, World Scientific, Singapore (U.-G- Meißner, ed.);
A. Pich, Introduction to chiral perturbation theory, Lectures given at the "5th Mexican School of Particles and Fields", Guanajuato, Mexico, Dec. 1992, preprint CERN–TH.6978/93;
E. de Rafael, Chiral Lagrangians and KP CP–violations. TASI-Lectures 1994, "CP Violation and the Limits of the Standard Model", preprint CPT-95/P.3161 (hep-ph/9502254); Chiral Perturbation Theory, preprint CPT-93/P.2967 (hep-ph/9312327);
J. Bijnens, "Chiral Perturbation Theory and anomalous Processes", Int. J. Mod. Phys. A8 (1993) 3045;
J.F. Donoghue, E. Golowich and B.R. Holstein, "Dynamics of the Standard Model", Cambridge Univ. Press, Cambridge, 1992;
M. Knecht and J. Stern, ref. [6];
J. Gasser, The QCD vacuum and chiral symmetry, in: Hadrons and Hadronic Matter, Eds. D. Vautherin et al., Plenum Publ. Co. (New York, 1990) ;
H. Georgi, Weak Interactions and Modern Particle Theory, Benjamin/Cumming, (Menlo Park,1984).

13. A. Bernstein and B.R. Holstein, eds., Proc. of the MIT Workshop:"Chiral Dynamics: Theory and Experiment", Cambridge, MA, July 1994. Springer, Heidelberg (1995).

14. J. Bijnens, G. Colangelo and J. Gasser, Nucl. Phys. B427 (1994) 427.

15. J. Bijnens, Nucl. Phys. B337 (1990) 635.

16. C. Riggenbach, J. Gasser, J.F. Donoghue and B.R. Holstein, Phys. Rev. D43 (1991) 127.

17. J. Bijnens and F. Cornet, Nucl. Phys. B296 (1988) 557.

18. D. Babusci et al., Phys. Lett. B277 (1992) 158.

19. S. Myint and C. Rebbi, Nucl. Phys. B421 (1994) 241.

20. G. Ecker, J. Gasser, A. Pich and E. de Rafael, Nucl. Phys. B321 (1989) 311.

21. G. Ecker, et al., Phys. Lett. B223 (1989) 425;
J.F. Donoghue, C. Ramirez and G. Valencia, Phys. Rev. D39 (1989) 1947;
M. Praszalowicz and G. Valencia, Nucl. Phys. B341 (1990) 27;
A. Bolokhov, V. Vereshagin and M. Polyakov, Sov. J. of Nucl. Phys. 53 (1991) 251;
A. Bolokhov et al., Phys. Rev. D48 (1993) 3090;
M.V. Polyakov and V.V. Vereshagin, preprint PNPI-TH-2068 (hep-ph/9509259);
D. Toublan, preprint UNIL-TP-3/95 (hep-ph/9509217).

22. J.F. Donoghue and E. Golowich, Phys. Rev. D49 (1994) 1513;
B. Moussallam and J. Stern, Chiral Symmetry Aspects of the Scalars, Talk given at the Workshop "Two-photon physics from DAΦNE to LEP200 and beyond", preprint IPNO/TH 94-26 (hep-ph/9404353).

23. J. Comellas, J.I. Latorre and J. Taron, preprint UB-ECM-PF-95-14 (hep-ph/9507258).

24. The literature may be traced from
J. Bijnens, Introduction to extended Nambu–Jona-Lasinio models, in ref. [2], p. 147;
E. Pallante and R. Petronzio, Quark–resonance models, in ref. [2], p. 157;

25. S. Weinberg, Phys. Rev. Lett. 18 (1967) 616; Phys. Rev. 166 (1968) 1568; ref. [3].

26. H.W. Fearing and S. Scherer, preprint TRI-PP-94-68 (hep-ph/9408346).

27. J. Gasser, M.E. Sainio and A. Švarc, Nucl. Phys. B307 (1988) 779.

28. G. Ecker, Phys. Lett. B336 (1994) 508;
G. Ecker and M. Mojžiš, preprint UWThPh-1995-22 (hep-ph/9508204).

29. J.A. Cronin, Phys. Rev. 161 (1967) 1483.

30. J. Kambor, J. Missimer and D. Wyler, Nucl. Phys. B346 (1990) 17.

31. A. Krause, Helvetica Phys. Acta 63 (1990) 3.

32. R. Urech, Nucl. Phys. B433 (1995) 234.

33. H. Neufeld and H. Rupertsberger, preprint UWThPh-1994-15; UWThPh-1995-18 (hep-ph/9506448).

34. For reviews of HBCHPT, see e.g. Ulf-G. Meißner, ref. [12].

35. N. Cabibbo and A. Maksymowicz, Phys. Rev. 137 (1965) B438; 168 (1968) 1926(E);
A. Pais and S.B. Treiman, Phys. Rev. 168 (18968) 1858;
G. Colangelo, M. Knecht and J. Stern, Phys. Lett. B336 (1994) 543; in ref. [2], p. 405;
M. Baillargeon and Paula J. Franzini, in ref. [2], p. 413.

36. J. Gasser and H. Leutwyler, Nucl. Phys. B259 (1985) 539.

37. J.F. Donoghue, B.R. Holstein and D. Wyler, Phys. Rev. D47 (1993) 2089;
J. Kambor et al., work in progress.

38. A. Anisovich and H. Leutwyler, work in progress.

39. J. Stern, H. Sazdjian and N.H. Fuchs, Phys. Rev. D47 (1993) 3814;
See also G. Mahoux, S.M. Roy and G. Wanders, Nucl. Phys. B70 (1974) 297.

40. D. Bessis and M. Pusterla, NC A 54 (1968) 243;
M. Knecht, B. Moussallam, J. Stern and N.H. Fuchs, preprint IPNO/TH 95-45, PURD-TH-95-05 (hep-ph/9507319);
Bijnens et al., work in progress.

41. S. Bellucci, J. Gasser and M.E. Sainio, Nucl. Phys. B423 (1994) 80; B 431 (1994) 413 (erratum);
U. Bürgi, Doctoral thesis, University of Bern, work in progress.

42. M. Jetter, preprint TRI-95-59 (hep-ph/9508407).

43. J.F. Donoghue, J. Gasser and H. Leutwyler, Nucl. Phys. B343 (1990) 341;
J.F. Donoghue, preprint UMHEP-417 (hep-ph/9506205).

44. H. Leutwyler, private communication.

45. J. Gasser and H. Leutwyler, Phys. Rep. 87C (1982) 77.

46. S. Weinberg, Strong Interactions at Low energies, in ref. [13], p. 3.

47. U.L. van Kolck, Thesis, University of Texas. Austin, 1993.

48. J.F. Donoghue, B.R. Holstein and D. Wyler, Phys. Rev. D47 (1993) 2089;
J. Bijnens, Phys. Lett. B306 (1993) 343;
K. Maltman and D. Kotchan, Mod. Phys. Lett. A5 (1990) 2457.

49. R. Baur and R. Urech, preprint ZU-TH-22/95, TTP95-31 (hep-ph/9508393).

50. M. Wicki, Diploma thesis, University of Bern, work in progress.

51. A. Gall, Doctoral thesis, University of Bern, work in progress.

52. A.-M. Diamant-Berger, Ph. D. thesis, University of Paris (Sud), Orsay, 1976.
L. Rosselet et al., Phys. Rev. D15 (1977) 574.

53. M. Goldberger and S.B. Treiman, Phys. Rev. 110 (1958) 1178.

54. H. Georgi, Phys. Lett. B240 (1990) 447;
E. Jenkins and A.V. Manohar, Phys. Lett. B255 (1991) 558.

55. J. Gasser and H. Leutwyler, unpublished.

56. R. Dashen, Phys. Rev. 183 (1969) 1245.

57. After my talk, I have learned from U.L. van Kolck that he had discussed this feature of isospin breaking in the $\pi\pi$ amplitude earlier in his thesis work [47].

58. L. Afanasyev et al., Phys. Lett. B308 (1993) 200.

59. B. Adeva et al, proposal to the SPSLC: Lifetime measurement of $\pi^+\pi^-$ atoms to test low-energy QCD predictions, preprint CERN/SPSLC 95-1. SPSLC/P 284.

60. J. Uretsky and J. Palfrey, Phys. Rev. 121 (1961) 1798.

61. U. Moor, G. Rasche and W.S. Wilcock, Nucl. Phys. A 587 (1995) 747.

62. U. Moor, Diploma thesis, University of Zurich (1994).

63. J. Gasser and H. Leutwyler, Phys. Lett. 125B (1983) 325.

64. J. Gasser, in preparation.

OPEN PROBLEMS IN MESON SPECTROSCOPY WHICH SHOULD BE SOLVED AT DAFNE

L.MONTANET

CERN

1 Introduction

We are today in possession of "models" which provide a rich list of rules, constraints and predictions on the hadronic world. Just to mention a few:

- the non relativistic quark model (NRQM);
- the OZI rule and, more generally, the Quark Line Rules(QLR);
- the Vector dominant model (VDM);
- the QCD sum rules and QCD anomalies;
- the Perturbative Chiral Theory (PCHT);
- Lattice calculations.

However, the relevant experimental information is unprecise, incomplete and, often, in a deplorable state.

We badly need high quality data, high statistics on interactions with a well defined initial state and "complete" information on the final state.

Crucial informations could be obtained, at DAFNE, on Pseudoscalar,Vector and Scalar mesons.We shall review here some of the main issues met in meson spectroscopy.

2 The $\rho(770)$ line shape

The Review of Particle Properties [1] lists as the two most precise determinations of the ρ^0 mass: L.Barkov et al.[2] :$m = 775.9 \pm 1.1$ MeV and M.Deutschmann et al. [3] $m = 768.0 \pm 1.0$ MeV. Clearly, these two results are not compatible, but one must note that one of them , [2], was obtained using the process: $e^+e^- \rightarrow \pi^+\pi^-$ whereas [3] used a complicated hadronic interaction. The origin of the difference between these two measurements must be due to the quite different production mechanisms involved in this comparison. All the mesurements of the ρ line-shape from hadronic interactions are model dependent: one usually write:

$$\sigma(m) = \frac{4\pi}{q^2} \frac{3\ m_\rho^2\ \Gamma_\rho^2(m)}{|D(m)|^2}$$

with

$$D(m) = (m_\rho^2 - m^2) - im_\rho\Gamma_\rho(m)$$

The width, $\Gamma_\rho(m)$, is mass dependent and can be written, quite generally:

$$\Gamma_\rho(m) = \Gamma_\rho \left(\frac{q(m)}{q(m_\rho)}\right)^3 \frac{g(m)}{g(m_\rho)}$$

where $g(m)$ is a function which depends on the left-hand cut singularities of the $\pi\ \pi$ P-wave scattering amplitude. Benayoun [4] introduced the parametrization:

$$g(m) = m^{-\lambda}$$

and found that λ may vary from 1 to values as large as 6 to reproduce the ρ line shape observed in hadronic processes. One has to conclude that the mass and width of ρ^0 are affected by large systematic errors in hadronic processes.

Using Benayoun parametrization (with λ free), most of the hadronic data can be reproduced with:

$$m_\rho \sim 764^{+20}_{-5} MeV$$

$$\Gamma_\rho \sim 147^{+9}_{-8} MeV$$

Considering now the process: $e^+e^- \rightarrow \pi^+\pi^-$, we write:

$$\sigma(m) = \frac{8\pi\alpha^2}{3}\frac{q^3(m)}{m^5}\ (A + \frac{g_{\rho\gamma}}{D_\rho(m)}\ G_\rho + \frac{g_{\omega\gamma}}{D_\omega(m)}\ e^{i\phi}\ G_\omega)^2$$

where

$$G_v = \frac{1}{q^{3/2}(m)}(6\ \pi\ _v m\ \Gamma_v(\pi^+\pi^-))^{1/2}$$

$$v = \rho, \omega$$

For $\Gamma_\rho(m)$, we use, as before, Benayoun λ parameter:

$$\Gamma_\rho(m) = \Gamma_\rho\ (\frac{q(m)}{q(m_\rho}\ )^3\ (\frac{m_\rho}{m}\ )^\lambda$$

For the ω, which is much narrower than the ρ, we use:

$$\Gamma_\omega(m) = B(\omega \rightarrow \pi^+\pi^-)\ \Gamma_\omega(\frac{q(m)}{q(m_\omega)}\ )^3\ \frac{m_\omega}{m}$$

$g_{\rho\gamma}$ and $g_{\omega\gamma}$ are given by the leptonic decay widths of the vector mesons. A is a non-VDM term introduced by Benayoun as a test of the VDM hypothesis. Setting first A=0, Benayoun obtains:

$$m_\rho = 780.8 \pm 0.5\ MeV$$

$$\Gamma_\rho = 153.0 \pm 2.0 \ MeV$$

$$\Lambda = 0.659 \pm 0.046 \ MeV$$

$$\varphi = 94^\circ \pm 3^\circ$$

in strong disagreement with the hadronic results and with the PDG reference values ($m_\rho = 769 MeV$). Allowing for a small non VDM contribution ($A \neq 0$) and fixing the mass to the PDG value (otherwise we have to face an essential ambiguity between A and m_ρ), one gets an excellent fit to the data with a small contribution of the non-VDM term ($\sigma \sim 6$ nb), the main effect being due to the interference between the ρ_0 and the non-VDM terms, and not so much to $\mid A \mid^2$ itself:

$$m_\rho = 768.7 \ MeV$$

$$\Gamma_\rho = 143. \pm 2. \ MeV$$

$$\lambda = 1.75$$

$$\varphi = 111^\circ \pm 3^\circ$$

$$A = c_0 + c_2 m^2$$

$$c_0 = -0.607 \pm 0.058$$

$$c_2 = 0.275 \pm 0.063 \ GeV^{-2}$$

It's clear that more accurate systematic measurements of $e^+e^- \rightarrow \pi^+\pi^-$ and $e^+e^- \rightarrow \mu^+\mu^-$ are needed, from threshold to $\sim 1 GeV$, to learn more on this non-VDM contribution and to solve the ρ^0 problem.

3 Radiative decay of Vector mesons

Recently, G.Morpurgo [5] has derived from relativistic field theories, say QCD, general parametrizations of several hadronic quantities (baryon magnetic moments, hadron masses [6], $V \to P\gamma$ transition moments [7]. which take unexpectedly simple forms and can be easily compared to the results of the "non relativistic quark model" (NRQM). This comparison clarifies why NRQM works so well, even for light quarks where v/c is not necessarily much smaller than one. Introducing (only) two assumptions: - the electromagnetic current is carried only by the quarks - the only flavour breaking term is λ_8 of SU3, G.Morpurgo shows that the eleven radiative transitions $V \to P\gamma$ which can be observed are governed by seven spin-flavour operators, four of them being due to quark contributions, the others being related to gluonic contributions (see table 1 of [7]). It turns out that the dominant quark contributions are precisely those selected by NRQM. The success of NRQM implies that the gluonic contributions are small. For example, NRQM predicts

$$\Gamma(\omega \to \pi\gamma)/\Gamma(\rho \to \pi\gamma) = 9$$

The exact prediction, given in [7], is:

$$\frac{\Gamma(\omega \to \pi\gamma)}{\Gamma(\rho \to \pi\gamma)} = (3 + \frac{2\mu_5 f_5(p)}{\mu_1 f_1(p)})^2$$

$\mu_5 f_5(p)$ being due to the gluonic contribution, $\mu_1 f_1(p)$ to the quark one. This ratio is therefore a measure of the gluonic annihilation to $\omega \to \pi\gamma$. The

present experimental results tell us that the contribution is small: but how much small? We need better data. The role of the gluonic contribution could also be tested with the accurate measurements of other ratios:

$$\Gamma(\omega \to \eta\gamma)/\Gamma(\rho \to \eta\gamma),$$

$$\Gamma(\eta' \to \rho\gamma)/\Gamma(\eta' \to \omega\gamma),$$

$$\Gamma(\Phi \to \eta\gamma)/\Gamma(\Phi \to \eta'\gamma).$$

The $\Phi \to \pi^0\gamma$ partial width is also providing interesting information on these gluonic contributions.Refering again to table 1 of [7],

$$\Gamma(\Phi \to \pi^0\gamma) = (\mu_1(sin(\theta_v - \theta_1) + \mu_5(2/9)^{1/2} + \mu_7(2/3)^{1/2})^2$$

μ_1 being determined from, say, $\rho \to \pi\gamma$, and knowing from other sources of information the value of Θ_v, the vector meson mixing angle, one could estimate the contribution of the gluonic terms (μ_5, μ_7) from an accurate measurements of $\Phi \to \pi^0\gamma$.

4 Meson radiative decays and QCD anomalies

One knows that the π^0,η and η' decays into $\gamma\gamma$ are governed, in QCD, by the triangle anomaly and how the QCD box anomaly could govern the non-resonant decays of η , η' into $\pi^+\pi^-\gamma$. Making use of all the experimental information presently available on $\pi^0/\eta/\eta' \to \gamma\gamma$, $\eta/\eta' \to \pi^+\pi^-\gamma$, $\eta/\eta' \to$

$\mu^+\mu^-\gamma$, $\eta/\eta' \to e^+e^-\gamma$, $J/\Psi \to \eta\gamma$, $J/\Psi \to \eta'\gamma$ and on all the vector meson radiative decays, Benayoun et al.[8] have shown, recently, that accurate data could provide a direct test of QCD via these QCD triangle and box anomalies. One compares, for instance, for η/η' decays into $\mu^+\mu^-\gamma$, the radiative decay $\eta/\eta' \to \rho\gamma$, with $\rho \to \mu^+\mu^-$, to the triangle anomaly contribution: $\eta/\eta' \to \gamma\gamma$, $\gamma \to \mu^+\mu^-$. Similarly, one may compare for η/η' decays into $\pi^+\pi^-\gamma$, the (same) radiative decay $\eta/\eta' \to \rho\gamma$ (with now $\rho \to \pi^+\pi^-$) to the box anomaly contribution which governs the non-resonant decays of $\eta/\eta' \to \pi^+\pi^-\gamma$.

For the J/Ψ decays into $\eta/\eta'\gamma$, Benayoun et al [8] make use of the Novikov - Akhovry - Frere relation [9].

For the radiative decays $V \to P\gamma$, $P \to V\gamma$, SU(3) relation are introduced, with five free parameters: the two mixing angles Θ_p and Θ_v, and the 3 coupling strengths $g(v8, p8, \gamma)$, $g(v1, p8, \gamma)$ and $g(v8, p1, \gamma)$. The results give rather sensible values for most of the physical couplings, and mixing angles which are introduced as free parameters:

$$g = g_{v8,P8,\gamma} = g_1 = g_{v1,P8,\gamma} = 0.70 \pm 0.02$$

$$g_1^1 = g_{v8,P1,\gamma} = 0.61 \pm 0.03$$

$$\theta_v = (38.6 \pm 0.2)^0$$

$$\theta_P = -(15.6 \pm 1.2)^0$$

The contribution of the QCD box anomaly is non zero both for η and η'. However, some radiative decays are in bad disagreement with the present

observation, for example: $\Phi \rightarrow \eta\gamma$ is predicted at $(2.85 \pm 0.18)10^{-2}$ and the yet unobserved decay $\Phi \rightarrow \eta'\gamma$ is predicted at $(132 \pm 10)10^{-6}$, not so far from the present upper limit (< 250 x 10^{-6} , latest BNPI results presented at this workshop).

It would be extremely interesting to measure accurately $e^+e^- \rightarrow \pi^0\gamma$,$e^+e^- \rightarrow \pi^+\pi^-\pi^0$, $e^+e^- \rightarrow \eta\gamma$ and $e^+e^- \rightarrow \pi^+\pi^-\eta$ from threshold to $\sim 1GeV$ to understand better the triangle and box anomalies.

5 The scalar mesons at DAFNE

The present experimental status of the scalar mesons is quite bad: In the I=1 sector, we have at least two candidates: $a_0(980)$ and $a_0(1470)$: they are both too low in mass to be simply taken as the ground state of the I=1 $J^{PC} = 0^{++}$ $q\bar{q}$ resonance and its first radial excitation, unless we follow N.Tornqvist [10] and move the "bare" pole of the $a_0(980)$ up to $\sim 1300MeV$ due to the $K\overline{K}$, $\eta'\pi$ channels unitary cut effects. Then the $a_0(1470)$ remains too low to be taken as the first radial excitation.

Another popular interpretation is to assume that $a_0(980)$ is not a pure $q\bar{q}$ state but rather a $K\overline{K}$ molecule or a four-quark state. Then $a_0(1470)$ could be the normal $q\bar{q}$ ground state. A better measurements of the $a_0(980)$ line shape to $\eta\pi$ and $K\overline{K}$ is necessary to remove the present ambiguities in its interpretation. This could be done at DAFNE, using the radiative ϕ decays: $\phi \rightarrow \eta\pi\gamma$ and $\phi \rightarrow K\overline{K}\gamma$. The I=0 sector is even more problematic. It's

well known that the $\pi\pi$ S-wave amplitude is described, in first approximation, by a slow rise of δ_0^0 from threshold to $\sim 1.4GeV$ superimposed to a rise by $\sim 180^0$ at the $K\overline{K}$ mass threshold.This $\pi\pi$ S-wave amplitude has been reanalyze, recently, by Morgan and Pennington [11] who conclude to the existence of a narrow resonance, the $f_0(980)$, and to a very broad one ($\Gamma \sim 700$ MeV) centred around 1000 MeV and purely elastic (whereas the $f_0(980)$ has a large relative coupling to $K\overline{K}$). At $\pi\pi$ threshold, the S-wave scattering is described by the $\pi\pi$ S-wave scattering length (a_0^0 and a_0^2 for I=0,2 respectively) - These quantities are badly determined, experimentally and, here too, accurate measurements are necessary. One way is to study (δ_0^0 - δ_1^1) in $K_{l4}^+ \rightarrow \pi^+\pi^-e^+\nu$ (see M.Knecht's and J.Stern's contribution to this workshop).

Above 1 GeV, there is now strong evidence for two more I=0 scalar resonances, both very inelastic: the $f_0(1350)$, mainly seen in 4π and $\eta\eta$ decays, and the $f_0(1500)$, with a relatively narrow width ($\sim$ 120 MeV), which is seen in $2\pi, \eta\eta, \eta\eta'$ and 4π decays [12]. The peculiar decay modes of this last resonance suggest an interpretation which involves a large gluonic component. At DAFNE, it would be very interesting to study the decay $\phi \rightarrow \pi^0\pi^0\gamma$ together with $\phi \rightarrow \eta\pi^0\gamma$ and $\phi \rightarrow K\overline{K}\gamma$ in order to disentangle the $f_0(980)/a_0(980)$ puzzle.

References

[1] RPM - Phys.Rev. D50(1994)

[2] L.Barkov et al. - Nucl.Phys. B256 (1985) 365

[3] M.Deutschmann et al. - Nucl.Phys. B103 (1976) 426

[4] M.Benayoun et al. - Z.Phys. C58 (1993) 31

[5] G.Morpurgo - Phys. Rev. D40 (1989) 2997

[6] G.Morpurgo - Phys. Rev. D40 (1989) 3111; Phys. Rev. D41 (1990) 2865; Phys. Rev. D45 (1992) 4068; Z.Phys. C62(1994)31.

[7] G.Morpurgo - Phys. Rev. D42 (1990) 1497

[8] M.Benayoun et al. - Z.Phys. C65 (1995) 399

[9] V.A.Novikov et al. - Nucl.Phys. B165 (1980) 55 R.Akhovry, J.M.Frere - Phys.Let. B220 (1989) 258

[10] N.Tornqvist - HU - SEFT R 1995-05

[11] D.Morgan and M.Pennington - Phys.Rev.D48 (1993) 1185

[12] The Crystal Barrel Collaboration - Cl.Amsler et al. (to appear in Phys.Let.B, 1995)

TWO-PHOTON PHYSICS AT DAΦNE[1]

A. Courau
Laboratoire de l'Accélérateur Linéaire
CNRS-IN2P3 et Université de Paris-sud
91405 Orsay France

ABSTRACT

The definition of $\gamma\gamma$ processes and various related notions are reviewed with the main characteristics and formulae. Next, taking into account the experimental conditions, it is shown that DAΦNE with KLOE gives a unique opportunity to study the $\gamma\gamma \to \pi\pi$ cross section near threshold, and the experimental design is briefly reported

1 Introduction

1.1 $\gamma\gamma$ process definitions

We call " $\gamma\gamma$ process" in e^+e^- collisions the configuration of a reaction $e^+e^- \to e^+e^-X$ such that the cross section is dominated by the following two-photon exchange graph [1) 2)] :

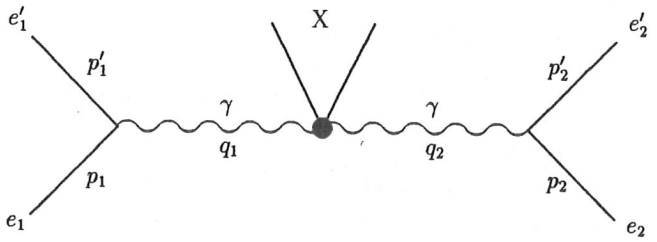

Figure 1: Two-photon exchange graph

If we compare such a graph with the one for $e^+e^- \to X$ annihilation one notices that the former X state can have any spin (J) and parity (P) with an even charge-conjugaison C=+1 instead of being a state $J^{PC} = 1^{--}$. The cross section is lower since there is of the order of α^4 instead of α^2 but it increases when the propagators are close to poles (*i.e.* $q^2 \to 0$).

[1]G.Alexander, F.Anulli, R.Baldini-Feroli, M.Bassetti, I.Cohen, A.Courau, A.Moalem, G.Pancheri, M.Preger, L.Razdolskaja, P.Sergio and A.Zallo

For $\mid q_1^2 \mid, \mid q_2^2 \mid << W_{\gamma\gamma}^2$, the photons are called "quasi-real" and in the cross section their longitudinal components can be neglected in front of the transverse ones. Then the differential cross section can be expressed as the product of both independant transverse photons spectra with the real $\gamma\gamma \rightarrow X$ cross section, leading to the so-called "Double Equivalent Photon Approximation" (DEPA) [3]. those conditions also involve that both electrons are scattered at very small angles. Furthermore, one can consider this process as produced through head-on collisions of γ spectra and one derives Williams-Weizsäcker type analytical approximations. Actually we generally measured only a small part of the total phase space and we must look very carefully to the various effect of the experimental acceptances [4].

In general, $\mid q_{1,2}^2 \mid << W_{\gamma\gamma}^2$ leads to a experimental configuration which is actually well overdominated by the two-photon exchange. But, let me emphasize that this graph is not the only one that contributes to the reaction $e^+e^- \rightarrow e^+e^-X$. One must take care that the experimental configuration considered includes no significant contribution from other graphs. Please do not confuse reaction, graph and process.

1.2 Notations

We use the following notations where momenta, energies and angles are defined in the e^+e^- c.m. frame. (The same quantities when they are defined in the $\gamma\gamma$ frame will be indicated by a star superscript) .

p_i and E are respectively the four-momentum and the energy of the incident electrons.

p_i' , E_i' , Θ_i' and Φ_i' are respectively the four-momentum , the energy, the polar and azimuthal angle of either scattered electrons $(i = 1, 2)$;

q_i , $E_{\gamma i}$, $\Theta_{\gamma,i}$ and $\Phi_{\gamma,i}$ are the same quantities for either virtual photon associated with a scattered electron $(i = 1, 2)$;

k_j , E_j , Θ_j and Φ_j are the same quantities for the outgoing particles of the hadronic system produced;

W , $E_{\gamma\gamma}$, β are respectively the invariant mass, the energy and the absolute value of the velocity of the $\gamma\gamma$ system in the ee frame;

Δ is the acolinearity angle between the two scattered electrons ($\Delta = 0$ when the two electrons are back to back in the ee frame).

In addition we define dimensionless quantities:

$$X_i = E_{\gamma i}/E \quad ; \quad Z = W/2E \quad ; \quad Q_i^2 = -q_i^2/E^2$$

with $$0 \leq X, Z \leq 1$$

Let us already note that m_π and m_e being respectively the pion and the electron mass, one has at DAΦNE [5] $m_e/E \simeq 10^{-3}$, while $W \sim 2m_\pi$ involves $Z \sim 0.3$; those values are two order of magnitude larger than the corresponding ones at LEP100.

2 Main characteritics : Quasi-real photon

2.1 Dynamics

In general the two-photon exchange process (fig.1) involves virtual photons which have both transverse (T) and longitudinal (L) components and the cross section can be descibed from 20 terms of helicity amplitudes. Integrating over the phase space of the outgoing particles of the system X produced (*i.e.* explicitely integrating over Φ_j^*), one derives the well-known expression [3] :

$$d\sigma = L_{TT}\,[\sigma_{TT} + \varepsilon\sigma_{LT} + \varepsilon'\sigma_{TL} + \varepsilon\varepsilon'(\sigma_{LL} + I_{TT}cos(2\varphi)) + \delta I_{TL}\cos\varphi]$$

where σ_{TT}, σ_{LT}, σ_{TL} and σ_{LL} are the virtual cross sections for $\gamma^*\gamma^* \to$ X; I_{TT} and I_{TL} are interference terms; ε, ε', δ are coefficients, smaller than 1, related to the polarisation of either photon ; φ is the azimuthal angle between the outgoing electrons in the $\gamma\gamma$ c. m. frame.

Now, it can be shown that if both photons satisfy the condition

$$|\,q_1^2\,|,|\,q_2^2\,| << W^2\,,$$

one can neglect all the terms with longitudinal component in front of σ_{TT}. Only survey σ_{TT} and I_{TT}. In such a case the photons are called as "quasi-real photons".

Moreover integrating over the azimuthal angle φ (which, in first approximation is the same in the $\gamma\gamma$ c.m. frame and in the overall c.m. frame) supresses the interference terms (mainly the remaining I_{TT}). One thus remains with

$$d\sigma \sim L_{TT}\;\sigma_{TT}\,,$$

while the same conditions ($|\,q_{1,2}^2\,| << W^2$) entail that generally one has :

$$\sigma_{TT}(W^2, q_1^2, q_2^2) = \sigma_{TT}(W^2, 0, 0) = \sigma_{\gamma\gamma}(W^2)$$

Therefore the $e^+e^- \to e^+e^-X$ cross section can be factorized as the product of two equivalent transverse photon spectra with a real $\gamma\gamma$ cross section and one gets the so called "Double Equivalent Photon Approximation" (DEPA) [3]:

$$d\sigma_{ee\to eeX} = d^2N(X_1Q_1^2)\;\; d^2N(X_2Q_2^2)\;\; \frac{d\sigma_{\gamma\gamma\to X}}{d\cos\Theta^*}d\cos\Theta^*$$

with :

$$dN(X_i, Q_i^2) = \frac{\alpha}{\pi}\left[(1 - X_i + \frac{X_i^2}{2}) - (1 - X_i)\frac{Q_{i,min}^2}{Q_i^2}\right]\frac{dX_i}{X_i}\frac{dQ_i^2}{Q_i^2}$$

Let us remark that in the DEPA one has only neglected terms of the order of $|\,q_1^2\,|\,/W^2$ and $|\,q_2^2\,|\,/W^2$, and integrated over all azimithal angles , but there is no other approximations (mainly no kinematical ones); in particular there remain Q_1^2 and Q_2^2 (Θ_1' and Θ_2') dependances.

2.2 Kinematics

In practice, Θ'_i should be relatively small so that :

$$\hat{\Theta} \equiv 2\sin\Theta'/2 \simeq \Theta' \quad \text{and} \quad \hat{\Delta} \equiv 2\sin\Delta/2 \simeq \Delta$$

Neglecting the electron mass ($E, E' \gg m_e$), from $W^2 = (p_1 + p_2 - p'_1 - p'_2)^2$, with $E'_i = (1 - X_i)E$, we obtain the relations :

$$Z^2 = X_1X_2 - \tfrac{1}{4}(1 - X_1)(1 - X_2)\hat{\Delta}^2$$
$$\beta^2 = \frac{(X_1 - X_2)^2 + (1 - X_1)(1 - X_2)\hat{\Delta}^2}{(X_1 + X_2)^2}$$

Now from $q_i^2 = (p_i - p'_i)^2$, using a m_e/E extansion at $\Theta' = 0$, and neglecting the mass at $\Theta' \gg m_e/E'$, one gets :

$$Q^2_{i,min} \cong \tilde{Q}^2_{i,min} = \frac{X_i^2}{1 - X_i}(\frac{m_e}{E})^2 \qquad \text{for } \Theta'_i = 0$$
$$Q_i^2 \cong \tilde{Q}_i^2 = (1 - X_i)\hat{\Theta}^2 \qquad \text{for } \Theta'_i \gg m_e/E'$$

Setting along the whole Θ'_i range (dropping the i index), $Q^2 = \tilde{Q}^2_{min} + \tilde{Q}^2$ one has

$$Q^2 \equiv -q^2/E^2 = \frac{X^2}{1 - X}\left[(\frac{m_e}{E})^2 + (\frac{1 - X}{X}\hat{\Theta})^2\right]$$
$$\hat{\Theta}^2 = \frac{1}{1 - X}Q^2 - (\frac{X}{1 - X}\frac{m_e}{E})^2$$

The quasi-reality condition $\mid q^2 \mid \ll W^2$ also implies that $p_\perp^2 = p' sin\Theta' \sim (1 - X) \mid q^2 \mid \ll W^2$ and $P_t^2 \ll W^2$ where P_t is the transverse momentum of the $\gamma\gamma$ system. Then, the transverse component of the Lorentz boost of the $\gamma\gamma$ system in the ee frame becomes negligible, and the direction of the boost as well as the $\gamma\gamma$ axis in the $\gamma\gamma$ frame remain close to the e^+e^- axis in the e^+e^- c.m. frame. Hence one derives the following simplified kinematical relations :

$$\Theta'_i \sim 0 \; ; \; \Phi'_i \simeq \Phi'^{\star}_i$$
$$Z^2 = X_1X_2 \; ; \; Y = \frac{1}{2}\ln\frac{X_1}{X_2}$$
$$y_j = Y + y_j^\star \; ; \; \Phi_j = \Phi_j^\star$$

while the space-phase limitations $X_1, X_2 \leq 1$ leads to

$$X^2 \leq Z \leq 1 \quad and \quad \ln(Z) \leq Y \leq \ln(1/Z)$$

where $Y \equiv \tanh^{-1}\beta = \tanh^{-1}\frac{\mid X_1 - X_2 \mid}{X_1 + X_2} \equiv \frac{1}{2}\ln\frac{X_1}{X_2}$, is the rapidity of the $\gamma\gamma$ system; $y, \beta_j, \cos\Theta_j$ and $y^\star, \beta_j^\star, \cos\Theta_j^\star$ are respectively the rapidity, the velocity, and the cosine along the e^+e^- axis, of the outgoing particles in the e^+e^- and $\gamma\gamma$ c.m. frames. ($y_j \equiv \tanh^{-1}(\tilde{\beta}_j\cos\Theta_j)$ and $y_j^\star \equiv \tanh^{-1}(\tilde{\beta}_j^\star\cos\Theta_j^\star)$)

Let us notice that the validity conditions of those kinematical approximations are just the same as the quasi-reality conditions $\mid q^2 \mid \ll W^2$ (rather than to be simply related to the angle of the scattered electrons).

2.3 Analytical approximation (Williams-Weizsäcker)

Now, assuming well defined limits of quasi-reality and acceptances and using the kinematical approximations, one can integrate analytically over the various parameters and one derives analytical approximation of the cross section similar to the classical Williams Weiszacker Approximation (WWA).

Integrating $d^2N(X,Q^2)$ over Q^2 for an electron scattering angle $0 \leq \Theta' \leq \Theta'_0$ with $Q^2_{max} = (1-X)\Theta'^2_0 \gg Q^2_{min} = \frac{X^2}{1-X}\frac{m_e{}^2}{E^2}$ one gets:

$$dN = 2\frac{\alpha}{\pi}\left[(1-X+\frac{X^2}{2})\ln(\frac{E}{m_e}\frac{1-X}{X}\Theta'_0) - \frac{1}{2}(1-X)\right]\frac{dX}{X}$$

We have previously shown that the quasi-reality condition for validity of the EPA is given by $\mid q^2 \mid << W^2$ (it means that, in the $\gamma\gamma$ center-of-mass frame, the mass of the virtual photon can be neglected versus its energy W/2). Just for convenience, let us change this condition only slightly and assume that the mass must be negligible in front of the energy in the e^+e^- c.m. frame. We then obtain the relation:

$$X \sin\Theta_\gamma = (1-X)\sin\Theta'$$

which implies $\sin\Theta' \leq X/(1-X)$ and, for $\Theta'_0 = X/(1-X)$, we get

$$dN = \frac{2\alpha}{\pi}(1-X+\frac{X^2}{2})(\ln\frac{E}{m} - \frac{1}{2})\frac{dX}{X}$$

This expression is practically the classical one found everywhere in the literature, but with only slight differences due to various approximations. Its main features are the $\ln(E/m_e)$ and dX/X dependances.

Changing the variables X_1 and X_2 to Z and Y according to the kinematical approximations ($Z^2 = X_1X_2$ and $2Y = \ln(X_2/X_1)$; *i.e.* $X = Ze^{\pm Y}$) one gets:

$$\frac{d^3\sigma_{ee\to eeX}}{dZ\,dY\,d\Omega^*} = \frac{d^2\mathcal{L}_{\gamma\gamma}}{dZ\,dY}\,\frac{d\sigma_{\gamma\gamma\to X}(W,\Omega^*)}{d\Omega^*}$$

with

$$d^2\mathcal{L}_{\gamma\gamma} = (\frac{2\alpha}{\pi})^2(\ln\frac{E}{m_e} - \frac{1}{2})^2 P(Z,Y)\frac{dZ}{Z}dY$$

$$P(Z,Y) = 4(1-Z\cosh Y)^2 + Z^2(2/\cosh Y - Z^2)^2)^2$$

while the integration of P(Z,Y)dY over Y from 0 to Y_0 leads to:

$$H(Z,Y_0) = (Z^2+2)^2Y_0 - 4Z(Z^2+2-Z\cosh Y_0)\sinh Y_0$$

Therefrom, assuming an ideal detector covering a 4π solid angle and integrating over the full phase phase $\Omega^* = 4\pi$ and $\mid Y \mid \leq ln(1/Z)$ one get

$$d\sigma_{ee\to eeX} = d\mathcal{L}_{\gamma\gamma}\ \sigma_{\gamma\gamma\to X}$$

$$d\mathcal{L}_{\gamma\gamma} = (\frac{2\alpha}{\pi})^2(\ln\frac{E}{m_e} - \frac{1}{2})^2\left[(Z^2+2)^2\ln\frac{1}{Z} - (1-Z^2)(3+Z^2)\right]dZ/Z$$

This expression, known as the Low formula, is the one reported for instance by the Particle Data Group. It main characteristics are both the logarithmic energy dependances so that the cross section is roughly given by

$$d\sigma_{ee\to eeX} \propto \left[ln\frac{E}{m_e}\right]^2\ ln\frac{2E}{W}\ \frac{dW}{W}\ \sigma_{\gamma\gamma\to X}\ .$$

Therefore, for the same integrated e^+e^- luminosity, the rates of $\pi\pi$ production near threshold (W $\sim$ 300 MeV) will be 10 times larger at PEP/PETRA than at DAFΦNE (25 times at LEP200).

3 Experimental limits and DAΦNE's opportunity

It is obvious that the results derived just above, implie approximations and integration ranges which are not always experimentally satisfied. Taking into account the experimental conditions and acceptances can lead to conclusions exactely opposite to the theoretical ones. It is, in particular, the case for the $\pi\pi$ production near threshold for the following reasons.

- The detectors of high energy machine are not suited to study very low invariant masses. It is particulary obvious, for example, that they could not trigger only on two charged pions of very low momenta or only 4 photons of very low energies. In the opposite way KLOE [6], particulary designed to study $\pi^+\pi^-$ and $\pi^0\pi^0$ decay of K^0 produced almost at rest, is vey well adapted to study pion pair production near threshold.

- The $\ln(2E/W)$ dependance is in fact obtained when integrating over the full space phase, namely over the full rapidity range and over a 4π angular acceptance. This increase of $\gamma\gamma$ luminosity with the beam energy for fixed W comes from a larger range of rapidity of the $\gamma\gamma$ system. But, the angular acceptance in the laboratory, strongly limits the allowed range of rapidity and it results that such energy dependance completely disappears.

- The $\ln(E/m_e)$ dependance comes from the integration over the Q^2 of the quasi-real photons spectra or, in other words, over the angles of the scattered electrons. However one can notice that the $\ln(E/m_e)$ increase of $\gamma\gamma$ luminosity with the beam energy is only due to scattering angles lower than m_e/E while the maximum scattering electron angle is of the order of $W/2E$ and tagging becomes impossible at high energy machine.

Now, let me in follows discuss in more details the two last points which are respectively related to the angular acceptances either of the central detector or of the scattered electrons.

3.1 angular acceptance of the central detector

The correlations between equivalent sets of independent variables relative either to the photon energies X_1, X_2 or to the $\gamma\gamma$ system Z,Y

$$Z^2 = X_1 X_2 \quad , \quad Y = \frac{1}{2} \ln \frac{X_1}{X_2}$$

as well as the phase-space limitations are visualized in the following figure, where X_1 and X_2 are plotted in logarithmic scales.

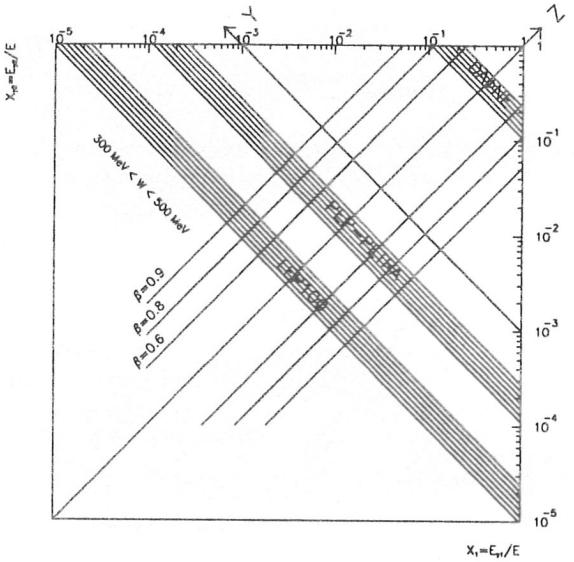

Figure 2: relations between X_1, X_2 and Z,Y

Since $\ln Z = \frac{1}{2}(\ln X_1 + \ln X_2)$ and, $Y = \frac{1}{2}(\ln X_1 - \ln X_2)$, The invariant mass and the rapidity of the $\gamma\gamma$ system are respectively plotted along the first and second bissectrix.

Since both photon spectra are proportional to dX/X, any area on this plot is also proportional to the $\gamma\gamma$ luminosity.

The hatched area show the allowed range for $300 \leq W \leq 500$ MeV for different colliders. One immediately see that the increase of $\gamma\gamma$ luminosity with the beam energy is only due to an increase of the rapidity of the $\gamma\gamma$ system.

Looking, for example, at a two body production with $y_{1,2} = Y \pm y^*$ and, assuming a symetrical angular acceptance of the central detector given by $|\cos\Theta_{1,2}| \leq \cos\Theta_0$, so that $|y_{1,2}| \leq y_0 \equiv \tanh^{-1}(\cos\Theta_0)$, one derives

$$|Y| = y_0 - y^* = \ln\frac{\tan(\theta^*/2)}{\tan(\Theta_0/2)},$$

so that one cannot separately integrate $d^2\mathcal{L}_{\gamma\gamma}$ over dY and $d\sigma_{\gamma\gamma}$ over $d\cos\theta^*$

The correlations and integration ranges of the 3 independants parameters $X_1, X_2, y^*(\cos\theta^*)$ and $Z, Y, y^*(\cos\theta^*)$ for $|\cos\Theta| \leq 0.998$, and $300\ MeV < W < 500\ MeV$, are visualized on the following plots where y^* $(\cos\theta^*)$ is perpendicular to the X_1, X_2 plane.

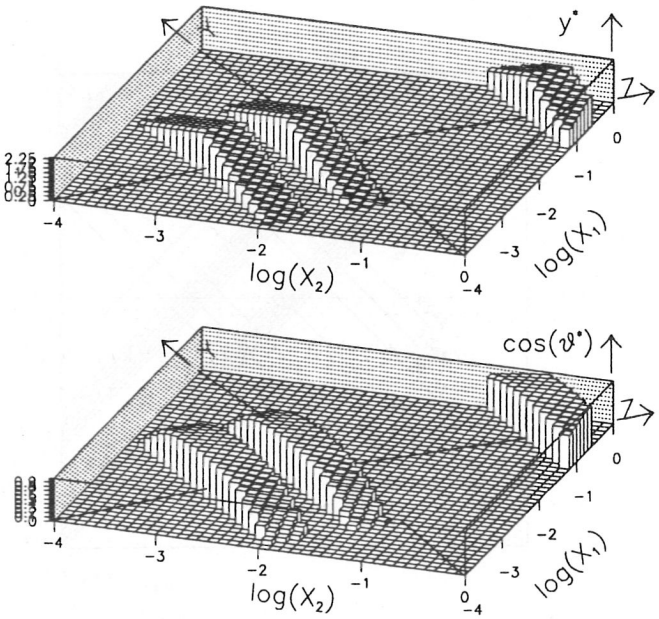

Figure 3: integration ranges over X_1, X_2, y^* and $X_1, X_2, \cos\theta^*$.

One notices that X_1, X_2 always remain defined on a limited range around Z, and that, for high energy machines, Y as y^* (or β as $\cos\theta^*$) are limited by the angular acceptance which tends to experimentally favour events with low β (Y) and low $\cos\theta^*$ (y^*) with

$$|Y|, y^* \leq y_0 \quad or \quad \beta, \cos\theta^* \leq \cos\Theta_0$$

$$X \sim Z$$

It results that one actually has:

$$d\sigma_{ee\to ee\pi\pi} = d\mathcal{L}_{\gamma\gamma} d\sigma_{\gamma\gamma\to\pi\pi}$$

$$d\mathcal{L}_{\gamma\gamma} = \varepsilon(W,\Theta^*)\frac{dW}{W} \quad ; \quad d\sigma_{\gamma\gamma\to\pi\pi} = \frac{d\sigma_{\gamma\gamma\to\pi\pi}(W,\Theta^*)}{d\cos\Theta^*} d\cos\Theta^*$$

where $$\varepsilon(W,\Theta^*) \sim Min\left[ln\frac{2E}{W}, \ln\frac{\tan\Theta^*/2}{\tan\Theta_0/2}\right]$$

is given, when integrating over the rapidity of the $\gamma\gamma$ system, either by the phase space limitation ($E_{\gamma 1,2} \leq E$) or by the limit due to the angular acceptance ($|\cos\Theta_{1,2}| \leq \cos\Theta_0$). Those values from the phase space at different values of Z and for $\cos\Theta_0 = 0.998$, are shown in the following figure

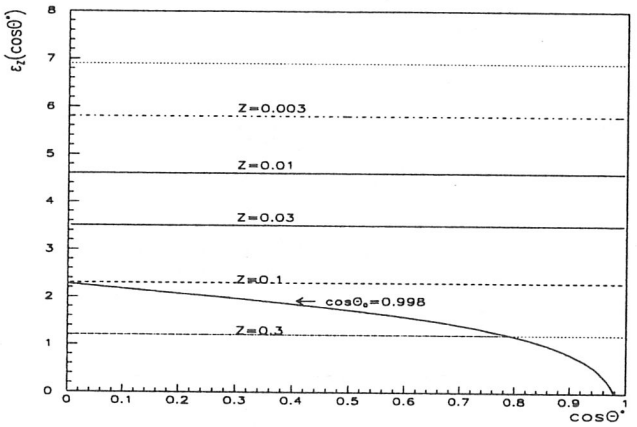

Figure 4: The $\varepsilon(\theta^*)$ function resulting from integration over Y limited either by the phase space or by the angular acceptance $|\cos\Theta_{1,2}| < 0.998$

Looking at the $\pi\pi$ threshold $W \sim 300\ MeV$, we notice that at DAΦNE, since $Z \sim 0.3$, $\varepsilon(W,\theta^*)$ remains defined by the phase space and flat up to large $\cos\theta^*$ values.

For other machines, from $E > 1.5$ GeV one has $Z > 0.1$ and $\varepsilon(W,\theta^*)$ becomes limited by the angular acceptance so that there is no more energy dependance (no $\ln(2E/W)$ increase).

Actually, from $W < 2E\ \tan(\Theta_0/2)$ the integration over Y only results in a angular acceptance efficiency in the $\gamma\gamma$ c.m. $\varepsilon(\theta^*)$ which is a decreasing function of $\cos\theta^*$. Experimental results presented as $\gamma\gamma$ cross section are unfolded from this acceptance efficiency. But, this procedure is not really independant of the choice of the angular distribution which is not so easy to check.

3.2 Tagging acceptance: photon flux

Figure 5 shows the correlations between the mass and energy of the photon (X, Q^2) and the scattering angle of the electron for various beam Energies

$$Q^2 \equiv -q^2/E^2 = \frac{X^2}{1-X}\left[(\frac{m_e}{E})^2 + (\frac{1-X}{X}\hat{\Theta})^2\right]$$

where X and Q^2 are plotted in logarithmic scales.

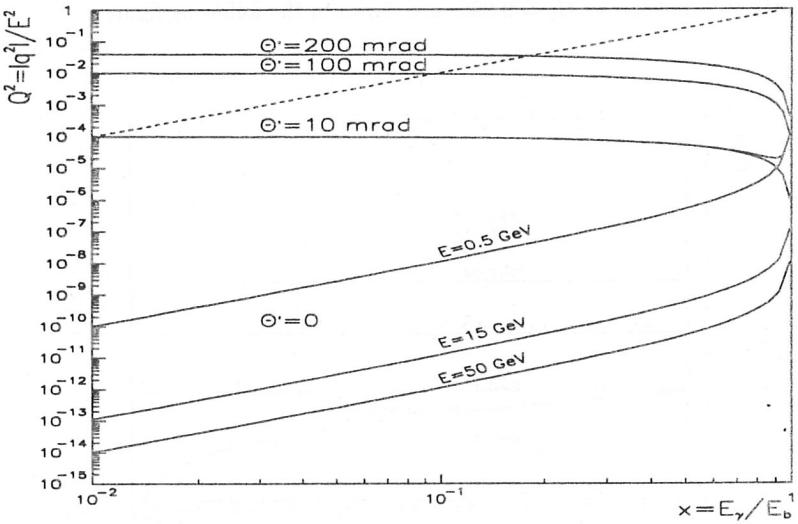

Figure 5: Relations between X , Q^2 and Θ'

The dashed line $Q^2 = X^2$ ($\mid q^2 \mid = E_\gamma^2$) roughly shows the limitation of quasi-reality of the photons. For those photons, any area on this plot is proportional to the intensity of the photon flux (since $d^2N(X,Q^2) \propto (dX/X)(dQ^2/Q^2)$.

One notices that the increase of the beam energy results in an increase of the intensity of the flux only at very small angles ($\Theta' \sim m_e/E$), while the increase of X suppresses the contribution of small angles but provides the photons to be quasi-real up to larger scattering angles.

Then it results that, for $W \sim 300$ MeV, the angular distribution of the scattered electrons is quite different for DAΦNE (E=0.5 GeV and $X \sim Z > 0.3$) and for machines of highest energy ($E > 10$ Gev with $X \sim Z < 0.1$)

The following table summarizes for $W \sim 300MeV$ the range of the energy lost and of the averaged and maximum scattering angles of the scattered electrons at various colliders.

	DAΦNE	PEP-PETRA	LEP100	LEP200
E (GeV)	0.510	15	50	100
Z=W/2E	0.3	0.01	0.003	0.0015
$< \Theta >= m_e/E$	1 mrad	0.03 mrad	0.01 mrad	0.005 mrad
$\Theta_{max} \sim Z$	300 mrad	10 mrad	3 mrad	1.5 mrad
$\Delta E/E = X$	0.3	0.01	0.003	0.0015
	2 rings	1 ring		

It is particulary obvious that, for high energy machine, not only the detectors are not suited for measuring very low masses but, it becomes impossible to tag quasi-real photon because the scattered electrons are emitted at very small angles with an energy close to the incident ones and remain in the closed orbit. This explains why there is only very few measurements of $\gamma\gamma \to \pi\pi$ near the threshold (DM1/DM2 at DCI [8], PLUTO at PETRA [9] , MARKII at PEP [10] for $\pi^+\pi^-$ and, crystal-ball at DORIS [11] for $\pi^0\pi^0$).

At DAΦNE, since W/2E and m_e/E becomes larger by order of magnitude, the scattered electrons have a quite unusual large lost of the incident energy and broad angular distribution untill large angle (see figure 6). Moreover DAΦNE is a two rings machine.

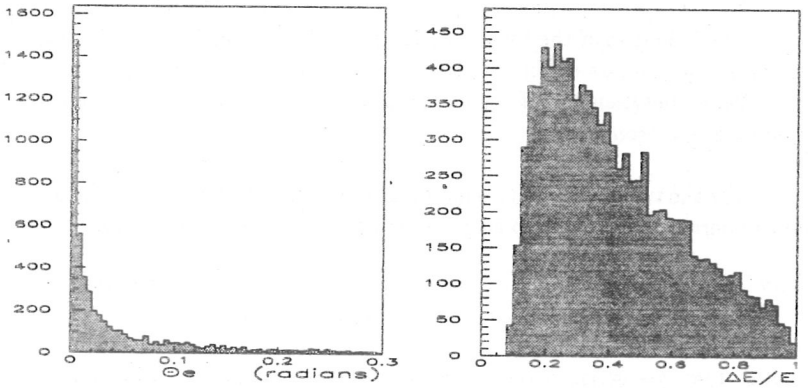

Figure 6: polar angle and energy lost distributions of the scattered electrons for $\gamma\gamma \to \pi^+\pi^-$ Monte-carlo simulation at DAΦNE

Therefore, in the one hand the large ratio of energy lost by the incident electrons makes possible a zero degree tagging system since those electrons can be extracted out of the closed orbit thanks to the splitter magnet; in the other hand, the broad angular distribution of the scattered electrons makes also possible tagging at large angle.

3.3 azimuthal correlations

This particulary high efficienccy for tagging quasi-real photon at large electron scattering angles gives an unique opportunity of measuring their azimuthal angles and then of testing various model by studying azimuthal correlations [7)]

Looking at quasi-real photons only γ helicities ± 1 contribute. If we does not integrate over the azimuthal angles as we did before, the general formula describing the helicity structure of the completely differentiated cross section of $e^+e^- \to e^+e^- AA'$ can be written as:

$$\begin{aligned} d\sigma \;\propto\;& I_{++,++} + I_{++,--} - 2\varepsilon\, \mathcal{R}e\, I_{++,+-} \cos 2\phi \\ &- 2\,\varepsilon'\, \mathcal{R}e\, I_{+-,++} \cos 2\phi' + \varepsilon\varepsilon'\, \mathcal{R}e\, I_{+-,+-} \cos 2(\phi+\phi') \\ &+ \varepsilon\varepsilon'\, \mathcal{R}e\, I_{+-,-+} \cos 2(\phi-\phi')\ , \end{aligned}$$

with

$$I_{m\bar{m},n\bar{n}} = \sum_{aa'} M^{aa'}_{mn} M^{aa'*}_{\bar{m}\bar{n}}$$

Where $M^{aa'}_{mn}$ ($M^{aa'}_{\bar{m}\bar{n}}$) the helicity amplitudes of the process $\gamma\gamma \to AA'$; $m(\bar{m})$ and $n(\bar{n})$ the helicities of the two photons and a, a' those of A, A'; ε, ε' are the polarization parameters of the photons; ϕ and ϕ' are azimuthal angles in the $\gamma\gamma$ c.m. frame, between one of the particles produced (either A or A') and the two outgoing electrons.

For the two-pion production (2 pseudoscalars production), the helicity terms are derived from the two amplitudes M_{++} and M_{+-} and one has:

$$\begin{aligned} d\sigma \;\propto\;& (\mid M_{++} \mid^2 + \mid M_{+-} \mid^2) - 2\mathcal{R}e(M_{++}M^*_{+-})[\varepsilon cos2\phi + \varepsilon cos2\phi'] \\ &+ \varepsilon\varepsilon'(\mid M_{++} \mid^2 cos2(\phi+\phi') + \mid M_{+-} \mid^2 cos2(\phi-\phi') \end{aligned}$$

We notice that $\phi + \phi'$ is, in the $\gamma\gamma$ c.m. frame, the azimuthal angle between the two electrons, while $\phi - \phi'$ is twice the angle between the bisectrix of the transverse momenta of the outgoing electrons and the transverse momentum of the pion. Those angles are obviously defined in the $\gamma\gamma$ c.m. frame but, contrary to the polar angles, the azimuthal ones remain almost identical in both the $\gamma\gamma$ and the e^+e^- systems.

The following figure shows the azimuthal correlations in e^+e^- system as they result from Monte-carlo simulations whether from Born term or chiral pertubation theory at DAΦNE with KLOE.

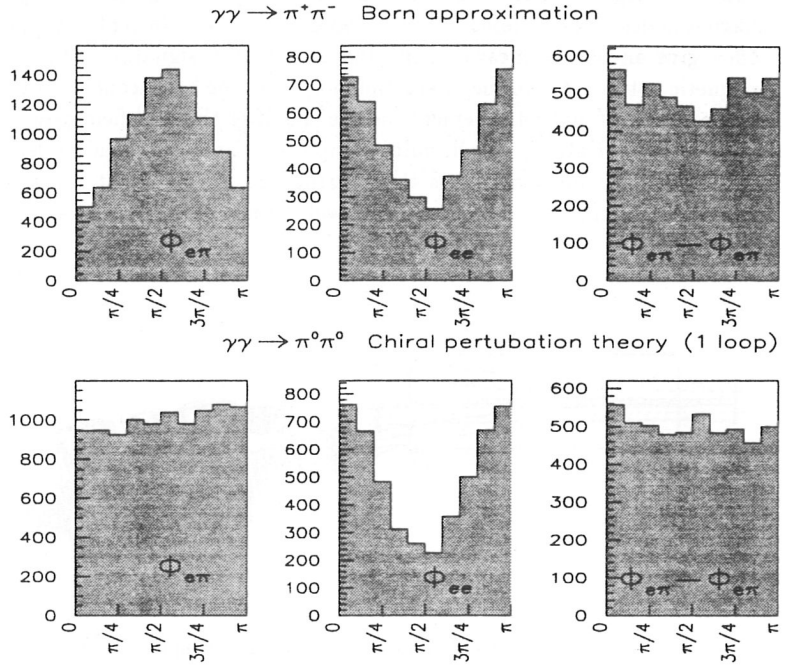

Figure 7: Azimuthal correlations in the e^+e^- center of mass

Let us notice that in the single tag mode, one azimuthal correlation $\Phi_{e\pi}$ (*i.e*: φ or φ') can be measured and still used to check the models.

4 The experimental design of $\gamma\gamma$ study at DAΦNE [12)]

Assuming an integrated e^+e^- luminosity of $5.10^{39} cm^{-2}$ (10^7 sec. at a nominal luminosity of $5.10^{32} cm^{-2} sec^{-1}$) one expects from $\gamma\gamma$ collisions about 10^6 $\pi^+\pi^-$ and 10^4 $\pi^0\pi^0$ events by year.

A prori, those events are well determined and constrained with a total transverse momentum close to zero. However DAΦNE runing at the Φ energy leads to a very high rate of annhilation events ($\sim 1\ MHz$) and the number of $\pi^+\pi^-$ and $\pi^0\pi^0$ observed from $K_S^0 K_L^0$ where one of them escapes to detection are respectively of about 3 and 6 10^8 events/year, i.e. 10^2 and 10^4 larger than the $\gamma\gamma$ signal. Thus, the tagging is not only very usefull but absolutely

needed in order to eliminate the large backgound remaining from the very high annihilation counting rates and to flag the small amount of $\gamma\gamma$ candidates.

4.1 tagging system

The "zero degree tagging" (SAT), is performed by setting after the split field magnet hodoscopes to detect e^+ or e^- which have lost sufficiently large energy. They give an energy measurement and an electron signature. However the magnetic optics between the interaction point and the hodoscopes is not simple. There is a lot of magnetic elements before and after the split field magnet. The acceptance is relatively small, quite complicated and can even be dependant of the runing conditions. It is thus particulary obvious that a control and normalisation through the similar but well known $\gamma\gamma \rightarrow \mu\mu$ process is very important.

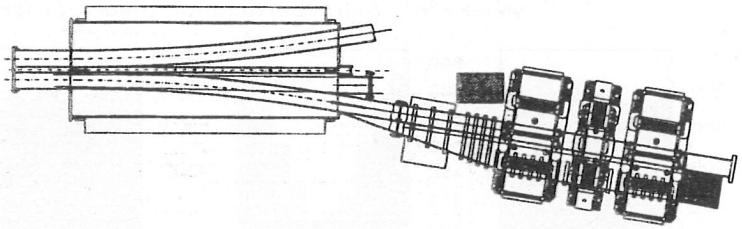

Figure 8: Zero degree tagging system

An other problem comes from the very high rate of Bremsstrahlung (Bhabba radiatif) which is strongly peacks at zero degree ($d\sigma/d\theta \sim 1/\theta^3$). Analytical evaluation [13] and exact calculation [14] show that, even for the maximum value of luminosity, there will be less than such an electron detected every 12 bunch crossing. Actually a bremsstrahlung device is designed in order to look for electron-gamma coincidence. However rates and possibly pile-up are particulary high.

The design of such a Zero degree tagging has been accepted and the necessary modifications of the machine, mainly for the vacuum pipe, has been take into account in the DAΦNE project.

Electrons scattered at angles larger than 150 mrad will be detected by KLOE itself. Obviously we would like to tag the quite large number of electrons emitted at smaller finite angles. However due to the presence inside

KLOE and close to the interaction point of the quadrupole producing the low beta, one cannot detect electrons emitted at finite angles lower than 70 mrad. One could only expect to detect them in front of the quadrupole (WAT) for $70 \leq \Theta_e \leq 150$ mrad by means of silicone strips leading to Θ, Φ measurements (no electron signature,no energy determination) . Such a wide angle tagging is not yet designed in a first step.

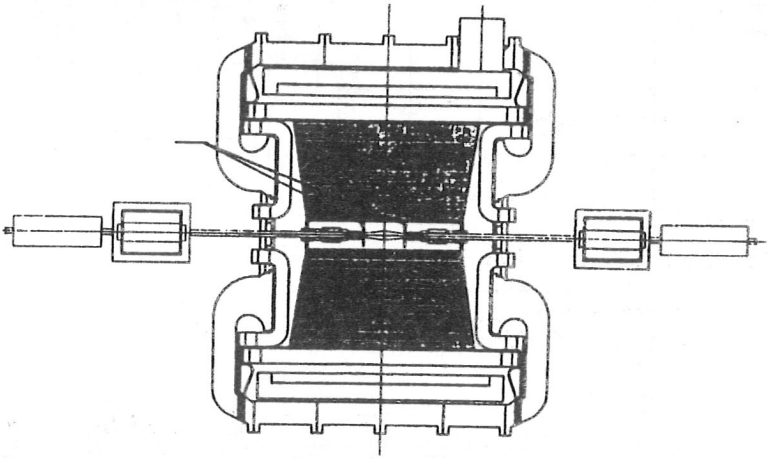

Figure 9: Wide angle tagging system

4.2 counting rates

The following table shows the number of $\pi^0\pi^0$ events per year expected for an integrated luminosity of $5.10^{39} cm^{-2}$

	double tagging			simple tagging
	KLOE	WAT	SAT	$e^+ or\ e^-$
KLOE	1			70
WAT	14	43		940
SAT	52	280	400	3200
	790			

Let us notice the particular importance of the WAT which allows the tagging to measure the azimuthal angle of the scattered electrons. With such a tagging, one can expect about 1500 $\pi^0\pi^0$ events with at least one azimuthal angle measured so that one can analysed the $\Phi_{e\pi}$ correlation and, about 60 events for wich we could measure all azimuthal angles and then all correlations.

The number of $\pi^0\pi^0$ events expected per year at DAΦNE is two order of magnitude larger than the one observed at crystal ball.

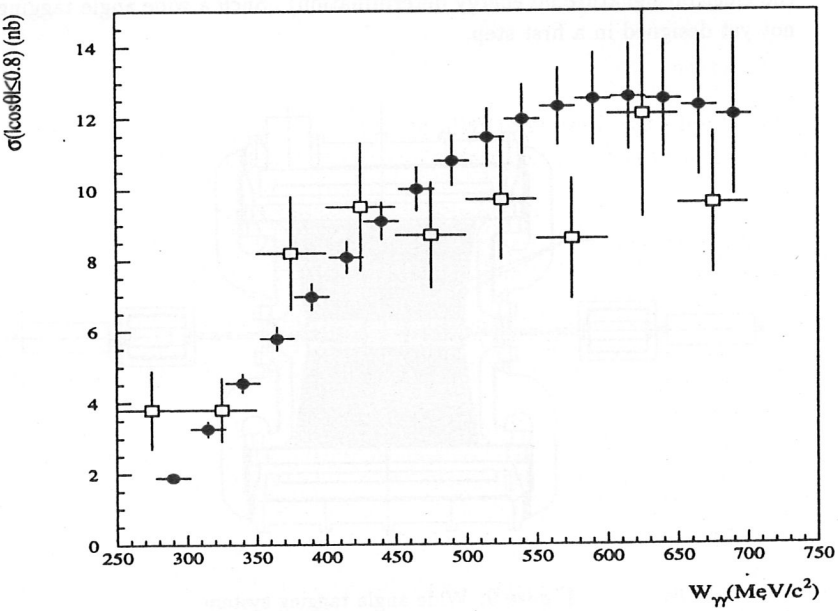

Figure 10: Number of $\gamma\gamma \to \pi^0\pi^0$ events expected per year at DaΦNE from the 2 loops Chiral pertubation theory compared with the Crystal ball data

The number of $\pi^+\pi^-$ is 100 times higher than the $\pi^0\pi^0$, number to be compared to the few ten events observed at DM1 for example.

5 Summary

DAΦNE and KLOE give the opportunity of studying the $\pi\pi$ production near threshold , measuring the $\gamma\gamma$ cross section including azimuthal correlations and, therefore, to check the predictions from various theoretical models using unitarity, dispersion relations or chiral pertubation theory. [15)]

One can also studied the light C^+ pseudoscalars to determine their internal structure and mixing angles.

The measurement of the total $\gamma\gamma$ cross section around 1 Gev is also designed but seems difficult : It could be not just derived from double Tagging coincidences because of the high rates of Bremsstrahlung.

Acknowledgements

I acknowledge financial support from the EEC human Capital and mobility Program. I would also like to thank all the people working on two-photon physics at DAΦNE with a special mention to Prof G.Pancheri, F.Annulli and A. Zallo.

References

1. F.Low, Phys. Rev. 120 (1960) 582.
   F.Calogero and Ch. Zemach, Phys.Rev. 120 (1960) 1860.

2. N.Arteaga-Romero, A.Jaccarini, J.Parisi, and P. Kessler, Lett.Nuovo Cim. 4 (1970) 388.
   V.E.Balakin, V.M. Budnev, and I.F. Ginnzburg, JETP Lett.11 (1970) 388.
   S.J. Brodsky, T.Kinoshita, and H. Terazawa, Phys. Rev. Lett 25 (1970) 1532.

3. V.M. Budnev, I.F. Ginzburg, G.V. Medelin, and V. Serbo, Phys. Rep. 15C (1975) 181.
   N.Arteaga-Romero, A.Jaccarini, P.Kessler and J.Parisi , Phys. Rev D3 (1971) 1569.
   C.Carimalo, P.Kessler, and J.Parisi, Phys. Rev. D20 (1979) 1057.

4. see for a more precise review A.Courau and G.Pancheri, in "The DAΦNE Physics Hanbook" , ed. by L.Maiani, G.Pancheri and N.Paver (INFN,Frascati,1992), and Ref. therein.

5. G. Vignola, in Proceedings of the Workshop on Physics and Detectors for DAΦNE, Frascati, Italy, April 1991, ed. G. Pancheri (INFN-Laboratori Nazionali di Frascati), p. 11.

6. "KLOE, A general purpose detector for DAΦNE", Frascati report LNF-92/019(R).

7. S. Ong and P. Kessler, Mod. Phys. Lett. A2 (1987) 683; Phys. Rev. D46 (1992) 944.
   S. Ong, P. Kessler and A. Courau, Mod. Phys. Lett. A4 (1989) 909.

8. A.Courau et al., Phys.Lett.,96B(1980)402; Nucl.Phys.,D271(1986) 1; Z.Ajaltouni et al.,Phys. Lett. 194B(1987) 573.

9. Ch.Berger et al.,Z. Phys. C26 (1984) 199.

10. J. Boyer et al.,Phys. Rev.D42(1990) 1350.

11. H. Marsiske et al.,Phys.Rev. D14(1990) 3324.

12. G. Alexander et al., Il Nuovo Cimento 107A (1994) 837.
F.Anulli et al, in "The Second $DA\Phi NE$ Physics Handbook" (ed. L.Maiani, G.Pancheri, N.Paver (INFN Frascati 1995)).

13. G. Pancheri,Phys.lett.315B(1993) 477.

14. M.Greco et al.Phys.lett.318B(1993)635.

15. see the various papers in "The Second $DA\Phi NE$ Physics Handbook" (ed. L.Maiani, G.Pancheri, N.Paver (INFN Frascati 1995)) from M.R.Pennington; J.Gasser and M.E.Saino; S.Bellucci, J.Gasser and M.E.Saino; S.Bellucci. A.Courau and S.Ong; M.Knecht, B.Moussalam and J.Stern; and the theoretical talks given at this workshop.

THE QED RUNNING COUPLING AND DAΦNE

Guido ALTARELLI
Theoretical Physics Division, CERN, Geneva, Switzerland

CONTENT

1. Introduction
2. The Muon Anomalous Magnetic Moment
3. The Hadronic Contribution to $\alpha(m_Z)$

1. Introduction.

The KLOE experiment at DAΦNE can be very useful in reducing the experimental errors on the hadronic cross section in e^+e^- annihilation at energies below 1.4 GeV. This in turn will allow a sizeable reduction of the theoretical errors associated with the hadronic contribution to the photon vacuum polarisation. This progress will be of great importance for reducing the theoretical error for the muon g-2, a_μ [1], and, to a lesser extent , for the determination of $\alpha(m_Z^2)$, which is very important for precision tests of the Standard Model [2]. In the following I will describe the status and the relevance of these problems.

2. The Muon Anomalous Magnetic Moment

The muon anomalous magnetic moment provides a very precise QED test. The present experimental value is [3]:

$$a_\mu^{exp} = (11659230 \pm 85)\ 10^{-10} \qquad (1)$$

The comparison with the theoretical prediction gives [4]:

$$a_\mu^{exp} - a_\mu^{th} = (38 \pm 87)\ 10^{-10} \tag{2}$$

A forthcoming Brookhaven experiment [5] aims at bringing the experimental accuracy down to

$$\Delta a_\mu^{exp} = \pm 4\ 10^{-10} \tag{3}$$

The theoretical prediction can be decomposed as follows

$$a_\mu^{th} = a_\mu^{QED} + a_\mu^{had} + a_\mu^{weak} + ? \tag{4}$$

where the dots stand for possible small exotic contributions. The weak interaction term is estimated to be [6]:

$$a_\mu^{weak} \sim 20\ 10^{-10} \tag{5}$$

The problem we address here is on the magnitude and the error associated to a_μ^{had}. In fig.1a-1b two typical diagrams contributing to a_μ^{had} are displayed: the hadronic vacuum

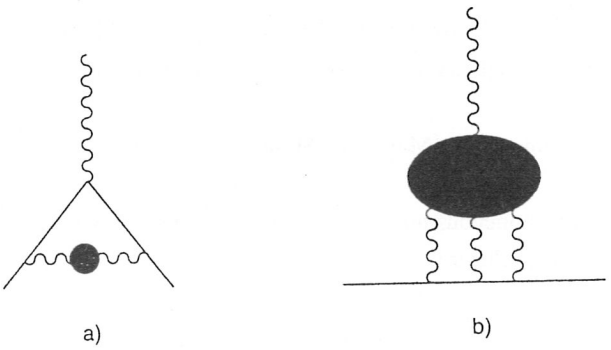

Fig. 1: Diagrams contributing to a_μ: a) photon vacuum polarisation, b) light by light scattering. The uncertainty is related to the corresponding hadronic contributions.

polarisation insertion (a) (multiple exchanges of the dressed photon line have also been considered) and the light by light scattering contribution (b). The largest term arises from the contribution in (a) which can be cast into the form [7]

$$a_\mu = (\frac{\alpha m_\mu}{3\pi})^2 \int_{4m_\pi^2}^{\infty} \frac{d\,s}{s^2} R(s)K(s) \qquad (6)$$

The kernel K(s) is a smooth function that varies monotonically from 0.63 to 1 in the integration range. R(s) is the ratio between the total hadronic cross section in e^+e^- annihilation and the pointlike $\mu^+\mu^-$ cross section. The s^2 denominator strongly emphasises the low energy part of the integration range. The integral can be evaluated starting from the existing data on e^+e^- annihilation into hadronic final states. The evolution of this procedure over the times is displayed in table 1, taken from ref.7.

Table 1

Author(s)	Year and Ref.	$a_\mu^{had}.10^{10}$
Barger et al	1975 [ref. 16 in ref.7]	663 ± 85
Barkov et al	1985 [ref. 17 in ref.7]	684 ± 11
Kinoshita et al	1985 [ref. 18 in ref.7]	707 ± 17
Casas et al	1985 [ref. 19 in ref.7]	710 ± 11
Dubnicka et al	1990 [ref. 20 in ref.7]	705 ± 8
Jegerlehner et al	1991 [ref. 21 in ref.7]	724 ± 27
Dubnickova et al	1992 [ref. 22 in ref.7]	699 ± 5
Eidelman et al	1995 [7]	702 ± 15
Eidelman et al (RG impr.)	1995 [7]	725 ± 16

The present best estimate is given by:

$$a_\mu = (725 \pm 16)\ 10^{-10} \qquad (7)$$

which corresponds to the last line of table1. The improvement from the Renormalisation Group consists in performing the Dyson resummation of the iterated vacuum polarisation bubbles leading to the replacement

$$\alpha\left(\frac{1}{k^2}+\frac{1}{k^2}\,\Pi\,\frac{1}{k^2}\;+\ldots\right)=\frac{1}{k^2}\,\frac{\alpha}{1-\Pi}=\frac{\alpha(k^2)}{k^2} \tag{8}$$

where Π is the vacuum polarisation function and $\alpha(k^2)$ is the running QED coupling.

A conspicous part of the error arises from the integration in the energy range $2m_\pi$ - 1.4 GeV that can be scanned at DAΦNE and also at VEPP-2M. This can be appreciated from table 2, also taken from ref.7.

Table 2: Contributions to $a_\mu^{had}\cdot 10^{10}$

final state	energy range (GeV)	contribution (stat) (syst)	rel. err.	abs. err.
ρ	(0.28, 0.81)	426.66 (5.61) (10.62)	2.8%	1.7%
ω	(0.42, 0.81)	37.76 (0.45) (1.02)	3.0%	0.2%
ϕ	(1.00, 1.04)	38.55 (0.54) (0.89)	2.7%	0.1%
J/ψ		8.60 (0.41) (0.40)	6.7%	0.1%
Υ		0.10 (0.00) (0.01)	6.7%	0.0%
hadrons	(0.81, 1.40)	112.85 (1.33) (5.49)	5.0%	0.8%
hadrons	(1.40, 3.10)	56.43 (0.45) (7.22)	12.8%	1.0%
hadrons	(3.10, 3.60)	4.47 (0.23) (0.86)	19.9%	0.1%
hadrons	(3.60, 9.46)	14.06 (0.07) (0.90)	6.5%	0.1%
hadrons	(9.46, 40.0)	2.70 (0.03) (0.13)	4.9%	0.0%
perturbative	(40.0, ∞)	0.16 (0.00) (0.00)	0.2%	0.0%
total		702.35 (5.85) (14.09)	2.2 %	2.2%

In particular a large uncertainty comes from the ρ region where some discrepancies among the existing data are present [7]. If DAΦNE succeeds to reduce to a negligible level the error from the energy range below 1.4 GeV, then the remaining uncertainty will be:

$$\Delta a_\mu = \pm 8\ 10^{-10} \qquad (9)$$

The light by light contribution shown in fig.1b is more model dependent. It cannot be determined directly starting from the data because there are no data. A theoretical prediction is difficult because it involves QCD in a non perturbative domain at small values of the energy scale. Back in 1985 Kinoshita et al [8] attempted to evaluate the contribution of the light by light contribution to a_μ from $\pi^\pm$ and π^0 exchange, while K and η exchange were neglected. Consistency with the alternative approach in terms of quark exchange was claimed. The result of ref.8 was:

$$a_\mu = (4.9 \pm 0.5)\ 10^{-10} \qquad (10)$$

Recently, at the DAΦNE Workshop in 1992, the quoted accuracy was questioned by Barbieri and Remiddi [9].They argued that, on the one hand, large cancellations take place among (external γ) gauge invariant terms in the evaluation in terms of $\pi^\pm$ and π^0 exchange. On the other hand the quark exchange determination is very much dependent of the quark mass values that are assumed. They concluded that the error in eq.10 is underestimated to such an extent as to possibly by far exceed the accuracy of the Brookhaven experiment. This important issue was reanalysed by Einhorn [10] and, independently, by de Rafael [11] in 1994. They agree that the error given by Kinoshita is underestimated but argue that the ambiguity is not as large as claimed in ref.9 In fact Einhorn points out that the large cancelling terms are gauge invariant for a gauge change on the external photon only. They are not gauge invariant under the separate transformations in all the four indices of the light by light scattering amplitude. In other words, the cancelling terms do not satisfy Bose statistics in the external photons. Thus the individual terms do not possess a definite physical significance. Einhorn considers the $\pi^\pm$ exchange amplitude more reliably computed than the one from π^0 exchange, because the latter is divergent in the point-like limit. But still there are residual sizeable cancellations between $\pi^\pm$ and π^0 exchange. The estimate of Einhorn for a_μ is around $a_\mu \sim 1.8\ 10^{-10}$. de Rafael uses the chiral perturbation theory formalism. He also agrees that the terms in the

expansion corresponding to the $\pi^{\pm}$ exchange amplitude are more reliably computed than the ones from π^0 exchange. However de Rafael goes beyond the pion exchange approximation by including higher order terms in the chiral expansion. He ends up with a value of a_μ around $a_\mu \sim 7.4\ 10^{-10}$.

Very recently, after my talk, two new studies have appeared, one by M.Hayakawa et al [12] and one by J.Bijnens et al [13]. These papers are based on two similar effective low energy QCD theories from an extended Nambu-Jona Lasinio model. Their results are $a_\mu \sim -3.6\ 10^{-10}$ and $a_\mu \sim 1\ 10^{-10}$.

In conclusion, the difference of the estimates in the second generation studies in refs.10-13 is significant for guessing at what the error can be. Certainly, at the beginning, Kinoshita was too optimist. However probably Barbieri and Remiddi exceeded in the opposite direction. From the combined analysis of refs. 10-13 something like $a_\mu = (2 \pm 5)\ 10^{-10}$ emerges. Clearly further studies could very much help in better clarifying this situation .

3. - The Hadronic Contribution to $\alpha(m_Z)$

The light quark masses are among the input parameters that must be fixed in order to compute the electroweak radiative corrections and compare the predictions with the data on precision tests of the Standard Model performed at LEP [2]. The only practically relevant terms where precise values of the light quark masses are needed are those related to the hadronic contribution to the photon vacuum polarisation diagrams. This correction is of order 6%, much larger than the accuracy of a few per mille of the precision tests. But, fortunately, one can use the actual data to almost completely solve the related ambiguity. But we shall see that the left over uncertainty is still one of the main sources of theoretical error.

According to eq.8 the QED running coupling is given by:

$$\alpha(s) = \frac{\alpha}{1-\Delta\alpha(s)} \qquad (11)$$

$$\Delta\alpha(s) = \Pi(s) = \Pi_\gamma(0) - \mathrm{Re}\,\Pi_\gamma(s) \tag{12}$$

In perturbation theory $\Delta\alpha(s)$ is given by [7]:

$$\Delta\alpha(s) = \frac{\alpha}{3\pi}\sum_f Q_f^2\, N_{Cf}\left(\log\frac{s}{m_f^2} - \frac{5}{3}\right) \tag{13}$$

where $N_{Cf}=3$ for quarks and 1 for leptons. However the perturbative formula is only reliable for leptons, not for quarks (because of the unknown values of the effective quark masses). Separating the leptonic, the light quark and the top quark contributions to $\Delta\alpha(s)$ we have:

$$\Delta\alpha(s) = \Delta\alpha(s)_l + \Delta\alpha(s)_h + \Delta\alpha(s)_t \tag{14}$$

with [7]:

$$\Delta\alpha(s)_l = 0.031421; \quad \Delta\alpha(s)_t = -\frac{\alpha}{3\pi}\frac{4}{15}\frac{m_Z^2}{m_t^2} = -0.000061 \tag{15}$$

Note that in QED there is decoupling so that the top quark contribution approaches zero in the large m_t limit. For $\Delta\alpha(s)_h$ one can use eq.12 and the Cauchy theorem to obtain the representation [7]:

$$\Delta\alpha(m_Z^2)_h = -\frac{\alpha m_Z^2}{3\pi}\,\mathrm{Re}\int_{4m_\pi^2}^{\infty}\frac{d\,s}{s}\,\frac{R(s)}{s-m_Z^2-i\varepsilon} \tag{16}$$

where R(s) has the same meaning as in eq.6. At s large one can use the perturbative expansion for R(s) while at small s one can use the actual data.

Recently there has been a lot of activity on this subject and a number of independent new estimates of $\Delta\alpha(m_Z^2)_h$ have appeared in the literature. In table 3 we report the results of these new computations together with the most significant earlier determinations (previously the generally accepted value was that of Jegerlehner in 1991 [17]).

Table 3

Author	Year and ref.	$\Delta\alpha(m_Z^2)_h$	$\alpha(m_Z^2)^{-1}$
Jegerlehner	1986 [14]	0.0285± 0.0007	128.83± 0.09
Lynn et al	1987 [15]	0.0283± 0.0012	128.86± 0.16
Burkhardt et al	1989[16]	0.0287± 0.0009	128.80± 0.12
Jegerlehner	1991 [17]	0.0282± 0.0009	128.87± 0.12
Swartz	1994 [18]	0.02666± 0.00075	129.08± 0.10
Swartz (rev.)	1995 [19]	0.0276± 0.0004	128.96± 0.06
Martin et al	1994 [20]	0.02732± 0.00042	128.99± 0.06
Nevzorov et al	1994 [21]	0.0280± 0.0004	128.90± 0.06
Krasnikov	1994 [22]	0.0275 ± 0.0009	128.97 ± 0.13
Eidelman et al	1995 [7]	0.0280± 0.0007	128.90± 0.09
Burkhardt et al	1995 [23]	0.0280± 0.0007	128.89± 0.09

The differences among the recent determinations are due to the procedures adopted for fitting the data and treating the errors, for performing the numerical integration etc. The differences are also due to the threshold chosen to start the application of perturbative QCD at large s and to the value adopted for $\alpha_s(m_Z)$. For example, in its first version Swartz [18] used parametric forms to fit the data, while most of the other determinations use a trapezoidal rule to integrate across the data points. It was observed that the parametric fitting introduces a definite bias [24]. In fact Swartz gets systematically lower results for all ranges of s. In its revised version Swartz improves his numerical procedure. Martin et al [20] use perturbative QCD down to $\sqrt{s}$ = 3 GeV (except in the upsilon region) with $\alpha_s(m_Z) = 0.118 \pm 0.007$. Eidelman et al [7] only use perturbative QCD for $\sqrt{s} > 40$ GeV and with $\alpha_s(m_Z) = 0.126 \pm 0.005$, i.e. the value found at LEP

[2]. They use the trapezoidal rule. Nevzorov et al [21] make a rather crude model with one resonance per channel plus perturbative QCD with $\alpha_s(m_Z) = 0.125 \pm 0.005$. Burkhardt et al [23] use perturbative QCD for $\sqrt{s} > 12$ GeV but with a very conservative error on $\alpha_s(m_Z) = 0.124 \pm 0.021$. This value was determined in ref.25 from e^+e^- data below LEP energies. My impression is that the excitement produced by the original claim by Swartz [18] of a relatively large discrepancy with respect to the value obtained by Jegerlehner [17] resulted in a useful debate. As a conclusion of this reevaluation of the problem the method of Jegerlehner has proven its solidity. As a consequence I think that the recent update by Eidelman and Jegerlehner [7] gives a quite reliable result. Also I do not think that a smaller error than quoted by these authors can be justified.

A partition of the magnitude of the $\Delta\alpha(m_Z)_h$ correction and of the related error is given in graphic form in fig.2 taken from ref.23. We see that the possible impact of

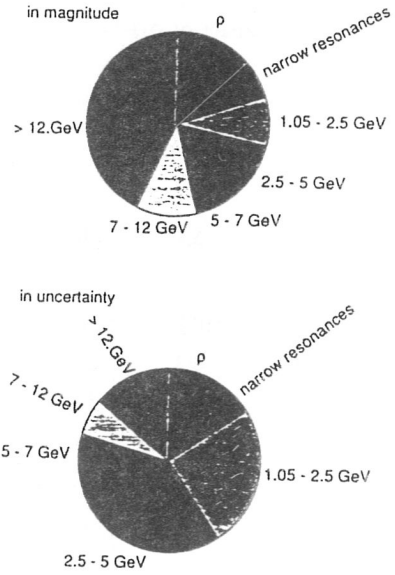

Fig. 2: Relative contributions to $\Delta\alpha(m_Z)$ in magnitude and uncertainty.

DAΦNE is less important than for the muon g-2. Even if the error from the region below 1.4 GeV is totally eliminated the advantage is not very large, given that the errors from the different regions are added in quadrature.

Finally, to give an idea of the impact of the ambiguity on the $\Delta\alpha(m_Z)_h$ correction on the theoretical errors for precision tests of the Standard Model, I report in table 4 a comparison of different sources of error for the most relevant observables. We see that the error from $\Delta\alpha(m_Z)_h$ is expecially important for $\sin^2\theta_W$ (this is the effective one determined from g_V/g_A for $Z\to l^+l^-$ [2]), which is very precisely measured by a combination of asymmetries, and also, to a lesser extent for Γ_Z and ε_3. A plot of the effect of a shift by $\Delta\alpha^{-1} = \pm 0.09$ in the ε_3-ε_1 plane is shown in fig.3. The resulting ambiguity is of the order of (but somewhat smaller than) the LEP-SLC discrepancy.

Table 4: Errors from different sources: Δ^{exp}_{now} is the present experimental error; Δ_∞ is the error at the end of LEP; $\Delta\alpha^{-1}$ is the impact of $\Delta\alpha^{-1} = \pm 0.09$; Δ_{th} is the estimated theoretical error from higher orders; Δm_t is from $\Delta m_t = \pm 12$ GeV; Δm_H is from Δm_H = 60-1000 GeV; $\Delta\alpha_s$ corresponds to $\Delta\alpha_s = \pm 0.006$. The epsilon parameters are defined in ref.2.

	Δ^{exp}_{now}	Δ_∞	$\Delta\alpha^{-1}$	Δ_{th}	Δm_t	Δm_H	$\Delta\alpha_s$
Γ_Z(MeV)	± 3.3	± 2	± 0.7	± 0.8	± 2.6	± 4.5	± 4
σ_h(pb)	81	60	1	4.3	6.4	4	3.3
$R_h.10^3$	35	30	4.3	5	3.2	15	42
$A^l_{FB}.10^4$	13	10	4.2	1.3	7.2	13	0
$\sin^2\theta.10^4$	4	3	2.5	0.8	3.5	8	0.6
m_W(MeV)	160	40	12	9	70	102	13
$R_{bh}.10^4$	19	15	0.1	1	4.4	0.35	0.6
$\varepsilon_1.10^3$	1.6	1.2	0	~0.1			0.5
$\varepsilon_3.10^3$	1.6	1.2	0.6	~0.1			0.3
$\varepsilon_b.10^3$	3.9	3.5	0	~0.1			2.3

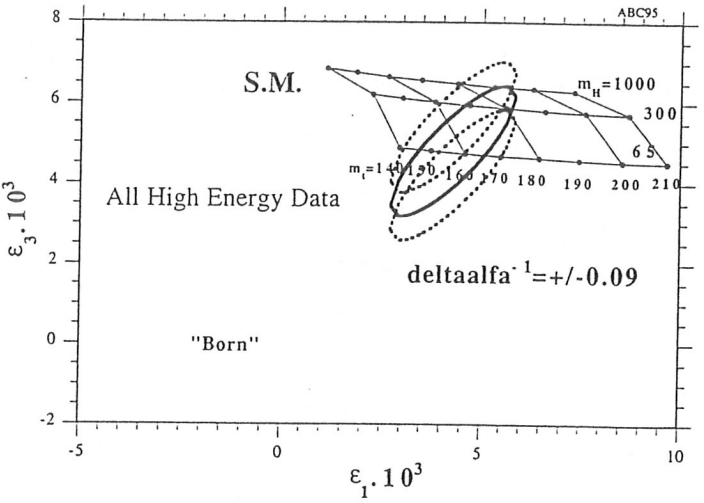

Fig. 3: The impact on the ε_3–ε_1 plane of an uncertainty $\Delta\alpha(m_Z)^{-1} = \pm 0.09$. The solid ellipse is the result of fitting the LEP data using the central value of $\alpha(m_Z)$, while the dotted ellipses correpond to 1σ shifts.

References

[1] See, for example, T. Kinoshita, Proceedings of the 10th Int. Symposium on High Energy Spin physics, Nagoya, Japan, 1992.

[2] See, for example, G. Altarelli, CERN-TH.7319/94;
G. Altarelli, F. Caravaglios and R. Barbieri, Phys. Lett. **B349** (1995) 145;
The LEP Electroweak Working Group, LEPEWWG/95-01, 1995.

[3] J. Bailey et al, Phys. Lett. **B68** (1977) 191;
F.J.M. Farley and E. Picasso, in Quantum Electrodynamics, ed. by T. Kinoshita, World Sci. 1990, p.479.

[4] T. Kinoshita, in Frontiers of High Energy Spin Physics, ed by T. Hasegawa et al, University Academic Press, Tokyo, 1992, p. 9.

[5] V.W. Hughes, in Frontiers of High Energy Spin Physics, ed by T. Hasegawa et al, University Academic Press, Tokyo, 1992, p. 717.

[6] R. Jackiw and S. Weinberg, Phys.Rev. **D5** (1972) 2473;
G. Altarelli, N. Cabibbo and L. Maiani, Phys.Lett. **B40** (1972) 415;
K. Fujikawa, B.W. Lee and A.I. Sanda, Phys.Rev. **D6** (1972) 2923;
I. Bars and M. Yoshimura, Phys.Rev. **D6** (1972) 374;
W.A. Bardeen,R. Gastmans and B.E. Lautrup, Nucl. Phys. **B46** (1972) 319;
T.V. Kukhto et al, Nucl. Phys. **B371** (1992) 3567.

[7] S. Eidelman and F. Jegerlehner, PSI-PR-95-01(1995).

[8] T. Kinoshita,B. Nizic and Y. Okamoto, Phys.Rev. **D31** (1985) 2108.

[9] R.Barbieri and E.Remiddi, in the DAΦNE Physics Handbook, ed by L. Maiani et al, INFN, Frascati, Vol. II, p.301.

[10] M.B.Einhorn, Phys.Rev. **D49** (1993) 1668.

[11] E. de Rafael, Phys.Lett. **B322** (1994) 239.

[12] M. Hayakawa, T. Kinoshita and A.I. Sanda, DPNU-94-21, hep-ph/9503463 (1995).

[13] J. Bijnens, E. Pallante and J. Prades, NORDITA-95/36 N/P (1995).

[14] F. Jegerlehner, Z.Phys. C32 (1986) 195.

[15] B.W. Lynn, G. Penso and C. Verzegnassi, Phys.Rev. **D35** (1987) 42.

[16] H. Burkhardt et al, Z.Phys. C42 (1989) 497.

[17] F. Jegerlehner, Progr. Part. Nucl. Phys. 27(1991)32.

[18] M.L. Swartz, Preprint SLAC-PUB-6710, 1994.

[19] M.L. Swartz, quoted by M.Peskyn at SUSY '95, Paris, May 1995.

[20] A.D. Martin and D. Zeppenfeld, Preprint MAD/PH/855, 1994.

[21] R.D. Nevzorov and A.V. Novikov, Preprint FTUV/94-27, 1994, Preprint MAD/PH /855, 1994.

[22] N.V. Krasnikov, Mod. Phys. Lett. **A9** (1994) 2825.

[23] H. Burkhardt and B. Pietrzyk, Preprint LAPP-EXP-95.05, 1995.

[24] G. D'Agostini, private communication.

[25] D. Haidt, in Precision Tests of the Standard Electroweak Model, ed. by P. Langacker, World. Sci. 1993.

EXPERIMENTAL SEARCH FOR ANTIMATTER IN THE UNIVERSE

Piero Spillantini
Dipartimento di Fisica dell'Università di Firenze, and Sezione INFN
Largo Fermi 2, I–50125 Firenze (Italy)

(No written contribution arrived)

MATTER LIFETIME

Carlo Rubbia
CERN – European Organization for Nuclear Reserch
CH–1211 Genèva (Switzerland)

(No written contribution arrived)

HADRONIC PHYSICS

PARALLEL SESSION

E.P. Solodov	Recent Results of the ϕ–Meson Study with CMD–2 at VEPP–2M and Relevance to Future CP, CPT Φ –Factory Studies	541
V.N. Ivanchenko	Review of Radiative Decays Study	559
G.V. Fedotovich	Measurement of the $e^+e^- \to \pi^+\pi^-$ Coss Section in the Energy Range Between ρ and Φ Meson	571
V. Fliaguine	Results in K Decays from Serpukhov PS	583
S. Dubnicka	An Improved Evaluation of Hadronic Contributions to the Anomalous Magnetic moment of Charged Leptons	593
J. Stern	How to see the Chiral Structure of QCD Vacuum in Low Energy π–π Scattering	609
M. Finkemeier	Radiative Corrections to π_{l2} and K_{l2}	623
P. Kokkas	Measuremet of the Difference of the K^o–$\overline{K}^o$ Forward Scattering Amplitudes in Carbon at Low Momentum with the CPLEAR Detector	635
N. Achasov	Do the Proofs of Appreciable $\varphi\omega$ Mixing Exist?	646

RECENT RESULTS OF THE ϕ-MESON STUDY WITH CMD-2 AT VEPP-2M AND RELEVANCE TO FUTURE CP,CPT ϕ FACTORY STUDIES

E. P. Solodov*

Budker Institute of Nuclear Physics, Novosibirsk, 630090, Russia

ABSTRACT

The general purpose detector CMD-2 is taking data at the e^+e^- collider VEPP-2M at Novosibirsk, with the luminosity $\approx 5. \times 10^{30} cm^{-2}s^{-1}$. Data from $\approx 1500 nb^{-1}$ of integrated luminosity around 1.02 GeV have been collected (about 1.7×10^6 of ϕ's were produced) and preliminary analyzed. We present progress on study of ϕ-meson and $K_S K_L$ system:

a) the measurement of the ϕ-meson parameters;

b) the search for the rare decays of ϕ. The new upper limits $\mathrm{B}(\phi \to \eta'\gamma) < 2.4 \times 10^{-4}$, $\mathrm{B}(\phi \to \pi^+\pi^-\pi^+\pi^-) < 1.0 \times 10^{-4}$ and $B(\phi \to f_0\gamma) < 8 \times 10^{-4}$ have been obtained;

c) the study of the K_L interactions in the CsI calorimeter.

d) with the help of 32,340 tagged K_S the semi-rare decay of $K_S \to \pi^+\pi^-\gamma$ has been observed with a branching ratio of $(1.82 \pm 0.49) \times 10^{-3}$;

e) the selection of events with $K_S K_L$ coupled decays and interactions. The regeneration cross section of the low momenta K_L was found to be $\sigma_{reg}^{Be} = 63 \pm 19$ mb.

[1]CMD-2 collaboration: Akhmetshin R.R., Aksenov G.A., Anashkin E.V., Astakhov V.A., Aulchenko V.M., Baibusinov B.O., Banzarov V.S., Barkov L.M., Baru S.E., Bondar A.E., Chernyak D.V., Danilov V.V., Eidelman S.I., Fedotovitch G.V., Gabyshev N.I., Grebeniuk A.A., Grigoriev D.N., Ivanov P.M., Khazin B.I., Koop I.A., Kuzmin A.S., Logashenko.I.B., Lysenko A.P., Maksimov A.V., Merzlyakov Yu.I., Monitch V.A., Nesterenko I.N., Okhapkin V.S., Perevedentsev E.A., Polunin A.A., Popkov E.V., Pozdeev E.G., Ptitzyn V.I., Purlats T.A., Redin S.I., Root N.I., Ruban A.A., Ryskulov N.M., Shatunov Yu.M., Sher A.E., Shubin M.A., Shwartz B.A., Sidorov V.A., Skrinsky A.N., Smakhtin V.P., Snopkov I.G., Solodov E.P., Sukhanov A.I., Titov V.M., Yudin Yu.V., Zavarzin V.G., Zverev S.G. - BINP,Novosibirsk, 630090, Russia; Brown D.H., Miller J.P., Roberts B.L., Worstell W.A.- Boston University; Thompson J.A., Valine C.M.- University of Pittsburgh; Cushman P.B.- University of Minnesota; Dhawan S.K., Hughes V.W.-Yale University.

1 Introduction

As it was realized at the very early steps of the ϕ-meson studies at the colliding beam machines, $K_S K_L$ pairs ($\approx 34\%$ of all ϕ decays) may be used as a new source for observing CP and CPT violation. These suggestions, including studies of quantum mechanical correlations, were discussed in papers [1], [2] when an electron-positron collider at Novosibirsk VEPP-2M with luminosity $\approx 5 \times 10^{30} cm^{-2} s^{-1}$, was under construction. The coupled decays of the $K_S K_L$ mesons will allow demonstration of the quantum mechanical correlations of the two particle decays (Einstein-Podolosky-Rosen paradox) [3].

The idea of constructing a more intensive source of ϕ mesons has been discussed by many authors [4], [5]. The flux of events at these so-called "ϕ-factories", now under construction [6], [7], will provide an opportunity to make new precise measurements of a possible direct component in the decay of the $K_L \to \pi^+\pi^-, \pi^0\pi^0$ (ϵ'/ϵ), as well as the observation of the CP-violating three pion decays of the K_S for the first time. The study of the oscillations in the joint decay distributions could give an information about real and imaginary parts of any CPT-violating amplitude.

At the VEPP-2M collider at Novosibirsk, which could be consider as a pre ϕ-factory. With the CMD-2 detector we have been proceeding step by step to prepare for work at the ϕ-factory which is under construction here. Studies of upgraded detectors and accelerators are in progress, including an intermediate $\approx 10^{32}$ luminosity collider for investigating the idea of the round beams, an important ingredient in the planned Novosibirsk ϕ-factory project [8], [9].

With the CMD-2 detector the neutral kaons from ϕ decays are under study and the coupled $K_S K_L$ decays have been observed for the first time. The attempt to select the $K_L \to \pi^+\pi^-$ stressed again problems of the semileptonic decay mode background as well as a high level of neutral kaon nuclear interactions including a regeneration of K_L into K_S. The opening of this kinematic region for the neutral kaon interactions study has been an additional argument for the ϕ factories construction, and we anticipate that the results obtained from the data now in hand will be important in planning ϕ-factory detectors and physics strategies.

A possible problem with a measurement of ϵ'/ϵ at the level of 10^{-4} - 10^{-5} would be an admixture of C=+1 into the final state, giving a component of $K_S K_S$ instead of the desired $K_S K_L$. Although efficient experimental cuts can reduce the effects of such an admixture [10, 11], a component as large as 5×10^{-5} of a C=+1 state would give a dominating contribution to the uncertainty of ϵ'/ϵ at the level of the planned ϕ-factory experiments [11]. The contamination from such a C-even K-$\overline{K}$ mode has been estimated by several authors giving generally lower values [4, 12, 13, 14], but there are no experiments confirming these results.

The decay of the ϕ to $f_0\ \gamma$ with f_0 decaying to two kaons is too small to be seen at the VEPP-2M collider and we hope to study the decay of ϕ to $f_0\ \gamma$ with a subsequent decay of the f_0 to two charged pions [15]. The two charged pion decay mode can be related to the two kaon decay and a limit on the C-even two kaon final state may be found. Estimates for the branching ratio of $\phi \to f_0\gamma$ range from a very small to as high as 2.5×10^{-4} [12, 13, 14].

The study of the f_0 is interesting by itself. The 20% decay probability into a two kaon final state seems puzzlingly high incase if f_0 is a member of the strangeness-0 and isospin-0 meson nonet. Various explanations for this large coupling to kaons have been advanced [12, 13, 14, 16], including the idea that f_0 is really made of four quarks, with a "hidden strangeness" component: $(f_0 = s\,\bar{s}(u\,\bar{u} + d\,\bar{d})/\sqrt{2})$, or that it may be a K-$\overline{K}$ molecule. A limit from VEPP-2M will help to distinguish between these different possibilities.

With expected high luminosity at the ϕ-factories the rare decay modes of ϕ can be measured with high accuracy. For example, a measurement of the $B(\phi \to \eta'\gamma)$ would give an important information about quark structure of light mesons and possible contributions from gluonium states (if any). Our new data obtained with the present statistic already improve upper limit for this process, as well as for $\phi \to \pi^+\pi^-\pi^+\pi^-$ and $\phi \to f_0\gamma$.

The analisys of the CMD-2 data is in progress and we expect new results in the ϕ-meson study.

2 The CMD-2 Detector And Data Sample

The CMD-2 detector has been described in more details elswhere [2, 17]. The CsI barrel calorimeter with 6x6x15 cm crystal size is placed outside a 0.4 r.l. superconducting solenoid with a 1 Tesla azimuthally symmetric magnetic field. The endcap calorimeter is made of 2.5 x 2.5 x 15 cm BGO crystals and was not installed for the data presented here. The drift chamber inside the solenoid has about 250 μ resolution transverse to the beam and 0.5-0.6 cm longitudinally.

The collected sample of the Bhabha events was used for the calibration and determination of the reconstruction efficiency in the drift chamber and in the calorimeter. A momentum resolution of 6-8% for 500 MeV/c charged particles, and energy resolution of about 10% for gammas in the CsI calorimeter have been obtained.

The luminosity integral collected in 1992-1993 at ϕ was mostly used for the detector study and software development. Not all detector systems were running properly and data peresented here are still preliminary – better detector understanding and better reconstruction programms available now will give results with less

systematic errors.

About 7.2×10^7 triggers were recorded. The total luminosity integral, determined by selection of Bhabha events, was found to be 1500 nb^{-1}.

The largest part of the integrated luminosity ($\approx 1200nb^{-1}$ in the 14 energy points around ϕ mass) have been collected during the 1993 summer runs and was used for study of rare decay modes of ϕ, coupled decays in the $K_S K_L$ sytem and nuclear interactions of neutral kaons.

3 ϕ-meson parameters

The main branching ratios of the ϕ have been measured using $\approx 300nb^{-1}$ of integrated luminosity, collected in 1992. It was the first time, when four major decay modes of ϕ were measured in one experiment. The events selection and other details may be found in paper [18]. The following results were obtained:

$$
\begin{aligned}
&m_\phi = 1019.380 \pm 0.034 \pm 0.048 \text{ MeV}, \\
&\Gamma_{tot} = 4.409 \pm 0.086 \pm 0.020 \text{ MeV}, \\
&\sigma(\phi \to K^+K^-) = 1993 \pm 65 \pm 82 \text{ nb}, \\
&\sigma(\phi \to K_S K_L) = 1360 \pm 25 \pm 49 \text{ nb}, \\
&\sigma(\phi \to 3\pi) = 656 \pm 24 \pm 30 \text{ nb}, \\
&\sigma(\phi \to \eta\gamma) = 47.9 \pm 3.5 \pm 3.2 \text{ nb}, \\
&\delta_{\omega-\phi} = (147 \pm 16)^\circ .
\end{aligned}
$$

The first error represents the statistical uncertainty and the second one the systematic uncertainty. The relative phase of $\omega - \phi$ mixing in three pion channel is in a good agreement with the most precise measerement presented in [22] $\delta_\phi = (155 \pm 15)^\circ$. The experimental cross-sections of the ϕ production in the different modes, together with fit functions are shown in Figure 1.

All the major decay modes were simultaneously measured in one experiment and therefore the branching ratios can be obtained as ratios of integrals over excitation curves independently of the width of the ϕ and the uncertainties due to the luminosity measurements:

$$
\begin{aligned}
&\mathrm{B}(\phi \to K^+K^-) = 49.1 \pm 1.2 \ \%, \\
&\mathrm{B}(\phi \to K_S K_L) = 33.5 \pm 1.0 \ \%, \\
&\mathrm{B}(\phi \to 3\pi) = 16.2 \pm 0.8 \ \%, \\
&\mathrm{B}(\phi \to \eta\gamma) = 1.18 \pm 0.11 \ \% .
\end{aligned}
$$

The electron width of the ϕ and its branching ratio to e^+e^- can also be calculated independently and were found to be

$\Gamma_{ee} = 1.27 \pm 0.05$ keV,
$B(\phi \rightarrow ee) = (2.87 \pm 0.09) \times 10^{-4}$.

All results are consistent with the Particle Data Group values [23].

Here we note, that in all parameters systematic errors dominate and using all available statistic will improve these results only after systematic errors study and better detector understanding.

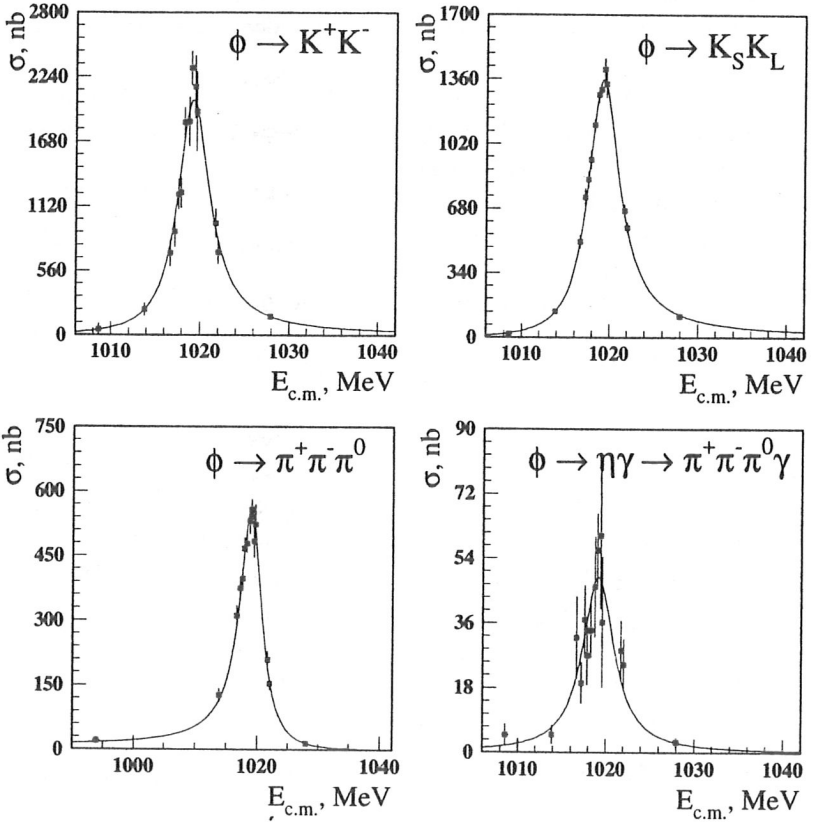

Figure 1: The excitation curves for ϕ-meson in different channels.

4 Study of $\phi \to \eta\gamma$ and Search for $\eta'\gamma$.

The decay of $\phi \to \eta\gamma$ was previosly observed in neutral modes ($\eta \to \gamma\gamma$, $\eta \to 3\pi^0$) only. Detector CMD-2 gives the possibility to study $\phi \to \eta\gamma$ decay in the channel with charged particles, when η decays into $\pi^+\pi^-\pi^0$. So, after $\pi^0 \to \gamma\gamma$ decay, the final state consists of two charged pions and three photons. Two photons in the final state are from π^0, the third one has the maximum energy of all three - 362 MeV at the ϕ-meson peak.

We select $\eta\gamma$ events using the information about momenta and angles from the Drift Chamber for both charged particles and about angle from CsI calorimeter for primary photon under suggestion that other photons are from π^0. The reconstructed invariant mass of 3 pions $M_{\pi^+\pi^-\pi^0}$ is the basic parameter we use to study the decay $\phi \to \eta\gamma$ and the distribution over it should have a peak around M_η = 547.45 MeV.

The distribution over $M_{\pi^+\pi^-\pi^0}$ for all 1993 ϕ-meson data after some simple cuts is presented in Figure 2. These distributions were used to get the numbers of $\eta\gamma$ events for the different beam energies.

The calculated cross-section $\sigma_{e^+e^-\to\phi\to\eta\gamma}$ with fit function is presented in Figure 2. Using the electron width of ϕ from [23] the $Br(\phi \to \eta\gamma)$ was found to be:

$$Br(\phi \to \eta\gamma) = (1.12 \pm 0.06 \pm 0.15)\%$$

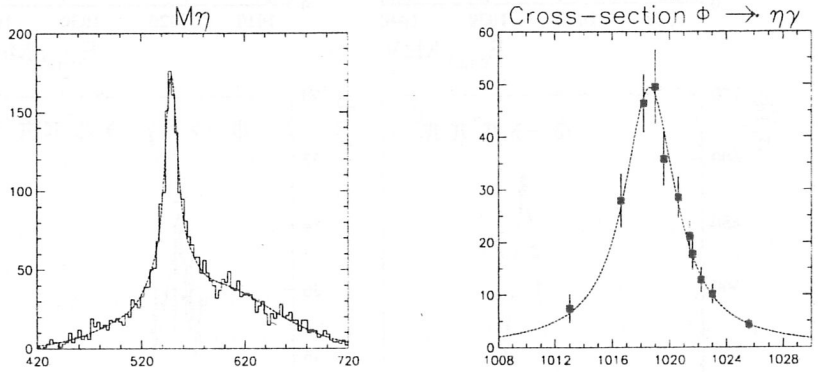

Figure 2: The study of $\phi \to \eta\gamma$: invariant mass $M_{\pi^+\pi^-\pi^0}$; $\phi \to \eta\gamma$ cross-section;

This result is preliminary because the work with efficiency determination is not finished and we hope significally decrease the systematic error.

The decay $\phi \to \eta'\gamma$ was searched in the mode, when η' decays into $\pi^+\pi^-\eta$ and $\eta \to \gamma\gamma$. So, both in $\eta\gamma$ and in $\eta'\gamma$ the final state there are 2 charged particles and

3 photons. The events with all these particles detected were used for the constrained fit.

The scatter plot of the invariant masses for two soft photons M_{23} versus the hardest photon energy ω_1 for the experimental data is presented in the Figure 3.

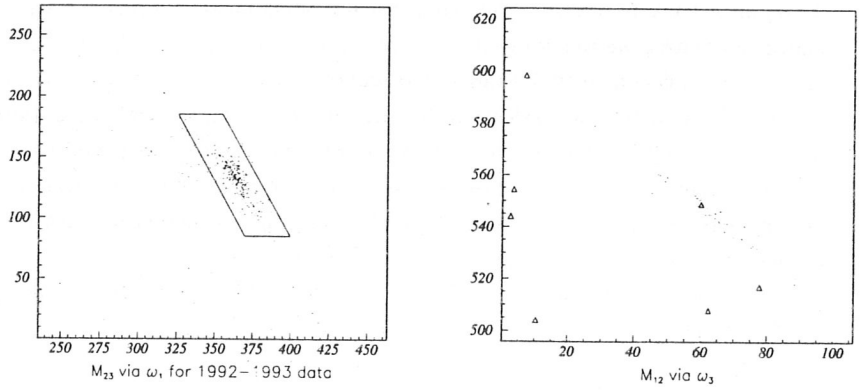

Figure 3: The search for $\phi \to \eta'\gamma$ (1993 data): Invariant mass M_{23} vs. ω_1 after constrained fit. Box shows $\eta\gamma$ cut; Invariant mass M_{12} vs. ω_3 after constrained fit. Dots are simulation, triangles - experiment

The decay into $\eta\gamma$ is the basic background for $\eta'\gamma$. Selecting 481 $\eta\gamma$ events at this plot one can make anti-$\eta\gamma$ cut.

Using this cut the scatter plot of the invariant masses for two hardest photons M_{12} versus the weakest photon energy ω_3 was studied. For $\eta'\gamma$ events M_{12} should be around η mass 547.5 MeV, while ω_3 is monochromatic 60 MeV photon. The Figure 3 presents the result of 1992–1993 data together with simulation of $\phi \to \eta'\gamma$. We have 1 candidate to $\eta'\gamma$ event with 1 event as estimated background. Using for the 90% C.L. upper limit $N_{\eta'\gamma} < 3$ and the ratio:

$$\frac{Br(\phi\to\eta'\gamma)}{Br(\phi\to\eta\gamma)} = \frac{N_{\eta'\gamma}}{N_{\eta\gamma}} \cdot \frac{Br(\eta\to\pi^+\pi^-\pi^0)}{Br(\eta'\to\pi^+\pi^-\eta)} \cdot \frac{Br(\pi^0\to\gamma\gamma)}{Br(\eta\to\gamma\gamma)} \cdot \frac{\varepsilon_{\eta\gamma}}{\varepsilon_{\eta'\gamma}},$$

with the efficiencies obtained from the simulation, $\varepsilon_{\eta\gamma} = 14.4\%$ and $\varepsilon_{\eta'\gamma} = 6.4\%$, the following result has been obtained:

$$Br(\phi \to \eta'\gamma) < 2.4 \cdot 10^{-4}.$$

5 Search for $\phi \to \pi^+\pi^-\pi^+\pi^-$

A sample of 3- and 4-tracks events was used for search for the process $\phi \to \pi^+\pi^-\pi^+\pi^-$. In this sample tracks have to originate from the beam-beam interaction point within 0.5 cm in r-ϕ plane and have at least 9 hits in the Drift Chamber. Total charge have to be ± 1 for 3-tracks events and 0 for 4-tracks events. To suppress background from the two-particle production and cosmic rays with some additional tracks, we reject events with at least two collinear tracks (mutual angle of any pair should be 0.16-3.0 rad in r-ϕ plane).

Even with these selection criteria we have a high background from the main channels of ϕ decaing into 3-tracks events. So, in the search for the process $\phi \to \pi^+\pi^-\pi^+\pi^-$ only 4-tracks events were used. The ratio of 3- and 4-tracks events at the energy points outside ϕ-meson region were used (along with simulation) for evaluation of a detection efficiency which was found to be 0.033 ± 0.012.

The scatter plot E_{tot} vs.P_{tot} for the selected 4-tracks events is shown on the Figure 4a.

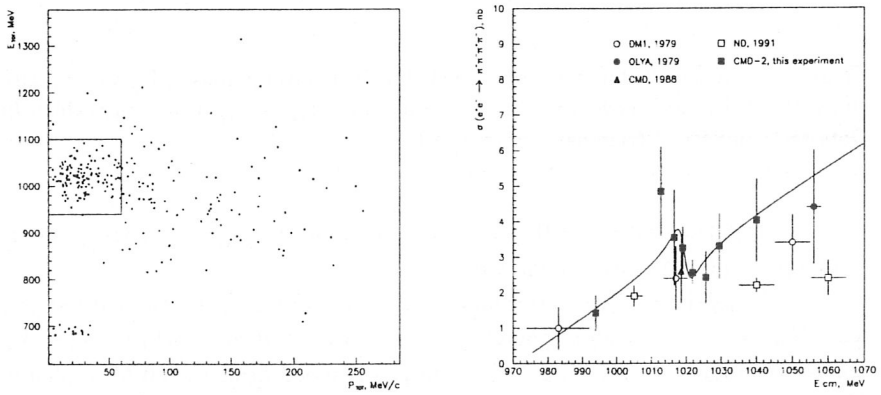

Figure 4: The search for $\phi \to \pi^+\pi^-\pi^+\pi^-$: E_{tot}vs.P_{tot} for 4 - track candidates; cross-section $e^+e^- \to \pi^+\pi^-\pi^+\pi^-$.

Here P_{tot} is the magnitude of the total momentum of 4 charged particles and E_{tot} is their total energy, assuming that all particles are pions. To extract number of events of the process $e^+e^- \to \pi^+\pi^-\pi^+\pi^-$ we apply a simple cut, shown on the Figure 4 by box.

The cross-section vs. energy for the process $e^+e^- \to \pi^+\pi^-\pi^+\pi^-$ is shown on the Figure 4. Only statistical errors are shown. A 4-parameters function which

contains linear background, amplitude and phase of the process $\phi \to \pi^+\pi^-\pi^+\pi^-$ was used for the fitting . Result of the fit is shown on the plot by a smooth line. Using this fit and the uncertanty in the efficiency, one can get

$$\mathrm{Br}(\phi \to \pi^+\pi^-\pi^+\pi^-) < 1. \cdot 10^{-4} \text{ for C.L.=90\%}.$$

This preliminary result is about 9 times lower then present upper limit for this process [23]. We plan to perform more simulation to improve both efficiency evaluation and data selection. Also we plan to evaluate and apply radiative corrections which are an order of 5%.

6 Search for $\phi \to f_0\gamma$

In order to extract the resonant contribution associated with the ϕ, two sets of data were used. Energy points at $E_{c.m.}$ from 1016 to 1023.2 MeV with integrated luminosity $660nb^{-1}$ were used for the ϕ region, and points at $E_{c.m.}$ = 996, 1013, 1026, 1030, 1040 MeV with integrated luminosity $440nb^{-1}$ were used for a background estimation (the "non-ϕ" region). The event candidates were selected by a requirement of only two charged tracks and only one photon with energy greater than 20 MeV in the detector. Total energy deposition was required to be less than 600 MeV, average momentum of two charged tracks to be higher than 240 MeV and the radial distance of the found vertex from the interaction region less than 0.15 cm. These cuts removed Bhabha events and charged and neutral kaons from ϕ decays. The requirement that the Z-coordinate of the vertex be within 10 cm at the detector center reduces cosmic ray background by a factorof two.

Each charged track required to have a corresponding cluster in the calorimeter. This requirement reduced the number of pions by about 14%, but avoided nuclear interactions of the pions before the calorimeter with clusters in the wrong place. However split clusters may still be presented.

The main visible background for the studied process is $\phi \to \pi^+\pi^-\pi^0$ decay, when one of the photons from π^0 escapes detection. To reduce this background a constrained fit was used. This fit required total energy and momentum conservation within detector resolutions for the three body decay. For χ^2/d.f. less than 3 only events with these requirements survived. But a three pion background was still presented, when one of the gammas from the π^0 had a very low energy and the event looked like a three body decay. Figure 5 shows the spectrum of the single gammas and the squared missing mass of two charged tracks (taken as pions) vs. detected gamma energy.

In the "ϕ region" data set a broad peak at 200-300 MeV in gamma spec-

trum, also seen as a broad distribution on the scatter plot at $M^2_{\pi^0}$, represents background from the three pion decays. Points concentrated at zero mass and low energy represent events with one gamma. To reduce the three pion and collinear events background, the cuts -15000 $\leq M^2_{inv} \leq$ 15000, $E_\gamma \leq$ 140 MeV and $\Delta\phi \geq 0.03$ rad. were applied. The sample of events, selected with above cuts, still contained about 30% of $e^+e^- \to \mu^+\mu^-\gamma$ events.

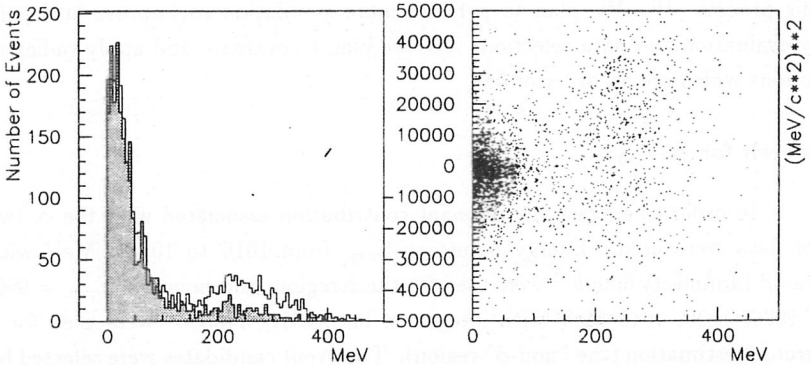

Figure 5: Search for $\phi \to f_0\gamma$: Single gamma spectra. The shaded histogram represents the "not ϕ" region; The squared missing mass vs. photon energy.

The visible cross section of the processes $e^+e^- \to \mu^+\mu^-\gamma + \pi^+\pi^-\gamma$ versus energy is presented in Figure 6a. With the cuts listed above the detection efficiency of these processes, obtained by simulation, was found to be 0.17, leaving 1.7 nb of the visible cross section. The observed 20% difference from average experimental cross section is due to the losses of the the low energy gammas, not correctly described by a simulation. A line shows a theoretical prediction of the cross section including influence of ϕ into photon propagator (vacuum polarization) and f_0 production, according to Achasov four quark model. The total branching ratio of $\phi \to \pi^+\pi^-\gamma$ could be extracted from this interference picture.

The signal from the decay of the $\phi \to f_0\gamma$ should be seen as a 30-40 MeV width structure at 45 MeV in the difference gamma spectra from "ϕ" region and "non-ϕ" region shown in Figure 6b together with the theoretical prediction calculated by Achasov model for the four quark state. With the present statistic only upper limit can be set.

Taking into account the effective number of ϕ's 1.1×10^6 and all inefficiencies described above, the upper limit was found to be

$$B(\phi \to f_0\gamma) \leq 8.0 \times 10^{-4} \; at \; C.L. = 90\%.$$

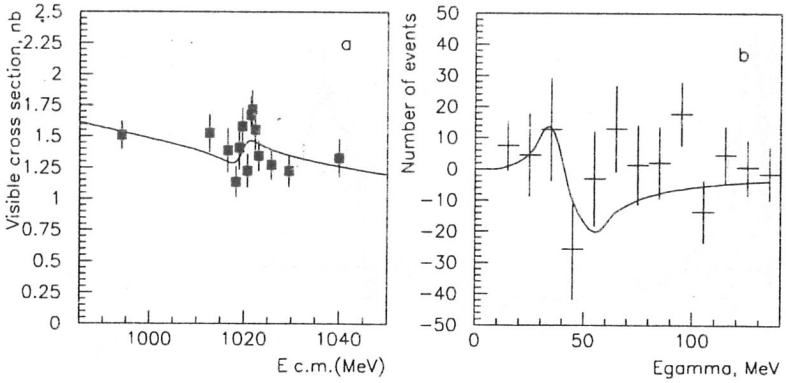

Figure 6: $\phi \to f_0\gamma$ search: a. Visible cross section for $e^+e^- \to \pi^+\pi^-\gamma + \mu^+\mu^-\gamma$ events; b. Normalized difference in photon spectra. A line is a prediction of the four quark model with distructive interference and $B(\phi \to f_0\gamma) = 2.5 \times 10^{-4}$.

7 The K_L nuclear interaction as a tag for K_S rare decay study

K_L candidates are selected by looking at calorimeter clusters opposite a 2-track vertex with an effective mass consistent with that of the kaon. Figure 7a shows the space angle between the predicted missing momentum direction of K_L and the cluster in the calorimeter. Figure 7b shows the energy deposition of the presumed K_L, Figure 7c shows the number of hit crystals, and Figure 7d shows the probability for a K_L to interact, corrected to interaction in the surrounding materials. The clusters from K_L are very broad and in 25 % cases are splitting to 2-4. Simulated distributions are shown shaded. Comparison of the data with the GEANT (with GHEISHA package) simulation shows definite disagreement. The difference is due to compleately incorrect cross sections for the low energy kaons, used by GHEISHA package.

Once the properties of the K_L clusters are understood, one can use the K_L cluster as a "tag" for K_S decays. Figures 8a shows the invariant mass distributions for the events with two charged tracks opposite to K_L clusters.

The constrained fit applied to the decay $K_S \to \pi^+\pi^-$ extracted 32340 events and they were used for a normalization. The rest is shown in Figure 8a by shaded histogramm. In order to search for the $\pi^+\pi^-\gamma$ mode, the sample of events with an acollinearity angle less than 2.4 radians, $M_{inv} \leq 450 MeV/c^2$, and $E_\gamma \geq 50$ MeV is taken.

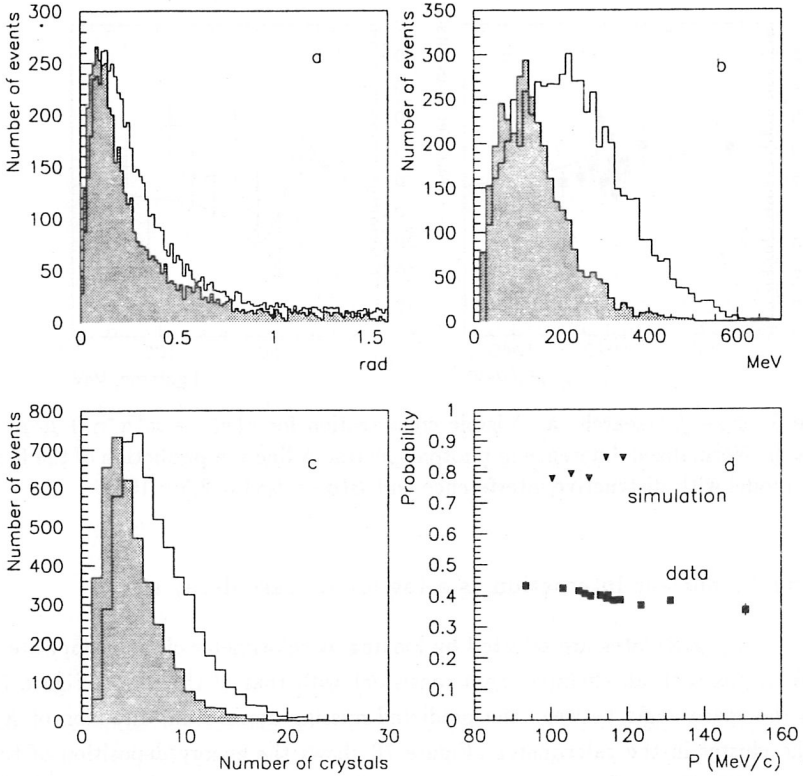

Figure 7: K_L interactions (dashed hists for simulation): a. Space angle between calorimeter cluster and P_{mis}; b. Energy deposition of K_L clusters; c. Number of hit crystals (dashed hists for simulation; d. Probability of K_L interactions in CsI.

Figure 8b shows the missing mass distribution for the two-track vertex, taking the K_S direction from the observed cluster, and the K_S momentum from the known center of mass energy, and assuming $\phi \to K_S K_L$. The 34.5 ± 8.0 events at zero mass, corresponding to the decay $K_S \to \pi^+\pi^-\gamma$ were found after fitting and background subtraction. The simulated ratio of the acceptances for $K_S \to \pi^+\pi^-$ and $K_S \to \pi^+\pi^-\gamma$ was found to be 2.49 ± 0.30, giving a branching ratio $\mathrm{Br}(K_S \to \pi^+\pi^-\gamma) = (1.82 \pm 0.49) \times 10^{-3}$.

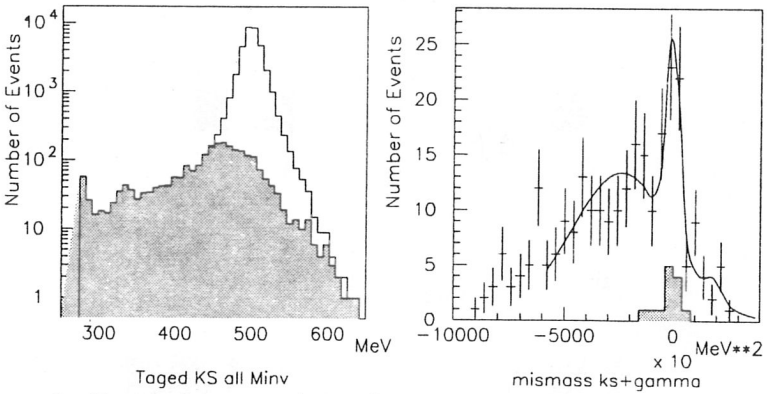

Figure 8: $K_S \to \pi^+\pi^-\gamma$ search: a. Invariant mass for vertecies oposite clusters; Events without K_S decaing to two pions are shown shaded; b. Missing mass in the frame of K_S. Events with real gamma found are shown shaded

8 The K_SK_L coupled decays study

The event candidates were selected from a sample in which two vertices, each of two opposite charged tracks, were seen. The example of this kind of events is shown in Figure 9.

Figure 10a,b show the invariant mass scatterplots of the two charged tracks, assuming that they are pions, vs. missing momentum for the closest to the beam vertex and to the other one. The concentration corresponding to K_S's dominates in the plot 10a and seen in 10b. A two dimensional cuts $470 < M_{inv} < 525$ and $90 < P_{mis} < 130$ with additional requirement to have another reconstructed vertex in the P_{mis} direction within detector resolution, select K_S's in any of the vertex, remaining K_L's in the other. Figure 10c,d show a characteristic M_{inv} and P_{mis} broad distributions, expected from the main 3-body K_L decays in good agreement with the simulation.

Figure 11a shows the distance from the point of origin to the decay point for selected K_S's. The exponential lifelength is seen with correct value 0.58 ± 0.03 cm with vertex position resolution 0.23 cm.

Figure 11b shows the vertex radius for the K_L decays. A loss of efficiency for these events is seen, since the K_L events should be approximately flat in this spatial region corresponding to the very early part of the K_L lifetime. A significant peak with 59 ± 16 events is also seen and is interpreted as the nuclear interactions of

K_L at the 0.077 cm Be vacuum beam pipe.

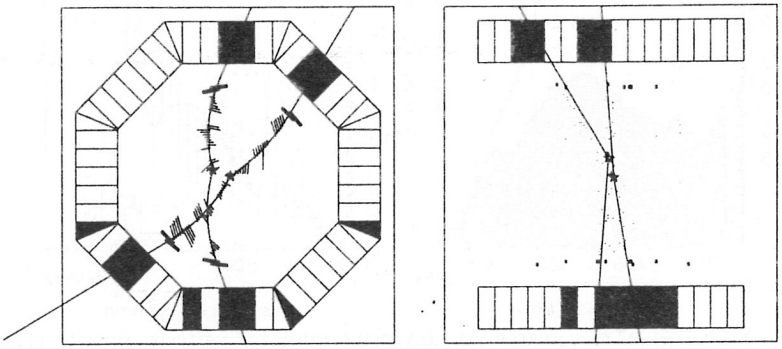

Figure 9: $\phi \rightarrow K_S K_L$ event with coupled decay.

The histogram in Figure 11d shows the events consistent with the two pion decay at the K_L vertices, when additional cut in M_{inv} was applied. With our resolution the suppression of the semileptonic K_L decays by a factor of 20 was expected, and these events dominated at all radii (only 2 CP violating K_L decays were expected with present sample), except beampipe, where 28±6 extra events survived. We interprete these events as regeneration of K_L into K_S.

The rest of the peak events may be explained by Σ and Λ production, when two pions are detected and recoil nucleon is unseen. With the applied M_{inv} cut about 10% of these events may be interpreted as pure two pions decay and should be extracted from the candidates for regenerated events.

Figure 11c shows the projected angle difference between the missing momentum derection and a line, connected K_L vertex with the beam position, for the events concentrated around the beam pipe. Dots with errors show expected distribution for semileptonic decays of K_L, normalized for expected number of these events. A peak at zero angle is seen, supporting expectation about regeneration of K_L into K_S.

Taking into account 10% corrections for DC mylar window and 10% from nuclear interaction processes background, the regeneration cross section is found to be $\sigma_{reg}^{Be} = 63 \pm 19$ mb. A visible nuclear interaction cross section (excluding regeneration) is found to be $\sigma_{nucl}^{Be} = 60 \pm 18$ mb.

The obtained regeneration cross section is in agreement with the calculations, performed in Frascati [24] that gave a value 40 mb for 114 MeV/c long lived kaons.

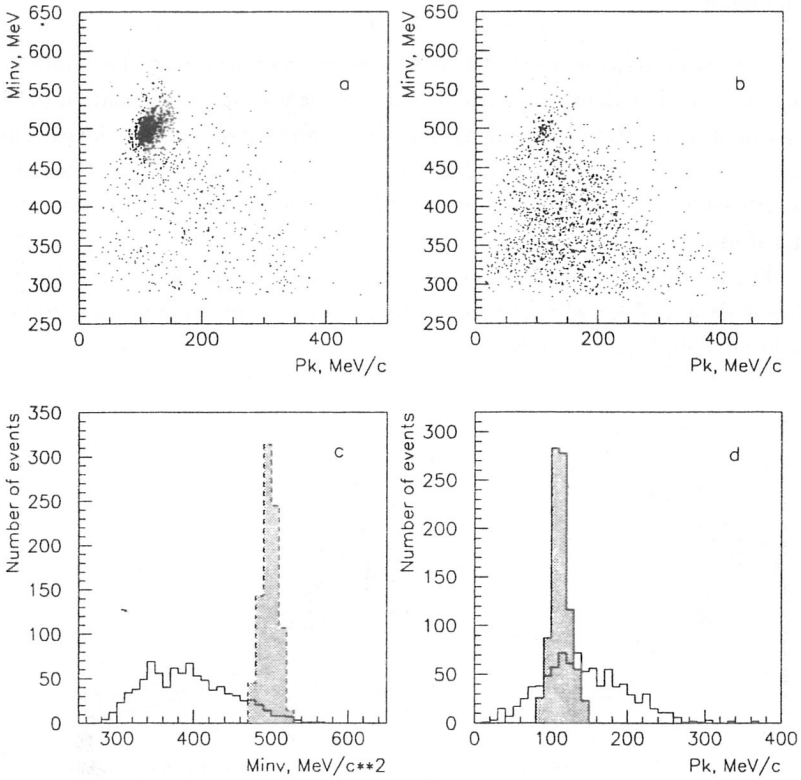

Figure 10: $K_S K_L$ coupled decays study: Invariant mass vs. missing momentum for 1-st (a) and 2-nd (b) vertex; c. Invariant mass for K_L and K_S (shaded) after K_S selection; d. Missing momentum for K_L and K_S (shaded) after K_S selection;

For the total nuclear interaction cross section of neutral kaons one can obtain a value 549±165 mbn, taking into account the ratio 0.21 of hyperon production to all other inelastic processes [25] and 0.52 as ratio of inelastic to elastic cross section [24]. It is also in good agreement with experimental data for higher momenta and calculation, done in [24].

9 Conclusion

The next stage in this work is to process the data with the improved detector resolution and to use all available particle identification information (drift chamber amplitudes, calorimeter energy deposition, and muon detector hits). The detector reconstruction efficiency is under intensive study and will reduce systematic errors in all results presented in this paper. Some other rare decay processes of ϕ are under study.

The presence of a regeneration and nuclear interaction background for the CP-violating decays of K_L will pose an additional background for ϕ factory studies and should be under carefull study.

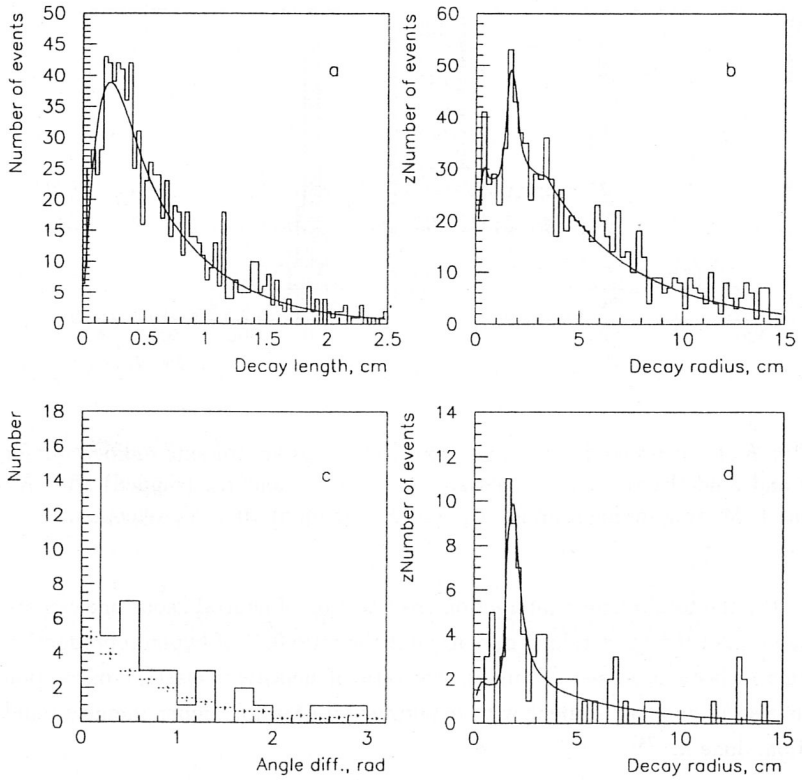

Figure 11: $K_S K_L$ coupled decays study: a. Decay length for K_Ss; b. Decay radius for K_Ls; c. Difference in angle of P_{mis} and vertex-beam line. d. Decay radius for K_Ls after M_{inv} cut; Crosses are from K_L semileptonic decays.

The data taking at ϕ is also planed with at least 10 times more integrated luminosity before reconstruction of VEPP-2M for round beam operation, what promises additional factor of 10 in data sample.

10 Acknowledgements

One of the authors (E.P.Solodov) should thank R. Baldini and A. Michetti for usefull discussion on nuclear interaction study and cooperation in this field.

This work is supported in part by the US Departament of Energy, US National Science Foundation and the International Science Foundation under the grant RPT000.

References

1. V.N.Bayer, ZETFP **17** (1973) 446.

2. G.A.Aksenov et al., Preprint BudkerINP 85-118, Novosibirsk, 1985.

3. P. Eberhard, Contribution to the ϕ Factory Workshop at UCLA, April, 1990.; G.Ghirardi, Proceedings of the Workshop on Physics and Detectors for DAΦNE, Frascati, April, 1991, p.261.

4. J.L. Rosner, I. Dunietz, J. Hauser, Phys. Rev. **D35** (1987) 2166.

5. A partial list of other major contributions includes: A.N.Skrinsky *et al.*, "Novosibirsk ϕ-factory project", F.J. Botella, J. Bernabeu and J. Roldan -Blois CP Violation Conference, FTUV/89-35,IFIC/89-11, May 1989.; G. Barbiellini and C. Santoni, CERN-EP/89-8 and CERN-PPE/90-124; J.A. Thompson, University of Pittsburgh preprint PITT-90-09; contributions by J.A. Thompson, D. Cline, and by C. Buchanan and others to the ϕ Factory Workshop at UCLA, April, 1990.; Y. Fukushima, *et al*,.KEK Preprint 89-159; summary talks by P. Franzini and M. Piccolo and others at the Workshop on Physics and Detectors for DAΦNE, Frascati, April, 1991.

6. A.N.Skrinsky, Proceedings of the Workshop on Physics and Detectors for DAΦNE, Frascati, April, 1991, p. 67.

7. G. Vignola, Proceedings of the Workshop on Physics and Detectors for DAΦNE, Frascati, April, 1991, p. 11.

8. A.N.Filippov et al., Proceedings of the XVth International Conference on High Energy Accelerators, Hamburg, Germany, 1991, World Scientific, V. II, p. 1145.

9. S. Eidelman, E. Solodov, and J. Thompson, Nuclear Physics B (Proceedings Supplement) **24A** (1991) 174.

10. D.Cocolicchio et al., Phys. Lett. **B238** (1990) p.417.

11. P. Franzini, Proceedings of the Workshop on Physics and Detectors for DAΦNE, Frascati, April, 1991.

12. N.N.Achasov & V.N.Ivanchenko, Nuclear Physics **B315**(1989) p.465.

13. S.Nussinov & Tran N. Truong, Phys. Rev. Lett. **63**(1989)1349; A.A. Pivovarov, Soviet Physics - Levedev Institute Reports **9**(1990) 12; N. Paver, contribution to ϕ Factory Workshop at UCLA, April, 1990.; J.L. Lucio & J.Pestieau, Phys. Rev. **D42**(1990)3253; and Oakes, *et al*, Phys. Rev. **D42**(1990).

14. F. Close, Plenary talk at the Workshop on Physics and Detectors for DAΦNE, Frascati, April, 1991, and F.E. Close, Nathan Isgur, and S. Kumano, Nuclear Phys.**B389** (1993) 513.

15. S. Eidelman, J.A.Thompson and C.H.Yang, Proceedings of the Workshop on Physics and Detectors for DAΦNE, Frascati, April 1991, p. 437.

16. The summary talks of L. Maiani and R. Baldini Ferroli and by N.N. Achasov and by M. Pennington at the Workshop on Physics and Detectors for DAΦNE, Frascati, April, 1991.

17. E.V. Anashkin et al., ICFA Instrumentation Bulletin 5 (1988), p.18.

18. Akhmetshin R.R et al., Preprint BudkerINP 95-35, Novosibirsk 1995.

19. J.Lee-Franzini et al., Phys. Lett. **B287** (1992)259.

20. A.Bramon et al., Phys. Lett. **B287**(1992)263.

21. J.Lee-Franzini et al., DAΦNE Physics Handbook, Frascati, 1992, V.II, p.513.

22. Dolinsky et al., Phys. Rep. Vol.202(1991)99.

23. L.Montanet et al., Phys.Rev.**D50**(1994)1173.

24. A. Michetti, Thesises, Roma University, 1993.

25. This value extracted from NUCRIN package.

REVIEW OF RADIATIVE DECAYS STUDY

V.N.Ivanchenko
Budker Institute of Nuclear Physics, 630090, Novosibirsk, Russia

ABSTRACT

Review of experimental studying on radiative decays of light vector mesons is presented. Analisys of magnetic dipole transitions in framework of the constituent quark model is performed.

1 – Introduction

Radiative decays of particles are an important source of information about their structure. The most accurate data on the radiative decays of ρ, ω, ϕ in e^+e^- production were obtained in experiments with the Neutral Detector (ND) at the e^+e^- collider VEPP-2M and was described in detail in the review [1]. Now a real possibility appeared to improve accuracy of radiative decays widths in e^+e^- experiments. After a reconstruction of the VEPP-2M [2] collider in Novosibirsk several runs with the CMD2 detector [3] have been performed and a new SND detector [4] at VEPP-2M has started his first run as well. Moreover, the projects of ϕ-factory DAΦNE in Frascati and ϕ-factory in Novosibirsk are in progress. Thus in this work the experimental status of the radiative decays of light vector mesons and models predictions are discussed from point of view of future experimental program.

2 – Experimental status

After the ND experiment only at this workshop new e^+e^- data from the CMD2 detector at VEPP-2M was reported [5]. Radiative decays of ω were studied for many years in pion production experiments [6, 7, 8] in the reaction $\pi^- p \to \omega n$. The widths of decays $\rho^- \to \pi^-\gamma$, $K^{*\pm} \to K^{\pm}\gamma$, $K^{*0} \to K^0\gamma$ and some other decays were measured using a Primakoff production in hadron-nuclei inelastic scattering [6]. Also one photoproduction experiment was performed [9].

Table 1: Experimental data on radiative decays of vector mesons to $\pi\gamma$.

Decay	Experiment	$\Gamma(keV)$
$\rho^0 \to \pi^0\gamma$	ND [1]	120±30
$\omega \to \pi^0\gamma$		746±50
$\phi \to \pi^0\gamma$		5.5±0.6
$\rho^\pm \to \pi^\pm\gamma$	PDG [6]	68±7
$\omega \to \pi^0\gamma$		717±42
$\phi \to \pi^0\gamma$		5.5±0.6

2.1 $\underline{\rho, \omega, \phi \to \pi\gamma}$

Decays of vector mesons into $\pi^0\gamma$ were studied by ND [1] in the reaction

$$e^+e^- \to \pi^0\gamma \to 3\gamma \tag{1}$$

In this process the recoil photon is monochromatic that enables selection of this reaction. The main background processes are

$$e^+e^- \to 3\gamma \quad (QED), \tag{2}$$

$$e^+e^- \to \phi \to K_S K_L \to neutrals. \tag{3}$$

The process (3) was excluded using selection cryteria for 3γ events. The background from the reaction (2) was calculated and substracted. After that radiative corrections and acceptance corrections were applied. Obtained cross section of the process (1) is shown in fig.1. It was fitted using the vector dominace model (VDM) approximation:

$$\sigma_{e^+e^-\to P\gamma}(s) = \frac{4\pi\alpha^2\omega^3}{s^{3/2}} \left| \sum_V A_V \right|^2, \quad V = \rho, \omega, \phi, \quad s = 4E^2, \quad V = \rho, \omega, \phi,$$

$$A_V = \frac{m_V^2 e^{i\delta_V} \sqrt{\Gamma_{V\to e^+e^-}(s)\Gamma_{V\to P\gamma}(s)}}{m_V^2 - s - i\sqrt{s}\Gamma_V(s)}, \quad P = \pi^0, \eta, \tag{4}$$

where ω is photon energy, δ_V is the relative phase shift, $\delta_\omega = 0$. As a result of the fit two different independent solutions were found according constructive and destructive interference of ρ and ω resonances. The ND data itself doesn't allow to choice one of them but taken into account the results of the Primakoff production experiments [6], in which the process $\rho^\pm \to \pi^\pm\gamma$ was studied, the solution corresponding to destructive interference is excluded on a level of 4 standard deviations. The results and PDG summary are presented in tab.1. One can see that in a e^+e^- experiment obtained width $\Gamma(V \to P\gamma)$ depends on values of m_V, Γ_V, and $\Gamma(V \to e^+e^-)$. Thus to improve accuracy of radiative decay widths these parameters are to be measured with higher accuracy. In this point e^+e^- experiments have real advantage to other type of experiments because beam energy resolution at e^+e^- mashines are much

Table 2: Experimental data on radiative decays of vector mesons to $\eta\gamma$.

Decay	Experiment	$\Gamma(keV)$
$\rho^0 \to \eta\gamma$	ND [1]	62±17
$\omega \to \eta\gamma$		6.1±2.5
$\phi \to \eta\gamma$		55±3
$\omega \to \eta\gamma$	GAM2 [7]	7.0±1.8
$\phi \to \eta\gamma$	CMD2 [5]	54±5
$\phi \to \eta\gamma$		50±7
$\rho \to \eta\gamma$	PDG [6]	57±11
$\omega \to \eta\gamma$		7.0±1.8
$\phi \to \eta\gamma$		56.7±2.7

higher than the widths of resonances. At a ϕ-factory an experimental accuracy in radiative decay widths will be determined both by quality of detectors and by theoretical uncertainty. It is obvious that the model description (4) is to be improved because in it the unitarity is broken. New ways for description of wide resonances are considered. N. N. Achasov and his collaborators have been developing field-theory-inspired approach [10]. M. Benayoun and his collaborators take into account triangle anomalies [11] and include s-dependence of coupling constants. In both cases parameters of resonances are changed significally, branching ratios are less sensitive to model modifications. But additional efforts in this field are necessary.

2.2 $\rho, \omega, \phi \to \eta\gamma$

In e^+e^- experiments decays of vector mesons into $\eta\gamma$ were studied in the following reactions:

$$e^+e^- \to \eta\gamma \to 3\gamma, \tag{5}$$

$$e^+e^- \to \eta\gamma \to 3\pi^0\gamma, \tag{6}$$

$$e^+e^- \to \eta\gamma \to \pi^+\pi^-\pi^0\gamma. \tag{7}$$

High statistic was collected in the ND experiment [1] for the process (5) in the energy region of ϕ and the reaction (6) was used for independent conrol. At the energy region $2E < 1\ GeV$ the reaction (6) was main because of high background for the process (5) from the processes (1) and (2). Cross section of $\eta\gamma$ production is shown in fig.2. Substraction of backgraund were performed. Radiative corrections, the acceptance, and the branching ratios of η decays were taken into account. It is clear from fig.2 that for the $\eta\gamma$ production in energy region of ϕ interference is much smaller than that for the $\pi^0\gamma$ production. The data were fitted using the VDM approximation (4). As in case of $\pi^0\gamma$, two different independent solutions were found according constructive and destructive interference of ρ and ω resonances. Using the data of the GAMS-2000 spectrometer [7] the solution corresponding to destructive interference is excluded on a level of 5 standard deviations. Results are

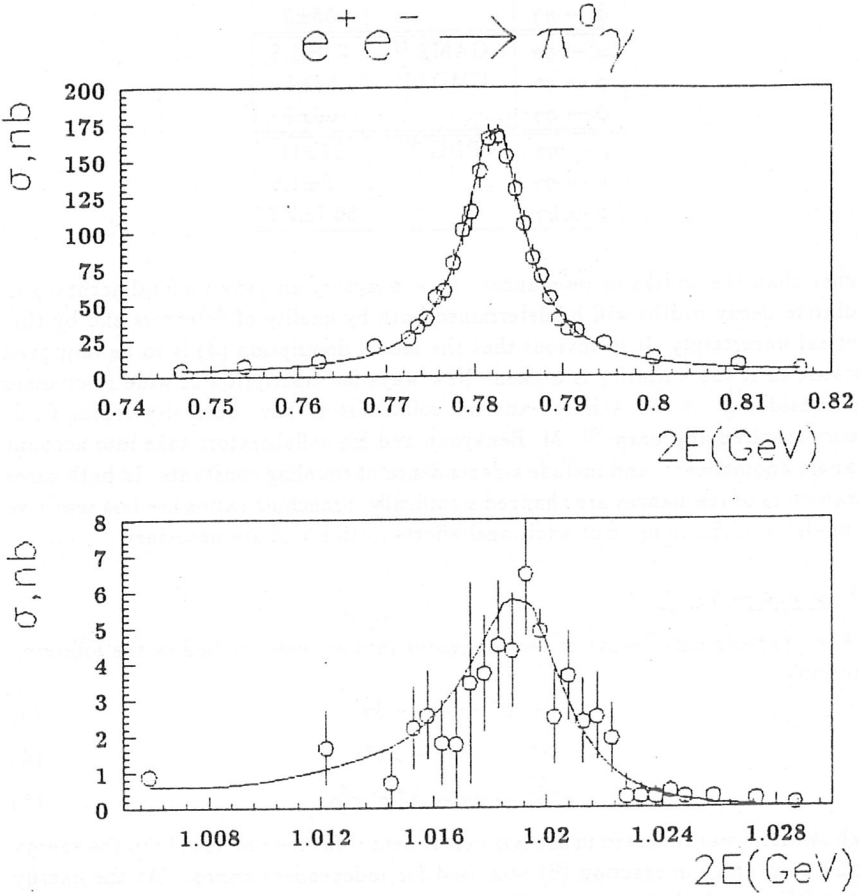

Figure 1: Cross section of the process $e^+e^- \to \pi^0\gamma$: a) energy region of ρ and ω mesons; b) energy region of ϕ meson; line - the best fit.

Table 3: The data and theory predictions on rare radiative decays of vector mesons.

Decay	Experiment	Branching ratio
$\rho^0 \to \pi^+\pi^-\gamma$	ND [1]	$(0.99 \pm 0.16)\%$
$\omega \to \pi^0\pi^0\gamma$		$< 4 \cdot 10^{-4}$
$\phi \to \pi^0\eta\gamma$		$< 2.5 \cdot 10^{-3}$
$\phi \to a_0(980)\gamma$		$< 5 \cdot 10^{-3}$
$\phi \to \pi^0\pi^0\gamma$		$< 10^{-3}$
$\phi \to f_0(975)\gamma$		$< 2 \cdot 10^{-3}$
$\omega \to \pi^0\pi^0\gamma$	GAMS-2000 [7]	$(7.2 \pm 2.6) \cdot 10^{-5}$
$\phi \to f_0(975)\gamma$	CMD2 [5]	$< 8 \cdot 10^{-4}$
Decay	Theory	Branching ratio
$\omega \to \pi^0\pi^0\gamma$	VDM [1]	$8 \cdot 10{-}5$
$\phi \to \rho\pi \to \pi^0\eta\gamma$	VDM [15]	$0.8 \cdot 10^{-5}$
$\phi \to a_0(980)\gamma \to \pi^0\eta\gamma$	4q [15]	$2 \cdot 10^{-4}$
	qq [15]	$2.4 \cdot 10^{-5}$
	KK molecula [16]	$2.4 \cdot 10^{-5}$
$\phi \to \rho\pi \to \pi\pi\gamma$	VDM [15]	$3 \cdot 10^{-5}$
$\phi \to f_0(975)\gamma \to \pi\pi\gamma$	4q [15]	$2.5 \cdot 10^{-4}$
	qq [15]	$5 \cdot 10^{-5}$
	KK molecula [16]	$5 \cdot 10^{-5}$
	glueball [16]	0

presented in tab.2. Note that in the CMD2 experiment [5] the alternate reaction (7) was stadied. Two independent runs were performed with CMD2 and the results of two independent analisys are presented in tab.2.

2.3 $\rho, \omega, \phi \to \pi\pi\gamma, \pi^0\eta\gamma$

Cross section of the process $e^+e^- \to \omega\pi^0 \to \pi^0\pi^0\gamma$ dominanted for the $\pi^0\pi^0\gamma$ production in the energy region below 1.5 GeV. In the ND experiment [1] the sample of these events is quite clean and there is a good coincidence of the ND data and the data of the DM2 experiment [12]. The CVC calculation [13] shows that the ARGUS data on correspondining τ decay [14] are in agreement with e^+e^- data as well. The shape of this cross section can be described via VDM sum of amplitudes of the ρ resonace and its radial exitations $\rho(1470)$ and $\rho(1700)$. As a result of the fit following value of the coupling constant was found:

$$g_{\rho\omega\pi} = 14.5 \pm 0.4 \pm 0.5, \qquad (8)$$

which is in an agreement with that obtained from the width of the ω resonance. Branching ratio of the ρ decay into $\omega\pi^0$ was not presented as a ND result because in the ρ pole this reaction is far below energy threshold and coupling constant is more

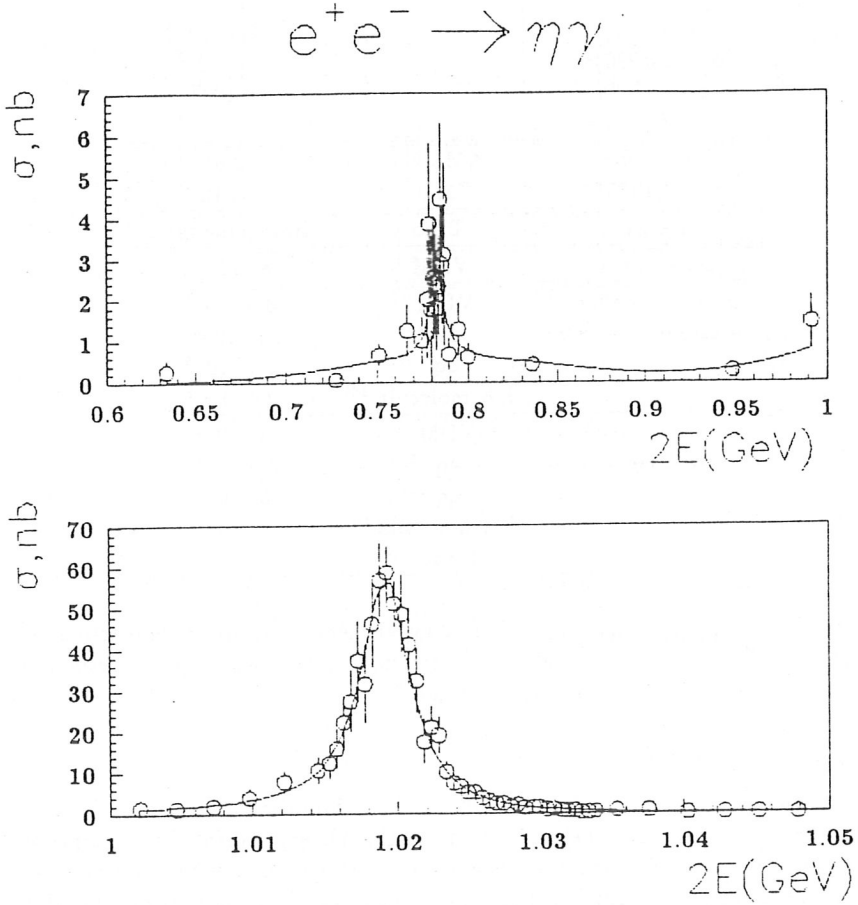

Figure 2: Cross section of the process $e^+e^- \to \eta\gamma$: a) energy region of ρ and ω mesons; b) energy region of ϕ meson; line - the best fit.

adequate value for description of this process. Opposit situation is in $\pi^+\pi^-\gamma$ production. Radiative decay of ρ meson dominates in the pole and the value of branching ratio are in agreement with the electromagnetic mecanism of the decay [1]. Another mechanisms of $\pi\pi\gamma$ production were not seen until new GAMS-2000 experiment [8] was performed in which the decay mode $\omega \to \pi^0\pi^0\gamma$ was observed. These data and upper limits on another decay modes are shown in tab.3. In tab.3 different model predictions for rare radiative decays of light vector mesons are presented as well. The decay modes

$$\phi \to \pi\pi\gamma, \pi^0\eta\gamma \tag{9}$$

can be realized by two different mechnisms. First one connects with $\rho\pi$ intermediate state and magnetic dipole transition of ρ, so it may be described by the VDM. Second is an electric dipole transition $V \to S\gamma$, where S is scalar state. The processes (9) provide studying of scalars $a_0(980)$ and $f_0(975)$. Structure of these mesons are not clear yet and one of the first tusks for VEPP-2M and DAΦNE is to put light on it. In the ND experiment [1] the backgraund from reactions (3) and (6) did not allow to extract decays (9) of any types. Buy the way, some sygnal was seen in the $\pi^0\eta\gamma$ channel on level of 2 standart deviations and preliminary results of the CMD2 experiment [5] show some evidence for the decay mode $\phi \to f_0(975) \to \pi^+\pi^-\gamma$ as well, but just now only upper limits can be established (tab.3).

3 – Analysis of magnetic dipole transitions

There are a lot of theoretical investigations on magnetic dipole transitions $V \to P\gamma$ and $P \to V\gamma$ in mesons consisted of u, d, s quarks [17, 18] and it is well known that the widths may be expressed as

$$\Gamma(V \to P\gamma) = \frac{4}{3}\pi\omega^3 M_{VP}, \quad \Gamma(P \to V\gamma) = 4\pi\omega^3 M_{VG}, \tag{10}$$

where ω is photon energy, M_{VP} is transition matrix element, which can be written in terms of the magnetic moments of the constituent quarks

$$M_{VP} = I_{VP} \sum_q \beta_q \cdot \mu_q, \quad q = u, d, s. \tag{11}$$

Here I_{VP} is overlap integral of the spatial wave functions of the initial and final states, β_q is a weight factors which can be expressed through the mixing angles α_P and α_V between basis states $s\bar{s}$ and $(u\bar{u} + d\bar{d})/\sqrt{2}$ in the vector and pseudoscalar octets [1]. If one assumes that in all decays under study the overlap integrals are equal, then there are 6 parameters of the model. Three of them are magnetic moments of the constituent quarks, which are well known [6] from the magnetic moments of proton, neutron and Λ baryon

$$\mu_u = 1.852, \quad \mu_d = -0.972, \quad \mu_s = -0.613 \pm 0.004. \tag{12}$$

Since one can suppose some difference between the magnetic moments of s quark in baryons and in mesons the data on decays $V \to P\gamma$ and $P \to V\gamma$ were fitted

with free parameters μ_s, α_P, α_V, I_{VP} (tab.4A). This fit confirms that the magnetic moment of s quark in mesons differs from (12), the value of mixing angle α_P is close to the prediction of the linear mass formula, and the value of α_V is in a good agreement with the quadratic mass formula prediction. On the other hand, within VDM, two-photon widths of the pseudoscalar mesons can be expressed via matrix elements of radiative decays

$$\Gamma(P \to \gamma\gamma) = \frac{3m_P^3}{4\alpha} \left| \sum_V \sqrt{\frac{\Gamma(V \to e^+e^-)}{m_V}} \cdot M_{VP} \right|^2, \quad V = \rho, \omega, \phi. \qquad (13)$$

Comparison of the results of such calculation (tab.4A) with the data shows coincidence for the widths of π^0, $\eta' \to \gamma\gamma$ and disagreement for the $\Gamma(\eta \to \gamma\gamma)$. The fit over all data yields value of $\chi^2/n_D = 46/9$ (tab.4B). Possible improvements of the theory are discussed for many years [18]. There are arguments for taking into account contribution of a glueball state into η' meson. In attempt to check such hypothesis the data were fitted with two additional parameters. First one was the quark-gluon mixture angle α_G. Second was amplitude of η' transition into $\gamma\gamma$ via gluonium M_G, which was added to the sum of amplitudes in the relation (13). χ^2 of this fit (tab.4C) is also poor, but this result is very interesting because we obtained the value of μ_s close to (12) and the value of α_P close to the quadratic mass formula prediction. Therefore the special fit was performed with fixed values μ_s from (12), α_P from quadratic mass formula, and I_{VP} from the value of $\Gamma(\omega \to \pi^0\gamma)$, which has small systematic uncertainty. The results of this calculation show (tab.4D) that practically for all decays there is good agreement between the data and model predictions. The gluonium contents in η' meson is $(20 \pm 5)\%$.

4 – Discussion

Thus simple phenomenological model including quark-gluon mixing can describe the main part of the data on magnetic dipole transitions, but all balk of data cannot be described simultaneously. Let us discuss the results from tab.4 taking into account future experiments in Novosibirsk and Frascati.

First of all one should mention that fitted value of $\Gamma(\omega \to \pi\gamma)$ depends on the model. Accuracy of this width can be increased up to 1% in the new generation of e^+e^- experiments. It will be limited by experimental systematic errors and by theoretical uncertainty in description of the interference of ρ, ω, and ϕ.

Statistic for the decays $\omega, \rho \to \eta\gamma$ is now very poor and obviously will be increased in new e^+e^- experiments, that will allow to have statistical errors for the decay widths about 10%. For such level of statistics the theoretical uncertainty will be small.

Estimated accuracy for the decay width $\phi \to \eta\gamma$ and $\phi \to \pi^0\gamma$ in the new e^+e^- experiments can be improved to $(1-3)\%$. For this aim studying of all decay modes of η in one experiment will be usefull. Energy resolution in e^+e^- experiments

is much higher than the total width of ϕ, that allows to perform accurate extraction of inputs of ρ and ω amplitude at ϕ energy range and to control the resonance shape.

It should be noted that the widths $\Gamma(K^{*\pm} \to K^{\pm}\gamma)$ and $\Gamma(K^{*0} \to K^{0}\gamma)$ depend only on quarks magnetic moments and overlap integrals and do not depend on mixture angles. Both this widths were measured only in Primakoff production experiments with low energy kaon beams. It seems that new independent experiments will be a good cross checking of the existing data and theoretical predictions.

The calculated value $\Gamma(\phi \to \eta'\gamma)$ is very sensitive to model assumptions and varies from 0.1 keV to 0.5 keV. But at the same time this decay is the most difficult for studying. Only upper limit on its width was placed in the ND experiment [1]. At this conference new upper limit was reported by CMD2 collaboration [5]

$$\Gamma(\phi \to \eta'\gamma) < 1 \ keV, \tag{14}$$

and for observation of the decay additional statistic is requiered.

$\Gamma(\eta \to \gamma\gamma)$ was obtained at colliders in two-photon production and also from Primakoff production at hadron beams. If only two-photon measurements are used for the PDG fit, then the average value is $\Gamma(\eta \to \gamma\gamma) = (0.510 \pm 0.026)$ [6], which is closer to the calculated value in tab.4D.

The value of α_V is in a good agreement with the quadratic mass formula prediction. The value of α_P depends on the model and set of new experiments to study radiative decays with η and η' can provide localization of the α_P.

5 – Conclusion

- New generation of e^+e^- experiments have a good perspective for radiative decays study. For these experiments additional theoretical investigations both on the radiative decays and on processes of the production of several wide resonaces in e^+e^- annihilation are necessary.
- Simple constituent quark model cannot describe all data on radiative widths of mesons consisted of u, d, s quarks. If one takes into account 20% admixture of gluonium into η' meson, then it is possible to describe main part of the data using the quadratic mass formula for mixture angles both for the vector and for the pseudoscalar octets. Widths of the decays $K^{*\pm} \to K^{\pm}\gamma$ and $\eta \to \gamma\gamma$ are in contradiction with such model.
- Width of the decay $\phi \to \eta'\gamma$ is very sensitive to model predictions.
- Electric dipole transitions will be extracted from decays into $\pi\pi\gamma$ and $\pi\eta\gamma$ if corresponding branching ratios are about $10^{-4} - 10^{-5}$. Decays of ϕ into these final states provide search on four quark states or kaonium contributions into $a_0(980)$ and $f_0(975)$ mesons.

Table 4: The data on radiative decays and fitting results.

Decay	PDG, $\Gamma(keV)$	Fitting results, $\Gamma(keV)$			
		A	B	C	D
$\rho \to \pi\gamma$	68±8	60	56	59	66
$\omega \to \pi\gamma$	717±42	652	611	648	717
$\phi \to \pi\gamma$	5.5±0.6	5.8	5.5	5.6	5.8
$\rho \to \eta\gamma$	57±11	54	44	40	45
$\omega \to \eta\gamma$	7.0±1.8	5.3	4.2	3.8	4.3
$\phi \to \eta\gamma$	57±3	57	59	61	64
$K^{*0} \to K^0\gamma$	116±10	131	116	114	124
$K^{*\pm} \to K^\pm\gamma$	50±5	55	56	66	75
$\eta' \to \rho\gamma$	59±6	59	71	60	61
$\eta' \to \omega\gamma$	5.9±0.8	6.1	6.9	5.6	5.6
$\phi \to \eta'\gamma$	< 1.7	0.45	0.31	0.15	0.15
$\pi^0 \to \gamma\gamma$	$(7.5\pm0.3)\cdot10^{-3}$	$6.8\cdot10^{-3}$	$6.4\cdot10^{-3}$	$6.7\cdot10^{-3}$	$7.5\cdot10^{-3}$
$\eta \to \gamma\gamma$	0.46±0.04	0.78	0.60	0.53	0.60
$\eta' \to \gamma\gamma$	4.3±0.5	4.5	4.9	4.3	4.3
μ_s	−0.613±0.004	−0.74±0.03	−0.69±0.02	−0.63±0.02	−0.613
α_P (deg.)		−55±2	−50±2	−45±2	−45
α_V (deg.)		3.55±0.20	3.6±0.2	3.5±0.2	3.4±0.2
α_G				35±4	38±3

Acknowledgements

The author is grateful to the organizers of the DAΦNE95 for an opportunity to present this talk and to S.I. Serednyakov for fruitful discussions. This work was supported by the International Science Foundation (grant number 4856/2).

References

1. S.I. Dolinsky et al., Physics Reports 202, **99** (1991).
2. V.V. Anashin et al., Preprint INP 84-123, Novosibirsk, 1984.
3. E.V. Anashkin et al., ICFA Instrum. Bull. **5**, 18 (1988); G.A. Aksenov et al., Preprint INP 85-118, Novosibirsk, 1985;
4. S. Serednyakov et al., SND-Detector for VEPP-2M and Φ-factory, in: Proc. Workshop on Physics and Detectors for DAΦNE (ed. G. Pancheri, Frascati, April 9–12, 1991), 605 (Frascati, 1991).
5. E.P. Solodov, this proceeding.
6. Review of Particle Properties, Phys. Rev. D **50**, 1177 (1994).
7. D. Alde et al., Z.Phys. C **61**, 35 (1994).
8. C. Amsler, Light Quark and Gluonium Spectroscopy, in: Proc. XXVII Inter. Conf. on High Energy Physics (ed.P.J. Bussey and I.G. Knowles, Glasgow, Scotland UK, July 20–27, 1994), **1**, 199 (Glasgow, 1994).
9. D.E. Andrews et al., Phys. Rev. Lett. **38**, 198 (1977).
10. N.N. Achasov, S.A. Devyanin and G.N. Shestakov, Sov. Phys. Usp. **142**, 361 (1984); N.N. Achasov et al., Int. Jour. Mod. Phys. A **7**, 3187 (1992); N.N. Achasov and A.A.Kozhevnikov, Particle World **3**, 125 (1993).
11. M. Benayoun et al., Z.Phys. C **58**, 31 (1993).
12. D. Bisello et al., Preprint LAL-91-64, Orsay, 1991.
13. S.I. Eidelman and V.N. Ivanchenko, Nucl. Phys. B (Proc. Suppl.) **40**, 131 (1995).
14. H. Albrecht et al., Phys. Lett. B**174**, 453 (1986).
15. N.N. Achasov and V.N. Ivanchenko, Nucl. Phys. B**315**, 465 (1989).
16. F.E. Close, N. Isgur and S. Kumano, RAL-92-026.
17. P.J. O'Donnell, Rev. Mod. Phys. **53**, 673 (1981); I.S. Sogami and Oh'Yamaguchi, Phys. Rev. Lett. **54**, 2295 (1985); R.C. Verma and M.P. Khanna, Phys. Lett. B **183**, 207 (1987); F. Gilman and R. Kauffman, Phys. Rev. D **36**, 2761 (1987); G. Morpugo, Phys. Rev. D **42**, 1497 (1990).
18. J.L. Rosner, Phys. Rev. D **27**, 1101 (1983); Sh.S. Eremyan and A.E. Nazaryan, Sov. J. Nucl. Phys. **43**, 863 (1986); **45**, 1758(1987); M.L. Nekrasov, Sov. J. Nucl. Phys. **51**, 1140 (1990); M. Benayoun et al., Z.Phys. C **65**, 399 (1995).

Measurement of the $e^+e^- \to \pi^+\pi^-$ Cross Section in the Energy Range between ρ and Φ Mesons

G.V.FEDOTOVICH*
Budker Institute of Nuclear Physics, Novosibirsk, 630090, Russia

ABSTRACT

The general purpose CMD-2 detector at the VEPP-2M collider in Novosibirsk has collected the luminosity integral of $\sim 300\ nb^{-1}$ in the energy range between ρ and Φ mesons. High accuracy measurements of the e^+e^- annihilation cross section in this energy region are required for the muon g-2 experiment at Brookhaven. The data are also important to interpret the fundamental Standard Model parameters known with high accuracy. Preliminary results of data analysis are presented.

1 – Introduction

The data on the cross section $e^+e^- \to \pi^+\pi^-$ in the energy range between ρ and Φ mesons were obtained with the CMD-2 detector [1, 2] at the VEPP-2M collider [3] at Budker Institute of Nuclear Physics in Novosibirsk. The data from the low energy region up to 1400 MeV (maximum energy provided by VEPP-2M) are important both for the search of rare decays of the light vector mesons and for the calculation

[1]CMD-2 collaboration:
R.R.Akhmetshin, G.A.Aksenov, E.V.Anashkin, V.M.Aulchenko, B.O.Baibusinov, V.S.Banzarov, L.M.Barkov, S.E.Baru, A.E.Bondar, D.V.Chernyak, V.V.Danilov, S.I.Eidelman, G.V.Fedotovich, N.I.Gabyshev, A.A.Grebeniuk, D.N.Grigoriev, P.M.Ivanov, B.I.Khazin, I.A.Koop, A.S.Kuzmin, I.B.Logashenko, A.P.Lysenko, A.V.Maksimov, Yu.I.Merzlyakov, V.A.Monich, I.N.Nesterenko, V.S.Okhapkin, E.A.Perevedentsev, A.A.Polunin, E.V.Popkov, E.G.Pozdeev, V.I.Ptitzyn, T.A.Purlatz, S.I.Redin, N.I.Root, A.A.Ruban, N.M.Ryskulov, Yu.M.Shatunov, A.E.Sher, M.A.Shubin, B.A.Shwartz, V.A.Sidorov, A.N.Skrinsky, V.P.Smakhtin, I.G.Snopkov, E.P.Solodov, A.I.Sukhanov, V.M.Titov, Yu.V.Yudin, V.G.Zavarzin, S.G.Zverev - *Budker Institute of Nuclear Physics, Novosibirsk, Russia*; D.H.Brown, J.P.Miller, B.L.Roberts, W.A.Worstell - *Boston University, USA*; J.A.Thompson, C.Valine - *University of Pittsburgh, USA*; S.Dhawan, V.Hughes *Yale University, USA*; P.Cushman *University of Minnesota, USA*

of the dispersion integral that relates the cross section of e^+e^- annihilation into hadrons to the value of the hadronic vacuum polarization. This value plays on important role in the interpretation of the fundamental Standard Model parameters and the evaluation of the anomalous magnetic moment of the muon [4, 5], which will be measured in the E821 experiment at BNL with an extremely high precision of 0.35 ppm. To evaluate the contribution of the hadronic vacuum polarization to the muon g-2 with the same accuracy a systematic error in hadronic cross section should be less than 0.5%, because the value of the total hadronic contribution is equal to 72 $\pm$1.6 ppm [6]. The main part of this contribution comes from the energy range which is provided by the VEPP-2M collider.

2 – Data Analysis

The data discussed in this talk were obtained by scanning the energy region between ϕ and ρ mesons with 10 MeV step. About 10^3 of pion pairs were sampled at every point. The main part of the luminosity integral $\sim$ 300 nb^{-1} was collected during 1994 runs. Using the resonance depolarization technique [7], the beam energy at each point was measured with the accuracy of 10^{-4}. The detector trigger is described in [8]. Events were recorded when:

* at least one track in the Drift Chamber was found by the tracking processor [9]
* the energy deposition in the CsI calorimeter was greater than 20 MeV.

About 20 million events were written on the magnetic tape. For off-line analysis only collinear two track events were selected. The cuts used for this selection are marked by arrows in Fig.1. Events were used in a maximum likelihood function fit with the following global optimization parameters:

* number of electrons N_e
* number of background events N_b
* $\frac{N_\pi}{N_e+N_\mu}$, where N_π - number of pions and N_μ - number of muons.

The ratio N_μ/N_e was fixed from the QED. The likelihood fit used information on the polar angle, longitudinal coordinate of the vertex and energies deposited in the CsI calorimeter. As it is seen from Fig.2 the experimental data are in a good agreement with the fit.

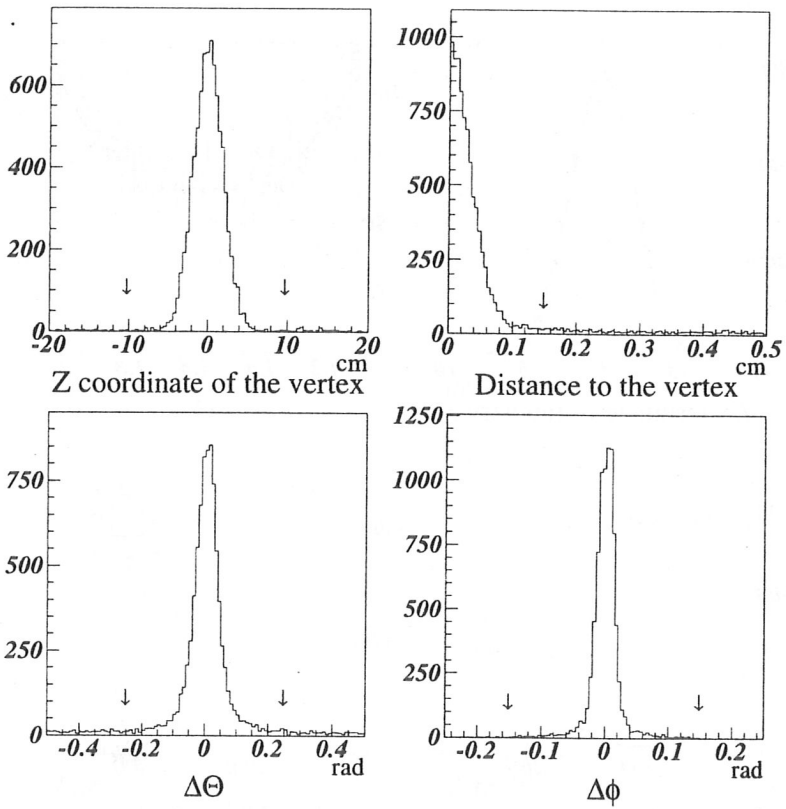

Figure 1: Two track events distributions and cuts imposed to select collinear events.

The ratio $\frac{N_\pi}{N_e+N_\mu}$ allows to express $e^+e^- \to \pi^+\pi^-$ cross section in a simple way:

$$\sigma_\pi = \frac{N_\pi}{N_e + N_\mu} \cdot \frac{\epsilon_e\sigma_e(1+\delta_e) + \epsilon_\mu\sigma_\mu(1+\delta_\mu)}{\epsilon_\pi(1+\delta_\pi)},$$

where ϵ_e, σ_e, δ_e, ϵ_μ, σ_μ, δ_μ, ϵ_π, σ_π, δ_π are detection efficiencies, cross sections and radiative corrections for electrons, muons and pions respectively. Pion formfactor values are presented in Fig.3 along with the results of the previous experiments.

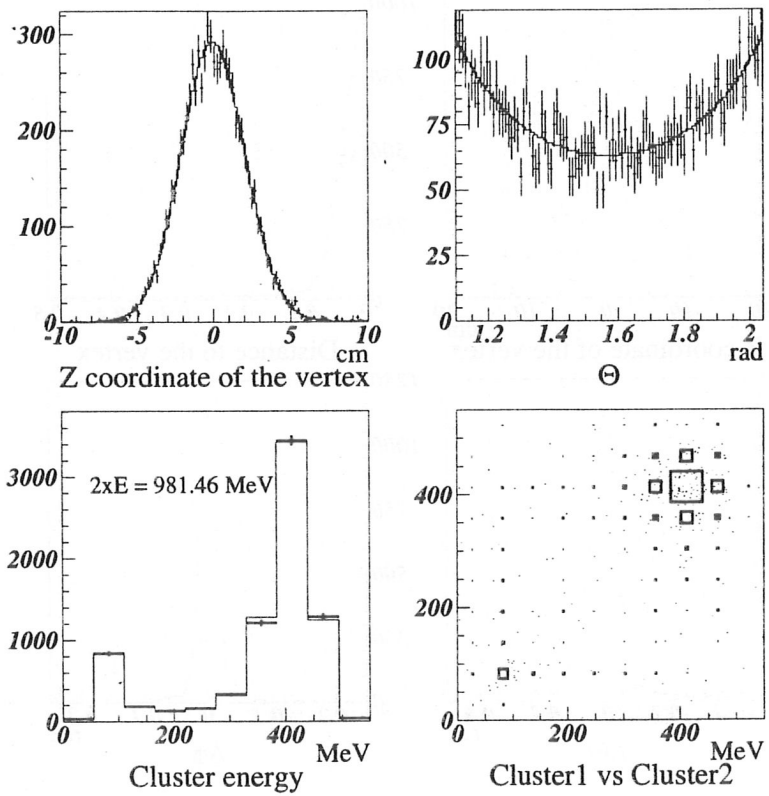

Figure 2: The comparison of the experimental data with a fit.

The statistical error of the $\pi^+\pi^-$ cross section at each energy point is better than 3%. At present the total systematic error is estimated to be $\sim$ 1.5%. The main part of this error comes from the detector solid angle uncertainty $\sim$ 1% and from the calculation of the radiative corrections for Bhabha events [10], which are known with accuracy $\sim$ 1%. Radiative corrections for all other channels of the e^+e^- annihilation into hadrons and muons were calculated with the accuracy about 0.2 - 0.5% [11, 12] which is sufficient for the purposes of the experiment. As an example, we describe very briefly the main idea and approach to calculation of the radiative corrections for the channel $e^+e^- \to \pi^+\pi^-$ in Appendix.

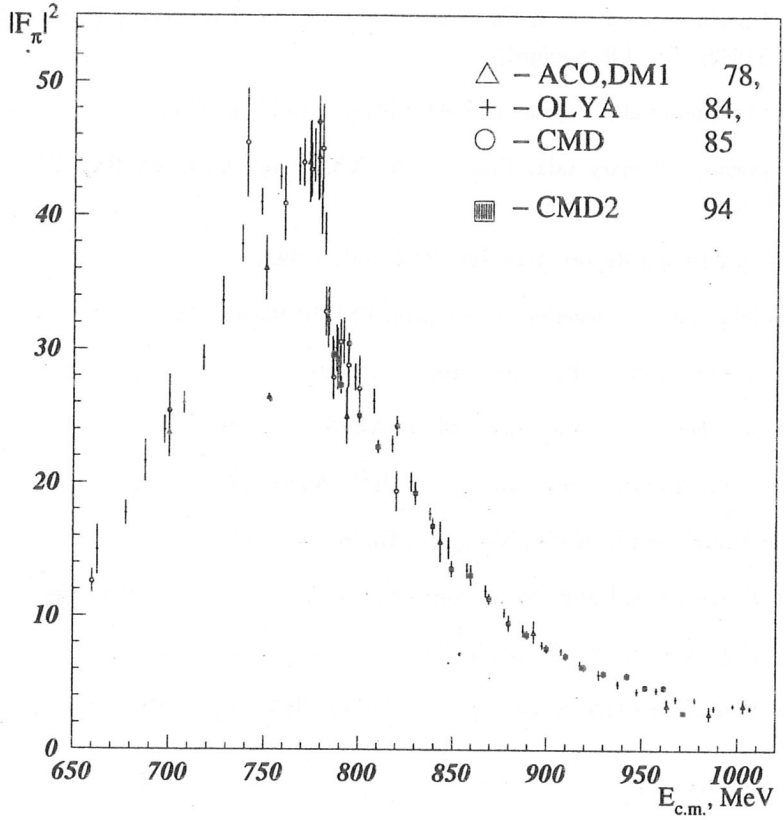

Figure 3: The experimental data for $|F_\pi|^2$.

The further improvement of the Drift Chamber parameters and more accurate calculations of the radiative corrections for Bhabha scattering events would decrease the systematic error to the level of 0.5%.

This work is supported in part by the US Department of Energy, US National Science Foundation and the International Science Foundation under the grant RPT000.

References

1. G.A. Aksenov et al., Preprint INP **85-118**, (Novosibirsk 1985).

2. B.I. Khazin et al., Proc. of the XXVI Int. Conf. on High Energy Physics, **2**, 1876,(1992) (Ed. J.R. Sanford).

3. V.V. Anashin et al., Preprint INP **84-114**, (Novosibirsk 1984).

4. M. Vysotski, Plenary talk, Proc. of the XXVII Int. Conf. on High Energy Physics.

5. Muon g-2 Design Report AGS 821, BNL, July (1992).

6. S. Eidelman and F. Jegerlehner, Preprint PSI-PR **95-01**, (1995).

7. Ya.S. Derbenev et al., Part. Acc. **10**, 177 (1980).

8. E.V. Anashkin et al., Nucl. Instr. Meth. **A323**, 178 (1992).

9. V.M. Aulchenko et al.,Nucl. Instr. and Meth.,**A252**, 299, (1986).

10. F.A. Berends and R. Kleiss, Nucl. Ph., **B228**, 537 (1983).

11. E.A. Kuraev, V.S. Fadin, Soviet Journal of Nuclear Physics,**41**, 466, (1985).

12. E.A. Kuraev al all. Will be published.

13. F.A. Berends and G.J. Komen, Physics Letters, **B63**, 432, (1976).

3 –Appendix

Our technique for the calculation of the radiative corrections is based primarily on two works [11, 12]. The first one gives an accuracy about 0.2% but the cross section is integrated over all final particles kinematics except for the total energy loss and furthermore is valid only for comparatively small energy losses (under 10% of the beam energy). The second one is less accurate (about 0.5%) and assumes that only one photon is emitted but it gives the angle distributions for the final particles, which is important when any selection criteria are applied to the events.

Our procedure for the calculation of the radiative corrections is combined both approaches in the following way: photons with the energy less than ΔE are simulated according to [11] while photons with the energy greater than ΔE are simulated according to [12]. The quantity ΔE is a free parameter and its selection will be discussed later. In order to get a smooth and continuous distributions over final particles kinematics, energy loss for a region under ΔE was assigned to a "hypothetical" single photon having the same angular distributions as follows from [12]. The dependence of the radiative corrections for the channel $e^+e^- \to \pi^+\pi^-$ on

the value of ΔE is shown in Fig.4 under selection criteria (mentioned above in the talk) for the collinear events.

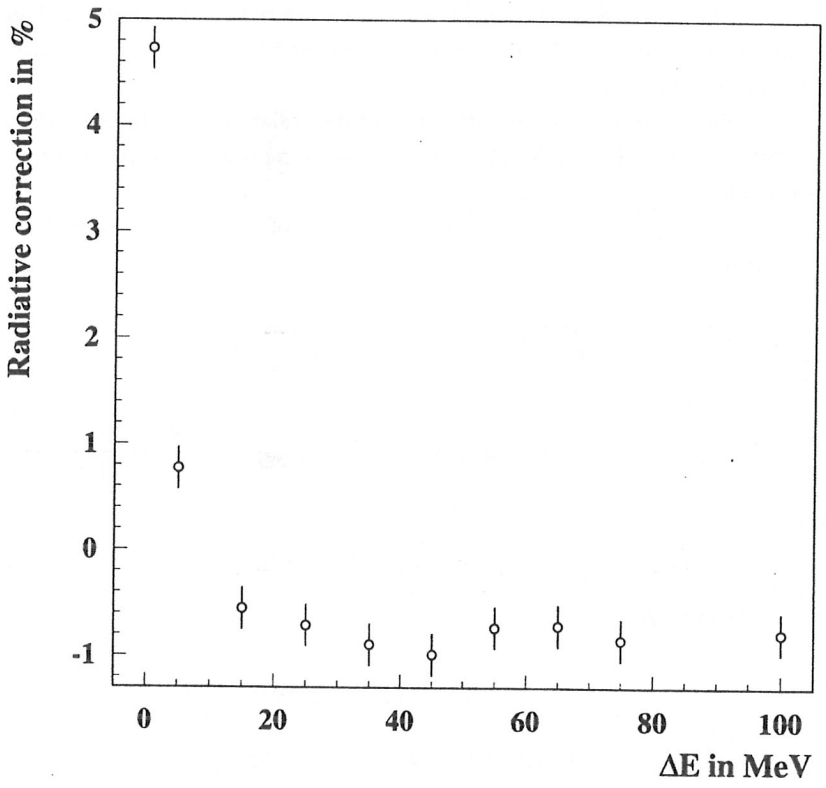

Figure 4: The dependence of the radiative corrections on ΔE for the energy 952 MeV.

One can see that in a wide region of the ΔE values the total cross section does not depend on ΔE with the accuracy of about $0.2 - 0.3\%$.

The possible values of ΔE are limited by the following factors:

* ΔE should not exceed the validity region of [11)]
* ΔE should be large enough for the approach of the single photon to be applicable
* it is desirable to have ΔE as large as possible to use the

better accuracy of [11]

* for large energy losses causing the events rejecting by the selection criteria an approach [12] should be used to take proper account of the final particles kinematic.

Thus the reasonable values of ΔE are limited on both sides and should be somewhere from 20 to 50 MeV depending on the beam energy and the selection criteria of the collinear events.

The expression for the calculation of the radiative corrections for the channel $e^+e^- \to \pi^+\pi^-$ is briefly described below. Calculations of the radiative corrections for the other channels were done in a similar way.

The cross section used for the calculation of the radiative corrections can be expressed as follow:

$$\frac{d\sigma_\pi(S)}{d\Omega_-} = \int_0^\Delta \frac{d\sigma_0(S_1)}{d\Omega_-} \cdot \frac{F(S,x_\gamma)}{|1-\Pi(S_1)|^2} dx_\gamma +$$

$$+\frac{2\alpha}{\pi} \int_\Delta^{X_\gamma{}^{max}} f_{en}(x_\gamma)dx_\gamma \int_{-1}^{1} f_{ang}(Z_\gamma)dZ_\gamma \frac{d\sigma_0(S_1)}{d\Omega_-} \left|\frac{F_\pi(S_1)}{F_\pi{}^{BW}(S_1)}\right|^2 \frac{R(S,Z_-,x_\gamma,Z_\gamma)}{|1-\Pi(S_1)|^2},$$

where

$$\frac{d\sigma_0(S)}{d\Omega_-} = \frac{\alpha^2}{8S}\beta_\pi{}^3(1-Z_-{}^2)$$

- is the Born cross section,

$$f_{en}(x_\gamma) = \frac{1}{x_\gamma(1-x_\gamma)[(1-\frac{S(1-x_\gamma)}{M_\rho{}^2})^2 + \frac{\Gamma\rho^2}{M_\rho{}^2}]}$$

- is a function used for the simulation of the photon energy,

$$f_{ang}(Z_\gamma) = \frac{1}{1-\beta_e{}^2 Z_\gamma{}^2}[1 - \frac{1}{1+\gamma_e{}^2(1-Z_\gamma{}^2)}]$$

- is a function used for the simulation of the polar angle of the photon emitted by the initial particles,

$|F_\pi(S)|^2$ - is the pion formfactor squared,

$\left|F_\pi{}^{BW}(S)\right|^2$ - is the pion formfactor squared in the simplest Breit-Wigner form,

$\Pi(S)$ - is the vacuum polarization due to leptons and hadrons [11, 13],

$F(S,x_\gamma)$ - is the structure function [11],

$$R(S,Z_-,x_\gamma,Z_\gamma) = \frac{1}{|1-\Pi(S_1)|^2} \cdot \frac{1}{\beta_\pi{}^3(1-Z_-{}^2)} \cdot [\frac{\beta_- x_-}{2-x_\gamma(1-cos(\Phi)/\beta_-)}] \cdot |M|^2.$$

The expression in the squared brackets is connected with the phase space of the final particles. $|M|^2$ is the dimensionless square of the matrix element for $e^+e^- \to \pi^+\pi^-$ process from which the main peculiarities ($f_{en}(x_\gamma)$ and $f_{ang}(Z_\gamma)$) are factored out.

$$|M|^2 = [1 + \frac{1}{\gamma_e{}^2(1 - Z_\gamma{}^2)}] \cdot \frac{R_1 + R_2}{1 - x_\gamma},$$

where [12]

$$R_1 = [(2 - x_\gamma)^2 + x_\gamma{}^2 Z_\gamma{}^2](\beta_\pi{}^2 - x_\gamma) - (1 - x_\gamma)[(x_+ - x_-)^2 + (x_+\beta_+ Z_+ - x_-\beta_- Z_-)^2]$$

and

$$R_2 = -\frac{1}{1 + \gamma_e{}^2(1 - Z_\gamma{}^2)}[4(1 - x_\gamma)(\beta_\pi{}^2 - x_\gamma) - (x_+(Z_\gamma + \beta_+ Z_+) - x_-(Z_\gamma + \beta_- Z_-))^2]$$

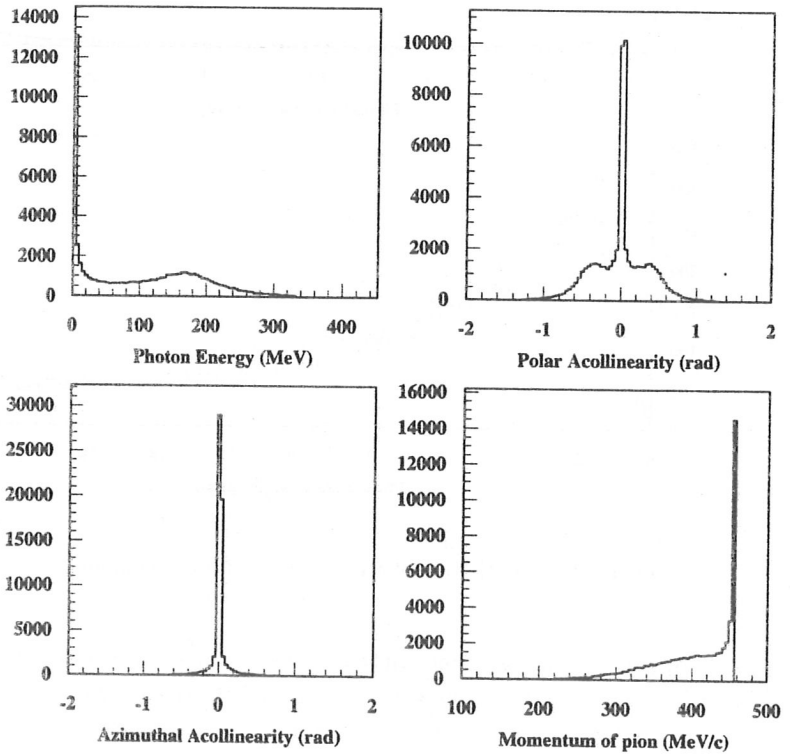

Figure 5: The distributions of the final state particles for the energy 952 MeV.

The following designations were used in the previous expressions: x_+, x_-, x_γ - energies of the final pions and photon divided by E_{beam} respectively; Z_-, Z_+, Z_γ - their polar angles cosines; β_+, β_- - velocities of pions; $S = 4E^2{}_{beam}$; S_1=S(1-x_γ); $\Delta \doteq \Delta E/E_{beam}$; $\gamma_e = E_{beam}/m_e$; $\beta_e = P_e/E_{beam}$; $\beta_\pi = P_\pi/E_{beam}$; E_{beam} - energy of the electron (positron); P_e - their momenta; m_e and m_π are the electron and pion masses.

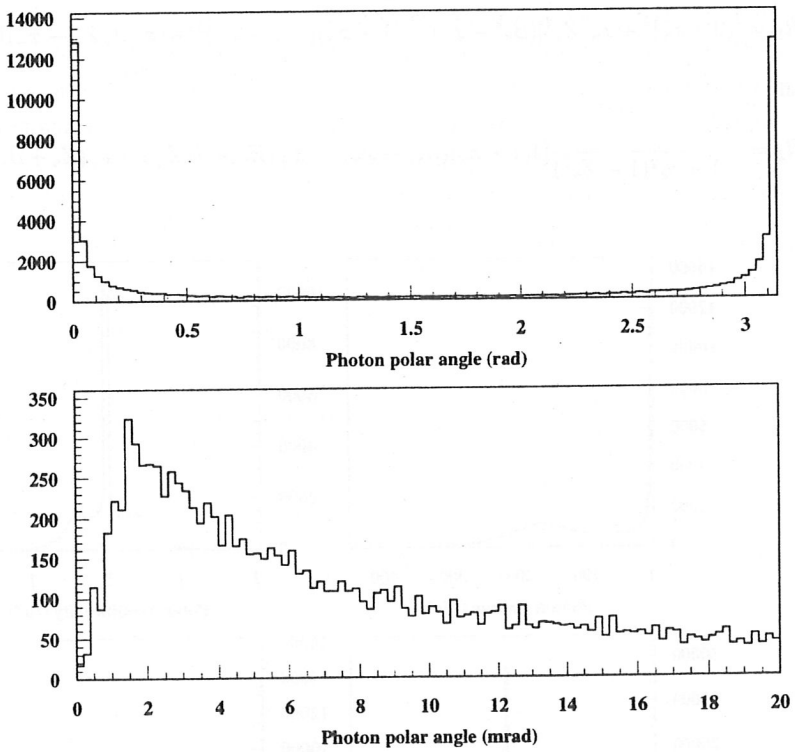

Figure 6: The photons distributions on the polar angle.

The $|M|^2$ is a smooth function that provides a high efficiency of the simulation. For the photons with the energies less than ΔE the efficiency is about 70-80% depending on the c.m.s. energy. For the photons with the energies more than ΔE the efficiency varies from 10 to 60% depending on the c.m.s. energy, reaction channel and selection criteria.

According to expressions described above 50000 events of the $e^+e^- \to \pi^+\pi^-\gamma$ process were simulated at the center of mass energy 952 MeV. Some of the distributions for the final state particles are shown in Fig.5-6. No selection criteria were used except that one of the charged particles should has the angles inside of the solid angle CMD-2 detector. On the first histogram of Fig.5 the energy spectrum of the emitted photons is represented. There is a bump near 160 MeV that corresponds to the dumping to ρ meson resonance. On the second histogram the polar acollinearity between two pions is shown. There are two symmetric bumps around the central peak that also correspond to the dumping to the resonance. On the third histogram the acollinearity between two pions in the azimuthal plane is shown. On the last histogram the momentum spectrum of pions is represented. The long tail can be explained by the emitted hard photons and by the dumping to the resonance. In Fig.6 two distributions over polar angles of the emitted photons are represented. The last one shows a small polar angles region in more details.

RESULTS IN K DECAYS FROM SERPUKHOV PS

V.Flyagin (V.Fliaguine)
Join Institute for Nuclear Research

ABSTRACT

The review of the latest Serpukhov experimental results on Kaon decays and other related data are presented. Of particular interest is possible tensor forces existence for K_{e3} decay. There are also other hints at tensor forces and that situation already became the subject of theoretical considerations beyond the Standard Model. The new data on the $K^+ \longrightarrow \pi^+\pi^0\pi^0$ decay Matrix element are presented, including h and k parameters. The new limit on $K_s^0 \longrightarrow e^+e^-$ decay is measured. New data on Kaon decays are expected from different Serpukhov experiments.

1 – Introduction

Although extensive experimental data are available on K meson decays, interest in this topic persists primarily for many reasons. One of them is a possibility of searching for so-called "new physics" beyond the Standard Model (SM).

We could draw up a long list of problems in which K decays provide very important information, such as CP violation understanding, $\Delta I = 1/2$ rule, "rare" and "forbidden" decays etc. Even common decay modes may yield unexpected new information. One of the cases, namely K_{e3} decay, is demonstrated below. There are also new theoretical ideas on the effective QCD Lagrangian approach to K decay physics which should be verified. Some good examples of this approach are demonstrated by calculations of semileptonic, non-leptonic K decays and the so-called structure dependent (SD) part of radiative decay modes.

At Serpukhov PS there are three experimental arrangements "on the floor" which provide or are expected to provide new results on Kaon decays. I shall not go into detail description of two of them and I offer an apology to colleagues if I give some not exact details below.

2 – Experimental situation

As I have mentioned, there are three experiments at the Serpukhov PS which provide new information on Kaon decays. The PS itself makes about two 1-1.5 months' runs per year for experimental physics purposes in spite of financial problems.

1. SERP-166 experiment (Spokesperson V.Bolotov). A set-up named "Istra M" is working reliably and this year we expect new information on some K^- decay features from this group. The results of this group obtained with the old experimental set-up "Istra" are very well known as they are included in the Review of Particle Properties [1]; the decay modes $\pi^0\pi^0 e^-\bar{\nu}_e$, $\pi^-\pi^0\pi^0\gamma$, and some other were observed for the first time. In the following discussion we shall compare some results of this group with our new ones.

   "Istra M" consists of many modern detectors situated in the unseparated 30 GeV/c beam. Its main components are: a beam part with Cherenkov counters to separate Kaons; a magnetic spectrometer with proportional chambers and drift tubes for charged secondary momentum measurements; e/m and hadron multichannel calorimeters and a muon identifier.

   The experiment continues data taking and processing. The main goals are: K^- decays into $\pi^-\pi^0\gamma$, $\pi^-e^+e^-$, $\pi^-\mu^+\mu^-$, $e^-\bar{\nu}_e\gamma$, and search for rare $K \longrightarrow \pi X^0$ decays, with X^0 as an unknown particle or $\nu\bar{\nu}$ system; and also search for Kaon decays into lepton plus heavy neutrino.

2. SERP-152 experiment (Spokesperson S.Denisov). Though the main tasks of the experiment are investigations of neutrino induced reactions using a tagged neutrino beam, the tagging station itself in principle can be used to study some K decays including CP violating parameter in K^+/K^- decay asymmetry.

3. SERP-167 experiment (cospokespersons J.Budagov,V.Flyagin,V.Kutjin). The aim of this experiment is to study some "common" and radiative Kaon decays.

Below I am going to describe briefly the set-up and some latest results of the experiment.

3 – Serpukhov-167 experiment

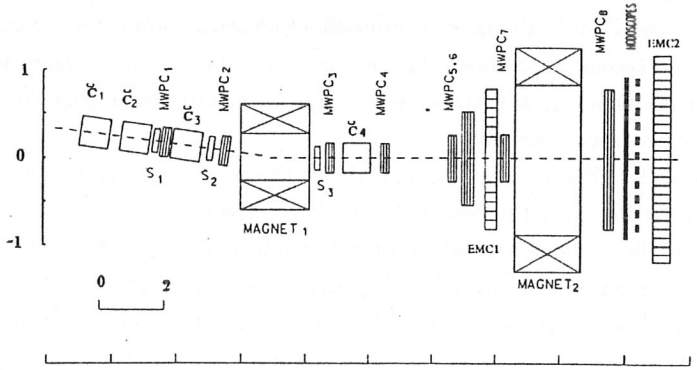

Figure 1:
Lay-out of the "Hyperon" spectrometer.

The experiment proposal aims to study the radiative and some other K^+ decays with neutral products using an one-arm spectrometer at the Serpukhov PS in the positive 10 GeV/c beam.

The main task is to search for and study the structure-dependent (SD) part of photon emission in semileptonic and nonleptonic K decays:

$$K^+ \longrightarrow \pi^+\pi^0\gamma, \quad 3\pi\gamma, \quad \pi^0 e^+ \nu_e \gamma \tag{1}$$

Within the same data taking runs the K_{e4} form factors which are also of interest will be measured. The SD part contains information on the internal quark structure of mesons. The verification of effective chiral Lagrangian models of low energy QCD, which are widely used now for the meson process description, is badly desirable.

Unfortunately, according to the latest theoretical estimations [3] there is a very little hope of finding a CP violating term in the $\pi^+\pi^0\gamma$ mode, as it was thought

possible earlier.

It must be mentioned that from the theoretical point of view the separation of the photon radiation structure part in $3\pi\gamma$ modes is more problematic than for $2\pi\gamma$ decays due to uncertainties in radiative corrections (there are no radiative corrections for $2\pi\gamma$ decay at all).

There are a few successful experimental attempts in search for direct photon emission (DE) in $\pi^+\pi^0\gamma$ mode [1]. No SD emission was found in other reactions (1). Our existing set-up of detectors in contrast to (not to a new set-up SERP-166) previous ones [4) 5) 6)] allows measuring all kinematical parameters: momenta of incoming and secondary charged particles, energies and emission angles of secondary gammas. Thus our advantage, as we expect, is better separation from the background (more constrained fit)

The collected experimental data are in the processing stage and at the moment I am not in position to report results on reactions (1).

As the first stage of investigations we made K_{e3} decay form factor measurement and estimated the upper limit for $K_s^0 \longrightarrow e^+e^-$ decay. These results are presented below. In both cases we did not yet use momentum measurement by magnetic field. Another decay we are to measure is $K^+ \longrightarrow \pi^+\pi^0\pi^0$, which is the main background source for decays (1) and should be studied carefully. On the other hand, the Dalitz plot slope parameters of this decay have recently attracted new theoretical interest [2]. The preliminary results will be shown below.

4 – Research design and methods

The experimental set-up was reconstructed and upgraded (we kept the old "Hyperon" spectrometer name for it) for Kaon decay study. It consists of beam facilities (see Fig.1), two magnetic spectrometer arrangements, two electromagnetic (e/m) calorimeters and is able to measure momenta of charged particles and γ-ray energies.

The unseparated 10 GeV/c positive particle beam contains about 5% of K^+ mesons, which can be picked out by 4 threshold gas Cherenkov counters. A typical K^+ intensity during a beam cycle is about 10^5/sec with a beam spill duration about 1-1.5 sec.

The beam spectrometer consists of a 4m long magnet and 16 multiwire plane proportional chambers (MWPC). The momentum measurement accuracy for an individual incoming particle is in 0.35-0.50% interval depending on the decay vertex position along the beam.

The spectrometer for charged secondary (SS) particles is based on a magnet with a 90 cm gap and pole dimensions 80×160 cm^2 (160 cm along the beam). The field usually used in K^+-decay experiments is 0.6 T. There are 19 MWPC planes in SS centered along one straight line in front of (12 MWPC) and behind (7 MWPC) the second magnet. The spectrometer provides secondary momentum measurement accuracy RMS=1.1% at 5 GeV/c, that is quite satisfactorily for our task.

Two hodoscopes behind the last MWPC allow an alternative trigger choice of requested charged particle amounts.

A distinctive feature of the whole arrangement is a set of two big (880 amplitude channels in total) lead glass hodoscopic e/m-calorimeters EMC1 and EMC2 which are used simultaneously. To let forward gammas and charge particles pass through the spectrometer the EMC1 has a 50×50 cm^2 hole in the center. All lead glass blocks have 14 radiation lengths in the longitudinal direction; their cross sections are different depending on location in the transversal plane.

The usual COMMON TRIGGER is defined by the requirements:

1) beam particle is K^+, chosen by Cherenkov threshold counters,

2) number of gammas Nγ >2,

3) threshold of gamma energy summed in individual cell groups is set to be the definite value within 0.3-1.1 GeV limits (adjustable).

These requirements suppress an incident beam to the level of 10^{-4}. In this case all decay modes (1) with one exception (3 charged pions) are taken simultaneously .

We make the e/m-calorimeter calibration in three ways for each beam exposure: by a positron beam or by fitting γ-quanta to π^0 and η meson masses. The $K^+ \longrightarrow \pi^+\pi^0$ decay (Fig.2) which is not completely suppressed by the trigger, gives us a very good possibility of calibrating data to a tagged π^0 momentum using data taken during the main exposures. This two-body decay is extremely useful for setting other processing parameters.

By now we have had a few runs with about 10^7 raw events written on tapes that are in processing now. During next two year period we intend to collect new data in two runs.

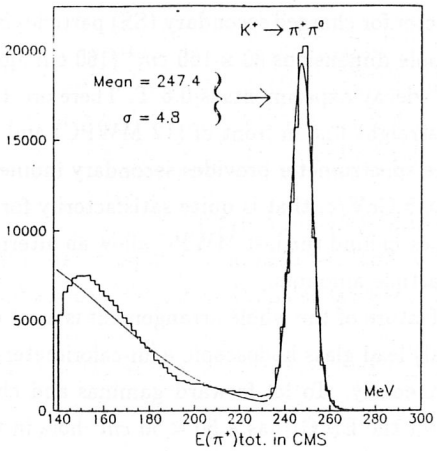

Figure 2:

π^+ energy spectrum in CM_System of K^+.

5 – Results on matrix element parameters for $K^\pm \longrightarrow \pi^\pm\pi^0\pi^0$ decay

We present here the Dalitz plot fit results based on 1/3 of total $K^+ \longrightarrow \pi^+\pi^0\pi^0$ decay statistics written on tapes. To make the most unambiguous sample we chose events with 4 gammas hitting the e/m calorimeters. The number of so chosen 6C-fit events in the Dalitz plot is 2×10^4.

Each Dalitz plot bin represents a ratio of observed event number to a number of events generated with the constant matrix element. The simulation takes into account the same trigger and reconstruction criteria and efficiencies of the detectors as for the real events. Using the standard matrix element form [1]:

$$|M|^2 = 1 + gU + hU^2 + kY^2 \quad \ldots . \tag{2}$$

where $U = \frac{(S_3 - S_0)}{m^2_{\pi^+}}$ $\quad Y = \frac{(S_1 - S_2)}{m^2_{\pi^+}}$

we obtained: (see Table 1.)

One can see the discrepancy between our data and world average parameters. The small errors of the PDG average are mainly due to the most precise data in the second column of Table 1. The spread of parameters given by other experiments is significant. We do not know the reason for these discrepancies; there is always of

Table 1:

Parameter	This experiment	Bolotov et al. [1]	PDG average
g	$0.753 \pm 0.014 \pm 0.010$	0.582 ± 0.021	0.594 ± 0.019
h	$0.126 \pm 0.019 \pm 0.010$	0.037 ± 0.024	0.035 ± 0.015
k	$-0.0194 \pm 0.0036 \pm 0.0040$	0.011 ± 0.007	

course a problem of possible systematic errors.

Having these not finalized data on the slope parameters I would prefer to leave comparison with theoretical calculations for the nearest future.

6 – Results of K_{e3} from factor measurements

The "Hyperon" spectrometer located before the second magnet was used in this experiment [8]. In this case the EMC-1 had a small $10 \times 10cm$ hole in the centre to let the beam through. The common trigger (see above) requirements were used during data taking. About 10^6 events were recorded on magnetic tapes. The acceptance of the set-up is a function of 4 momentum transfer q^2 to the dilepton pair and ranges from 12 to 19%.

Events with three e/m showers above the 1.0 GeV threshold each were accepted with one shower initiated by a secondary decay track (e^+).

The main background source was the $K^+ \longrightarrow \pi^+\pi^0$ decay, with one shower produced by π^+ interaction in EMC-1 lead glass . The events satisfying this hypothesis (4C-fit) were rejected.

The number of events accepted by the 2C-fit K_e3 hypothesis was found to be 3.2×10^4.

The form factor dependence on q^2 can be extracted in a model-independent way described above for $\pi^+\pi^0\pi^0$ decay, that is using Monte Carlo generated events with the constant matrix element and applying the same reconstruction program as for the real events.

The measured q^2 dependence of the vector form factor f_+ was approximated by the well known linear function :

$$f_+(q^2) = f_+(0)(1 + \lambda_+ q^2/m_\pi^2) \qquad (3)$$

and after fit we obtained one of the most precise value :

$$\lambda_+ = 0.0284 \pm 0.0027 \pm 0.0020$$

The confidence level is $P(\chi^2) = 21\%$.

This approximation (3) represents the standard V-A theory; one can also apply the

most general form for the matrix element, which would contain [1], in addition to the terms in (3), the elements

$$+ 2m_K f_s \bar{l}(1+\gamma_5)\nu + (2f_t/m_K)(P_K)_\lambda (P_K)_\nu \bar{l}\sigma_{\lambda\mu}(1+\gamma_5)\nu \qquad (4)$$

where f_s is the scalar form factor and f_t is the tensor form factor. In the case of K_{e3} decay, where f_- is negligible, the experiment yields limits on f_s/f_+ and $f_t/_+$ The result of our Dalitz plot fit to the general matrix element is shown in Table 2.

Table 2: General matrix element fit results.

Parameter	World average	Experiment [9] *	This experiment*
λ_+	---	$0.012^{+0.011}_{-0.014}$	$0.024^{+0.003}_{-0.003}$
$\|f_s/f_+\|$	$0.12^{+0.04}_{-0.05}$	$0.14^{+0.03}_{-0.04}$	$0.070^{+0.016}_{-0.016}$
$\|f_t/f_+\|$	$0.12^{+0.15}_{-0.13}$	$0.24^{+0.16}_{-0.14}$	$0.53^{+0.09}_{-0.10}$
$\Phi_{s\,t}$	---	$0.00^{+0.95}_{-0.95}$	$0.00^{+0.52}_{-0.52}$

*statistical errors only

The confidence level is $P(\chi^2) = 16\%$.

Our estimate indicates that the systematic errors were not larger than the statistical ones; so that due to systematical errors addition in ref. [1] the form factors are shown as:

$$f_s/f_+ = 0.070 \pm 0.16 \pm 0.16 \quad \text{and} \quad f_t/f_+ = 0.53^{+0.09}_{-0.10} \pm 0.10$$

Though both ratios are not equal to zero in this fit, we cannot definitely say that we observe the fact. Actually the result is: we have used two matrix element hypotheses and they are equally good. But let us assume for the moment that the tensor form factor exists (keeping in mind that the scalar one is too small) and look for other experimental manifestations of the tensor force. There is at least one more example, which indicates possible existence of this kind of force. The investigations of the $\pi \longrightarrow e\nu\gamma$ decay with the "Istra" set-up [10] indicate deviations from the Standard Model and again correct description is possible if effective quark lepton tensor interaction is involved [11].

To describe all above-mentioned experiments and avoid some theoretical problems, in ref. [12] two doublets of new tensor particles were introduced. This tensor interaction can play an important role in the nonleptonic weak interactions, particularly, it gives a contribution to $K_s - K_l$ mass difference [13]. It also affects e^+ spectrum parameters of μ^+ decay [14]. All these theoretical predictions give us a possibility of the experimental verification of this theory. In this context new precise experiments ought to be done to check the above-mentioned K_{e3} decay parameters. It is possible in new KLOE experiments.

7 – Upper limit for the branching of $K_S^0 \longrightarrow e^+e^-$ decay

The $K_S^0 \longrightarrow e^+e^-$ decay is suppressed by the flavor changing neutral current absence to a very low level, perhaps less than 10^{-14}. But it is worth looking for it as one of possible new physics manifestation beyond the Standard Model. A previous experimental value of the branching ratio is $\mathrm{Br}(K_S^0 \longrightarrow e^+e^-) < 1. \times 10^{-5}$.

A search for $K_S^0 \longrightarrow e^+e^-$ decay is performed by means of a 624 channel lead glass shower hodoscope EMC-2 and a set of proportional chambers behind the main magnet (M2). Neutral Kaons were produced in the quasi binary charge exchange reaction. A 9cm thick Cu target was exposed to a K^+- tagged (by Cherenkov counters) beam. It was followed by anti-coincidence counters to suppress the charged secondaries in the forward direction. The trigger was set to a 3 GeV threshold in the EMC-2. A total suppression of the incident Kaon beam was 4×10^{-4}.

The data obtained correspond to 3.5×10^9 incident K^+ mesons.

The main background is due to $K_S^0 \longrightarrow \pi^+\pi^-$ decay followed by hadron-e/m showers in lead glass. All possible e^+e^- events were killed by mass, minimum opening angle and "track-shower distance" in EMC criteria. The normalization was done by reconstruction of the observed $K_s^0 \longrightarrow \pi^0\pi^0$ and $K_s^0 \longrightarrow \pi^+\pi^-$ decays and Monte Carlo calculation of the acceptances shown in Table 3.

Table 3:

Decay	Ev.Nb.	Accept.	Br. [1)]	$\mathrm{Br}(e^+e^-)$
$\pi^+\pi^-$	6.4×10^5	0.794	0.686	$< 2.81 \times 10^{-6}$
$\pi^0\pi^0$	2.1×10^5	0.545	0.314	$< 2.75 \times 10^{-6}$
e^+e^-	none	0.697	$< 10^{-5}$	—

So we set the new upper limit to [7)]:

$$\mathrm{Br}(K_s^0 \longrightarrow e^+e^-) < 2.8 \times 10^{-6} \text{ at } 90\% \text{ CL}$$

It is still far off the Standard Model theoretical predictions. And we need more precise experiments which in principal can be carried out at new Φ factory facilities like DAFNE. Who knows. may be on this way we could find some "new physics".

8 – Conclusions

1. There are three experiments at the Serpukhov PS which provide new information on Kaon decays.

2. Two experiments provided new precise results in charged Kaon decays and

entered the Review of Particle Properties Tables.

3. Some of these data, for example on K_{e3} and even usual 3π decays, ought to be verified in future KLOE experiments in spite of existence of the first priority CP violation problem.

4. The search for "forbidden" and very rare decays like $K_s^0 \longrightarrow e^+e^-$ seems to be very important in future experiments.

Acknowledgements

I am grateful to V.Batusov and I.Liba for help in preparation the report.

References

1. Review of Particle Properties Phys.Rev. **45**,Numb. 11,1992.
2. A.A. Bel'kov et al. Interner Bericht DESY-Zeuten **93-04** ,1993.
3. A.A. Bel'kov et al. Prepr. DESY **93-060**, 1993.
4. B.P. Bolotov et al. Yadern. Phizika. **45**,1652, 1987.
5. R.J. Abrams et al. PRL **29** ,1118,1972.
6. K.M. Smith et al. NP **B109**,173,1976.
7. A. Blick et al Phys.Let. **B334** ,234,1994
8. S. Akimenko et al. Phys.Lett.,**B259**,225,1991.
9. H. Steiner et al. Phys.Lett.,**B36**,521.1971.
10. V.N. Bolotov et al. Phys.Lett. B243,108.1990; Sov.Nuc.Phys.**51**,455,1990.
11. A.A. Poblaguev. Phys.Lett. **B286**,169,1992.
12. M.V. Chizhov. Mod.Phys.Lett.A8,2753,1993.
13. M.V. Chizhov. Prepr JINR E2-94 **253**,1994. Subm. to PL.B.
14. M.V. Chizhov. Prepr JINR E2-94 **254**.1994. Subm. to Mod.PL.A.

AN IMPROVED EVALUATION OF HADRONIC CONTRIBUTIONS TO THE ANOMALOUS MAGNETIC MOMENT OF CHARGED LEPTONS

Stanislav Dubnička
Inst.of Physics, Slovak Acad.of Sci., Dúbravská cesta 9, 842 28 Bratislava, Slovakia
Anna Zuzana Dubničková
Dept.of Theor. Physics, Comenius Univ., Mlynská dolina, 842 15 Bratislava, Slovakia
Pavol Stríženec
Lab.of Theor. Physics, JINR, Dubna, Russia

ABSTRACT

The most precise up to now evaluation of the lowest-order hadronic vacuum-polarization contribution to the anomalous magnetic moment of the electron, muon and tau-lepton is achieved by analysing new additional data on some exclusive processes under consideration, by applying more accomplished models for a description of the pion and kaon electromagnetic structure, by calculating the external covariance matrix as given by the HESSE subroutine of the MINUIT program without any bounds on free parameters of models used in a description of existing data and by using the revised value of the coefficient of the third power of QCD formula for $R(s)$.

In the very topical case of the muon, the evaluated error is four times as small as the one-loop weak interaction contribution and it becomes comparable with an accuracy expected in the new Brookhaven National Laboratory E821 $g-2$ muon experiment.

1 – Introduction

Charged leptons are described by the Dirac equation and their magnetic moments are related to the spin by

$$\mu_\ell = g_\ell \frac{e}{2m_\ell \cdot \mathrm{c}} \cdot \frac{\hbar}{2}, \tag{1}$$

where the value of the gyromagnetic ratio g_ℓ is predicted (in the absence of the Pauli term) to be exactly 2 and in the QED language this number corresponds just to the simplest Feynman diagram (Fig.1) of an interaction of a charged lepton with an external magnetic field.

Practically, however, the interactions existing in nature modify (through radiative corrections) g_ℓ to be different from 2 because of the emission and absorption

of virtual photons (electromagnetic effects), intermediate vector and Higgs bosons (weak interaction effects) and the vacuum polarization into virtual hadronic states (strong interaction effects).

To describe this modification of g_ℓ, the magnetic anomaly was introduced by the relation

$$a_\ell \equiv \frac{g_\ell - 2}{2} = a_\ell^{(1)} \cdot \frac{\alpha}{\pi} + (a_\ell^{(2)\mathrm{QED}} + a_\ell^{(2)\mathrm{had}}) \cdot (\frac{\alpha}{\pi})^2 + a_\ell^{(2)\mathrm{weak}} + O(\frac{\alpha}{\pi})^3, \qquad (2)$$

where $\alpha = 1/137.0359895(61)$ is the fine-structure constant.

A comparison of a_ℓ^{exp} with a_ℓ^{th} provides one of the most rigorous tests of the standard model (SM) that unifies the electromagnetic, weak and strong interactions.

2 – Experimental situation

At present there are only experimental values on the anomalous magnetic moment of the electron and the muon.

The average of the most accurate measurements [1] for the electron

$$a_{e^-}^{\mathrm{exp}} = 1159652188.4(4.3) \times 10^{-12} \qquad (3)$$

and for the positron

$$a_{e^+}^{\mathrm{exp}} = 1159652187.9(4.3) \times 10^{-12} \qquad (4)$$

is

$$a_e^{\mathrm{exp}} = 1159652188.2(3.0) \times 10^{-12}. \qquad (5)$$

The average of the most accurate measurements [2] for the μ^+

$$a_{\mu^+}^{\mathrm{exp}} = 1165910(12) \times 10^{-9} \qquad (6)$$

and for the μ^-

$$a_{\mu^-}^{\mathrm{exp}} = 1165936(12) \times 10^{-9} \qquad (7)$$

is

$$a_\mu^{\mathrm{exp}} = 1165923(9) \times 10^{-9} \qquad (8)$$

which is in a perfect agreement with the definitive value

$$a_\mu^{\mathrm{exp}} = 1165922.9(8.5) \times 10^{-9} \qquad (9)$$

of the series of CERN experiments quoted just recently [3].

Up to now, there is no experimental value for the τ-lepton anomalous magnetic moment, though an experiment of that type has already been proposed [4]

to be realized at the Tau-charm factory, where cca 10^8 τ pairs would be produced via the reaction $e^+e^- \to \tau^+\tau^-$ at a c.m. energy of 3.67 GeV. Only the upper bound

$$a_\tau^{\rm exp} \leq 0.11 \tag{10}$$

was estimated experimentally from a low-statistics analysis of the $Z \to \tau^+\tau^-\gamma$ process [5].

3 – Theoretical situation

As one can see from (2), the anomalous magnetic moment of charged leptons consists of electromagnetic-, strong- and weak-interaction contributions. However, they do not contribute equally to every charged lepton.

The anomalous magnetic moment of the electron is almost completely described by electromagnetic contributions and therefore the electron anomaly a_e is still primarily concerned with the test of QED.

In the case of the muon, the hadronic contribution is adequately large to be identified experimentally and the weak-interaction contribution will likely be measurable in the new $g-2$ muon Brookhaven National Laboratory (BNL) E821 experiment [6] that is aimed at obtaining a factor of 20 in a precision above that of the previous CERN measurements [3], i.e. it is expected to be performed with an accuracy of

$$\Delta a_\mu^{\rm exp} = \pm 43 \times 10^{-11}. \tag{11}$$

So, the latter could provide a good test of the SM of electroweak interactions assuming that the hadronic part will be evaluated sufficiently precisely.

An experimental measurement of the anomalous magnetic moment of the τ-lepton seems to be the best candidate for the discovery of the new physics beyond the SM, as the hadronic contribution $a_\tau^{\rm had}$ and the weak-interaction contribution $a_\tau^{\rm weak}$ are significant (in comparison with the electron and muon) because of the large mass scale m_τ. However, due to a large instability of the τ-lepton (mean life time $= 2.956(0.031) \times 10^{-13}$s) the latter is not a simple task.

There is a remarkable progress in a precision of the theoretical prediction of the anomalous magnetic moments of charged leptons.

The QED contributions were calculated up to the eighth-order in vertices giving for the electron the value [7]

$$a_e^{\rm QED} = 1159652140.7(5.3)(4.1)(27.1) \times 10^{-12}, \tag{12}$$

where the first and second errors come from the theoretical uncertainties in the sixth- and eighth-order terms, while the third one reflects the uncertainty in the best available value of α.

For the muon the value

$$a_\mu^{\mathrm{QED}} = 1165846984(17)(28) \times 10^{-12} \tag{13}$$

is predicted [8], where the first error is a composite of uncertainties in theoretical calculations and the experimental uncertainty in the muon-electron mass ratio, and the second error comes from the uncertainty in the value of α.

Both the values, (12) and (13), were verified [9] by improved QED predictions using Padè Approximants.

By using the value a_e^{QED} of (12), also the QED contribution for the τ-lepton was calculated [10] to be

$$a_\tau^{\mathrm{QED}} = 1173.19(0.01) \times 10^{-6}. \tag{14}$$

As for the hadronic contributions, they are evaluated to be poorer. Listed below are the recent evaluations of the second-order charged lepton vertex (Fig.2):

for the electron [9]

$$a_e^{(2)\mathrm{had}} = 1600(200) \times 10^{-15} \tag{15}$$

for the muon

$$a_\mu^{(2)\mathrm{had}} = 7068(59)(164) \times 10^{-11} \quad [11] \tag{16}$$

$$a_\mu^{(2)\mathrm{had}} = 7100(105)(49) \times 10^{-11} \quad [12] \tag{17}$$

$$a_\mu^{(2)\mathrm{had}} = 7052(60)(46) \times 10^{-11} \quad [13] \tag{18}$$

and

for the τ-lepton [10]

$$a_\tau^{(2)\mathrm{had}} = 3600(300)(100) \times 10^{-9}. \tag{19}$$

The weak-interaction contributions were evaluated in the one-loop approximation to be:

for the electron [8, 9]

$$a_e^{\mathrm{weak}} = 0.05 \times 10^{-12} \tag{20}$$

for the muon [14, 15]

$$a_\mu^{\mathrm{weak}} = 195(1) \times 10^{-11} \tag{21}$$

and

for the τ-lepton it was estimated [10] just recently

$$a_\tau^{\mathrm{weak}} = 5.560(0.002) \times 10^{-7} \tag{22}$$

by scaling the corresponding contribution for the muon.

By comparing the theoretical values for the QED-, strong- and weak-interaction contributions, one can see immediately that the largest uncertainty in total theoretical values is caused by the strong-interaction contributions.

In the most interesting case of the muon the error of the strong-interaction contribution is only 1-2 times as small as that of the weak-interaction contribution. Therefore, a more accurate evaluation of the hadronic contributions is urgently needed before the new $g-2$ muon BNL E821 experimental result becomes available.

In what follows, we will just try to realize the latter program, taking into account a new additional experimental information on the processes under consideration and some theoretical improvements too.

The total hadronic contribution a_ℓ^{had} consists of the diagram (Fig.2) of $(\frac{\alpha}{\pi})^2$ order and the higher corrections of $(\frac{\alpha}{\pi})^3$ order presented in Fig.3 and Fig.4. Since the contributions of Fig.3 and Fig.4 seem to be smaller than errors of $a_\mu^{(2)\mathrm{had}}$ at present evaluated, we concentrate ourselves only on an evaluation of the diagram in Fig.2.

The latter can be represented by the integral

$$a_\ell^{(2)\mathrm{had}} = \frac{1}{4\pi^3}\int_{4m_\pi^2}^{\infty}\sigma^h(s)K_\ell(s)ds, \tag{23}$$

where $\sigma^h(s) \equiv \sigma_{tot}(e^+e^- \to \text{hadrons})$ and

$$K_\ell(s) = \int_0^1 \frac{x^2(1-x)}{x^2+(1-x)s/m_\ell^2}dx. \tag{24}$$

The integral (24) can be calculated explicitly. Since $m_e,\ m_\mu < m_\pi$, then for $\ell = e, \mu$ the latter takes the form

$$\begin{aligned} K_{e,\mu}(s) &= (\frac{1}{2}-A)-(A-\frac{A^2}{2})\ln A - \\ &- \frac{A(A^2-4A+2)}{2\sqrt{A^2-4A}}\ln\frac{\left[(2-A)-\sqrt{A^2-4A}\right]\left[-A+\sqrt{A^2-4A}\right]}{\left[(2-A)+\sqrt{A^2-4A}\right]\left[-A-\sqrt{A^2-4A}\right]} \end{aligned} \tag{25}$$

for all $4m_\pi^2 < s < \infty$, where $A = s/m_{e,\mu}^2$.

At the same time, as $m_\tau > m_\pi$, then for the τ-lepton, the explicit form of the function (24) depends on the relation of s to $4m_\tau^2$. If $4m_\pi^2 < s < 4m_\tau^2$, then

$$\begin{aligned} K_\tau(s) &= (\frac{1}{2}-A)-(A-\frac{A^2}{2})\ln A - \\ &- \frac{A(A^2-4A+2)}{\sqrt{4A-A^2}}\left[\arctan\frac{2-A}{\sqrt{4A-A^2}} - \arctan\frac{-A}{\sqrt{4A-A^2}}\right] \end{aligned} \tag{26}$$

and for all $s > 4m_\tau^2$ $K_\tau(s)$ is identical in form with (25), where now $A = s/m_\tau^2$.

From the practical point of view it is advantageous to separate the low-energy region ($4m_\pi^2 < s < s_0$) from the high-energy region ($s_0 < s < \infty$) in the integral (22) as follows

$$a_\ell^{(2)\mathrm{had}} = \frac{1}{4\pi^3}\left\{\int_{4m_\pi^2}^{s_0}\left[\sum_F \sigma_{tot}(e^+e^- \to \mathrm{F})\right] K_\ell(s)ds + \right.$$
$$\left. + \int_{s_0}^{\infty} \mathrm{R}(e^+e^- \to \mathrm{had})\sigma_{\mathrm{tot}}(\mathrm{e^+e^-} \to \mu^+\mu^-)\mathrm{K}_\ell(\mathrm{s})\mathrm{ds}\right\}. \qquad (27)$$

Here s_0 was fixed at $2\mathrm{GeV}^2$, where an overlap of the data on total cross sections of exclusive processes $e^+e^- \to \mathrm{F}$ and the data on $\mathrm{R} = \sigma_{tot}(e^+e^- \to \mathrm{had})/\sigma_{\mathrm{tot}}(\mathrm{e^+e^-} \to \mu^+\mu^-)$ already exists.

4 – Numerical evaluations

We have taken into account the following exclusive channels

$$\sum_F \sigma_{tot}(e^+e^- \to \mathrm{F}) = \sigma_{tot}(e^+e^- \to \pi^+\pi^-) + \sigma_{tot}(e^+e^- \to K^+K^-) +$$
$$+ \sigma_{tot}(e^+e^- \to K^0\bar{K}^0) + \sigma_{tot}(e^+e^- \to \pi^+\pi^-\pi^0) + \qquad (28)$$
$$+ \sigma_{tot}(e^+e^- \to \pi^0\omega) + \sigma_{tot}(e^+e^- \to \pi^+\pi^-2\pi^0) +$$
$$+ \sigma_{tot}(e^+e^- \to 2\pi^+2\pi^-) + \sigma_{tot}(e^+e^- \to 2\pi^+2\pi^-\pi^0) +$$
$$+ \sigma_{tot}(e^+e^- \to 3\pi^+3\pi^-).$$

All other known exclusive channels with higher thresholds are not considered here because they give negligible contributions on the level of estimated errors. There are two reasons for the latter. First, the cross sections of channels like $K^0K^\pm\pi^\pm$, $K^+K^-\pi^0$, $K^+K^-\pi^+\pi^-$ are of order 1 - 3 nb. Second, as can be seen from (24), $K_\ell(s)$ behaves like $\approx m_\ell^2/s$ for $s >> m_\ell^2$, thus suppressing the contributions from higher-energy regions.

To achieve realistic estimates, we have included, into our analysis, the uncertainties coming from the experimental input as well as the ones induced by the models of $\sigma_{tot}(e^+e^- \to \mathrm{F})$. Then the total error $\Delta a_\ell^{(2)\mathrm{had}}$ consists of three parts as follows

$$\Delta a_\ell^{(2)\mathrm{had}} = \sqrt{[\Delta a_\ell^{(2)\mathrm{had}}(\mathrm{stat})]^2 + [\Delta a_\ell^{(2)\mathrm{had}}(\mathrm{syst})]^2 + [\Delta a_\ell^{(2)\mathrm{had}}(\mathrm{mod})]^2} \qquad (29)$$

where $\Delta a_\ell^{(2)\mathrm{had}}(\mathrm{stat})$ is a statistical error, $\Delta a_\ell^{(2)\mathrm{had}}(\mathrm{syst})$ is a systematic error and $\Delta a_\ell^{(2)\mathrm{had}}(\mathrm{mod})$ is the model error defined as a deviation of the value of a contribution, obtained by the integration over experimental points using the trapezoidal rule, from the value obtained by the integration based on the model parametrization.

The total cross section for the first three processes $e^+e^- \to M\bar{M}$ ($M = \pi, K$) is given by the relation

$$\sigma_{tot}(e^+e^- \to M\bar{M}) = \frac{\pi\alpha^2\beta_M^3}{3s}|\mathrm{F}_M(s)|^2 \quad \text{with} \quad \beta_M = (1-4m_M^2/s)^{1/2}. \tag{30}$$

For charged pions $\mathrm{F}_\pi(s) = \mathrm{F}_\pi^{I=1}(s) + \mathrm{Re}^{i\phi}\frac{m_\omega^2}{m_\omega^2 - s - im_\omega\Gamma_\omega}$, where R and ϕ are the $\rho - \omega$ interference amplitude and phase, respectively, and $\mathrm{F}_\pi^{I=1}(s)$ is given by a more accomplished unitary and analytic model [16] (see Fig.5) with three excited states of the $\rho(770)$ meson. Analogous models for kaons [16] are presented in Fig.6 and Fig.7, where also new DM2 data [17] on the $e^+e^- \to K^+K^-$ total cross section have been included into the analysis.

For all other exclusive channels in (28) there are no theoretical models used and their contributions were evaluated only numerically by means of the trapezoidal integration over experimental points. Here new data [18] on $\pi^+\pi^-\pi^0$ and the data [18] on the new $\pi^0\omega$ channel together with corrected data [18] on the $\pi^+\pi^-\pi^0\pi^0$ channel were included into the analysis.

For $\pi^+\pi^-\pi^+\pi^-$, 5π and 6π, we used the same data as in [13].

The high-energy contributions to $a_\ell^{(2)\mathrm{had}}$ are obtained by means of the second integral in (27). For parametrization of $\mathrm{R}(e^+e^- \to \mathrm{had})$ we used the corrected QCD formula up to the third order of α_s, where the coefficient of the third power of α_s is changed from the value (+64) used in [13] to the value (-12) [19, 20]. Moreover, the electroweak corrections are taken into account in the sense of the Marshall analysis [21], but with electroweak parameters to be fixed at the table values and only $\Lambda_{\overline{MS}}$ is left as a free parameter.

The contributions of all resonances that appeared up to now in the region described by $\mathrm{R}(s)$ were evaluated in the narrow-width approximation like in [13].

Then all partial contributions to $a_\ell^{(2)\mathrm{had}}$ from the low-energy and high-energy regions are summarized in Tables1-3. Comparing Table 2 for the muon with results in [13] we see a drastic improvement for the model error of the $\pi^+\pi^-$ channel, as a consequence of the used more-accomplished unitary and analytic pion-form-factor model. Also diminution of experimental errors for $\pi^+\pi^-$, K^+K^- and $K_\mathrm{S}^0K_\mathrm{L}^0$ channels was achieved by a more thorough calculation of the external covariance matrix C_{ij} (as given by the HESSE subroutine of the MINUIT program with UP adjusted to the number of fitted parameters) determining the experimental error to be given by

$$\sigma^2 = \sum_{i,j} C_{ij}D_iD_j, \tag{31}$$

where $D_i = \partial a_\ell/\partial A_i$ and A_i are fitted parameters. For parameters A_i we do not use any upper and lower limits in finding the definitive minimum. The latter leads to C_{ij} that produces a smaller error in (31) in comparison with the contrary approach.

The same procedure was used in a description of the high-energy region. The latter, together with the above-mentioned correction of the coefficient of the third power of α_s in the QCD formula for R(s), diminished errors as shown in Table 2.

The summation of all contributions presented in Tables 1-3 gives the following values

$$a_e^{(2)\mathrm{had}} = 1810(11)(2) \times 10^{-15} \quad (32)$$

$$a_\mu^{(2)\mathrm{had}} = 6986(42)(16) \times 10^{-11} \quad (33)$$

$$a_\tau^{(2)\mathrm{had}} = 3436(24)(24) \times 10^{-9} \quad (34)$$

which are (compare them with (15)-(19)) the most precise up to now determined values of the lowest-order (Fig.2) hadronic vacuum polarization contributions to the anomalous magnetic moment of charged leptons. In the case of the muon we have achieved diminution of the error

$$\Delta a_\mu^{(2)\mathrm{had}} = 45 \times 10^{-11} \quad (35)$$

to be more than four times as small as the one-loop weak-interaction contribution (21) and it becomes comparable with the accuracy (14) expected in the new $g-2$ muon BNL E821 experiment [6].

5 – Summary and outlook

So, in the case of the muon, we have achieved the precision of theoretical predictions when higher-order contributions of strong- and weak- interactions are starting to play an important role in a comparison of theory with the expected experimental value to be measured in BNL E821 experiment.

The strong-interaction corrections of $(\frac{\alpha}{\pi})^3$ order are presented in Fig.3 and Fig.4. All contributions of Fig.3 can fortunately be evaluated without the knowledge of the underlying theory of strong interactions, as they can be directly related [22] to $\sigma_{tot}(e^+e^- \to \mathrm{had})$ measured in colliding-beam experiments, and they give [23] the value

$$a_\mu^{(3)\mathrm{had}}(3a-c) = -90(5) \times 10^{-11}. \quad (36)$$

By far the most difficult to evaluate theoretically is the contribution of hadronic light-by-light (Fig.4) scattering. No way has been found up to now to relate this contribution to observable quantities. Therefore, at present, the hadronic light-by-light contribution to the anomalous magnetic moment of the muon can be evaluated only in a model-dependent way. Such a calculation was carried out

previously [22] assuming that the blob in Fig.4 can be approximated by quark loops of various flavours and colors. Then one obtains the following value

$$a_\mu^{(3)\mathrm{had}}(\mathrm{light-by-light}) = -260(100) \times 10^{-11}. \tag{37}$$

The second approach [11] is based on the assumption that the blob in Fig.4 can be approximated by charged-pion loops and various low-energy resonances. Then one obtains the value

$$a_\mu^{(3)\mathrm{had}}(\mathrm{light-by-light}) = 49(5) \times 10^{-11}. \tag{38}$$

Finally, the light-by-light-scattering diagram (Fig.4) contribution was calculated [24] within the low-energy effective theory of QCD, the Nambu-Jona-Lasinio model and hidden local chiral symmetry as guides. As a result, one gets

$$a_\mu^{(3)\mathrm{had}}(\mathrm{light-by-light}) = -36(16) \times 10^{-11}. \tag{39}$$

In view of the contradicting values (37)-(39), it is highly desirable to find a better and a more reliable estimate of the light-by-light-scattering contribution.

On the other hand, it has been pointed out recently that the $\gamma\gamma Z$ electron triangular anomaly diagrams induce [25] a relative large two-loop contribution

$$a_\mu^{\mathrm{weak}}(\gamma\gamma Z) = -10 \times 10^{-11} \tag{40}$$

to the anomalous magnetic moment of the muon. They are no more negligible and it is desirable to complete carefully all the two-loop calculations before the new result from the BNL E821 experiment becomes available.

From all discussed here it follows that the weak-interaction contribution to the anomalous magnetic moment of the muon is very likely to be confirmed by the BNL E821 experiment. If the latter will be achieved, then the comparison of theory with experiment will impose very strict constraints on the new physics, such as extra gauge bosons, additional Higgs scalars, supersymmetry and a compositeness of leptons.

References

1. R.S. Van Dyck, Jr., P.B. Schwinberg and H.G. Dehmelt, Phys. Rev. Lett. **59**, 26 (1987).

2. J. Bailey et al., Phys. Lett. **68B**, 191 (1977).

3. F.J.M. Farley, Z. Phys. **C56**, S88 (1992).

4. M.L. Perl, in Proceedings of the Lake Louise Winter Institute, February (1991).

5. J.A. Grifols and A. Méndez, Phys. Lett. **255B**, 611 (1991).

6. B. Lee Roberts, Z. Phys. **C56**, S101 (1992).

7. T. Kinoshita and W.B. Lindguist, Phys. Rev. **D42**, 636 (1990).

8. T. Kinoshita, Cornell Univ. Preprint CLNS 93/1187, Ithaka (1993).

9. J. Ellis, M Karliner, M.A. Samuel and E. Steinfelds, Preprint SLAC-PUB-6670, Stanford (1994).

10. M. Samuel, G. Li and R. Mendel, Phys. Rev. Lett. **67**, 668 (1991).

11. T. Kinoshita, B. Nizic and Y. Okamoto, Phys. Rev. **D31**, 2108 (1985).

12. J.A. Casas, C. Lopez and F.J. Yndurain, Phys. Rev. **D32**, 736 (1985).

13. Ľ. Martinovič and S. Dubnička, Phys. Rev. **D42**, 884 (1990).

14. G. Altarelli, N. Cabibbo and L. Maiani, Phys. Lett. **40B**, 415 (1972).

15. R. Jackiw and S. Weinberg, Phys. Rev. **D5** 2473 (1972) and ibid. **D16**, 3596 (1977).

16. M.E. Biagini, S. Dubnička, E. Etim and P. Kolář, Nuovo Cimento **A104**, 363 (1991).

17. D. Bisello et al, Z. Phys. **C39**, 13 (1988).

18. D. Bisello et al, Z.Phys. **C56**, 15 (1992)
S.I. Dolinsky et al, Phys.Lett. **174B**, 453 (1986)
N. Albrecht et al, Phys.Lett. **185B**, 223 (1987).

19. S.G. Gorishny, A.L. Kataev and S.A. Larin, Phys.Lett. **B259**, 144 (1991).

20. L.R. Surguladze and M.A. Samuel, Phys. Rev. Lett. **66**, 560 (1991).

21. R. Marshall, Z.Phys. **C43**, 595 and 607 (1989).

22. J. Calmet, S. Narison, M. Perrotet and E.de Rafael, Rev. Mod. Phys. **49**, 21 (1977).

23. T. Kinoshita, Z. Phys. **C56**, S80 (1992).

24. M. Hayakawa, T. Kinoshita and A.I. Sanda, Preprint DPNU-94-21, Nagoya (1995).

25. E.A. Kuraev, T.V. Kukhto and A. Schiller, Sov. J. Nucl. Phys. **51**, 1031 (1990).

Channel	Central value $\times 10^{-12}$	Exp. error $\times 10^{-15}$	Model error $\times 10^{-15}$
$\pi^+\pi^-$	1.3610	5.614	0.31
K^+K^-	0.0593	2.386	1.42
$K_S^0K_L^0$	0.0325	1.592	1.42
$\pi^+\pi^-\pi^0$	0.1350	6.769	-
$\omega\pi^0$	0.0187	1.719	-
$\pi^+\pi^-\pi^0\pi^0$	0.0336	5.080	-
$\pi^+\pi^-\pi^+\pi^-$	0.0147	1.534	-
5π	0.0008	0.247	-
6π	0.00003	0.064	-
QCD 1.reg. $2\ \text{GeV}^2 \le s \le 9.61\ \text{GeV}^2$	0.0633	0.974	0.002
QCD 2.reg. $20.2\ \text{GeV}^2 \le s \le 81.0\ \text{GeV}^2$	0.0208		0.003
QCD 3.reg. $s \ge 196.0\ \text{GeV}^2$	0.0248		0.004
$c\bar{c}$ reg. $9.61\ \text{GeV}^2 \le s \le 20.2\ \text{GeV}^2$	0.0217	0.581	-
$b\bar{b}$ reg. $81.0\ \text{GeV}^2 \le s \le 196.0\ \text{GeV}^2$	0.0045	0.025	-
Resonances	0.0197	1.147	-

Table 1: Partial contributions to $a_e^{(2)\text{had}}$

Channel	Central value $\times 10^{-11}$	Exp. error $\times 10^{-11}$	Model error $\times 10^{-11}$
$\pi^+\pi^-$	4942.16	20.59	0.86
K^+K^-	232.53	9.34	5.54
$K_S^0K_L^0$	127.31	6.23	5.54
$\pi^+\pi^-\pi^0$	512.36	25.57	-
$\omega\pi^0$	74.15	6.74	-
$\pi^+\pi^-\pi^0\pi^0$	133.82	20.23	-
$\pi^+\pi^-\pi^+\pi^-$	59.99	10.45	-
5π	3.17	0.99	-
6π	1.30	0.44	-
QCD 1.reg. $2\ \text{GeV}^2 \le s \le 9.61\ \text{GeV}^2$	604.78	2.00	8.22
QCD 2.reg. $20.2\ \text{GeV}^2 \le s \le 81.0\ \text{GeV}^2$	89.98		11.76
QCD 3.reg. $s \ge 196.0\ \text{GeV}^2$	10.70		1.68
$c\bar{c}$ reg. $9.61\ \text{GeV}^2 \le s \le 20.2\ \text{GeV}^2$	92.48	2.40	-
$b\bar{b}$ reg. $81.0\ \text{GeV}^2 \le s \le 196.0\ \text{GeV}^2$	19.40	0.22	-
Resonances	83.03	4.83	-

Table 2: Partial contributions to $a_\mu^{(2)\text{had}}$

Channel	Central value $\times 10^{-8}$	Exp. error $\times 10^{-8}$	Model error $\times 10^{-8}$
$\pi^+\pi^-$	170.10	0.73	0.38
K^+K^-	12.68	0.50	0.84
$K_S^0K_L^0$	6.80	0.33	0.84
$\pi^+\pi^-\pi^0$	21.84	1.08	-
$\omega\pi^0$	4.62	0.42	-
$\pi^+\pi^-\pi^0\pi^0$	8.62	1.30	-
$\pi^+\pi^-\pi^+\pi^-$	3.93	1.01	-
5π	0.21	0.06	-
6π	0.11	0.04	-
QCD 1.reg. $2\ \text{GeV}^2 \le s \le 9.61\ \text{GeV}^2$	59.72	0.40	1.04
QCD 2.reg. $20.2\ \text{GeV}^2 \le s \le 81.0\ \text{GeV}^2$	17.72		1.84
QCD 3.reg. $s \ge 196.0\ \text{GeV}^2$	2.79		0.42
$c\bar{c}$ reg. $9.61\ \text{GeV}^2 \le s \le 20.2\ \text{GeV}^2$	14.66	0.36	-
$b\bar{b}$ reg. $81.0\ \text{GeV}^2 \le s \le 196.0\ \text{GeV}^2$	4.64	0.05	-
Resonances	12.54	0.71	-

Table 3: Partial contributions to $a_\tau^{(2)\text{had}}$

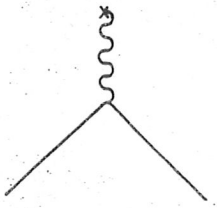

Fig.1. The simplest Feynmam diagram of an interaction of a charged lepton with an external magnetic field.

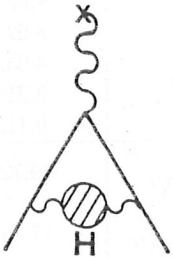

Fig.2. The lowest-order hadronic vacuum-polarization contribution to the anomalous magnetic moment of charged leptons.

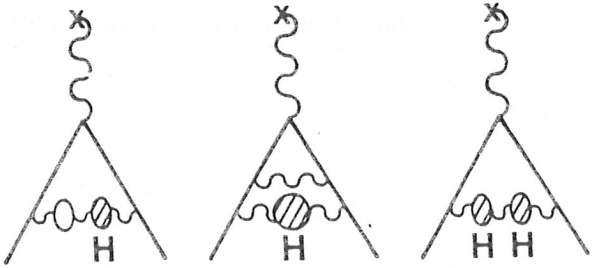

Fig.3. The third-order hadronic vacuum-polarization contributions to the anomalous magnetic moment of charged leptons.

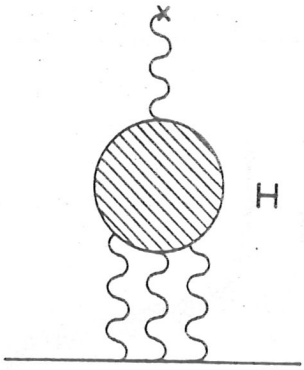

Fig.4. Hadronic light-by-light scattering contributions to the anomalous magnetic moment of charged leptons.

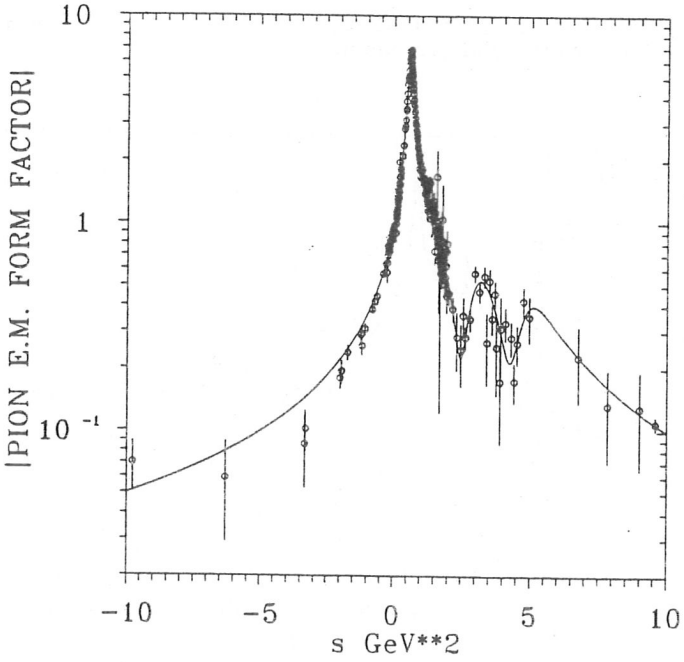

Fig.5. The unitary and analytic pion form factor model with three excited states of the rho-meson.

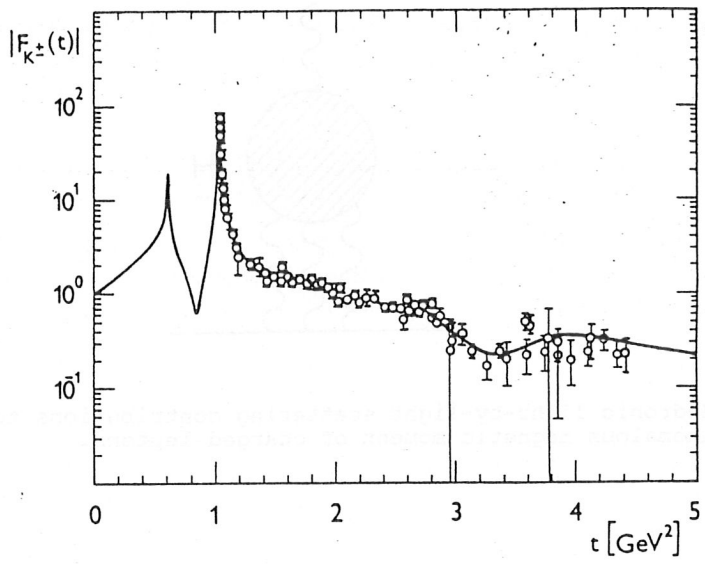

Fig.6. The unitary and analytic model of the electromagnetic form factor of charged kaons.

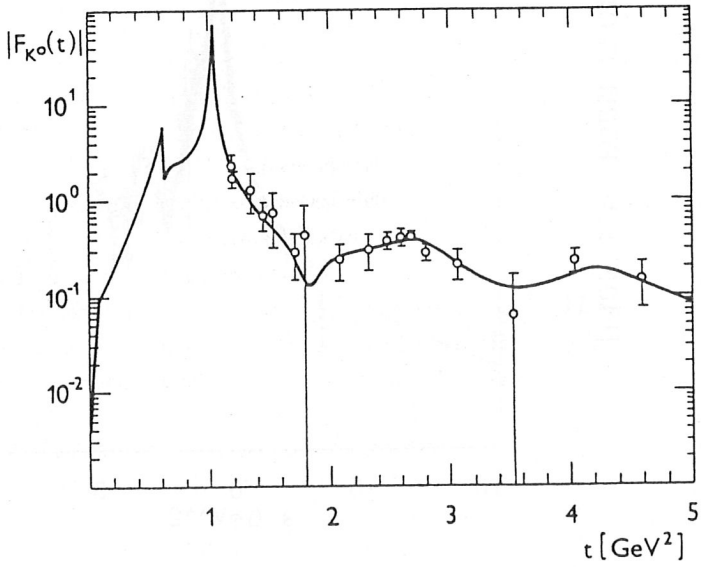

Fig.7. The unitary and analytic model of the electromagnetic form factor of neutral kaons.

HOW TO SEE THE CHIRAL STRUCTURE OF QCD VACUUM IN LOW ENERGY $\pi - \pi$ SCATTERING [1]

Jan STERN
Division de Physique Théorique[2] *, Institut de Physique Nucléaire, 91406 Orsay Cedex*

Abstract

Precise measurement of the $\pi\pi$-phase shift $\delta_0^0(E)$ at very low energies would provide, for the first time, the experimental evidence in favour of or against the existence of a large quark condensate in the QCD vacuum, which is standardly postulated as the mechanism of the spontaneous breakdown of chiral symmetry in QCD. The contribution of Daϕne to this discovery could be decisive.

1 – INTRODUCTION

The origin and the dynamics of the spontaneous breakdown of various symmetries in the Standard Model is not yet fully understood. Different theoretical scenarios are conceivable and crucial experimental tests are still missing. In the electroweak sector, these tests require energies not reached so far : The question is that of the existence of an elementary Higgs field, of its self-interaction and of its coupling to fermions. In the QCD sector, one meets a similar situation concerning the spontaneous breakdown of chiral symmetry (SBCHS). Here too, the standardly postulated mechanism of symmetry breaking - the formation of a condensate of quark-antiquark pairs in the QCD vacuum - has not so far been tested experimentally. Such tests are possible within new low-energy experiments requiring a precision not reached so far. In this talk this point will be illustrated on the example of low-energy $\pi\pi$-scattering which is experimentally accessible in K_{e4} decays. In this domain Daϕne-Kloe can reach a decisive improvement and provide the first experimental evidence in favour of or against the existence of a strong quark condensation in the QCD vacuum.

[1] Invited talk at the "Workshop on Physics and Detectors for DaΦne", Frascati 4-7 April 1995
[2] Unité de Recherche des Universités Paris XI et Paris VI associée au CNRS

2 – CHIRAL SYMMETRY IN QCD

In the limit $m_u = m_d = m_s = 0$ of massless light quarks, the QCD Lagrangian is invariant under the group of transformations

$$\psi \equiv \begin{pmatrix} u \\ d \\ s \end{pmatrix} \to \left\{ \frac{1}{2}(1-\gamma_5)g_L + \frac{1}{2}(1+\gamma_5)g_R \right\} e^{i\omega_v} \psi \tag{1}$$

that consists of two independent $SU(3)$ rotations g_L and g_R of the left-handed and right-handed components of quark fields and of a common phase factor $e^{i\omega_v}$. This global chiral symmetry $SU(3)_L \times SU(3)_R \times U(1)_v$ implies the existence of 9 vector ($a = 0, 1 \ldots 8$) and 8 axial ($i = 1 \ldots 8$) Noether currents

$$J^a_\mu(x) = \bar{\psi}\gamma_\mu \frac{\lambda^a}{2}\psi(x), \quad J^i_{\mu 5}(x) = \bar{\psi}\gamma_\mu\gamma_5 \frac{\lambda^i}{2}\psi(x) \tag{2}$$

which are conserved

$$\partial^\mu J^a_\mu(x) = \partial^\mu J^i_{\mu 5}(x) = 0 \; . \tag{3}$$

Provided the physical spectrum of the theory does not involve massless quarks (confinement), the chiral symmetry $SU(3)_L \times SU(3)_R \times U(1)_v$ must be spontaneously broken down to the subgroup $U(3)_v$ generated by the 9 vector currents J^a_μ. This is known to be a mathematical consequence of anomalous Ward identities[1] and of the vectorial character of the coupling of quarks and gluons[2]. The statement of SBCHS has a double meaning : First, the vacuum state $|0>$ does not share all the symmetries of the Lagrangian. In particular, the 8 axial charges do not annihilate the vacuum :

$$\int d^3\vec{x} \; J^i_{05}(\vec{x}, t)|0> \neq 0 \; . \tag{4}$$

Next, there exist 8 massless $J^p = 0^-$ particles $|\pi^i, \vec{p}>$ coupled to the 8 conserved axial currents :

$$<0|J^i_{\mu 5}|\pi^j, \vec{p}> = i\delta^{ij} F_0 p_\mu, \; p^2 = 0 \; . \tag{5}$$

The quantity F_O, which coincides with the chiral limit $m_u = m_d = m_s = 0$ of the pion decay constant $F_\pi = 92.4$ MeV, plays a fundamental role. It measures a long-range correlation between the Noether currents in the vacuum of the massless theory :

$$F_0^2 \delta^{ij} = \frac{i}{3} \int d^4x < 0|T\left\{ J^i_{\mu 5}(x) J_5^{\mu,j}(0) - J^i_\mu(x) J^{\mu,j}(0) \right\}|0> \; . \tag{6}$$

The existence of this correlation implies the asymmetry of the vacuum, c.f. Eq. (4). Indeed, the operator in the curly bracket on r.h.s. of Eq. (6) transforms as the irreducible representation $\{8, 8\}$ of the symmetry group $SU(3)_L \times SU(3)_R$. Consequently, if the vacuum was invariant, the matrix element (6) would necessarily vanish.

In other words, F_0 is an **order parameter** : its non zero value implies SBCHS. In fact, Goldstone theorem guarantees that also the inverse statement is true : $F_0 \neq 0$ is not only a sufficient but also a **necessary** condition of SBCHS.

The 8 Goldstone bosons are identified with the 8 lightest $J^p = 0^-$ particles π, K, $\bar{K}$ and η. The non zero but small masses of pseudoscalar mesons reflect the nonvanishing (running) masses of the light quarks u, d, s. The mass term in the QCD Lagrangian

$$\mathrm{L} = \mathrm{L}_0 - \bar{\psi}\, \mathcal{M}\, \psi, \quad \mathcal{M} = \mathrm{diag}(m_u, m_d, m_s) \tag{7}$$

breaks the chiral symmetry explicitly. However, the chiral symmetry still remains a good approximation and the mass term in Eq.(7) can be treated as a small perturbation, since, in the real world,

$$m_u, m_d, m_s \ll \Lambda_H \sim 1\mathrm{GeV} \tag{8}$$

where Λ_H represents the mass scale of the first massive bound states of the theory $(\rho, N \ldots)$.

3 – THE QUARK CONDENSATE

The theoretical facts summarized above represent unavoidable consequences of the QCD Lagrangian. In spite of their importance, these statements remain on a rather general level. In particular, the basic fact of SBCHS, i.e. the non-zero value of the correlator F_0^2 (6), does not by itself imply a particular chiral structure in the QCD vacuum, nor does it clarify the dynamical origin of SBCHS in QCD. Further progress in this direction requires a consideration of other order parameters. This point can be illustrated by an analogy with the spin systems. In the latter case, the spontaneous breakdown of rotation symmetry can be realized by means of rather different types of magnetic order in the ground state. **Ferromagnets** are characterized by aligned spins

$$\uparrow \uparrow \uparrow \uparrow \uparrow \uparrow \ ,$$

whereas **antiferromagnets** exhibit a rather different magnetic structure of the type

$$\uparrow \downarrow \uparrow \downarrow \uparrow \downarrow \ .$$

The order parameter which makes the distinction between these two extreme cases is the average spontaneous magnetization $< \vec{m} >$: For ferromagnets $< \vec{m} > \neq 0$ and this parameter plays a crucial role in the description of the response of the system to an external magnetic field. On the other hand, the magnetization of an antiferromagnet

is marginal or even vanishing to the extent that the ground state approaches the Néel-type magnetic order. Hence, the spontaneous magnetization is an example of order parameter whose non-zero value is not necessary for the spontaneous breakdown of symmetry to occur. Rather, it describes the nature of the order in the ground state, i.e. the structural details of the dynamics of symmetry breaking.

In QCD, the simplest order parameter which plays a similar role as the spontaneous magnetization of spin systems is the vacuum condensate $< 0|\bar{q}q|0 >$ $(q = u, d, s)$ defined in the chiral limit. (In this limit, the definition of the quark condensate is free of ultraviolet ambiguities.) It is convenient to describe quark condensation by a parameter B_0

$$B_0 = -\frac{1}{F_0^2} < 0|\bar{u}u|0 >= -\frac{1}{F_0^2} < 0|\bar{d}d|0 >= -\frac{1}{F_0^2} < 0|\bar{s}s|0 > , \tag{9}$$

which has the dimension of mass. Since the operator $\bar{q}q$ carries anomalous dimension, B_0 is actually a running quantity depending on the renormalization scale μ. In order to get a renormalization group invariant quantity, B_0 has to be multiplied by the quark mass. This fact explains, why it is so difficult to detect quark condensation experimentally : B_0 enters physical observables only multiplied by a quark mass and consequently, it manifests itself exclusively through tiny symmetry breaking effects.

One should, of course, understand within the framework of QCD the interplay between SBCHS and quark condensation. In particular, one should check and clarify the theoretical possibility (suggested by the example of antiferromagnetism) of SBCHS without formation of a quark condensate. The first (rather modest) step in this direction can be reached, expressing the order parameters F_O^2 (c.f. Eq. 6) and B_0 (Eq. 9) in terms of the Euclidean functional integral of QCD in a four-dimensional box of size L. Integrating over quarks first (giving them a small mass m) one finds, that for large volume and small masses, the order parameters of SBCHS F_O^2 and B_0 are both determined by the small eigenvalues of the Dirac operator

$$H(A)\phi_n = \lambda_n(A)\phi_n, \quad H(A) = \gamma_\mu(i\partial_\mu + A_\mu^a t^a) \tag{10}$$

averaged over all gluonic configurations $A_\mu^a(x)$.[2]. (Notice that in Euclidean space, $H^+ = H$. Since $\{\gamma_5, H\} = 0$, the spectrum λ_n is symmetric around 0.) In particular, the crucial question is how dense does the spectrum become at the infrared end as $L \to \infty$[3]. Three types of behavior appear as particularly interesting. They are all characterized by different thermodynamical properties (different dependence on L and on m) and, in this sense, they appear as possible distinct phases.

I. $\lambda(L) \sim \frac{1}{L}$ In this case, both F_0 and the quark condensate vanish. Chiral symmetry is not spontaneously broken (i.e. quarks cannot be confined.)

II. $\lambda(L) \sim 1/L^2 F_0$ In this case[5] one can have $F_0 \neq 0$, but the quark condensate still vanishes as L^{-2} in the limit $L \to \infty$, $m \to 0$. Goldstone bosons are formed, SBCHS takes place but quarks do not condense.

III. $\lambda(L) \sim 1/L^4\psi$ This is the minimal level density that is needed for quarks to start condense[4]. Both F_0 and B_0 are different from zero : $< \bar{q}q > \sim -\psi$.

This discussion does not tell us what actually does happen in the QCD vacuum. However, it collects theoretical possibilities and it illustrates how SBCHS (i.e. $F_0 \neq 0$) without quark condensation can naturally arise within QCD. In fact, it is conceivable that in practice, the "phases" II. and III. coexist and compete, giving rise to a marginal quark condensate of the order $B_0 \sim 100$ MeV, or so.

It is standardly postulated that in QCD, SBCHS is triggered by a strong quark condensation[6] with the parameter B_0 of the order or even larger than the bound-state scale $\Lambda_H \sim 1$ GeV. (A typical value at $\mu = 1$ GeV would be $B_0 \sim 1.6$ GeV[7]. This believe is usually motivated by the Nambu, Jona-Lasinio model[8] in which, indeed, SBCHS and quark condensation can hardly be dissociated. However, the chiral structure of the NJL model differs from that of QCD : In the NJL model, the mechanism of SBCHS is not related to the spectral properties of the Dirac operator (10). It is conceivable that the previous discussion and the emergence of the "phase II" as a theoretical possibility are in fact limited to vector - like theories such as QCD.

The standard scenario of a large quark condensate seems to be supported by existing lattice simulations performed at finite m and L and subsequently, extrapolated to the limit $m \to 0$, $L \to \infty$ following extrapolation formulae valid exclusively in the phase III. Lattice regularization is known to mistreat chiral symmetry in one way or another, especially in the quenched approximation in which the most significant results are obtained. (For a recent review see Ref. 9)). For these reasons, the lattice results concerning the size of $< \bar{q}q >$ deserve an independent experimental test.

The question of the strength of quark condensation has to be settled experimentally. At present, none of the characteristic consequences of the standard strong condensation scenario has been experimentally tested. Actually, there is no single experimental fact available that would allow to eliminate the alternative possibility II of SBCHS without quark condensation.

4 – QUARK MASSES

The amount of quark condensation has immediate consequences for the relationship between pseudoscalar meson and (current) quark masses. For $m_q \ll \Lambda_H$, one has for instance

$$\begin{aligned} M^2_{\pi^+} &= (m_u + m_d)B_0 + (m_u + m_d)^2 A_0 + \dots \\ M^2_{K^+} &= (m_u + m_s)B_0 + (m_u + m_s)^2 A_0 + \dots \end{aligned} \tag{11}$$

where the dots stand for chiral log's (irrelevant for the present, merely qualitative discussion) and for higher order terms. A similar expression holds for the η-mass, except that at the quadratic level, a new constant appears reflecting the axial U(1) anomaly and the $\eta - \eta'$ mixing. A_0 is yet another order parameter of SBCHS : $F_0^2 A_0$ represents a long range correlation between scalar and pseudoscalar quark densities of the type similar to (6). A_0 can be roughly estimated using sum rules : $A_0 \sim 1 \div 5$.

In view of the previous discussion, let us distinguish three cases : i) The (standard) case of a **large condensate** characterized by the condition

$$m_q \ll m_0 = \frac{B_0}{2A_0} \sim \Lambda_H \tag{12}$$

i.e. by the dominance of the first term in the expansion (11). ii) The case of **vanishing condensate**, $B_0 = 0$ and finally, iii) the "mixed case" of a **marginal condensate** defined by

$$m_q \sim m_0 = \frac{B_0}{2A_0} \ll \Lambda_H \ . \tag{13}$$

In the latter case the first and second terms in Eq. (11) may become of a comparable size.

4.1 The quark mass ratio $r = \frac{m_s}{\widehat{m}}, \widehat{m} = \frac{1}{2}(m_u + m_d)$

In the large condensate case this ratio is predicted[10),12)] to be

$$r = r_2 = 2\frac{M_K^2}{M_\pi^2} - 1 + \text{small corrections} \simeq 26 \ . \tag{14}$$

If the condensate vanishes, Eq. (11) implies

$$r = r_1 = 2\frac{M_K}{M_\pi} - 1 + \text{small corrections} \simeq 6.3 \ . \tag{15}$$

In the case of a marginal condensate, the ratio r can take any value between the two extremes r_1 and r_2.

$$r_1 \leq r \leq r_2 \ . \tag{16}$$

4.2 The Gell-Mann, Oakes, Renner ratio $x = \frac{(m_u+m_d)B_0}{M_\pi^2}$.

In the large condensate alternative, x is predicted to be close to 1[6),11)]:

$$x = 1 + \frac{1}{32\pi^2}\frac{M_\pi^2}{F_\pi^2}\bar{l}_3 + \cdots , \tag{17}$$

where $\bar{l}_3$ is one of the $SU(2) \times SU(2)$ low energy constants introduced by Gasser and Leutwyler[11)]. It is expected to be of the order of unity. Comparing with Eq. (11), one finds

$$\bar{l}_3 = -32\pi^2 F_\pi^2 \frac{A_0}{B_0^2} . \tag{18}$$

Hence, for $B_0 \to 0$, $\bar{l}_3$ is naturally expected to be large and negative ($A_0 > 0$). In this case the expansion (17) breaks down, since it treats m_q/m_0 as a small quantity. In the case of a marginal condensate, the GOR ratio can actually take any value between 0 ($B_0 = 0$) and 1, depending on the quark mass ratio r :

$$x = \frac{(r - r_1)(r + r_1 + 2)}{r^2 - 1} + \text{small corrections} . \tag{19}$$

4.3 The η-mass

In the case of a large condensate, the η-mass is related to the π and K-masses by the well-known Gell-Mann Okubo formula, modulo higher order corrections (including the $\eta - \eta'$ mixing) which are hard to estimate in advance. For smaller B_0 this relationship is lost. The reason is that in this case, the unknown anomaly and $\eta - \eta'$ mixing contributions are, in principle, of a comparable size as the quark condensate contribution.

4.4 The running quark mass $\widehat{m}(\mu)$

The standard source of information on the magnitude of running quark masses are the QCD sum rules (see e.g. [7),14)]). A model independent evaluation of the sum rule for $\widehat{m}$ is at present problematic, due to the complete absence of experimental informations on the size and shape of the spectral function associated with the divergence of the axial current $\bar{u}\gamma_\mu\gamma_5 d$, beyond the one-pion contribution. Models for this spectral function that are **based on the large condensate hypothesis** lead to the value[7)] $\widehat{m}$ (1 GeV) = (6 ± 2) MeV. In the low-condensate alternative, the spectral function is expected to be considerably larger[13)] leading to a value of $\widehat{m}$ $3 \div 4$ times the value given above. On the other hand, the sum rule determination of $m_s - \widehat{m}$ involves the divergence of the vector current $\bar{s}\gamma_\mu u$ for which more experimental informations are available. The resulting value[14)] $m_s - \widehat{m} = (184 \pm 32)$ MeV (at $\mu = 1$ GeV) is likely

to be rather independent of the strength of quark condensation. The question of the size of $\widehat{m}$ thus becomes closely related to the question of the magnitude of the ratio $r = m_s/\widehat{m}$:

$$\widehat{m}\ (1\ \text{GeV}) \simeq \frac{184 \pm 32}{r-1}\ (\text{MeV})\ . \tag{20}$$

5 – CHIRAL PERTURBATION THEORY

We have seen that different alternatives of quark condensation manifest themselves through different values of the quark mass ratio $r = m_s/\widehat{m}$, the GOR ratio $x = \frac{2\widehat{m}B_0}{M_\pi^2}$ and, last but not least, the running quark mass $\widehat{m}(\mu)$. Up to higher order corrections, the ratio r can be, for instance, measured comparing the observed deviations form the Goldberger-Treimann relation in 3 different channels[15]. The current data suggest a value of r smaller by at least a factor 2 than the standard $r \simeq 26$, but the uncertainties of this "determination" are large. Similarly, the issue of the magnitude of $\widehat{m}$ can, in principle, be settled, measuring with a high degree of accuracy the tiny azimuthal asymmetries in the decay $\tau \to 3\pi + \nu_\tau$[13] - a project requiring a Tau-Charm-Factory or a similar device. In addition to such projects, the experimental determination of the strength of quark condensation requires a systematic model independent parametrization of various low-energy observables in terms of the quark mass ratio r and/or the GOR ratio x. Such a prametrization is provided by the (generalized) Chiral Perturbation Theory.

Chiral perturbation theory (CHPT) is a systematic low-energy expansion of QCD correlation functions in powers of external momenta p and quark masses m_q such that the ratio p/M_π is kept of the order of 1. It is based on the Ward identities of the therory, SBCHS and on generalities such as analyticity, crossing symmetry and unitarity. It is completely model independent. The unknown features of the low-energy QCD dynamics are parametrized by a set of low-energy constants such as F_0, $\widehat{m}B_0$, m_sB_0, etc.

At low energies the only relevant degrees of freedom are those of Goldstone bosons. This fact has allowed a reformulation of CHPT as a low-energy effective theory (LEET) based on the most general effective Lagrangian compatible with the chiral symmetry[16]. The use of this technical device has greatly simplified the practice of CHPT and it is at the origin of its rapid development during the last 12 years[11),12),17]. LEET is still completely model independent and it is equivalent to QCD, provided the low-energy constants of L_{eff} are properly associated with the order parameters of SBCHS in QCD. However, the identification of all terms in L_{eff} contributing to a given chiral order $0(p^d)$ depends on the strength of quark condensation.

The standard version of CHPT[11),12)] is based on the hypothesis of a large quark condensate, as defined by the condition (12) : symmetry breaking effects are expanded in powers of both m_q/Λ_H **and** m_q/m_0. In the case of a marginal or vanishing condensate, the condition (12) breaks down and the expansion of the effective Lagrangian has to be reformulated in a way which does not treat m_q/m_0 as a small quantity. This leads to the generalized chiral perturbation theory[18)] (GCHPT), which at each chiral order $0(p^d)$ includes more terms of L_{eff} than its standard counterpart. GCHPT constitutes the proper theoretical framework for an unbiased experimental determination of $r = m_s/\widehat{m}$ and/or of the GOR ratio $x = \frac{2\widehat{m}B_0}{M_\pi^2}$.

6 – LOW ENERGY $\pi\pi$ SCATTERING

The chiral expansion of the $\pi\pi$ amplitude $A(s|tu)$ starts at the order $0(p^2)$.

The first step in this expansion goes back to the 1966 work of Weinberg[19)]:

$$A(s|tu) = \frac{1}{F_\pi^2}(s - 2\widehat{m}B_0) + 0(p^4) \ . \tag{21}$$

The $\pi\pi$ scattering is the priviledged place to investigate quark condensation precisely because the amplitude A explicitly depends on B_0 already at the leading order[18)]. In the large condensate alternative, $2\widehat{m}B_0$ in Eq. (21) is replaced by M_π^2 (yielding the original Weinberg's formula). In this case Eq. (21) leads to the $I = 0$ s-wave scattering length $a_0^0 = 0.16$ whereas in the alternative of vanishing condensate, one would have $a_0^0 = 0.27$. Let us recall that the current experimental value is[20)]

$$a_0^0|_{exp} = 0.26 \pm 0.05 \ . \tag{22}$$

The second step was performed in 1983 by Gasser and Leutwyler[11),22)] who have computed the $0(p^4)$ corrections to A **within the framework of the large condensate hypothesis**. At order $0(p^4)$, the amplitude A depends on 4 low-energy constants $\bar{l}_1, \bar{l}_2, \bar{l}_3, \bar{l}_4$. Three of them $(\bar{l}_1, \bar{l}_2, \bar{l}_4)$ can be determined from other sources (d-waves, K_{e4} form-factors, scalar radius of the pion, $F_K/F_\pi \cdots$). The constant $\bar{l}_3$ measures the deviation of the GOR ratio x from 1, see Eq. (18). Assuming the latter not to exceed a few %, $(\bar{l}_3 = 2.9 \pm 2.4)$[11)] the scattering length increases from the Weinberg's value 0.16 towards $a_0^0 = 0.20 \pm 0.01$. In order to reach the central experimental value $a_0^0 = 0.26$, $\bar{l}_3$ would have to be as large and negative as $\bar{l}_3 \sim -70$. Notice that within the low-condensate altenative, a large negative value of $\bar{l}_3$ is naturally expected, due to Eq. (19).

The third step was completed only very recently[23)] by Knecht, Moussallam, Fuchs and Stern. The amplitude A has been calculated up to and including order

$0(p^6)$ (i.e. to the two-loop accuracy) **independently of any prejudice about the strength of quark condensation.** At this order, A depends on 6 parameters $\alpha, \beta, \lambda_1, \lambda_2, \lambda_3, \lambda_4$. It is of the form

$$\begin{aligned} A(s|t,u) &= \alpha\tfrac{M_\pi^2}{3F_\pi^2} + \tfrac{\beta}{F_\pi^2}(s - \tfrac{4}{3}M_\pi^2) + \\ &+ \tfrac{1}{F_\pi^4}\Big\{\lambda_1(s-2M_\pi^2)^2 + \lambda_2[(t-2M_\pi^2)^2 + (u-2M_\pi^2)^2]\Big\} + \\ &+ \tfrac{1}{F_\pi^6}\Big\{\lambda_3(s-2M_\pi^2)^3 + \lambda_4[(t-2M_\pi^2)^3 + (u-2M_\pi^2)^3]\Big\} + \\ &+ K_{\alpha,\beta,\lambda_1,\lambda_2}(s|t,u) + 0[(\tfrac{p}{\Lambda_H})^8] \,, \end{aligned} \tag{23}$$

where K is a non-trivial two-loop function (displayed in Ref. 23)), which depends non-linearly on the parameters α, β, λ_1 and λ_2. The $0(p^4)$ amplitude can be obtained from Eq. (23), setting $\lambda_3 = \lambda_4 = 0$ and reducing the function K to its one-loop counterpart[23] : There is a one to one correspondence between Gasser- Leutwyler's $0(p^4)$ constants $\bar{l}_1, \bar{l}_2, \bar{l}_3, \bar{l}_4$ and the parameters $\alpha, \beta, \lambda_1, \lambda_2$ to the $O(p^4)$ accuracy.

The parameters $\lambda_1, \lambda_2, \lambda_3, \lambda_4$ can be determined from the sum rules, using the existing $\pi\pi$-scattering data at energies $E > 500$ MeV[23] :

$$\begin{aligned} \lambda_1 &= (-5.3 \pm 2.5) \times 10^{-3} \,, & \lambda_2 &= (+9.7 \pm 1.0) \times 10^{-3} \,, \\ \lambda_3 &= (+2.9 \pm 0.9) \times 10^{-4} \,, & \lambda_4 &= (-1.4 \pm 0.2) \times 10^{-4} \,. \end{aligned} \tag{24}$$

The remaining two parameters α and β encode the information on the strength of quark condensation. Given (24), α and β have to be determined experimentally. For instance, the fit to the existing K_{l4} data[21] gives

$$\alpha = 2.16 \pm 0.86 \quad \beta = 1.074 \pm 0.053 \,, \tag{25}$$

reflecting the large experimental error bars. (The data points are shown on the Figure.) This fit corresponds to the value of the scattering length $a_0^0 = 0.263 \pm 0.052$ in a perfect agreement with the previous determination[20] from the same data analyzed using Roy equations.

The parameter α strongly depends on the quark mass ratio $r = \frac{m_s}{\hat{m}}$

$$\alpha = 1 + 6\frac{r_2 - r}{r^2 - 1} + \delta\alpha \,, \tag{26}$$

whereas β stays close to 1 for all r :

$$\beta = 1 + \frac{1}{r-1}(\frac{F_K^2}{F_\pi^2} - 1) + \delta\beta \,. \tag{27}$$

$\delta\alpha$ and $\delta\beta$ contain (small) Zweig rule violating terms and the (small) higher order chiral corrections - they are discussed in Ref. 23). In the large condensate alternative, one has $r \simeq r_2$ (c.f. Eq. (14) and α is close to 1. Standard version of CHPT gives

$$\alpha_{st} = 1.04 \pm 0.15 \,, \quad \beta_{st} = 1.08 \pm 0.03 \,. \tag{28}$$

In the case of a marginal or vanishing condensate, r gets closer to $r_1 \simeq 6.3$ (Eq. (15)) and α can be as large as 4. Hence the problem is to distinguish experimentally between the cases i) $1 < \alpha \leq 1.2$ (large condensate) ii) $1.5 \leq \alpha \leq 3$ (marginal condensate) and iii) $\alpha \gtrsim 3.5$ which might be considered as a signature of the pure phase II with no quark condensation.

Since now the expression of the amplitude is available to orders $0(p^2)$, $0(p^4)$ and $0(p^6)$, one can check the convergence of the chiral expansion. In the case of a large condensate, the scattering length a_0^0 takes, for instance, the values 0.16, 0.20 and 0.21 at order $0(p^2)$, $O(p^4)$ and $0(p^6)$ respectively. A similar convergence rate is observed for other threshold parameters and for other values of α and β. Actually, a rather good convergence persists even above threshold, in particular, in the low-energy range accessible in K_{l4} decays. This is shown in Fig. a, where the difference $\delta_0^0 - \delta_1^1$ (for $\alpha = 2$, $\beta = 1.08$) is drawn for three successive orders $0(p^2)$, $O(p^4)$ and $0(p^6)$. The overall good convergence rate suggests that the two-loop formula (23) is enough accurate to serve as a basis for the analysis of low-energy $\pi\pi$ data.

The last step will be hopefully performed in a near future by experimentalists. The difference of phase shifts $\delta_0^0(E) - \delta_1^1(E)$ is accessible in a model independent way in a K_{l4}^+ experiment. In Fig. b are plotted 3 predictions for $\delta_0^0 - \delta_1^1$ corresponding to $\alpha = 1.04$, $\alpha = 2$ and $\alpha = 3$ respectively. The data points are those of the last 1977 K_{l4}^+ experiment[21]. The figure shows the accuracy that is needed in order to clearly distinguish between these 3 cases. A preliminary study shows[24] that this accuracy could well be reached in the Daϕne-Kloe K_{l4}^+ experiment.

An interesting independent project exists at CERN[25] : It aims to determine the difference of scattering lengths $\Delta = a_0^0 - a_0^2$ to a 5% accuracy, measuring the lifetime of the $\pi^+\pi^-$ atom. Such independent information would be extremely useful. For $\alpha = 1.04$, $\alpha = 2.16$ and $\alpha = 3$, Δ is predicted to take values $\Delta = 0.253$, $\Delta = 0.290$ and $\Delta = 0.327$ respectively, with a typical error bar (not including uncertainty due to electromagnetic corrections) ± 0.007.

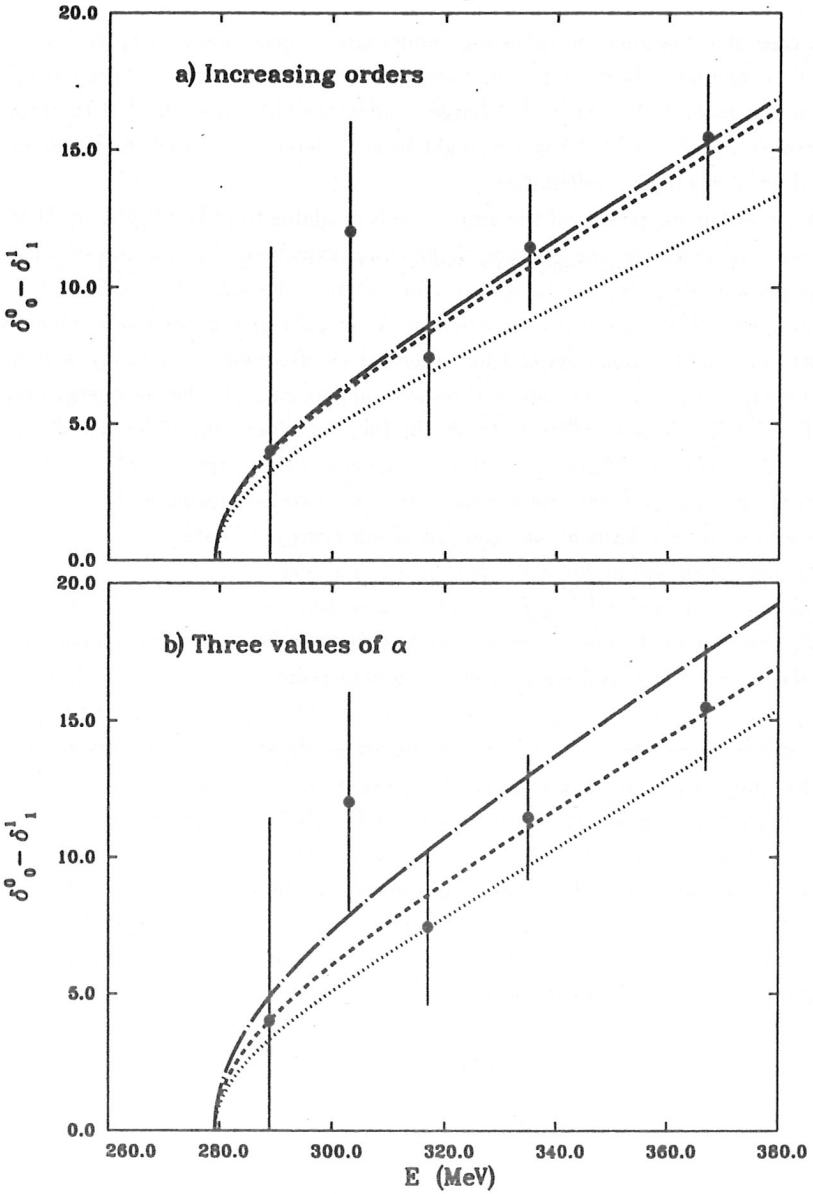

Figure 1: *The phase shift difference $\delta_0^0 - \delta_1^1$ in the range of energies accessible in the K_{l4} decays is shown a) for increasing chiral orders, and b) for several values of α and β*

References

[1] G.'t Hooft,in: Recent developments in gauge theories, eds. G.'t Hooft et *al.* (Plenum, NY 1980); Y. Frishman, A. Schwimmer, T. Banks and S. Yankielowicz, Nucl. Phys. **B177**, 157 (1981) ; S. Coleman and B. Grossman, Nucl. Phys. **B203**, 205 (1982).

[2] C. Vafa and E. Witten, Nucl. Phys. **B234**, 173 (1984) ; Comm. Math. Phys. **95**, 257 (1984).

[3] T. Banks and A. Casher, Nucl. Phys. **B168**, 103 (1980).

[4] H. Leutwyler and A. V. Smilga, Phys. Rev. D46, 5607 (1992).

[5] J. Stern, to be published.

[6] M. Gell-Mann, R. J. Oakes and B. Renner, Phys. Rev. **175**, 2195 (1968).

[7] J. Gasser and H. Leutwyler, Phys. Rep. **87**, 77 (1982) ; J. Bijnens, J. Prades and E. de Rafael, Phys. Lett. **B348**, 226 (1995).

[8] Y. Nambu and G. Jona-Lasinio, Phys. Rev. **122**, 345 (1961) ; **124**, 246 (1961).

[9] R. Gupta in LATTICE 94, Nucl. Phys. **B** (Proc. Supp.) **42**, 85 (1995).

[10] S. Weinberg, in: Festschrift for I.I. Rabi, ed. L. Motz (New York Academy of Sciences, New York, 1977), p. 185.

[11] J. Gasser and H. Leutwyler, Ann. Phys. **158**, 142 (1984).

[12] J. Gasser and H. Leutwyler, Nucl. Phys. **B250**, 465 (1985).

[13] J. Stern, N.H. Fuchs and M. Knecht, in : Proceedings of the Third workshop on the Tau-Charm-Factory, Marbella, Spain, June 1993, eds. J. Kirkby and R. Kirkby (Editions Frontières, 1994).

[14] M. Jamin and M. Münz, Z. Phys. **C66**, 633 (1995).

[15] N. H. Fuchs, H. Sazdjian and J. Stern, Phys. Lett. **B238**, 380 (1990).

[16] S. Weinberg, Physica **96A**, 327 (1979).

[17] J. Gasser, these proceedings.

[18] N. H. Fuchs, H. Sazdjian and J. Stern, Phys. Lett. **269**, 183 (1991) ; J. Stern, H. Sazdjian and N. H. Fuchs, Phys. Rev. **D47**, 3814 (1993) ; M. Knecht and J. Stern, in Second DAϕNE Physics Handbook, L. Maiani, N. Paver and G. Pancheri, eds. (Frascati, May 1995).

[19] S. Weinberg, Phys. Rev. Lett. **17**, 616 (1966).

[20] M. M. Nagels et *al.*, Nucl. Phys. **B147**, 189 (1979).

[21] L. Rosselet et *al.*, Phys. Rev. **D1** 574, (1977).

[22] J. Gasser and H. Leutwyler, Phys. Lett. **B125**, 325 (1983).

[23] M. Knecht, B. Moussallam and J. Stern, in Second DAϕNE Physics Handbook, L. Maiani, N. Paver and G. Pancheri, eds. (Frascati, May 1995) ; M. Knecht, B. Moussallam, J. Stern and N.H. Fuchs : "The low-energy $\pi\pi$-amplitude to one and two loops", preprint IPNO/TH 95-45 and PURD-TH-95-05 also hep-ph/9507319, to be published in Nucl. Phys. **B**.

[24] M. Baillargeon and P. J. Franzini, in Second DAϕNE Physics Handbook, L. Maiani, N. Paver and G. Pancheri, eds. (Frascati, May 1995).

[25] B. Adeva et *al.* : "Lifetime measurement of $\pi^+\pi^-$ atoms to test low-energy QCD predictions", preprint CERN/SPSLC 95-1.

RADIATIVE CORRECTIONS TO π_{l2} AND K_{l2} DECAYS

Markus Finkemeier*
INFN - L.N.F., C.P. 13, 00044 Frascati (Roma), Italy

ABSTRACT

We report on our reexamination of the radiative corrections to π_{l2} and K_{l2} decays. We perform a matching calculation, using a specific model with vector meson dominance in the long distance part and the parton model in the short distance part. By considering the dependence on the matching scale and on the hadronic parameters, and by comparing with model independent estimates, we scrutinize the model dependence of the results. For the pseudoscalar meson decay constants, we extract the values $f_\pi = (92.1 \pm 0.3)\,\mathrm{MeV}$ and $f_K = (112.4 \pm 0.9)\,\mathrm{MeV}$. For the ratios R_π and R_K of the electronic and muonic decay modes, we predict $R_\pi = (1.2354 \pm 0.0002) \cdot 10^{-4}$ and $R_K = (2.472 \pm 0.001) \cdot 10^{-5}$.

1 – Introduction

1.1 What is interesting about π_{l2}, K_{l2} decays?

Interest in π_{l2} and K_{l2} comes from two different sources. On the one hand, the decay widths of the pion and the kaon into muon and neutrino are used to extract the decay constants f_π and f_K,

$$\begin{aligned} \Gamma(\pi \to \mu\nu_\mu) &\longrightarrow f_\pi \\ \Gamma(K \to \mu\nu_\mu) &\longrightarrow f_K \end{aligned}$$

which are important input parameters for chiral perturbation theory. And so the question arises how $O(\alpha)$ radiative corrections affect these these parameters.

*Address from July 1995: Lyman Laboratory of Physics, Harvard University, Cambridge MA 02138, USA

On the other hand, the ratios R_π and R_K of the electronic and muonic decay modes

$$R_\pi = \frac{\Gamma(\pi \to e\nu_e)}{\Gamma(\pi \to \mu\nu_\mu)} \qquad R_K = \frac{\Gamma(K \to e\nu_e)}{\Gamma(K \to \mu\nu_\mu)} \tag{1}$$

can be predicted by theory. What makes R_π and R_K very interesting is that hadronic uncertainties cancel to a very large extent in these ratios and that the electronic decay channels are strongly helicity suppressed in the standard model due to the $V-A$ structure of the weak interaction. Thus the ratios R_π and R_K are very sensitive to non standard model effects (such as multi-Higgses, leptoquarks or other [1]), which might induce an effective pseudoscalar hadronic weak current. And so π_{l2} and K_{l2} decays allow for low-energy precision tests of the standard model, if we are able to understand the radiative corrections δR_{QED},

$$R_M = \frac{m_e^2\,(m_M^2 - m_e^2)^2}{m_\mu^2\,(m_M^2 - m_\mu^2)^2}\Big(1 + \delta R_{QED}\Big)\Big(1 + \delta R_{non-SM}\Big) \tag{2}$$

The experimental precision tends to be better for π_{l2} decays. However, non standard model effects δR_{non-SM} might be enhanced in R_K by a factor of m_K/m_π, and therefore K_{l2} decays are of comparable interest in testing the standard model.

1.2 Current Experimental Situation

For R_π, there are recent results (from 1992/93), obtained by TRIUMF and PSI [2], resulting in [3] a relative precision of

$$\frac{\Delta R_\pi}{R_\pi} = 3 \times 10^{-3} \tag{3}$$

The precision of R_K as quoted by the 1994 particle data book

$$\frac{\Delta R_K}{R_K} = 4 \times 10^{-2} \tag{4}$$

is one order of magnitude worse, but one should note that this number is based on 1972–76 data. It would be very interesting indeed to receive some new experimental information on this important quantity R_K.

1.3 Theory

There is a vast literature on the radiative corrections to π_{l2} decays. In 1958/59, Berman and Kinoshita [4] calculated the radiative corrections to π_{l2} decays using a model with an effective pointlike pion. There have been numerous later attempts to improve this simple model in order to take into account hadronic structure effects. Important milestones in the understanding of these effects were the 1973 paper

by Terent'ev [5], who derived a general theorem on the leading hadronic structure dependent correction, and the 1976 paper by Marciano and Sirlin [6], who proved that the leading logarithm of the radiative correction is not affected by the strong interaction, if one considers the inclusive decay rate $\Gamma(\pi \to \mu\nu_\mu) + \Gamma(\pi \to \mu\nu_\mu\gamma)$ integrated over all photons. In 1977, Goldman and Wilson [7] considered various models for the strong interaction effects in the context of gauge theories of the weak interaction. In 1990, Holstein [8] was the first to point to the importance of short distance radiative corrections in the extraction of f_π, and in 1993, Marciano and Sirlin reconsidered π_{l2} decays from a modern point of view, collection all the leading model-independent corrections and giving rough order of magnitude estimates for the remaining model dependent corrections.

Last year, we have performed an improved matching calculation [9] of π_{l2} and K_{l2} decays. In this calculation we include vector mesons as explicit degrees of freedom (instead of matching simply the point pion/kaon with the short distance part), calculate the full short distance correction (instead of including only the leading logarithm) and we scrutinize the size of the model-dependent corrections by explicitly calculating them within a reasonable model (instead of just roughly estimating their order of magnitude). This calculation allows to obtain improved values both for the pseudoscalar decay constants f_π and f_K, and for the ratios R_π and R_K, with a clear control over the (small) model-dependent contributions.

2 – Outline of the Calculation

2.1 General Considerations

To obtain the $O(\alpha)$ radiative corrections to $\pi \to \mu\nu_\mu$, we have to evaluate Feynman diagrams with one photon loop, where the photon can be contracted twice, once or not at all to the leptonic side. Because of the infra-red divergences, we have to add to this the tree diagrams for $\pi \to \mu\nu_\mu\gamma$, where the photon couples either to the leptonic or to the hadronic side. The essential task is then to understand the coupling of a (real or virtual) photon to the hadrons.

In the treatment of the strong interaction, one can distinguish three different regimes. In the low energy regime, where momentum transfers are small compared with a typical hadronic scale of about 1 GeV, there are the low energy theorems of QCD which give model independent predictions. In the high energy regime, where the virtual photon momentum is large on a hadronic scale, we can use the parton model and calculate the QED corrections to the $l\nu_l ud$ operator. In the intermediate energy regime of momentum transfers of the order of 1 GeV, however, there is no way to obtain model independent predictions. This energy regime

is dominated by the physics of vector meson resonances and can be described by phenomenological models only.

And so in order to evaluate the loop diagrams, one separates the integration over the loop momentum into a long distance part $k_E^2 = 0 \cdots \mu_{cut}^2$ and the short distance part $k_E^2 = \mu_{cut}^2 \cdots m_Z^2$, where μ_{cut} is a hadronic scale of about $\mu_{cut} \approx 1\,\mathrm{GeV}$.

Then one can either choose to neglect the problem of the vector meson energy regime and match the low energy regime and the short distances directly at a scale of about $\mu_{cut} = m_\rho^2$, as has been done by Holstein [8] and by Marciano and Sirlin [10]. A matching scale of m_ρ^2, however, is somewhat too large for the low energy regime, on the one hand, because for $P^2 \to m_\rho^2$, all the neglected higher orders $O(P^6)$, $O(P^8)$, ... become large. On the other hand, m_ρ^2 is somewhat too small for the short distance part, where, after all, one is using asymptotically free quarks.

Therefore we used the alternative approach of including the vector mesons as explicit degrees of freedom in the long distance part. This allows to push up the matching scale up to $\mu_{cut} = 1 \cdots 2\,\mathrm{GeV}$, rendering the short distance part more reliably.

However, this unavoidably introduces model-dependence. Thus we then scrutinize the size of the model dependence in different ways. Firstly we vary the matching scale from $\mu_{cut} = 0.75 \cdots 3\,\mathrm{GeV}$ and the parameters of the hadronics within their experimental uncertainties. Secondly, we determine the full size of the contribution to the loop integral from intermediate scales ($0.5 \cdots 3\,\mathrm{GeV}$), which is the regime where the model dependence is large. Thirdly, we compare our result with the leading model independent contributions and then take the full size of the model dependent contribution as a measure of the uncertainty.

2.2 Long Distance Part

For the long distance part, we start from a model with an effective point meson model, which should be a good approximation for very small momentum transfers. These point meson amplitudes are then modified along the lines of vector meson dominance in order to account explicitly for the vector meson degrees of freedom. Consider, for example, the coupling $V(p,p')^\mu$ of the photon to a pion line. In the point meson approximation, this coupling is given by scalar QED as

$$V(p,p')^\mu_{point} = ie(p+p')^\mu \tag{5}$$

where p and p' are the ingoing and outgoing pion momenta. But actually this coupling *defines* the pion electromagnetic form factor F_π via

$$V(p,p')^\mu_{phys} = ieF_\pi(k^2)(p+p')^\mu \tag{6}$$

where V^{μ}_{phys} denotes the physical photon-pion-pion coupling and $k = p' - p$ is the photon momentum. $F_\pi(k^2)$ is known experimentally rather well in the relevant regime of k^2 up to 1 or 2 GeV. Thus in the point pion amplitudes, we replace $V(p,p')^{\mu}_{point}$ by $V(p,p')^{\mu}_{phys}$, using the parameterization of F_π determined in [11]. This modification determines in turn the appropriate modification of the pion-photon-W boson seagull coupling, viz. by the requirement of gauge invariance. In the case of the kaon, the scalar QED point kaon-kaon-photon coupling has to be replaced by a coherent superposition of ρ, ω and Φ vector meson dominance. In addition to these modified point meson diagrams, there are loops which correspond to the so-called structure dependent (SD) radiation in the radiative decays $\pi(K) \to l\nu_l\gamma$, where the emitted photon becomes contracted with the leptonic side.

2.3 Short Distance Corrections

For photons with large virtuality, $|k^2| \gtrsim (1 \ldots 2\,\mathrm{GeV})^2$, we can use the parton model. Thus the first step is to calculate the one-loop photonic corrections $\delta\mathcal{A}$ to $\mathcal{A}_0 = \frac{G_F}{\sqrt{2}}[\bar{u}_\nu \gamma^\mu \gamma_- u_l][\bar{u}_d \gamma_\mu \gamma_- u_u]$.

Neglecting all masses except for m_l and μ_{cut}, we obtain the leading logarithm of the radiative correction

$$\delta\mathcal{A} = \frac{\alpha}{\pi} \frac{1}{m_l^2 - \mu_{cut}^2} \left(m_l^2 \ln \frac{m_Z}{m_l} - \mu_{cut}^2 \ln \frac{m_Z}{\mu_{cut}^2} \right) + \cdots \tag{7}$$

where the dots indicate corrections which are not leading in the limit $m_Z^2 \to \infty$.

In the radiative corrections to the individual decay rates $M \to l\nu_\tau(\gamma)$, this leading logarithm clearly dominates, and so for the extraction of f_π and f_K its consideration is sufficient. It depends, however, only very little on the lepton mass and thus cancels almost completely in the ratios R_π and R_K. In view of the very high precision of the theoretical prediction for these ratios, we therefore go beyond the leading logarithm and calculate the full $\delta\mathcal{A}$. This full result for $\delta\mathcal{A}$ is firstly no longer proportional to the Born amplitude $\mathcal{A}_0$ and secondly it depends on the relative momentum of the two quarks. Therefore we firstly project onto the $J^P = 0^-$ component of the two quarks, and secondly we integrate over the relative momentum up of the quarks in the infinite momentum frame ($u = -1 \ldots +1$). This leads to a result

$$\left(\delta R_M\right)_{short\,dist} = \frac{3}{2 f_M} \int_{-1}^{+1} du\, \Phi_M(u)\, r_M(u) \tag{8}$$

Here $\Phi_M(u)$ denotes the parton distribution function, whereas $r_M(u)$ is calculated from the projected short distance diagrams. We find that $r_\pi(u)$ and $r_K(u)$ depend

only very little on u, and so we can approximate them by their values at $u = 0$, where the wave function is presumably peaked:

$$\left(\delta R_M\right)_{short\ dist} \approx r_M(0) \underbrace{\frac{3}{2f_M} \int_{-1}^{+1} du\, \Phi_M(u)}_{=1} = r_M(0) \tag{9}$$

where the last equation follows from a sum rule [12].

In matter of fact, we find that R_π and R_K are also dominated by the leading logarithm,

$$\left(\delta R_M\right)_{short\ dist} \approx \frac{2\alpha}{\pi} \frac{m_\mu^2}{m_\mu^2 - \mu_{cut}^2} \ln \frac{m_\mu}{\mu_{cut}} \tag{10}$$

2.4 Treatment of Real Photons

Because of the infra-red divergences, one has to add some or all real photons to the virtual corrections and to consider inclusive decay rates

$$\Gamma(M \to l\nu_l) + \Gamma(M \to l\nu_l\gamma)$$

Whether one includes only soft photons or all real radiation is a matter of convention. Our convention, which appears to be in accord with the one used by experimentalists, is to include all photons in the pion decays $\Gamma(\pi \to l\nu_l(\gamma))$. In the case of the kaon decays $\Gamma(K \to l\nu_l(\gamma))$, we include all the internal bremsstrahlung (IB) photons, but exclude completely the structure dependent (SD) radiation.

For $K \to \mu\nu_\mu\gamma$ this SD radiation is completely negligible, but for the electronic mode it is extremely large, $\Gamma_{SD}(K \to e\nu_e\gamma) \approx \Gamma_0(K \to e\nu_e)$, where Γ_0 denotes the Born amplitude. Therefore it is useful to consider the SD radiation as a separate decay mode and not to include it in the radiative correction to $K \to e\nu_e$.

Of course it is not possible to tell definitely whether a radiated photon is due to internal bremsstrahlung or to structure dependent radiation. However, if suitable experimental cuts are used, which put a small upper limit onto the photon energy, the measured rate of $K \to e\nu_e(\gamma)$ will include only a very small SD background, and only very little of the IB part will have been discarded. Using the predicted differential distributions [13, 14], the SD background can be subtracted and the missing IB part added. Because of the smallness of this correction, it does not give rise to any important uncertainties.

3 – Numerical Results

3.1 The pseudoscalar decay constants

Adding up the long and short distance corrections, we obtain the full radiative correction. The numerical result depends on the choice of the matching scale μ_{cut} and

Figure 1: Radiative correction to $\Gamma(K \to \mu\nu_\mu)$, using different choices for the hadronic parameters: Standard choice (I, solid) and variations (II, dashed and III, dotted)

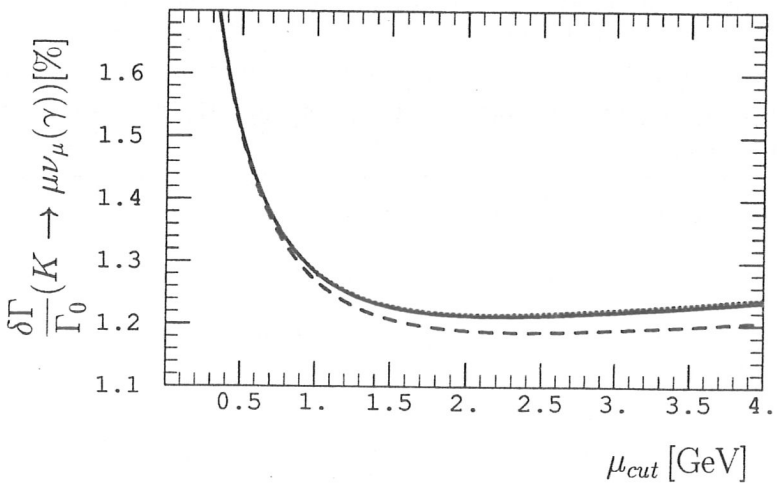

on the parameters of the hadronics, which are known only with limited experimental precision.

In Fig. 1 we display the correction to the decay rate $\Gamma(K \to \mu\nu_\mu(\gamma))$ in variation with μ_{cut}, using three different choices for the hadronic parameters. The solid line (I) corresponds to the central values of the hadronic parameters, whereas the dashed (II) and the dotted (III) lines are obtained by varying these parameters within reasonable ranges. From this, we obtain

$$\frac{\delta\Gamma}{\Gamma_0}(K \to \mu\nu_\mu(\gamma)) = (1.23 \pm 0.13 \pm 0.02)\% + O(\alpha^2) + O(\alpha\alpha_s) \qquad (11)$$

The central value 1.23% of the radiative correction of order $O(\alpha)$ has been obtained with $\mu_{cut} = 1.5\,\mathrm{GeV}$ and the central values of the hadronics. The first error quoted, $\pm 0.13\%$ is the matching uncertainty, obtained from varying the matching scale up and down by a factor of two, $\mu_{cut} = 0.75 \cdots 3\,\mathrm{GeV}$. The second error, $\pm 0.02\%$ estimates the uncertainty induced by the hadronic parameters.

In view of the smallness of the error, one has to worry about higher order corrections. In [10], the authors have summed up the leading $O(\alpha^n)$ corrections for the leading logs in the short distance part, which leads to an enhancement of $+0.13\%$. Furthermore they considered the leading QCD short distance corrections of order $O(\alpha\alpha_s)$, which decrease the short distance part by -0.03%. Similarly, $O(\alpha)^n$ effects

should be considered in the long distance part.

Furthermore, note that we employ m_Z as an ultra-violet cut-off for the short distance corrections, according to the general theorems by Sirlin [15] on short-distance electroweak corrections to semileptonic processes. But this implies that there is an uncertainty of the order of $\alpha/(2\pi) \times O(1) \approx 0.1\%$ in the definition of the radiative correction, because a change of the cut-off scheme would induce a change of the result of this order. Note that the error of the $O(\alpha)$ correction which we have determined is of the same order of magnitude as this inherent uncertainty.

Taking into account the higher order corrections and these uncertainties, we use the following value in order to extract f_K:

$$\frac{\delta\Gamma}{\Gamma_0}(K \to \mu\nu_\mu(\gamma)) = (1.3 \pm 0.2)\% \tag{12}$$

Using the 1994 particle data group values for the decay rates and the V_{us} matrix element, this yields

$$f_K = (112.4 \pm 0.9)\,\mathrm{MeV} \tag{13}$$

From a similar analysis, we obtain

$$f_\pi = (92.1 \pm 0.1)\,\mathrm{MeV} \tag{14}$$

Two comments are in order:

- f_π is not defined unambiguous at the order $O(\alpha)$. One could decide to absorb part of the radiative correction into f_π. Here we have by definition factored out *all* radiative corrections from f_π. Holstein [8] used a different definition which absorbs terms proportional to $\ln(m_\pi/m_\mu)$ into f_π. Use of his definition would yield a slightly lower value of $f_\pi = (91.9 \pm 0.1)\,\mathrm{MeV}$.

- We have estimated the model dependence from the matching uncertainty and the hadronic parameter dependence, and so the $\pm 0.1\,\mathrm{MeV}$ uncertainty is actually a lower limit.

Taking the full size of the model dependent part as uncertainty, a conservative error estimate is

$$f_\pi = (92.1 \pm 0.3)\,\mathrm{MeV} \tag{15}$$

Note that the error on f_K is dominated by the error on $|V_{us}|$ rather than by model dependence.

Our number on f_π is to be compared with the particle data group value [3], which is based on [10]. Dividing by $\sqrt{2}$ in order to conform with our convention, it reads

$$f_\pi^{RPP} = (92.4 \pm 0.07 \pm 0.25)\,\mathrm{MeV} \tag{16}$$

Figure 2: Radiative correction to the ratio R_K, using different choices for the hadronic parameters: Standard choice (I, solid) and variations (II, dashed and III, dotted)

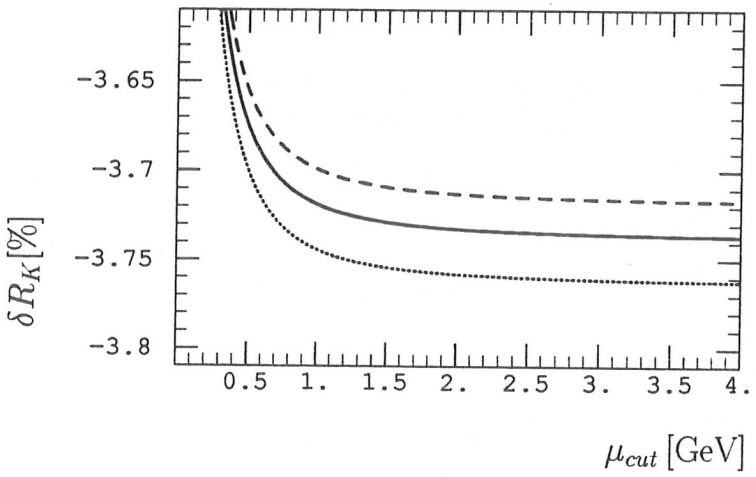

where the first error ± 0.07 comes from the experimental uncertainty on $|V_{ud}|$ and the second ± 0.25 from the matching uncertainty. The numbers are compatible within the error bars. Our number has a smaller central value due to the improved matching procedure (our matching dependence is in fact an order of magnitude smaller.)

3.2 The ratios R_π and R_K

Let us consider next the ratio R_K of the electronic and muonic modes in kaon decay. From Fig. 2 we obtain

$$\delta R_K = -(3.73 \pm 0.02 \pm 0.03)\% + O(\alpha^2) \tag{17}$$

where the error given are the matching uncertainty $\pm 0.02\%$ and the uncertainty from the hadronic parameters $\pm 0.03\%$. These errors give a lower limit of the model dependence of the result.

To get a reliable understanding of the model dependence, we have compared our evaluation with the leading model-independent contributions and added up the full sizes of the various model dependent parts. This leads to an error estimate of $\pm 0.04\%$.

Furthermore we have determined the contribution to the loop integral from intermediate scales $\sqrt{|k^2|} = 0.5 \cdots 3\,\mathrm{GeV}$. This also leads to an error estimate of $\pm 0.04\%$.

Finally higher order corrections have to be discussed. In [10] the authors sum up the leading logs in m_e/m_μ to all orders in α, leading to an enhancement of $+0.05\%$. Next-to-leading corrections are unknown, and so we allow for an additional $\pm 0.01\%$ uncertainty. This leads to our final result

$$\delta R_K = -(\underbrace{3.73 \pm 0.04}_{O(\alpha)} + \underbrace{0.05 \pm 0.01}_{O(\alpha^n), n \geq 2})\% = -(3.78 \pm 0.04)\% \tag{18}$$

and

$$R_K = (2.472 \pm 0.001) \times 10^{-5} \tag{19}$$

Similarly, we obtain

$$R_\pi = (1.2354 \pm 0.0002) \times 10^{-4} \tag{20}$$

4 – Summary

Performing an improved matching calculation, we have extracted

$$\begin{aligned} f_\pi &= (92.1 \pm 0.3)\,\text{MeV} \\ f_K &= (112.4 \pm 0.9)\,\text{MeV} \end{aligned} \tag{21}$$

where we have, by definition, factored out all $O(\alpha)$ effects from f_π and f_K.

Furthermore we found

$$\begin{aligned} R_\pi = \frac{\Gamma(\pi \to e\nu_e(\gamma))}{\Gamma(\pi \to \mu\nu_\mu(\gamma))} &= (1.2354 \pm 0.0002) \times 10^{-4} \\ R_K = \frac{\Gamma(K \to e\nu_e(\gamma))}{\Gamma(K \to \mu\nu_\mu(\gamma))} &= (2.472 \pm 0.001) \times 10^{-5} \end{aligned} \tag{22}$$

These are model independent predictions in the sense that the full model dependence is included in the error bars given.

R_π and R_K can be predicted reliably within the standard model, with relative uncertainties of a few 10^{-4}. Thus they allow for very sensitive low energy precision tests of the standard model.

Acknowledgements

The author gratefully acknowledges financial support by the HCM program under EEC contract number CHRX-CT90026

References

1. O. Shanker, Nucl. Phys. **B204**, 375 (1982)
2. D.I. Britton et al., Phys. Rev. Lett. **68**, 3000 (1992); C. Czapek et al., Phys. Rev. Lett. **70**, 12 (1993)
3. Review of Particle Properties, L. Montanet *et al.*, Phys. Rev. **D50** 1173, (1994)
4. S. M. Berman, Phys. Rev. Lett. **1**, 468 (1958); T. Kinoshita, Phys. Rev. Lett. **2**, 477 (1959)
5. M.V. Terent'ev, Yad. Fiz. **18**, 870 (1973), Sov. J. Nucl. Phys. **18**, 449 (1974)
6. W.J. Marciano, A. Sirlin, Phys. Rev. Lett. **36**, 1425 (1976)
7. T. Goldman and W.J. Wilson, Phys. Rev. **D15**, 709 (1977)
8. B.R. Holstein, Phys. Lett. **B244**, 83 (1990)
9. M. Finkemeier, "Radiative Corrections to π_{l2} and K_{l2} decays", LNF-94/076(IR), hep-ph/9501286
10. W.J. Marciano, A. Sirlin, Phys. Rev. Lett. **71**, 3629 (1993)
11. J. H. Kühn and A. Santamaria, Z. Phys. **C48**, 445 (1990)
12. R. Brandt and G. Preparata, Phys. Rev. Letters **25**, 1530 (1970)
13. S. G. Brown, S. A. Bludman, Phys. Rev. **136**, B1160 (1964)
14. J. Bijnens, G. Ecker, J. Gasser, Nucl. Phys. **B396**, 81 (1993)
15. A. Sirlin, Rev. Mod. Phys. **50**, 573 (1978)

MEASUREMET OF THE DIFFERENCE OF THE K^O-$\overline{K}^O$ FORWARD SCATTERING AMPLITUDES IN CARBON AT LOW MOMENTUM WITH THE CPLEAR DETECTOR

Panagiotis Kokkas
Institute for Physics, University of Basel, Klingelbergstr. 82, CH-4056 Basel, Switzerland
For the CPLEAR Collaboration [1].

ABSTRACT

We propose to measure the difference $\Delta f = f(0) - \overline{f}(0)$ of the $K^\circ - \overline{K^\circ}$ forward scattering amplitudes in carbon at low momenta (250-750 MeV/c) with the CPLEAR detector. We expect to determine Δf with a precision of $\pm 2\%$ for the modulus and $\pm 2^\circ$ for the phase. The two results are correlated for K° momenta higher than 350 MeV/c. The systematic error on the CPLEAR measurement of φ_{+-} connected with the regeneration effect will be decreased to about 0.1°.

1 INTRODUCTION

The difference $\Delta f = f(0) - \overline{f}(0)$ between the forward scattering amplitudes of K° and $\overline{K^\circ}$ is important for the determination of regeneration effects in high precision CP-violation experiments [1, 2, 3, 4]. For the experiments working with neutral kaons of low energy [3, 4], only semi-theoretical calculations can be used at present to

[1]The CPLEAR Collaboration
A. Angelopoulos[1], A. Apostolakis[1], E. Aslanides[11], G. Backenstoss[2], C.P. Bee[2], O. Behnke [17], A. Benelli [9], V. Bertin[11], F. Blanc[7,13], P. Bloch[4], P. Carlson[15], M. Carroll[9] J. Carvalho[5], E. Cawley[9], S. Charalambous[16], G. Chardin[14], M.B. Chertok[3], A. Cody[9], M. Danielsson[15], M. Dejardin[14], J. Derre[14], A. Ealet[11], C. Eleftheriadis[16], I. Evangelou[8], L. Faravel [7], R. Ferreira-Marques[5], W. Fetscher[17], M. Fidecaro[4], A. Filipčič[10], D. Francis[3], J. Fry[9], E. Gabathuler[9], R. Gamet[9], D. Garreta[14], H.-J. Gerber[17], A. Go[15], C. Guyot[14], A. Haselden[9], P.J. Hayman[9], F. Henry-Couannier[11], E. Hubert[11], K. Jon-And[15], P.-R. Kettle[13], C. Kochowski[14], P. Kokkas[2], R. Kreuger[6], R. Le Gac[11], F. Leimgruber[2],A. Liolios[16], E. Machado[5], I. Mandić[10], N. Manthos[8], G. Marel[14], M. Mikuž[10], J. Miller[3], F. Montanet[11], T. Nakada[13], B. Pagels [17], I. Papadopoulos[16], P. Pavlopoulos[2], J. Pinto da Cunha[5], A. Policarpo[5], G. Polivka[2], R. Rickenbach[2], B.L. Roberts[3], E. Rozaki[1], T. Ruf[4], L. Sakeliou[1], P. Sanders[9], M. Schäfer[17], L.A. Schaller[7], A. Schopper[4], P. Schune[14], A. Soares[14], L. Tauscher[2], C. Thibault[12], F. Touchard[11], C. Touramanis[4], F. Triantis[8], E. Van Beveren[5], C.W.E. Van Eijk[6], G. Varner[3], S. Vlachos[2], P. Weber[17], O. Wigger[13], M. Wolter[17], C. Yeche[14], D. Zavrtanik[10] and D. Zimmerman[3]

[1]University of Athens, [2]University of Basel, [3]Boston University, [4]CERN, [5]LIP and University of Coimbra, [6]Delft University of Technology, [7]University of Fribourg, [8]University of Ioannina, [9]University of Liverpool, [10]J. Stefan Inst. and Phys. Dep., University of Ljubljana, [11]CPPM, IN2P3-CNRS et Université d'Aix-Marseille II, [12]CSNSM, IN2P3-CNRS, Orsay, [13]Paul-Scherrer-Institut(PSI), [14]CEA, DSM/DAPNIA, CE-Saclay, [15]KTH Stockholm, [16]University of Thessaloniki, [17]ETH-IPP Zürich

estimate Δf. This introduces large systematic uncertainties in the correction for regeneration effects. In the CPLEAR experiment [3, 5], the latter induces an uncertainty of $\pm 0.6°$ on the phase of the CP-violating parameter η_{+-}. It is the largest source of systematic errors and of the same order as the statistical error expected at the end of the experiment.

Direct measurements of Δf are available for various materials from many experiments [6, 7, 8] using K_L beams, at momenta above 2 GeV/c. Experimental results are shown in fig. 1 and 2 for hydrogen and carbon respectively. Below 2 GeV/c the quantity Δf can be calculated using measured K^+ and K^- cross sections with protons and neutrons (due to isospin symmetry in strong interactions, the K° and $\overline{K^\circ}$ scattering amplitudes with protons and neutrons are related to those of K^+ and K^-). The imaginary part of the forward scattering amplitude is related to the total cross section through the Optical Theorem. Measurements [9] of total cross sections exist in all interesting kaon momentum regions for $K^\pm p$ scattering, but only above 800 MeV/c kaon momentum for $K^\pm n$. Measurements of the real part of the $K^\pm p$ and of the $K^\pm n$ forward scattering amplitudes are rare and poor, and their values are obtained, in particular for momenta below 1 GeV/c, from an integral over total cross section with the help of dispersion relations [10], or other more elaborate methods [11, 12]. The same procedure is used for the imaginary part in the momentum range where experimental data on total cross sections do not exist [10, 12].

We have assumed the average of these values, with an error given by their standard deviation, to calculate Δf and its error in hydrogen. The results are shown together with the experimental data at high momenta in fig. 3. In the momentum region between 350 to 800 MeV/c, the average uncertainty in $|\Delta f|$ and $\arg(\Delta f)$ is $\pm 13\%$ and $\pm 9°$ respectively. In fig. 3 the values given by Eberhard [13], and by Michetti and Baldini [14] are also shown. Both sets are in good agreement with our average values.

The corresponding scattering amplitudes for a nucleus are calculated as the convolution of the proton and neutron contributions in the framework of an optical model calculation. Recent theoretical estimations [13] of $\Re(\Delta f)$ and $\Im(\Delta f)$ for various materials and kaon momenta between 0.35 and 2.6 GeV/c are based on the optical model of ref. [15], and on values of $\Re(\Delta f)$ and $\Im(\Delta f)$ for hydrogen shown in fig. 3.

2 EXPERIMENTAL METHOD

In the CPLEAR experiment, the dominant contribution to the regeneration effect in the 2π decay arises from the interference of the inherent K_S amplitude with the K_S amplitude regenerated from the K_L component of the neutral kaon. For a better understanding of the regenerated K_S amplitude $\rho = |\rho| e^{i\varphi_\rho}$ (which is proportional to Δf [16, 17]) we intend to enhance the regeneration effect by introducing an additional amount of material (absorber, regenerator) into the decay volume of the detector.

The time dependent decay rate asymmetry between the initially pure K° and $\overline{\mathrm{K}^\circ}$

$$A_{+-}(\tau) = \frac{R\left(\overline{\mathrm{K}^\circ}_{\tau=0} \to \pi^+\pi^-\right)(\tau) - R\left(\mathrm{K}^\circ_{\tau=0} \to \pi^+\pi^-\right)(\tau)}{R\left(\overline{\mathrm{K}^\circ}_{\tau=0} \to \pi^+\pi^-\right)(\tau) + R\left(\mathrm{K}^\circ_{\tau=0} \to \pi^+\pi^-\right)(\tau)} \qquad (1)$$

measured for decays behind the absorber is:

$$A_{+-}(\tau) \approx 2Re(\varepsilon) -$$

The interference term I is ideally measured by placing the absorber in such a way that the inherent K_S amplitude is comparable to the regenerated K_S amplitude. Fig. 4 shows the expected decay rate asymmetry with a 2 cm carbon absorber compared to the one expected in the absence of absorber for five different K° momentum regions, between 250 and 750 MeV/c, which is the region covered in the CPLEAR experiment.

2.1 Experimental Setup

The neutral kaons are produced in $\overline{\mathrm{p}}$p-annihilations at rest through the two channels $\overline{\mathrm{p}}\mathrm{p} \to \mathrm{K}^\pm\pi^\mp\overline{\mathrm{K}^\circ}(\mathrm{K}^\circ)$ both with a branching ratio of $2 \cdot 10^{-3}$. The strangeness of the neutral kaon is tagged by the charge of the accompanying charged kaon. A carbon absorber, shaped as a cylinder sector of 2 cm thickness, will be put inside the CPLEAR detector at about 7 cm from the target (see fig. 5), where about 90% of the K_S available at $\tau = 0$ have already decayed. The absorber will cover only 120° of the azimuthal angle providing thus the possibility of selecting primary charged particles which did not cross the absorber.

The weight of the absorber material is approximately 2.4 kg. It will be mounted together with the target on an extraction tube made of inox, so that the regenerator can easily be put in and taken out through the downstream side of the detector. The position of the absorber can be determined by reconstructing the vertex of converted photons [20].

We plan to equip the absorber with a thin veto counter. It would allow us to reject, at an early trigger stage, the events with charged tracks traversing the absorber, thus reducing trigger and readout deadtime, with an increase in the trigger rate by 30% with respect to the present one. Possible solutions for this counter are either a flat scintillator with flexible light guides or a plane of 2 mm thin scintillating fibers (as used in the electromagnetic calorimeter of the KLOE detector [18]).

2.2 Simulation Studies and Statistical Errors

In 1994 the CPLEAR experiment collected a total of 11×10^6 fully reconstructed events $\mathrm{K}^\circ(\overline{\mathrm{K}^\circ}) \to \pi^+\pi^-$ with a lifetime above 1 τ_S. The average $\overline{\mathrm{p}}$p-rate was 650 kHz and the average efficiency of LEAR during the 70 days of running was 60% [21]. With the same amount of beam time and efficiency for the regeneration measurement, we expect about $4 \times 10^6\ \pi^+\pi^-$ decays above 1 τ_S where the primary charged tracks

do not cross the absorber and the neutral kaon momentum direction points to the regenerator.

The central values of the modulus $|\Delta f|$ and the phase $\varphi_{\Delta f}$ of Δf for carbon taken from ref. [13] are shown in table 1. Using these values as input, a detailed simulation was done taking into account the K° and $\overline{K^\circ}$ propagation through the detector material [19], the kaon momenta and angular distributions, and the acceptance as a function of the lifetime, as measured by the CPLEAR detector. "Experimental" asymmetries for five different momentum intervals with altogether $4 \cdot 10^6$ events were generated. The asymmetries are shown in fig. 4 together with the asymmetry without regenerator. Due to the necessary integrations over different regenerator thicknesses and kaon momenta only a *numerical fit* is possible to obtain the modulus and phase of Δf. In order to perform this numerical fit the shape of the asymmetries corresponding to different values of $|\Delta f|$ and $\varphi_{\Delta f}$ have to be known. Therefore we calculated the K° and $\overline{K^\circ}$ decay rate asymmetries for different values of $|\Delta f|$ and $\varphi_{\Delta f}$ (40×40 sets in steps of ± 0.1 fm and $\pm 0.5°$), and five different kaon momentum bins. By comparing in each momentum bin these asymmetries with the "experimental" asymmetry we obtain the χ^2-distribution for $|\Delta f|$ and $\varphi_{\Delta f}$. From this distribution we extract at $\chi^2 = \chi^2_{\min}$ the pair $|\Delta f|$ and $\varphi_{\Delta f}$, whereas the errors and correlations for $|\Delta f|$ and $\varphi_{\Delta f}$ are given by the values at $\chi^2 = (\chi^2_{\min} + 1)$ (see table 2). Except for the first momentum region, the measurements of the modulus and phase are strongly correlated as can be understood from eq. 3. However the fact that the absorber has a cylindrical geometry results in values for τ_R which depend on the K° momentum direction, and therefore decouples partially $|\Delta f|$ and $\varphi_{\Delta f}$.

It turns out that by using the complete covariance matrix the error on φ_{+-} due to the regeneration corrections remains small despite of the large correlation of $|\Delta f|$ and $\varphi_{\Delta f}$. We estimated the dependence of the CPLEAR measurement of φ_{+-} in first order to $|\Delta f|$ and $\varphi_{\Delta f}$ (see table 3). The remaining uncertainties on the measurement of φ_{+-} due to regeneration corrections are shown in table 4 together with the presently estimated uncertainty. We conclude that the measurement of Δf would eliminate the regeneration corrections as the dominating source of the systematic error of the φ_{+-} measurement.

2.3 Systematic Errors

The effect of multiple scattering inside the absorber material on the momentum and vertex resolution was studied with a Monte Carlo simulation and was found to be small compared to the measurement error of the drift chambers. The number of wrongly identified decays outside the absorber amounts to about 3% causing only a small dilution of the measured asymmetry. The systematic error resulting from the uncertainty of Δm should be less than 0.6° for $\varphi_{\Delta f}$ and negligible for $|\Delta f|$.

3 SUMMARY

To strongly reduce the systematic error due to regeneration effects in the measurement of the phase φ_{+-} in the CPLEAR experiment, we propose to measure Δf, the difference of the forward scattering amplitudes, for low K° and $\overline{\mathrm{K}^0}$ momenta. With 70 days of running in '96 we expect to determine Δf in carbon for a K° momentum between 250 and 350 MeV/c with a precision of 2% for the modulus and 2° for the phase. At higher K° momenta (up to 750 MeV/c) we will obtain correlated information on the modulus and the phase of Δf. This will enable us to reduce the systematic error on our measurement of φ_{+-} induced by the regeneration effect to about 0.1°.

Table 1: Central values for the difference of scattering amplitudes in carbon used in the simulation

Momentum interval [MeV/c]	$\lvert\Delta f\rvert$ [fm]	$\varphi_{\Delta f}$ [°]
[250 – 350]	5.09	−136.1
[350 – 450]	5.82	−130.5
[450 – 550]	6.24	−140.5
[550 – 650]	7.46	−143.7
[650 – 750]	10.63	−144.4

Table 2: Covariance matrix

Momentum interval [MeV/c]	$\sigma(\lvert\Delta f\rvert)$ [fm]	$\sigma(\varphi_{\Delta f})$ [°]	correlation coefficient
[250 – 350]	0.13	2.1	−0.01
[350 – 450]	0.24	3.5	0.90
[450 – 550]	0.49	6.0	0.97
[550 – 650]	0.47	3.2	0.96
[650 – 750]	0.55	2.2	0.92

Table 3: Dependence of φ_{+-} on Δf amplitude and phase

Momentum interval [MeV/c]	$\partial\varphi_{+-}/\partial\lvert\Delta f\rvert$ [°][fm^{-1}]	$\partial\varphi_{+-}/\partial\varphi_{\Delta f}$ [%]
[250 – 350]	−0.89	3.3
[350 – 450]	−0.62	7.0
[450 – 550]	−0.45	5.1
[550 – 650]	−0.29	4.8
[650 – 750]	−0.23	5.0

Table 4: Systematic error of φ_{+-} from regeneration

Momentum interval [MeV/c]	present [°]	1996 [°]
[250 – 350]	0.66	0.14
[350 – 450]	0.78	0.13
[450 – 550]	0.58	0.11
[550 – 650]	0.51	0.04
[650 – 750]	0.55	0.05

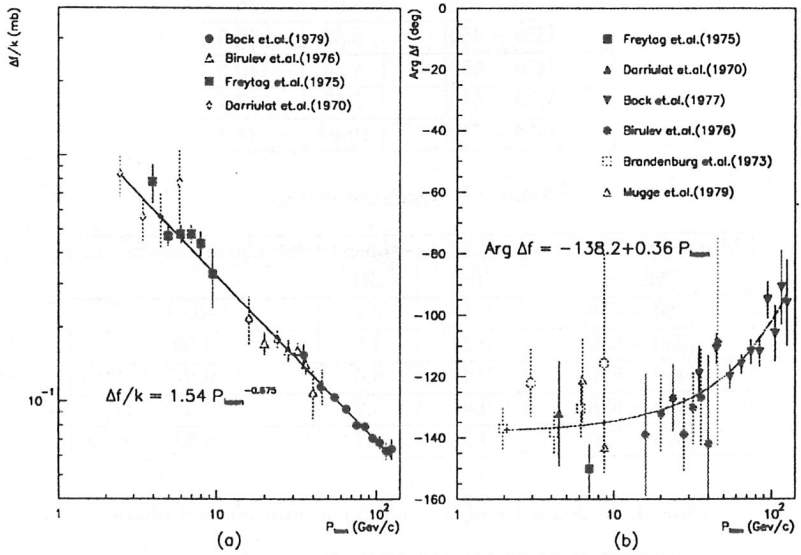

Figure 1: Measured difference of the K° and $\overline{\text{K°}}$ forward scattering amplitudes in hydrogen as function of the kaon momentum, a) modulus and b) phase

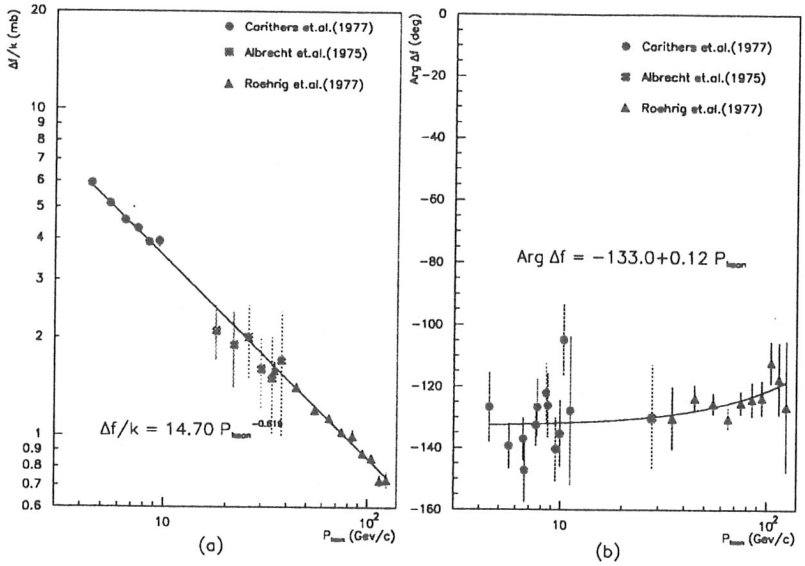

Figure 2: Measured difference of the K° and $\overline{\text{K}^\circ}$ forward scattering amplitudes in carbon as function of the kaon momentum, a) modulus and b) phase

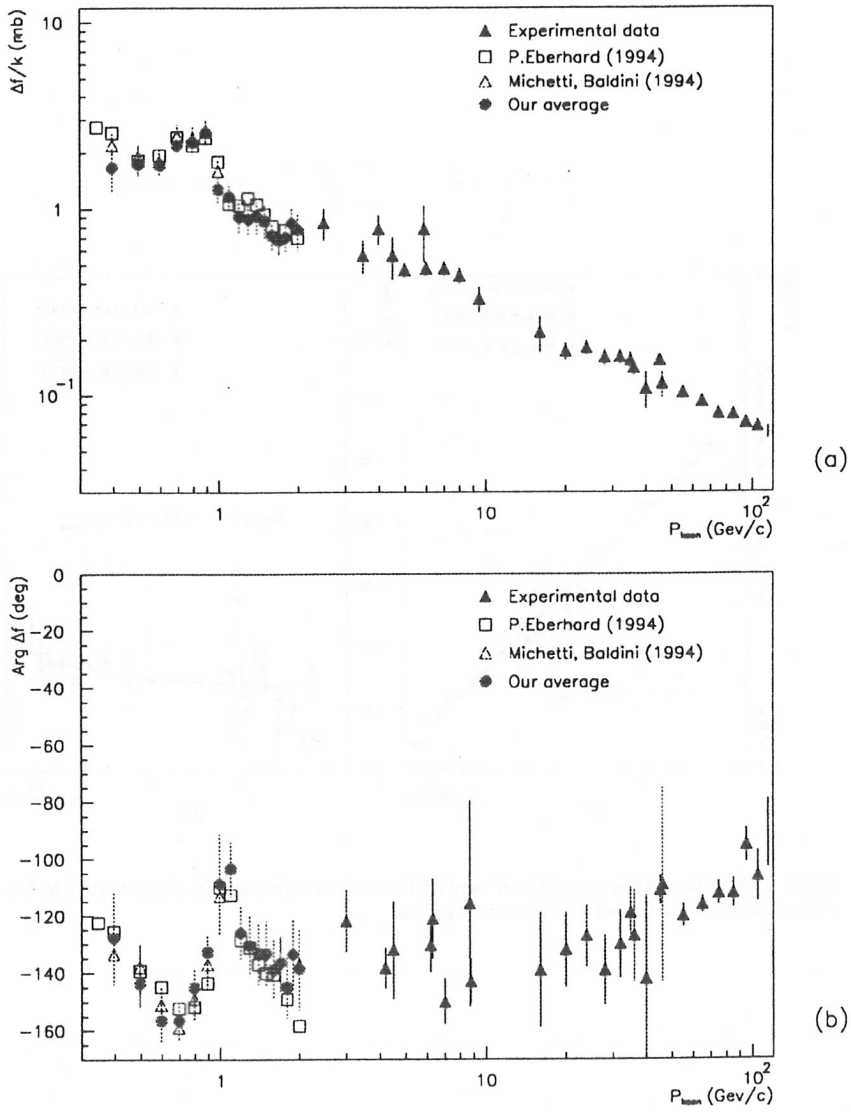

Figure 3: Difference of the K^0 and $\overline{K^0}$ forward scattering amplitudes in hydrogen as function of the kaon momentum, calculated and measured values for the modulus (a) and phase (b)

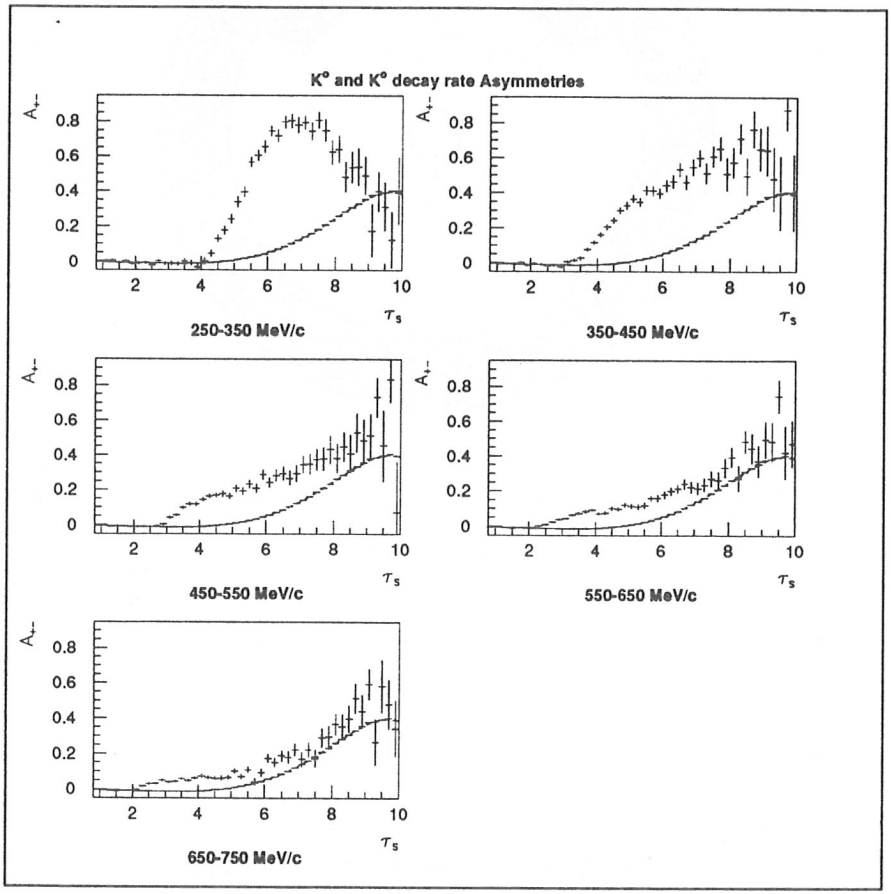

Figure 4: $\overline{\mathrm{K^0}}$ – $\mathrm{K^0}$ decay to $\pi^+\pi^-$ rate asymmetries for 5 intervals of the kaon momentum, as a function of the proper time τ (in units of the K_S mean lifetime τ_S). The dashed line is the asymmetry without regenerator (Eq. 2 with I=0) and the points are Monte Carlo data with a 2 cm carbon regenerator at 7 cm from the target.

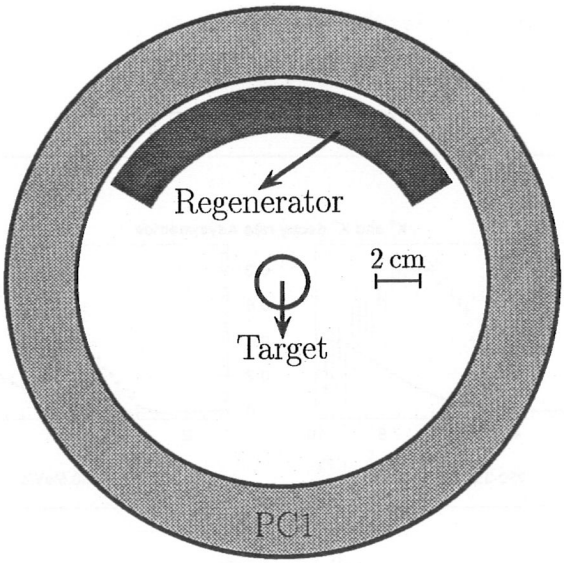

Figure 5: Schematic view of the regenerator inserted in front of the inner proportional chamber (PC1)

References

1. R.Carosi et al., Phys. Lett. B237 (1990) 303.

2. L.K.Gibbons et al., Phys. Rev. Lett. 70 (1993) 1199.

3. 'Measurement of the CP Violation Parameter η_{+-} using tagged K° and $\overline{\text{K°}}$', R.Adler et al., to be submitted to Phys. Lett.

4. The DAFNE Physics handbook, ed. L.Maiani, G.Pancheri and N.Paver, INFN Frascati

5. 'The CPLEAR detector at CERN', R.Adler et al., to be submitted to Nucl. Instr. and Methods.

6. A.Gsponer et al., Phys. Rev. Lett. 42 (1979) 13;
H.Faissner et al., Phys. Lett. 30B, (1969) 204;
H.Foeth et al., Phys. Lett. 31B, (1970) 544;
F.Dydak et al., Nucl. Phys. B102, (1976) 253.

7. D.Freytag et al., Phys. Rev. Lett. 35 (1975) 412;
P.Darriulat et al., Phys. Lett. 33B, (1970) 433;
G.J.Bock et al., Phys. Rev. Lett. 42 (1979) 350;
V.K.Birulev et al., Nucl. Phys. B115 (1976) 249;
G.W.Brandenburg et al., Phys. Rev. 9D (1974) 1939;
M.Mugge et al., Phys. Rev. 20D (1979) 2105.

8. W.C.Carithers et al., Phys. Rev. Lett. 34 (1975) 1240;
K.F.Albrecht et al., Nucl. Phys. B93 (1975) 237;
J.Roehrig et al. Phys. Rev. Lett. 38 (1977) 1116.

9. A.Baldini et al., Landolt-Börnstein New Series I/12b,
'Data an Kaon total cross sections'

10. P.Baillon et al., Nucl. Phys. B105 (1976) 365;
P.Baillon et al., Nucl. Phys. B107 (1976) 189;
P.Baillon et al., Nucl. Phys. B134 (1978) 31.

11. A.D.Martin, Nucl. Phys. B179 (1981) 33.

12. J.Antolin, Phys. Rev. 35D (1987) 122;
J.Antolin, J.Math.Phys. 31 (1990) 791;
J.Antolin and A.Cruz, J.Phys. G:Nucl. Phys. 12 (1986) 297.

13. P.H.Eberhard and F.Uchiyama, Nucl. Instr. and Methods A 350 (1994) 144.

14. A.Michetti and R.Baldini, KLOE Collaboration, private communication.

15. W.L.Wang and F.Uchiyama, Nucl. Phys. B73 (1974) 23.
F.Uchiyama, Phys. Rev 9D (1974) 673.

16. K.Kleinknecht, Fortschritte der Physik 21 (1973) 57.

17. 'Determination of regeneration amplitudes with K° and $\overline{\mathrm{K}^{\circ}}$ beams',
W.Fetscher, P.Kokkas, P.Pavlopoulos and T.Ruf, in preparation.

18. S.Bellucci, KLOE Collaboration, private communication.

19. 'The effect on regeneration for the 2π decays',
P.Kokkas, CPLEAR note CP/PHY-034 (1994).

20. 'Status of the $\pi^{\circ}\pi^{\circ}$-analysis using Dalitz decays and converted photons',
T.Ruf and M.Wolter, CPLEAR note CP/NFS/007.

21. see CERN SPSLC 94-30, october 1994.

DO THE PROOFS OF APPRECIABLE $\varphi\omega$ MIXING EXIST?

N.N. ACHASOV
Laboratory of Theoretical Physics, S.L. Sobolev Inst. Math.
630090, Novosibirsk-90, Russian Federation *)
A.A. KOZHEVNIKOV
Laboratory of Theoretical Physics, S.L. Sobolev Inst. Math.
630090, Novosibirsk-90, Russian Federation

ABSTRACT

Modern data on the decays $\varphi, \omega \to e^+e^-$ are shown to point to the essential role of the direct transition in comparison with the standard picture of the $\varphi\omega$ mixing. Invoking the arguments based on QCD, we argue in favor of the direct transition being equally probable origin of the decay $\varphi(1020) \to \rho(770)\pi \to \pi^+\pi^-\pi^0$ as the $\varphi\omega$ mixing.

At present, new investigations of the $\varphi(1020)$ meson decays with the detector CMD-2 [1] are under way at an upgraded e^+e^- facility VEPP-2M in Novosibirsk. Another detector, SND, aiming to study the same energy range should soon be put into the operation at the same facility. Moreover, the φ factory DAΦNE in Frascati is also expecting to start the operation. In connection with this development, we would like to raise at a new level the old classic problem of the $\varphi\omega$ mixing and of the decay $\varphi(1020) \to \rho(770)\pi$.

In the conventional picture of the $\varphi\omega$ mixing of the ideally mixed states,

$$\begin{aligned} \omega^{(0)} &= (u\bar{u} + d\bar{d})/\sqrt{2}, \\ \varphi^{(0)} &= s\bar{s}, \end{aligned} \tag{1}$$

the decay $\varphi(1020) \to \rho(770)\pi \to \pi^+\pi^-\pi^0$ is caused by a small admixture of the non-strange quarks in the wave function of the φ meson,

$$\varphi(1020) = s\bar{s} + \varepsilon_{\varphi\omega}(u\bar{u} + d\bar{d})/\sqrt{2}, \tag{2}$$

where $\varepsilon_{\varphi\omega}$ is the complex parameter of the $\varphi\omega$ mixing, $|\varepsilon_{\varphi\omega}| \ll 1$. It can be expressed through the nondiagonal polarization operator $\Pi_{\varphi\omega}$ according to the relation

$$\varepsilon_{\varphi\omega} = -\frac{\mathrm{Re}\Pi_{\varphi\omega} + i\mathrm{Im}\Pi_{\varphi\omega}}{m_\varphi^{(0)2} - m_\omega^{(0)2} - i\sqrt{s}(\Gamma_\varphi^{(0)}(s) - \Gamma_\omega^{(0)}(s))}. \tag{3}$$

Here $m_V^{(0)}$, $\Gamma_V^{(0)}(s)$ are, respectively, the mass and width of the ideally mixed state $V = \omega^{(0)}, \varphi^{(0)}$. [See Eq. (1) and Ref. [2] for more detail.] The magnitude of $\mathrm{Re}\varepsilon_{\varphi\omega} \simeq 0.05$ necessary to explain the branching ratio $B(\varphi(1020) \to \rho(770)\pi) = 12.9 \pm 0.7\%$ [3] and the sign of the $\varphi\omega$ interference near the φ resonance is considered to arise in QCD due to the nonperturbative effects of the type shown in Fig. 1(a) [4],

$$\varepsilon_{\varphi\omega} \propto \alpha_s \frac{\langle 0|s\bar{s}|0\rangle\langle 0|u\bar{u} + d\bar{d}|0\rangle}{M^6}, \tag{4}$$

where M is the Borel mass entering into the QCD sum rule [4]. Note that the imaginary part, $\mathrm{Im}\Pi_{\varphi\omega}$, is determined above the $K\bar{K}$ threshold, by the unitarity relation, through common decay modes of the states $\omega^{(0)}$, $\varphi^{(0)}$, mainly $K\bar{K}$. This model-independent contribution is always present, however, corresponding $B(\varphi(1020) \to \rho(770)\pi)$ is by two orders of magnitude lower than that observed.

Let us inspect the question of how good is the basis of the conventional picture of the $\varphi\omega$ mixing. To this end we write the effective $\varphi\rho\pi$ coupling constant,

$$g_{\varphi\rho\pi} = g_{\varphi\rho\pi}^{(0)} + \varepsilon_{\varphi\omega} g_{\omega\rho\pi}^{(0)}, \tag{5}$$

where the first term describes the direct transition while the second one corresponds to the $\varphi\omega$ mixing. Analogous expression is valid also for other decay modes of the φ and ω mesons. If the mass difference of these mesons were small, the $\varphi\omega$ mixing would dominate, similar to the system of the neutral K-mesons. In the present case, however, the mass squared difference, $m_\varphi^{(0)2} - m_\omega^{(0)2} \simeq 0.4$ GeV^2, amounts to 40% of the characteristic scale 1 GeV^2, so that there are no serious reasons to expect the mixing prevails the direct transition.

The ratio of the leptonic widths [5]

$$R_{e^+e^-} \equiv \frac{\Gamma(\varphi \to e^+e^-, \sqrt{s} = m_\varphi)}{\Gamma(\omega \to e^+e^-, \sqrt{s} = m_\omega)} = \left|\frac{g_{\gamma\varphi}^{(0)} + \varepsilon_{\varphi\omega} g_{\gamma\omega}^{(0)}}{g_{\gamma\omega}^{(0)} - \varepsilon_{\varphi\omega} g_{\gamma\varphi}^{(0)}}\right|^2 \left(\frac{m_\omega}{m_\varphi}\right)^3, \tag{6}$$

is sensitive to the magnitude of $\varepsilon_{\varphi\omega}$. Here $g_{\gamma V}^{(0)} = e m_V^{(0)2}/f_V^{(0)}$ and m_ω, m_φ are the masses of the states with the $\varphi\omega$ mixing being taken into account. Approximately, they are equal to, respectively, $m_\omega^{(0)}$, $m_\varphi^{(0)}$, if one neglects the terms of second order in the mixing parameter. Assuming the ratio of the coupling constants implied by the nonrelativistic quark model [6],

$$f_\omega^{(0)}/f_\varphi^{(0)} = -\sqrt{2}, \tag{7}$$

one obtains that $R_{e^+e^-} = 2.0$ at $\mathrm{Re}\varepsilon_{\varphi\omega} \approx 0.05$ and $R_{e^+e^-} = 2.6$ at $\mathrm{Re}\varepsilon_{\varphi\omega} \approx 0$.

Until 1988, an experiment gave $R_{e^+e^-} = 1.9 \pm 0.4$ and seemingly witnessed in favor of the sizeable amplitude of the $\varphi\omega$ mixing. Modern data [3] give $R_{e^+e^-} = 2.3 \pm 0.1$, pointing to a rather weak mixing. In fact, one gets from $R_{e^+e^-} = 2.3$ that $\mathrm{Re}\varepsilon_{\varphi\omega} \approx 0.02$, provided the ratio Eq. (7) is fulfilled, resulting in an unacceptable low $B(\varphi(1020) \to \rho(770)\pi) = 2\%$. Hence, in view of Eq. (5), the coupling constant of the direct transition $\mathrm{Re}g^{(0)}_{\varphi\rho\pi} \simeq 0.5\ \mathrm{GeV}^{-1} \approx \frac{1}{29}\mathrm{Re}g^{(0)}_{\omega\rho\pi}$ is required to reconcile the data on the e^+e^- and $\rho\pi$ decay modes of the $\varphi(1020)$. Note that the current fits [7, 8] give $\mathrm{Re}g^{(0)}_{\omega\rho\pi} = 14.3\ \mathrm{GeV}^{-1}$.

As is clear from the expression [6]

$$f_V^{(0)} = \frac{m_V^{3/2}}{2\sqrt{3}C_V|\psi(0,m_V)|}, \tag{8}$$

where C_V is expressed through the charge of the quark q as $C_\varphi = e_s = -1/3$, $C_\omega = (e_u + e_d)/\sqrt{2} = 1/3\sqrt{2}$, the magnitude of the $\varphi\omega$ mixing can be extracted from the e^+e^- data only in the case of the specific assumptions about the mass behavior of the wave function of the $q\bar{q}$ bound state $\psi(0,m_V)$ at the origin. Side by side with Eq. (7), which is valid in the case of the nonrelativistic behavior $|\psi(0,m_V)|^2 \propto m_V^3$ and corresponds to the Coulomb-like $q\bar{q}$ potential [9], currently popular is the behavior $|\psi(0,m_V)|^2 \propto m_V^2$. It is valid for heavy quarkonia J/ψ and $\Upsilon(1S)$, and predicts

$$\Gamma(V \to e^+e^-, \sqrt{s} = m_V) \propto C_V^2 \tag{9}$$

in the absence of the mixing, independent of m_V. The resulting ratios

$$\Gamma(\varphi \to e^+e^-) : \Gamma(J/\psi \to e^+e^-) : \Gamma(\Upsilon(1S) \to e^+e^-) = e_s^2 : e_c^2 : e_b^2 = 1 : 4 : 1, \tag{10}$$

perfectly agree with the data [3]. Corresponding $q\bar{q}$ potential varies like $r^{-1/2}$ [9], incorporating the property of the asymptotic freedom at the short distances. Extrapolating Eq. (9) to the $\omega\varphi$ mass range, one gets that

$$f_\omega^{(0)}/f_\varphi^{(0)} = -\sqrt{2m_\omega/m_\varphi} = -1.24, \tag{11}$$

giving $R_{e^+e^-} = 2.0$ in the absence of the $\varphi\omega$ mixing, $\mathrm{Re}\varepsilon_{\varphi\omega} \approx 0$, which coincides with the prediction of conventional $\varphi\omega$ mixing and the behavior $|\psi(0,m_V)|^2 \propto m_V^3$.

In order to explain the experimental magnitude of $R_{e^+e^-} = 2.3$, the extrapolation Eq. (11) demands $\mathrm{Re}\varepsilon_{\varphi\omega} \approx -0.026$ leading to a too low $B(\varphi \to \rho\pi)$ amounting to one fourth of the observed. Moreover, due to the minus sign, this sharply contradicts the measurements of the cross section of the reaction $e^+e^- \to \pi^+\pi^-\pi^0$ [7],

$$\sigma = \frac{4\pi\alpha W(s)}{s^{3/2}} \left| \frac{(g^{(0)}_{\gamma\omega} - \varepsilon_{\varphi\omega}g^{(0)}_{\gamma\varphi})g^{(0)}_{\omega\rho\pi}}{m_\omega^2 - s - i\sqrt{s}\Gamma_\omega(s)} + \frac{(g^{(0)}_{\gamma\varphi} + \varepsilon_{\varphi\omega}g^{(0)}_{\gamma\omega})g_{\varphi\rho\pi}}{m_\varphi^2 - s - i\sqrt{s}\Gamma_\varphi(s)} \right|^2, \tag{12}$$

[$\alpha = 1/137$] since results in the wrong sign of the interference pattern. Here s is the total center of mass energy squared, $\Gamma_\omega(s)$ and $\Gamma_\varphi(s)$ are the total widths of the ω and φ mesons with the $\varphi\omega$ mixing being taken into account while $W(s)$ is [8] the phase space factor for the 3π decay. To remove this contradiction, one should introduce, in view of Eq. (5), a sizable coupling constant of the direct transition $\mathrm{Re}g^{(0)}_{\varphi\rho\pi} \simeq 1.1\ \mathrm{GeV}^{-1} \approx \frac{1}{13}\mathrm{Re}g^{(0)}_{\omega\rho\pi}$.

From the other hand, to obtain the acceptable $\rho\pi$ branching ratio, the correct interference pattern in the cross section of the reaction $e^+e^- \to \omega, \varphi \to \pi^+\pi^-\pi^0$ and the experimental magnitude of $R_{e^+e^-} = 2.3$ in the case of conventional $\varphi\omega$ mixing, $\mathrm{Re}\varepsilon_{\varphi\omega} \approx 0.05$, one should change $f^{(0)}_\omega/f^{(0)}_\varphi$ to -1.53. The latter value corresponds to $|\psi(0, m_V)|^2 \propto m_V^{3.6}$ which follows from the $q\bar{q}$ potential $V(r) \propto r^{-1.2}$ [9] and means the increase of effective QCD coupling at the short distances in a contradiction with the property of the asymptotic freedom.

Thus, the existing data on the decays $\varphi(1020) \to e^+e^-$, $\rho(770)\pi$ and the interference pattern seem to point to a sizable, or even dominant, coupling constant $\mathrm{Re}g^{(0)}_{\varphi\rho\pi}$ of the direct transition as compared to the conventional $\varphi\omega$ mixing.

Note that an old theoretical phenomenology [see e.g. [10]] gave a broad spectrum of the possible values $-0.07 \le \mathrm{Re}\varepsilon_{\varphi\omega} \le +0.07$ [$-0.03 \le \mathrm{Re}\Pi_{\varphi\omega} \le +0.03\ \mathrm{GeV}^2$]. As for the QCD estimate, Eq. (4), the results of the papers [11, 12] show that the magnitudes of the quark condensates $\langle 0|q\bar{q}|0\rangle$ are known only up to a factor ranging from 0.1 to 8.0. The magnitude of the Borel mass entering into the sum rule as M^{-6} is also uncertain. Taken together, these facts demonstrate the lack of the firm basis for a sizable $\varphi\omega$ mixing in QCD. But if the mixing is unessential, how can one explain the decay $\varphi(1020) \to \rho(770)\pi$? Or, in other words, what is the direct transition?

To this end let us note [13] that the meson $\varphi(1020)$ composed of mainly $s\bar{s}$ quark pair lies at the borderline between the domains of light [$u\bar{u}$, $d\bar{d}$] and heavy [$c\bar{c}$, $b\bar{b}$] quarkonia. Hence, the mechanism of the three-gluon annihilation, which describes the Okubo-Zweig-Iizuka [OZI] rule [14, 15, 16] violating decays of heavy quarkonia J/ψ and $\Upsilon(1S)$ into hadrons containing no heavy quarks, cannot be excluded for this state. In fact, treating s quarks as heavy and applying to the φ meson the expression for the three-gluon width [17],

$$\Gamma(\varphi \to 3g) = \frac{10}{9\pi}(\pi^2 - 9)\frac{\alpha_s^3(m_\varphi)}{\alpha^2}\Gamma(\varphi \to e^+e^-), \tag{13}$$

one can obtain that the branching ratio of the decay $\varphi(1020) \to \rho(770)\pi \to \pi^+\pi^-\pi^0$ corresponds to the QCD coupling constant $\alpha_s(m_\varphi) = 0.43$, in agreement with the QCD estimate, namely, $\alpha_s(m_\varphi) = 0.43$ at $\Lambda = 200$ MeV. [In the case of $\Lambda = 100$ MeV the partial width of the three-gluon annihilation amounts to 1/3 of the $\varphi(1020) \to$

$\rho(770)\pi \to 3\pi$ partial width.] Note that the $\rho\pi$ is essentially the only final hadronic state not suppressed by the phase space volume, to which three gluons can convert, e.g., by means of the process shown in Fig. 1(b), exactly in the same manner as it takes place in the decays of heavy quarkonia. The precise magnitude of the probability of this conversion cannot be evaluated at present. However, there seems to be no reasons to expect it severely suppressed, since the gluon conversion into the hadrons composed of light quarks occurs at large distances, where the quark-gluon coupling constant is not small.

Evidently, such a diagram is not reduced to the $\varphi\omega$ mixing. In the meantime, the contribution of the three-gluon mechanism to the $\varphi\omega$ mixing shown in Fig. 1(c) is negligible and has a wrong sign [18, 19] in the sense that in contradiction with the experiment [7] it results in the interference minimum in the energy dependence of the cross section of the reaction $e^+e^- \to \omega, \varphi \to \pi^+\pi^-\pi^0$ [see Eq. (12)] below the φ resonance but not above it.

The experimental elucidation of the situation is necessary, first, by means of the improvement of the accuracy of the measurement of the ω and φ leptonic widths by a factor of $5 - 10$.

We, however, believe that the study of the nature of the decay $\varphi(1020) \to \rho(770)\pi$ is equally important. As is shown in [2], to this end one should investigate the energy dependence of the cross section of the reaction $e^+e^- \to \omega, \varphi \to \pi^+\pi^-\pi^0$ in the vicinity of the $\varphi\omega$ interference minimum, $\sqrt{s} = 1.05$ GeV, where the cross section is very sensitive to a small difference between the $\varphi\rho\pi$ coupling constants in the variants of the strong [$\mathrm{Re}\Pi_{\varphi\omega} \neq 0$, $\mathrm{Re}g^{(0)}_{\varphi\rho\pi} = 0$] and weak [$\mathrm{Re}\Pi_{\varphi\omega} = 0$, $\mathrm{Re}g^{(0)}_{\varphi\rho\pi} \neq 0$] $\varphi\omega$ mixing.

Acknowledgements

The present work is partially supported by the grant 94-02-05 188 from the Russian Foundation for Basic Research.

Nikolai Achasov is grateful to organizers of DAΦNE'95 and especially to Giulia Pancheri for invitation and for financial support.

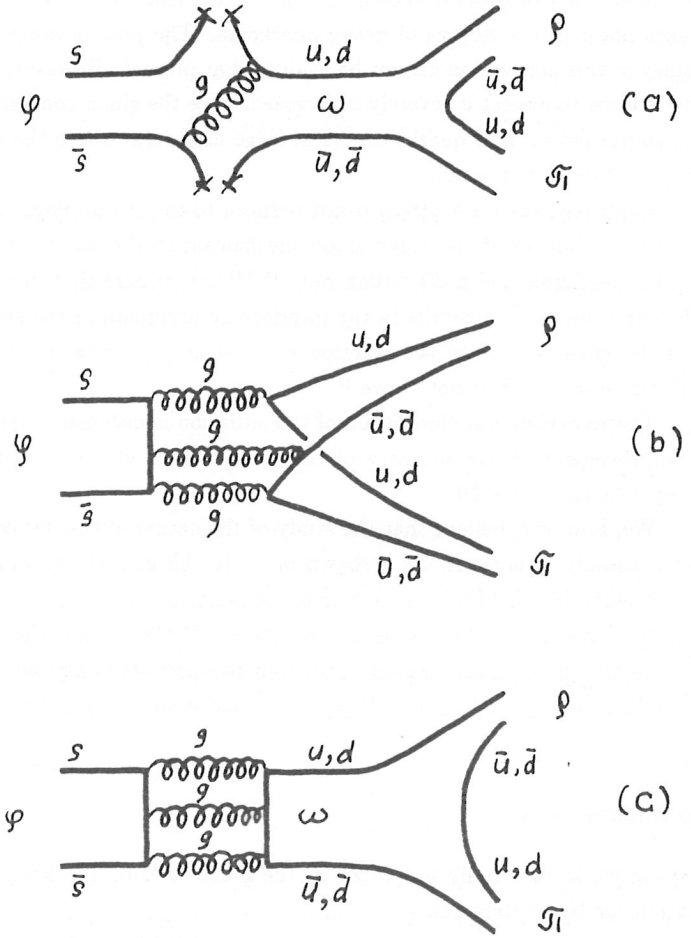

Figure 1: Possible mechanisms of the decay $\varphi(1020) \to \rho(770)\pi$. (a)The $\varphi\omega$ mixing due to the nonperturbative QCD effects. (b)The three-gluon mechanism of the direct transition $\varphi \to \rho\pi$. (c)The $\varphi\omega$ mixing caused by the three-gluon mechanism. Crosses mean the quark condensate, g denotes the gluon.

References

* . E-mail address: achasov@math.nsk.su

1. R.R. Akhmetshin *et al.*, CMD2 Collaboration, Pittsburg Preprint PITT 94-05 (1994) (unpublished).

2. N.N. Achasov and A.A. Kozhevnikov, Particle World, **3**, 125 (1993); Yad. Fiz. **55**, 3086 (1992).

3. M. Agiular-Benitez *et al.*, (Particle Data Group), Phys. Rev. D**50**, 1173 (1994).

4. M.A. Shifman, A.I. Vainshtein and V.I. Zakharov, Nucl. Phys., **B147**, 448 (1979).

5. N.M. Kroll, T.D. Lee and B. Zumino, Phys. Rev., **157**, 1376 (1967).

6. R. Van Royen and V.F. Weisskopf, Nuovo Cimento, **LA3**, 617 (1967).

7. S.I. Dolinsky *et al.*, Phys. Rep. C**202**, 99 (1991).

8. N.N. Achasov *et al.*, Int. Journ. Mod. Phys. A**7**, 3187 (1992).

9. F.E. Close, *Introduction to Quarks and Partons*, (Academic Press, 1979) chap. 16.

10. J.J. Sakurai, *Currents and Mesons*, (The University of Chicago Press, Chicago and London) chap.3.

11. A.G. Grozin and Yu.F. Pinelis, Mod. Phys. Lett., **A3**, 735 (1988).

12. R.A. Bertelman *et al.*, Z. Phys. C-Particles and Fields, **39**, 231 (1988).

13. N.N. Achasov, in: II EURODAΦNE Collaboration Meeting, (Frascati, 19-22 April, 1994, eds. L. Maiani, G. Pancheri and N. Paver) p. 628.

14. S. Okubo, Phys. Lett., **5**, 165 (1963).

15. G. Zweig, CERN Report 8419/TH412 (1964) (unpublished).

16. J. Iizuka, Progr. Theor. Phys. Suppl., **37-38**, 21 (1966).

17. T. Appelequist and H.D. Politzer, Phys. Rev. Lett., **34**, 43 (1975).

18. J. Arafune, M. Fukugita and Y. Oyanagy, Phys. Lett., **B70**, 221 (1977).

19. B.V. Geshkenbein and B.L. Ioffe, Nucl. Phys. **B166**, 340 (1980).

Participants

Nikolai N. ACHASOV	Novosibirsk
Michelangelo AGNELLO	Torino
Roy ALEKSAN	SLAC
Gedeon ALEXANDER	Tel Aviv
Ahmed ALI	DESY
Wolfgang ALLES	Bologna
Guido ALTARELLI	CERN
Renzo ALZETTA	Cosenza
Lluis AMETLLER	Barcelona
Balasubramanian ANANTHANARAYAN	Lausanne
Antonella ANTONELLI	LNF
Katsushi ARISAKA	UCLA
Vincente AZCOITI	LNF
Emili BAGAN	Barcelona
Rinaldo BALDINI-FERROLI	LNF
Ted BARNES	Oak Ridge
Roger C. BARRETT	Guildford
Giorgio BELLETTINI	Pisa
Stefano BELLUCCI	LNF
Karl BERKELMAN	Cornell
Monica BERTANI	LNF
Sergio BERTOLUCCI	LNF
Maria Enrica BIAGINI	LNF
Nicola BIANCHI	LNF
Stefano BIANCO	LNF
Caterina BLOISE	LNF
Jerzy BOGDANOWICZ	Warsaw
Fabio BOSSI	LNF
Francisco J. BOTELLA	Valencia
Elena BOTTA	Torino
Tullio BRESSANI	Torino
Cristophe BRUNO	Bern
Marco BRUSCHI	Bologna
Nicola CABIBBO	ENEA
Alessandro CALCATERRA	LNF
Mario CALVETTI	Perugia
Daniela CALVO	Torino
Giorgio CAPON	LNF
Claudio CATTANEO	Pavia
Augusto CECCUCCI	Torino
Luigina CELANO	Bari
Patrizia CENCI	Perugia
Rosanna CESTER	Torino
Maxwell CHERTOK	CERN
Decio COCOLICCHIO	Milano
Nicola COLONNA	Bari
Fernando CORNET	Granada

Andre' COURAU	LAL
Giancarlo D'AMBROSIO	Napoli
Ginevra D'ERASMO	Bari
Riccardo DE SANGRO	LNF
Pascal DEBU	Saclay
Achim DENIG	Karlsruhe
Antonio DI DOMENICO	Roma I
Claudio DIB	Valparaiso
Stanislav DUBNICKA	Bratislava
Jean DUCLOS	CERN
Alex DZIERBA	Indiana
Phillippe EBERHARD	Berkeley
Jean Pierre EGGER	Neuchâtel
Onofrio ERRIQUEZ	Bari
Franco L. FABBRI	LNF
Ada FARILLA	LNF
Guenadi V. FEDOTOVICH	Novosibirsk
Alessandro FELICIELLO	Torino
Maria Lorenza FERRER	LNF
Alessandra FILIPPI	Torino
Rosa Anna FINI	Bari
Markus FINKEMEIER	LNF
Luigi FIORE	Bari
Vladimir FLIAGUINE	Dubna
Paolo FRANZINI	LNF
Avraham GAL	Jerusalem
Juerg GASSER	Bern
Ugo GASTALDI	LNL
Paolo GENSINI	Perugia
Paola GIANOTTI	LNF
Carlo GOBBI	Pavia
Viatcheslav GOLOVATIUK	Lecce
Edoardo GORINI	Lecce
Peter GOSDZINSKY	Barcelona
Ines GRAU	Granada
Mario GRECO	LNF
Carlo GUARALDO	LNF
Paola GUARNACCIA	Bari
Peter HAYMAN	Liverpool
Barry R. HOLSTEIN	Amherst
Enzo IAROCCI	LNF
Toru IIJIMA	Tsukuba
Markus IMHOF	Karlsruhe
Gino ISIDORI	Roma I
Vladimir M. IVANCHENKO	Novosibirsk
Masa IWASAKI	Tokyo
Leonid KHALFIN	St. Petersburg

Marc KNECHT	Orsay
Panagiotis KOKKAS	CERN
Ivan KOOP	Novosibirsk
Yury KUDENKO	Moskva
Oleg KUZNETSOV	Genova
Paolo LAURELLI	LNF
Juliet LEE-FRANZINI	LNF
Massimo LENTI	Firenze
Harry J. LIPKIN	Rehovot
Jose L. LUCIO	Guanajuato
Juris LUKSTINS	Dubna
Luciano MAIANI	INFN
Lubomir MAJLING	Dubna
Simonetta MARCELLO	Torino
Guido MARTINELLI	Roma I
Mara MARTINI	CERN
Nikolaos MAVROMATOS	CERN
Bruno MINETTI	Torino
Stefano MISCETTI	LNF
Amnon MOALEM	Beer-Sheva
Alfredo MOLINARI	Torino
Fabio MONITTOLA	Lecce
Lucien MONTANET	CERN
Ombretta MORRA	Torino
Giampaolo MURTAS	LNF
Helmut NEUFELD	Wien
Marek NOWAKOWSKI	LNF
Jona OBERSKI	NIKHEF
Art OLIN	TRIUMF
Saro ONG	Paris
Haruhiko OUTA	Tokyo
Elisabetta PALLANTE	NORDITA
Marco PANAREO	Lecce
Giulia PANCHERI	LNF
Ambrogio PANTALEO	Bari
Luciano PAOLUZI	Roma II
Daniela PARENA	Torino
Emmanuel PASCHOS	Dortmund
Vincenzo PATERA	LNF
Nello PAVER	Trieste
Noulis PAVLOPOULOS	CERN
Roberto PECCEI	UCLA
Bernard PEYAUD	Saclay
Maurizio PICCININI	Bologna
Marcello PICCOLO	LNF
Ludovico PONTECORVO	Roma I
Jorge PORTOLES	Didcot

Joaquim PRADES	NORDITA
Margherita PRIMAVERA	Lecce
Angels RAMOS	Barcelona
Giulia RICCIARDI	Napoli
Elena ROSSETTO	Torino
Patrich ROUDEAU	Orsay
Carlo RUBBIA	CERN
Thomas RUF	CERN
Federico RUGGIERI	LNF
Bijan SAGHAI	Saclay
Mikko SAINIO	Helsinki
Alessandra SAINO	Pavia
Giorgio SALVINI	Roma I
Shahzad SARWAR	LNF
Reyad I. SAWAFTA	Upton
Frank SCHOENLEBER	Karlsruhe
Andreas SCHWARZ	DESY
Eugeni SHABALIN	Moscow
Archana SHARMA	Torino
Yuri SHATUNOV	Novosibirsk
Alexande N. SKRINSKY	Novosibirsk
Evgeny P. SOLODOV	Novosibirsk
Stefania SPAGNOLO	Lecce
Josef SPETH	Juelich
Piero SPILLANTINI	Firenze
Yogendra SRIVASTAVA	Perugia
Jan STERN	Orsay
Leo STODOLSKI	Muenchen
Pere TALAVERA	Bellaterra
Hirokazu TAMURA	Tokyo
Dominique TOUBLAN	Lausanne
Vincenzo VALENTE	LNF
Luca VENTURELLI	Brescia
Gaetano VIGNOLA	LNF
Uwe VON HAGEL	Karlsruhe
Dieter WALTHER	Bochum
Siegfried WESELER	Karlsruhe
Bruce D. WINSTEIN	Chicago
Toshimitsu YAMAZAKI	Tokyo
Aldo ZENONI	Brescia
David ZIMMERMAN	CERN
Antonio ZOCCOLI	Bologna
Andy ZOTT	Karlsruhe